LHCb-ANA-2013-097
December 15, 2015

Angular analysis of $B^0 \to K^{*0}\mu^+\mu^-$ decays using 3 fb^{-1} of integrated luminosity

E. Ben-Haim[4], T. Blake[1], E. Bowen[2], M. Chrzaszcz[2], M. De Cian[3], S. Coquereau[4], S. Cunliffe[5], U. Egede[5], M. McCann[5], C. Langenbruch[1], T. Nikodem[3], M. Patel[5], K. Petridis[6], F. Polci[4], N. Serra[2], B. Storaci[2], M. Tresch[2]

[1] *Department of Physics, University of Warwick, Coventry, United Kingdom*

[2] *Physik-Institut, Universität Zürich, Zürich, Switzerland*

[3] *Physikalisches Institut, Ruprecht-Karls-Universität Heidelberg, Heidelberg, Germany*

[4] *LPNHE, Université Pierre et Marie Curie, Université Paris Diderot, CNRS/IN2P3, Paris, France*

[5] *Imperial College London, London, United Kingdom*

[6] *University of Bristol, Bristol, United Kingdom*

Abstract

We present an angular analysis of the $B^0 \to K^{*0}\mu^+\mu^-$ decay using the full data sample collected by the LHCb experiment during Run I and corresponding to an integrated luminosity of $3\,\text{fb}^{-1}$. We determine angular observables in two different q^2 binnings, using an unbinned maximum likelihood fit and the method of moments. In addition, we determine the K^{*0} helicity amplitudes in the q^2 range $1.1 < q^2 < 6\,\text{GeV}^2/c^4$ using a q^2 dependent ansatz.

Contents

0 Information on the review process

0.1 Version history

v1	12. 11. 2014	Initial release
v2	26. 11. 2014	WG approval

- Added two-dimensional likelihood scans for the angular observables in Sec. 6.2.5.
- S-wave pollution can be constrained using the $m_{K\pi}$ distribution. The method is described in Sec. 6.2.12.
- Added further discussion on accidental symmetry in Sec. 6.4.4
- Completed list of 1D profile plots of amplitude coefficients in Sec. 6.4.11
- Expanded discussion of how the $m_{K\pi}$ dependence of the amplitudes is treated in Sec. 6.4.6

v3	16. 01. 2015	1st comments

- Implemented 1st round of referee comments.
- Re-written description of the fits to the amplitudes in Sec. 6.4.
- Added section on expected sensitivity to model with $\mathcal{C}_9^{NP} = -1.5$ for the amplitude fits in Sec. 6.4.12.
- Added systematic uncertainties related to acceptance correction, background parametrisation and $m_{K\pi}$ dependence for amplitude fits.
- Added (almost) complete set of 2D profiles for amplitude fits.
- Evaluated additional systematic uncertainties for the observables fit: Peaking backgrounds, angular background description, higher order acceptance model, signal mass model
- Performed first blind fits of observables
- Improved description of simultaneous angular and $m_{K\pi}$ fit, the plots of allowed parameter regions, table of previous $B^0 \to J/\psi\, K^{*0}$ results, profile likelihood scans for the observables fit

v3c	22. 01. 2015	update

- Implemented referees' comments in the method of moments sections
- Added $B^0 \to J/\psi K^*$ validation with the method of moments
- Added S-wave studies with the method of moments
- Added blinded results for the method of moments
- Added first coverage corrected results from the observables fit
- Added $m_{K\pi}$ systematics for the observables fit

v4 07. 07. 2015 update

- Added result for the method of moments. Including bootstrapping of the dataset to determine the statistical uncertainty on the angular observables and fit to $m(K^+\pi^-)$ to determine $F_{\rm S}$.
- Added systematic unertainties for the method of moments.
- Added *CP* asymmetries A_i and full $P_i^{(\prime)}$ basis from the observables fit.
- Added systematic uncertainties for *CP* asymmetries.
- Increased FC statistics for the observables fit. Updated $B^0 \to J/\psi K^{*0}$ numbers. Updated toy studies.

0.2 To-do list

Here we summarize the main ongoing open studies:

- General ongoing studies:
- Specific for the amplitude fit:
  - Test the statistical coverage of the bootstraps.
  - Complete zero crossing point studies.

1 Introduction

The decay $B^0 \to K^{*0}(\to K^+\pi^-)\mu^+\mu^-$ is a $b \to s$ flavour changing neutral current (FCNC) process and in the Standard Model (SM) is therefore forbidden at tree-level and only allowed at loop level.[1] In extensions of the SM, new heavy particles can appear, potentially both at tree- and loop level, and significantly change the branching fraction of this process, as well as the angular distributions of the particles in the final state.

This note describes the analysis of the angular distribution of the final state particles with the full Run I data sample, corresponding to an integrated luminosity of $3\,\mathrm{fb}^{-1}$ and taken at center of mass energies of 7 and 8 TeV. Two previous angular analyses have been performed of the decay [1, 2] using the data taken by LHCb in 2011, corresponding to an integrated luminosity of $1\,\mathrm{fb}^{-1}$. In the first publication, the CP-averaged angular observables S_i described in Ref. [3] have been determined, in the second paper, the less form-factor dependent observables $P'_{4,5,6,8}$ proposed in Ref. [4] have been measured. The angular observables show good agreement with the SM predictions, with the exception of the observable P'_5, which shows a local deviation corresponding to $3.7\,\sigma$. Assuming no correlations the p-value for such a deviation for four observables in six bins is 0.5%.

There is currently intense discussion in the theory community about the observed discrepancy. Several publications studied possible New Physics (NP) scenarios that could cause the observed shift using global fits of the underlying Wilson coefficients [5–8]. One possible explanation, which was first proposed in Ref. [5] would be a Z' of $\mathcal{O}(1\,\mathrm{TeV})$. In addition to possible NP explanations of the observed deviation, the uncertainty of the SM prediction has been under scrutiny. In particular the influence of non-factorisable corrections has been discussed [9, 10]. Recently, the influence of the $c\bar{c}$ resonances on the SM prediction has come under question [11], following the publication of a precise branching fraction measurement of the decay $B^+ \to K^+\mu^+\mu^-$ [12]. This angular analysis using LHCb's full Run I data sample is a central building block needed to clarify our picture of $b \to s\mu^+\mu^-$ transitions.

The analysis note is structured as follows: Section 2 introduces the analysis strategy, Sec. 3 presents the samples of data and simulated events used for the analysis and Sec. 4 summarizes the selection. Section 5 details the modeling of the reconstructed B^0 mass and Sec. 6 the different approaches to the analysis of the angular distributions. Section 8 discusses the angular acceptance effects and Sec. 9 gives the results for the angular observables. Systematic uncertainties are determined in Sec. 10. Finally, conclusions are presented in Sec. 12.

[1] Charge conjugation is implied throughout this note unless explicitly stated.

2 Strategy

The decay $B^0 \to K^{*0}(\to K^+\pi^-)\mu^+\mu^-$ is first selected using the cut-based Stripping and preselection, after which a multivariate classifier, a BDT, is applied. Specific vetoes are applied to reject peaking backgrounds. The $q^2 = m^2_{\mu^+\mu^-}$ regions $[8.0, 11.0]\,\text{GeV}^2$ and $[12.5, 15.0]\,\text{GeV}^2$ that contain the J/ψ and $\psi(2S)$ resonances are removed from the analysis since the tree-level decays $B^0 \to J/\psi\, K^{*0}$ and $B^0 \to \psi(2S)K^{*0}$ dominate in these regions. The selection is detailed in Ref. [13], in this note only the most important points are summarised. The reconstruction and selection results in a distortion of the angular distributions of the final state particles. This angular acceptance effect needs to be accounted for in the the angular analysis as described in Sec. 8.

There are three complementary methods for the angular analysis of the final state of the signal decay.

- *Maximum likelihood method (main proponents: C. Langenbruch, T. Nikodem, M. De Cian)* The angular observables can also be determined using an unbinned maximum likelihood fit. This method has been shown to be more sensitive than the *method of moments* in larger bins of q^2. However, for narrow q^2 bins, the method is affected by the presence of physical boundaries for the parameters which lead to a non-Gaussian behaviour of the likelihood function. The *maximum likelihood method* is the preferred method for larger q^2 bins. It is described in detail in Sec. 6.2

- *Method of moments (main proponents: M. Chrzaszcz, N. Serra)* Due to the orthogonality of the angular terms, it is possible to determine the angular observables introduced in Sec. 6.1 using a weighted counting approach, the *method of moments*. The main advantage of this method is that it is very stable and robust and allows to perform the angular analysis in narrow q^2 bins of $1\,\text{GeV}^2$. This allows to better resolve the q^2 dependency of the observables, which is of interest in theory. The *method of moments* is described in Sec. 6.3.

- *Amplitude fit (main proponents: U. Egede, M. Patel, K. Petridis, T. Blake)* Instead of the angular observables it is also possible to determine the decay amplitudes. The q^2 dependent unbinned *amplitude fit* in the $1.1 < q^2 < 6\,\text{GeV}^2/c^4$ region is interesting since the observables vary strongly here. This method allows to obtain the p-value of the SM in the most precise manner and provide the zero-crossing point of many observables. The presence of resonances outside this region make this method only applicable within $1.1 < q^2 < 6\,\text{GeV}^2/c^4$. The added benefit of fitting for the amplitudes is that the angular distribution remains positive irrespective of the values of the amplitudes. The *amplitude fit* is detailed in Sec. 6.4.

The availability of the three different approaches allows to thoroughly crosscheck the results. All methods of angular analysis provide also the linear correlations between the determined observables. This is a major improvements compared to the previous publications [1, 2], where, due to different angular foldings, no correlation matrix could be quoted.

Throughout the analysis, the tree-level decay $B^0 \to J/\psi K^{*0}$ is used as control-channel. The decay is used for the training of the multivariate selection and to ensure good agreement of simulation with data as detailed in Ref. [13]. It also allows an important cross-check for the description of the angular acceptance as discussed in Sec. 6.2.11.

As a further cross-check, at least two separate implementations have been prepared for each of the fit strategies described above and for the determination of the angular acceptance. Results from the different implementations are fully consistent.

To conclude the discussion of our analysis strategy, we give a specific list of the results we aim to provide in the paper.

- Figures showing the 8 CP-averaged observables F_L, A_{FB} and $S_{3,4,5,7,8,9}$ as well as the 7 CP-asymmetries $A_{3,4,5,6,7,8,9}$. We will present the observables in the $2\,\mathrm{GeV}^2/c^4$ bins, as well as the two large bins $1.1-6\,\mathrm{GeV}^2/c^4$ and $15-19\,\mathrm{GeV}^2/c^4$, for the observables fit and in the narrow $1\,\mathrm{GeV}^2/c^4$ bins for the method of moments. The results from the q^2 dependent amplitudes in the $1.1-6\,\mathrm{GeV}^2/c^4$ bin will be overlaid.

- Tables showing the CP-averaged observables and the CP-asymmetries in the $2\,\mathrm{GeV}^2/c^4$ and $1\,\mathrm{GeV}^2/c^4$ bins and the observables in the $1.1-6\,\mathrm{GeV}^2/c^4$ and $15-19\,\mathrm{GeV}^2/c^4$ bins. The covariance matrices should be additional information.

- Tables showing the amplitude fit parameters for the amplitude fit in the $1.1-6\,\mathrm{GeV}^2/c^4$ bin. The covariance matrices should be additional information.

- The zero crossing points for the different observables extracted from the amplitude fit, with their uncertainties.

- The observables $P_i^{(\prime)}$ etc. should appear as additional information, derived from the S_i results, unless we find something very non-SM like after unblinding.

3 Data and simulation

3.1 Data

The angular analysis described in this note is based on data corresponding to an integrated luminosity of $3\,\mathrm{fb}^{-1}$, collected by the LHCb experiment in pp collisions. The dataset comprises $1\,\mathrm{fb}^{-1}$ of integrated luminosity collected at $\sqrt{s} = 7\,\mathrm{TeV}$ in 2011 and $2\,\mathrm{fb}^{-1}$ collected at $\sqrt{s} = 8\,\mathrm{TeV}$ in 2012. Described extensively in Ref. [13], the data have been reconstructed with `Reco14` and stripped with `Stripping 20r0` and `Stripping 20r1`.

3.2 Simulated events

Fully Monte Carlo simulated $B^0 \to K^{*0}\mu^+\mu^-$ events generated according to a phase-space model are used to determine the acceptance effect of the selection and reconstruction. This sample was filtered on the `StrippingB2XMuMu` stripping line (the same as the `Stripping 20r0` and `Stripping 20r1` data) allowing for a relatively large sample to be generated. The acceptance of the full selection on the decay angles is accounted for in the analyses as described in Sec. 6.2.3. The systematic uncertainty due to the determination of the acceptance using simulation is determined as described in Sec. 10.1. Possible pollution from peaking backgrounds are estimated using several exclusive b-hadron decays. Fully simulated samples are generated for these backgrounds with `MC12` settings and reconstructed using `Reco14a`. They are combinations of `Sim08b` and `Sim08e` with an approximately equal mix of events generated using Pythia 6 and 8. The samples used in this analysis are summarised in Tab. 1.

In addition to fully simulated events, the analysis uses simulated signal events generated according to an updated full theory calculation of the decay $B^0 \to K^{*0}\mu^+\mu^-$ [14, 15] to validate the angular analysis methods used. The calculation is implemented in the publicly available `EOS` software package [16]. Two different sets of Wilson coefficients are used for the generation, the SM setting ($\mathcal{C}_7 = -0.331$, $\mathcal{C}_9 = 4.27$, $\mathcal{C}_{10} = -4.173$) and the NP setting ($\mathcal{C}_7 = -0.331$, $\mathcal{C}_9 = 4.27 - 1.5$, $\mathcal{C}_{10} = -4.173$). The choice of $\mathcal{C}_9 = 4.27 - 1.5$ in the NP setting is motivated by the best fit point of the Wilson coefficients in Ref. [5]. The `EOS` software package also is able to calculate the angular observables for the given parameters, so the simulated samples are useful to validate the methods of angular analysis. Tables 2 and 3 give the angular observables which will be introduced in Sec. 6.1.2 for two q^2 binnings. The reconstructed B^0 mass is modelled by the sum of two crystal ball functions generated using the parameters in Tab. 4. Background is modelled to be flat in the angles, exponential in the mass and parabolic in q^2. The q^2 dependence of the background fraction is taken from an extended maximum likelihood fit of the background yields in data, as shown in Fig. 1. The four dimensional acceptance described in Sec. 8.2 is applied using an accept-reject method. In addition, samples without acceptance are also generated.

Table 1: Simulated samples used in the analysis. Sample (a) is used for deriving the acceptance correction. It is filtered on the `StrippingB2XMuMu` line, number of events in this case corresponds to the statistics after stripping. Sample (b) is used to derive data-simulation corrections. Samples (b-c) are used to assess background levels. Samples (d) are used for validation of fitters and comparison of fit techniques.

	Decay	DecFile event type	Number of events
(a)	$B^0 \to K^{*0}\mu^+\mu^-$ (phase-space)	`11114005`	5.5M (stripped)
(b)	$B^0 \to J/\psi K^{*0}$ (physics)	`11144001`	2M
(c)	$B^0 \to K^{*0}\mu^+\mu^-$ (physics)	`11114001`	1M
(c)	$\Lambda_b^0 \to \Lambda(1530)\mu^+\mu^-$	`15114000`	1M
(c)	$\Lambda_b^0 \to pK^-\mu^+\mu^-$	`15114011`	2M
(c)	$B_s^0 \to \phi\mu^+\mu^-$	`13114002`	0.6M
(c)	$B^+ \to K^+\mu^+\mu^-$	`12113001`	1M
(d)	`EOS` SM Wilson coefficients, no acceptance	-	10 M
(d)	`EOS` SM Wilson coefficients, with acceptance	-	10 M
(d)	`EOS` NP Wilson coefficients, no acceptance	-	10 M
(d)	`EOS` NP Wilson coefficients, with acceptance	-	10 M

Table 2: Observables predicted by `EOS` using the 1 GeV^2 binning and the SM Wilson coefficients.

q^2[GeV^2]	S_1^s	S_1^c	S_2^s	S_2^c	S_3	S_4	S_5	S_6^s	S_6^c	S_7	S_8	S_9
$[0.1, 0.98]$	0.5599	0.2450	0.1448	−0.1953	0.0003	−0.0885	0.2251	0.1210	0.0000	0.0215	−0.0039	0.0001
$[1.1, 2.0]$	0.2580	0.6641	0.0832	−0.6258	0.0000	−0.0483	0.1651	0.2664	0.0000	0.0389	−0.0108	0.0002
$[2.0, 3.0]$	0.1648	0.7870	0.0544	−0.7591	−0.0016	0.0479	−0.0287	0.1995	0.0000	0.0382	−0.0124	0.0003
$[3.0, 4.0]$	0.1547	0.7988	0.0515	−0.7787	−0.0038	0.1254	−0.1896	0.0763	0.0000	0.0343	−0.0122	0.0003
$[4.0, 5.0]$	0.1800	0.7637	0.0600	−0.7488	−0.0062	0.1764	−0.2969	−0.0459	0.0000	0.0308	−0.0115	0.0003
$[5.0, 6.0]$	0.2159	0.7150	0.0719	−0.7037	−0.0088	0.2088	−0.3653	−0.1515	0.0000	0.0285	−0.0110	0.0003
$[6.0, 7.0]$	0.2526	0.6654	0.0841	−0.6565	−0.0117	0.2294	−0.4083	−0.2397	0.0000	0.0278	−0.0110	0.0003
$[7.0, 8.0]$	0.2869	0.6192	0.0955	−0.6120	−0.0150	0.2425	−0.4350	−0.3129	0.0000	0.0293	−0.0118	0.0003
$[15.0, 16.0]$	0.4825	0.3570	0.1606	−0.3553	−0.1273	0.2822	−0.3654	−0.5805	0.0000	−0.0000	−0.0002	0.0003
$[16.0, 17.0]$	0.4915	0.3450	0.1636	−0.3435	−0.1587	0.2888	−0.3356	−0.5641	0.0000	−0.0000	−0.0002	0.0003
$[17.0, 18.0]$	0.4981	0.3360	0.1658	−0.3347	−0.2016	0.2987	−0.2911	−0.5191	0.0000	−0.0000	−0.0001	0.0002
$[18.0, 19.0]$	0.5012	0.3318	0.1668	−0.3308	−0.2621	0.3139	−0.2124	−0.4018	0.0000	0.0000	−0.0001	0.0002

Table 3: Observables predicted by `EOS` using the 2 GeV^2 binning and the SM Wilson coefficients.

q^2[GeV^2]	S_1^s	S_1^c	S_2^s	S_2^c	S_3	S_4	S_5	S_6^s	S_6^c	S_7	S_8	S_9
$[0.1, 0.98]$	0.5599	0.2450	0.1448	−0.1953	0.0003	−0.0885	0.2251	0.1210	0.0000	0.0215	−0.0039	0.0001
$[1.1, 2.5]$	0.2312	0.6996	0.0749	−0.6639	−0.0003	−0.0245	0.1175	0.2537	0.0000	0.0390	−0.0113	0.0002
$[2.5, 4.0]$	0.1546	0.7993	0.0514	−0.7774	−0.0032	0.1074	−0.1521	0.1078	0.0000	0.0354	−0.0123	0.0003
$[4.0, 6.0]$	0.1986	0.7384	0.0662	−0.7254	−0.0076	0.1932	−0.3323	−0.1006	0.0000	0.0296	−0.0112	0.0003
$[6.0, 8.0]$	0.2704	0.6414	0.0900	−0.6334	−0.0134	0.2362	−0.4221	−0.2776	0.0000	0.0286	−0.0114	0.0003
$[15.0, 17.0]$	0.4867	0.3513	0.1620	−0.3497	−0.1422	0.2853	−0.3513	−0.5727	0.0000	−0.0000	−0.0002	0.0003
$[17.0, 19.0]$	0.4994	0.3344	0.1662	−0.3332	−0.2253	0.3046	−0.2603	−0.4732	0.0000	−0.0000	−0.0001	0.0002

Table 4: Parameters used to describe the massmodel for the generation of simulated events using EOS. These parameters are determined from a fit integrated over the full q^2 range, which is dominated by $B^0 \to J/\psi\, K^{*0}$ events.

Parameter	value
m_B^0	5279.6
$f_{m,1}^{\rm sig}$	0.73
$\sigma_{\rm m,1}$	15.5
$\sigma_{\rm m,2}$	27.0
$\alpha_{\rm CB}$	1.5
$n_{\rm CB}$	5.6
$\alpha_{\rm m}$	6.6×10^{-3}

Figure 1: The background yield in bins of q^2 as seen in data. The fitted quadratic polynomial is used to describe the q^2 dependence of the background contribution for events simulated using EOS.

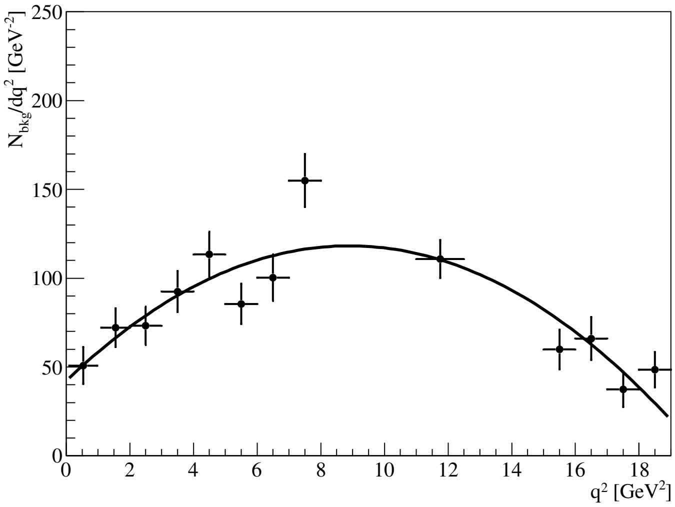

4 Selection

The selection is described in detail in Ref. [13]. Therefore only a short overview of the main parts of the selection is given below.

4.1 Stripping and preselection

Reconstructed B^0 candidates are selected from the `StrippingB2XMuMu` stripping line in `Stripping-20r0` and `Stripping-20r1`. The Stripping cuts are summarised in Tab. 5. In addition the preselection cuts given in Tab. 6 are applied. The $m_{K\pi}$ mass window used for the analysis is given by $(795.9 < m_{K\pi} < 995.9)\,\mathrm{MeV}/c^2$.

4.2 Peaking backgrounds

Several cuts are applied to reject peaking backgrounds from $\Lambda_b^0 \to pK^-\mu^+\mu^-$, $B_s^0 \to \phi\mu^+\mu^-$, and $B^0 \to J/\psi K^{*0}$ decays, as well as $B^0 \to K^{*0}\mu^+\mu^-$ signal swaps. The most significant of these is a requirement that

$$\mathrm{DLL}_{K\pi}(K) > \mathrm{DLL}_{K\pi}(\pi)$$

to remove $K \to \pi$ and $\pi \to K$ double misidentification and backgrounds from $\Lambda_b^0 \to pK^-\mu^+\mu^-$ where the proton is misidentified as a pion. Unless the contributions of the peaking backgrounds are found to be negligible, systematic uncertainties are evaluated

Table 5: Stripping selection criteria in `StrippingB2XMuMu` for Stripping `20` and Stripping `20r1`.

Candidate	Selection
B meson	IP $\chi^2 < 16$ (best PV)
B meson	$4600\,\mathrm{MeV}/c^2 < M < 7000\,\mathrm{MeV}/c^2$
B meson	DIRA angle $< 14\,\mathrm{mrad}$
B meson	flight distance $\chi^2 > 121$
B meson	vertex $\chi^2/\mathrm{ndf} < 8$
$\mu^+\mu^-$	$m(\mu^+\mu^-) < 7100\,\mathrm{MeV}/c^2$
$\mu^+\mu^-$	vertex $\chi^2/\mathrm{ndf} < 9$
K^{*0}	$m(K^+\pi^-) < 6200\,\mathrm{MeV}/c^2$
K^{*0}	vertex $\chi^2/\mathrm{ndf} < 9$
K^{*0}	flight distance $\chi^2 > 9$
tracks	ghost Prob < 0.4
tracks	min IP $\chi^2 > 9$
muon	`IsMuon`
muon	$\mathrm{DLL}_{\mu\pi} > -3$
GEC	SPD Mult. < 600

Table 6: Pre-selection cuts applied to stripped candidates. In this table only: θ is the opening angle from the beam; θ_{pair} is the opening angle between two track pairs.

Candidates	Selection
Track	$0 < \theta < 400$ mrad
Track Pairs	$\theta_{pair} > 1$ mrad
$\mu^+\mu^-$	`IsMuon` True
K	`hasRich` True
K	$\mathrm{DLL}_{K\pi} >$ -5
π	`hasRich` True
π	$\mathrm{DLL}_{K\pi} < 25$
PV	$\lvert X - < X > \rvert < 5\,\mathrm{mm}$
PV	$\lvert Y - < Y > \rvert < 5\,\mathrm{mm}$
PV	$\lvert Z - < Z > \rvert < 200\,\mathrm{mm}$

using toy studies. The largest source of peaking background is $\Lambda_b^0 \to pK^-\mu^+\mu^-$ at the level of 1% of the signal.

4.3 Trigger

The analysis relies on the `L0muon` trigger at `L0`. At `Hlt1` candidates are selected using the `Hlt1TrackMuon` and `Hlt1TrackAllL0` trigger lines. The main `Hlt2` trigger lines are the `Hlt2Topo(Mu)[2,3,4]BodyBBDT` topological trigger lines. Only signal candidates that are triggered on (`TOS`) are accepted. Table 7 gives the fraction of stripped data triggered by the different `TCKs` used during data taking. The trigger efficiency in simulation is checked using the `TISTOS` method on the $B^0 \to J/\psi K^{*0}$ control channel, see e.g. Fig 2 and Fig. 3. Table 8 gives the fraction of events passing through each trigger lines.

4.4 Multivariate selection

The majority of the combinatorial background is rejected using a BDT. In comparison to the previous angular analysis [17] the new BDT contains uses fewer input variables and is trained on a larger data sample. The variables used in the BDT are:

- the B^0 candidate lifetime;
- the B^0 momentum and p_{T};
- the B^0 direction angle (DIRA);
- the $K^+\pi^-\mu^+\mu^-$ vertex χ^2;
- the $\mathrm{DLL}_{K\pi}$ of the kaon and pion;

- the $\mathrm{DLL}_{\mu\pi}$ of the muons;
- the isolation of the four final state particles.

The B^0 variables are be only weakly correlated to q^2 and the angular distribution of the final state particles. No correlation is observed with the $K^+\pi^-\mu^+\mu^-$ invariant mass.

Table 7: Fraction of Stripped data sample selected by different L0 and HLT TCKs. Only TCKs selecting more than 1% of the data sample are shown. Data taking conditions were stable for `L0Muon`, `Hlt1Track` and `Hlt2Topo` for the majority of the data taken in 2011 and 2012.

L0 TCK	%	HLT TCK	%
42	19.1	990042	19.1
3d	19.0	a30044	10.7
44	16.5	790038	10.1
37	10.2	97003d	9.6
38	10.1	94003d	9.4
46	8.8	760037	9.1
35	5.6	730035	5.5
32	4.6	990044	4.9
45	3.4	ac0046	3.8
40	2.4	6d0032	2.9
		a10045	2.5
		8c0040	2.2
		a90046	2.2
		ab0046	1.8
		5a0032	1.6
		a30046	1.1
		790037	1.1

Table 8: Fraction of events passing through each trigger lines in $B^0 \to J/\psi K^{*0}$ data ($B^0 \to J/\psi K^{*0}$ MC).

	L0Muon and Hlt1TrackAllL0	L0Muon and Hlt1TrackMuon
Hlt2TopoMu2BodyBBDT	78.06 (79.95)%	85.13 (87.08)%
Hlt2TopoMu3BodyBBDT	72.29 (77.10)%	79.32 (84.32)%
Hlt2TopoMu4BodyBBDT	39.97 (46.02)%	43.27 (49.64)%
Hlt2Topo2BodyBBDT	68.65 (71.01)%	73.97 (76.54)%
Hlt2Topo3BodyBBDT	68.34 (73.52)%	74.41 (79.89)%
Hlt2Topo4BodyBBDT	39.21 (45.29)%	42.34 (48.75)%
Hlt2SingleMuon	23.92 (49.41)%	27.60 (55.91)%
Hlt2DiMuon	0.08 (0)%	0.09 (0)%

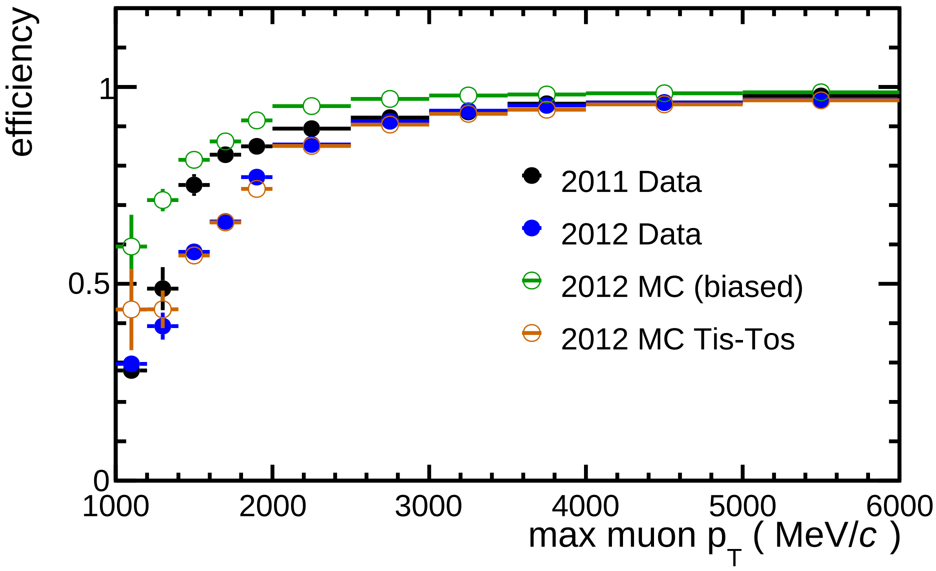

Figure 2: Trigger efficiency of `L0Muon` as a function of the maximum p_{T} of the μ^+ or μ^- for offline selected $B^0 \to J/\psi\, K^{*0}$ candidates that are TOS in `Hlt 1` and `Hlt 2`. The MC is filtered according to the 2012 `TCK 0x409F0045`.

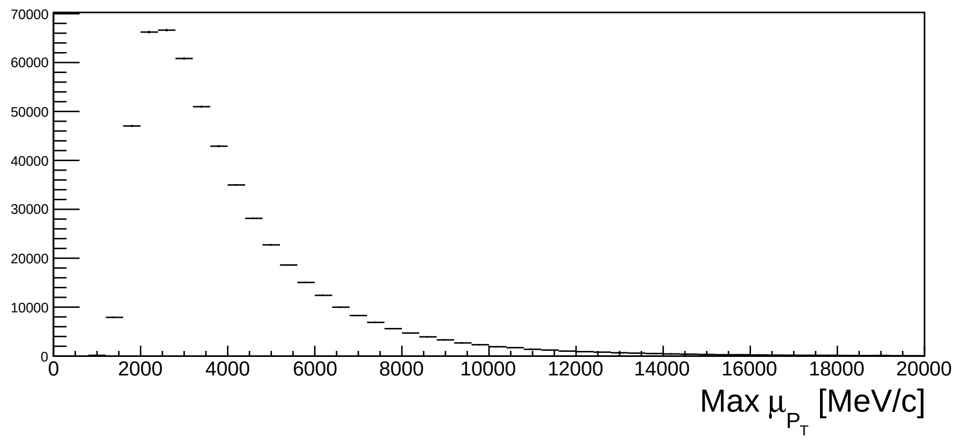

Figure 3: Distribution of the maximum p_{T} of the μ^+ or μ^- for offline selected $B^0 \to J/\psi\, K^{*0}$ candidates.

4.5 q^2 binnings

As will be discussed in Sec. 6 the different methods of angular analysis have different strength and weaknesses that determine where they are most useful. Table 9 gives two binnings with q^2 bin widths of $1\,\mathrm{GeV}^2/c^4$ and $2\,\mathrm{GeV}^2/c^4$, respectively. They will henceforth be known as the $1\,\mathrm{GeV}^2$ and $2\,\mathrm{GeV}^2$ binnings. In addition, the two larger

Table 9: q^2 binnings with (left) $1\,\mathrm{GeV}^2$ and (right) $2\,\mathrm{GeV}^2$ bins.

Bin	$q^2[\mathrm{GeV}^2]$
1	$[0.1, 0.98]$
2	$[1.1, 2.0]$
3	$[2.0, 3.0]$
4	$[3.0, 4.0]$
5	$[4.0, 5.0]$
6	$[5.0, 6.0]$
7	$[6.0, 7.0]$
8	$[7.0, 8.0]$
9	$[11.0, 11.75]$
10	$[11.75, 12.5]$
11	$[15.0, 16.0]$
12	$[16.0, 17.0]$
13	$[17.0, 18.0]$
14	$[18.0, 19.0]$

Bin	$q^2[\mathrm{GeV}^2]$
1	$[0.1, 0.98]$
2	$[1.1, 2.5]$
3	$[2.5, 4.0]$
4	$[4.0, 6.0]$
5	$[6.0, 8.0]$
6	$[11.0, 12.5]$
7	$[15.0, 17.0]$
8	$[17.0, 19.0]$

q^2 bins $1 < q^2 < 6\,\mathrm{GeV}^2/c^4$ and $15 < q^2 < 19\,\mathrm{GeV}^2/c^4$ are used which are preferred by some theory groups. The region between $8\,\mathrm{GeV}^2/c^4$ and $11\,\mathrm{GeV}^2/c^4$ as well as between $12.5\,\mathrm{GeV}^2/c^4$ and $15\,\mathrm{GeV}^2/c^4$ contain the charmonium resonances and are therefore vetoed. In the low q^2 region additionally the range $[0.98, 1.1]\,\mathrm{GeV}^2/c^4$ is vetoed to protect against possible pollution from $\phi \to \mu^+\mu^-$ decays.

5 Mass fits

5.1 $K^+\pi^-\mu^+\mu^-$ invariant mass distribution

The strategy for modeling the $K^+\pi^-\mu^+\mu^-$ invariant mass shape of the $B^0 \to K^{*0}\mu^+\mu^-$ candidates is to exploit the large sample of $B^0 \to J/\psi K^{*0}$ in data. Monte Carlo simulated $B^0 \to K^{*0}\mu^+\mu^-$ and $B^0 \to J/\psi K^{*0}$ events are then used to study (and correct for) possible q^2 dependence of the mass shape parameters.

The $K^+\pi^-\mu^+\mu^-$ invariant mass, m, of the signal is described by the sum of two Crystal Ball functions with common mean (μ) and tail parameters (α and n) but different widths. Explicitly, the reconstructed B^0 mass is parameterised as

$$\mathcal{P}_{\rm sig}(m|\vec{\lambda}) = f_{\rm core}\mathcal{P}_{\rm CB}(m|\mu,\sigma_1,\alpha,n) + (1-f_{\rm core})\mathcal{P}_{\rm CB}(m|\mu,\sigma_2,\alpha,n). \tag{1}$$

The shape of the Crystal Ball is given by

$$\mathcal{P}_{\rm CB}(m|\mu,\sigma,\alpha,n) = \begin{cases} e^{-\frac{1}{2}\left(\frac{m-\mu}{\sigma}\right)^2} & \frac{m-\mu}{\sigma} > \alpha \\ \frac{a}{\left(b-\left(\frac{m-\mu}{\sigma}\right)\right)^n} & \frac{m-\mu}{\sigma} < \alpha \end{cases}, \tag{2}$$

i.e. a Gaussian distribution above $\alpha\sigma$ and a power law tail below, where

$$\begin{aligned} a =& \left(\frac{n}{|\alpha|}\right)^n e^{-\frac{1}{2}\alpha^2} \\ b =& \frac{n}{|\alpha|} + \alpha \ . \end{aligned} \tag{3}$$

The invariant distribution of the background is described by an exponential distribution. For the $B^0 \to J/\psi K^{*0}$ decay a second signal component is included for the $B_s^0 \to J/\psi K^{*0}$ decay, it is expressed with the same signal parametrisation with a shift on the mean (μ) by $\Delta m = m(B_s^0) - m(B^0)$.

The parameters to describe the $B^0 \to K^{*0}\mu^+\mu^-$ signal mass shape, are determined from a fit to the control decay $B^0 \to J/\psi K^{*0}$, which is shown in Fig. 4. The resulting mass parameters for the angular analysis of the signal decay $B^0 \to K^{*0}\mu^+\mu^-$ are given in Tab. 10. To account for possible changes of the signal mass shape with q^2 we include a single scaling factor s_σ for every q^2 bin which is applied to both widths σ_1 and σ_2. This scaling factor is determined from a fit to MC simulated $B^0 \to K^{*0}\mu^+\mu^-$ signal events. The scaling factor for the two q^2 binnings can been see in Fig. 5, the numerical values are given in the Tab. 11

5.2 Event yields

The $K^+\pi^-\mu^+\mu^-$ invariant mass distribution of $B^0 \to K^{*0}\mu^+\mu^-$ candidates for the different q^2 bins are shown in Fig. 6, Fig. 7 and Fig. 8. Table. 12 lists the signal and background yield in each q^2 bin for the two binning schemes. In total, 2390 signal candidates are seen within the range $0.1 < q^2 < 19\,{\rm GeV}^2/c^4$.

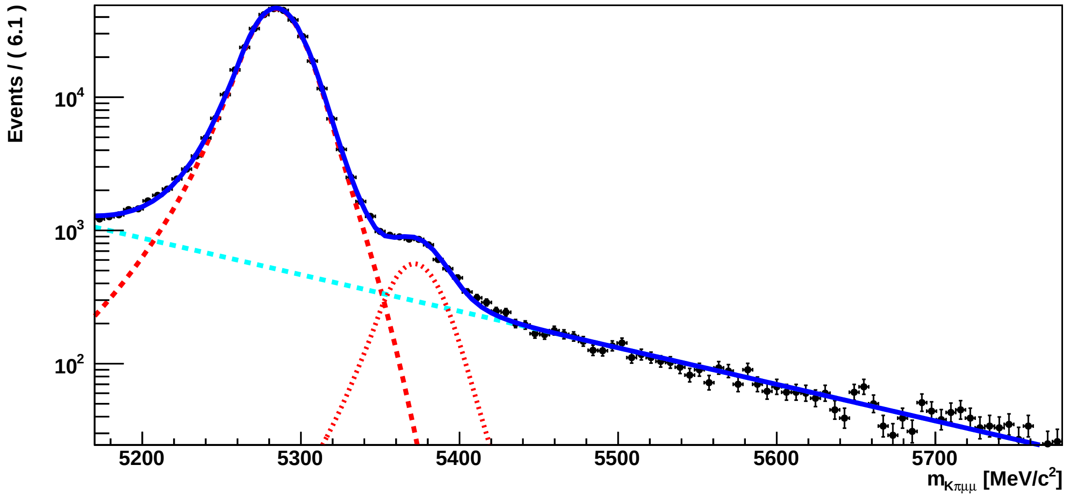

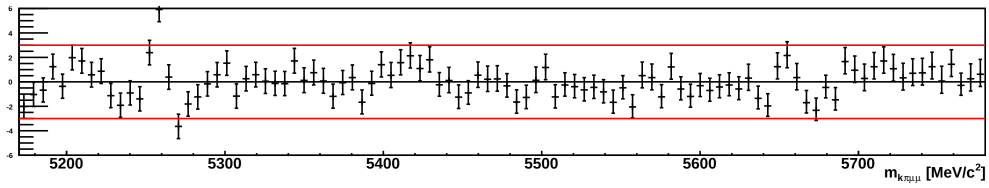

Figure 4: Fit to the control channel $B^0 \to J/\psi\, K^{*0}$. The full line is the overall PDF, the dashed red line is the PDF of the $B_d^0 \to J/\psi\, K^{*0}$ decay, the dashed-dotted red line is the PDF of the $B_s^0 \to J/\psi\, K^{*0}$ decay, and the dashed blue line represent the exponential background.

Parameter	Value
α_{CB}	1.533 ± 0.033
n	4.23 ± 0.6
σ_1	15.36 ± 0.19
σ_2	25.85 ± 0.82
f_{core}	0.704 ± 0.031
B_d mass (μ)	5284.339 ± 0.043
Δm	87.21 ± 0.83
exp. slope	-0.006319 ± 0.0001
N_{sig}	343763 ± 822
$N_{B_s^0}$	4199 ± 162
N_{bkg}	26877 ± 649

Table 10: Mass model parameters determined from a fit of the control channel $B^0 \to J/\psi\, K^{*0}$.

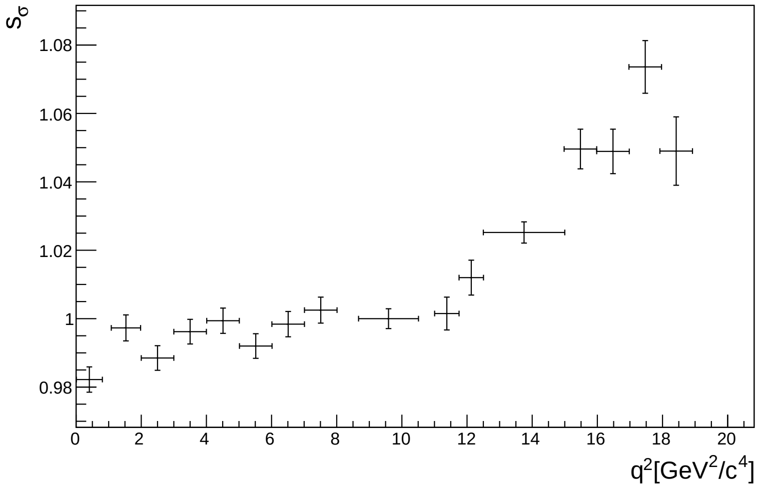

(a) 1 GeV^2 bins

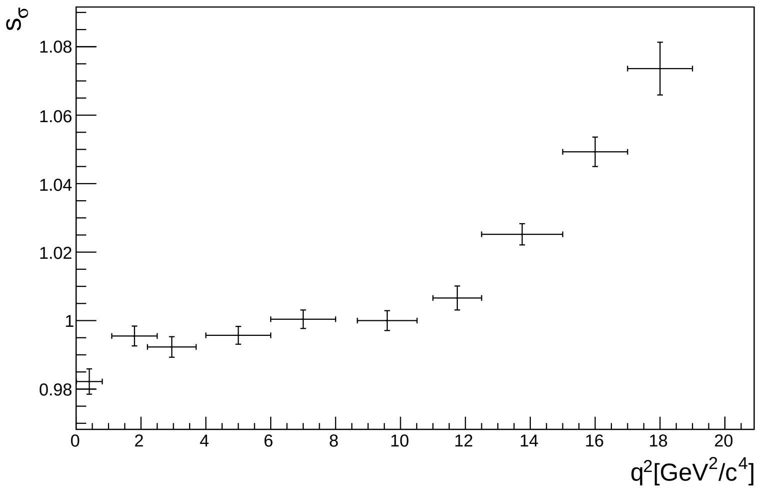

(b) 2 GeV^2 bins

Figure 5: Scaling factor s_σ in 1 GeV^2 (a) and 2 GeV^2 q^2 bins (b) and the $J/psi(1S)$ and $/psi(2S)$bins, fitted in the MC simulated $B^0 \to K^{*0}\mu^+\mu^-$ signal events.

$q^2\,[\,\mathrm{GeV}^2]$	Scaling factor
$[0.1, 0.98]$	0.982
$[1.1, 2.0]$	0.997
$[2.0, 3.0]$	0.989
$[3.0, 4.0]$	0.996
$[4.0, 5.0]$	0.999
$[5.0, 6.0]$	0.992
$[6.0, 7.0]$	0.998
$[7.0, 8.0]$	1.003
$[11.0, 11.75]$	1.002
$[11.75, 12.5]$	1.001
$[15.0, 16.0]$	1.050
$[16.0, 17.0]$	1.050
$[17.0, 18.0]$	1.074
$[18.0, 19.0]$	1.049

$q^2\,[\,\mathrm{GeV}^2]$	Scaling factor
$[0.1, 0.98]$	0.982
$[1.1, 2.5]$	0.996
$[2.5, 4.0]$	0.992
$[4.0, 6.0]$	0.996
$[6.0, 8.0]$	1.000
$[11.0, 12.5]$	1.007
$[15.0, 17.0]$	1.049
$[17.0, 19.0]$	1.074

Table 11: Scaling factor s_σ for the two q^2 binnings: (left) $1\,\mathrm{GeV}^2$ and (right) $2\,\mathrm{GeV}^2$ bins.

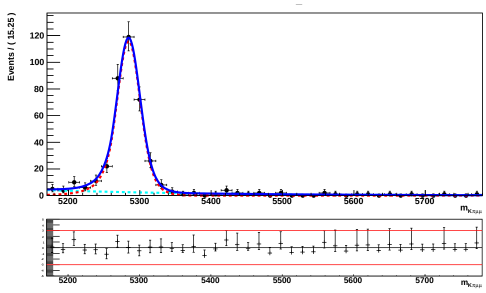

(a) $[0.10, 0.98]$

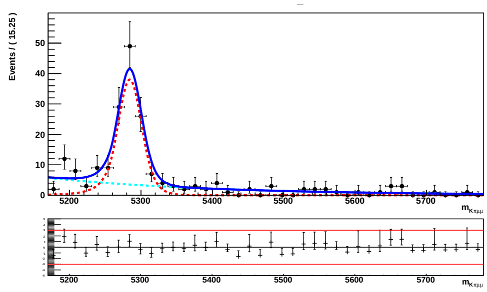

(b) $[1.1, 2.0]$

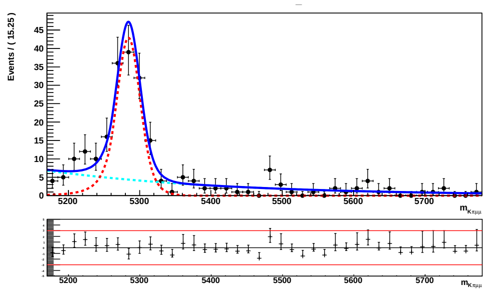

(c) $[2.0, 3.0]$

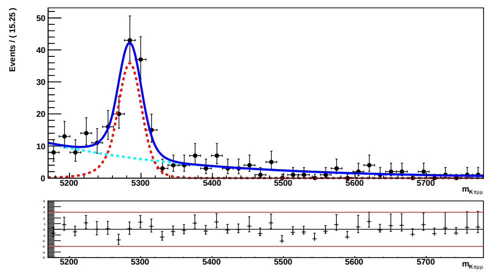

(d) $[3.0, 4.0]$

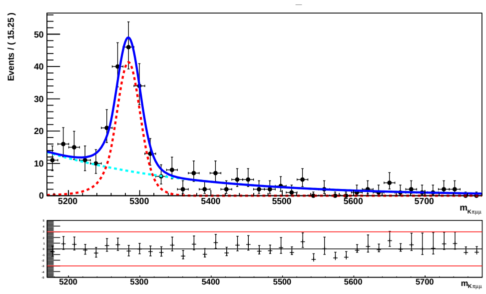

(e) $[4.0, 5.0]$

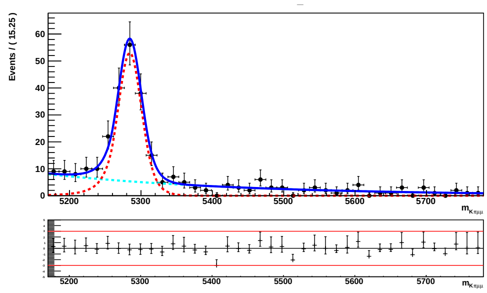

(f) $[5.0, 6.0]$

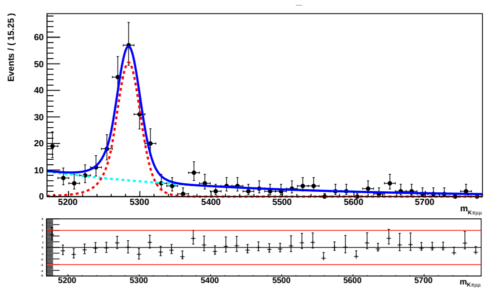

(g) $[6.0, 7.0]$

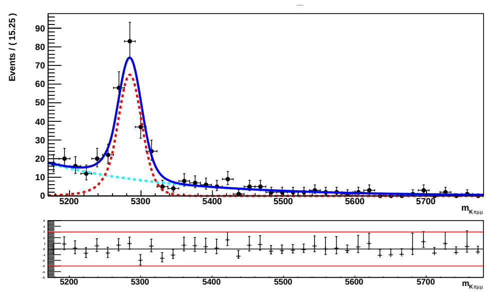

(h) $[7.0, 8.0]$

Figure 6: The $K^+\pi^-\mu^+\mu^-$ invariant mass distribution of $B^0 \to K^{*0}\mu^+\mu^-$ candidates of the first 8 bins in the $1\,\mathrm{GeV}^2/c^4$ q^2 binning.

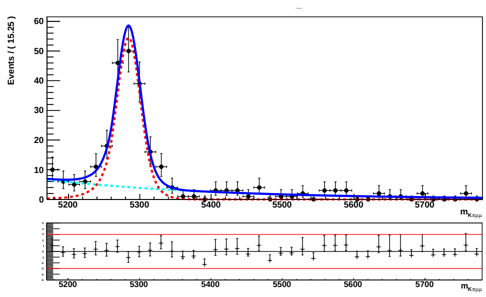

(a) $[11.0, 11.75]$

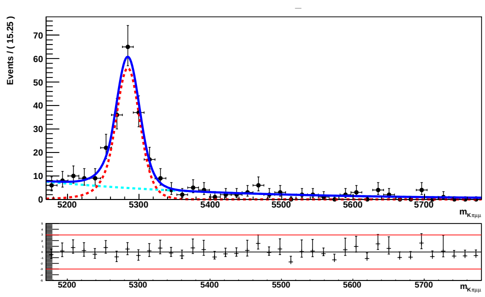

(b) $[11.75, 12.50]$

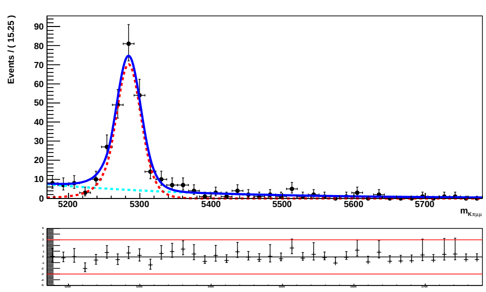

(c) $[15.0, 16.0]$

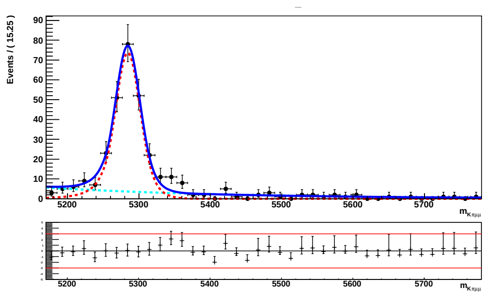

(d) $[16.0, 17.0]$

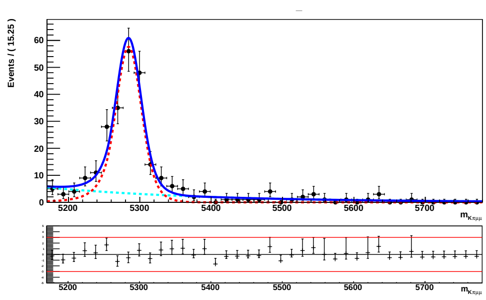

(e) $[17.0, 18.0]$

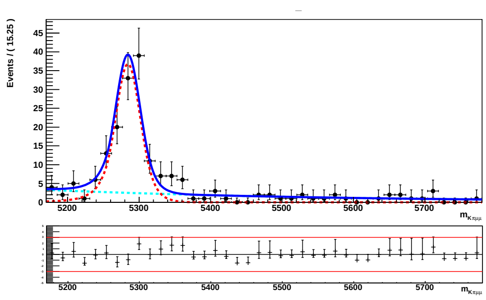

(f) $[18.0, 19.0]$

Figure 7: The $K^+\pi^-\mu^+\mu^-$ invariant mass distribution of $B^0 \to K^{*0}\mu^+\mu^-$ candidates of the last 6 bins in the $1\,\mathrm{GeV}^2/c^4$ q^2 binning.

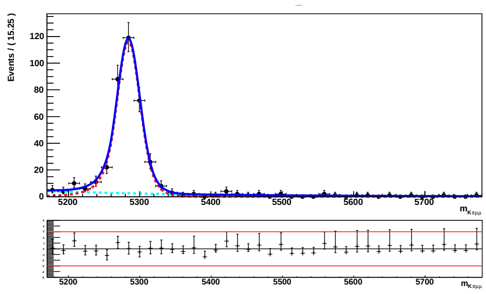

(a) $[0.10, 0.98]$

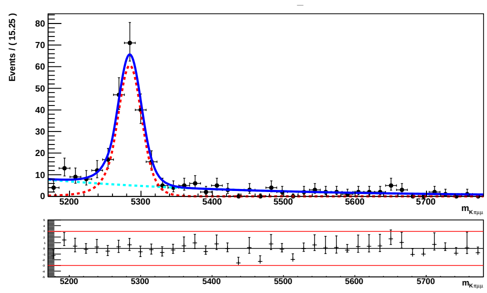

(b) $[1.1, 2.5]$

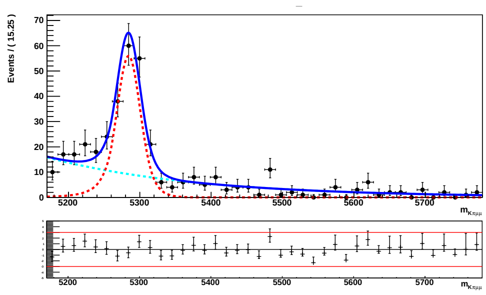

(c) $[2.5, 4.0]$

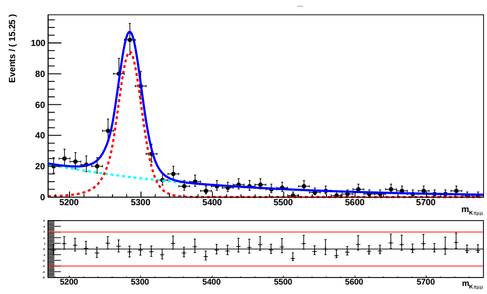

(d) $[4.0, 6.0]$

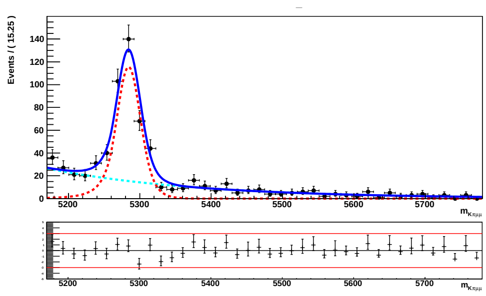

(e) $[6.0, 8.0]$

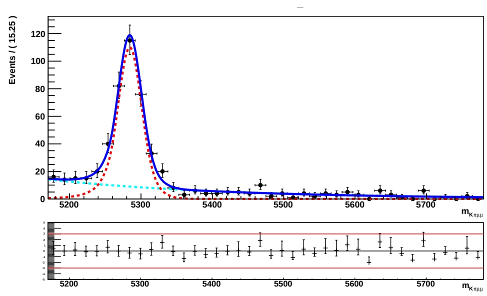

(f) $[11.0, 12.5]$

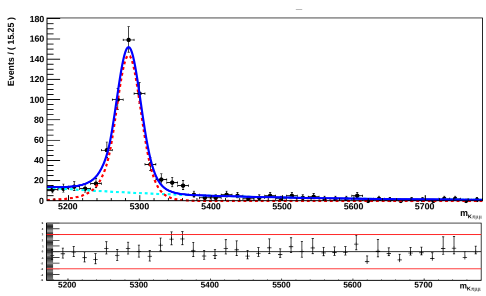

(g) $[19.0, 17.0]$

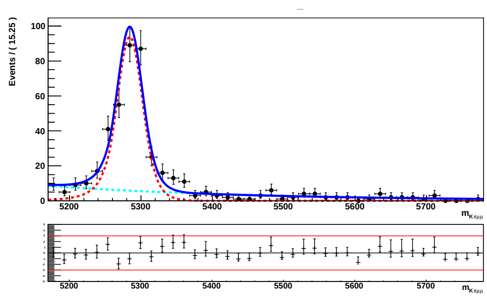

(h) $[17.0, 19.0]$

Figure 8: The $K^+\pi^-\mu^+\mu^-$ invariant mass distribution of $B^0 \to K^{*0}\mu^+\mu^-$ candidates of the first 8 bins in the $2\,\mathrm{GeV}^2/c^4$ q^2 binning

.

$q^2\,[\,\mathrm{GeV}^2]$	signal yield	background yield
$[0.1, 0.98]$	339.1 ± 19.6	58.9 ± 10.3
$[1.1, 2.0]$	113.0 ± 12.2	82.0 ± 10.9
$[2.0, 3.0]$	126.3 ± 13.3	103.7 ± 12.4
$[3.0, 4.0]$	106.4 ± 12.8	144.6 ± 14.2
$[4.0, 5.0]$	123.1 ± 13.9	169.9 ± 15.5
$[5.0, 6.0]$	156.6 ± 14.6	130.4 ± 13.7
$[6.0, 7.0]$	150.3 ± 14.5	146.7 ± 14.4
$[7.0, 8.0]$	194.2 ± 16.7	197.8 ± 16.8
$[11.0, 11.75]$	162.5 ± 14.7	96.5 ± 12.2
$[11.75, 12.5]$	166.9 ± 15.0	116.1 ± 13.2
$[15.0, 16.0]$	219.5 ± 16.7	102.5 ± 12.8
$[16.0, 17.0]$	229.8 ± 16.9	87.1 ± 12.0
$[17.0, 18.0]$	184.1 ± 15.4	75.9 ± 11.5
$[18.0, 19.0]$	114.9 ± 12.2	69.1 ± 10.2

$q^2\,[\,\mathrm{GeV}^2]$	signal yield	background yield
$[0.1, 0.98]$	339.1 ± 19.6	58.9 ± 10.3
$[1.1, 2.5]$	179.7 ± 15.4	124.4 ± 13.5
$[2.5, 4.0]$	165.4 ± 15.9	206.6 ± 17.1
$[4.0, 6.0]$	279.5 ± 20.2	300.4 ± 20.7
$[6.0, 8.0]$	344.3 ± 22.1	344.8 ± 22.1
$[11.0, 12.5]$	329.8 ± 21.0	212.1 ± 18.0
$[15.0, 17.0]$	449.2 ± 23.8	189.8 ± 17.5
$[17.0, 19.0]$	299.9 ± 19.8	144.1 ± 15.3

Table 12: Signal and background yields with the two q^2 binnings: (top) $1\,\mathrm{GeV}^2/c^4$ and (bottom) $2\,\mathrm{GeV}^2/c^4$ bins.

6 Methods

6.1 Angular description of the decay $B^0 \to K^{*0}\mu^+\mu^-$

6.1.1 The angular basis

The decay angles are defined differently by experimentalists and theorists. Details on the differences between the convention chosen by a majority of the theory publications [3,18] and the convention adopted by LHCb for this analysis and the previous publications [1,2] are given in Ref. [19].

The angular basis used in this paper is illustrated in Fig. 9. The angle θ_ℓ is defined as the angle between the direction of the μ^+ (μ^-) in the dimuon rest frame and the direction of the dimuon in the B^0 ($\overline{B}^0$) rest frame. The angle θ_K is defined as the angle between the direction of the kaon in the K^{*0} ($\overline{K}^{*0}$) rest frame and the direction of the K^{*0} ($\overline{K}^{*0}$) in the B^0 ($\overline{B}^0$) rest frame. The angle ϕ is the angle between the plane containing the μ^+ and μ^- and the plane containing the kaon and pion from the K^{*0}. Explicitly, $\cos\theta_\ell$ and $\cos\theta_K$ are defined as

$$\cos\theta_\ell = \left(\hat{p}^{(\mu^+\mu^-)}_{\mu^+}\right)\cdot\left(\hat{p}^{(B^0)}_{\mu^+\mu^-}\right) = \left(\hat{p}^{(\mu^+\mu^-)}_{\mu^+}\right)\cdot\left(-\hat{p}^{(\mu^+\mu^-)}_{B^0}\right) \;, \tag{4}$$

$$\cos\theta_K = \left(\hat{p}^{(K^{*0})}_{K^+}\right)\cdot\left(\hat{p}^{(B^0)}_{K^{*0}}\right) = \left(\hat{p}^{(K^{*0})}_{K^+}\right)\cdot\left(-\hat{p}^{(K^{*0})}_{B^0}\right) \tag{5}$$

for the B^0 and

$$\cos\theta_\ell = \left(\hat{p}^{(\mu^+\mu^-)}_{\mu^-}\right)\cdot\left(\hat{p}^{(\overline{B}^0)}_{\mu^+\mu^-}\right) = \left(\hat{p}^{(\mu^+\mu^-)}_{\mu^-}\right)\cdot\left(-\hat{p}^{(\mu^+\mu^-)}_{\overline{B}^0}\right) \;, \tag{6}$$

$$\cos\theta_K = \left(\hat{p}^{(K^{*0})}_{K^-}\right)\cdot\left(\hat{p}^{(\overline{B}^0)}_{K^{*0}}\right) = \left(\hat{p}^{(K^{*0})}_{K^-}\right)\cdot\left(-\hat{p}^{(K^{*0})}_{\overline{B}^0}\right) \tag{7}$$

for the $\overline{B}^0$ decay. The definition of the angle ϕ is given by

$$\cos\phi = \left(\hat{p}^{(B^0)}_{\mu^+}\times\hat{p}^{(B^0)}_{\mu^-}\right)\cdot\left(\hat{p}^{(B^0)}_{K^+}\times\hat{p}^{(B^0)}_{\pi^-}\right) \;, \tag{8}$$

$$\sin\phi = \left[\left(\hat{p}^{(B^0)}_{\mu^+}\times\hat{p}^{(B^0)}_{\mu^-}\right)\times\left(\hat{p}^{(B^0)}_{K^+}\times\hat{p}^{(B^0)}_{\pi^-}\right)\right]\cdot\hat{p}^{(B^0)}_{K^{*0}} \tag{9}$$

for the B^0 and

$$\cos\phi = \left(\hat{p}^{(\overline{B}^0)}_{\mu^-}\times\hat{p}^{(\overline{B}^0)}_{\mu^+}\right)\cdot\left(\hat{p}^{(\overline{B}^0)}_{K^-}\times\hat{p}^{(\overline{B}^0)}_{\pi^+}\right) \;, \tag{10}$$

$$\sin\phi = -\left[\left(\hat{p}^{(\overline{B}^0)}_{\mu^-}\times\hat{p}^{(\overline{B}^0)}_{\mu^+}\right)\times\left(\hat{p}^{(\overline{B}^0)}_{K^-}\times\hat{p}^{(\overline{B}^0)}_{\pi^+}\right)\right]\cdot\hat{p}^{(\overline{B}^0)}_{\overline{K}^{*0}} \tag{11}$$

for the $\overline{B}^0$ decay. The $\hat{p}^{(Y)}_X$ are unit vectors describing the direction of a particle X in the rest frame of the system Y. In every case the particle momenta are first boosted to the B^0 (or $\overline{B}^0$) rest frame. In this basis, the angular definition for the $\overline{B}^0$ decay is a CP transformation of that for the B^0 decay.

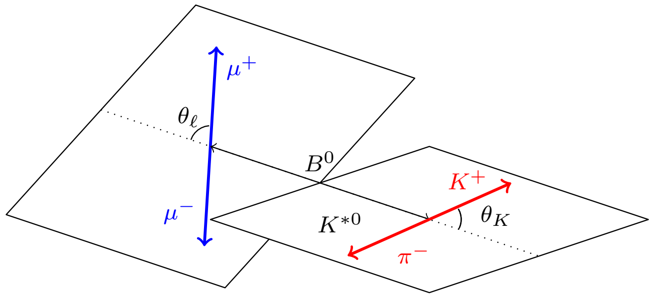

(a) θ_K and θ_ℓ definitions for the B^0 decay

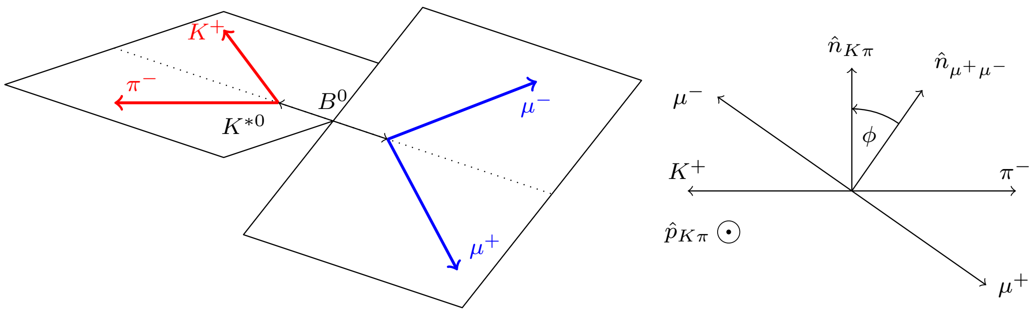

(b) ϕ definition for the B^0 decay

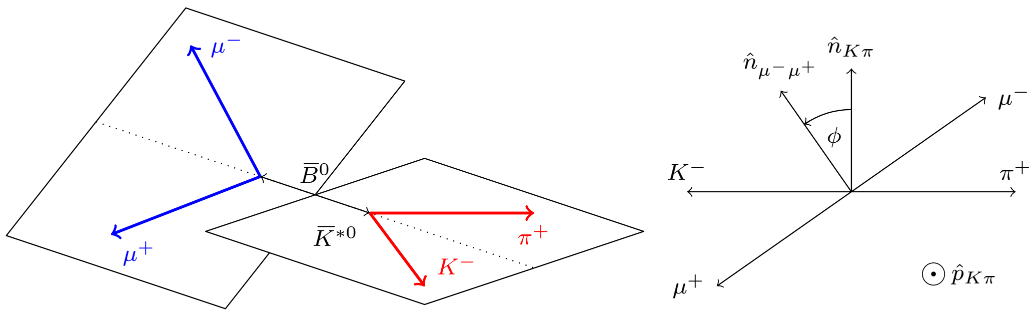

(c) ϕ definition for the $\overline{B}^0$ decay

Figure 9: Graphical representation of the angular basis used for $B^0 \to K^{*0}\mu^+\mu^-$ and $\overline{B}^0 \to \overline{K}^{*0}\mu^+\mu^-$ decays in this paper. The notation $\hat{n}_{ab}$ is used to represent the normal to the plane containing particles a and b in the B^0 (or $\overline{B}^0$) rest frame. An explicit description of the angular basis is given in the text.

6.1.2 The differential decay rate

The four-differential decay rate, for a $K\pi$ system in a P-wave configuration and ignoring scalar[2] contributions, is given by

$$
\begin{aligned}
\frac{\mathrm{d}^4\Gamma[\overline{B}^0 \to \overline{K}^{*0}\mu^+\mu^-]}{\mathrm{d}\cos\theta_\ell\,\mathrm{d}\cos\theta_K\,\mathrm{d}\phi\,\mathrm{d}q^2} =& \frac{9}{32\pi}\sum_i J_i(q^2) f_i(\cos\theta_\ell, \cos\theta_K, \phi) \\
=& \frac{9}{32\pi}\Big[\, J_1^s \sin^2\theta_K + J_1^c \cos^2\theta_K + \\
& J_2^s \sin^2\theta_K \cos 2\theta_\ell + J_2^c \cos^2\theta_K \cos 2\theta_\ell + \\
& J_3 \sin^2\theta_K \sin^2\theta_\ell \cos 2\phi + J_4 \sin 2\theta_K \sin 2\theta_\ell \cos\phi + \\
& J_5 \sin 2\theta_K \sin\theta_\ell \cos\phi + J_6^s \sin^2\theta_K \cos\theta_\ell + \\
& J_7 \sin 2\theta_K \sin\theta_\ell \sin\phi + J_8 \sin 2\theta_K \sin 2\theta_\ell \sin\phi + \\
& J_9 \sin^2\theta_K \sin^2\theta_\ell \sin 2\phi \,\Big].
\end{aligned}
\tag{12}
$$

Here, the q^2 dependent angular observables $J_i(q^2)$ are given by

[2]This refers to a scalar configuration of the dimuon system, not to be confused with an S-wave contribution to the $K\pi$ system as will be discussed later

$$
\begin{aligned}
J_1^s &= \frac{(2+\beta_\mu^2)}{4}\left[|A_\perp^L|^2 + |A_\parallel^L|^2 + (L\to R)\right] + \frac{4m_\mu^2}{q^2}\Re e(A_\perp^L A_\perp^{R*} + A_\parallel^L A_\parallel^{R*}) \\
J_1^c &= |A_0^L|^2 + |A_0^R|^2 + \frac{4m_\mu^2}{q^2}\left[|A_t|^2 + 2\Re e(A_0^L A_0^{R*})\right] \\
J_2^s &= \frac{\beta_\mu^2}{4}\left[|A_\perp^L|^2 + |A_\parallel^L|^2 + (L\to R)\right] \\
J_2^c &= -\beta_\mu^2\left[|A_0^L|^2 + (L\to R)\right] \\
J_3 &= \frac{\beta_\mu^2}{2}\left[|A_\perp^L|^2 - |A_\parallel^L|^2 + (L\to R)\right] \\
J_4 &= \frac{\beta_\mu^2}{\sqrt{2}}\left[\Re e(A_0^L A_\parallel^{L*}) + (L\to R)\right] \\
J_5 &= \sqrt{2}\beta_\mu\left[\Re e(A_0^L A_\perp^{L*}) - (L\to R)\right] \\
J_6^s &= 2\beta_\mu\left[\Re e(A_\parallel^L A_\perp^{L*}) - (L\to R)\right] \\
J_7 &= \sqrt{2}\beta_\mu\left[\Im m(A_0^L A_\parallel^{L*}) - (L\to R)\right] \\
J_8 &= \frac{\beta_\mu^2}{\sqrt{2}}\left[\Im m(A_0^L A_\perp^{L*}) + (L\to R)\right] \\
J_9 &= \beta_\mu^2\left[\Im m(A_\parallel^{L*} A_\perp^L) + (L\to R)\right]
\end{aligned} \tag{13}
$$

with $\beta_\mu^2 = (1 - 4m(\mu)^2/q^2)$. The angular distribution therefore depends on 7 q^2 dependent complex amplitudes ($A_0^{L,R}$, $A_\parallel^{L,R}$, $A_\perp^{L,R}$ and A_t) corresponding to different polarisation states of the $B\to K^*V^*$ decay. The K^{*0} is on-shell and has three polarisation states, $\epsilon(+,-,0)$. The V^* is off-shell and has 4 possible states, $\epsilon(+,-,0,t)$. The amplitude A_t corresponds to a longitudinal polarisation of the K^{*0} and time-like polarisation of the dimuon system. It is suppressed and can be safely neglected, leaving six complex amplitudes.

The labels L and R refer to the chirality of the dimuon system. In the limit that the decay is dominated by a vector current $A^L_{\parallel,\perp,0} = A^R_{\parallel,\perp,0}$ which implies $J_{5,6,7} = 0$ and the angular expression collapses to the familiar expression for $B^0\to J/\psi\, K^{*0}$.

$$
\begin{aligned}
\frac{\mathrm{d}^3\Gamma[\overline{B}^0 \to J/\psi\, \overline{K}^{*0}]}{\mathrm{d}\cos\theta_\ell\,\mathrm{d}\cos\theta_K\,\mathrm{d}\phi} = \frac{9}{32\pi} \Big[& 2|A_0|^2 \cos^2\theta_K \sin^2\theta_\ell \; + \\
& \frac{1}{2}\left(|A_\parallel|^2 + A_\perp|^2\right) \sin^2\theta_K (1+\cos^2\theta_\ell) \; + \\
& \frac{1}{2}\left(|A_\perp|^2 - |A_\parallel|^2\right) \sin^2\theta_K \sin^2\theta_\ell \cos 2\phi \; + \\
& \sqrt{2}\Re e(A_0 A_\parallel^*) \sin 2\theta_K \sin 2\theta_\ell \cos\phi \; + \\
& \frac{1}{\sqrt{2}}\Im(A_0 A_\perp^*) \sin 2\theta_K \sin 2\theta_\ell \sin\phi \; + \\
& \Im(A_\parallel A_\perp^*) \sin^2\theta_K \sin^2\theta_\ell \sin 2\phi \Big]
\end{aligned} \tag{14}
$$

which in terms of helicity amplitudes H_0, H_+ and H_- is identical to

$$
\begin{aligned}
\frac{\mathrm{d}^3\Gamma[\overline{B}^0 \to J/\psi\, \overline{K}^{*0}]}{\mathrm{d}\cos\theta_\ell\,\mathrm{d}\cos\theta_K\,\mathrm{d}\phi} = \frac{9}{16\pi} \Big[& |H_0|^2 \cos^2\theta_K \sin^2\theta_\ell \; + \\
& \frac{1}{4}\left(|H_+|^2 + H_-|^2\right) \sin^2\theta_K (1+\cos^2\theta_\ell) \; - \\
& \frac{1}{2}\Re(H_+ H_-^*) \sin^2\theta_K \sin^2\theta_\ell \cos 2\phi \; + \\
& \frac{1}{2}\Im(H_+ H_-^*) \sin^2\theta_K \sin^2\theta_\ell \sin 2\phi \; + \\
& \frac{1}{2}\Re((H_+ + H_-) H_0^*) \sin 2\theta_K \sin 2\theta_\ell \cos\phi \; - \\
& \frac{1}{2}\Im((H_+ + H_-) H_0^*) \sin 2\theta_K \sin 2\theta_\ell \sin\phi \Big]
\end{aligned} \tag{15}
$$

In the limit of $q^2 \gg 4m(\mu)^2$ the factor $\beta_\mu^2 \to 1$ and

$$
\frac{\mathrm{d}\Gamma}{\mathrm{d}q^2} = |A_\perp^L|^2 + |A_\parallel^L|^2 + |A_0^L|^2 + (L \to R)
$$

In this limit, $J_2^c = -J_1^c$ and $J_2^s = J_1^s/3$. While the differential decay rate in Eq. 12 is defined for the the decay of the $\overline{B}^0$ meson, the decay of the the B^0 is given in complete analogy by

$$
\frac{\mathrm{d}^4\Gamma[B^0 \to K^{*0}\mu^+\mu^-]}{\mathrm{d}\cos\theta_\ell\,\mathrm{d}\cos\theta_K\,\mathrm{d}\phi\,\mathrm{d}q^2} = \frac{9}{32\pi}\sum_i \bar{J}_i(q^2) f_i(\cos\theta_\ell, \cos\theta_K, \phi). \tag{16}
$$

The identical form of this equation compared to Eq. 12 is a consequence of our angular definition described in Sec. 6.1.1. vcFollowing Ref. [3], it is customary to define CP-averaged observables S_i and CP-violating observables A_i according to

$$S_i = \frac{J_i + \bar{J}_i}{\left(\mathrm{d}\Gamma + \mathrm{d}\bar{\Gamma}\right)/\mathrm{d}q^2} \tag{17}$$

$$A_i = \frac{J_i - \bar{J}_i}{\left(\mathrm{d}\Gamma + \mathrm{d}\bar{\Gamma}\right)/\mathrm{d}q^2}. \tag{18}$$

The normalisation condition implies $\frac{3}{4}\left(2S_1^s + S_1^c\right) - \frac{1}{4}\left(2S_2^s + S_2^c\right) = 1$. In the limit of massless leptons, the CP-averaged observables are related by $S_2^c = -S_1^c$ and $S_2^s = S_1^s/3$ as discussed above.

Often, the forward-backward asymmetry A_{FB}, and the longitudinal (transverse) polarisation fraction F_L (F_T) are referred to in the literature. These quantities are related to the CP-averaged observables S_i according to

$$\begin{aligned} A_{\mathrm{FB}} &= \frac{3}{4} S_6^s \\ F_{\mathrm{L}} &= S_1^c = -S_2^c \\ F_{\mathrm{T}} &= 4 S_2^s. \end{aligned}$$

6.1.3 Interference with other $K^+\pi^-$ states

Eq. 12 is valid if the $K^+\pi^-$ system is in a P-wave configuration, as is the case for the $K^{*0}(892)$ vector meson. If the $K^+\pi^-$ system is in an S-wave configuration or in a configuration with higher angular momentum up to $J_{\max}$ the replacements

$$A(J=1)_0^{L,R} \cdot Y_1^0(\theta_K, 0) \to \sum_{i=0}^{J_{\max}} A_0^{L,R}(i) \cdot Y_i^0(\theta_K, 0) \text{ and} \tag{19}$$

$$A(J=1)_{\parallel,\perp}^{L,R} \cdot Y_1^0(\theta_K, 0) \to \sum_{i=1}^{J_{\max}} A_0^{L,R}(i) \cdot Y_i^{-1}(\theta_K, 0) \tag{20}$$

need to be made, where the $Y_l^m(\theta_K)$ are spherical harmonics. The relevant spherical harmonics for S, P and D-wave are

$$
\begin{aligned}
Y_0^0(\theta_K) &= \frac{1}{2\sqrt{\pi}} \\
Y_1^0(\theta_K) &= \frac{1}{2}\sqrt{\frac{3}{\pi}}\cos\theta_K \\
Y_2^0(\theta_K) &= \frac{1}{4}\sqrt{\frac{5}{\pi}}(3\cos^2\theta_K - 1) \\
Y_1^{-1}(\theta_K) &= \frac{1}{2}\sqrt{\frac{3}{2\pi}}\sin\theta_K \\
Y_2^{-1}(\theta_K) &= \frac{1}{2}\sqrt{\frac{15}{2\pi}}\sin\theta_K\cos\theta_K .
\end{aligned}
$$

6.1.4 S-wave interference

For the decay $B^0 \to J/\psi K^{*0}$ the S-wave fraction was determined to be $(6.4 \pm 0.3 \pm 1.0)\%$ in a mass window of $\pm 70\,\mathrm{MeV}$ around the known K^{*0} mass using $1\,\mathrm{fb}^{-1}$ of LHCb data [20]. In the previous publications [1, 2] the presence of an S-wave contribution was accounted for by assigning a systematic uncertainty. In this analysis, the S-wave parameters are determined in the full angular analysis. Therefore, Eq. 12 needs to be modified according to

$$
\begin{aligned}
\frac{\mathrm{d}^4\Gamma}{\mathrm{d}\cos\theta_\ell\,\mathrm{d}\cos\theta_K\,\mathrm{d}\phi\,\mathrm{d}q^2} \;\rightarrow\; & \frac{\mathrm{d}^4\Gamma}{\mathrm{d}\cos\theta_\ell\,\mathrm{d}\cos\theta_K\,\mathrm{d}\phi\,\mathrm{d}q^2} \\
& + \frac{9}{32\pi}\Big[\, {J'}_1^c + {J''}_1^c\cos\theta_K + \\
& \quad {J'}_2^c\cos 2\theta_\ell + {J''}_2^c\cos\theta_K\cos 2\theta_\ell + \\
& \quad {J'}_4\sin 2\theta_\ell\sin\theta_K\cos\phi + \\
& \quad {J'}_5\sin\theta_\ell\sin\theta_K\cos\phi + \\
& \quad {J'}_7\sin\theta_\ell\sin\theta_K\sin\phi + \\
& \quad {J'}_8\sin 2\theta_\ell\sin\theta_K\sin\phi \Big]
\end{aligned}
\tag{21}
$$

with

$$
\begin{aligned}
{J'}^c_1 &= \frac{1}{3}|A^L_{J=0}|^2 + \frac{1}{3}|A^R_{J=0}|^2 \\
{J''}^c_1 &= \frac{2}{\sqrt{3}}\Big[\Re e(A^L_{J=0}A^{L*}_0) + (L \to R)\Big] \\
{J'}^c_2 &= -\Big[\frac{1}{3}|A^L_{J=0}|^2 + \frac{1}{3}|A^R_{J=0}|^2\Big] \\
{J''}^c_2 &= -\frac{2}{\sqrt{3}}\Big[\Re e(A^L_{J=0}A^{L*}_0) + (L \to R)\Big] \\
{J'}_4 &= \sqrt{\frac{2}{3}}\Big[\Re e(A^L_{J=0}A^{L*}_\parallel) + (L \to R)\Big] \\
{J'}_5 &= 2\sqrt{\frac{2}{3}}\Big[\Re e(A^L_{J=0}A^{L*}_\perp) - (L \to R)\Big] \\
{J'}_7 &= 2\sqrt{\frac{2}{3}}\Big[\Im m(A^L_{J=0}A^{L*}_\parallel) - (L \to R)\Big] \\
{J'}_8 &= \sqrt{\frac{2}{3}}\Big[\Im m(A^L_{J=0}A^{L*}_\perp) + (L \to R)\Big]
\end{aligned} \tag{22}
$$

and

$$
\begin{aligned}
\frac{\mathrm{d}\Gamma}{\mathrm{d}q^2} &= \frac{\mathrm{d}\Gamma_P}{\mathrm{d}q^2} + \frac{\mathrm{d}\Gamma_S}{\mathrm{d}q^2} \\
&= |A^L_{J=0}|^2 + |A^L_{J=1,0}|^2 + |A^L_{J=1,\parallel}|^2 + |A^L_{J=1,\perp}|^2 + (L \to R)
\end{aligned} \tag{23}
$$

The fraction of longitudinal polarisation is given by

$$
F_{\mathrm{S}} = |A^L_{J=0}|^2 \cdot \frac{1}{\mathrm{d}\Gamma/\mathrm{d}q^2} \tag{24}
$$

6.1.5 Less form-factor dependent observables

The angular observables can be reparametrized such that leading form-factor uncertainties cancel to first order. The authors of Ref. [4] propose the basis consisting of F_{L} (or A_{FB})

and the observables $P_i^{(\prime)}$ that can be calculated from the observables S_i according to

$$\begin{aligned}
P_1 &= 2\frac{S_3}{1-F_\mathrm{L}} \\
P_2 &= \frac{1}{2}\frac{S_6^s}{1-F_\mathrm{L}} = \frac{2}{3}\frac{A_\mathrm{FB}}{1-F_\mathrm{L}} \\
P_3 &= -\frac{S_9}{1-F_\mathrm{L}} \\
P_4' &= \frac{S_4}{\sqrt{F_\mathrm{L}(1-F_\mathrm{L})}} \\
P_5' &= \frac{S_5}{\sqrt{F_\mathrm{L}(1-F_\mathrm{L})}} \\
P_6' &= \frac{S_7}{\sqrt{F_\mathrm{L}(1-F_\mathrm{L})}} \\
P_8' &= \frac{S_8}{\sqrt{F_\mathrm{L}(1-F_\mathrm{L})}}.
\end{aligned}$$

It should be noted that $P_{1,2,3}$ are related to the previously proposed observables A_T^Re, A_T^Im [21] and A_T^2 [22] according to

$$\begin{aligned}
P_1 &= A_\mathrm{T}^2 \\
P_2 &= \frac{1}{2}A_\mathrm{T}^\mathrm{Re} \\
P_3 &= -\frac{1}{2}A_\mathrm{T}^\mathrm{Im}
\end{aligned}$$

The PDF used to fit the angular observables can be reparametrised to use the basis $(F_\mathrm{L}, P_{1,2,3}, P'_{4,5,6,8})$. The shapes of the allowed parameter regions simplify compared to the basis $(F_\mathrm{L}, A_\mathrm{FB}, S_{3,4,5,7,8,9})$, however the reparametrisation introduces additional correlations between observables since the PDF is no longer linear in the parameters. For this analysis, the CP-averaged observables S_i and the CP-asymmetries A_i will be considered the nominal observables. However, we aim to provide also the less form-factor dependent observables, which can be either fit directly or constructed from the observables S_i and A_i.

We would like to note that theorists use a different convention of the P_i definitions. For completeness we give the definition for the P_i which are different:

$$\begin{aligned}
P'_{4,theory} &= 2\frac{S_4}{\sqrt{F_\mathrm{L}(1-F_\mathrm{L})}} \\
P'_{6,theory} &= -\frac{S_7}{\sqrt{F_\mathrm{L}(1-F_\mathrm{L})}}.
\end{aligned}$$

6.2 Fitting for angular observables

This method of angular analysis of the decay $B^0 \to K^{*0}\mu^+\mu^-$ determines the angular observables S_i (or A_i) in bins of q^2 using an unbinned maximum likelihood fit of the reconstructed B^0 mass and the decay angles $\vec{\Omega} = (\cos\theta_l, \cos\theta_K, \phi)$.

The analysis needs to describe the the signal and background components using probability density functions (PDFs) depending on the the angular observables and nuisance parameters. The total PDF is given by

$$\mathcal{P}_{\mathrm{tot}} = f_{\mathrm{sig}}\mathcal{P}_{\mathrm{sig}}(\vec{\Omega}, m) + (1 - f_{\mathrm{sig}})\mathcal{P}_{\mathrm{bkg}}(\vec{\Omega}, m). \tag{25}$$

Both signal and background component are assumed to factorise in the decay angles $\vec{\Omega}$ and the reconstructed B^0 mass m (see appendix H)

$$\mathcal{P}_{\mathrm{sig}}(\vec{\Omega}, m) = \mathcal{P}_{\mathrm{sig}}(\vec{\Omega}) \times \mathcal{P}_{\mathrm{sig}}(m) \tag{26}$$

$$\mathcal{P}_{\mathrm{bkg}}(\vec{\Omega}, m) = \mathcal{P}_{\mathrm{bkg}}(\vec{\Omega}) \times \mathcal{P}_{\mathrm{bkg}}(m). \tag{27}$$

To determine the angular observables, the negative logarithmic likelihood

$$-\log\mathcal{L} = -\sum_{\text{events } e} \log\mathcal{P}_{\mathrm{tot}}(\vec{\Omega}_e, m_e | \vec{\lambda}_{\mathrm{phys}}, \vec{\lambda}_{\mathrm{nuisance}}) \tag{28}$$

is minimised with respect to the physics parameters $\vec{\lambda}_{\mathrm{phys}}$ and the nuisance parameters $\vec{\lambda}_{\mathrm{nuisance}}$. The minimisation is performed using the MINUIT software package. Uncertainties on the parameters can be either determined using the second derivative matrix (HESSE) or the $-2\Delta\log\mathcal{L} = 1$ rule (MINOS), which allows asymmetric uncertainties.

6.2.1 Angular distributions

The angular description of the signal component of the PDF is given by the differential decay rate given by Eq. 12. The data are binned in q^2, thereby effectively averaging the observables over the width of the q^2 bins. The resulting three-differential decay rate is given by

$$\begin{aligned}\frac{1}{\mathrm{d}(\Gamma+\bar{\Gamma})/\mathrm{d}q^2}\frac{\mathrm{d}(\Gamma+\bar{\Gamma})}{\mathrm{dcos}\theta_l\,\mathrm{dcos}\theta_K\,\mathrm{d}\phi}\bigg|_{\mathrm{P}} = \tfrac{9}{32\pi}\big[&\tfrac{3}{4}(1-F_{\mathrm{L}})\sin^2\theta_K \\ &+ F_{\mathrm{L}}\cos^2\theta_K + \tfrac{1}{4}(1-F_{\mathrm{L}})\sin^2\theta_K\cos 2\theta_l \\ &- F_{\mathrm{L}}\cos^2\theta_K\cos 2\theta_l + S_3\sin^2\theta_K\sin^2\theta_l\cos 2\phi \\ &+ S_4\sin 2\theta_K\sin 2\theta_l\cos\phi + S_5\sin 2\theta_K\sin\theta_l\cos\phi \\ &+ \tfrac{4}{3}A_{\mathrm{FB}}\sin^2\theta_K\cos\theta_l + S_7\sin 2\theta_K\sin\theta_l\sin\phi \\ &+ S_8\sin 2\theta_K\sin 2\theta_l\sin\phi + S_9\sin^2\theta_K\sin^2\theta_l\sin 2\phi\big].\end{aligned} \tag{29}$$

As discussed in Sec. 6.1.4, the inclusion of an S-wave contribution, where the $K^+\pi^-$ system is in a spin 0 configuration, leads to additional angular terms. The PDF needs to be changed to include both the S-wave and interference between S- and P-wave resulting in

$$\left.\frac{1}{\mathrm{d}(\Gamma+\bar{\Gamma})/\mathrm{d}q^2}\frac{\mathrm{d}(\Gamma+\bar{\Gamma})}{\mathrm{dcos}\theta_l\,\mathrm{dcos}\theta_K\,\mathrm{d}\phi}\right|_{\mathrm{S+P}} = (1-F_S)\left.\frac{1}{\mathrm{d}(\Gamma+\bar{\Gamma})/\mathrm{d}q^2}\frac{\mathrm{d}(\Gamma+\bar{\Gamma})}{\mathrm{dcos}\theta_l\,\mathrm{dcos}\theta_K\,\mathrm{d}\phi}\right|_{\mathrm{P}} \\ +\tfrac{3}{16\pi}\big[F_S\sin^2\theta_l + S_{S1}\sin^2\theta_l\cos\theta_K \\ + S_{S2}\sin 2\theta_l\sin\theta_K\cos\phi \\ + S_{S3}\sin\theta_l\sin\theta_K\cos\phi \\ + S_{S4}\sin\theta_l\sin\theta_K\sin\phi \\ + S_{S5}\sin 2\theta_l\sin\theta_K\sin\phi\big]. \tag{30}$$

The background component in the maximum likelihood fit is modelled using Chebyshev polynomials. The angular parametrisation of the background is assumed to factorise, For the angular parametrisation of the background using Chebyshev polynomials T_i of second order and lower, the PDF is given by

$$\mathcal{P}_{\mathrm{bkg}}(\cos\theta_l,\cos\theta_K,\phi) = \left[\sum_{i=0}^{2} c_i T_i(\cos\theta_l)\right]\times\left[\sum_{j=0}^{2} c_j T_j(\cos\theta_K)\right]\times\left[\sum_{k=0}^{2} c_k T_k(\phi)\right] \tag{31}$$

6.2.2 Mass modeling

The reconstructed B^0 mass of the signal is modelled using the sum of two Crystal Ball functions with common tail parameters for the low mass side, as described in Sec. 5. The parameters describing the signal mass shape are determined from a fit to the control-decay $B^0 \to J/\psi\, K^{*0}$ and the q^2 dependency is accounted for by a q^2 dependent scale factor determined from Monte Carlo simulation. The mass distribution of the background is modelled using an exponential function. For the fits of the $B^0 \to K^{*0}\mu^+\mu^-$ signal only τ_m, the inverse of the exponential decay constant as well as the signal fraction f_{sig} are floated. The other mass parameters are taken from the control decay and fixed in the fit of the signal decay.

6.2.3 Acceptance effect

The reconstruction and selection of the signal decay distorts the angular distributions and needs to be accounted for when determining the angular observables. This acceptance effect, depending on q^2 and the decay angles can be parameterised using multidimensional polynomials

$$\epsilon(q^2,\cos\theta_l,\cos\theta_K,\phi) = \sum_{hijk} c_{hijk}\times(q^2)^h\times(\cos\theta_l)^i\times(\cos\theta_K)^j\times(\phi)^k. \tag{32}$$

The determination of the polynomial coefficients and the resulting angular description is discussed in Sec. 8. This efficiency can be included in the fit in two ways, either by performing a weighted fit in which the events are weighted by $1/\epsilon$, of by including the effect in the signal PDF.

In the first option, the distributions are effectively unfolded, therfore the original signal PDF without acceptance can be used. It should be noted that the background component will be weighted in the same way. The per-event weight is included in the likelihood as follows

$$\begin{aligned}\mathcal{L} &= -\sum_{\text{event } e} w_e \times \log \mathcal{P}(\vec{\Omega}_e, m_e) \\ &= -\sum_{\text{event } e} \frac{1}{\epsilon(q_e^2, \vec{\Omega}_e)} \times \log \mathcal{P}(\vec{\Omega}_e, m_e).\end{aligned}$$

Special care needs to be taken for the estimation of the parameter uncertainties, since weighted fits in general are not guaranteed correct coverage. However, an approximate methods exists. The corrected covariance matrix V' for the weighted fit can be calculated according to

$$V' = VC^{-1}V,$$

where V is the covariance matrix calculated with the weights w_e and C the covariance matrix calculated using the squared weights w_e^2 [23]. The unfolding using acceptance weights is the preferred approach for the large q^2 bins $1.1 < q^2 < 6$ and $15.0 < q^2 < 19.0$, since the method can account for possible variation of the acceptance with q^2. Furthermore the expected signal yield in these bins is sufficiently large to reduce possible fluctuations from the weighting procedure.

The second option requires to include the efficiency in the signal PDF. The main difficulty with this approach is the correct determination of the norm of the signal component which will be affected by the acceptance[3]. The norm $\mathcal{N}_{\text{sig}}$ is given by

$$\begin{aligned}\mathcal{N}_{\text{sig}} &= \int \epsilon(q^2, \vec{\Omega}) \mathcal{P}_{\text{sig}}(\vec{\Omega}) \mathrm{d}\vec{\Omega} \\ &= \int \epsilon(q^2, \vec{\Omega}) \frac{9}{32\pi} \sum_i S_i f_i(\vec{\Omega}) \mathrm{d}\vec{\Omega} \\ &= \frac{9}{32\pi} \sum_i S_i \xi_i(q^2),\end{aligned} \tag{33}$$

with $\xi_i = \int \epsilon(q^2, \vec{\Omega}) f_i(\vec{\Omega}) \mathrm{d}\vec{\Omega}$, and where the angular terms $f_i(\vec{\Omega})$ are defined by the Eqs. 29 and 30. This is the preferred approach for the $2\,\mathrm{GeV}^2/c^4$ q^2 bins, where the acceptance does not vary significantly over the (narrow) q^2 bin.

6.2.4 Physical boundaries of the observables

Eqs. 29 and 30 imply certain boundaries for the angular observables since the PDF is not allowed to become negative for any combination of angles. If the values of the angular

[3] Note that the factor $\epsilon(q^2, \vec{\Omega})$ in the numerator can be omitted when determining $-\log \mathcal{L}$.

observables lie close to these constraints the likelihood function becomes non-Gaussian. Technically, a large penalty term is added in the fit for every event for which $\mathcal{P}_{\mathrm{tot}}(\vec{\Omega}_e, m_e)$ becomes negative. It is instructive to explore the particular shape of the allowed parameter regions by performing parameter scans and using toys to find wether the PDF can become negative for a certain parameter set. Figures 10 and 11 show the allowed parameter range for different combinations of angular observables in dark gray. The red points are the SM values for the seven bins of the $2\,\mathrm{GeV}^2/c^4$ q^2 binning. Particularly striking are the constraints on combinations of F_L with the other observables, that can be expressed by the following relations

$$|S_3| \leq \frac{1}{2}(1 - F_L) \tag{34}$$

$$|A_{\mathrm{FB}}| \leq \frac{3}{4}(1 - F_L) \tag{35}$$

$$|S_9| \leq \frac{1}{2}(1 - F_L). \tag{36}$$

Due to the large dependence of the allowed parameter range on F_L, the allowed regions for parameter combinations not containing F_L are integrated over all possible F_L values (we iterate over the full available F_L range from zero to one in 40 steps). The other parameters not shown are either assumed to be zero or equal to one of the seven SM points of the $2\,\mathrm{GeV}^2/c^4$ q^2 binning. If the studied point is allowed for one of these eight possibilities it is marked as allowed. The parameter boundaries can affect the coverage negatively. To ensure correct coverage we therefore rely on the Feldman-Cousins method described in Sec. 6.2.10.

6.2.5 Likelihood scans

The effects of the physical boundaries on the observables discussed in Sec. 6.2.4 can also be seen when performing two-dimensional profile likelihood scans for `EOS` toy data. Figs. 113-116 give two-dimensional profile likelihood scans for combinations of F_L with all other observables for all q^2 bins. The 68.3% and 90% confidence level regions are given by the solid black lines. It should be noted that the given likelihood scans are of course dependending on the specific toy that is being studied, different toys will exhibit different shapes due to statistical fluctuations. The profile likelihood scans can be used to determine correlations between the observables according to the method described in Sec. 7.1.

6.2.6 CP-asymmetries $\mathbf{A_i}$

There is significant theoretical interest in the CP-asymmetries A_i defined in Eq. 18, particularly the T-odd asymmetries $A_{7,8,9}$, where significants effects of new weak phases could be seen. To determine the angular observables, Eq. 29 needs to be modified, replacing $S^{(s)}_{3,\ldots,9}$ by $A_{3,\ldots,9}$ for the $\overline{B}^0$ decay and $-A_{3,\ldots,9}$ for the B^0 decay flavour. The CP-asymmetry corresponding to F_{L} cannot be determined in this way, since this would require both the angular signal PDF $\mathcal{P}_{\mathrm{sig}}(\vec{\Omega})$ as well as $-\mathcal{P}_{\mathrm{sig}}(\vec{\Omega})$ to be positive. F_{L} (or equivalently

$S_1^{s/c}$) is therefore treated as a nuisance parameter in these fits. Since the SM values of all asymmetries are close to zero as shown in Fig. 111 and 112, the CP-asymmetries are expected to be less affected by the physical boundaries.

6.2.7 The $\mathbf{P_i^{(\prime)}}$ basis

The PDF can also be expressed in the $P_i^{(\prime)}$ basis detailed in Sec. 6.1.5. The varied signal parameters in this case are F_{L}, $P_{1,2,3}$ and $P'_{4,5,6,8}$. Since the $P_i^{(\prime)}$ are nonlinear combinations of the angular coefficients S_i, the uncertainties are expected to be generally more asymmetric.

6.2.8 Fit validation using `EOS` toys

The fit is validated using simulated events generated according to an updated theory calculation as described in Sec. 3.2. Pull studies are performed to ensure the fit is unbiased and estimates the uncertainties correctly. The pull of the observable p is defined as $(p_{\text{fitted}} - p_{\text{generated}})/\sigma(p)_{\text{fitted}}$. In the ideal case the pull is distributed according to a Gaussian distribution with mean compatible with 0 and width compatible with 1. For low statistics and non-Gaussian PDFs this is not necessarily the case and can lead to incorrect coverage. For the toy studies, the P-wave observables S_i, the signal fraction f_{sig}, the parameter τ_m describing the exponential shape of the combinatorial background, and six coefficients describing the angular distribution of the combinatorial background as detailed in Sec. 6.2.1 are floated. The `EOS` toys do not contain an S-wave component.

Tables 13 and 14 give toy studies for the $2\,\mathrm{GeV}^2$ binning. For every q^2 bin 1000 toys are performed. It should be noted that the fit converges successfully for all toys (Migrad status 0, Hesse status 3). Generally the toys behave well, however there are some observables where sizeable biases larger than 0.1 are seen, which are shaded in gray. A particularly large deviation from the `EOS` value is observed for the first bin for S_1^s. This deviation is understood since the fit assumes that the lepton masses can be neglected, which is not the case close to $q^2 = 0\,\mathrm{GeV}^2$. All other deviations seen are smaller than 0.20. To ensure correct coverage for the $2\,\mathrm{GeV}^2$ binning, the Feldman-Cousins method will be used for the determination of the confidence intervals.

The corresponding CP-asymmetries A_i have been determined from the `EOS` toy MC as well. The results are given in Tab. 116. No CP-asymmetries are showing significant biases. As discussed in Sec. 6.2.6 this is due to the SM values being further away from physical parameter boundaries.

6.2.9 Fit validation using toy studies

It is also possible to validate the fitter using events that are generated by the PDFs themselves. This is particularly useful for validating the determination of the S-wave parameters since `EOS` does not generate the S-wave amplitude A_S out of the box. For these toy studies, we do include the S-wave component according to Eq. 30. Parameters floating in the fits are the P-wave observables S_i, the signal fraction f_{sig}, the S-wave fraction F_S

Table 13: Results from pull studies on `EOS` toys in bins of q^2. A background component is included. The acceptance effect is included and assumed to be constant over the q^2 bins. Observables that show biases larger than 0.1 are shaded gray. Nuisance parameters are omitted.

$0.1 < q^2 < 1.0\,\mathrm{GeV}^2$	sensitivity	pull mean	pull width
S_1^s	0.028 ± 0.001	0.80 ± 0.03	1.00 ± 0.03
S_3	0.053 ± 0.001	-0.01 ± 0.03	0.99 ± 0.02
S_4	0.065 ± 0.002	-0.04 ± 0.03	1.02 ± 0.02
S_5	0.051 ± 0.001	0.06 ± 0.03	1.03 ± 0.03
S_6^s	0.071 ± 0.002	0.02 ± 0.03	0.98 ± 0.03
S_7	0.051 ± 0.001	-0.01 ± 0.03	0.99 ± 0.03
S_8	0.067 ± 0.002	0.02 ± 0.03	1.05 ± 0.03
S_9	0.057 ± 0.001	-0.00 ± 0.03	1.02 ± 0.03

$1.1 < q^2 < 2.5\,\mathrm{GeV}^2$	sensitivity	pull mean	pull width
S_1^s	0.047 ± 0.001	0.01 ± 0.03	1.05 ± 0.03
S_3	0.074 ± 0.002	-0.07 ± 0.03	1.10 ± 0.03
S_4	0.097 ± 0.003	-0.02 ± 0.03	1.02 ± 0.03
S_5	0.085 ± 0.002	0.01 ± 0.03	1.03 ± 0.03
S_6^s	0.082 ± 0.002	-0.16 ± 0.03	1.00 ± 0.03
S_7	0.084 ± 0.002	-0.01 ± 0.03	0.99 ± 0.03
S_8	0.105 ± 0.003	0.02 ± 0.04	1.10 ± 0.03
S_9	0.071 ± 0.002	0.02 ± 0.03	1.08 ± 0.03

$2.5 < q^2 < 4.0\,\mathrm{GeV}^2$	sensitivity	pull mean	pull width
S_1^s	0.045 ± 0.001	-0.06 ± 0.03	1.01 ± 0.03
S_3	0.072 ± 0.002	0.02 ± 0.04	1.10 ± 0.03
S_4	0.096 ± 0.003	0.06 ± 0.03	1.04 ± 0.03
S_5	0.089 ± 0.002	0.03 ± 0.03	1.05 ± 0.03
S_6^s	0.072 ± 0.002	-0.13 ± 0.03	0.98 ± 0.03
S_7	0.088 ± 0.002	0.06 ± 0.03	1.04 ± 0.03
S_8	0.103 ± 0.002	-0.08 ± 0.03	1.08 ± 0.03
S_9	0.072 ± 0.002	0.09 ± 0.03	1.06 ± 0.03

$4.0 < q^2 < 6.0\,\mathrm{GeV}^2$	sensitivity	pull mean	pull width
S_1^s	0.033 ± 0.001	0.03 ± 0.03	0.96 ± 0.03
S_3	0.059 ± 0.002	-0.01 ± 0.03	1.03 ± 0.03
S_4	0.074 ± 0.002	0.07 ± 0.03	1.05 ± 0.03
S_5	0.067 ± 0.002	0.11 ± 0.03	0.99 ± 0.03
S_6^s	0.057 ± 0.001	-0.04 ± 0.03	1.05 ± 0.03
S_7	0.065 ± 0.002	-0.10 ± 0.03	0.96 ± 0.02
S_8	0.074 ± 0.002	0.00 ± 0.03	1.02 ± 0.03
S_9	0.057 ± 0.001	-0.04 ± 0.03	1.03 ± 0.03

and the five angular terms S_{Si}. As before, we also float the parameter τ_m describing the exponential shape of the combinatorial background, and six coefficients describing the

Table 14: Results from pull studies on `EOS` toys in bins of q^2. A background component is included. The acceptance effect is included and is assumed to be constant over the q^2 bins. Observables that show biases larger than 0.1 are shaded gray. Nuisance parameters are omitted.

$6.0 < q^2 < 8.0\,\mathrm{GeV}^2$	sensitivity	pull mean	pull width
S_1^s	0.032 ± 0.001	0.01 ± 0.03	1.05 ± 0.03
S_3	0.051 ± 0.001	-0.02 ± 0.03	1.00 ± 0.03
S_4	0.062 ± 0.002	0.10 ± 0.03	1.07 ± 0.03
S_5	0.056 ± 0.001	0.07 ± 0.03	1.00 ± 0.03
S_6^s	0.047 ± 0.001	0.02 ± 0.03	1.02 ± 0.03
S_7	0.063 ± 0.002	-0.05 ± 0.03	0.98 ± 0.03
S_8	0.063 ± 0.002	-0.03 ± 0.03	0.99 ± 0.03
S_9	0.052 ± 0.001	-0.01 ± 0.03	1.02 ± 0.03

$15.0 < q^2 < 17.0\,\mathrm{GeV}^2$	sensitivity	pull mean	pull width
S_1^s	0.029 ± 0.001	-0.03 ± 0.03	1.04 ± 0.03
S_3	0.048 ± 0.001	-0.10 ± 0.03	1.04 ± 0.03
S_4	0.053 ± 0.001	0.13 ± 0.04	1.14 ± 0.03
S_5	0.044 ± 0.001	-0.00 ± 0.03	1.02 ± 0.03
S_6^s	0.045 ± 0.001	0.03 ± 0.03	1.03 ± 0.03
S_7	0.056 ± 0.002	-0.02 ± 0.03	1.00 ± 0.03
S_8	0.058 ± 0.002	-0.00 ± 0.03	1.02 ± 0.03
S_9	0.048 ± 0.001	-0.01 ± 0.04	1.09 ± 0.03

$17.0 < q^2 < 19.0\,\mathrm{GeV}^2$	sensitivity	pull mean	pull width
S_1^s	0.039 ± 0.001	0.09 ± 0.04	1.11 ± 0.03
S_3	0.071 ± 0.002	-0.13 ± 0.03	1.10 ± 0.03
S_4	0.073 ± 0.002	0.19 ± 0.04	1.15 ± 0.03
S_5	0.065 ± 0.002	0.09 ± 0.03	1.10 ± 0.03
S_6^s	0.065 ± 0.002	0.18 ± 0.03	1.00 ± 0.02
S_7	0.075 ± 0.002	0.02 ± 0.03	1.01 ± 0.03
S_8	0.073 ± 0.002	-0.01 ± 0.03	1.00 ± 0.03
S_9	0.070 ± 0.002	0.08 ± 0.04	1.13 ± 0.03

angular distribution of the combinatorial background as detailed in Sec. 6.2.1.

Tables 15 and 16 give the results of the toy studies including 10% S-wave contribution. For every q^2 bin 1000 toys are performed. As expected, the sensitivities to the observables decreases, however the fit does successfully converge (MIGRAD returns 0 and HESSE returns 3) for all toys, even with the six additional observables F_S and $S_{S1...5}$. Biases on the angular observables larger than 0.1 are shaded gray. All biases seen are smaller than 0.3. The parameter F_S exhibits a bias in all bins. This is due to the asymmetric pull distribution from the requirement $F_S \geq 0$. In addition, results of toy studies for the the two large q^2 bins $[1, 6]\,\mathrm{GeV}^2$ and $[15, 19]\,\mathrm{GeV}^2$ are given in Tab. 17 and 18. In Tab. 17, the toy study is performed including the acceptance in the fit, for the results in Tab. 18 event weights were used to unfold the distribution. No large biases are seen in either case due to the larger statistics compared to the smaller $2\,\mathrm{GeV}^2$ bins.

The results from the toy studies for the CP-asymmetries A_i, including the S-wave component, are given in Tab. 117 and 118. Again the toy studies for the CP-asymmetries behave better than the toy studies for the CP-averaged observables.

6.2.10 Coverage correction

To guarantee correct coverage, even for non-Gaussian PDFs, the Feldman-Cousins method [24] is employed. This method is a specific Neyman construction using likelihood ratios as ordering principle. The nuisance parameters are included using the plugin method [25].

Technically the parameter of interest is scanned at a number of equidistant points. For every point the likelihood ratio on data, $\Delta \log \mathcal{L}_{\mathrm{data}} = \log \mathcal{L}^{\mathrm{data}}_{\mathrm{fixed}} - \log \mathcal{L}^{\mathrm{data}}_{\mathrm{floated}}$, is determined, where the parameter of interest is fixed at the point for $\log \mathcal{L}^{\mathrm{data}}_{\mathrm{fixed}}$, but allowed to float for $\log \mathcal{L}^{\mathrm{data}}_{\mathrm{floated}}$. Then N_{toys} toys are thrown for the point, determining N_{toys} toy likelihood ratios $\Delta \log \mathcal{L}_{\mathrm{toy}\ i} = \log \mathcal{L}^{\mathrm{toy}}_{\mathrm{fixed}\ i} - \log \mathcal{L}^{\mathrm{toy}}_{\mathrm{floated}\ i}$. The confidence level of the point under study is then given by the fraction of toys for which $\Delta \log \mathcal{L}_{\mathrm{toy}\ i} > \Delta \log \mathcal{L}_{\mathrm{data}}$.

Fig. 12 shows the results for a single toy, generated with `EOS` as described in Sec. 3.2 with signal and background yields corresponding to the $3\,\mathrm{fb}^{-1}$ data sample. The observable S_5 is determined in seven bins of q^2. For every bin, 500 toys are generated for 100 equidistant points of the observable of interest. The resulting coverage-corrected 68.3% confidence interval is given in red. The blue line denotes the coverage from the likelihood method, the 68.3% confidence interval from the likelihood is given by the blue vertical line. As is apparent for bins three and seven, for certain parameter configurations the likelihood method undercovers.

6.2.11 Fit validation on data using $B^0 \to J/\psi\, K^{*0}$

The angular distributions of the tree-level decay $B^0 \to J/\psi\, K^{*0}$ was studied previously by BaBar [26], Belle [27] and CDF [28] experiment. Most recently, LHCb analysed the decay using $1\,\mathrm{fb}^{-1}$ of data recorded in 2011 [20]. The decay $B^0 \to J/\psi\, K^{*0}$ is selected using the full selection for the $B^0 \to K^{*0}\mu^+\mu^-$ signal decay and requiring that the invariant mass of the dimuon system is $\pm 60\,\mathrm{MeV}$ around the known J/ψ mass. The parameter n_{CB} is fixed

Table 15: Results from pull studies on toys including S-wave constribution in bins of q^2. A background component is included as well. The acceptance effect is included and is assumed to be constant over the q^2 bins. Observables that show biases larger than 0.1 are shaded gray. Nuisance parameters are omitted.

$0.1 < q^2 < 1.0\,\mathrm{GeV}^2$	sensitivity	pull mean	pull width
S_1^s	0.036 ± 0.001	0.03 ± 0.03	0.97 ± 0.03
S_3	0.066 ± 0.002	0.04 ± 0.03	0.97 ± 0.03
S_4	0.068 ± 0.002	0.03 ± 0.03	0.95 ± 0.02
S_5	0.072 ± 0.002	-0.07 ± 0.03	0.92 ± 0.03
S_6^s	0.083 ± 0.002	0.01 ± 0.03	1.07 ± 0.03
S_7	0.061 ± 0.002	-0.01 ± 0.03	0.96 ± 0.03
S_8	0.071 ± 0.002	-0.05 ± 0.03	0.98 ± 0.03
S_9	0.063 ± 0.002	0.08 ± 0.03	0.95 ± 0.02
F_S	0.166 ± 0.007	0.24 ± 0.03	0.89 ± 0.02
S_{S1}	0.093 ± 0.003	0.06 ± 0.03	1.01 ± 0.03
S_{S2}	0.091 ± 0.002	0.02 ± 0.03	1.06 ± 0.03
S_{S3}	0.070 ± 0.002	-0.09 ± 0.03	0.99 ± 0.03
S_{S4}	0.075 ± 0.002	0.02 ± 0.03	1.03 ± 0.03
S_{S5}	0.087 ± 0.002	-0.10 ± 0.03	0.97 ± 0.02

$1.1 < q^2 < 2.5\,\mathrm{GeV}^2$	sensitivity	pull mean	pull width
S_1^s	0.069 ± 0.002	-0.28 ± 0.03	0.98 ± 0.03
S_3	0.102 ± 0.003	-0.02 ± 0.03	1.05 ± 0.03
S_4	0.139 ± 0.004	-0.12 ± 0.03	1.08 ± 0.03
S_5	0.113 ± 0.003	-0.13 ± 0.03	1.03 ± 0.03
S_6^s	0.114 ± 0.003	-0.15 ± 0.03	1.00 ± 0.02
S_7	0.116 ± 0.003	-0.09 ± 0.03	1.01 ± 0.02
S_8	0.133 ± 0.004	0.02 ± 0.03	1.07 ± 0.03
S_9	0.106 ± 0.003	-0.03 ± 0.03	1.04 ± 0.03
F_S	0.216 ± 0.009	0.20 ± 0.03	1.05 ± 0.03
S_{S1}	0.170 ± 0.004	-0.05 ± 0.03	1.03 ± 0.03
S_{S2}	0.139 ± 0.004	-0.03 ± 0.04	1.17 ± 0.03
S_{S3}	0.104 ± 0.002	-0.00 ± 0.03	1.05 ± 0.03
S_{S4}	0.111 ± 0.003	-0.03 ± 0.04	1.14 ± 0.03
S_{S5}	0.130 ± 0.003	-0.02 ± 0.03	1.11 ± 0.03

$2.5 < q^2 < 4.0\,\mathrm{GeV}^2$	sensitivity	pull mean	pull width
S_1^s	0.073 ± 0.002	-0.23 ± 0.03	1.05 ± 0.03
S_3	0.095 ± 0.002	-0.04 ± 0.03	1.07 ± 0.03
S_4	0.133 ± 0.004	0.09 ± 0.03	1.10 ± 0.03
S_5	0.110 ± 0.003	0.09 ± 0.03	0.94 ± 0.02
S_6^s	0.099 ± 0.003	-0.11 ± 0.03	1.05 ± 0.03
S_7	0.121 ± 0.003	-0.02 ± 0.04	1.07 ± 0.03
S_8	0.129 ± 0.003	-0.11 ± 0.04	1.10 ± 0.03
S_9	0.101 ± 0.003	0.04 ± 0.03	1.03 ± 0.02
F_S	0.187 ± 0.008	0.24 ± 0.03	1.03 ± 0.03
S_{S1}	0.176 ± 0.005	0.04 ± 0.03	1.05 ± 0.03
S_{S2}	0.134 ± 0.003	0.08 ± 0.04	1.17 ± 0.03
S_{S3}	0.114 ± 0.003	0.04 ± 0.03	1.09 ± 0.03
S_{S4}	0.115 ± 0.003	0.07 ± 0.03	1.09 ± 0.03
S_{S5}	0.132 ± 0.003	-0.01 ± 0.04	1.17 ± 0.03

$4.0 < q^2 < 6.0\,\mathrm{GeV}^2$	sensitivity	pull mean	pull width
S_1^s	0.047 ± 0.001	-0.11 ± 0.03	0.99 ± 0.03
S_3	0.072 ± 0.002	0.04 ± 0.03	0.97 ± 0.03
S_4	0.093 ± 0.002	0.06 ± 0.03	1.06 ± 0.03
S_5	0.095 ± 0.003	0.04 ± 0.03	1.02 ± 0.03
S_6^s	0.063 ± 0.002	0.06 ± 0.03	0.98 ± 0.02
S_7	0.085 ± 0.002	-0.01 ± 0.03	0.98 ± 0.03
S_8	0.092 ± 0.002	-0.07 ± 0.03	1.05 ± 0.03
S_9	0.073 ± 0.002	0.04 ± 0.03	1.02 ± 0.03
F_S	0.128 ± 0.005	0.24 ± 0.02	0.84 ± 0.03
S_{S1}	0.135 ± 0.003	-0.08 ± 0.03	1.03 ± 0.03
S_{S2}	0.101 ± 0.003	0.06 ± 0.04	1.15 ± 0.03
S_{S3}	0.087 ± 0.002	0.02 ± 0.03	1.09 ± 0.03
S_{S4}	0.088 ± 0.002	0.07 ± 0.03	1.07 ± 0.03
S_{S5}	0.092 ± 0.002	-0.04 ± 0.03	1.05 ± 0.03

to 4.23, determined from a fit in the q^2 region $[8.0, 11.0]\,\mathrm{GeV}^2$ where the fit is more stable. In contrast to the fit of the signal decay $B^0 \to K^{*0}\mu^+\mu^-$, the contribution from the B_s^0 decay $B_s^0 \to J/\psi\, K^{*0}$, which is suppressed by $f_s/f_d|V_{\rm cd}/V_{\rm cs}|^2$, is modelled in the fit as well. Its angular and mass distribution are assumed to be identical to $B^0 \to J/\psi\, K^{*0}$, with the mass distribution of the B_s^0 shifted by Δm. As angular acceptance the parametrisation described in Sec. 8.2 is used, included in the fit as discussed in Sec. 6.2.3. Figure 13 gives the projections for the fit of $B^0 \to J/\psi\, K^{*0}$ in the $m_{K\pi}$ mass range $[795.9, 995.9]\,\mathrm{MeV}$. Table 19 gives the result of a full anguar fit in different bins of $m_{K\pi}$. For comparison, Tab. 20 gives the angular terms that were previously measured by LHCb [20]. Since Ref. [20] gives the magnitudes of the amplitudes $|A_{0,\|,\perp,S}|$ and the strong phases $\delta_{\|,\perp,S}$ as results, they are converted to the angular observables according to Eqs. 13 and 22. The observables are found to be consistent with the previous measurement of $B^0 \to J/\psi\, K^{*0}$.

Table 16: Results from pull studies on toys including S-wave constribution in bins of q^2. A background component is included as well. The acceptance effect is included and is assumed to be constant over the q^2 bins. Observables that show biases larger than 0.1 are shaded gray. Nuisance parameters are omitted.

$6.0 < q^2 < 8.0\,\mathrm{GeV}^2$	sensitivity	pull mean	pull width
S_1^s	0.038 ± 0.001	-0.04 ± 0.03	0.98 ± 0.03
S_3	0.067 ± 0.002	-0.03 ± 0.03	1.03 ± 0.03
S_4	0.074 ± 0.002	0.11 ± 0.03	1.04 ± 0.03
S_5	0.087 ± 0.002	0.07 ± 0.03	0.94 ± 0.03
S_6^s	0.057 ± 0.001	0.11 ± 0.03	1.00 ± 0.03
S_7	0.073 ± 0.002	0.02 ± 0.03	1.02 ± 0.03
S_8	0.076 ± 0.002	0.10 ± 0.03	1.05 ± 0.03
S_9	0.068 ± 0.002	-0.01 ± 0.03	1.01 ± 0.03
F_S	0.116 ± 0.005	0.27 ± 0.02	0.79 ± 0.02
S_{S1}	0.119 ± 0.003	0.06 ± 0.03	1.04 ± 0.03
S_{S2}	0.081 ± 0.002	-0.06 ± 0.04	1.11 ± 0.03
S_{S3}	0.075 ± 0.002	0.06 ± 0.03	1.05 ± 0.03
S_{S4}	0.075 ± 0.002	0.01 ± 0.03	1.01 ± 0.03
S_{S5}	0.082 ± 0.002	0.01 ± 0.03	1.08 ± 0.03

$15.0 < q^2 < 17.0\,\mathrm{GeV}^2$	sensitivity	pull mean	pull width
S_1^s	0.033 ± 0.001	-0.05 ± 0.03	0.95 ± 0.02
S_3	0.060 ± 0.001	-0.17 ± 0.03	1.02 ± 0.03
S_4	0.065 ± 0.002	0.07 ± 0.03	1.04 ± 0.03
S_5	0.063 ± 0.002	-0.00 ± 0.03	0.97 ± 0.03
S_6^s	0.064 ± 0.002	0.07 ± 0.03	1.01 ± 0.03
S_7	0.064 ± 0.002	-0.03 ± 0.03	0.98 ± 0.02
S_8	0.065 ± 0.002	0.06 ± 0.03	1.03 ± 0.03
S_9	0.060 ± 0.001	-0.03 ± 0.03	1.05 ± 0.03
F_S	0.105 ± 0.004	0.26 ± 0.03	0.79 ± 0.02
S_{S1}	0.092 ± 0.002	-0.04 ± 0.03	0.99 ± 0.02
S_{S2}	0.068 ± 0.002	-0.06 ± 0.03	1.09 ± 0.03
S_{S3}	0.063 ± 0.002	-0.06 ± 0.03	1.03 ± 0.03
S_{S4}	0.077 ± 0.002	0.04 ± 0.03	1.01 ± 0.03
S_{S5}	0.074 ± 0.002	-0.00 ± 0.03	1.04 ± 0.03

$17.0 < q^2 < 19.0\,\mathrm{GeV}^2$	sensitivity	pull mean	pull width
S_1^s	0.044 ± 0.001	0.03 ± 0.03	0.99 ± 0.03
S_3	0.091 ± 0.002	-0.24 ± 0.03	0.99 ± 0.03
S_4	0.102 ± 0.003	0.24 ± 0.04	1.09 ± 0.03
S_5	0.082 ± 0.002	0.03 ± 0.03	1.02 ± 0.03
S_6^s	0.085 ± 0.003	0.19 ± 0.03	0.96 ± 0.02
S_7	0.088 ± 0.002	-0.01 ± 0.03	1.03 ± 0.03
S_8	0.088 ± 0.002	-0.02 ± 0.03	1.03 ± 0.03
S_9	0.086 ± 0.002	0.01 ± 0.03	1.02 ± 0.02
F_S	0.152 ± 0.006	0.24 ± 0.03	0.93 ± 0.02
S_{S1}	0.119 ± 0.003	0.04 ± 0.03	1.03 ± 0.03
S_{S2}	0.099 ± 0.003	0.04 ± 0.04	1.13 ± 0.03
S_{S3}	0.087 ± 0.002	-0.04 ± 0.04	1.11 ± 0.03
S_{S4}	0.102 ± 0.003	0.01 ± 0.03	1.04 ± 0.03
S_{S5}	0.107 ± 0.003	-0.06 ± 0.03	1.06 ± 0.03

6.2.12 Constraining the S-wave using the $m_{K\pi}$ distribution

As mentioned in Sec. 6.2.9 including the S-wave contribution results in a reduction of sensitivity to the physically interesting P-wave observables. This is because, according to Eq. 30, all P-wave parameters are scaled by the factor $(1 - F_S)$ which is not known a priori. Neglecting the S-wave in the fit and correcting the P-wave parameters using F_S from the dedicated S-wave analysis which is in preparation is problematic since it partially uses the same data distributions ($m_{K\pi\mu\mu}$ and $\cos\theta_K$). A possibility to circumvent these difficulties is to include the $m_{K\pi}$ projection in a simultaneous fit. Since the P-wave is peaking in $m_{K\pi}$ while the S-wave contribution is relatively flat this gives an additional constraint on F_S and therefore also allows a better determination of the P-wave observables. Ref. [29] gives details on the dependence of the decay amplitudes on $m_{K\pi}$. To parameterize the

Table 17: Results from pull studies on toys including S-wave constribution in bins of q^2. A background component is included as well. The acceptance effect is included and is assumed to be constant over the q^2 bins. Observables that show biases larger than 0.1 are shaded gray. Nuisance parameters are omitted.

	$1.0 < q^2 < 6.0\,\mathrm{GeV}^2$				$15.0 < q^2 < 19.0\,\mathrm{GeV}^2$		
	sensitivity	pull mean	pull width		sensitivity	pull mean	pull width
S_1^s	0.033 ± 0.001	-0.03 ± 0.03	1.01 ± 0.02	S_1^s	0.028 ± 0.001	0.01 ± 0.03	1.02 ± 0.02
S_3	0.047 ± 0.001	-0.02 ± 0.03	1.02 ± 0.02	S_3	0.053 ± 0.001	0.03 ± 0.03	1.03 ± 0.02
S_4	0.057 ± 0.001	0.03 ± 0.03	1.00 ± 0.02	S_4	0.052 ± 0.001	0.07 ± 0.03	1.04 ± 0.02
S_5	0.056 ± 0.001	0.05 ± 0.03	1.01 ± 0.02	S_5	0.049 ± 0.001	0.07 ± 0.03	0.98 ± 0.02
S_6^s	0.044 ± 0.001	0.08 ± 0.03	0.99 ± 0.02	S_6^s	0.053 ± 0.001	0.00 ± 0.03	1.01 ± 0.02
S_7	0.055 ± 0.001	-0.06 ± 0.03	1.02 ± 0.02	S_7	0.054 ± 0.001	-0.01 ± 0.03	1.03 ± 0.02
S_8	0.058 ± 0.001	-0.02 ± 0.03	1.01 ± 0.02	S_8	0.052 ± 0.001	-0.03 ± 0.03	1.02 ± 0.02
S_9	0.046 ± 0.001	-0.00 ± 0.03	1.00 ± 0.02	S_9	0.047 ± 0.001	-0.03 ± 0.03	0.99 ± 0.02
F_S	0.073 ± 0.002	0.07 ± 0.03	1.00 ± 0.02	F_S	0.072 ± 0.002	0.07 ± 0.03	1.00 ± 0.02
S_{S1}	0.088 ± 0.002	-0.03 ± 0.03	0.99 ± 0.02	S_{S1}	0.075 ± 0.002	-0.05 ± 0.03	1.04 ± 0.02
S_{S2}	0.057 ± 0.001	0.01 ± 0.03	1.02 ± 0.02	S_{S2}	0.053 ± 0.001	-0.03 ± 0.03	1.06 ± 0.02
S_{S3}	0.051 ± 0.001	0.03 ± 0.03	0.98 ± 0.02	S_{S3}	0.049 ± 0.001	-0.02 ± 0.03	1.02 ± 0.02
S_{S4}	0.053 ± 0.001	-0.01 ± 0.03	1.02 ± 0.02	S_{S4}	0.060 ± 0.001	0.03 ± 0.03	1.02 ± 0.02
S_{S5}	0.057 ± 0.001	0.01 ± 0.03	1.00 ± 0.02	S_{S5}	0.060 ± 0.001	0.01 ± 0.03	1.04 ± 0.02

Table 18: Results from pull studies on toys including S-wave contribution for two large q^2 bins using event weights. A background component is included. Observables that show biases larger than 0.1 are shaded gray. Nuisance parameters are omitted.

	$1.0 < q^2 < 6.0\,\mathrm{GeV}^2$				$15.0 < q^2 < 19.0\,\mathrm{GeV}^2$		
	sensitivity	pull mean	pull width		sensitivity	pull mean	pull width
S_1^s	0.034 ± 0.001	0.06 ± 0.03	0.82 ± 0.02	S_1^s	0.026 ± 0.001	0.04 ± 0.04	1.18 ± 0.03
S_3	0.048 ± 0.001	0.03 ± 0.03	1.01 ± 0.02	S_3	0.052 ± 0.001	0.06 ± 0.03	0.96 ± 0.02
S_4	0.060 ± 0.001	0.04 ± 0.03	1.01 ± 0.02	S_4	0.052 ± 0.001	0.03 ± 0.03	1.08 ± 0.02
S_5	0.054 ± 0.001	-0.01 ± 0.03	0.93 ± 0.02	S_5	0.055 ± 0.001	-0.06 ± 0.03	1.06 ± 0.02
S_6^s	0.046 ± 0.001	0.04 ± 0.03	1.00 ± 0.02	S_6^s	0.056 ± 0.001	0.01 ± 0.04	1.22 ± 0.03
S_7	0.055 ± 0.001	0.03 ± 0.03	0.97 ± 0.02	S_7	0.053 ± 0.001	0.02 ± 0.03	1.02 ± 0.02
S_8	0.058 ± 0.001	-0.02 ± 0.03	0.95 ± 0.02	S_8	0.053 ± 0.001	0.00 ± 0.03	1.04 ± 0.02
S_9	0.047 ± 0.001	0.05 ± 0.03	0.97 ± 0.02	S_9	0.045 ± 0.001	-0.01 ± 0.03	0.94 ± 0.02
F_S	0.080 ± 0.002	-0.00 ± 0.02	0.74 ± 0.02	F_S	0.077 ± 0.002	0.03 ± 0.03	1.09 ± 0.02
S_{S1}	0.094 ± 0.002	-0.02 ± 0.03	1.02 ± 0.02	S_{S1}	0.073 ± 0.002	-0.04 ± 0.03	1.00 ± 0.02
S_{S2}	0.058 ± 0.001	0.02 ± 0.03	1.01 ± 0.02	S_{S2}	0.054 ± 0.001	0.02 ± 0.03	1.07 ± 0.02
S_{S3}	0.056 ± 0.001	0.01 ± 0.03	1.05 ± 0.02	S_{S3}	0.052 ± 0.001	0.04 ± 0.03	1.04 ± 0.02
S_{S4}	0.053 ± 0.001	-0.04 ± 0.03	1.00 ± 0.02	S_{S4}	0.060 ± 0.001	0.08 ± 0.03	1.01 ± 0.02
S_{S5}	0.058 ± 0.001	0.04 ± 0.03	1.00 ± 0.02	S_{S5}	0.061 ± 0.001	0.00 ± 0.03	1.02 ± 0.02

$m_{K\pi}$ dependence of the P-wave a Breit-Wigner distribution is used

$$\begin{aligned}\mathcal{A}_P(m_{K\pi}) = \sqrt{pq} \times B'_{L_B}(p, p_0, d) \left(\frac{p}{m_B}\right)^{L_B} \times B'_{L_{K^*}}(q, q_0, d) \left(\frac{q}{m_{K\pi}}\right)^{L_{K^*}} \\ \times \frac{1}{m_{K^*}^2 - m_{K\pi}^2 - i m_{K^*}\Gamma(m_{K\pi})},\end{aligned} \tag{37}$$

where p (q) denote the K^{*0} (K^+) momentum in the B^0 (K^{*0}) rest frame, p_0 (q_0) are the corresponding quantities at the resonance peak. L_B (L_{K^*}) are the orbital angular momenta and B'_{L_B} $(B'_{L_{K^*}})$ the Blatt-Weisskopf functions given in Ref. [30]. For the S-wave

Table 19: Results of the angular fit of the decay $B^0 \to J/\psi K^{*0}$ in different bins of $m_{K\pi}$, using the full available data set corresponding to $3\,\mathrm{fb}^{-1}$. The angular terms that have been previously determined in Ref. [20] are given in Tab. 20.

	$m_{K\pi}$ range in MeV/c^2					
parameter	$[795.9, 995.9]$	$[825.9, 965.9]$	$[826.0, 861.0]$	$[861.0, 896.0]$	$[896.0, 931.0]$	$[931.0, 966.0]$
S_{1s}	0.331 ± 0.001	0.329 ± 0.001	0.326 ± 0.004	0.324 ± 0.002	0.333 ± 0.002	0.334 ± 0.003
S_3	-0.000 ± 0.002	0.000 ± 0.002	-0.009 ± 0.006	0.000 ± 0.003	0.000 ± 0.003	0.004 ± 0.006
S_4	-0.255 ± 0.002	-0.255 ± 0.002	-0.258 ± 0.007	-0.258 ± 0.003	-0.254 ± 0.003	-0.251 ± 0.006
S_5	-0.001 ± 0.002	-0.002 ± 0.002	-0.002 ± 0.007	0.000 ± 0.003	-0.007 ± 0.003	0.002 ± 0.006
S_6^s	0.000 ± 0.002	0.000 ± 0.002	-0.005 ± 0.006	-0.000 ± 0.003	0.001 ± 0.003	0.004 ± 0.005
S_7	0.001 ± 0.002	0.001 ± 0.002	-0.000 ± 0.007	0.001 ± 0.003	0.002 ± 0.003	0.002 ± 0.006
S_8	-0.053 ± 0.002	-0.052 ± 0.002	-0.064 ± 0.007	-0.055 ± 0.003	-0.051 ± 0.003	-0.045 ± 0.006
S_9	-0.089 ± 0.002	-0.089 ± 0.002	-0.088 ± 0.007	-0.084 ± 0.003	-0.094 ± 0.003	-0.090 ± 0.006
F_S	0.087 ± 0.003	0.072 ± 0.003	0.12 ± 0.01	0.051 ± 0.005	0.061 ± 0.005	0.119 ± 0.009
S_{S1}	-0.234 ± 0.003	-0.233 ± 0.004	-0.75 ± 0.01	-0.363 ± 0.006	-0.091 ± 0.006	0.15 ± 0.01
S_{S2}	0.023 ± 0.002	0.027 ± 0.002	0.159 ± 0.007	0.065 ± 0.004	-0.006 ± 0.004	-0.091 ± 0.007
S_{S3}	0.003 ± 0.002	0.003 ± 0.002	-0.004 ± 0.007	0.003 ± 0.003	0.004 ± 0.004	0.009 ± 0.006
S_{S4}	0.001 ± 0.002	0.001 ± 0.002	0.015 ± 0.007	-0.003 ± 0.003	0.000 ± 0.004	0.007 ± 0.006
S_{S5}	-0.068 ± 0.002	-0.064 ± 0.002	0.037 ± 0.008	-0.031 ± 0.004	-0.091 ± 0.004	-0.166 ± 0.007

Table 20: Results of the full angular fit of the decay $B^0 \to J/\psi K^{*0}$ in Ref. [20], translated to the angular observables.

	$m_{K\pi}$ range in MeV/c^2				
parameter	$[825.9, 965.9]$	$[826.0, 861.0]$	$[861.0, 896.0]$	$[896.0, 931.0]$	$[931.0, 966.0]$
S_1^s	0.321 ± 0.006	0.321 ± 0.006	0.321 ± 0.006	0.321 ± 0.006	0.321 ± 0.006
S_3	-0.013 ± 0.010	-0.013 ± 0.010	-0.013 ± 0.010	-0.013 ± 0.010	-0.013 ± 0.010
S_4	-0.250 ± 0.006	-0.250 ± 0.006	-0.250 ± 0.005	-0.250 ± 0.006	-0.250 ± 0.006
S_5	0	0	0	0	0
S_6^s	0	0	0	0	0
S_7	0	0	0	0	0
S_8	-0.048 ± 0.007	-0.048 ± 0.007	-0.048 ± 0.007	-0.048 ± 0.007	-0.048 ± 0.007
S_9	0.084 ± 0.006	0.084 ± 0.006	0.084 ± 0.006	0.084 ± 0.006	0.084 ± 0.006
F_S	0.064 ± 0.010	0.115 ± 0.021	0.049 ± 0.008	0.052 ± 0.011	0.105 ± 0.016
S_{S1}	-	-0.887 ± 0.082	-0.514 ± 0.030	-0.216 ± 0.044	0.035 ± 0.096
S_{S2}	-	0.192 ± 0.018	0.100 ± 0.007	0.022 ± 0.012	-0.045 ± 0.021
S_{S3}	-	0	0	0	0
S_{S4}	-	0	0	0	0
S_{S5}	-	0.028 ± 0.023	-0.034 ± 0.012	-0.105 ± 0.015	-0.176 ± 0.013

509 component the LASS parameterisation [31] is used

$$\mathcal{A}_S(m_{K\pi}) = \sqrt{pq} \times B'_{L_B}(p, p_0, d)\left(\frac{p}{m_B}\right)^{L_B} \times B'_{L_{K_0^*}}(q, q_0, d)\left(\frac{q}{m_{K\pi}}\right)^{L_{K_0^*}} \times \left(\frac{1}{\cot\delta_B - i} + e^{2i\delta_B}\frac{1}{\cot\delta_R - i}\right), \tag{38}$$

where $\cot\delta_B = \frac{1}{aq} + \frac{1}{2}rq$ and $\cot\delta_R = (m^2_{K_0^*} - m^2_{K\pi})/(m_{K_0^*}\Gamma_0(m_{K\pi}))$. Accounting for the $m_{K\pi}$ dependence, Eq. 30, integrated over the three decay angles $\cos\theta_l$, $\cos\theta_K$ and ϕ, becomes

$$\begin{aligned}\frac{1}{\mathrm{d}(\Gamma+\bar{\Gamma})/\mathrm{d}q^2}\frac{\mathrm{d}(\Gamma+\bar{\Gamma})}{\mathrm{d}m_{K\pi}}\bigg|_{\mathrm{S+P}} = {} & (1-F_S)\sum_{i=1}^{9}\tfrac{9}{32\pi}\xi_i S_i^{(s,c)}|\mathcal{A}'_P(m_{K\pi})|^2 \\ & +\tfrac{3}{16\pi}\big[F_S\xi_{F_S}|\mathcal{A}'_S(m_{K\pi})|^2 \\ & \quad + (S_{S1}\xi_{S1} + S_{S2}\xi_{S2} + S_{S3}\xi_{S3})\,\Re\left(\mathcal{A}'_S(m_{K\pi})\mathcal{A}^{*\prime}_P(m_{K\pi})\right) \\ & \quad + (S_{S4}\xi_{S4} + S_{S5}\xi_{S5})\,\Im\left(\mathcal{A}'_S(m_{K\pi})\mathcal{A}^{*\prime}_P(m_{K\pi})\right)\big]\end{aligned} \tag{39}$$

where $\xi_{(S)i}$ denote the angular integrals $\xi_{(S)i} = \int \epsilon(\cos\theta_l, \cos\theta_K, \phi) f_{(S)i}(\cos\theta_l, \cos\theta_K, \phi)\mathrm{d}\vec{\Omega}$ and the amplitudes are appropriately normalized according to

$$\begin{aligned}\mathcal{A}'_P(m_{K\pi}) &= \frac{\mathcal{A}_P(m_{K\pi})}{\sqrt{\int_{795.9\,\mathrm{MeV}/c^2}^{995.9\,\mathrm{MeV}/c^2}|\mathcal{A}_P(m_{K\pi})|^2\mathrm{d}m_{K\pi}}}, \\ \mathcal{A}'_S(m_{K\pi}) &= \frac{\mathcal{A}_S(m_{K\pi})}{\sqrt{\int_{795.9\,\mathrm{MeV}/c^2}^{995.9\,\mathrm{MeV}/c^2}|\mathcal{A}_S(m_{K\pi})|^2\mathrm{d}m_{K\pi}}}.\end{aligned}$$

In the case of flat acceptance the integrated terms $\xi_{S1\ldots5}$ evaluate to $\xi_{S1\ldots5} = 0$ such that the interference terms drop out. For the nominal acceptance these terms are of the order of a few percent and are included for completeness.

The simultaneous fit of the angles and the $m_{K\pi}$ projection is tested using the control decay $B^0 \to J/\psi K^{*0}$. Table 21 gives the results of a fit of the full $3\,\mathrm{fb}^{-1}$ data sample in the $m_{K\pi}$ mass region $\pm100\,\mathrm{MeV}$ around the K^{*0} mass. Fig. 14 shows the corresponding projections on the decay angles, $m_{K\pi\mu\mu}$ and $m_{K\pi}$. The result is in good agreement with the results in Tab. 19 where only the decay angles are used.

To illustrate the effect of the additional constraint on F_S on the sensitivity of the P-wave observables subsets of the $B^0 \to J/\psi K^{*0}$ data are fitted. These subsets consists of 300 events which roughly corresponds to the expected signal yield for the signal decay $B^0 \to K^{*0}\mu^+\mu^-$. Since the signal fraction for the decay $B^0 \to J/\psi K^{*0}$ is $f_{\mathrm{sig}} \approx 0.95$, higher than what is expected for the decay $B^0 \to K^{*0}\mu^+\mu^-$, the background is modeled using only first order polynomials. All other PDFs are modeled in complete analogy to the toys in Sec. 6.2.9. First purely angular fits are performed. The results are given in Tab. 22 (left). Then the fits are performed using the additional constraint from the $m_{K\pi}$ distribution in a simultaneous fit. The corresponding results in Tab. 22 (right) show a much better sensitivity for F_S (by more than a factor two) and in consequence also an improved sensitivity for all P-wave parameters (by around 10% each). The constraint from the $m_{K\pi}$ distribution also protects the fit against rare statistical fluctuations resulting in very large (unphysical) values of F_S. This is shown in Fig. 15 that shows large fluctuation in F_S for the purely angular fit and much better behaviour when adding the constraint from the $m_{K\pi}$ distribution.

Table 21: Result of the simultaneous fit of the decay angles, $m_{K\pi\mu\mu}$ and $m_{K\pi}$ for the full $B^0 \to J/\psi\, K^{*0}$ data sample.

parameter	value
S_{1s}	0.332 ± 0.001
S_3	-0.000 ± 0.002
S_4	-0.251 ± 0.002
S_5	-0.001 ± 0.002
S_{6s}	0.000 ± 0.002
S_7	0.001 ± 0.002
S_8	-0.052 ± 0.002
S_9	-0.086 ± 0.002
F_S	0.068 ± 0.002
S_{S1}	-0.231 ± 0.003
S_{S2}	0.023 ± 0.002
S_{S3}	0.003 ± 0.002
S_{S4}	0.001 ± 0.002
S_{S5}	-0.068 ± 0.002

Table 22: Results from fitting 1000 samples of 300 $B^0 \to J/\psi\, K^{*0}$ events each, using the purely angular fit (left) and adding the constraint from a simultaneous fit of the $m_{K\pi}$ distribution (right). The true values for used for the pull distributions are determined from a fit to the full data sample.

	sensitivity	pull mean	pull width
S_{1s}	0.038 ± 0.001	-0.10 ± 0.03	1.01 ± 0.02
S_3	0.075 ± 0.002	-0.03 ± 0.03	1.03 ± 0.02
S_4	0.092 ± 0.002	-0.24 ± 0.04	1.11 ± 0.02
S_5	0.081 ± 0.002	0.00 ± 0.03	1.07 ± 0.02
S_{6s}	0.062 ± 0.001	0.01 ± 0.03	1.02 ± 0.02
S_7	0.077 ± 0.002	0.00 ± 0.03	1.01 ± 0.02
S_8	0.083 ± 0.002	-0.09 ± 0.03	1.07 ± 0.02
S_9	0.080 ± 0.002	-0.10 ± 0.03	1.04 ± 0.02
F_S	0.095 ± 0.002	0.25 ± 0.03	0.98 ± 0.02
S_{S1}	0.123 ± 0.003	-0.10 ± 0.03	1.03 ± 0.02
S_{S2}	0.088 ± 0.002	-0.06 ± 0.04	1.11 ± 0.02
S_{S3}	0.080 ± 0.002	0.02 ± 0.03	1.09 ± 0.02
S_{S4}	0.080 ± 0.002	-0.00 ± 0.03	1.05 ± 0.02
S_{S5}	0.088 ± 0.002	-0.02 ± 0.03	1.09 ± 0.02

	sensitivity	pull mean	pull width
S_{1s}	0.036 ± 0.001	-0.02 ± 0.03	1.02 ± 0.02
S_3	0.068 ± 0.002	-0.03 ± 0.03	1.06 ± 0.02
S_4	0.081 ± 0.002	-0.13 ± 0.04	1.15 ± 0.03
S_5	0.074 ± 0.002	0.01 ± 0.03	1.09 ± 0.02
S_{6s}	0.058 ± 0.001	0.01 ± 0.03	1.02 ± 0.02
S_7	0.072 ± 0.002	0.00 ± 0.03	1.02 ± 0.02
S_8	0.078 ± 0.002	-0.07 ± 0.03	1.08 ± 0.02
S_9	0.071 ± 0.002	-0.03 ± 0.03	1.10 ± 0.02
F_S	0.049 ± 0.001	-0.29 ± 0.03	1.01 ± 0.02
S_{S1}	0.121 ± 0.003	-0.05 ± 0.03	1.02 ± 0.02
S_{S2}	0.088 ± 0.002	-0.06 ± 0.03	1.10 ± 0.02
S_{S3}	0.078 ± 0.002	0.02 ± 0.03	1.09 ± 0.02
S_{S4}	0.078 ± 0.002	-0.00 ± 0.03	1.05 ± 0.02
S_{S5}	0.088 ± 0.002	-0.02 ± 0.03	1.08 ± 0.02

6.2.13 Toy studies using the $m_{K\pi}$ distribution

To ensure that the fit including the simultaneous fit of the $m_{K\pi}$ distribution is unbiased and estimates the uncertainties correctly, toy studies are performed. The settings for the toy studies are identical to the description in Sec. 6.2.9, with the exception of the inclusion of the simultaneous $m_{K\pi}$ fit. This results in the inclusion of one additional parameter describing the linear parametrisation of the background in $m_{K\pi}$. The sensitivities and pull distributions for the CP averages S_i, the CP asymmetries A_i and the $P_i^{(\prime)}$ are given in Tab. 122-127 in appendix F. It is evident that the behaviour of the toys improves with the inclusion of the $m_{K\pi}$ constraint. Still, for the nominal results the Feldman-Cousins method [24] will be employed to ensure correct coverage.

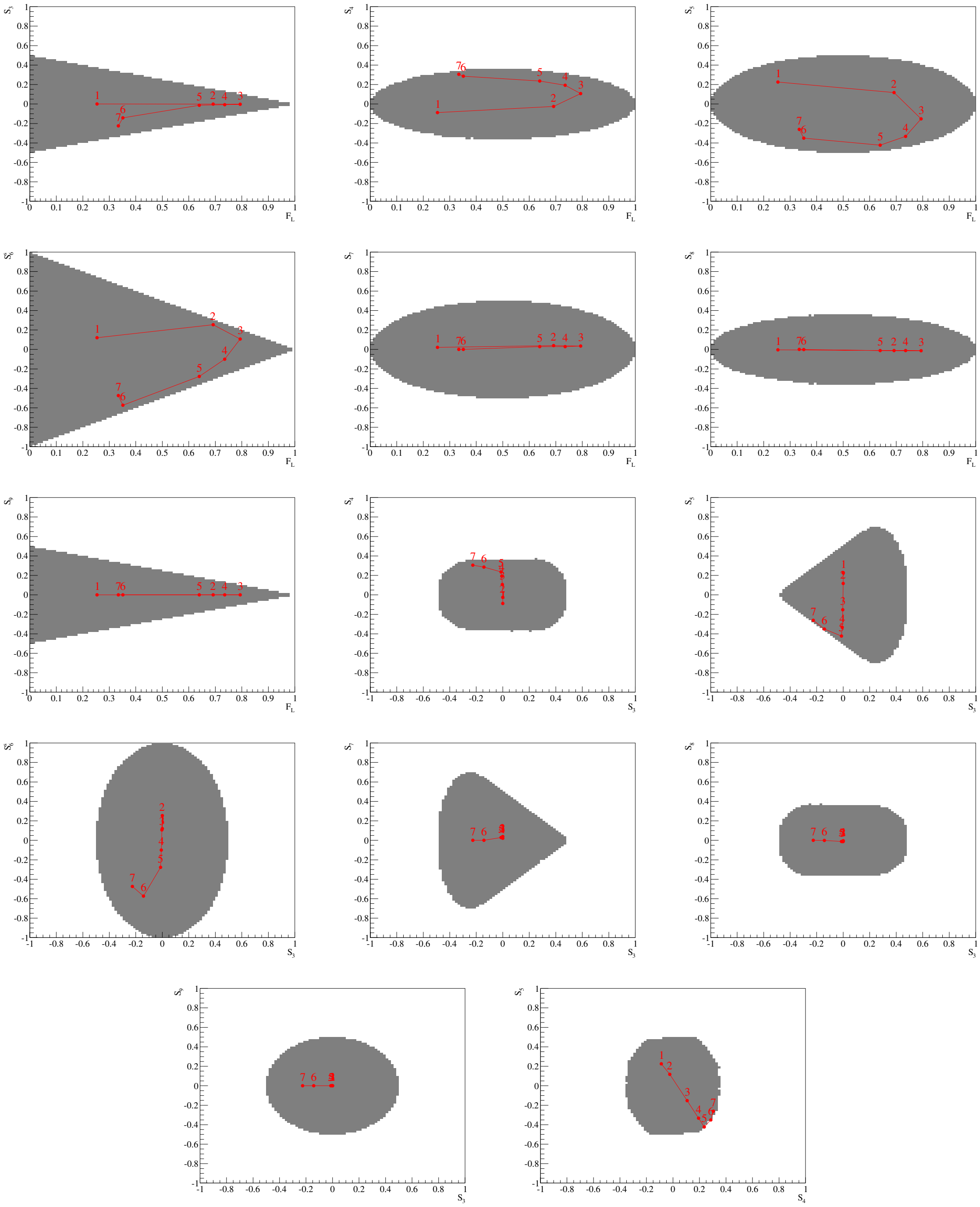

Figure 10: Projection of the allowed parameter range, where the PDF is positive, for different combinations of parameters. Particularly striking are the triangles in the combinations of F_L with S_3, S_6^s and S_9.

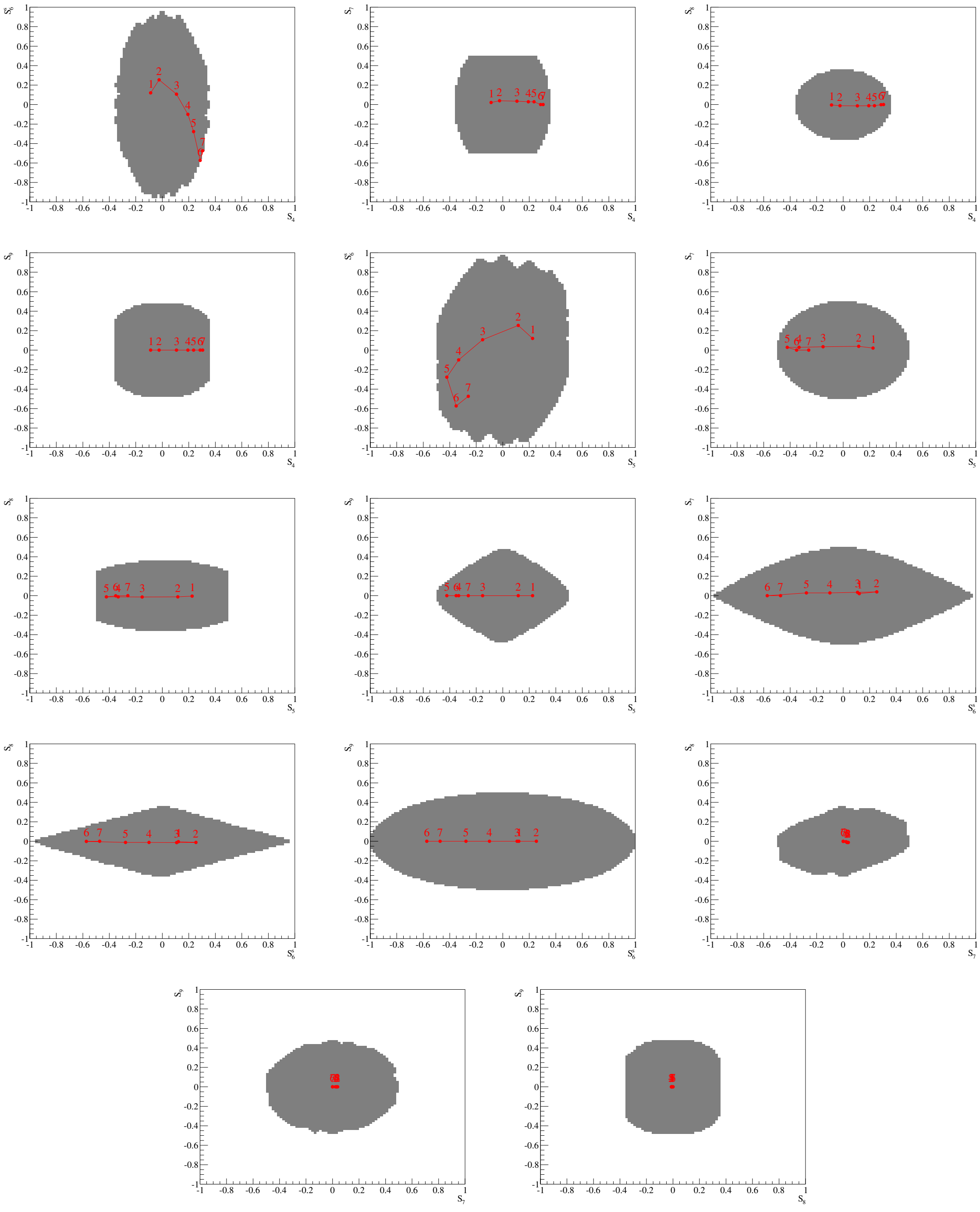

Figure 11: Projection of the allowed parameter range, where the PDF is positive, for different combinations of parameters.

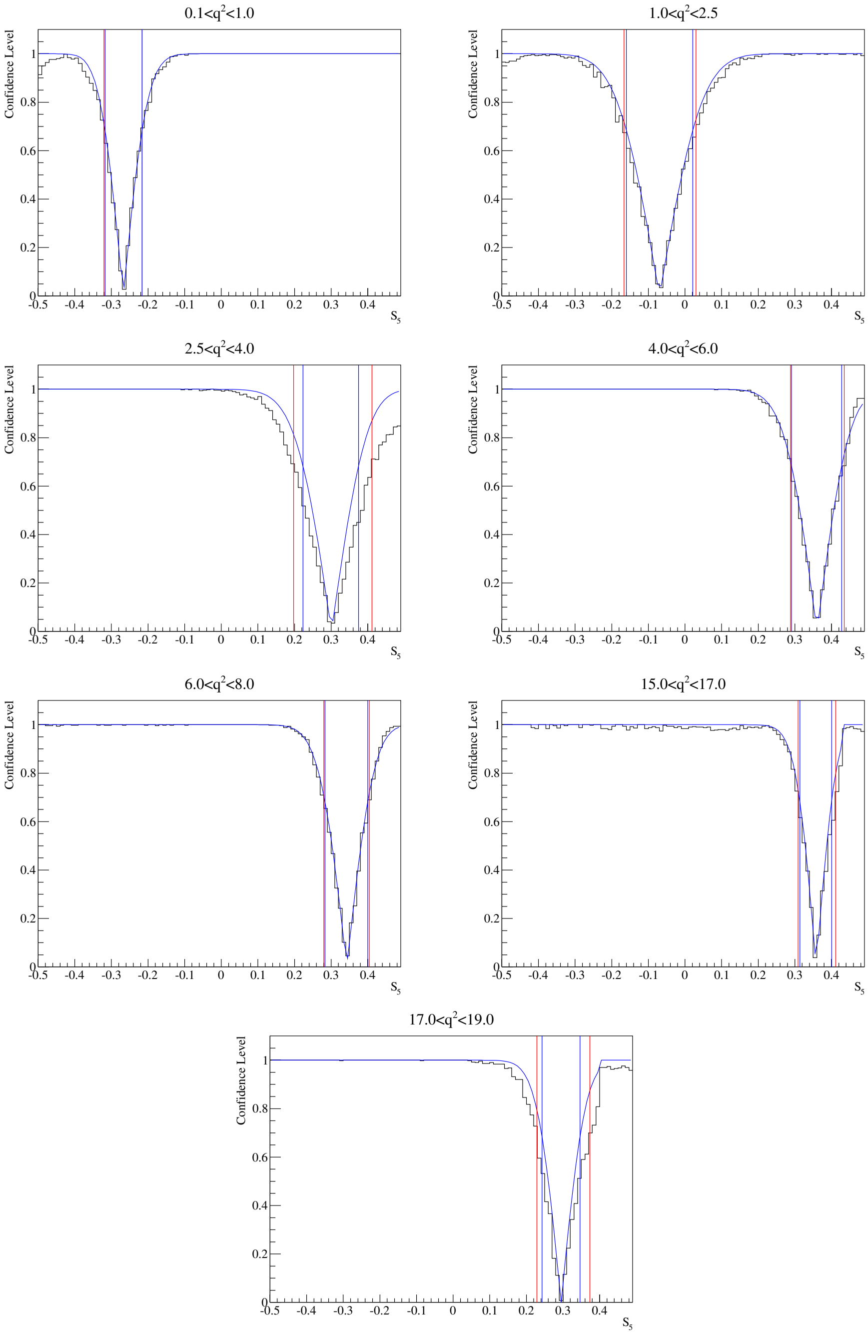

Figure 12: Feldman-Cousins results for the observable S_5 using an `EOS` toy in seven bins of q^2. The Feldman-cousins confidence level is given by the black histogram. The red vertical lines denote the 68.3% confidence interval from the Feldman-Cousins method. As comparison the blue line gives the confidence level using the likelihood method. The blue vertical lines give the 68.3% from the likelihood method.

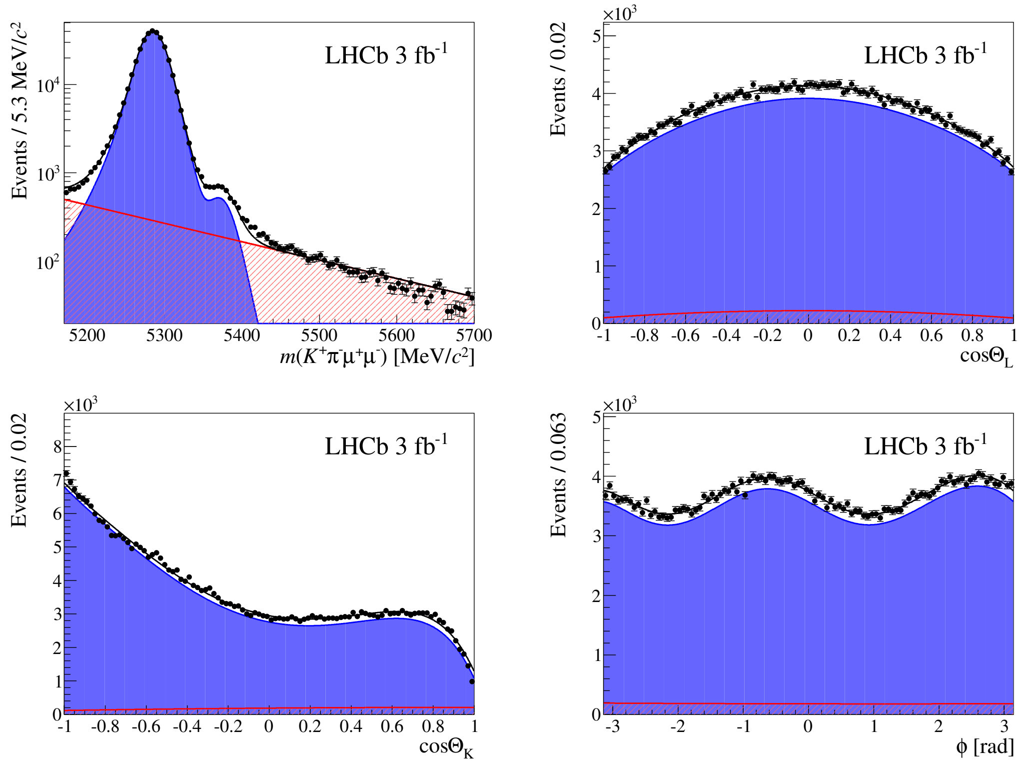

Figure 13: Fit projections of the angular fit of the decay $B^0 \to J/\psi\, K^{*0}$ in the $m_{K\pi}$ mass range $[795.9, 995.9]$ MeV. The slight mismodeling of the reconstructed B^0 mass is due to the narrow $\pm 60\,\mathrm{MeV}/c^2$ cut around the known J/ψ mass which cuts away the radiative tails. This however does not affect the angular observables significantly.

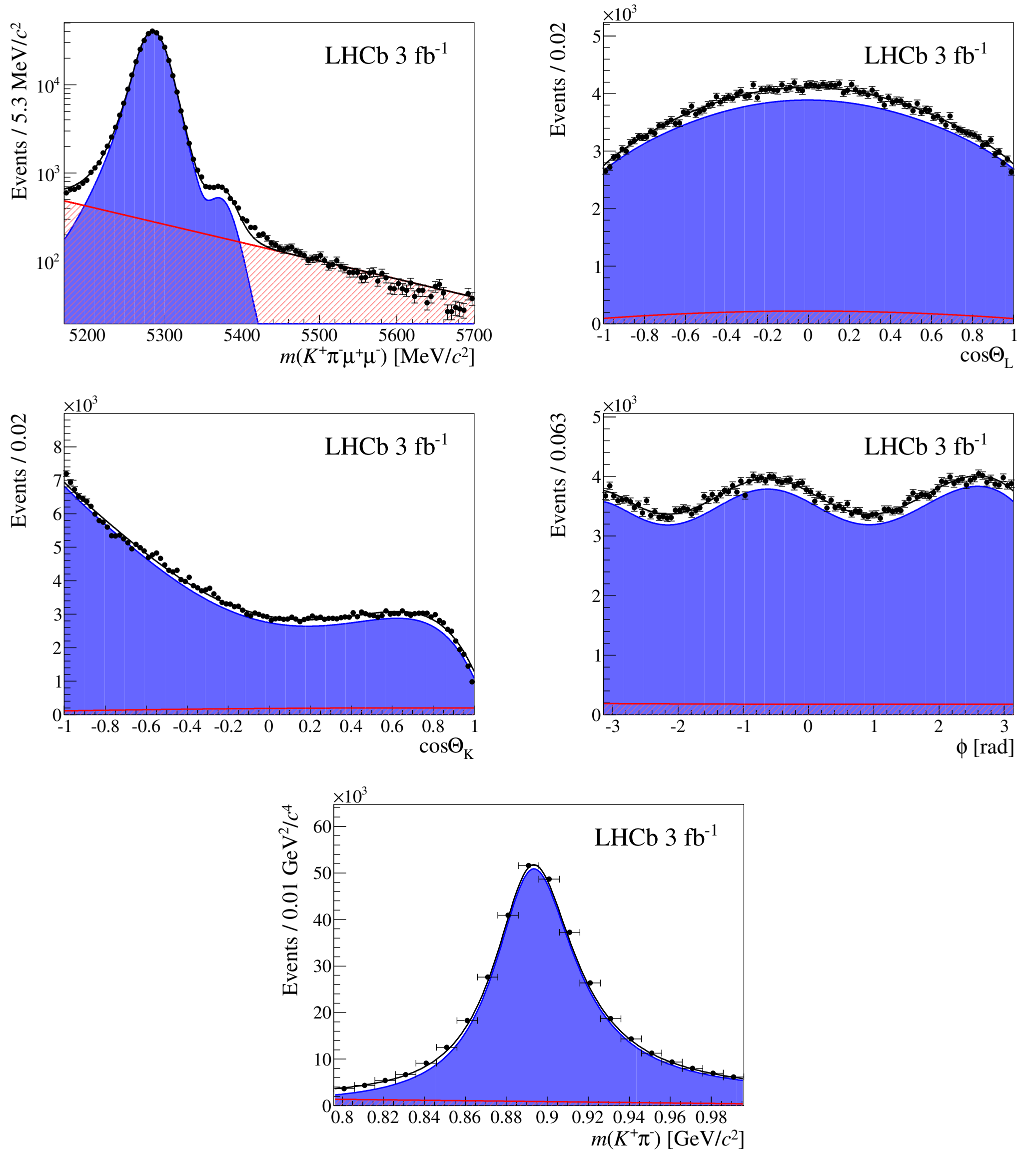

Figure 14: Angular, $m_{K\pi\mu\mu}$ and $m_{K\pi}$ projections after the fit of the full $B^0 \to J/\psi\, K^{*0}$ data sample. The fit is performed as described in Sec. 6.2.12, simultaneously in the decay angles and $m_{K\pi\mu\mu}$, and $m_{K\pi}$, in the $m_{K\pi}$ mass range $[795.9, 995.9]$ MeV. The slight mismodeling of the reconstructed B^0 mass is due to the narrow $\pm 60\,\mathrm{MeV}/c^2$ cut around the known J/ψ mass which cuts away the radiative tails. This however does not affect the angular observables significantly.

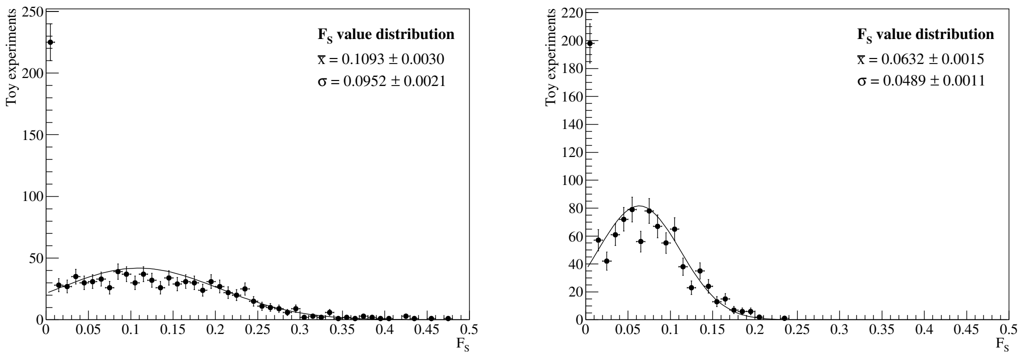

Figure 15: Results on the parameter F_S from fitting 1000 samples of 300 $B^0 \to J/\psi\, K^{*0}$ events each, using the purely angular fit (left) and adding the constraint from a simultaneous fit of the $m_{K\pi}$ distribution (right).

6.2.14 Angular folding

In the previous publications [1, 2], the number of angular observables to fit was reduced by performing angular foldings which are discussed below. While this analysis will be performed without angular foldings, retaining the full information of the angular distributions, it is useful to compare the results also with results from folded fits. In the folding method, the angular distributions are simplified by performing transformations of the decay angles ϕ, θ_ℓ or θ_K,

$$\phi \to \hat{\phi} \ \text{ and } \ \theta_\ell \to \hat{\theta}_\ell \ \text{ and } \ \theta_K \to \hat{\theta_K} \ . \tag{40}$$

These transformation can cancel contributions from certain observables. For example, the angular terms S_4, S_5, S_7 and S_8 cancel when transforming the angles as

$$\hat{\phi} = \begin{cases} \phi & \text{if } \phi \geq 0 \\ \phi + \pi & \text{if } \phi < 0 \end{cases} \tag{41}$$

leaving only F_L, S_3, S_6 and S_9 in the angular distribution. The angle $\hat{\phi}$ is defined in the range

$$0 < \hat{\phi} < \pi \ . \tag{42}$$

This is the angular folding chosen for Ref. [1] where, due to the low signal yield available when analysing the $1\,\mathrm{fb}^{-1}$ of data taken in 2011, an angular folding was necessary to reduce the number of observables.

There are other angular foldings that are applied to determine the remaining observables in Ref. [2]. Firstly, the angular distribution can be transformed as

$$\hat{\phi} = \begin{cases} \phi & \text{if } \phi \geq 0 \text{ and } \theta_\ell \leq \pi/2 \\ -\phi & \text{if } \phi < 0 \text{ and } \theta_\ell \leq \pi/2 \\ \pi - \phi & \text{if } \phi \geq 0 \text{ and } \theta_\ell > \pi/2 \\ \pi + \phi & \text{if } \phi < 0 \text{ and } \theta_\ell > \pi/2 \end{cases} \quad \text{and} \quad \hat{\theta}_\ell = \begin{cases} \theta_\ell & \text{if } \theta_\ell \leq \pi/2 \\ \pi - \theta_\ell & \text{if } \theta_\ell > \pi/2 \end{cases} \tag{43}$$

to leave only F_L, S_3 and S_4, where

$$0 < \hat{\phi} < \pi \ \text{ and } \ 0 < \hat{\theta}_\ell < \pi/2 \ . \tag{44}$$

The angular distribution can also be transformed as

$$\hat{\phi} = \begin{cases} \phi & \text{if } \phi \geq 0 \\ -\phi & \text{if } \phi < 0 \end{cases} \quad \text{and} \quad \hat{\theta}_\ell = \begin{cases} \theta_\ell & \text{if } \theta_\ell \leq \pi/2 \\ \pi - \theta_\ell & \text{if } \theta_\ell > \pi/2 \end{cases} \tag{45}$$

to leave only F_L, S_3 and S_5, where

$$0 < \hat{\phi} < \pi \ \text{ and } \ 0 < \hat{\theta}_\ell < \pi/2 \ . \tag{46}$$

The angular distribution can be transformed as

$$\hat{\phi} = \begin{cases} \phi & \text{if } -\pi/2 \leq \phi \leq \pi/2 \\ \pi - \phi & \text{if } \phi > \quad \pi/2 \\ -\pi - \phi & \text{if } \phi < -\pi/2 \end{cases} \quad \text{and} \quad \hat{\theta}_\ell = \begin{cases} \theta_\ell & \text{if } \theta_\ell \leq \pi/2 \\ \pi - \theta_\ell & \text{if } \theta_\ell > \pi/2 \end{cases} \tag{47}$$

to leave only F_{L}, S_3 and S_7, where

$$0 < \hat{\phi} < \pi \quad \text{and} \quad 0 < \hat{\theta}_\ell < \pi/2\ . \tag{48}$$

Finally, it can be transformed as

$$\hat{\phi} = \begin{cases} \phi & \text{if } -\pi/2 \leq \phi \leq \pi/2 \\ \pi - \phi & \text{if } \phi > \quad \pi/2 \\ -\pi - \phi & \text{if } \phi < -\pi/2 \end{cases} \tag{49}$$

$$\hat{\theta}_\ell = \begin{cases} \theta_\ell & \text{if } \theta_\ell \leq \pi/2 \\ \pi - \theta_\ell & \text{if } \theta_\ell > \pi/2 \end{cases} \quad \text{and} \quad \hat{\theta_K} = \begin{cases} \theta_K & \text{if } \theta_\ell \leq \pi/2 \\ \pi - \theta_K & \text{if } \theta_\ell > \pi/2 \end{cases} \tag{50}$$

to leave only F_{L}, S_3 and S_8, where

$$0 < \hat{\phi} < \pi \quad \text{and} \quad 0 < \hat{\theta}_\ell < \pi/2 \quad \text{and} \quad 0 < \hat{\theta_K} < \pi\ . \tag{51}$$

6.3 Extracting angular observables using the method of moments

Due to the orthogonality of the spherical harmonics (and consequently the angular terms), it is possible to extract the angular observables from a moment analysis [32, 33]. The angular distribution has the form

$$\frac{\mathrm{d}^4\Gamma}{\mathrm{d}q^2\mathrm{d}\vec{\Omega}} = \frac{9}{32\pi}\sum_i S_i(q^2) f_i(\vec{\Omega}) \ , \tag{52}$$

which averaged over q^2 is

$$\frac{\mathrm{d}^3\Gamma}{\mathrm{d}\vec{\Omega}} = \frac{9}{32\pi}\sum_i S_i f_i(\vec{\Omega}) \ , \tag{53}$$

and is normalised such that

$$\int \frac{\mathrm{d}^3\Gamma}{\mathrm{d}\vec{\Omega}}\mathrm{d}\vec{\Omega} = \int_{-1}^{+1}\int_{-1}^{+1}\int_{-\pi}^{+\pi} \frac{\mathrm{d}^3\Gamma}{\mathrm{d}\cos\theta_K\,\mathrm{d}\cos\theta_l\,\mathrm{d}\phi}\mathrm{d}\cos\theta_K\,\mathrm{d}\cos\theta_l\,\mathrm{d}\phi = 1, \tag{54}$$

where $\vec{\Omega} = (\cos\theta_K, \cos\theta_l, \phi)$ and

$$\begin{aligned}
f_{1s}(\cos\theta_K, \cos\theta_l, \phi) &= \sin^2\theta_K \\
f_3(\cos\theta_K, \cos\theta_l, \phi) &= \sin^2\theta_K \sin^2\theta_l \cos 2\phi \\
f_4(\cos\theta_K, \cos\theta_l, \phi) &= \sin 2\theta_K \sin 2\theta_l \cos\phi \\
f_5(\cos\theta_K, \cos\theta_l, \phi) &= \sin 2\theta_K \sin\theta_l \cos\phi \\
f_{6s}(\cos\theta_K, \cos\theta_l, \phi) &= \sin^2\theta_K \cos\theta_l \\
f_7(\cos\theta_K, \cos\theta_l, \phi) &= \sin 2\theta_K \sin\theta_l \sin\phi \\
f_8(\cos\theta_K, \cos\theta_l, \phi) &= \sin 2\theta_K \sin 2\theta_l \sin\phi \\
f_9(\cos\theta_K, \cos\theta_l, \phi) &= \sin^2\theta_K \sin^2\theta_l \sin 2\phi
\end{aligned} \tag{55}$$

Since the angular functions are orthogonal we have:

$$\int f_i(\vec{\Omega}) f_j(\vec{\Omega})\mathrm{d}\vec{\Omega} = \alpha\delta_{ij}, \tag{56}$$

for $i = 3\ldots 9$ and where α is a normalisation constant. The mean (or expectation value) of the f_i can be used to determine the S_i, i.e.

$$M_i = \int \frac{\mathrm{d}^4\Gamma}{\mathrm{d}q^2\,\mathrm{d}\vec{\Omega}} f_i(\vec{\Omega})\mathrm{d}\vec{\Omega} = \begin{cases} \frac{8}{25} S_{i=3,4,8,9} \\ \frac{2}{5} S_{i=5,6,7} \ . \end{cases} \tag{57}$$

Note, the f_i for f_{1s}, f_{2s}, f_{1c} and f_{2c} are not orthogonal. The corresponding moments are linear combinations of S_{1s}, S_{2s}, S_{1c} and S_{2c}, with

$$M_{1s} = \frac{2}{5}(2 - F_{\mathrm{L}}) \quad , \tag{58}$$

under the assumption that $q^2 \gg 4m(\mu)^2$. Re-arranging gives

$$F_{\mathrm{L}} = 2 - \frac{5}{2} M_{1s} \tag{59}$$
$$S_i = \frac{5}{2} M_{5,6,7} \tag{60}$$
$$S_i = \frac{25}{8} M_{3,4,8,9} \tag{61}$$
$$\tag{62}$$

In the absence of background, M_i can be estimated as

$$\langle M_i \rangle = \frac{1}{N} \sum_{\text{event } e} f_i(\vec{\Omega}_e) \tag{63}$$

where N is the number of events in the data sample. An estimate for the error can be evaluated as a normal variance

$$\delta\langle M_i \rangle = \sqrt{\frac{1}{N(N-1)} \sum_{\text{event } e} \left(\langle M_i \rangle - f_i(\vec{\Omega}_e)\right)^2} \tag{64}$$

6.3.1 Measurement of S_{6c}

In the SM, the term S_{6c} is vanishingly small. It only exists in the presence of large scalar operators and is suppressed by $m_\mu/\sqrt{q^2}$. The method of moments can be used to determine the S_{6c} coefficient. The corresponding angular term is

$$f_{6c}(\cos\theta_K, \cos\theta_l, \phi) = \cos^2\theta_K \cos\theta_l \ , \tag{65}$$

which appears mixed with S_{6s} when evaluating the raw moments,

$$M_{6c} = \frac{1}{20}(3S_{6c} + 2S_{6s}) \tag{66}$$
$$M_{6s} = \frac{1}{10}(S_{6c} + 4S_{6s}). \tag{67}$$
$$\tag{68}$$

The solution to this linear system is

$$S_{6c} = 2(4S_{6c} - S_{6s}), \tag{69}$$
$$S_{6s} = 2S_{6c} + 3S_{6s}. \tag{70}$$
$$\tag{71}$$

This allows to determine both S_{6c} and S_{6s}.

6.3.2 Method of moments in the presence of background

In the presence of background, the moments M_i in the signal mass window will be an admixture of the moments for pure signal ($M_{i,\mathrm{sig}}$) and pure background ($M_{i,\mathrm{bkg}}$). The mixed moment

$$M_{i,\mathrm{mix}} = \frac{N_{\mathrm{sig}} M_{i,\mathrm{sig}} + N_{\mathrm{bkg}} M_{i,\mathrm{bkg}}}{N_{\mathrm{sig}} + N_{\mathrm{bkg}}} \ , \tag{72}$$

where N_{sig} and N_{B} are the number of signal and background events in the signal mass window, respectively. The yields N_{sig} and N_{bkg} can be estimated from an extended unbinned maximum likelihood fit to the $K^+\pi^-\mu^+\mu^-$ invariant mass and $M_{i,\mathrm{bkg}}$ can be estimated from the upper mass sideband. The upper mass sideband is chosen to be $m(K^+\pi^-\mu^+\mu^-) > 5350\ \mathrm{MeV}/c^2$. It would also be possible to determine $M_{i,\mathrm{sig}}$ by sWeighting the events.

6.3.3 Acceptance corrections of the method of moments

When including the angular acceptance, the measured moments (raw moments) are no longer proportional to the observables S_i. To correct for the acceptance, each event is weighted according to a weight

$$w_e = \frac{1}{\epsilon(\vec{\Omega}_e, q_e^2)} \ , \tag{73}$$

where $\epsilon(\vec{\Omega}_e, q_e^2)$ is the efficiency function derived in Sec. 8.1. The corresponding formula to obtain the raw moments is then

$$\widehat{M_i} = \frac{1}{\sum_e w_e} \sum_{\mathrm{event}\ e} w_e f_i(\vec{\Omega}_e) \ . \tag{74}$$

The angular acceptance does not need to be treated as constant over the q^2 bin and the full q^2 dependence can be accounted for. The absolute normalisation of the weights does not matter, since it appears in the numerator and denominator of Eq. 74, i.e. the weights can be re-scaled for an arbitrary constant.

An estimate for the uncertainty on the moments can be derived from the weighted variance

$$V_{ij} = \frac{\sum_e w_e}{(\sum_e w_e)((\sum_e w_e)^2 - \sum_e w_e^2)} \sum_e w_e \left(\widehat{M_i} - f_i(\vec{\Omega}_e)\right)\left(\widehat{M_j} - f_j(\vec{\Omega}_e)\right) . \tag{75}$$

6.3.4 Statistical uncertainty on the method of moments

The statistical uncertainty on the raw moments (and the observables) is evaluated in data using the bootstrapping method. This method consists of obtaining an ensemble of pseudo-experiments by Poisson fluctuating each event. This method is described in Ref. [34]. We checked that this method gives the same uncertainty as the weighted standard deviation (Eq. 75) by performing toy studies. An example is shown in Fig. 16

for the observables F_{L}, S_3 and S_4. Here, the bootstrapping distribution of a single toy experiment is shown. The 68% C.L. is shown for the weighted standard deviation and for the bootstrapping. Excellent agreement is observed between the two. The coverage of the statistical uncertainty has been checked with toy experiments.

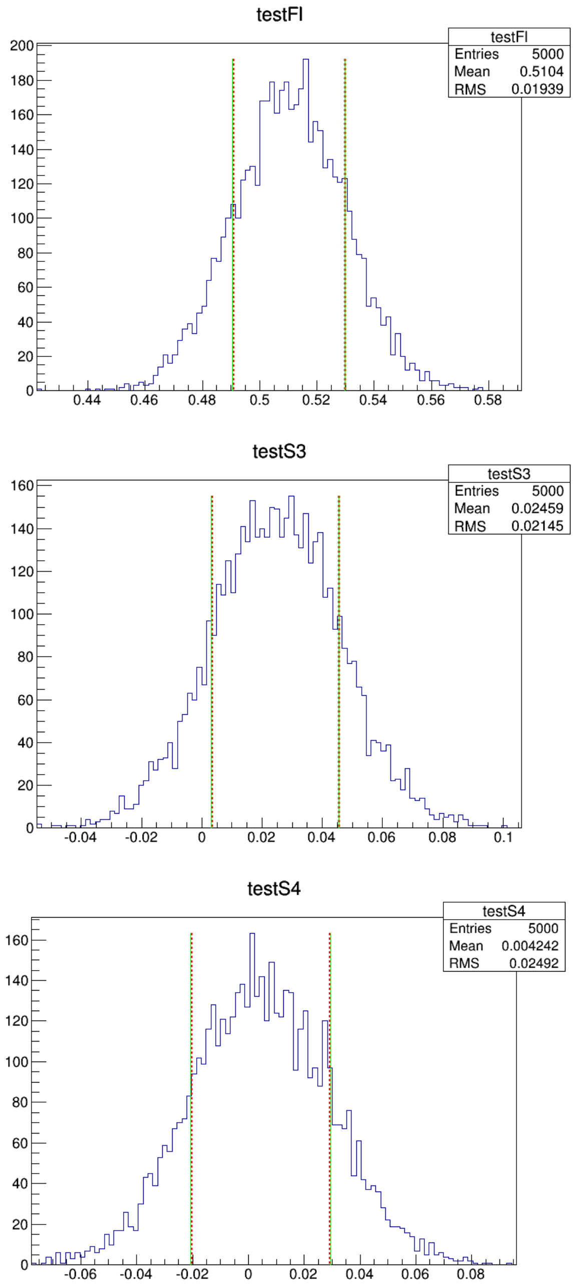

Figure 16: The bootstrapping distribution of a specific pseudo-experiment. The 68% C.L. is indicated in red for the bootstrap and green for the weighted standard deviation.

6.3.5 Toy studies for method of moments

Toy studies for the method of moments were performed in the same way as for the fits for the angular observables. Signal events were generated using `EOS` predictions for the different q^2 bins. Toy studies were performed in three different configurations:

- pure signal without detector acceptance;
- mixture of signal and background without detector acceptance;
- and a mixture of signal and background with detector acceptance.

The results of the pseudo-experiment studies for the latter case (signal mixed with background and acceptance) are presented in Tab. 23 and 24 and in Appendix G. These studies are performed using the reweighing method for the acceptance and without including any S-wave component (studies with S-wave are described in Sec. 6.3.7). No bias, apart for the evident large bias in the value of F_{L}, is observed. This bias, at the level of 0.5 standard deviations in the $0.1 < q^2 < 0.98$ bin, comes from neglecting lepton mass terms in the angular distribution.

6.3.6 Error dependence of number of events

As the moments are determined from a simple counting experiment, one expects the error to scale as $1/\sqrt{N}$, where N is the number of events in the dataset. This behaviour has been verified using signal only toy experiments, see Fig. 20, using signal only samples without acceptance.

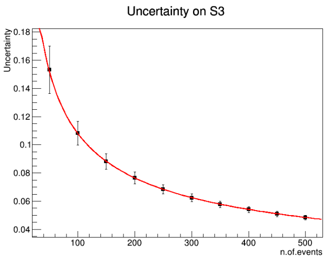

(a) S_3

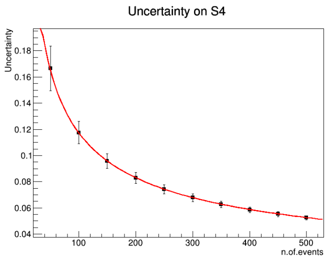

(b) S_4

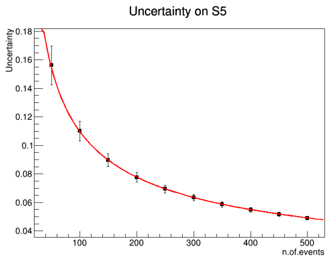

(c) S_5

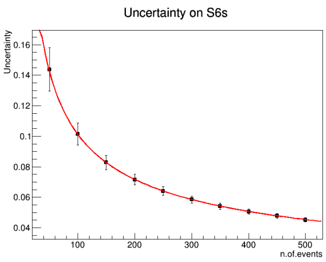

(d) S_6

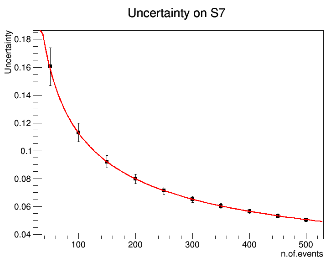

(e) S_7

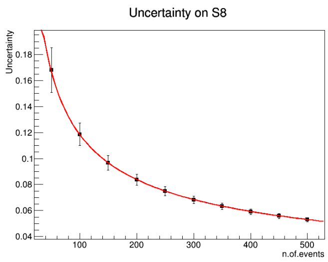

(f) S_8

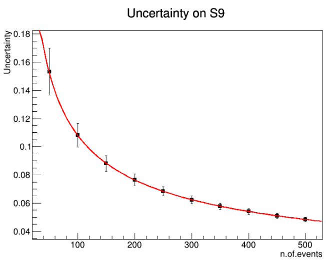

(g) S_9

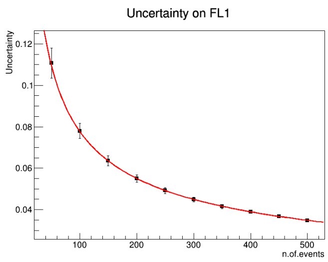

(h) F_{L}

Figure 17: Error dependence on the number of events in the sample. The data points correspond to the mean uncertainty on a large ensemble of SM toy experiments, generated without background or acceptance. The error bars are taken as 68% spread of the error on the toy experiments. Points are fitted with $\alpha/\sqrt{N}$.

Table 23: Results for the mean of the pull distribution of toys in bins of q^2, when a background component and acceptance is included. The acceptance is assumed to be constant over the q^2 bins. In brackets we note the significance of the deviation from zero.

q^2[GeV]	F_L	S_3	S_4	S_5	S_{6s}	S_7	S_8	S_9
$0.1-0.98$	-0.50 ± 0.02 (18.4)	0.00 ± 0.02 (0.02)	$+0.06\pm0.02$ (2.48)	0.00 ± 0.02 (0.01)	$+0.04\pm0.02$ (1.78)	-0.00 ± 0.02 (0.36)	-0.00 ± 0.02 (0.11)	0.00 ± 0.02 (0.11)
$1.1-2.0$	-0.04 ± 0.02 (1.71)	$+0.01\pm0.02$ (0.67)	$+0.04\pm0.02$ (1.53)	-0.01 ± 0.02 (0.45)	0.00 ± 0.02 (0.28)	-0.07 ± 0.02 (2.77)	-0.06 ± 0.02 (2.32)	$+0.03\pm0.02$ (1.12)
$2.0-3.0$	-0.01 ± 0.02 (0.45)	-0.04 ± 0.02 (1.64)	-0.01 ± 0.02 (0.39)	-0.05 ± 0.02 (1.87)	-0.00 ± 0.02 (0.24)	$+0.00\pm0.02$ (0.05)	-0.04 ± 0.02 (1.54)	$+0.02\pm0.02$ (0.94)
$3.0-4.0$	-0.05 ± 0.02 (1.78)	-0.02 ± 0.02 (1.08)	$+0.03\pm0.02$ (1.11)	-0.01 ± 0.02 (0.44)	-0.06 ± 0.02 (2.37)	$+0.04\pm0.02$ (1.53)	$+0.03\pm0.02$ (1.14)	$+0.00\pm0.02$ (0.09)
$4.0-5.0$	-0.04 ± 0.02 (1.72)	$+0.02\pm0.02$ (0.81)	-0.01 ± 0.02 (0.50)	0.00 ± 0.02 (0.20)	$+0.03\pm0.02$ (1.18)	-0.00 ± 0.02 (0.14)	-0.07 ± 0.02 (2.76)	$+0.01\pm0.02$ (0.71)
$5.0-6.0$	-0.06 ± 0.02 (2.29)	$+0.02\pm0.02$ (0.95)	0.00 ± 0.02 (0.31)	$+0.02\pm0.02$ (0.79)	-0.01 ± 0.02 (0.45)	-0.01 ± 0.02 (0.39)	-0.03 ± 0.02 (1.18)	$+0.04\pm0.02$ (1.58)
$6.0-7.0$	-0.00 ± 0.02 (0.28)	$+0.04\pm0.02$ (1.51)	$+0.01\pm0.02$ (0.60)	-0.01 ± 0.02 (0.59)	$+0.02\pm0.02$ (0.78)	0.00 ± 0.02 (0.04)	$+0.02\pm0.02$ (0.80)	-0.00 ± 0.02 (0.14)
$7.0-8.0$	$+0.03\pm0.02$ (1.31)	$+0.01\pm0.02$ (0.47)	-0.00 ± 0.02 (0.34)	0.00 ± 0.02 (0.14)	0.00 ± 0.02 (0.02)	$+0.01\pm0.02$ (0.62)	$+0.01\pm0.02$ (0.60)	$+0.03\pm0.02$ (1.15)
$15.0-16.0$	-0.02 ± 0.02 (1.11)	0.00 ± 0.02 (0.06)	-0.05 ± 0.02 (1.79)	$+0.02\pm0.02$ (0.98)	$+0.02\pm0.02$ (0.93)	$+0.02\pm0.02$ (0.73)	-0.04 ± 0.02 (1.71)	0.00 ± 0.02 (0.08)
$16.0-17.0$	-0.02 ± 0.02 (1.06)	0.00 ± 0.02 (0.25)	-0.01 ± 0.02 (0.69)	$+0.01\pm0.02$ (0.38)	$+0.03\pm0.02$ (1.14)	-0.01 ± 0.02 (0.41)	-0.06 ± 0.02 (2.34)	-0.04 ± 0.02 (1.64)
$17.0-18.0$	0.00 ± 0.02 (0.04)	-0.01 ± 0.02 (0.44)	-0.05 ± 0.02 (2.05)	0.00 ± 0.02 (0.10)	-0.03 ± 0.02 (1.39)	0.00 ± 0.02 (0.16)	$+0.04\pm0.02$ (1.75)	0.00 ± 0.02 (0.15)
$18.0-19.0$	0.00 ± 0.02 (0.27)	$+0.08\pm0.02$ (3.16)	0.00 ± 0.02 (0.36)	-0.06 ± 0.02 (2.32)	0.00 ± 0.02 (0.26)	-0.02 ± 0.02 (0.94)	-0.01 ± 0.02 (0.55)	0.00 ± 0.02 (0.15)

Table 24: Results for the width of the pull distribution of toys in bins of q^2, when a background component is included. The acceptance is assumed to be constant over the q^2 bins. In brackets we note the significance of the deviation from unity.

q^2[GeV]	F_L	S_3	S_4	S_5	S_{6s}	S_7	S_8	S_9
$0.1-0.98$	0.99 ± 0.02 (0.19)	0.95 ± 0.01 (2.23)	0.96 ± 0.01 (1.91)	0.97 ± 0.02 (1.42)	0.99 ± 0.02 (0.40)	0.97 ± 0.02 (1.19)	0.99 ± 0.02 (0.18)	0.95 ± 0.02 (2.37)
$1.1-2.0$	0.96 ± 0.02 (1.57)	1.01 ± 0.02 (0.77)	0.99 ± 0.02 (0.08)	1.01 ± 0.02 (0.49)	0.99 ± 0.02 (0.24)	1.00 ± 0.02 (0.06)	0.97 ± 0.01 (1.23)	1.00 ± 0.02 (0.15)
$2.0-3.0$	0.94 ± 0.02 (2.55)	0.96 ± 0.02 (1.66)	0.95 ± 0.01 (2.19)	0.98 ± 0.02 (0.54)	0.93 ± 0.01 (3.53)	0.96 ± 0.02 (1.70)	0.95 ± 0.01 (2.26)	1.03 ± 0.02 (1.34)
$3.0-4.0$	1.01 ± 0.02 (0.77)	0.96 ± 0.02 (1.60)	0.99 ± 0.02 (0.32)	1.00 ± 0.02 (0.29)	0.99 ± 0.02 (0.48)	0.98 ± 0.02 (0.49)	0.99 ± 0.02 (0.25)	1.00 ± 0.02 (0.01)
$4.0-5.0$	1.00 ± 0.02 (0.26)	0.96 ± 0.02 (1.72)	0.97 ± 0.01 (1.48)	1.00 ± 0.02 (0.12)	0.93 ± 0.02 (2.98)	1.00 ± 0.02 (0.18)	0.97 ± 0.01 (1.37)	0.97 ± 0.02 (1.37)
$5.0-6.0$	0.94 ± 0.01 (2.70)	1.04 ± 0.02 (1.79)	0.96 ± 0.02 (1.67)	1.00 ± 0.02 (0.46)	0.96 ± 0.01 (1.67)	0.95 ± 0.02 (1.95)	0.99 ± 0.01 (0.06)	0.98 ± 0.01 (0.85)
$6.0-7.0$	0.98 ± 0.02 (0.79)	0.96 ± 0.02 (1.84)	0.99 ± 0.01 (0.41)	0.99 ± 0.02 (0.01)	1.02 ± 0.02 (1.22)	0.99 ± 0.02 (0.16)	0.97 ± 0.01 (1.33)	0.97 ± 0.02 (1.24)
$7.0-8.0$	1.02 ± 0.02 (1.03)	0.96 ± 0.02 (1.74)	0.97 ± 0.01 (1.45)	0.94 ± 0.02 (2.47)	0.93 ± 0.02 (3.21)	0.95 ± 0.01 (2.56)	0.94 ± 0.02 (2.57)	0.97 ± 0.02 (1.05)
$15.0-16.0$	0.95 ± 0.02 (2.42)	0.93 ± 0.02 (3.08)	1.01 ± 0.02 (0.51)	0.98 ± 0.01 (0.91)	1.00 ± 0.02 (0.02)	1.00 ± 0.02 (0.23)	0.97 ± 0.02 (1.13)	0.95 ± 0.02 (2.28)
$16.0-17.0$	0.98 ± 0.02 (0.83)	0.96 ± 0.02 (1.50)	0.94 ± 0.02 (2.66)	0.95 ± 0.02 (2.20)	0.95 ± 0.02 (2.06)	0.96 ± 0.02 (1.7)	0.97 ± 0.02 (1.20)	0.98 ± 0.02 (0.89)
$17.0-18.0$	1.00 ± 0.02 (0.31)	0.96 ± 0.02 (1.57)	0.93 ± 0.01 (3.37)	0.95 ± 0.01 (2.45)	0.97 ± 0.01 (1.14)	0.97 ± 0.02 (1.02)	0.98 ± 0.02 (0.82)	1.02 ± 0.02 (0.92)
$18.0-19.0$	0.95 ± 0.01 (2.38)	0.98 ± 0.01 (0.76)	0.97 ± 0.01 (1.40)	0.97 ± 0.01 (1.38)	0.96 ± 0.02 (1.49)	0.96 ± 0.02 (1.58)	0.97 ± 0.02 (0.98)	0.98 ± 0.02 (0.85)

6.3.7 Method of moments with S-wave contribution

The addition of an S-wave component to the $K^+\pi^-$ system modifies the angular distribution according to

$$\frac{\mathrm{d}^3\Gamma}{\mathrm{d}\vec{\Omega}} = \frac{9}{32\pi}(1-F_{\mathrm{S}})\sum_i S_i f_i(\vec{\Omega}) + \frac{3}{16\pi}\sum_j S_j f_j(\vec{\Omega}) \ , \tag{76}$$

where the first sum is the sum over the P-wave angular terms and the second includes the S-wave terms and S-P-wave interference.

This distribution is normalised such that

$$\int_{-1}^{+1}\int_{-1}^{+1}\int_{-\pi}^{+\pi}\frac{\mathrm{d}^3\Gamma}{\mathrm{d}\vec{\Omega}}\mathrm{d}\cos\theta_K\,\mathrm{d}\cos\theta_l\,\mathrm{d}\phi = 1 \ . \tag{77}$$

Therefore, we have the additional functions

$$\begin{aligned}
f_{F_s}(\cos\theta_K,\cos\theta_l,\phi) &= \sin^2\theta_l \\
f_{S_{S1}}(\cos\theta_K,\cos\theta_l,\phi) &= \sin^2\theta_l\cos\theta_K \\
f_{S_{S2}}(\cos\theta_K,\cos\theta_l,\phi) &= \sin\theta_K\sin 2\theta_l\cos\phi \\
f_{S_{S3}}(\cos\theta_K,\cos\theta_l,\phi) &= \sin\theta_K\sin\theta_l\cos\phi \\
f_{S_{S4}}(\cos\theta_K,\cos\theta_l,\phi) &= \sin\theta_K\sin\theta_l\sin\phi \\
f_{S_{S5}}(\cos\theta_K,\cos\theta_l,\phi) &= \sin\theta_K\sin 2\theta_l\sin\phi
\end{aligned} \tag{78}$$

and in order to completely solve the system we need to calculate the additional moments

$$M_i = \int_{-1}^{+1}\int_{-1}^{+1}\int_{-\pi}^{+\pi}\frac{d^3\Gamma}{\mathrm{d}\cos\theta_K\,\mathrm{d}\cos\theta_l\,\mathrm{d}\phi}f_i(\cos\theta_K,\cos\theta_l,\phi) = \begin{cases}\frac{8}{25}S_{3,4,8,9}(1-F_{\mathrm{S}}) \\ \frac{2}{5}S_{5,6,7}(1-F_s) \\ \frac{2}{5}(2-F_{\mathrm{L}})(1-F_s) \ , \ i=1s \\ \frac{1}{5}(3+F_{\mathrm{S}}+F_{\mathrm{L}}-F_{\mathrm{L}}F_{\mathrm{S}}) \ , \ i=F_{\mathrm{S}} \\ \frac{4}{15}S_{S1,S2,S5} \\ \frac{1}{3}S_{S3,S4}\end{cases} \tag{79}$$

The system is no longer orthogonal, however the solution can easily be found

$$
\begin{aligned}
F_{\mathrm{S}} &= \frac{15}{4}(2M_{F_{\mathrm{S}}} + M_{F_{\mathrm{L}}} - 2) \\
F_{\mathrm{L}} &= \frac{10M_{F_{\mathrm{S}}} + 15M_{1s} - 18}{30M_{F_{\mathrm{S}}} + 15M_{1s} - 34} \\
S_{S3,S4} &= 3M_{S3,S4} \\
S_{S1,S2,S5} &= \frac{15}{4}M_{S1,S2,S5} \\
S_{5,6,7} &= \frac{5}{2}M_{5,6,7}/(1 - F_{\mathrm{S}}) \\
S_{3,4,8,9} &= \frac{25}{8}M_{3,4,8,9}/(1 - F_{\mathrm{S}}) \; .
\end{aligned}
\tag{80}
$$

While it is possible to solve Eq. 80 to extract the S-wave, simulation studies have shown that a fit of the $m_{K\pi}$ mass give a better resolution, so the method described in Sec. 6.2.12 is used as input of the S-wave for the method of moments.

6.3.8 Toy studies including S-wave

When we include the S-wave, the raw moment for M_{1s}, M_{1c} etc are not orthogonal to the moments for the S-wave. However, the raw moments are still unbiased so long as the S-wave fraction can be extracted in an unbiased way. We performed a toy studies to demonstrate this using a wide range of values for F_{S} from 0.01 to 0.5. The toys have the normal SM P-wave component with additional S-wave component added. In all cases no biases was observed. The pulls for the raw moments are shown in Tables 25 and 26.

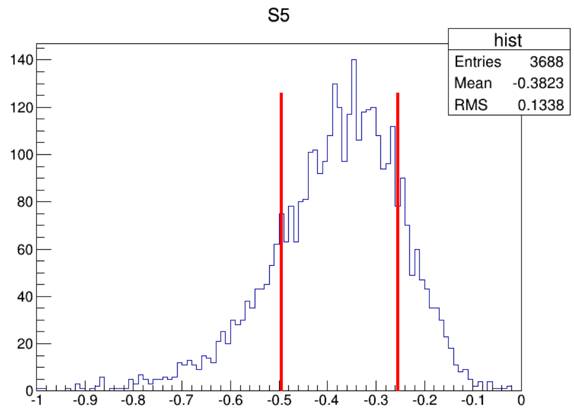

Figure 18: 68% confidence belt obtained using MC method.

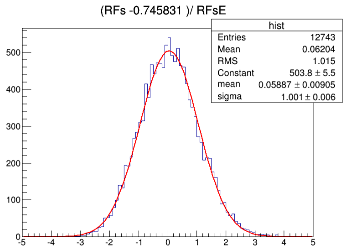

(a) M_{F_S}

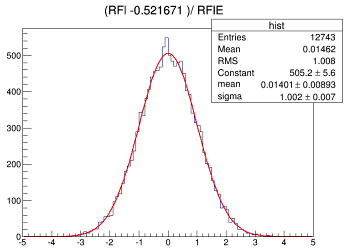

(b) M_{F_L}

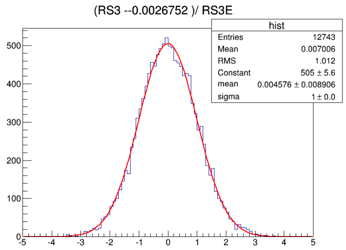

(c) M_{S_3}

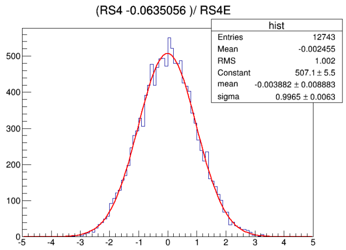

(d) M_{S_4}

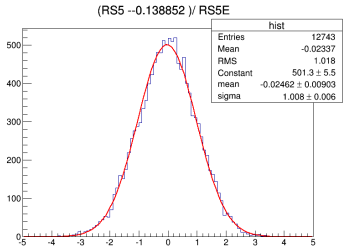

(e) M_{S_5}

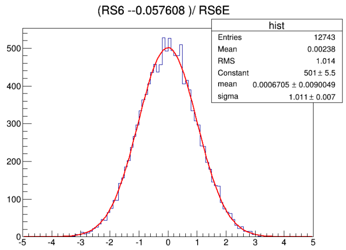

(f) M_{S_6}

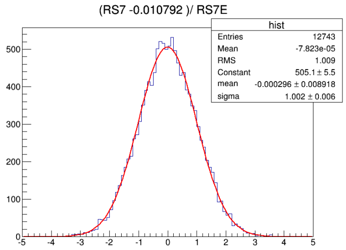

(g) M_{S_7}

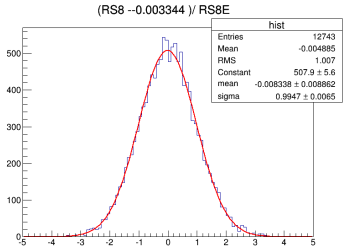

(h) M_{S_8}

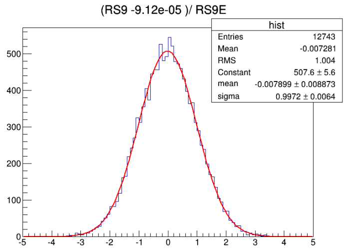

(i) M_{S_9}

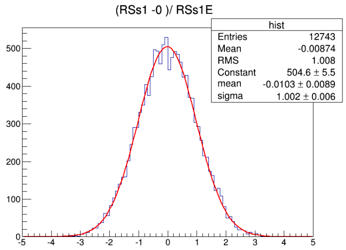

(j) M_{S1}

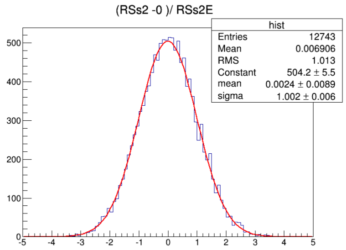

(k) M_{S2}

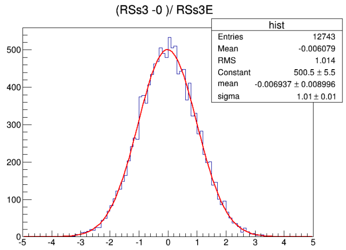

(l) M_{S3}

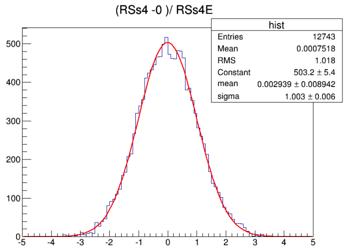

(m) M_{S4}

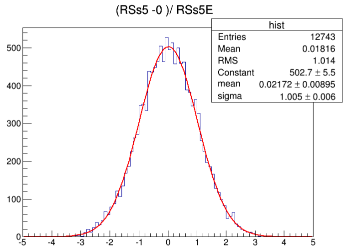

(n) M_{S5}

Figure 19: Pull plots of raw moments defined in (79). These toys were generated with SM predictions for the P wave observables and $F_S = 0.05$.

Table 25: Results for the mean of the pull distribution for the raw moments in bins of q^2. The toy experiments were generated with background and S-wave included. In brackets we note the significance of the deviation from zero.

q^2 (GeV$^2/c^4$)	F_L	S_3	S_4	S_5	S_{6s}	S_7	S_8	S_9
[0.1, 0.98]	$-0.48 \pm 0.04(-10.95)$	$0.00 \pm 0.04(0.01)$	$0.06 \pm 0.04(1.53)$	$0.02 \pm 0.04(0.54)$	$0.03 \pm 0.04(0.85)$	$-0.03 \pm 0.04(-0.74)$	$-0.04 \pm 0.04(-1.14)$	$-0.00 \pm 0.04(-0.12)$
[1.1, 2.0]	$-0.04 \pm 0.04(-1.05)$	$0.02 \pm 0.04(0.61)$	$0.08 \pm 0.04(2.04)$	$0.04 \pm 0.04(1.00)$	$0.05 \pm 0.04(1.13)$	$-0.08 \pm 0.04(-2.19)$	$-0.07 \pm 0.04(-1.78)$	$0.01 \pm 0.05(0.18)$
[2.0, 3.0]	$-0.01 \pm 0.04(-0.20)$	$0.01 \pm 0.04(0.29)$	$0.06 \pm 0.04(1.49)$	$-0.09 \pm 0.04(-2.38)$	$0.06 \pm 0.04(1.54)$	$-0.06 \pm 0.04(-1.70)$	$-0.02 \pm 0.04(-0.59)$	$0.03 \pm 0.04(0.70)$
[3.0, 4.0]	$-0.07 \pm 0.04(-1.90)$	$-0.04 \pm 0.04(-0.99)$	$-0.01 \pm 0.04(-0.33)$	$-0.01 \pm 0.04(-0.17)$	$-0.01 \pm 0.04(-0.29)$	$0.05 \pm 0.04(1.42)$	$-0.01 \pm 0.04(-0.25)$	$-0.03 \pm 0.04(-0.70)$
[4.0, 5.0]	$-0.05 \pm 0.04(-1.28)$	$0.03 \pm 0.04(0.74)$	$-0.00 \pm 0.04(-0.09)$	$0.04 \pm 0.05(0.80)$	$0.00 \pm 0.03(0.13)$	$-0.02 \pm 0.04(-0.50)$	$-0.01 \pm 0.04(-0.15)$	$0.04 \pm 0.04(0.98)$
[5.0, 6.0]	$-0.01 \pm 0.04(-0.32)$	$0.03 \pm 0.04(0.69)$	$-0.02 \pm 0.04(-0.44)$	$-0.04 \pm 0.04(-0.86)$	$-0.02 \pm 0.04(-0.57)$	$-0.02 \pm 0.04(-0.41)$	$-0.00 \pm 0.04(-0.04)$	$0.02 \pm 0.04(0.56)$
[6.0, 7.0]	$-0.00 \pm 0.04(-0.05)$	$0.07 \pm 0.04(1.60)$	$-0.05 \pm 0.04(-1.19)$	$-0.06 \pm 0.04(-1.55)$	$0.03 \pm 0.04(0.84)$	$-0.05 \pm 0.04(-1.39)$	$0.01 \pm 0.04(0.31)$	$0.02 \pm 0.04(0.39)$
[7.0, 8.0]	$0.03 \pm 0.04(0.80)$	$0.04 \pm 0.04(0.94)$	$-0.02 \pm 0.04(-0.40)$	$-0.03 \pm 0.04(-0.85)$	$0.07 \pm 0.04(2.09)$	$0.01 \pm 0.04(0.36)$	$0.02 \pm 0.04(0.55)$	$-0.04 \pm 0.04(-0.95)$
[15.0, 16.0]	$0.02 \pm 0.04(0.49)$	$-0.03 \pm 0.04(-0.86)$	$-0.08 \pm 0.04(-2.11)$	$0.02 \pm 0.05(0.46)$	$-0.01 \pm 0.04(-0.21)$	$0.00 \pm 0.04(0.06)$	$-0.06 \pm 0.04(-1.45)$	$-0.06 \pm 0.04(-1.50)$
[16.0, 17.0]	$0.04 \pm 0.04(0.90)$	$-0.03 \pm 0.04(-0.67)$	$-0.01 \pm 0.04(-0.30)$	$-0.00 \pm 0.04(-0.06)$	$-0.00 \pm 0.04(-0.12)$	$-0.01 \pm 0.04(-0.16)$	$-0.06 \pm 0.03(-1.69)$	$-0.02 \pm 0.04(-0.51)$
[17.0, 18.0]	$-0.01 \pm 0.04(-0.19)$	$-0.02 \pm 0.04(-0.55)$	$-0.04 \pm 0.04(-1.08)$	$0.01 \pm 0.04(0.27)$	$-0.04 \pm 0.04(-1.03)$	$0.00 \pm 0.04(0.03)$	$0.03 \pm 0.04(0.96)$	$-0.06 \pm 0.04(-1.46)$
[18.0, 19.0]	$0.01 \pm 0.04(0.33)$	$0.07 \pm 0.04(1.79)$	$0.05 \pm 0.04(1.20)$	$-0.02 \pm 0.04(-0.41)$	$0.02 \pm 0.04(0.43)$	$0.04 \pm 0.04(0.89)$	$-0.01 \pm 0.04(-0.15)$	$-0.01 \pm 0.04(-0.16)$

Table 26: Results for the width of the pull distribution for the raw moments in bins of q^2. The toy experiments were generated with background and S-wave included. In brackets we note the significance of the deviation from unity.

q^2 (GeV$^2/c^4$)	F_L	S_3	S_4	S_5	S_{6s}	S_7	S_8	S_9
[0.1, 0.98]	$1.00 \pm 0.02(-0.10)$	$0.97 \pm 0.02(1.66)$	$0.95 \pm 0.02(2.61)$	$0.97 \pm 0.02(1.55)$	$1.00 \pm 0.02(0.24)$	$0.97 \pm 0.02(1.25)$	$0.99 \pm 0.02(0.38)$	$0.93 \pm 0.02(3.57)$
[1.1, 2.0]	$0.95 \pm 0.02(2.24)$	$1.01 \pm 0.02(-0.31)$	$0.99 \pm 0.02(0.56)$	$1.02 \pm 0.02(-0.78)$	$0.99 \pm 0.02(0.59)$	$0.99 \pm 0.02(0.54)$	$0.97 \pm 0.02(1.62)$	$1.00 \pm 0.02(-0.09)$
[2.0, 3.0]	$0.95 \pm 0.02(2.37)$	$0.97 \pm 0.02(1.41)$	$0.97 \pm 0.02(1.71)$	$0.98 \pm 0.02(0.80)$	$0.95 \pm 0.02(2.88)$	$0.97 \pm 0.02(1.38)$	$0.96 \pm 0.02(2.27)$	$1.01 \pm 0.02(-0.53)$
[3.0, 4.0]	$1.01 \pm 0.02(-0.30)$	$0.99 \pm 0.02(0.53)$	$0.99 \pm 0.02(0.24)$	$1.01 \pm 0.02(-0.33)$	$0.99 \pm 0.02(0.36)$	$0.99 \pm 0.02(0.39)$	$1.00 \pm 0.02(-0.12)$	$1.00 \pm 0.02(-0.23)$
[4.0, 5.0]	$1.01 \pm 0.02(-0.25)$	$0.98 \pm 0.02(1.10)$	$0.98 \pm 0.02(1.17)$	$1.01 \pm 0.02(-0.61)$	$0.95 \pm 0.02(2.50)$	$0.99 \pm 0.02(0.62)$	$0.97 \pm 0.02(1.43)$	$0.97 \pm 0.02(1.67)$
[5.0, 6.0]	$0.94 \pm 0.02(2.94)$	$1.02 \pm 0.02(-1.15)$	$0.96 \pm 0.02(1.97)$	$1.01 \pm 0.02(-0.46)$	$0.99 \pm 0.02(0.41)$	$0.97 \pm 0.02(1.35)$	$0.99 \pm 0.02(0.27)$	$0.98 \pm 0.02(1.06)$
[6.0, 7.0]	$0.97 \pm 0.02(1.25)$	$0.94 \pm 0.02(3.30)$	$1.00 \pm 0.02(0.19)$	$1.00 \pm 0.02(-0.12)$	$1.01 \pm 0.02(-0.53)$	$0.98 \pm 0.02(0.78)$	$0.95 \pm 0.02(2.60)$	$0.96 \pm 0.02(2.25)$
[7.0, 8.0]	$1.02 \pm 0.02(-0.82)$	$0.97 \pm 0.02(1.38)$	$0.98 \pm 0.02(1.19)$	$0.96 \pm 0.02(1.74)$	$0.95 \pm 0.02(2.51)$	$0.95 \pm 0.02(2.45)$	$0.96 \pm 0.02(2.14)$	$0.98 \pm 0.02(0.85)$
[15.0, 16.0]	$0.95 \pm 0.02(2.23)$	$0.96 \pm 0.02(1.68)$	$0.98 \pm 0.02(0.90)$	$1.00 \pm 0.02(0.24)$	$0.99 \pm 0.02(0.36)$	$1.01 \pm 0.02(-0.59)$	$0.97 \pm 0.02(1.30)$	$0.97 \pm 0.02(1.38)$
[16.0, 17.0]	$0.97 \pm 0.02(1.37)$	$0.98 \pm 0.02(1.07)$	$0.97 \pm 0.02(1.41)$	$0.95 \pm 0.02(2.45)$	$0.97 \pm 0.02(1.41)$	$0.97 \pm 0.02(1.72)$	$0.94 \pm 0.02(3.25)$	$0.97 \pm 0.02(1.36)$
[17.0, 18.0]	$1.00 \pm 0.02(-0.23)$	$0.96 \pm 0.02(2.11)$	$0.93 \pm 0.02(3.53)$	$0.97 \pm 0.02(1.53)$	$0.96 \pm 0.02(2.14)$	$1.00 \pm 0.02(-0.02)$	$0.98 \pm 0.02(0.90)$	$1.00 \pm 0.02(0.08)$
[15.0, 19.0]	$0.96 \pm 0.02(2.08)$	$0.97 \pm 0.02(1.53)$	$0.99 \pm 0.02(0.55)$	$0.97 \pm 0.02(1.51)$	$0.98 \pm 0.02(0.88)$	$0.98 \pm 0.02(1.25)$	$0.98 \pm 0.02(1.10)$	$0.99 \pm 0.02(0.46)$

Table 27: Pull distribution for F_s extracted with the $m(K^+\pi^-)$ mass fit. The toy study has been done including a linear background with parameters taken from data. Toy studyes are here reported for $F_S = 0.1$.

q^2 (GeV^2/c^4)	mean	sigma
$[0.1, 0.98]$	0.038 ± 0.029	0.918 ± 0.021
$[1.1, 2.0]$	-0.024 ± 0.031	0.998 ± 0.022
$[2.0, 3.0]$	-0.025 ± 0.029	0.942 ± 0.021
$[3.0, 4.0]$	-0.069 ± 0.030	0.971 ± 0.022
$[4.0, 5.0]$	0.062 ± 0.030	0.955 ± 0.021
$[5.0, 6.0]$	0.081 ± 0.032	0.992 ± 0.022
$[6.0, 7.0]$	-0.031 ± 0.031	0.992 ± 0.022
$[7.0, 8.0]$	-0.054 ± 0.030	0.962 ± 0.021
$[11.0, 11.75]$	0.002 ± 0.030	0.947 ± 0.021
$[11.75, 12.50]$	-0.027 ± 0.031	0.979 ± 0.022
$[15.0, 16.0]$	0.011 ± 0.029	0.933 ± 0.021
$[16.0, 17.0]$	0.02 ± 0.029	0.929 ± 0.020
$[17.0, 18.0]$	-0.054 ± 0.030	0.962 ± 0.021
$[18.0, 19.0]$	-0.075 ± 0.030	0.964 ± 0.021

In data F_s fraction will be determined from a fit to $m_{K\pi}$ mass spectrum with the same method as the likelihood fit. The method is described in Sec. 6.2.12. We performed a toy study to check if the method is stable in 1 GeV^2/c^4 q^2 bins. The $m_{K\pi}$ distribution is generated with a linear background (with parameters taken from data). The results of the pulls are shown in Tab. 27 for $F_S = 0.1$. As can be seen no bias is observed. We observed a small overestimation of the error, however this has negligible effect on the P-wave observables.

6.3.9 Method of moments applied to $B^0 \to J/\psi K^{*0}$

In order to check our method with data, we use the decay $B^0 \to J/\psi K^{*0}$ as a control channel. In additional to preselection cuts described in [13] we required that the dimuon mass to be within 60 MeV/c^2 around the J/ψ nominal invariant mass. The measured angular observables are presented in Tab. 28. In general we observe agreement in the P-wave angular observables between these measurements and the angular parameters determined in Ref. [20], small discrepancies are negligible with respect to the expected statistical uncertainty in the $B^0 \to K^{*0}\mu^+\mu^-$ decay.

6.3.10 Measuring asymmetries with the method of moments

The method described here is also used to measure the *CP*-asymmetries (the A_i). These observables are defined as the asymmetries of the corresponding J_i for B^0 and $\overline{B}^0$, nor-

Table 28: Results of the angular fit of the decay $B^0 \to J/\psi K^{*0}$ in different bins of $m(K^+\pi^-)$, using the full available data set corresponding to $3\,\text{fb}^{-1}$. The angular terms that have been previously determined in Ref. [20] are given in Tab. 20.

parameter	$m_{K\pi}$ range in MeV/c^2 [795.9, 995.9]	[825.9, 965.9]	[826.0, 861.0]	[861.0, 896.0]	[896.0, 931.0]	[931.0, 966.0]
$F_{\rm L}$	0.558 ± 0.003	0.558 ± 0.003	0.566 ± 0.006	0.561 ± 0.004	0.549 ± 0.004	0.562 ± 0.005
S_3	0.000 ± 0.002	0.001 ± 0.002	-0.006 ± 0.006	0.000 ± 0.004	0.001 ± 0.003	0.004 ± 0.006
S_4	-0.280 ± 0.003	-0.282 ± 0.004	-0.278 ± 0.007	-0.288 ± 0.005	-0.279 ± 0.004	-0.275 ± 0.006
S_5	-0.002 ± 0.003	-0.002 ± 0.003	-0.004 ± 0.007	0.000 ± 0.005	-0.006 ± 0.003	0.003 ± 0.006
S_6^s	0.001 ± 0.003	0.002 ± 0.003	-0.004 ± 0.008	0.001 ± 0.003	0.003 ± 0.004	0.003 ± 0.005
S_7	0.001 ± 0.003	0.001 ± 0.003	-0.003 ± 0.007	0.001 ± 0.004	0.001 ± 0.004	0.007 ± 0.006
S_8	-0.053 ± 0.003	-0.054 ± 0.003	-0.072 ± 0.008	-0.058 ± 0.004	-0.051 ± 0.004	-0.047 ± 0.006
S_9	-0.089 ± 0.003	-0.088 ± 0.004	-0.089 ± 0.008	-0.086 ± 0.004	-0.091 ± 0.004	-0.086 ± 0.006
F_S	0.080 ± 0.004	0.068 ± 0.003	0.10 ± 0.012	0.053 ± 0.006	0.061 ± 0.005	0.108 ± 0.009
S_{S1}	-0.240 ± 0.004	-0.245 ± 0.004	-0.70 ± 0.01	-0.387 ± 0.007	-0.109 ± 0.006	0.160 ± 0.010
S_{S2}	0.003 ± 0.003	0.007 ± 0.003	0.140 ± 0.008	0.045 ± 0.004	-0.028 ± 0.004	-0.108 ± 0.006
S_{S3}	0.004 ± 0.003	0.004 ± 0.003	-0.005 ± 0.007	0.003 ± 0.003	0.004 ± 0.003	0.012 ± 0.006
S_{S4}	0.001 ± 0.003	0.001 ± 0.003	0.014 ± 0.008	-0.003 ± 0.003	0.000 ± 0.004	0.005 ± 0.006
S_{S5}	-0.065 ± 0.003	-0.061 ± 0.003	0.040 ± 0.008	-0.027 ± 0.004	-0.091 ± 0.004	-0.157 ± 0.007

malised with respect to the total width $\Gamma_{\rm tot}$ as defined in Eq. 18. In order to measure these observables, B^0 candidates (only) are multiplied by a factor -1 for the angular terms $f_{i=4\ldots9}$ when determining the moments.

6.3.11 Determination of $F_{\rm S}$ using BW phase shift

The value of $F_{\rm S}$ obtained from the mass fit can be cross-checked using the method described in Ref [17]. This method exploits the phase change of $\mathcal{A}_0$ between the left- and right-hand side of the Breit-Wigner and its interference with the S-wave. Assuming $\text{Re}(\mathcal{A}_0^0)$ and $\text{Im}(\mathcal{A}_0^0)$ to be constant (or slowly varying) in $\pm 100\,\text{MeV}$ mass window, then $F_{\rm S}$ can be written as a function of the θ_K forward-backward asymmetry (S_{S1}). Defining S_{S1}^- and S_{S1}^+ as the value of the moment S_{S1} respectively at the left and the right of the Breit-Wigner pole, we can write $F_{\rm S}$ as

$$F_{\rm S} = \frac{[(S_{S1}^+ + S_{S1}^-)^2/16 + (S_{S1}^+ - S_{S1}^-)^2/(16 \times 1.23)]\dfrac{3.24}{3F_{\rm L}}}{1 - [(S_{S1}^+ + S_{S1}^-)^2/16 + (S_{S1}^+ - S_{S1}^-)^2/(16 \times 1.23)]\dfrac{3.24}{3F_{\rm L}}} \tag{81}$$

Applying this procedure to the $B^0 \to J/\psi K^{*0}$ dataset, yields

$$S_{S1}^+ = -0.046 \pm 0.006\ , \tag{82}$$
$$S_{S1}^- = -0.506 \pm 0.006 \tag{83}$$
$$\tag{84}$$

and

$$F_{\mathrm{S}} = 0.060 \pm 0.003 \tag{85}$$

The result is consistent with the one obtained using the procedure described in Sec. 6.3.7.

6.3.12 Expected difference between the likelihood fit and the method of moments

The method of moments estimator is strongly, but not completely, correlated to the maximum likelihood estimator. This correlation between the two estimators was studied using the `EOS` SM toy MC. Example scatter plots for S_5 and F_{L} in one q^2 bin are given in Fig. 21. Whilst the distributions are strongly correlated the spread of the data points is larger than one might naively expect (approximately 50% of the statistical uncertainty). This effect is mainly statistical is largely independent on the level of background and on the acceptance.

Small differences between the two estimators are also seen in the data. For a global comparison, we calculate the difference between the two estimates of each observable in every q^2 bin, then divide it by the expected difference from toy MC. The result is shown in Fig. 22. The resulting distribution is consistent with having a mean of zero and a width of one, i.e. the moments/likelihood fit are consistent with each other when accounting for the expected differences between the two methods.

6.3.13 Determination of the P_i observables with the MoM

The less form factor dependent observables (P_i) are related to the measured observables via relations defined in Sec 6.1.5. As can be seen in the denominator in all the equations a factor of $1 - F_L$ appears. If F_L is sufficiently large the normal error propagation does not work as the first derivative in the Taylor expansion is insufficient to describe the transformation. Due to this we used bootstrap technique to determine the appropriate intervals using quantiles. For each of the P_i bootstrap distribution a interval from $-\infty$ to P_i^{min} is constructed in a way that it contains 16 % of events. In the same manner the interval (P_i^{max}, ∞) is constructed. The error that will be quoted is simply (P_i^{min}, P_i^{max}). We decided to use this method as the quantiles are invariant under PDF re-parametrization.

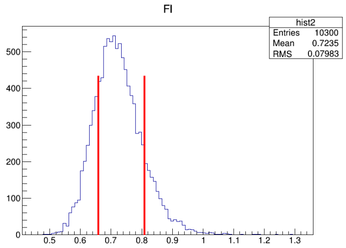

(a) F_l

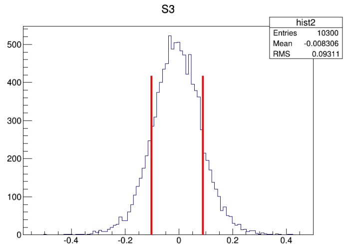

(b) S_3

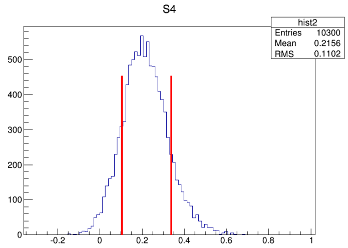

(c) S_4

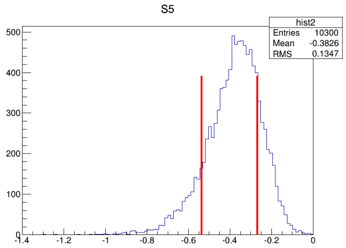

(d) S_5

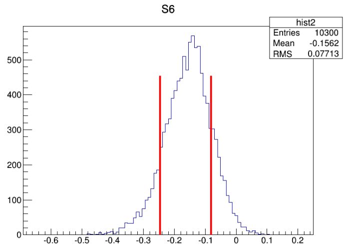

(e) S_6

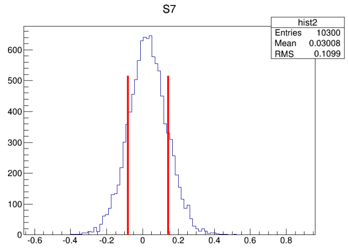

(f) S_7

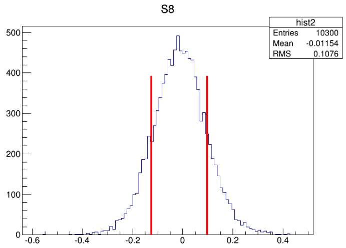

(g) S_8

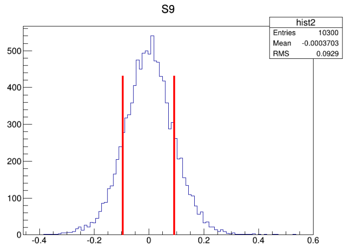

(h) S_9

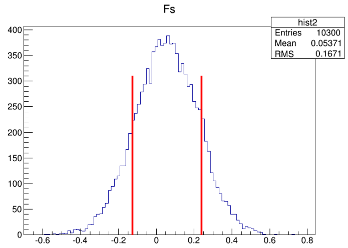

(i) F_s

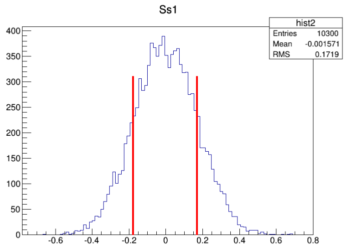

(j) S_{1s}

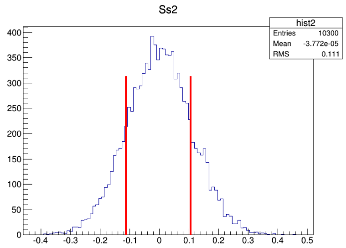

(k) S_{2s}

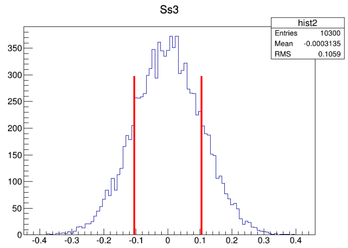

(l) S_{3s}

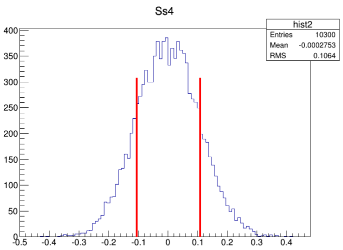

(m) S_{4s}

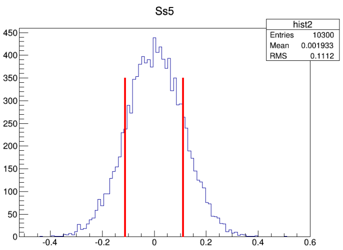

(n) S_{5s}

Figure 20: 68.3% belt on measured $F_{\rm S}$, $F_{\rm L}$, S_i. Error is propagated using MC method.

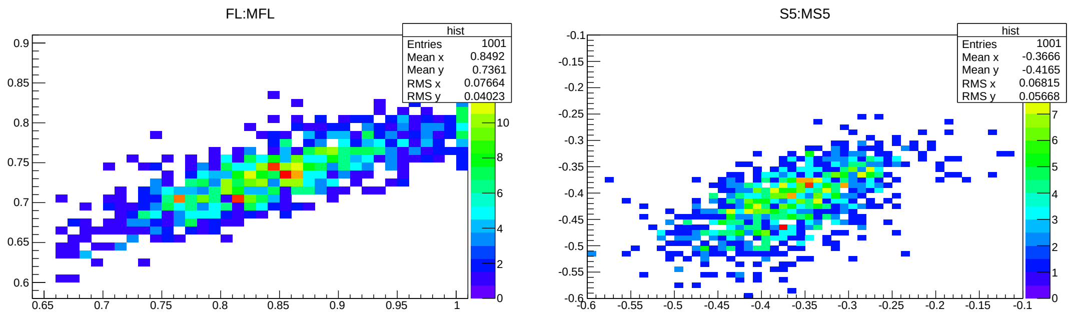

Figure 21: An example illustration of difference between the maximum likelihood and method of moments, when applied to SM MC.

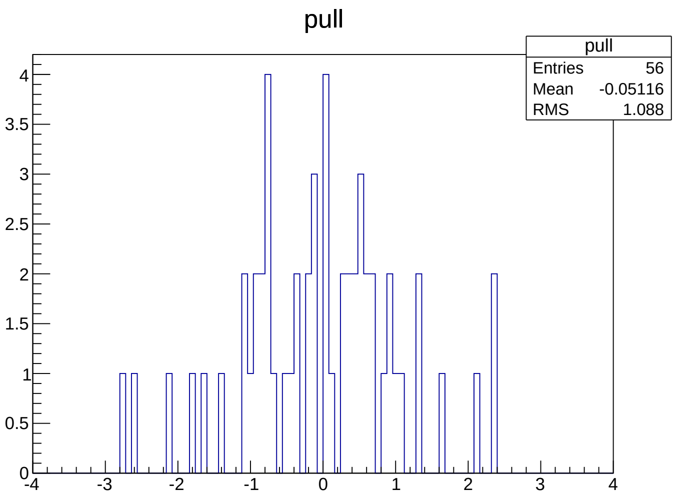

Figure 22: Pull distribution of difference between the method of moments and the log-likelihood fit.

6.4 Fitting for the K^{*0} amplitudes

6.4.1 Introduction

The main goal of this method is to perform a measurement of the q^2 dependent K^{*0} spin amplitudes using a three-coefficient ansatz per real amplitude component. In princple, the values of these coefficients as well as their correlations can be provided. Theorists can then be able to construct observables of their choice out of these amplitude coefficients and compare to their predictions. In reality, as will be discussed in Sec. 9.4, the best fit point of the fit to the 3 fb^{-1} data results in multiple closely separated minima. These multiple solutions make the approximation of the likelihood surface using an error matrix invalid and therefore will require a more sophisticated treatment.

One of the main benefits for fitting for the q^2 dependent K^{*0} spin amplitudes is that we make use of all the possible relations between the angular coefficients (J_i) thus reducing the number of degrees of freedom we extract. In addition, the angular distribution remains positive definite for any amplitude value and there are consequently no boundary issues. Finally, the fact that the amplitudes are extracted continuously in q^2 can increase the sensitivity to the effects of physics beyond the SM. This is because new physics can change the q^2 dependence of the angular observables. This q^2 dependence also means that the zero-crossing point of observables can be analytically extracted.

The S-wave amplitude components are included in the signal angular pdf as will be discussed below. However the S-wave amplitude components will be treated as nuisance parameters and not parameters of interest. That means that it will be made clear to theorists that they will need to marginalise over these when performing their studies.

6.4.2 Infinitesimal symmetries of the angular distribution

As discussed in Sec. 6.1.2, the angular distribution of the decay can be described by eleven parameters J_i $(\bar{J}_i)$ for each B^0 flavour. These J_i $(\bar{J}_i)$ are made up of bilinear combinations of the K^{*0} spin amplitudes and represent the "experimental" degrees of freedom. Then the experimental degrees of freedom should match the number of real amplitude components which represent the "theoretical" degrees of freedom. Another way of saying this is that the amount of independent information that one can extract from the angular distribution should be independent of whether one parametrises the distribution using the angular coefficients or the spin amplitudes. Just like the case of the $B^0 \to J/\psi K^{*0}$ analysis of Ref. [20], where the amplitudes could only be obtained up to a global phase rotation of all the amplitudes, there are continuous symmetry transformations of the amplitudes that leave the decay rate invariant. In order for the degrees of freedom to match we require

$$n_j - n_d = n_a - n_s, \tag{86}$$

where n_j is the number of J_i terms, n_d the number of relations between the J_i, n_a is the number of real amplitude components and n_s is a number of continuous symmetry transformations of the amplitudes that leave the decay rate invariant. In contrast to the $B^0 \to J/\psi K^{*0}$ analysis of Ref. [20], we now have both Left- and Right-handed spin amplitudes which can introduce additional symmetries under certain conditions. In particular, in the massless limit ($q^2 \gg 4m(\mu)^2$), and ignoring scalar contributions to the dimuon system, there are four continuous symmetry transformations of the amplitudes ($n_s = 4$) that leave each of the J_i and therefore the decay rate invariant [35]. More on the continuous symmetry transformation can be found in Appendix I.

The existence of these symmetries means that a likelihood function including all twelve real amplitude components, would therefore exhibit a “valley” of continuous maxima in amplitude space, rendering minimisation techniques for the determination of the amplitude components from data impossible. The symmetries of the angular distribution allow for the transformation of the amplitudes to a particular basis where four of the amplitude components are fixed to some arbitrary value at every point in q^2. The choice of the basis, referred to as “basis-fixing”, is exactly what lifts the degeneracy. This basis-fixing has two requirements: firstly that values for transformation exists for every point in q^2, and secondly the amplitudes in this transformed basis are slowly varying in q^2 such that they can be described by a simple functional form. This second requirement restricts the q^2 range where the amplitudes can be extracted. The presence of potential light resonances below ~ 1 GeV$^2/c^4$ and of $c\bar{c}$ resonances above 8 GeV$^2/c^4$ motivates the use of the resonance-free and theoretically preferred region of $1 < q^2 < 6$ GeV$^2/c^4$.

A previous study described in [35] used the following basis-fixing,

$$\mathrm{Re}(A_\parallel^L) = \mathrm{Im}(A_\parallel^L) = \mathrm{Im}(A_\parallel^R) = \mathrm{Im}(A_\perp^R) = 0. \tag{87}$$

This basis however suffers from a discontinuity in $\mathrm{Re}(A_0^L)$ at $q^2 \sim 2\,\mathrm{GeV}^2/c^4$. In Ref. [35], the problems caused by this discontinuity where avoided by ignoring the q^2 region below $2.5\,\mathrm{GeV}^2/c^4$. This is clearly highly undesirable. For the present analysis a better basis-fixing was devised,

$$\mathrm{Re}(A_0^R) = \mathrm{Im}(A_0^R) = \mathrm{Im}(A_0^L) = \mathrm{Im}(A_\perp^R) = 0. \tag{88}$$

The amplitudes in the improved fixed-basis exhibit a smooth behaviour in q^2 both in the SM as well as in a range of new physics models, including ones discussed in [35]. Figure 24 shows the effect of the improved basis-fixing for SM amplitudes calculated using the `EOS` package [16].

6.4.3 Exact discrete symmetries

In addition to the continuous transformations of the amplitudes that leave the angular distribution invariant, there are is also the discrete symmetry transformation, $A_i \to -A_i$, that leaves the angular distribution invariant, even after the basis-fixing transformation has been applied. This symmetry can be seen simply by inspecting Eq. 13 and noting that even after the conditions of Eq. 88 have been applied, all angular observables are still constructed out of products of spin-amplitudes in the fixed-basis. Note that in the SM, the statistical precision of the amplitudes means that this discrete symmetry can be broken by requiring $\mathrm{Re}(A_0^L) < 0$ at any q^2 value for the left-handed amplitudes, and $\mathrm{Re}(A_\perp^R) > 0$ at $q^2 = 2.0$ GeV$^2/c^4$ for the right-handed amplitudes.

6.4.4 Accidental discrete symmetries

The limited amount of signal candidates available in experiment data, can also give rise to approximate symmetries under discrete transformations of the amplitudes. The exact form of these approximate symmetries can depend on the basis-fixing transformations discussed in Sec. 6.4.2. Given the basis-fixing condition of Eq. 88, a clear example occurs in the transformed basis of the SM, where the lack of right handed currents can give rise to an approximate symmetry under the transformation

$$\begin{aligned} A_{\parallel}^{L} &\to -A_{\perp}^{L} \\ A_{\perp}^{L} &\to -\frac{A_{\parallel}^{L}}{2}. \end{aligned} \tag{89}$$

The effect of this accidental approximate symmetry can be demonstrated by generating samples based on the SM and in a model with large right handed Wilson coefficients, with a size equivalent to that of the LHCb Run-I dataset. Figure 23 shows the effect of the discrete transformation of Eq. 89 $\cos\theta_\ell$, both in the SM and in a model with large right handed currents. It is clear that the aforementioned transformation is an approximate discrete symmetry of the angular distribution in the SM and models with no right handed currents.

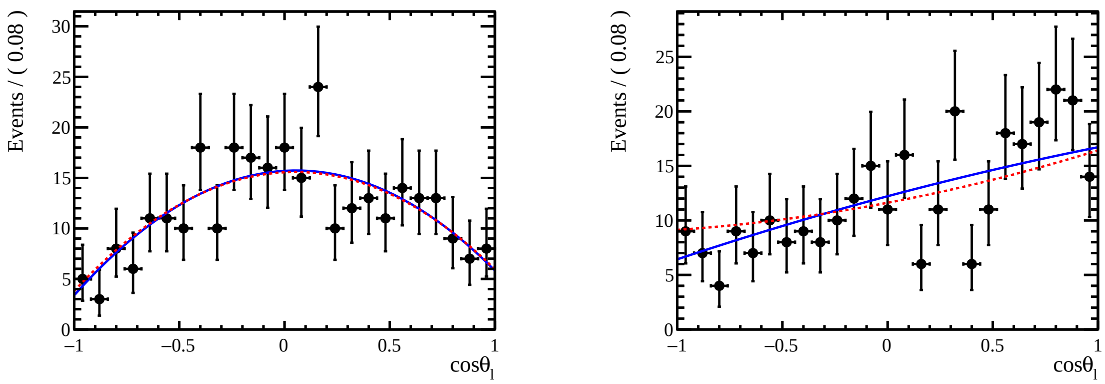

Figure 23: Demonstration of the effect of the transformation of Eq. 89 in the SM (left) and in a model with large right handed Wilson Coefficients (right). The amount of data corresponds to the expected number of $\overline{B}^0 \to \overline{K}^{*0}\mu^+\mu^-$ candidates in LHCb's Run-I dataset. The blue line denotes the model that the data is generated from. The right line denotes the model with the aforementioned transformation applied. The difference in χ^2 of the two curves with respect to the data are 0.01 for the SM and 0.1 for the model with right handed currents.

An additional approximate discrete symmetry exists under the transformation of the right handed amplitudes in the transformed basis

$$A_{\parallel}^{R} \leftrightarrow -A_{\perp}^{R}. \tag{90}$$

As for the left-handed amplitudes, the transformation of Eq. (90) is an approximate discrete symmetry of the angular distribution only in the SM and in other models with no right-handed currents.

6.4.5 Parameterised amplitudes

The second ingredient in performing a q^2 dependent fit to extract the K^{*0} spin amplitudes is the choice of the q^2 parametrisation of the amplitudes in the transformed basis. A three parameter ansatz of the form

$$A_i^{L,R} = \alpha_i^{L,R} + \beta_i^{L,R} q^2 + \gamma_i^{L,R}/q^2 \tag{91}$$

for both real and imaginary amplitude parameters is chosen. No attempt is made to interpret these α, β and γ coefficients in terms of short- or long-distance parameters. The choice of this ansatz is justified by fitting the transformed spin amplitudes, as provided by `EOS` in the SM as well as numerous physics models, using the parametrisation described above. Figure 24 shows the result of this fit. It is clear that this ansatz is a reasonable choice and any bias coming from this choice will be dwarfed by the statistical uncertainty of our current data sample.

The basis-fixing reduces the number of amplitude components that need to be determined to eight per B^0 flavour. Considering that each such component is described by three parameters to account for the q^2 dependence, in total there are twenty-four amplitude parameters per B^0 flavour that need to be extracted. This parameter counting ignores any S-wave amplitudes. Such amplitudes are discused further in Sec. 6.4.6. Alternatively, one can make the model dependent assumption that the only weak phases present in the amplitudes come from the CKM matrix elements, which are negligibly small. This assumption leads to the B^0 and $\overline{B}^0$ amplitudes being identical. Accounting for the experimental angular convention of the decay rate described in Sec. 6.1.2, the decay distribution of both the B^0 and $\overline{B}^0$ decays can be described using a single set of amplitude parameters. The approaches with separate and identical B^0 and $\overline{B}^0$ amplitude parameters are both discussed below.

6.4.6 S-wave contribution

Previous studies have discussed both the potential size as well as the impact of the S-wave contribution in the angular analysis of $B^0 \to K^{*0}\mu^+\mu^-$ decays [36–39]. In particular, it has been shown that with 3 fb^{-1} of LHCb data, ignoring the S-wave contribution can have a significant effect on some angular observables. It is therefore critical that the q^2 dependent S-wave amplitude components are also accounted for in the fit to the angular distribution of $B^0 \to K^{*0}\mu^+\mu^-$ decays.

The S-wave amplitudes are included in the angular distribution of the signal by default based on Eq. 21 and are treated as nuisance parameters. The $K^+\pi^-$ mass range considered corresponds to 100 MeV/c^2 around the $K^{*0}(892)$ pole mass. The $m_{K\pi}$ dependence is

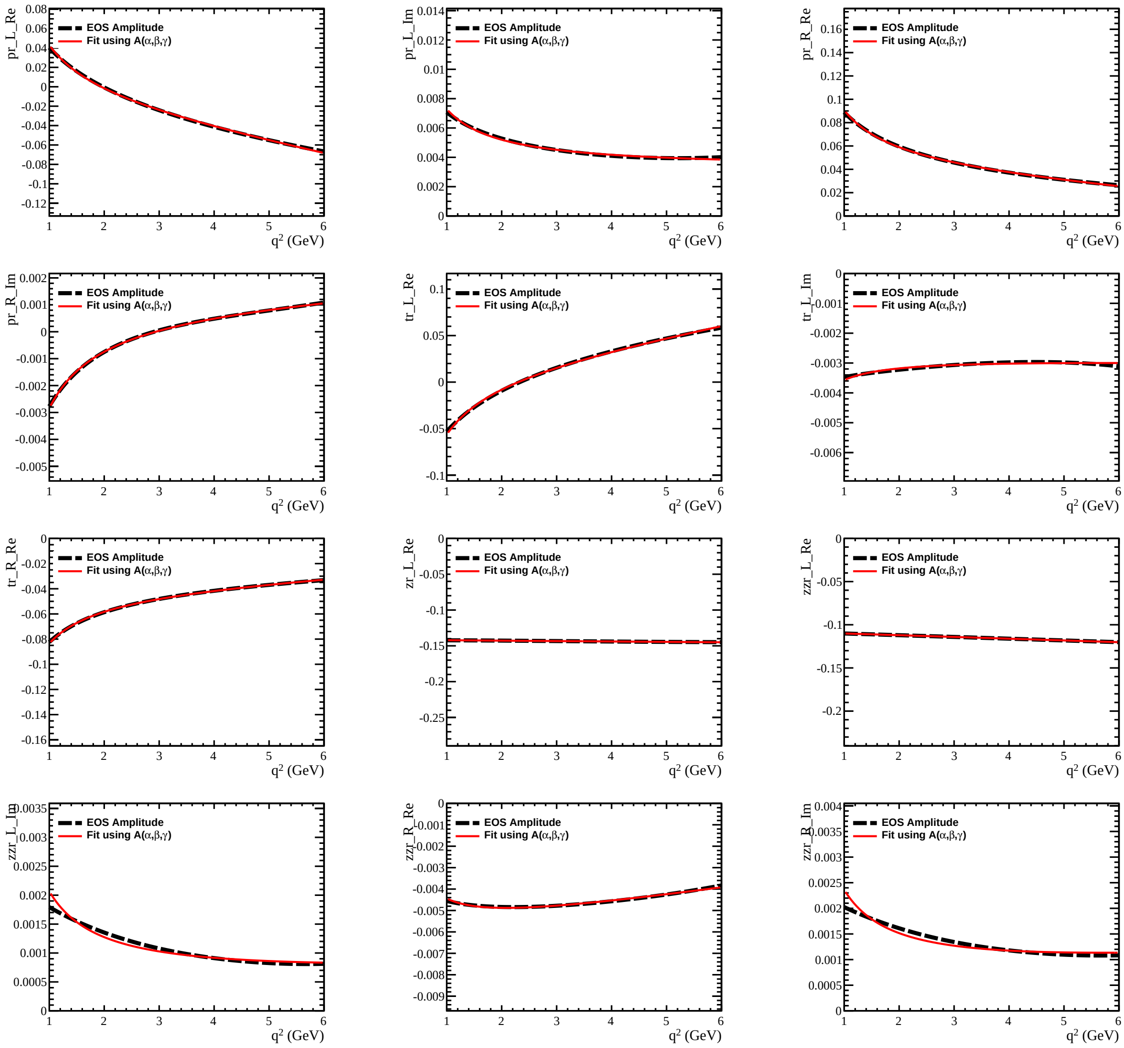

Figure 24: Distribution of transformed SM amplitudes and their fit to the q^2 dependent ansatz. Only the non-zero amplitude components in the transformed basis are shown. "pr"=$A_{\parallel}$,"tr"=$A_{\perp}$,"zr"=A_0, "zzr"=A_{00}.

accounted for by modifying each J_i term in Eq. 21 by

$$J_{ij} = A_i A_j^* \to A_i A_j^* \int g_i(m_{K\pi}) g_j^*(m_{K\pi}) dm_{K\pi}, \tag{92}$$

where $g_i(m_{K\pi})$ represents the $m_{K\pi}$ line-shape of either a P-wave or an S-wave amplitude.

For the fit to actual data, the $K^{*0}(892)$ is modelled using a relativistic Breit-Wigner with a running width, including phase space and Blatt-Weiskopff factors both for the breakup of the $K\pi$ system and the decay of the B^0, as shown in Eq. 37. For the S-wave, two models are considered. The default model used is the LASS parametrisation, as described in Eqn. 38. The Isobar model is used as a systematic variation, including

Table 29: Table summarising the various integrals of the S and P wave line shapes that are used both in the generation of the toys and in the fit for the amplitudes

Term	Value Toys	Isobar	LASS
$\int_{796}^{996} \lvert g_{K^{*0}}\rvert^2 dm_{K\pi}$	0.70	0.87	0.87
$\int_{796}^{996} \lvert g_{\text{S-wave}}\rvert^2 dm_{K\pi}$	0.16	0.10	0.08
$\int_{796}^{996} g_{\text{S-wave}} g^*_{K^{*0}} dm_{K\pi}$	$0.19 - 0.2i$	$-0.12 + 0.16i$	$0.09 - 0.11i$

relativistic Breit-Wigners with running widths, for the $\kappa(600)$ and the $K_0^*(1430)$ with mass and width parameters as given in Ref. [40]. The relative phase and magnitude these two S-wave resonances is set to $0.51e^{3.127}$, as obtained from a fit to the $m_{K\pi}$ spectrum of $B^0 \to J/\psi K^{*0}$ data in the region of $644 < m_{K\pi} < 1200$ MeV/c^2.

For both the nominal and systematically varied models, the integrals $\int g_i(m_{K\pi})g_j^*(m_{K\pi})dm_{K\pi}$ are computed 100 MeV around the $K^{*0}(892)$ pole mass, and their values are insterted into the angular distribution. The values of these integrals are summarised in Tab. 29

6.4.7 The S-wave in the simulation studies

The q^2 dependence of the S-wave amplitudes used in the generation of the simulated events are calculated following Ref. [41]. Given the lack of form factor predictions for the S-wave, in the simulations studies, only the $\kappa(600)$ is considered to contribute to the S-wave in the $K^+\pi^-$ mass range considered. This means that for the simulations studies only the line-shape of the κ is considered to contribute to the S-wave $g_i(m_{K\pi})$ of Eq. 92. The line-shape of both the $\kappa(600)$ and the $K^{*0}(892)$, are taken as relativistic Breit-Wigner distributions with mass and width parameters as given in Ref. [40]. The form-factor of the $\kappa(600)$ is taken from Ref. [42]. The values of the corresponding $\int g_i(m_{K\pi})g_j^*(m_{K\pi})dm_{K\pi}$ are shown in Tab. 29. The resulting value of F_S as a function of q^2 in the SM is shown in Fig. 25. Using this simplistic approach, the predicted value of F_S is approximately $\leq 10\%$ which is similar to the values obtained using a more sophisticated treatment such as that of Refs. [37, 38].

Given the size of the data sample in hand and the fact that the S-wave fraction is expected to be small ($\mathcal{O}(10\%)$), one can approximate the q^2 dependence of the S-wave amplitudes to be flat in q^2. This is a good approximation since the q^2 shape of the S-wave amplitude is expected to be the same as that of $A_0^{L,R}$ which approximately flat in the region $1 < q^2 < 6$ GeV^2/c^4.

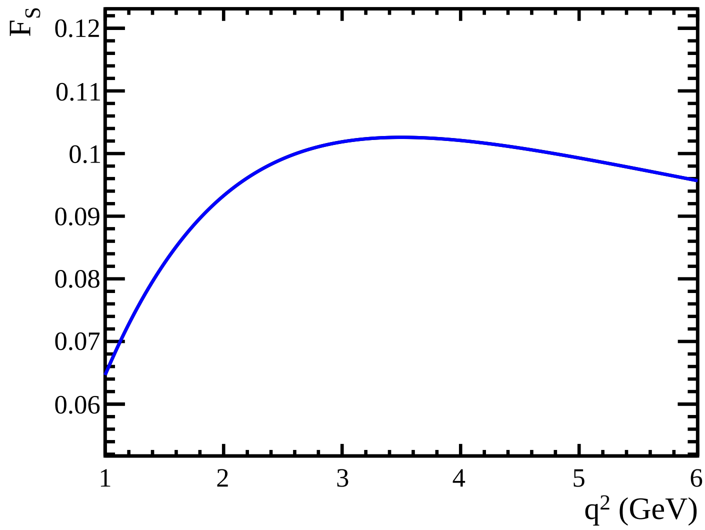

Figure 25: Estimate of the S-wave fraction F_S in the SM as a function of q^2 using the simplistic approach as described in the text.

6.4.8 Extracting the amplitudes

The stability and sensitivity of a fit for the q^2 dependent amplitudes is determined using simulated data with sample sizes equivalent to those expected at LHCb with 3 fb^{-1}. The angular distribution of the signal is described using Eq. 13 where the q^2 dependent amplitudes are again calculated using the `EOS` package for both the SM and new physics models. Similar to the method of fitting the observables directly, the angular distribution of the background is described by a product of three Chebyshev polynomials of second order. An additional first order Chebyshev polynomial is used to describe the q^2 dependence. The B^0 mass line-shape of the signal and background candidates is described using functional forms discussed in Sec. 5. Equation 93 shows the total background model.

$$\frac{\mathrm{d}^5\Gamma[\mathrm{Bkg}]}{\mathrm{d}\cos\theta_\ell\,\mathrm{d}\cos\theta_K\,\mathrm{d}\phi\,\mathrm{d}q^2\mathrm{d}m_B} = f(\cos\theta_\ell)\times g(\cos\theta_K)\times h(\phi)\times l(q^2)\ \times k(m_B), \tag{93}$$

where $f,\ g,\ h,\ l$ are polynomials and k are the B^0 and $\overline{B}^0$ mass line-shapes. The effects that the trigger, reconstruction and selection criteria have on the angular distribution of the signal, are accounted for by multiplying the angular distribution of the signal by the four dimensional (unfactorised) acceptance correction discussed in Sec. 8. Writing this explicitly we have:

$$\frac{\mathrm{d}^5\Gamma'[\mathrm{Sig}]}{\mathrm{d}\cos\theta_\ell\,\mathrm{d}\cos\theta_K\,\mathrm{d}\phi\,\mathrm{d}q^2\mathrm{d}m_B} = \frac{\mathrm{d}^5\Gamma[\mathrm{Sig}]}{\mathrm{d}\cos\theta_\ell\,\mathrm{d}\cos\theta_K\,\mathrm{d}\phi\,\mathrm{d}q^2\mathrm{d}m_B}\times\epsilon(\cos\theta_\ell,\cos\theta_K,\phi,q^2), \tag{94}$$

where $\epsilon(\cos\theta_\ell,\cos\theta_K,\phi,q^2)$ denotes the efficiency to trigger, reconstruct and select a $B^0\to K^{*0}\mu^+\mu^-$ decay.

For each simulated dataset, the amplitude coefficients α, β and γ (see Eq. 91) are determined using an extended maximum likelihood fit. The probability distribution functions for the signal and background, $P_{\mathrm{Sig(Bkg)}}$, are formed from the decay rate functions of Eq. 94, where the signal amplitudes are written in terms of the three-parameter ansatz of Eq. 91. The likelihood function used is shown in Eq. 95,

$$\begin{aligned} -\log\mathcal{L} &= \sum_{i}^{N_{\mathrm{Dat}}} -\log[N_{\mathrm{Sig}}(\alpha_j,\beta_j,\gamma_j)P_{\mathrm{Sig}}(\cos\theta_\ell,\cos\theta_K,\phi,q^2|\alpha_j,\beta_j,\gamma_j)+ \\ &\qquad N_{\mathrm{Bkg}}P_{\mathrm{Bkg}}(\cos\theta_\ell,\cos\theta_K,\phi,q^2)]+ \\ &\quad -N_{\mathrm{Dat}}\log[N_{\mathrm{Sig}}(\alpha_j,\beta_j,\gamma_j)+N_{\mathrm{Bkg}}]+[N_{\mathrm{Sig}}(\alpha_j,\beta_j,\gamma_j)+N_{\mathrm{Bkg}}], \end{aligned} \tag{95}$$

where N_{Dat} is the total number of events in the dataset, N_{Bkg} is a parameter in the fit that gives the number of background events, and $N_{\mathrm{Sig}}(\alpha_j,\beta_j,\gamma_j)$ is the number of signal events written in terms of the integrated signal decay rate:

$$N_{\mathrm{Sig}}(\alpha_j,\beta_j,\gamma_j) = \frac{\bar{N}_{sig}}{\Delta q^2}\times\int_{-1}^{1}\int_{-1}^{1}\int_{-\pi}^{\pi}\int_{1\,\mathrm{GeV}^2/c^4}^{6\,\mathrm{GeV}^2/c^4}\frac{\mathrm{d}^4\Gamma[\mathrm{Sig}]}{\mathrm{d}\cos\theta_\ell\,\mathrm{d}\cos\theta_K\,\mathrm{d}\phi\,\mathrm{d}q^2}\,\mathrm{d}\cos\theta_\ell\,\mathrm{d}\cos\theta_K\,\mathrm{d}\phi\,\mathrm{d}q^2, \tag{96}$$

where $\Delta q^2 = 5\ \mathrm{GeV}^2/c^4$ representing the size of the q^2 range considered and $\bar{N}_{sig}/\Delta q^2$ is just a constant scaling which for simplicitly is chosen to be related to the expected number of signal events in 3 fb^{-1} of data multiplied by the q^2 interval in question.

The last term of Eq. 95 denotes the extended term in the likelihood where the signal yield is explicitely related to the integral of the angular distribution of the signal. This term is what sets the overall scale of the amplitudes[4].

6.4.9 Validation of amplitude fits using `EOS` toys

An ensemble of 10^4 simulated data sets is generated containing signal and background events as described in Sec. 6.4.8. A maximum likelihood fit is performed to each of the data sets, to extract the q^2 dependent P- and S-wave spin amplitudes. Therefore at a given value of q^2, 10^4 determinations of each amplitude and thus of each angular observable are performed. The starting point for each fit is randomised, such that the amplitude coefficients are fluctuated around their SM values, according to a Gaussian distribution centred at their SM values with a width of 300 times the SM value. The fits exhibit a very stable behaviour, with $> 97\%$ converging succesfully with a positive definite error

[4] One could in principle set the overall scale of the amplitudes by fixing a component to a value such as unity, as the normalisation of the angular distribution to convert into a probability density function allows to cancel the dependence to a single component, or equivalently reparametrise all amplitude coefficients relative to a particular one. However practically this does not work as well as having an explicit extended term to set the scale, due to the large correlations between the α, β and γ coefficients of each of the amplitudes.

matrix. The remaining 3% of the fits succesfully converge if a different random starting value is chosen.

Originally the plan was to fit for B^0 and $\overline{B}^0$ amplitudes separately, which would allow for the simultaneous extraction of both the CP averaged and CP-asymmetric observables S_i and A_i. the limited signal candidates expected in 3 fb^{-1} however would not guarantee a correct statistical coverage. The analysis therefore is de-scoped and the assumption that B^0 and $\overline{B}^0$ amplitudes are the same, which it turn means that all weak-phases are assumed to be negligible (ie only effectively only considering real Wilson coefficients).

6.4.10 Fits to combined B^0 and $\overline{B}^0$ decays

Assuming B^0 and $\overline{B}^0$ amplitudes are the same, there are 8 real amplitude P-wave components each of which is parametrised using the α, β, γ ansatz. In addition there are 4 real amplitude S-wave components, each parametrised as a constant in q^2. This gives a total of $8 \times 3 + 4 \times 1 = 28$ signal parameters. **In what follows, amplitudes obtained from fits to combined B^0 and $\overline{B}^0$ decays assuming no weak-phases, will be referred to as $\overline{B}^0$ amplitudes**. In addition there are 7 Chebyshev coefficients used to describe the angular and q^2 dependence of the background. These background parameters are common between B^0 and $\overline{B}^0$. Finally the B^0 mass shape parameters are fixed in the fits to the toy data to the values obtained from fits to $B^0 \to J/\psi\, K^{*0}$ accounting for the correction to the resolution of the lineshpae due to the q^2 dependence of the resolution. A correction factor of 0.995, constantin the q^2 range between 1.1 and 6 GeV^2/c^4 is used. This value is obtained by inspecting Fig. 5.

The results of the fits for the q^2 dependent $\overline{B}^0$ amplitudes are shown in Fig. 26. A clear degeneracy is observed under reflections about the x-axis. This is effect is a consequence of the discrete symmetry $A_i \to -A_i$ as discussed in Sec. 6.4.3. When making plots of the amplitudes resulting from an ensemble of toys, the median and mean of the distribution of the toys would be zero for every point in q^2 due to this symmetry. Therefore in order to be able to make sensible comparisons in the plots, the degeneracy is broken by requiring the $\text{Re}(A_0^L) < 0$ and $\text{Re}(A_\perp^{Re}) < 0$ at $q^2 = 2.6\,\text{GeV}^2/c^4$.

The resulting angular observables, as defined in Secs 6.1.2 and 6.1.4, from fits to toy data are shown in Fig. 27. By looking at the point where 34% and 47.5% of results lie within either side of the most likely value of the ensembles at a given q^2 point (peak position), asymmetric 1 σ and 2 σ errors can be computed. Connecting these at different q^2 values gives us the 1 σ and 2 σ bands for the experimental errors on the observable.

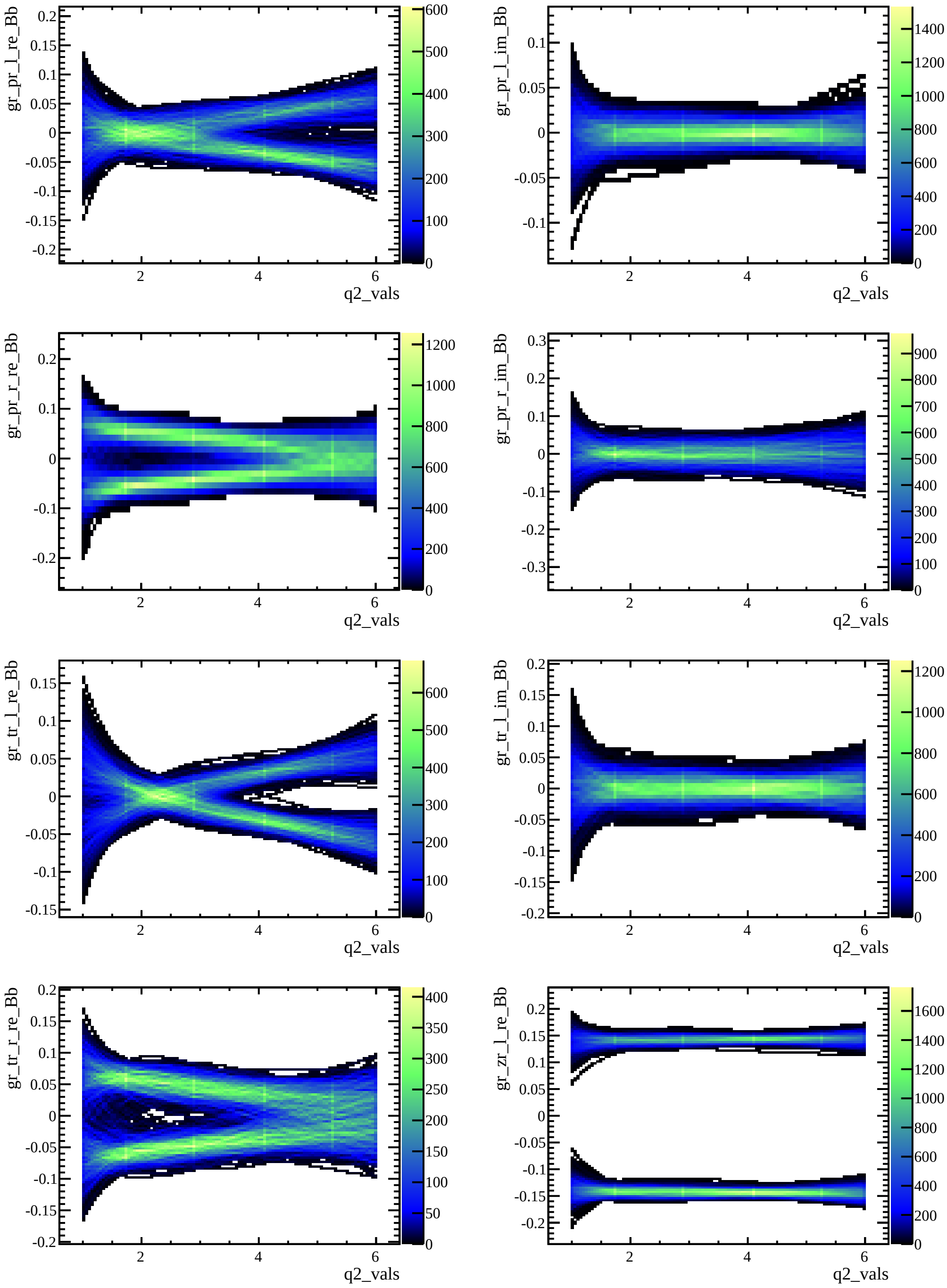

Figure 26: Two dimensional histograms of the amplitudes as a function of q^2 resulting from 10^4 fits to generated signal and background toy data as described in the text. A discrete symmetry of reflections about zero is observed due to the fact that the J_i terms are bilinear coefficients of the amplitudes. "pr"$=A_\parallel$,"tr"$=A_\perp$,"zr"$=A_0$.

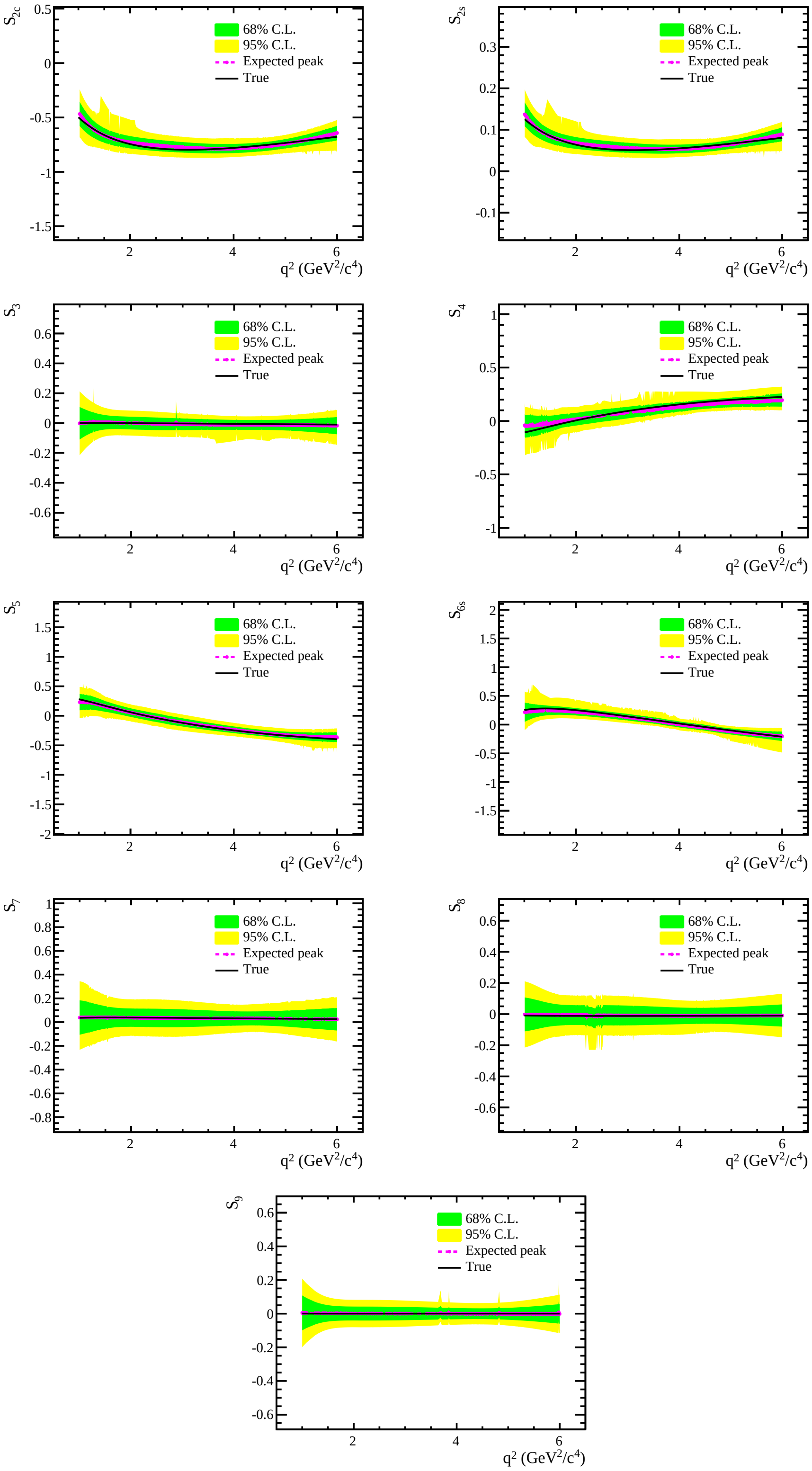

Figure 27: Resulting CP averaged observables as functions of q^2 from simulataneous fits to B^0 and $\overline{B}^0$ amplitudes in ensembles of simulated data generated according to the SM with.

A bias at the level of 0.5σ is apparent in some observables, most notably S_4, S_{2s} and S_{2c}. All of these observables contain the amplitude $\mathrm{Re}(A_{\parallel}^{L})$. For example the S_4 observable is related to J_4 which in turn can be written in terms of the amplitudes in the fixed-basis as $J_4 = \mathrm{Re}(A_{\parallel}^{L})\mathrm{Re}(A_0^L)$. As such it is instructive to look for potential biases in $A_{\parallel}^{L}$ and A_0^L. Fig. 28 shows the peak position, 1 and 2 σ bands of these two amplitudes resulting from the ensemble of fits to the simulated data. It is evident that the bias in S_4 is arising from the bias in $A_{\parallel}^{L}$.

The main reason behind this bias arises from an accidental approximate discrete symmetry of Eq. 89, as discussed in Sec. 6.4.4. This accidental symmetry is most evident in models where the right handed Wilson Coefficients are zero, such as the SM. A systematic uncertainty given by the difference between the peak position of the ensemble fits and the true value derived from the SM, is a conservative estimate of this uncertainty. Fig. 29 shows the comparison of the results of $\mathrm{Re}(A_{\parallel}^{L})$ from fits to ensembles of simulated data generated according to the SM and to a model with large right handed Wilson coefficients. However since this bias arises due to a genuine degenaracy of the angular distribution, such a systematic uncertainty would not be required if all the two-dimensional profiles between all the parameterers of interest where provided, as the likelihood surface itself would encode the second solution.

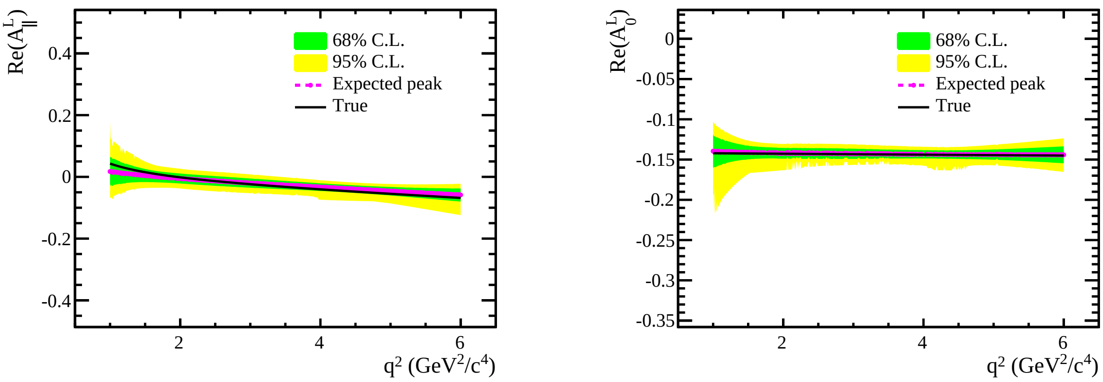

Figure 28: Resulting amplitudes as a functions of q^2 from fits to ensembles of simulated data generated according the SM which enter int the calculation of J_4 and therefore S_4. Left for $\mathrm{Re}(A_{\parallel}^{L})$ and right for $\mathrm{Re}(A_0^L)$. There is a clear bias in $\mathrm{Re}(A_{\parallel}^{L})$ as discussed in the text.

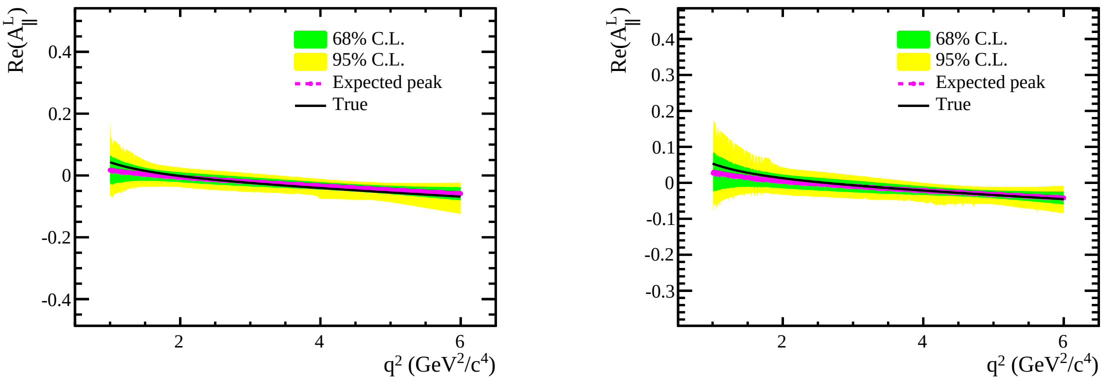

Figure 29: Resulting $\mathrm{Re}(A_{\parallel}^{L})$ amplitudes as a functions of q^2 from fits to ensembles of simulated data generated according the SM (left) to a model with large right handed Wilson coefficients (right). The level of bias is reduced in models with non-zero right handed Wilson coefficients.

6.4.11 Uncertainty estimation

Table 30 summarises the pull mean and width of the amplitudes at a point in q^2. In order to discern any statistical bias from the bias originating from the approximate symmetries discussed in Sec. 6.4.4, a point in q^2 is chosen such that minimises the bias from the approximate symmetries.

The pull means and widths are largely consistent with zero and unity, respectively, indicating that the likelihood is a good estimator of the uncertainty of the amplitudes. The residual bias in $A_{\parallel}^{R}$ arises from the additional approximate symmetry between $A_{\parallel}^{R}$ and $A_{\perp}^{R}$ discussed in Sec. 6.4.4.

The one dimensional profile likelihoods of the individual $\overline{B}^0$ amplitude coefficients from a fit to $\overline{B}^0$ amplitudes to a single toy dataset, are shown in Figs. 30 and 31 . The red lines indicate the 1,2 and 3 σ intervals as given by the HESSE error.

The two dimensional profile likelihoods for $\mathrm{Im}(A_{\parallel}^{L})$ of the $\bar{B}$ are shown in Figs. 32, 33, 34 . More can be found in Appendix J. The ellipse corresponds to the one standard deviation value provided by HESSE. It is clear that the HESSE matrix gives a good approximation to the likelihood surface. However there are cases where the error is asymmetric. As long as the shape of the likelihood surface faithfully represents the statistical uncertainty obtained from fits to ensembles of toy-data, these profiles an be used to determine the uncertainty of the amplitude parameters. Otherwise a technique such as Feldman-Cousins will need to be employed in order to guarantee correct statistical coverage. Given the large correlations between the parameters of interest, a multidimensional Feldman-Cousins technique would have to be employed, which can be computationally expensive.

Unfortunately post unblinding has revealed multiple minima closely separated. This fact makes the use of the correlations obtained from 2D likelihood surfaces close to a single minimum a bad approximation. Techniques such as bootstraping the data in order to obtain the coverage of the observables is

Table 30: Means and widths of the pull distributions of the P-wave amplitudes at $q^2 = 2.4\ \mathrm{GeV}^2/c^4$, obtained from fits to ensembles of simulated data samples in Scenario-I. The pull is defined as (Fit-SM)/$\sigma_{\mathrm{Meas.}}$ where $\sigma_{\mathrm{Meas.}}$ is the error on the measured quantity obtained using the error matrix of the fit. The deviation of the pull mean of $\mathrm{Re}(A_{\parallel}^{R})$ from zero arises due to the residual bias from the approximate symmetry of the angular distribution.

Parameter	Pull mean	Pull width
$\mathrm{Re}(A_0^L)\overline{B}^0$	-0.03 ± 0.02	0.97 ± 0.03
$\mathrm{Re}(A_{\parallel}^L)\overline{B}^0$	0.00 ± 0.02	1.01 ± 0.03
$\mathrm{Im}(A_{\parallel}^L)\overline{B}^0$	0.01 ± 0.02	1.02 ± 0.03
$\mathrm{Re}(A_{\parallel}^R)\overline{B}^0$	0.22 ± 0.02	0.90 ± 0.03
$\mathrm{Im}(A_{\parallel}^R)\overline{B}^0$	-0.02 ± 0.02	0.94 ± 0.03
$\mathrm{Re}(A_{\perp}^L)\overline{B}^0$	0.02 ± 0.02	0.97 ± 0.03
$\mathrm{Im}(A_{\perp}^L)\overline{B}^0$	-0.04 ± 0.02	0.95 ± 0.03
$\mathrm{Re}(A_{\perp}^R)\overline{B}^0$	-0.05 ± 0.02	0.94 ± 0.03

under investigation

6.4.12 Sensitivity to new physics

The expected sensitivity to the effects of new physics is estimated by generating a large number of simulated data samples according to the SM (null dataset) and a NP model (test dataset) where $C_9^{NP} = -1.5$. The `EOS` program is used to generate these two models using their central value predictions. Two fits are then performed to each of these two separate ensembles. One where all the amplitude parameters are fixed to their SM values (null hypothesis) and one where the amplitude parameters are fixed to the values given by the model with $C_9^{NP} = -1.5$ (test hypothesis). The background components, yields and S-wave amplitude parameters are treated as nuisances and are left floating in each fit. The test statistics are defined as

$$
\begin{aligned}
Q^{NP} &= -2(\mathrm{NLL}_1^{NP} - \mathrm{NLL}_0^{NP}) \\
Q^{SM} &= -2(\mathrm{NLL}_1^{SM} - \mathrm{NLL}_0^{SM}),
\end{aligned}
\tag{97}
$$

where $\mathrm{NLL}_{0,1}^{SM,NP}$ corresponds to the negative log likelihood value of the test or null hypothesis on a test or null dataset. The expected sensitivity to a model with $C_9^{NP} = -1.5$ is then estimated by counting the fraction of the toys with a value of $Q^{SM} \leq \bar{Q}^{NP}$, where $\bar{Q}^{NP}$ is the median of the Q^{NP} distribution. Figure 35 shows the distribution of the test statistic for both the null and test hypotheses in simultaneous fits to B and $\bar{B}$ candidates. The probability for the null hypothesis to fluctuate such that it gives a test statistic as

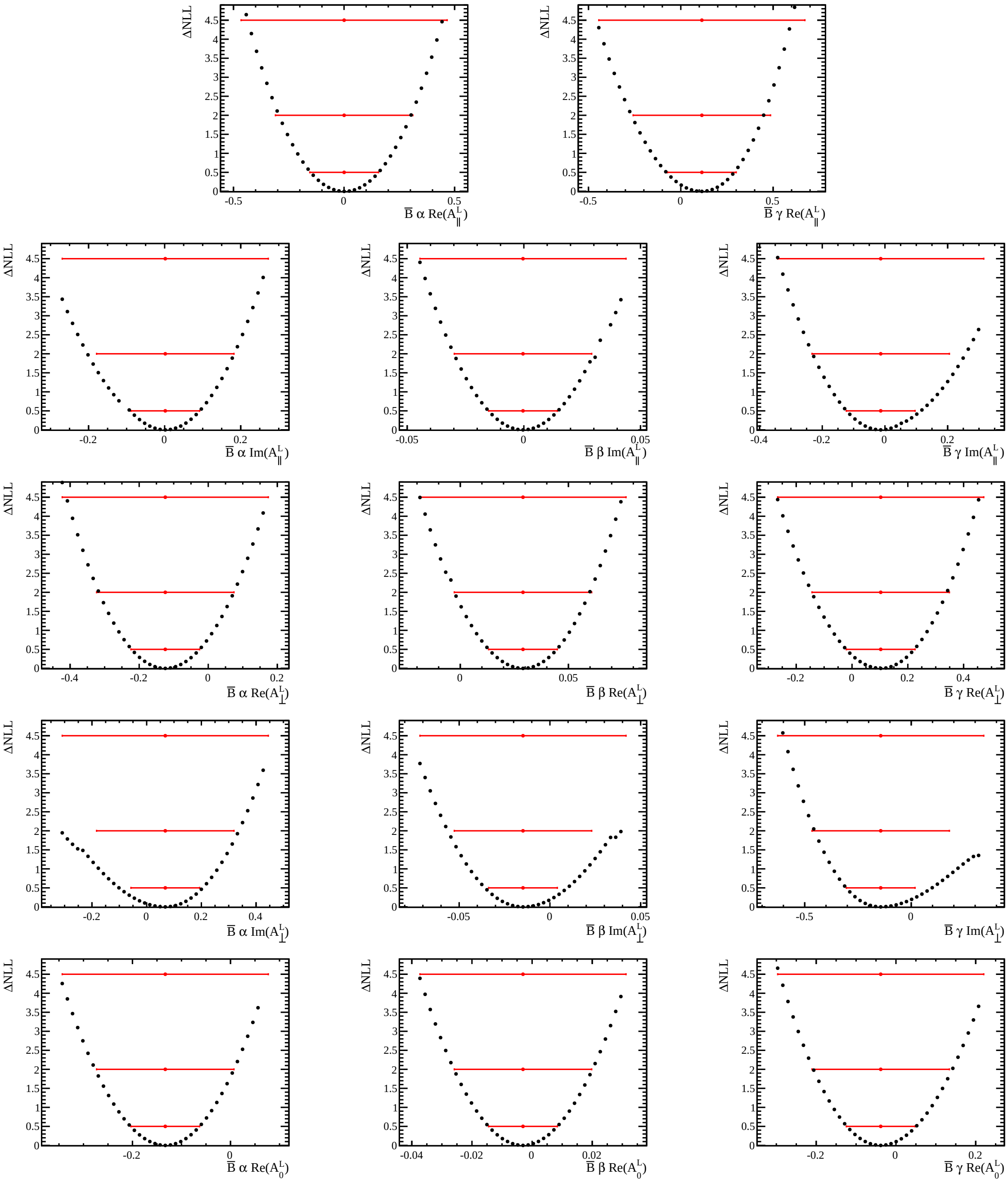

Figure 30: One dimensional profile likelihoods of left handed $\overline{B}^0$ amplitude coefficients from a fit to a single toy dataset. A good agreement between the HESSE errors (red lines) and the likelihood profile is observed up to at least 2 standard deviations.

low or lower than the median of the test hypothesis (i.e $Q^{SM} \leq \bar{Q}^{NP}$) corresponds to a significance of $\sim 6.5\sigma$. It must be stressed at this point that the theory uncertainties related to each model are not accounted for. Including these theory uncertainties is beyond

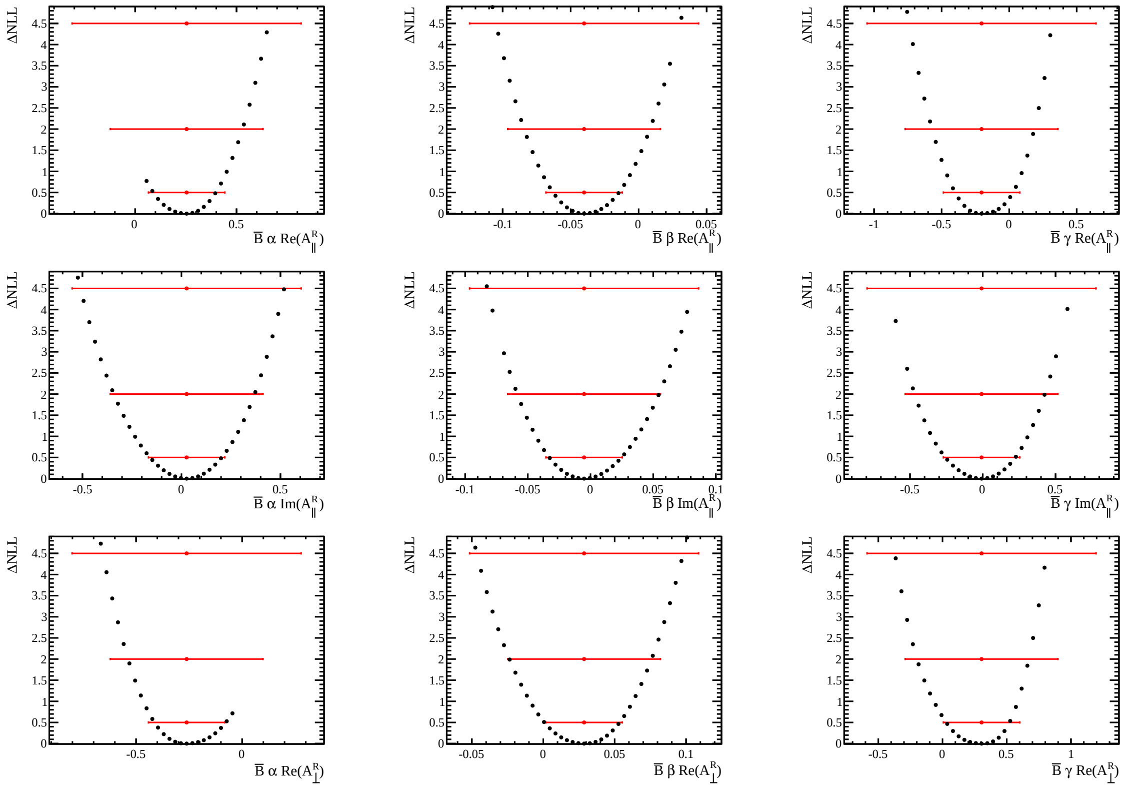

Figure 31: One dimensional profile likelihoods of right handed $\overline{B}^0$ amplitude coefficients from a fit to a single toy dataset. A good agreement between the HESSE errors (red lines) and the likelihood profile is observed up to at least 2 standard deviations.

the scope of the current analysis. In order to maximise the sensitivity to models that have real Wilson coefficients, the B and $\bar{B}$ candidats could be combined doubling the available statistical precision and thus, increasing the statistical sensitivity by a factor of $\sqrt{2}$.

6.4.13 Fit validation on data using $B^0 \to J/\psi K^{*0}$

Just as in Sec. 6.2.11, the fit model is validated by fitting $B^0 \to J/\psi K^{*0}$ data and comparing to the published LHCb result [20]. The q^2 parametrisation of the amplitudes cannot describe the J/ψ line-shape. In order to maintain the q^2 parametrisation of the fit without having to integrate over q^2, a flat q^2 distribution is generated to replace the J/ψ lineshape. The results of the fit in the region $796 < m_{K\pi} < 996$ GeV$^2/c^4$ to angular observables according to Eqs. 13 and 22. The uncertainties are estimated by propagating the error matrix of the fit to the expresion of the angular observables. Fig. 36 shows the mass and angular distribution projections of the data. The small descrepancy observed in $\cos\theta_K$ around -0.5 is compatible with the presence of an exotic Z state decaying to $J/\psi\pi$.

Table 31 summarises the results of fits to $B^0 \to J/\psi K^{*0}$ data obtained from fits to observables taken from Tab. 31 and from fits to spin amplitudes. Both methods are in good

Table 31: Comparison of results of the angular fit of the decay $B^0 \to J/\psi K^{*0}$ from fits to observables taken from Tab. ??, with the results obtained from fits to the spin amplitudes.

	$m_{K\pi}$ range $[796, 996]$ MeV/c^2	
parameter	Observables	Amplitudes
S_1^s	0.331 ± 0.001	0.330 ± 0.001
S_3	0.000 ± 0.002	0.000 ± 0.002
S_4	-0.256 ± 0.002	-0.245 ± 0.001
S_5	-0.002 ± 0.002	-0.002 ± 0.002
S_6^s	0.000 ± 0.002	0.000 ± 0.002
S_7	0.001 ± 0.002	0.001 ± 0.002
S_8	-0.053 ± 0.002	-0.052 ± 0.002
S_9	-0.090 ± 0.002	-0.092 ± 0.002
F_S	0.087 ± 0.003	0.089 ± 0.002
S_{S1}	-0.234 ± 0.003	-0.302 ± 0.002
S_{S2}	0.023 ± 0.002	0.022 ± 0.002
S_{S3}	0.003 ± 0.002	0.002 ± 0.002
S_{S4}	0.001 ± 0.002	0.001 ± 0.002
S_{S5}	-0.068 ± 0.002	-0.051 ± 0.002

agreement. Some small descrepancy remains in S_{1s} however this is a nuisance parameter in our fit.

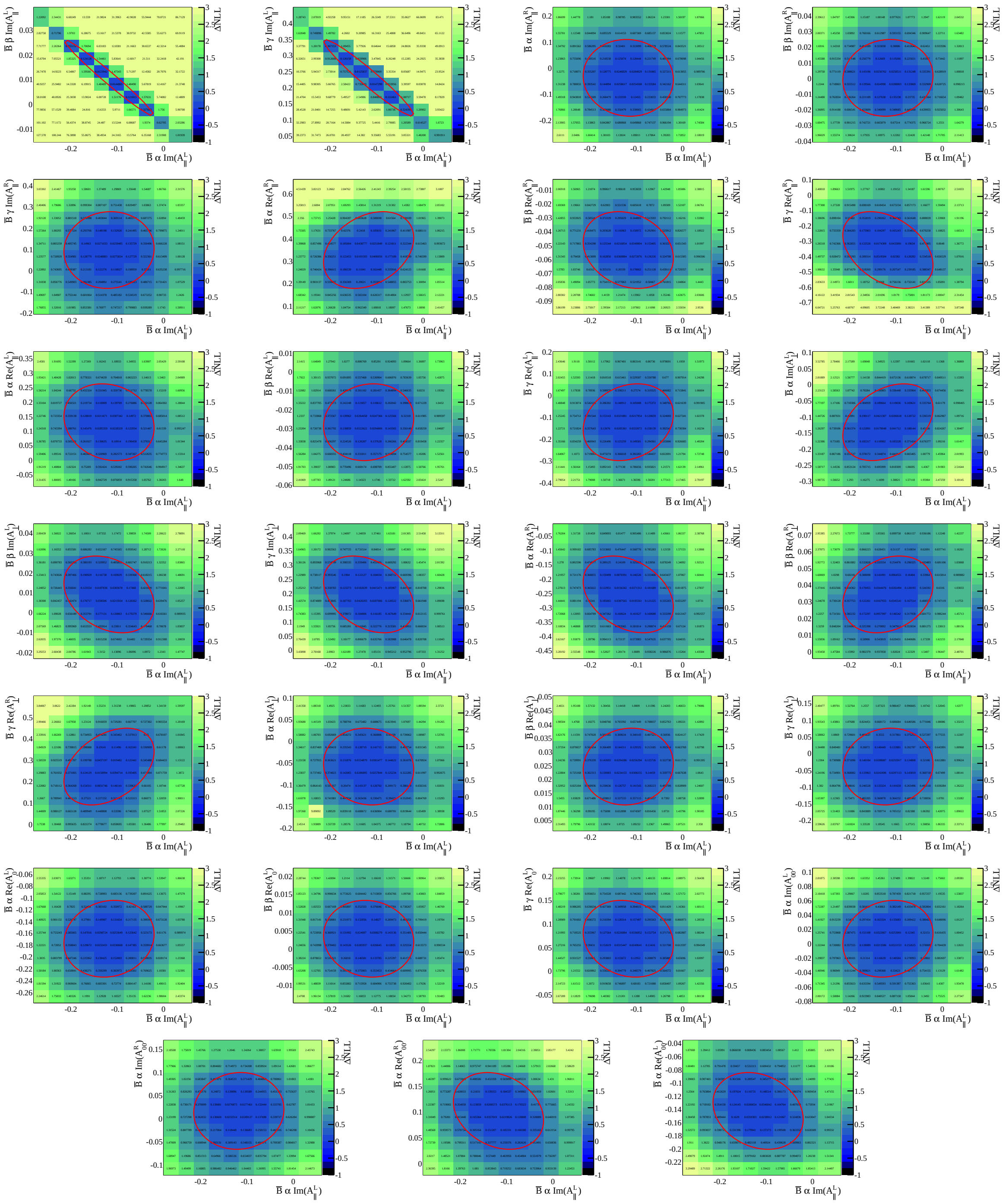

Figure 32: Two dimensional profile likelihoods of a of $Im(A_{\parallel}^{L})$ of $\bar{B}$ with other amplitude parameters. The ellipse corresponds to the one standard deviation value provided by HESSE. Values at -0.5 denote failed fits which need to be rerun with a different starting value.

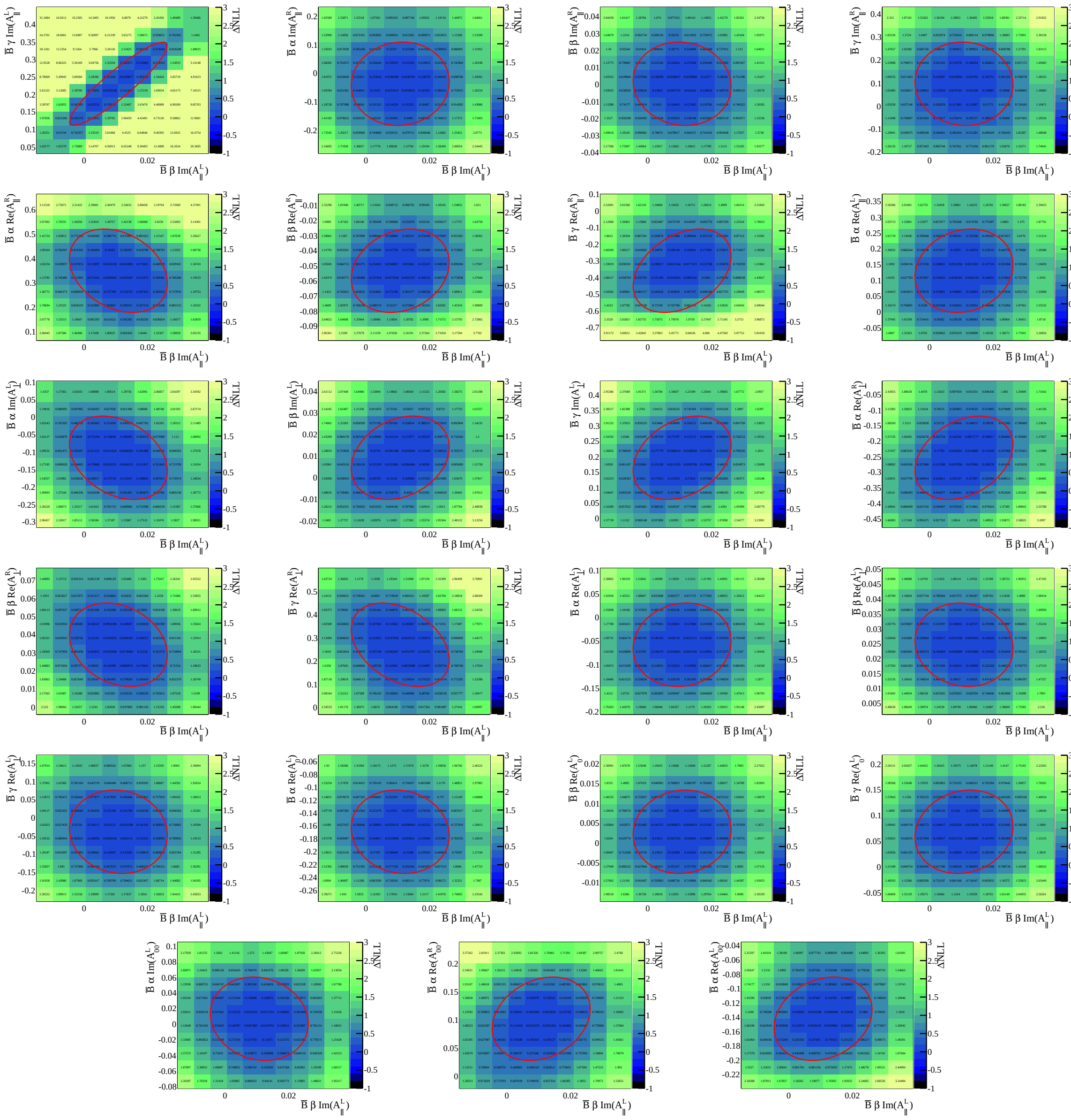

Figure 33: Two dimensional profile likelihoods of b of $Im(A_{\parallel}^{L})$ of $\bar{B}$ with other amplitude parameters. The ellipse corresponds to the one standard deviation value provided by HESSE. Values at -0.5 denote failed fits which need to be rerun with a different starting value.

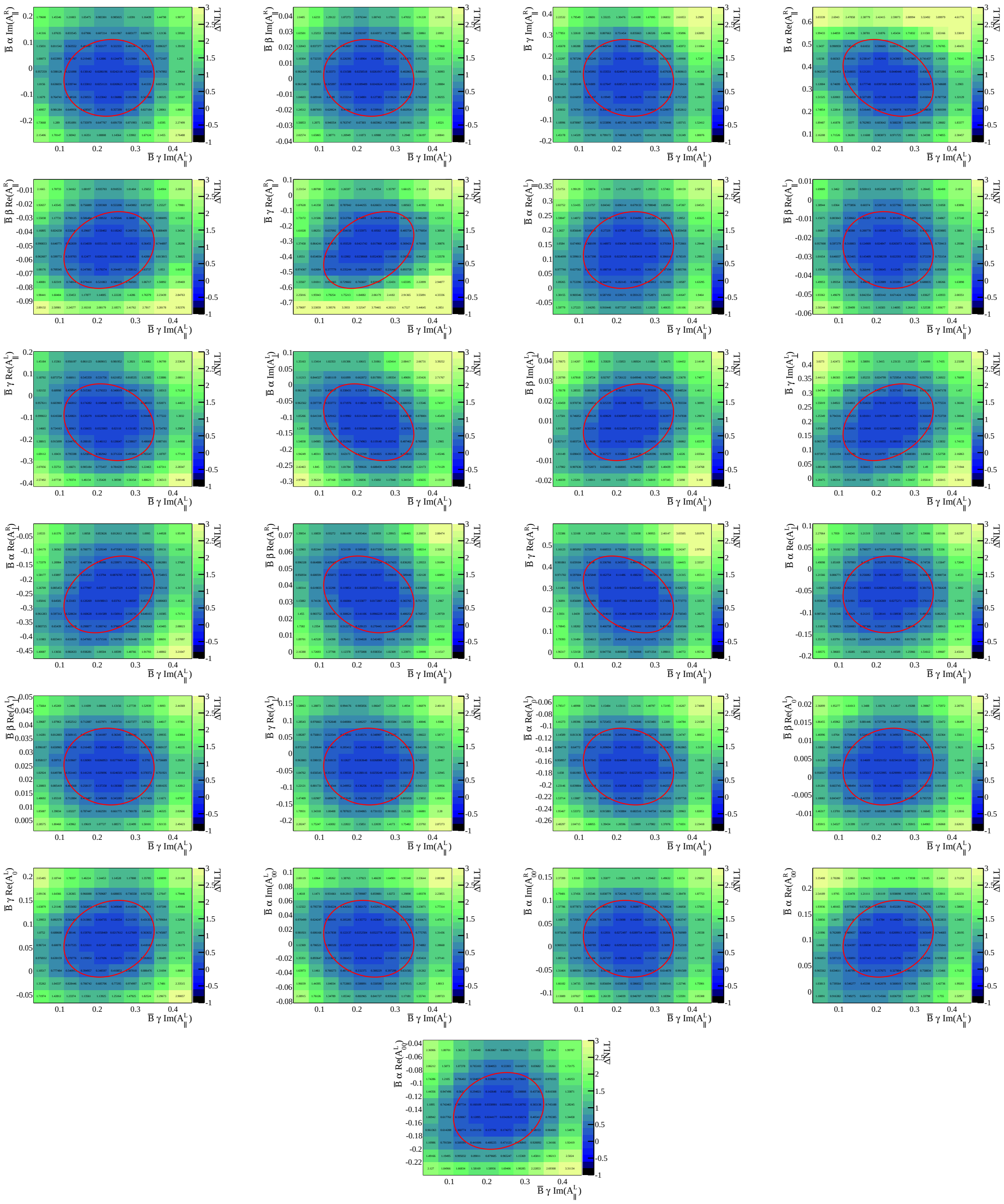

Figure 34: Two dimensional profile likelihoods of c of $Im(A_{\|}^{L})$ of $\bar{B}$ with other amplitude parameters. The ellipse corresponds to the one standard deviation value provided by HESSE. Values at -0.5 denote failed fits which need to be rerun with a different starting value.

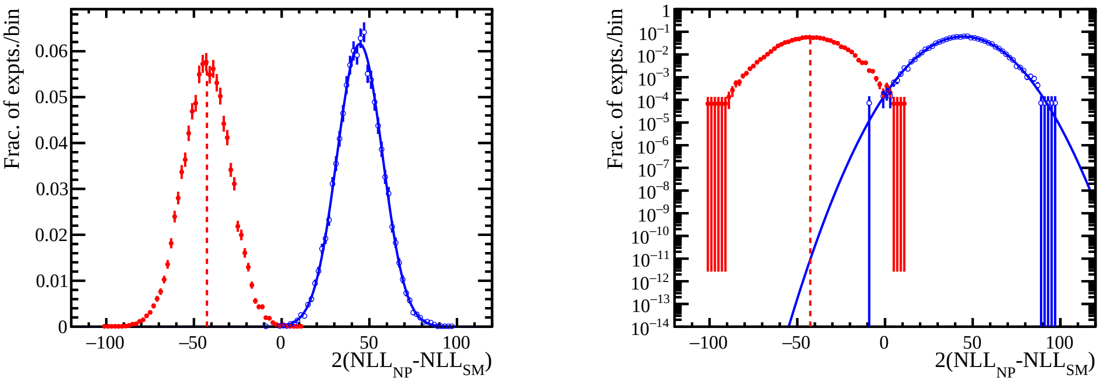

Figure 35: Distribution of the test statistic for fits to the test hypothesis (red full points) and null hypothesis (blue open points). The dashed red line denotes the median of the test statistic from fits to the test hypothesis. The solid blue curve is a fit of a gaussian distribution to the distribution of the test statistic from fits to the null hypothesis. The left and right plot are for a linear and log y-axis scale respectively.

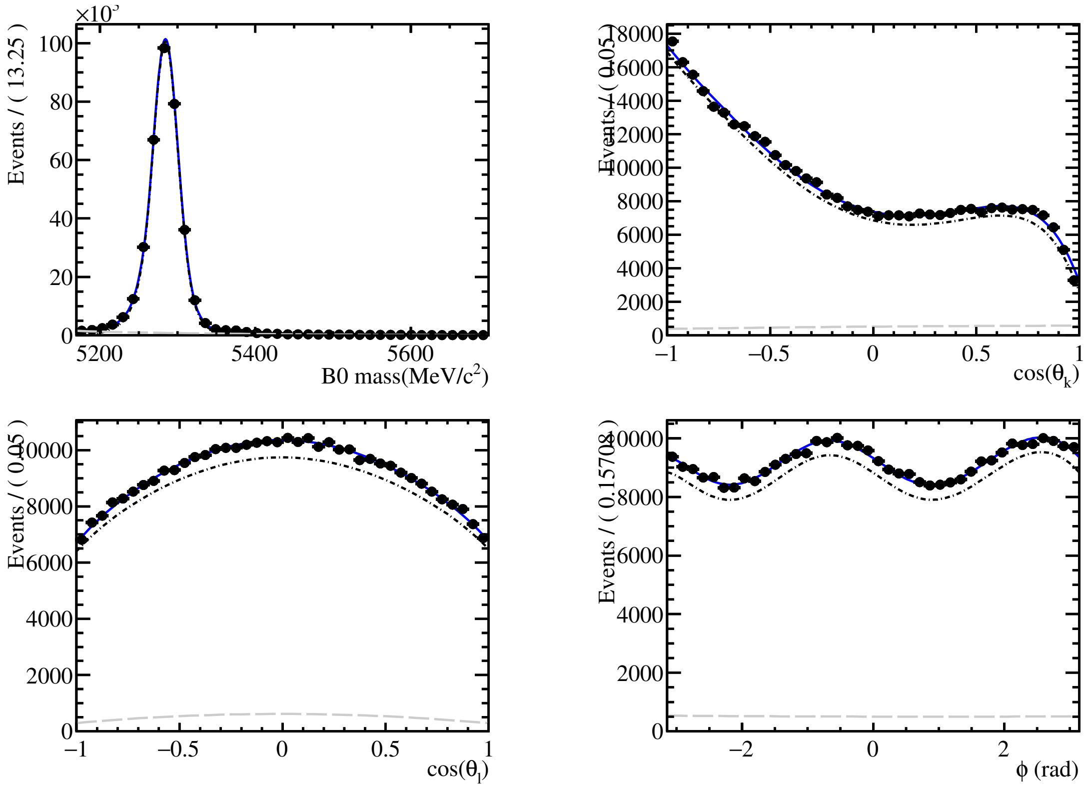

Figure 36: Mass and angular projections of the results of the fit to $B^0 \to J/\psi\, K^{*0}$ data in $796 < m_{K\pi} < 996$ MeV/c^2.

7 Correlations

The correlation between two random variables X,Y is defined as

$$\mathrm{cor}(X,Y) = \frac{\mathrm{cov}(X,Y)}{\sigma_X \sigma_Y} = \frac{\langle (X - \langle X \rangle)(Y - \langle Y \rangle) \rangle}{\sigma_X \sigma_Y} \tag{98}$$

where cov is the covariance between the two random variables, σ the standard deviation and $\langle\rangle$ the expectation value operator. Although most of the angular terms in Eq. 13 are orthogonal this does not mean that they are also uncorrelated. The correlation of the different angular terms can be calculated analytically using their moments:

$$\mathrm{cor}(S_i, S_k) = \frac{\langle f_i f_k \rangle - \langle f_i \rangle \langle f_k \rangle}{\sqrt{\langle f_i^2 \rangle - \langle f_i \rangle^2} \sqrt{\langle f_k^2 \rangle - \langle f_k \rangle^2}} \tag{99}$$

The correlation matrix of the angular terms for the different q^2 bins is shown in Figs. 37-39. A detailed calculation can be found in appendix W.

The correlation can also be determined performing toy studies. The mean correlation of multiple toys can be calculated from the individual results. The process is separated in two steps. In a first step the mean value of the observable is calculated. Afterwards the correlation can be calculated via the following formula:

$$\mathrm{cor}(S_i, S_k) = \frac{1}{N_{\mathrm{toys}}} \sum_{\mathrm{toys}} \frac{(S_i - \langle S_i \rangle)(S_k - \langle S_k \rangle)}{\sigma_{S_i} \sigma_{S_k}} \tag{100}$$

The toy studies performed to measure the correlation are based on the official MC sample and the nominal observable fit. In Fig. 40 the correlation for two sets of variables which have a significant correlation is shown, using signal decays only. Besides the analytical calculation from the PDF also the correlation determined with toy studies using the method of moments and the likelihood fit is shown. The method of moments seems to better reproduce the analystical predictions, possibly due to the presence of the physical boundaries for the likelihood fit of the observables.

The correlation of background and signal events is different. Thus including background in the toy studies modifies also the measured correlation, as can be seen in Fig. 41. The background is mainly uncorrelated which makes the total correlations smaller.

There is an intrinsic correlation between the angular terms which originates directly from the PDF. However, there can be also an additional correlation introduced in the measurement by the angular acceptance and statistical fluctuations of the data set.

7.1 Measuring Correlation with the Fit Likelihood profile

A correlation matrix is provided by Hesse. This matrix is the inverse of the second derivate matrix at the minimum. However, if the minimum is near a (physical) boundary the likelihood becomes highly non-Gaussian and the calculation by `Minuit` via the second derivatives no longer accurately reflects the correlations.

A possibility to take the boundaries into account is to scan the 2D likelihood profile. For each set of two parameters the 2D likelihood profile is sampled and the correlation is calculated via the following formula:

$$cor(S_i, S_k) = \frac{1}{\sum p_{\text{point}}} \sum\nolimits_{\text{point}} p_{\text{point}} \frac{(S_{i,\text{point}} - S_i)(S_{k,\text{point}} - S_k)}{\sigma_{S_i}\sigma_{S_k}} \tag{101}$$

where p_{point} is the likelihood at the sampled point.

In Fig. 42 the different methods are compared in a toy study. The mean of the correlation factors of Hesse and the likelihood scan method are compared to the measured correlation of the fit (as explained in the previous chapter). Whereas in some regions the mean of the matrix from `Hesse` shows deviations from the measured correlation of the fit, the likelihood scan method performs significantly better.

7.2 Measuring Correlation with the Bootstrapping Method

The full covariance matrix and therefore the correlation between observables can be easily determined with the Bootstrapping method. Detailed information on this method can be found in Ref. [34]. The ensamble of pseudo-experiments determined with the bootstrapping method can be used to estimate the experimental covariance matrix statistically according with the following formula:

$$cor(S_i, S_k) = \frac{1}{N_{\text{samples}}} \sum\nolimits_{\text{samples}} \frac{(S_{i,\text{sample}} - S_{]})(S_{k,\text{sample}} - S_k)}{\sigma_{S_{i,\text{sample}}}\sigma_{S_{k,\text{sample}}}}. \tag{102}$$

The result of a toy study comparing this method to the measured correlation can be seen in Fig. 43. There is a good agreement between the mean of the Bootstrap results and the measured correlation of the results from the Method of Moments.

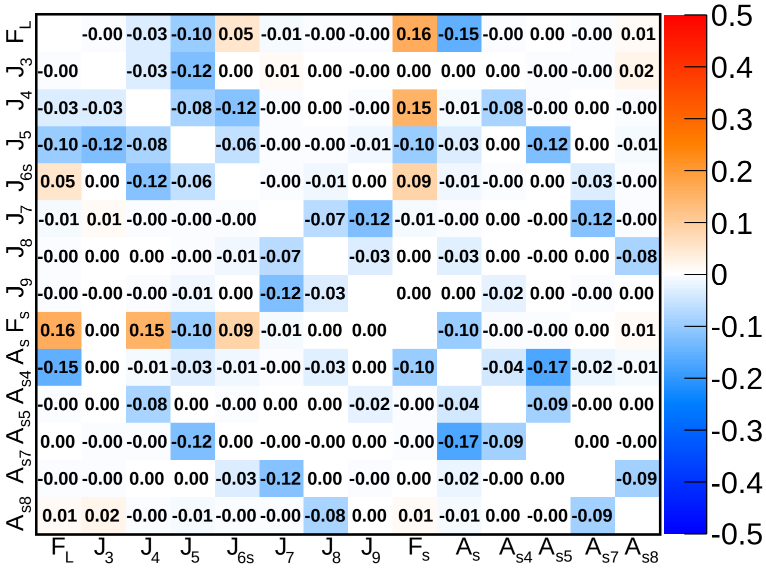

Figure 37: Correlation Matrix for the different angular terms calculated analytically from the pdf for $0.1\,\mathrm{GeV}^2/c^4 < q^2 < 0.98\,\mathrm{GeV}^2/c^4$.

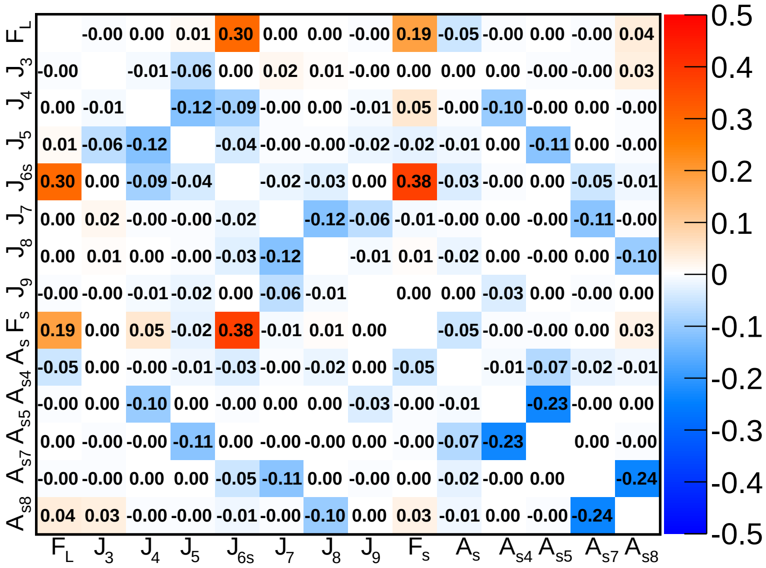

Figure 38: Correlation matrix for the different angular terms calculated analytically from the pdf for $1.1\,\mathrm{GeV}^2/c^4 < q^2 < 2.5\,\mathrm{GeV}^2/c^4$.

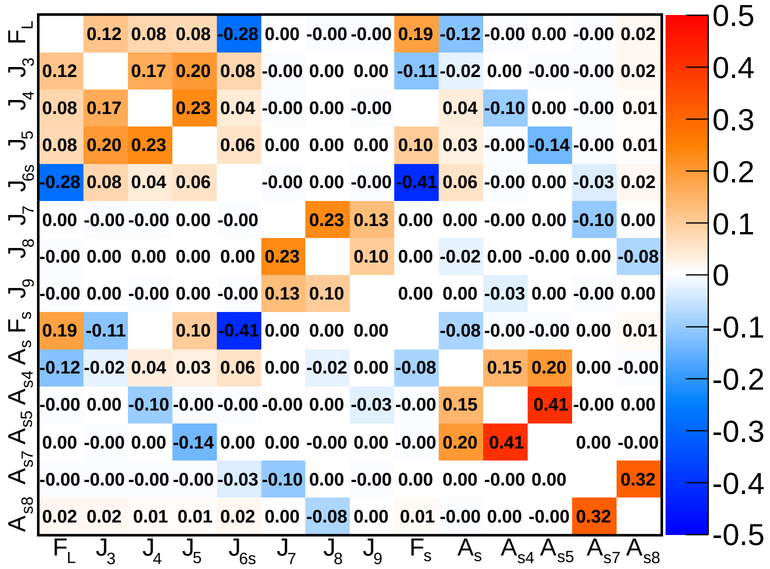

Figure 39: Correlation Matrix for the different angular terms calculated analytically from the pdf for $17\,\mathrm{GeV}^2/c^4 < q^2 < 19\,\mathrm{GeV}^2/c^4$.

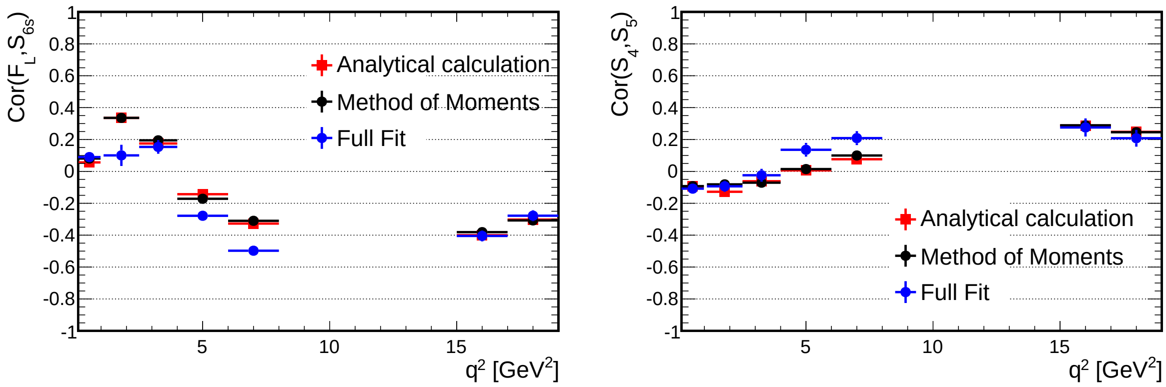

Figure 40: Correlation between two sets of variables which have a significant correlation, in bins of q^2. Both the analytical calculation and the toy studies (MoM, Fit) are signal only.

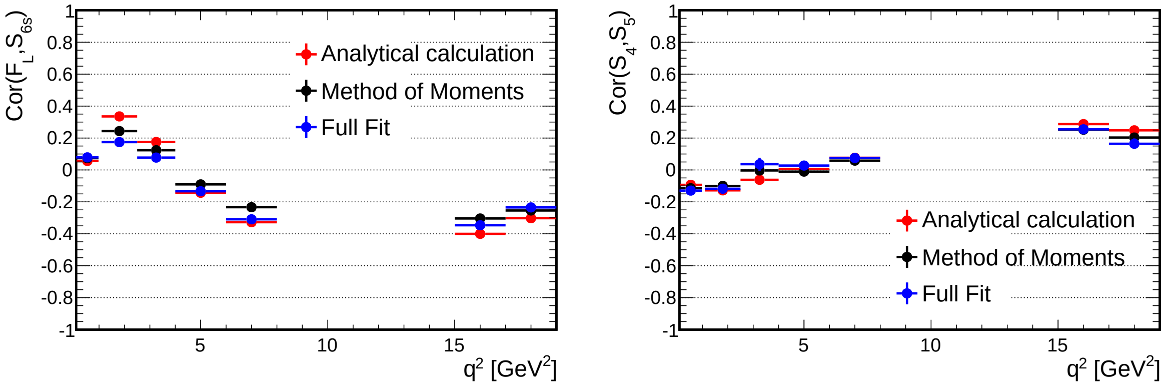

Figure 41: Correlation between two sets of variables which have a significant correlation, in bins of q^2. The toys are done including background, in the analytical calculation the effect of background is ignored.

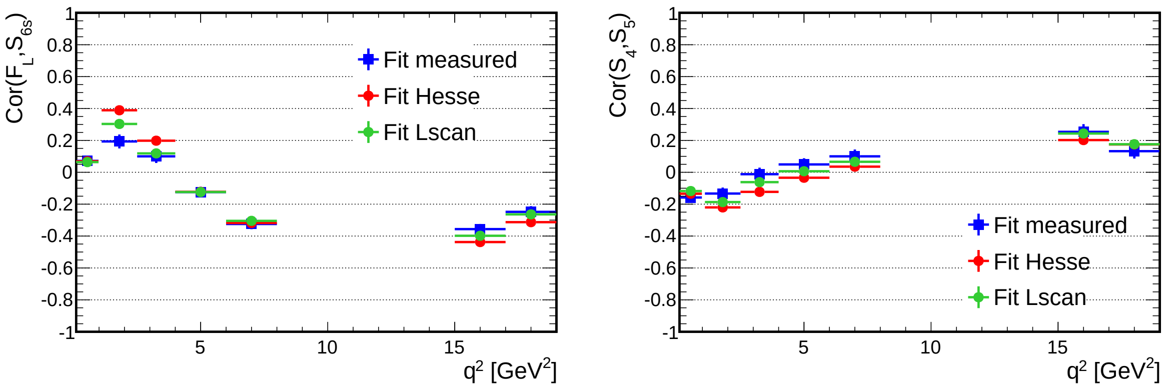

Figure 42: Correlation between two sets of variables which have a significant correlation, in bins of q^2. Shown is the measured correlation of the fit and the mean of the Hesse matrix and the Likelihood scan method.

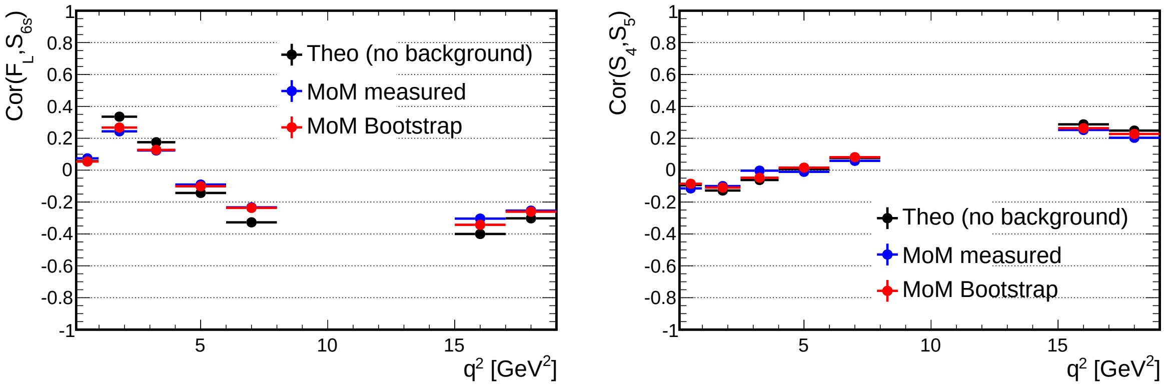

Figure 43: Correlation between two sets of variables which have a significant correlation, in bins of q^2. Shown is the measured correlation of the Method of Moments (over all toys) and the mean of correlations calculated with the Bootstrapping method.

8 Efficiencies

8.1 Acceptance parametrisation

To correct for the distortion caused by reconstruction and selection of the signal decay, Monte Carlo simulated signal events are used. The acceptance effect can be parameterised using Legendre polynomials. While in the previous analyses [1, 2], the acceptance effect was assumed to factorise in the three decay angles, *i.e.* $\varepsilon(\cos\theta_l, \cos\theta_K, \phi) = \varepsilon(\cos\theta_l) \times \varepsilon(\cos\theta_K) \times \varepsilon(\phi)$, in this iteration of the angular analysis, factorisation in the angles is not assumed. Instead, the acceptance can be parameterised in four dimensions, q^2, $\cos\theta_l$, $\cos\theta_l$ and ϕ according to

$$\varepsilon(\cos\theta_\ell, \cos\theta_K, \phi, q^2) = \sum_{k,l,m,n} c_{k,l,m,n} P(\cos\theta_\ell, k) P(\cos\theta_K, l) P(\phi, m) P(q^2, n). \tag{103}$$

where $P(x, m)$ are Legendre polynomials in x of order m and $-1 \leq x \leq 1$. The coefficicients $c_{k,l,m,n}$ are determined from a moment analysis of $B^0 \to K^{*0}\mu^+\mu^-$ phase-space MC

$$\begin{aligned} c_{k,l,m,n} = \frac{1}{N'} \sum_{i=1}^{N} w_i \Bigg[& \left(\frac{2k+1}{2}\right) \left(\frac{2l+1}{2}\right) \left(\frac{2m+1}{2}\right) \left(\frac{2n+1}{2}\right) \\ & \times P(\cos\theta_\ell, k) P(\cos\theta_K, l) P(\phi, m) P(q^2, n) \Bigg] \end{aligned} \tag{104}$$

where N is the number of candidates in the MC sample, w_i is a per-candidate weight used to correct for the non-flat phasespace distribution of events in q^2 and the data-driven corrections for $p_{\mathrm{T}}(B^0)$, χ^2_{Vtx} and track multiplicity. The normalisation is given by

$$N' = \sum_{i=1}^{N} w_i \quad . \tag{105}$$

The factors of $(2k + 1)/2$ etc. arise from the orthogonality of the Legendre Polynomials,

$$\int_{-1}^{+1} P(x, m) P(x, m') \mathrm{d}x = \frac{2}{2m+1} \delta_{mm'} \ . \tag{106}$$

8.2 Four-dimensional acceptance

The acceptance is modeled using Legendre polynomials of the lowest order that show good description of the angular acceptance effect. For q^2, Legendre polynomials of order five and lower are used. For the decay angles polynomials of order four and lower are used for $\cos\theta_l$, order five and lower for $\cos\theta_K$ and order six and lower for the angle ϕ.

This results in a total of 720 coefficients that are determined according to Sec. 8.1 using a total of 1.406 M reconstructed and selected Monte Carlo simulated signal events. The resulting one-dimensional projections of the efficiency on q^2 and the three decay

Figure 44: One-dimensional projections of the four-dimensional efficiency parametrisation on q^2, $\cos\theta_l$, $\cos\theta_K$, and ϕ.

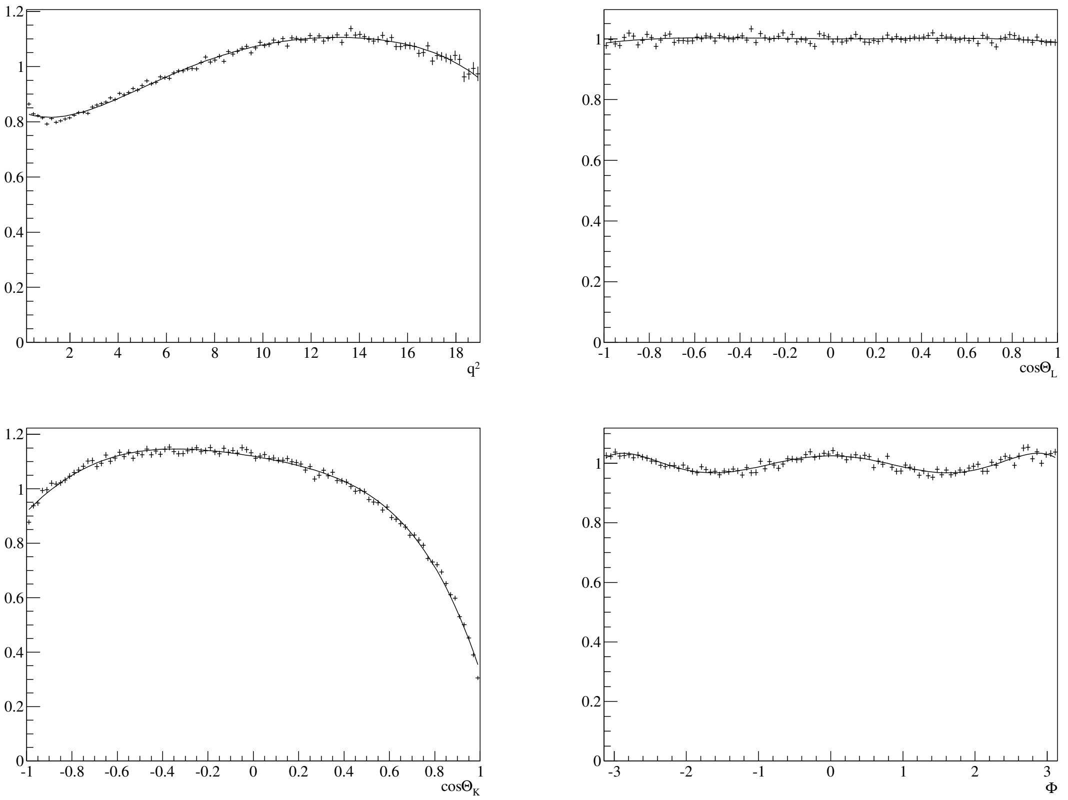

angles is given in Fig. 44. Good agreement is seen for the one-dimensional projections. Figs. 45, 46 and 47 show the one-dimensional projections in bins of q^2 which illustrates the change of the efficiency with q^2. In addition, Fig. 48 gives two-dimensional projections of the efficiency parameterisation and the two-dimensional efficiency determined from a four-dimensional histogram. Again, the four-dimensional parametrisation seems to describe the acceptance effect well. It should be noted that the efficiency drops towards zero for some corners, visible for example in Fig. 48 for $|\cos\theta_l| \to 1$ and very low q^2. It is possible that the parametrisation becomes negative which is problematic for an efficiency. For toy events that are distributed flat in q^2 and the three decay angles this is the case for less than 0.2% of events.

Figure 45: One-dimensional projections of the four-dimensional efficiency parametrisation on $\cos\theta_l$ in bins of q^2.

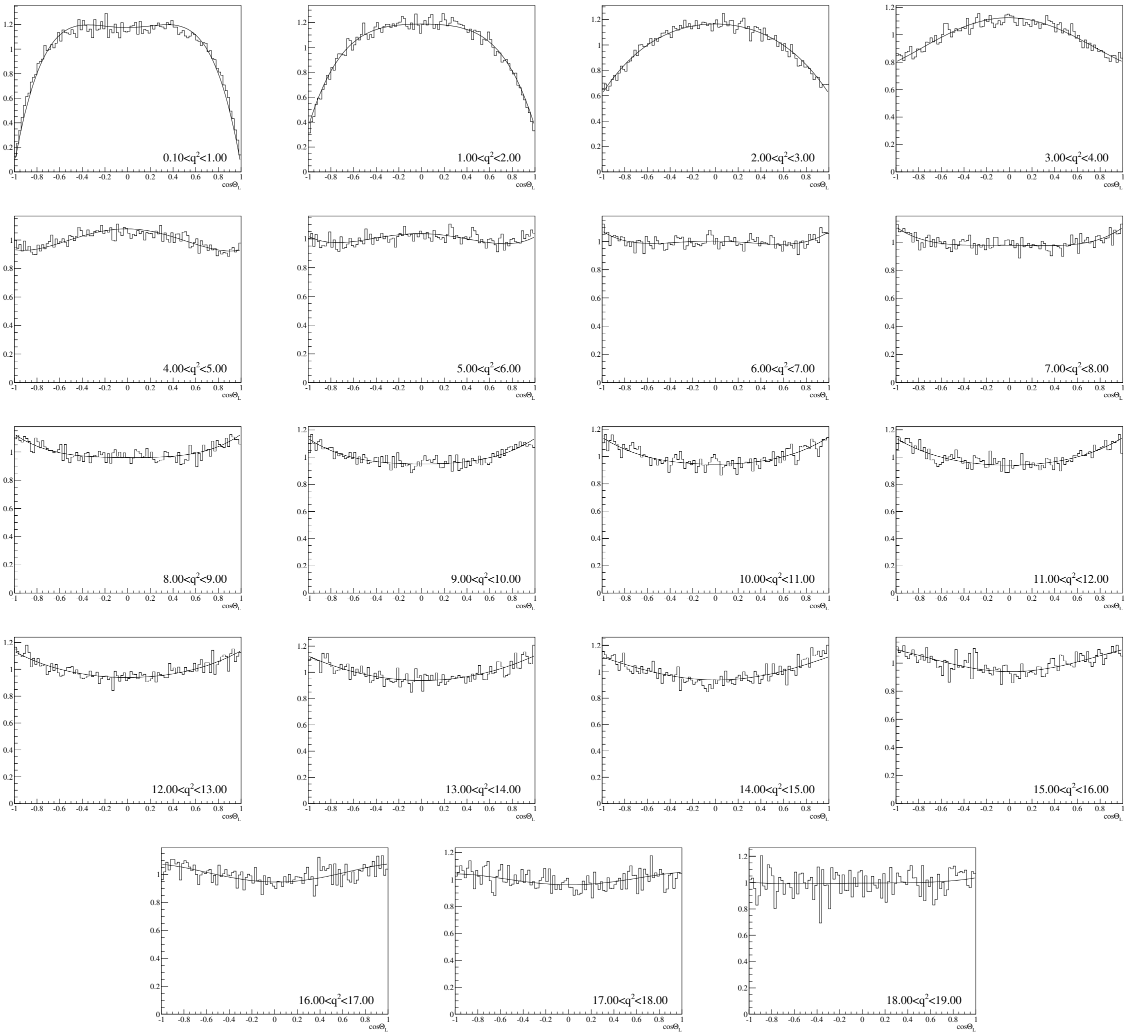

8.3 Further tests of the four-dimensional acceptance parametrisation

As already discussed in Sec. 6.2.3, the change of normalisation of the PDF is the main effect of the acceptance and the quantities

$$\xi_i = \int \varepsilon(q^2, \vec{\Omega}) f_i(\vec{\Omega}) \mathrm{d}\vec{\Omega} \tag{107}$$

can be used to determine the changed normalisation. It is therefore important to crosscheck these quantities for different acceptance parametrisations. In Fig. 49 the ξ_i determined

Figure 46: One-dimensional projections of the four-dimensional efficiency parametrisation on $\cos\theta_K$ in bins of q^2.

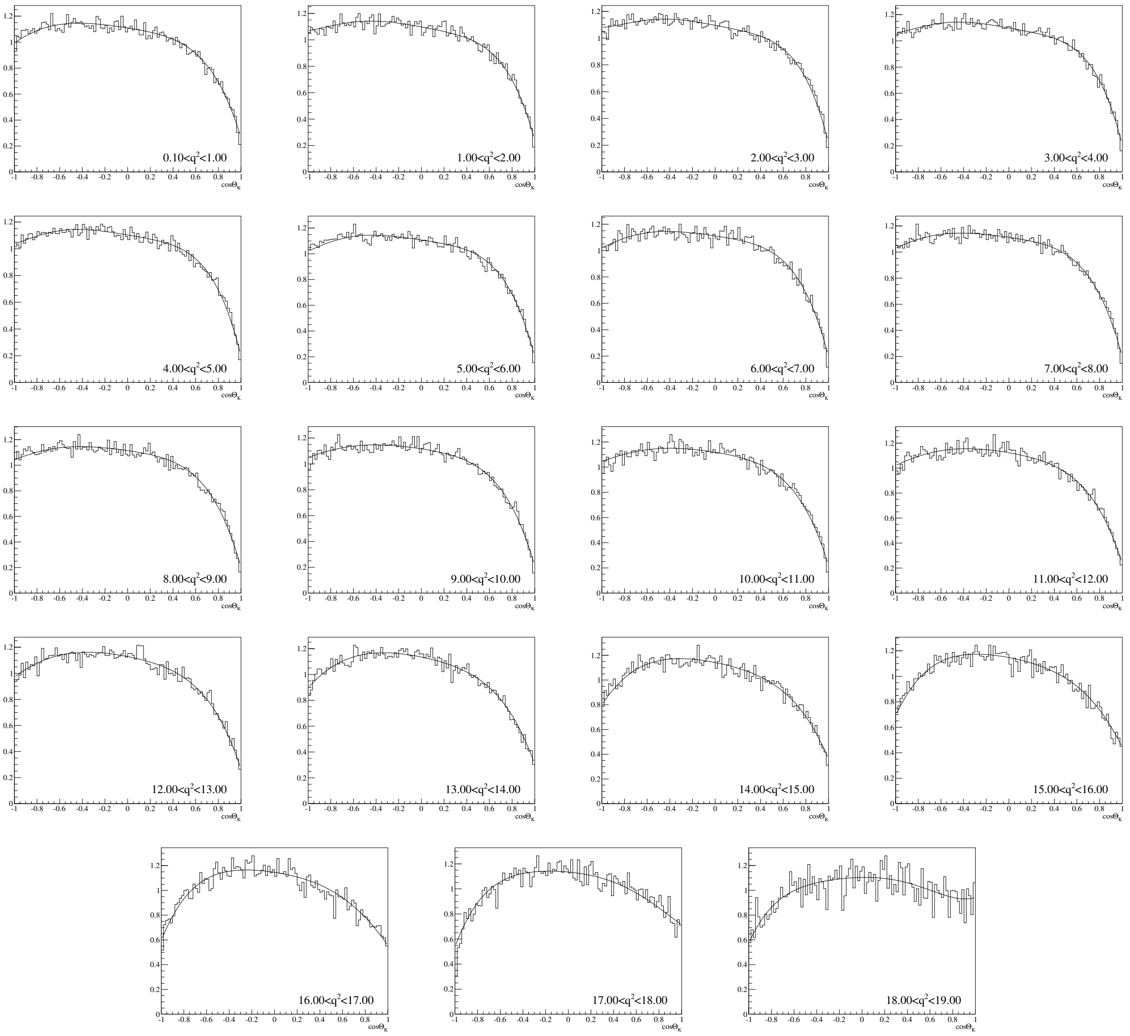

from the four-dimensional acceptance parametrisation (black line) are compared to ξ_i determined using four-dimensional histograms (black histogram) and ξ_i determined using the so-called *unbinned method* (blue histogram). The *unbinned method* determines the ξ_i according to

$$\xi_i = \frac{2^3\pi}{N_{\text{events}}}\sum_e f_i(\vec{\Omega}_e). \tag{108}$$

The results from all approaches are in very good agreement.

In addition, it is useful to compare the performance of the four-dimensional Legendre parametrisation with other parametrisations. To determine wether the parametrisation

Figure 47: One-dimensional projections of the four-dimensional efficiency parametrisation on ϕ in bins of q^2.

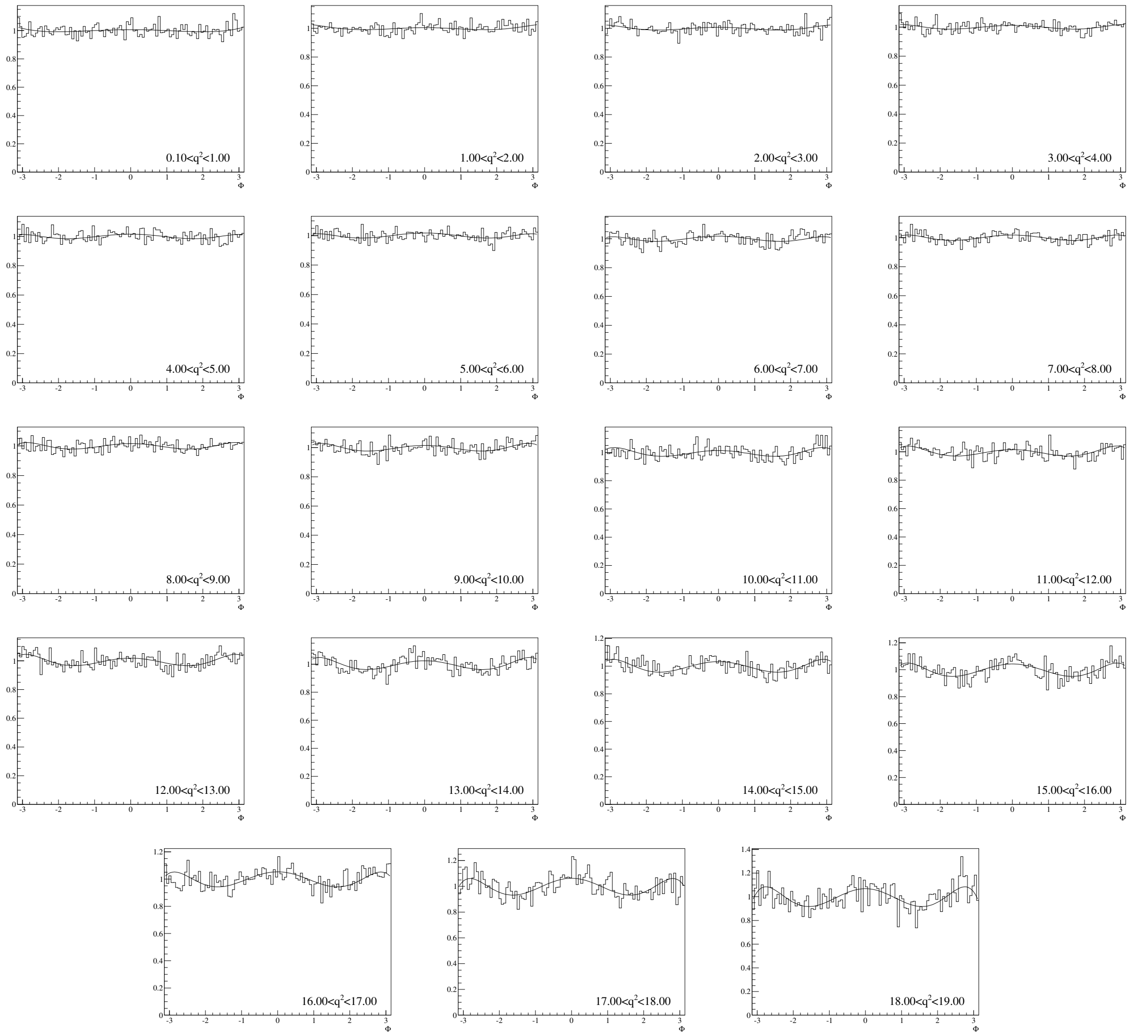

describes the efficiency in simulation well, the modified χ^2 given by

$$\frac{\chi^2}{N_{\text{bins}}} = \sum_{\text{bin } i} \frac{(N_{\text{sel } i} - \varepsilon_{\text{bin } i} N_{\text{tot}})^2}{N_{\text{bins}}} \tag{109}$$

is a helpful quantity. Here, N_{bins} gives the number of bins which is $N_{\text{bins}} = 19_{q^2} \times 10_{\cos\theta_l} \times 10_{\cos\theta_K} \times 10_{\phi} = 19\,000$. For the four-dimensional efficiency this yields $\chi^2/N_{\text{bins}} = 1.53$. This compares favourably with the assumption of factorisation in 19 q^2 which results in $\chi^2/N_{\text{bins}} = 1.64$.

Figure 48: Two-dimensional projections of the four-dimensional efficiency parametrisation on q^2, $\cos\theta_l$, $\cos\theta_K$, and ϕ and comparison with the corresponding efficiency projection determined from histograms.

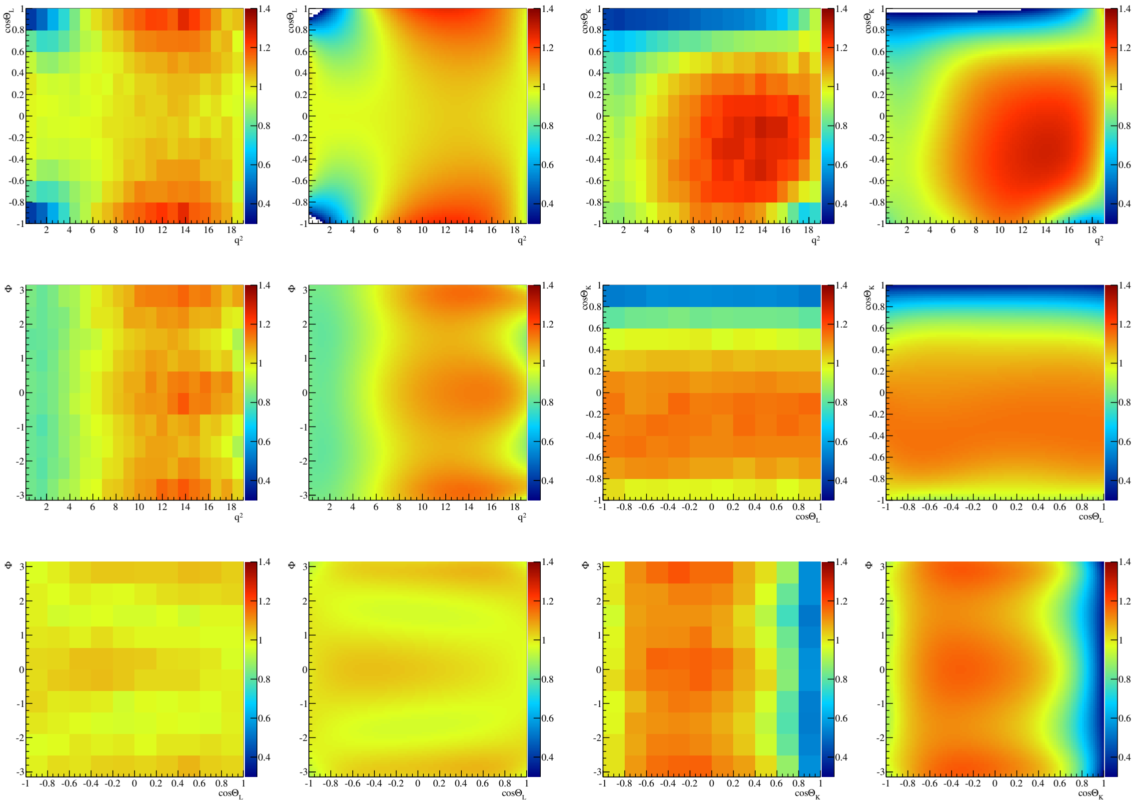

Figure 49: Integrated angular terms $\xi_i = \int \varepsilon(q^2, \vec{\Omega}) f_i(\vec{\Omega}) \mathrm{d}\vec{\Omega}$ needed to account for the change in normalisation due to the acceptance effect. The ξ_i are shown for the four-dimensional parametrisation (black line), the determination from four-dimensional histograms (black histogram) and the *unbinned method* (blue histogram). The red dashed lines show flat acceptance in all variables.

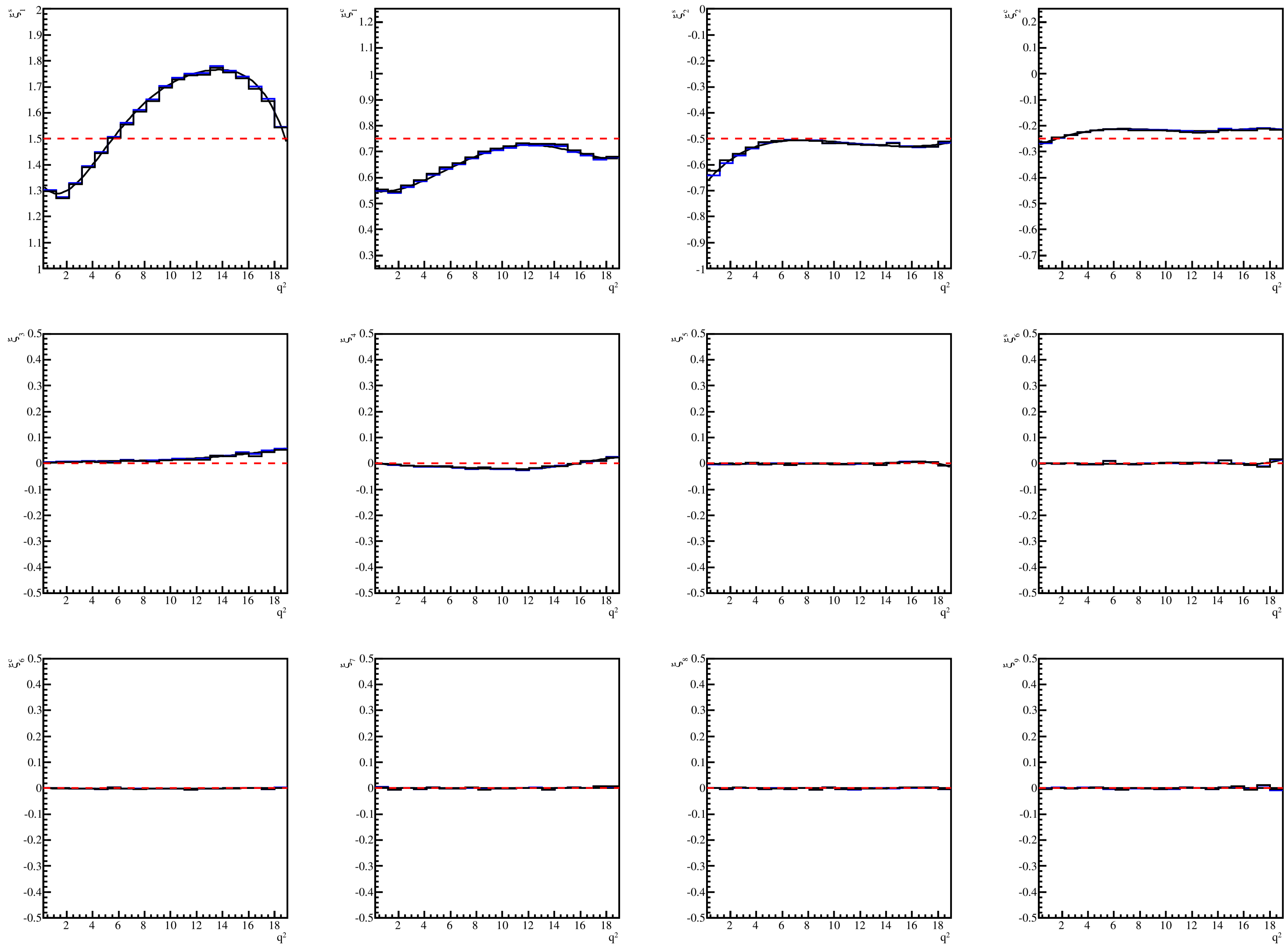

9 Results

This section will contain the results of the angular analysis on data. It will be filled when blinded results from the different methods of angular analysis become available.

9.1 Results of the fits for the observables

The angular observables are determined using an angular maximum likelihood fit as described in Sec. 6.2, including the simulaneous fit of the $m_{K\pi}$ distribution as described in Sec. 6.2.12. The varied parameters for every q^2 bin are the signal fraction $f_{\rm sig}$, the parameter τ_m describing the exponential slope of the mass distribution of the combinatorial background, six coefficients to describe the background angular distribution, one parameter to describe the background distribution in $m_{K\pi}$ and finally the P-wave observables $F_{\rm L}, A_{\rm FB}, S_{3,4,5,7,8,9}$ and the S-wave parameters $F_S, S_{S1,\ldots,S5}$. The four dimensional acceptance correction described in Sec. 8 is included. For the two large q^2 bins $[1.1, 6.0]\,{\rm GeV}^2/c^4$ and $[15.0, 19.0]\,{\rm GeV}^2/c^4$ a weighted fit approach is used, since the acceptance significantly varies over these large bins. For all other bins, the acceptance is evaluated at the bin center as described in Sec. 6.2.3. The projections of the probability density function on the decay angles, the reconstructed B^0 mass and $m_{K\pi}$ are given in Figs. 50-54 for the signal region, $\pm 50\,{\rm MeV}/c^2$ around the nominal B^0_s mass. The results for the CP-averaged observables from the likelihood fit method are given in Tab. 32. The first given uncertainty is statistical, determined using the Feldman-cousing method [24], with 4 000 toys for each point. The corresponding Feldman-Cousins confidence intervals are shown in Figs. 117-124 in Appendix D. The second uncertainty is the quadratic sum of the systematic uncertainties, which are detailed in Sec. 10.1. The linear correlations are given in Tab. 119 in Appendix E.

The CP asymmetries A_i are given in Tab. 33 with the corresponding Feldman-Cousins confidence intervals in Figs. 125-131 in Appendix D. For the Feldman-Cousins method 4 000 toys are generated at each point. The linear correlations between these observables are given in Tab. 120 in Appendix E. Finally, the results for the $P_i^{(\prime)}$ basis described in Sec. 6.1.5 are given in Tab. 34, with Feldman-Cousins confidence intervals given in Figs. 132-138 in Appendix D. For the Feldman-Cousins method 4 000 toys are generated at each point, with the exception of P_5', where 10 000 toys are generated. Linear correlations are available in Tab. 121 in Appendix E.

$0.1 < q^2 < 0.98\,\mathrm{GeV}^2/c^4$

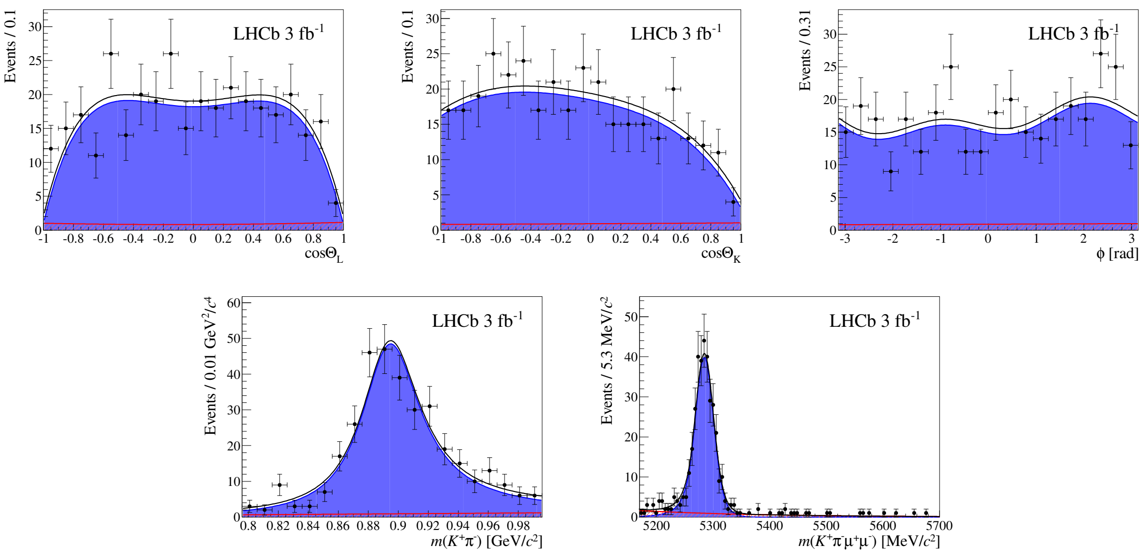

$1.1 < q^2 < 2.5\,\mathrm{GeV}^2/c^4$

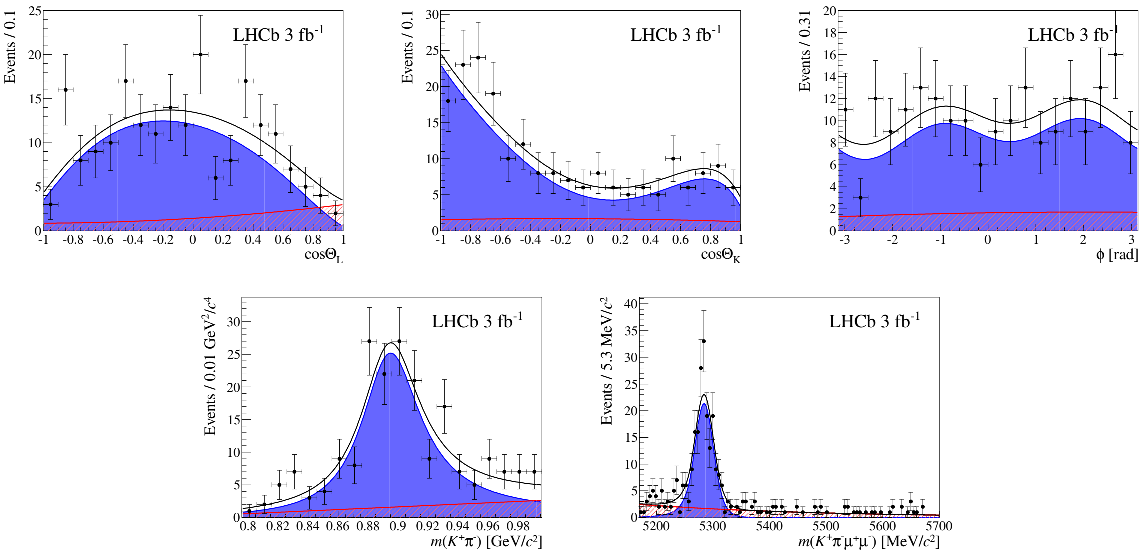

Figure 50: Projections of the fitted probability density function on the decay angles, $m_{K\pi}$ and the reconstructed B^0 mass in bins of q^2.

$2.5 < q^2 < 4.0\,\text{GeV}^2/c^4$

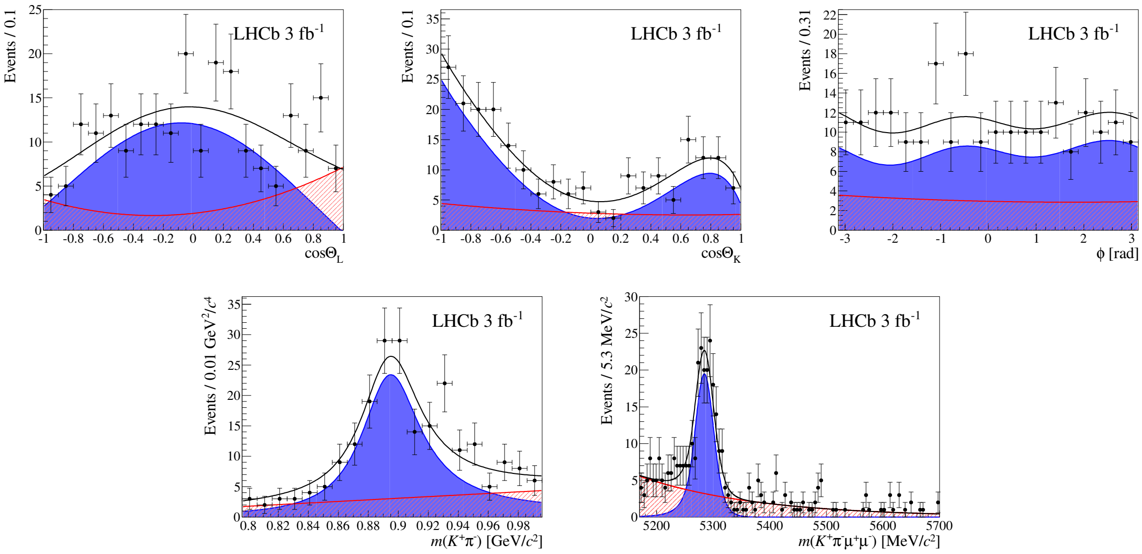

$4.0 < q^2 < 6.0\,\text{GeV}^2/c^4$

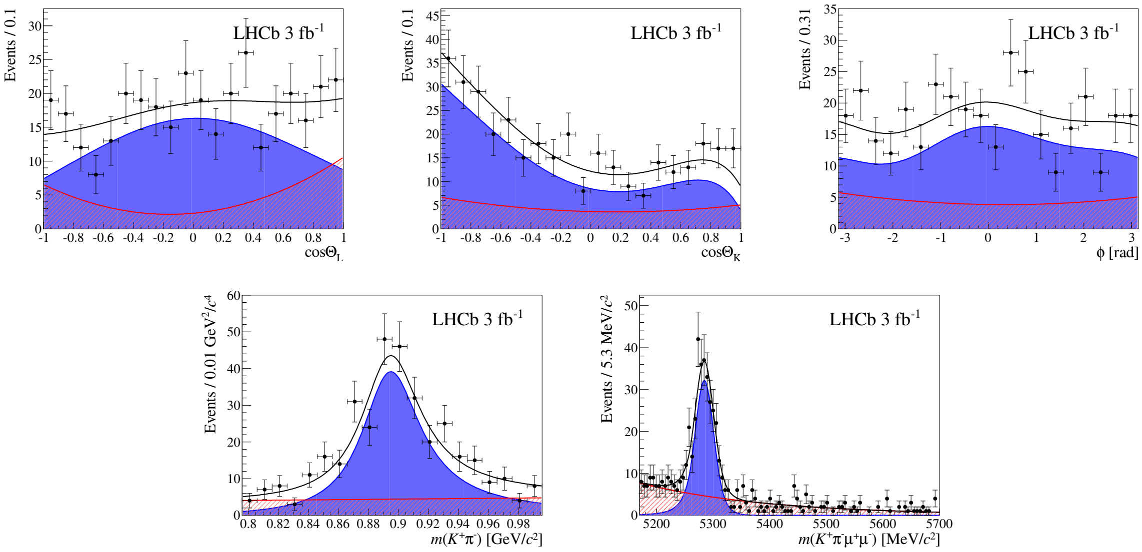

Figure 51: Projections of the fitted probability density function on the decay angles, $m_{K\pi}$ and the reconstructed B^0 mass in bins of q^2.

$6.0 < q^2 < 8.0\,\mathrm{GeV}^2/c^4$

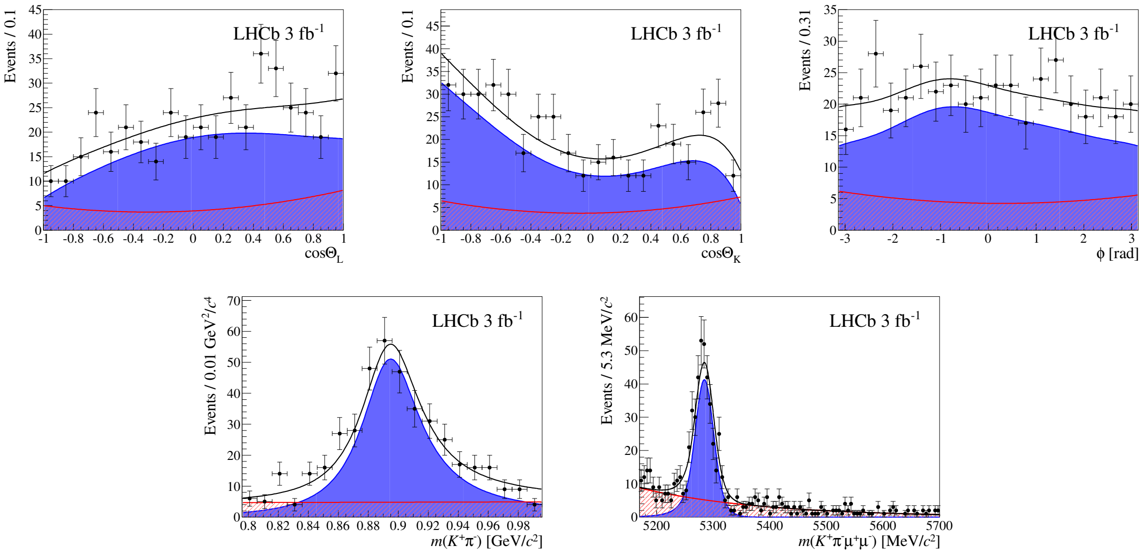

$11.0 < q^2 < 12.5\,\mathrm{GeV}^2/c^4$

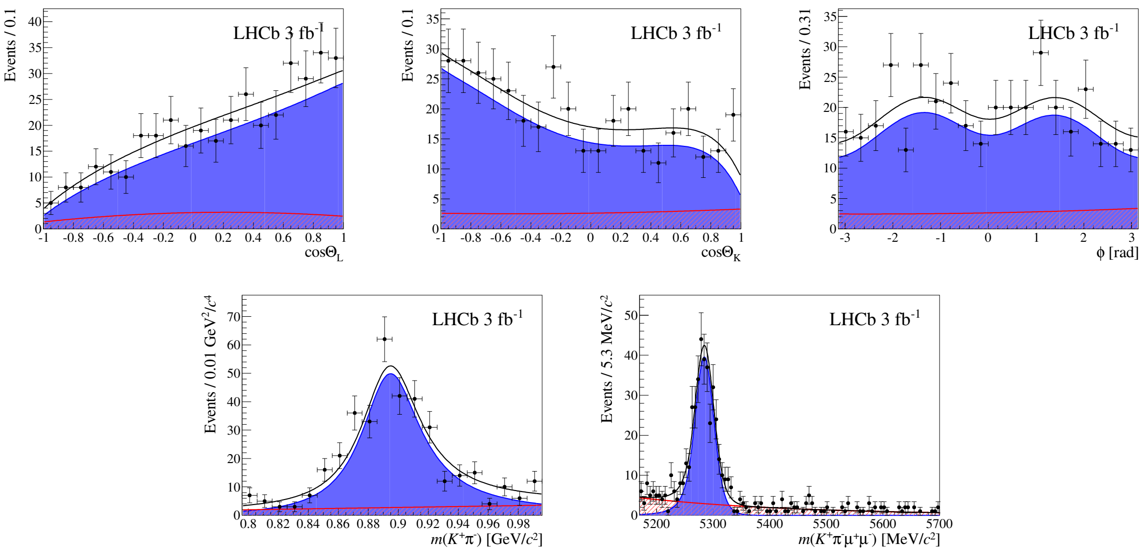

Figure 52: Projections of the fitted probability density function on the decay angles, $m_{K\pi}$ and the reconstructed B^0 mass in bins of q^2.

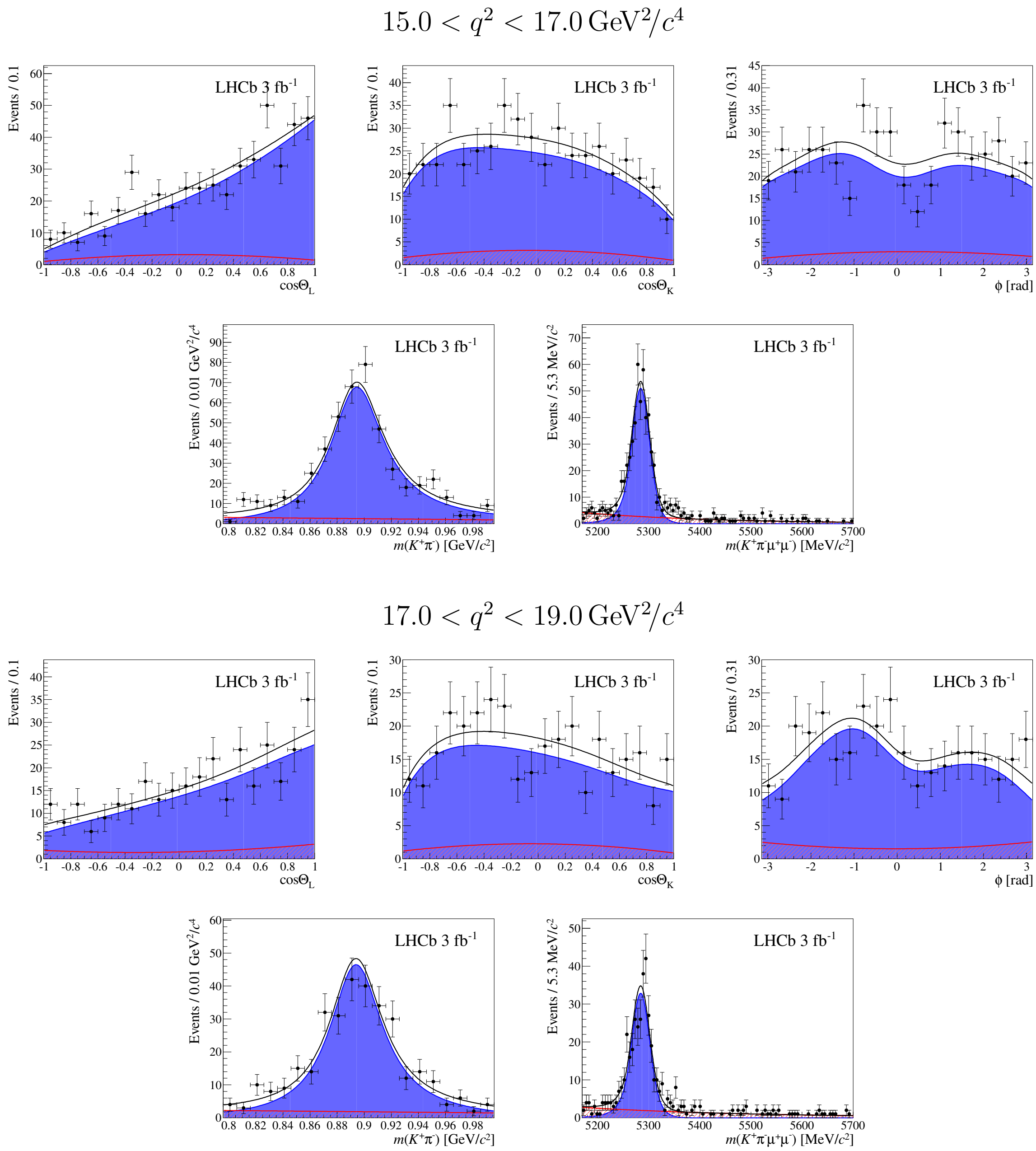

Figure 53: Projections of the fitted probability density function on the decay angles, $m_{K\pi}$ and the reconstructed B^0 mass in bins of q^2.

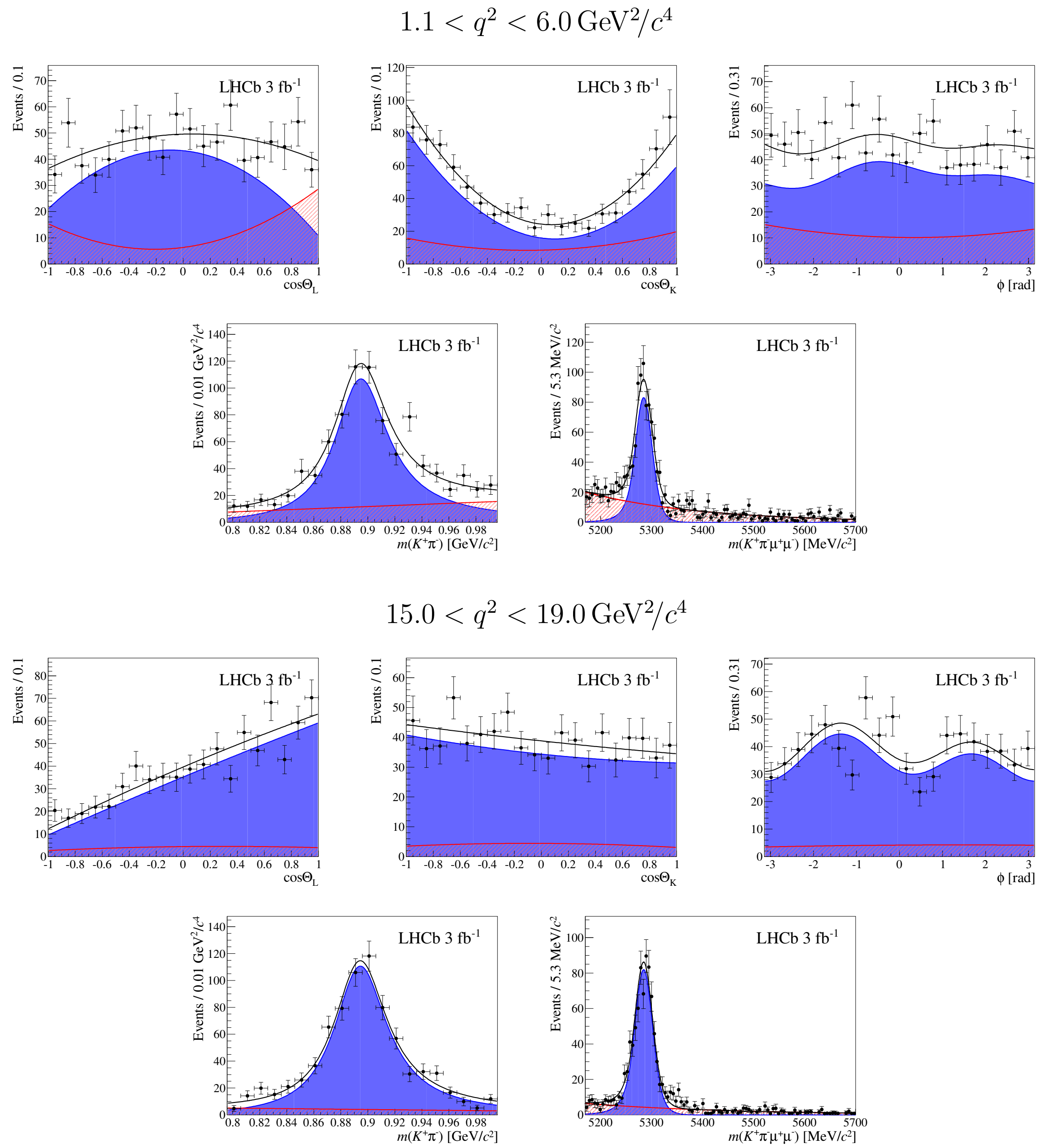

Figure 54: Projections of the fitted probability density function on the decay angles, $m_{K\pi}$ and the reconstructed B^0 mass in bins of q^2.

Table 32: Results for the CP-averaged observables S_i.

$0.1 < q^2 < 0.98\,\mathrm{GeV}^2/c^4$	
Obs.	Value
F_L	$0.263^{+0.045}_{-0.044} \pm 0.017$
S_3	$-0.036^{+0.063}_{-0.063} \pm 0.005$
S_4	$0.082^{+0.068}_{-0.069} \pm 0.009$
S_5	$0.170^{+0.059}_{-0.058} \pm 0.018$
A_FB	$-0.003^{+0.058}_{-0.057} \pm 0.009$
S_7	$0.015^{+0.059}_{-0.059} \pm 0.006$
S_8	$0.079^{+0.076}_{-0.075} \pm 0.007$
S_9	$-0.083^{+0.058}_{-0.057} \pm 0.004$

$1.1 < q^2 < 2.5\,\mathrm{GeV}^2/c^4$	
Obs.	Value
F_L	$0.660^{+0.083}_{-0.077} \pm 0.022$
S_3	$-0.077^{+0.087}_{-0.105} \pm 0.005$
S_4	$-0.077^{+0.111}_{-0.113} \pm 0.005$
S_5	$0.137^{+0.099}_{-0.094} \pm 0.009$
A_FB	$-0.191^{+0.068}_{-0.080} \pm 0.012$
S_7	$-0.219^{+0.094}_{-0.104} \pm 0.004$
S_8	$-0.098^{+0.108}_{-0.123} \pm 0.005$
S_9	$-0.119^{+0.087}_{-0.104} \pm 0.005$

$2.5 < q^2 < 4.0\,\mathrm{GeV}^2/c^4$	
Obs.	Value
F_L	$0.876^{+0.109}_{-0.097} \pm 0.017$
S_3	$0.035^{+0.098}_{-0.089} \pm 0.007$
S_4	$-0.234^{+0.127}_{-0.144} \pm 0.006$
S_5	$-0.022^{+0.110}_{-0.103} \pm 0.008$
A_FB	$-0.118^{+0.082}_{-0.090} \pm 0.007$
S_7	$0.068^{+0.120}_{-0.112} \pm 0.005$
S_8	$0.030^{+0.129}_{-0.131} \pm 0.006$
S_9	$-0.092^{+0.105}_{-0.125} \pm 0.007$

$4.0 < q^2 < 6.0\,\mathrm{GeV}^2/c^4$	
Obs.	Value
F_L	$0.611^{+0.052}_{-0.053} \pm 0.017$
S_3	$0.035^{+0.069}_{-0.068} \pm 0.007$
S_4	$-0.219^{+0.086}_{-0.084} \pm 0.008$
S_5	$-0.146^{+0.077}_{-0.078} \pm 0.011$
A_FB	$0.025^{+0.051}_{-0.052} \pm 0.004$
S_7	$-0.016^{+0.081}_{-0.080} \pm 0.004$
S_8	$0.167^{+0.094}_{-0.091} \pm 0.004$
S_9	$-0.032^{+0.071}_{-0.071} \pm 0.004$

$6.0 < q^2 < 8.0\,\mathrm{GeV}^2/c^4$	
Obs.	Value
F_L	$0.579^{+0.046}_{-0.046} \pm 0.015$
S_3	$-0.042^{+0.058}_{-0.059} \pm 0.011$
S_4	$-0.296^{+0.063}_{-0.067} \pm 0.011$
S_5	$-0.249^{+0.059}_{-0.060} \pm 0.012$
A_FB	$0.152^{+0.041}_{-0.040} \pm 0.008$
S_7	$-0.047^{+0.068}_{-0.066} \pm 0.003$
S_8	$-0.085^{+0.072}_{-0.070} \pm 0.006$
S_9	$-0.024^{+0.059}_{-0.060} \pm 0.005$

$11.0 < q^2 < 12.5\,\mathrm{GeV}^2/c^4$	
Obs.	Value
F_L	$0.493^{+0.049}_{-0.047} \pm 0.013$
S_3	$-0.189^{+0.054}_{-0.058} \pm 0.005$
S_4	$-0.283^{+0.084}_{-0.095} \pm 0.009$
S_5	$-0.327^{+0.076}_{-0.079} \pm 0.009$
A_FB	$0.318^{+0.044}_{-0.040} \pm 0.009$
S_7	$-0.141^{+0.072}_{-0.074} \pm 0.005$
S_8	$-0.007^{+0.070}_{-0.072} \pm 0.005$
S_9	$-0.004^{+0.070}_{-0.073} \pm 0.006$

$15.0 < q^2 < 17.0\,\mathrm{GeV}^2/c^4$	
Obs.	Value
F_L	$0.349^{+0.039}_{-0.039} \pm 0.009$
S_3	$-0.142^{+0.044}_{-0.049} \pm 0.007$
S_4	$-0.321^{+0.055}_{-0.074} \pm 0.007$
S_5	$-0.316^{+0.051}_{-0.057} \pm 0.009$
A_FB	$0.411^{+0.041}_{-0.037} \pm 0.008$
S_7	$0.061^{+0.058}_{-0.058} \pm 0.005$
S_8	$0.003^{+0.061}_{-0.061} \pm 0.003$
S_9	$-0.019^{+0.054}_{-0.056} \pm 0.004$

$17.0 < q^2 < 19.0\,\mathrm{GeV}^2/c^4$	
Obs.	Value
F_L	$0.354^{+0.049}_{-0.048} \pm 0.025$
S_3	$-0.188^{+0.074}_{-0.084} \pm 0.017$
S_4	$-0.266^{+0.063}_{-0.072} \pm 0.010$
S_5	$-0.323^{+0.063}_{-0.072} \pm 0.009$
A_FB	$0.305^{+0.049}_{-0.048} \pm 0.013$
S_7	$0.044^{+0.073}_{-0.072} \pm 0.013$
S_8	$0.013^{+0.071}_{-0.070} \pm 0.005$
S_9	$-0.094^{+0.065}_{-0.067} \pm 0.004$

$1.1 < q^2 < 6.0\,\mathrm{GeV}^2/c^4$	
Obs.	Value
F_L	$0.690^{+0.035}_{-0.036} \pm 0.017$
S_3	$0.012^{+0.038}_{-0.038} \pm 0.004$
S_4	$-0.155^{+0.057}_{-0.056} \pm 0.004$
S_5	$-0.023^{+0.050}_{-0.049} \pm 0.005$
A_FB	$-0.075^{+0.032}_{-0.034} \pm 0.007$
S_7	$-0.077^{+0.050}_{-0.049} \pm 0.006$
S_8	$0.028^{+0.058}_{-0.057} \pm 0.008$
S_9	$-0.064^{+0.042}_{-0.041} \pm 0.004$

$15.0 < q^2 < 19.0\,\mathrm{GeV}^2/c^4$	
Obs.	Value
F_L	$0.344^{+0.028}_{-0.030} \pm 0.008$
S_3	$-0.163^{+0.033}_{-0.033} \pm 0.009$
S_4	$-0.284^{+0.038}_{-0.041} \pm 0.007$
S_5	$-0.325^{+0.036}_{-0.037} \pm 0.009$
A_FB	$0.355^{+0.027}_{-0.027} \pm 0.009$
S_7	$0.048^{+0.043}_{-0.043} \pm 0.006$
S_8	$0.028^{+0.044}_{-0.045} \pm 0.003$
S_9	$-0.053^{+0.039}_{-0.039} \pm 0.002$

Table 33: Results for the CP asymmetries A_i.

$0.1 < q^2 < 0.98\,\mathrm{GeV}^2/c^4$ Obs.	Value
A_3	$0.006^{+0.064}_{-0.065} \pm 0.005$
A_4	$-0.068^{+0.071}_{-0.073} \pm 0.009$
A_5	$0.001^{+0.061}_{-0.059} \pm 0.018$
A_6	$0.122^{+0.076}_{-0.075} \pm 0.011$
A_7	$0.076^{+0.061}_{-0.060} \pm 0.006$
A_8	$-0.031^{+0.074}_{-0.074} \pm 0.007$
A_9	$0.030^{+0.062}_{-0.061} \pm 0.004$

$1.1 < q^2 < 2.5\,\mathrm{GeV}^2/c^4$ Obs.	Value
A_3	$0.042^{+0.097}_{-0.087} \pm 0.005$
A_4	$0.235^{+0.125}_{-0.109} \pm 0.005$
A_5	$-0.114^{+0.099}_{-0.105} \pm 0.009$
A_6	$0.037^{+0.102}_{-0.091} \pm 0.016$
A_7	$-0.087^{+0.091}_{-0.093} \pm 0.004$
A_8	$-0.044^{+0.108}_{-0.113} \pm 0.005$
A_9	$-0.004^{+0.092}_{-0.098} \pm 0.005$

$2.5 < q^2 < 4.0\,\mathrm{GeV}^2/c^4$ Obs.	Value
A_3	$-0.111^{+0.087}_{-0.109} \pm 0.006$
A_4	$-0.007^{+0.130}_{-0.135} \pm 0.007$
A_5	$-0.005^{+0.107}_{-0.106} \pm 0.008$
A_6	$0.022^{+0.115}_{-0.096} \pm 0.010$
A_7	$-0.032^{+0.109}_{-0.115} \pm 0.005$
A_8	$-0.071^{+0.124}_{-0.131} \pm 0.006$
A_9	$-0.228^{+0.114}_{-0.152} \pm 0.007$

$4.0 < q^2 < 6.0\,\mathrm{GeV}^2/c^4$ Obs.	Value
A_3	$-0.173^{+0.070}_{-0.079} \pm 0.006$
A_4	$-0.168^{+0.086}_{-0.085} \pm 0.008$
A_5	$-0.059^{+0.071}_{-0.073} \pm 0.011$
A_6	$-0.023^{+0.082}_{-0.075} \pm 0.005$
A_7	$0.041^{+0.083}_{-0.082} \pm 0.004$
A_8	$0.004^{+0.093}_{-0.095} \pm 0.005$
A_9	$0.062^{+0.078}_{-0.072} \pm 0.004$

$6.0 < q^2 < 8.0\,\mathrm{GeV}^2/c^4$ Obs.	Value
A_3	$0.064^{+0.067}_{-0.064} \pm 0.011$
A_4	$-0.037^{+0.073}_{-0.073} \pm 0.011$
A_5	$0.129^{+0.067}_{-0.066} \pm 0.012$
A_6	$0.047^{+0.062}_{-0.060} \pm 0.011$
A_7	$0.035^{+0.065}_{-0.067} \pm 0.003$
A_8	$-0.043^{+0.070}_{-0.069} \pm 0.006$
A_9	$0.110^{+0.061}_{-0.060} \pm 0.005$

$11.0 < q^2 < 12.5\,\mathrm{GeV}^2/c^4$ Obs.	Value
A_3	$0.132^{+0.075}_{-0.073} \pm 0.005$
A_4	$-0.100^{+0.082}_{-0.077} \pm 0.009$
A_5	$0.027^{+0.077}_{-0.076} \pm 0.010$
A_6	$0.024^{+0.069}_{-0.067} \pm 0.013$
A_7	$-0.008^{+0.073}_{-0.073} \pm 0.005$
A_8	$0.014^{+0.075}_{-0.073} \pm 0.005$
A_9	$-0.057^{+0.057}_{-0.059} \pm 0.006$

$15.0 < q^2 < 17.0\,\mathrm{GeV}^2/c^4$ Obs.	Value
A_3	$-0.034^{+0.056}_{-0.055} \pm 0.007$
A_4	$-0.071^{+0.064}_{-0.064} \pm 0.008$
A_5	$-0.076^{+0.065}_{-0.063} \pm 0.010$
A_6	$-0.085^{+0.062}_{-0.060} \pm 0.012$
A_7	$-0.105^{+0.058}_{-0.059} \pm 0.005$
A_8	$0.048^{+0.063}_{-0.063} \pm 0.003$
A_9	$0.091^{+0.059}_{-0.059} \pm 0.004$

$17.0 < q^2 < 19.0\,\mathrm{GeV}^2/c^4$ Obs.	Value
A_3	$-0.056^{+0.075}_{-0.073} \pm 0.017$
A_4	$-0.071^{+0.073}_{-0.073} \pm 0.011$
A_5	$0.008^{+0.073}_{-0.075} \pm 0.010$
A_6	$-0.127^{+0.080}_{-0.076} \pm 0.018$
A_7	$0.047^{+0.070}_{-0.069} \pm 0.013$
A_8	$0.022^{+0.072}_{-0.073} \pm 0.005$
A_9	$0.043^{+0.066}_{-0.067} \pm 0.005$

$1.1 < q^2 < 6.0\,\mathrm{GeV}^2/c^4$ Obs.	Value
A_3	$-0.072^{+0.038}_{-0.038} \pm 0.004$
A_4	$0.012^{+0.057}_{-0.056} \pm 0.005$
A_5	$-0.044^{+0.049}_{-0.047} \pm 0.005$
A_6	$0.020^{+0.061}_{-0.060} \pm 0.009$
A_7	$-0.045^{+0.050}_{-0.050} \pm 0.006$
A_8	$-0.047^{+0.058}_{-0.057} \pm 0.008$
A_9	$-0.033^{+0.040}_{-0.042} \pm 0.004$

$15.0 < q^2 < 19.0\,\mathrm{GeV}^2/c^4$ Obs.	Value
A_3	$-0.035^{+0.043}_{-0.042} \pm 0.010$
A_4	$-0.079^{+0.047}_{-0.048} \pm 0.008$
A_5	$-0.035^{+0.047}_{-0.047} \pm 0.010$
A_6	$-0.110^{+0.052}_{-0.051} \pm 0.013$
A_7	$-0.040^{+0.045}_{-0.044} \pm 0.006$
A_8	$0.025^{+0.048}_{-0.047} \pm 0.003$
A_9	$0.061^{+0.043}_{-0.044} \pm 0.002$

Table 34: Results for the CP-averaged observables $P_i^{(\prime)}$.

$0.1 < q^2 < 0.98\,\mathrm{GeV}^2/c^4$ Obs.	Value
P_1	$-0.099^{+0.168}_{-0.163} \pm 0.014$
P_2	$-0.003^{+0.051}_{-0.052} \pm 0.007$
P_3	$0.113^{+0.079}_{-0.079} \pm 0.006$
P_4'	$0.185^{+0.158}_{-0.154} \pm 0.023$
P_5'	$0.387^{+0.132}_{-0.133} \pm 0.052$
P_6'	$0.034^{+0.134}_{-0.135} \pm 0.015$
P_8'	$0.180^{+0.174}_{-0.169} \pm 0.007$

$1.1 < q^2 < 2.5\,\mathrm{GeV}^2/c^4$ Obs.	Value
P_1	$-0.451^{+0.519}_{-0.636} \pm 0.038$
P_2	$-0.373^{+0.146}_{-0.199} \pm 0.027$
P_3	$0.350^{+0.330}_{-0.254} \pm 0.015$
P_4'	$-0.163^{+0.232}_{-0.240} \pm 0.021$
P_5'	$0.289^{+0.220}_{-0.202} \pm 0.023$
P_6'	$-0.463^{+0.202}_{-0.221} \pm 0.012$
P_8'	$-0.208^{+0.224}_{-0.270} \pm 0.024$

$2.5 < q^2 < 4.0\,\mathrm{GeV}^2/c^4$ Obs.	Value
P_1	$0.571^{+2.404}_{-1.714} \pm 0.045$
P_2	$-0.636^{+0.444}_{-1.735} \pm 0.015$
P_3	$0.745^{+2.587}_{-0.861} \pm 0.030$
P_4'	$-0.713^{+0.410}_{-1.305} \pm 0.024$
P_5'	$-0.066^{+0.343}_{-0.364} \pm 0.023$
P_6'	$0.205^{+0.962}_{-0.341} \pm 0.013$
P_8'	$0.091^{+0.650}_{-0.432} \pm 0.025$

$4.0 < q^2 < 6.0\,\mathrm{GeV}^2/c^4$ Obs.	Value
P_1	$0.180^{+0.364}_{-0.348} \pm 0.027$
P_2	$0.042^{+0.088}_{-0.087} \pm 0.011$
P_3	$0.083^{+0.187}_{-0.184} \pm 0.023$
P_4'	$-0.448^{+0.169}_{-0.172} \pm 0.020$
P_5'	$-0.300^{+0.158}_{-0.159} \pm 0.023$
P_6'	$-0.032^{+0.167}_{-0.166} \pm 0.007$
P_8'	$0.342^{+0.188}_{-0.185} \pm 0.009$

$6.0 < q^2 < 8.0\,\mathrm{GeV}^2/c^4$ Obs.	Value
P_1	$-0.199^{+0.281}_{-0.275} \pm 0.025$
P_2	$0.241^{+0.061}_{-0.062} \pm 0.013$
P_3	$0.057^{+0.148}_{-0.139} \pm 0.013$
P_4'	$-0.599^{+0.131}_{-0.135} \pm 0.010$
P_5'	$-0.505^{+0.122}_{-0.122} \pm 0.024$
P_6'	$-0.095^{+0.135}_{-0.135} \pm 0.011$
P_8'	$-0.171^{+0.142}_{-0.143} \pm 0.006$

$11.0 < q^2 < 12.5\,\mathrm{GeV}^2/c^4$ Obs.	Value
P_1	$-0.745^{+0.207}_{-0.230} \pm 0.015$
P_2	$0.418^{+0.053}_{-0.046} \pm 0.005$
P_3	$0.007^{+0.141}_{-0.138} \pm 0.010$
P_4'	$-0.567^{+0.169}_{-0.187} \pm 0.014$
P_5'	$-0.655^{+0.147}_{-0.160} \pm 0.015$
P_6'	$-0.282^{+0.146}_{-0.151} \pm 0.007$
P_8'	$-0.015^{+0.145}_{-0.142} \pm 0.005$

$15.0 < q^2 < 17.0\,\mathrm{GeV}^2/c^4$ Obs.	Value
P_1	$-0.436^{+0.134}_{-0.147} \pm 0.018$
P_2	$0.421^{+0.042}_{-0.035} \pm 0.005$
P_3	$0.029^{+0.082}_{-0.084} \pm 0.006$
P_4'	$-0.672^{+0.113}_{-0.151} \pm 0.016$
P_5'	$-0.662^{+0.109}_{-0.127} \pm 0.017$
P_6'	$0.127^{+0.119}_{-0.122} \pm 0.006$
P_8'	$0.007^{+0.125}_{-0.129} \pm 0.005$

$17.0 < q^2 < 19.0\,\mathrm{GeV}^2/c^4$ Obs.	Value
P_1	$-0.581^{+0.225}_{-0.263} \pm 0.037$
P_2	$0.314^{+0.046}_{-0.048} \pm 0.007$
P_3	$0.145^{+0.107}_{-0.102} \pm 0.008$
P_4'	$-0.556^{+0.133}_{-0.156} \pm 0.016$
P_5'	$-0.676^{+0.133}_{-0.152} \pm 0.017$
P_6'	$0.092^{+0.148}_{-0.152} \pm 0.025$
P_8'	$0.027^{+0.147}_{-0.147} \pm 0.009$

$1.1 < q^2 < 6.0\,\mathrm{GeV}^2/c^4$ Obs.	Value
P_1	$0.080^{+0.248}_{-0.245} \pm 0.044$
P_2	$-0.162^{+0.072}_{-0.073} \pm 0.010$
P_3	$0.205^{+0.135}_{-0.134} \pm 0.017$
P_4'	$-0.336^{+0.124}_{-0.122} \pm 0.012$
P_5'	$-0.049^{+0.107}_{-0.108} \pm 0.014$
P_6'	$-0.166^{+0.108}_{-0.108} \pm 0.021$
P_8'	$0.060^{+0.122}_{-0.124} \pm 0.009$

$15.0 < q^2 < 19.0\,\mathrm{GeV}^2/c^4$ Obs.	Value
P_1	$-0.497^{+0.102}_{-0.099} \pm 0.027$
P_2	$0.361^{+0.025}_{-0.026} \pm 0.010$
P_3	$0.081^{+0.060}_{-0.059} \pm 0.005$
P_4'	$-0.597^{+0.080}_{-0.085} \pm 0.015$
P_5'	$-0.684^{+0.078}_{-0.081} \pm 0.020$
P_6'	$0.101^{+0.090}_{-0.092} \pm 0.011$
P_8'	$0.059^{+0.094}_{-0.093} \pm 0.008$

9.2 Results of the method of moments

In this section, the results of the method of moments (described in Sec. 6.3) applied to data are reported. The $m(K^+\pi^-\mu^+\mu^-)$ mass fits are performed in the nominal range $5170 < m(K^+\pi^-\mu^+\mu^-) < 5700\,\mathrm{MeV}/c^2$. The $m(K^+\pi^-)$ mass fit (described in Sec. 5) is performed in the nominal range $795.9 < m(K^+\pi^-) < 995.9\,\mathrm{MeV}/c^2$ The fits to the mass distributions are shown inn Figs. 55 to 75.

The results for the P-wave observables, S_i and P_i, are shown in Tables 35,36 and 37 for the narrow $1\,\mathrm{GeV}^2/c^4$ q^2-bins. Results are also presented in Tables 35,36 and 37 for the same q^2-binning ($\sim 2\,\mathrm{GeV}^2/c^4$) used in the likelihood fit. The errors are purely statistical in nature, sources of systematic errors are discussed in Sec. 10.2. The distribution of the pseudo-experiments obtained from bootstrapping the data is shown in Appendix L. The correlation matrixes, obtained with the bootstrapping method for all q^2 bins is shown in Tables 128 through 185 in Appendix M.

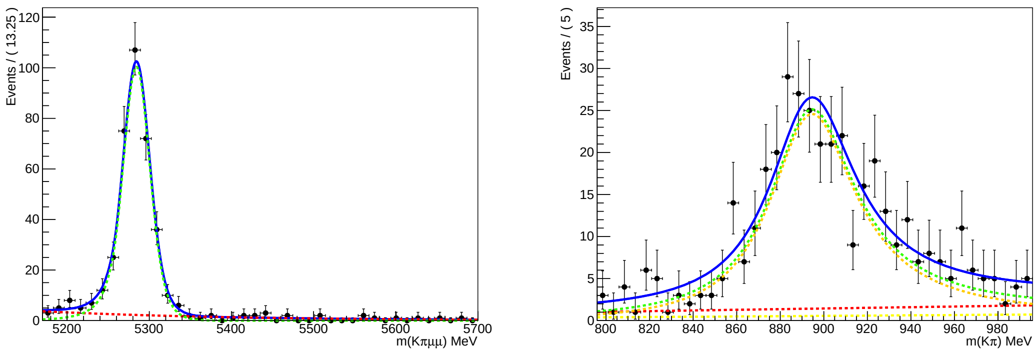

Figure 55: Results of the mass fit to $m(K^+\pi^-\mu^+\mu^-)$ mass and $m(K^+\pi^-)$ in $0.1 < q^2 < 0.98$ GeV^2/c^4. The red dashed component is the background, the green component is the sum of the P and S-wave, the dark yellow component is the P-wave and the lighter yellow component the S-wave.

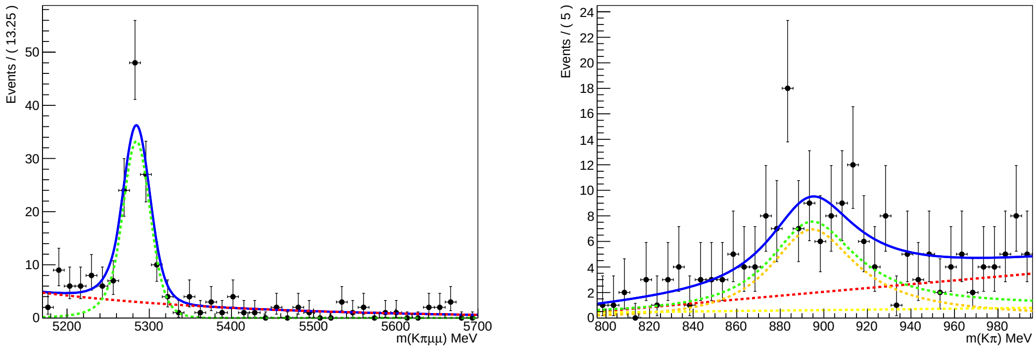

Figure 56: Results of the mass fit to $m(K^+\pi^-\mu^+\mu^-)$ mass and $m(K^+\pi^-)$ in $1.1 < q^2 < 2.0$ GeV^2/c^4. The red component is the background, the green component is the sum of the P and S-wave, the dark yellow component is the P-wave and the lighter yellow component the S-wave.

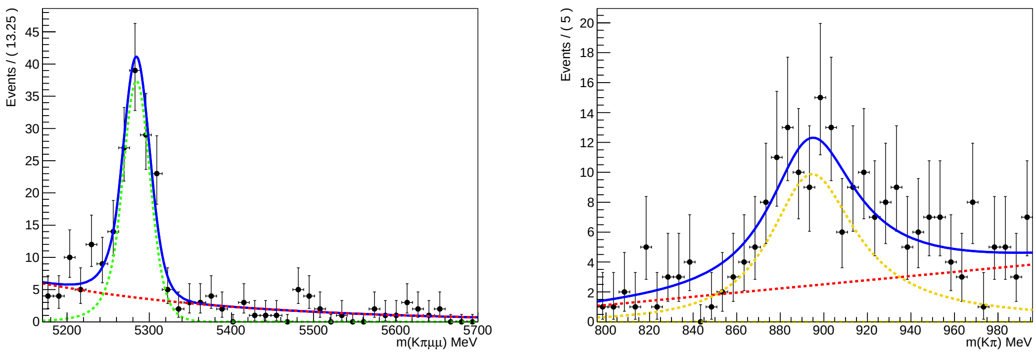

Figure 57: Results of the mass fit to $m(K^+\pi^-\mu^+\mu^-)$ mass and $m(K^+\pi^-)$ in $2.0 < q^2 < 3.0$ GeV^2/c^4. The red component is the background, the green component is the sum of the P and S-wave, the dark yellow component is the P-wave and the lighter yellow component the S-wave.

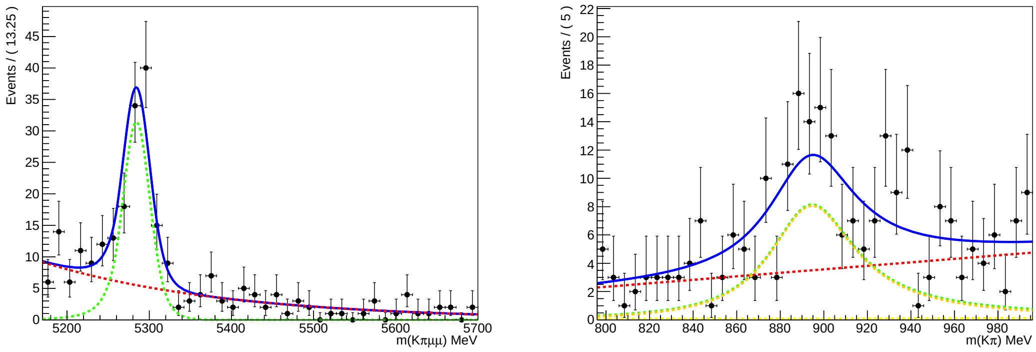

Figure 58: Results of the mass fit to $m(K^+\pi^-\mu^+\mu^-)$ mass and $m(K^+\pi^-)$ in $3.0 < q^2 < 4.0$ GeV$^2/c^4$. The red component is the background, the green component is the sum of the P and S-wave, the dark yellow component is the P-wave and the lighter yellow component the S-wave.

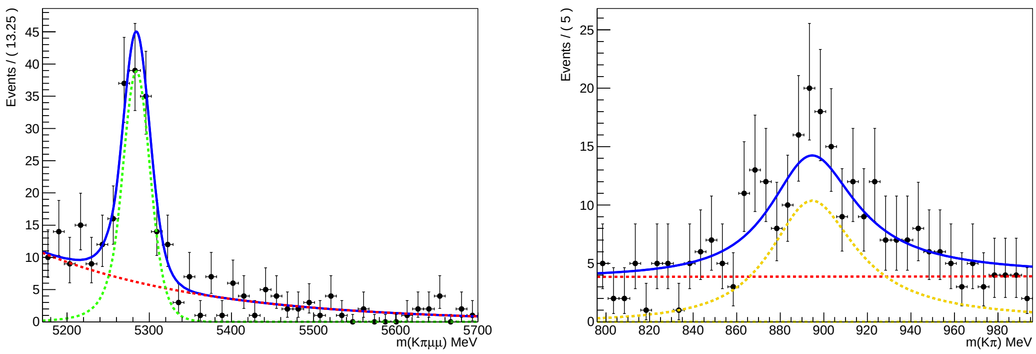

Figure 59: Results of the mass fit to $m(K^+\pi^-\mu^+\mu^-)$ mass and $m(K^+\pi^-)$ in $4.0 < q^2 < 5.0$ GeV$^2/c^4$. The red component is the background, the green component is the sum of the P and S-wave, the dark yellow component is the P-wave and the lighter yellow component the S-wave.

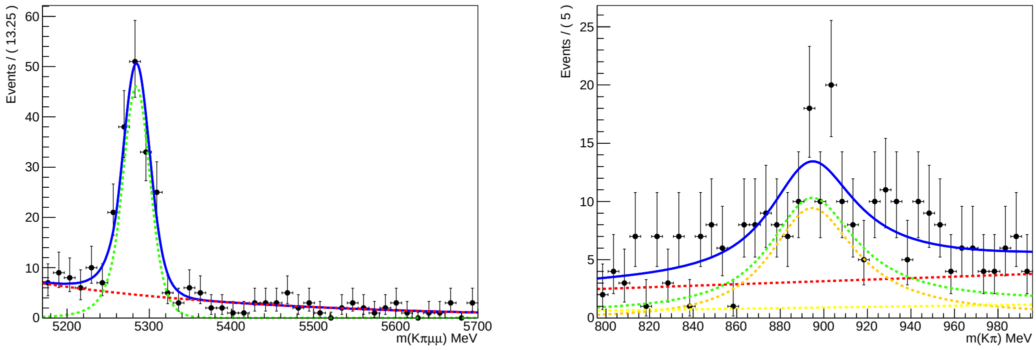

Figure 60: Results of the mass fit to $m(K^+\pi^-\mu^+\mu^-)$ mass and $m(K^+\pi^-)$ in $5.0 < q^2 < 6.0\ \mathrm{GeV}^2/c^4$. The red component is the background, the green component is the sum of the P and S-wave, the dark yellow component is the P-wave and the lighter yellow component the S-wave.

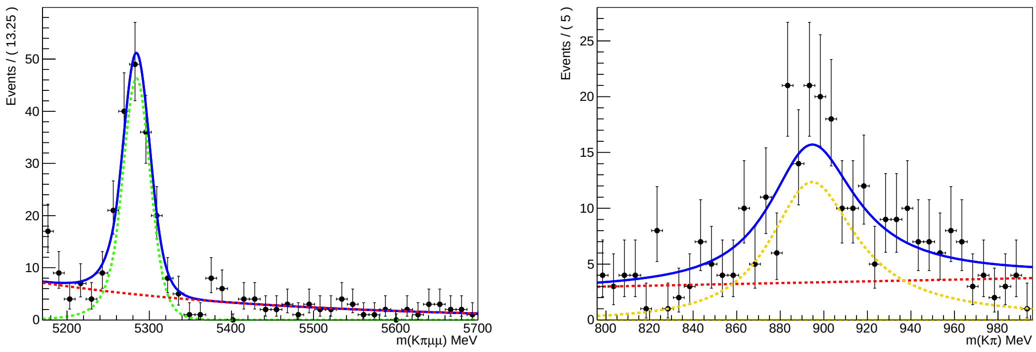

Figure 61: Results of the mass fit to $m(K^+\pi^-\mu^+\mu^-)$ mass and $m(K^+\pi^-)$ in $6.0 < q^2 < 7.0\ \mathrm{GeV}^2/c^4$. The red component is the background, the green component is the sum of the P and S-wave, the dark yellow component is the P-wave and the lighter yellow component the S-wave.

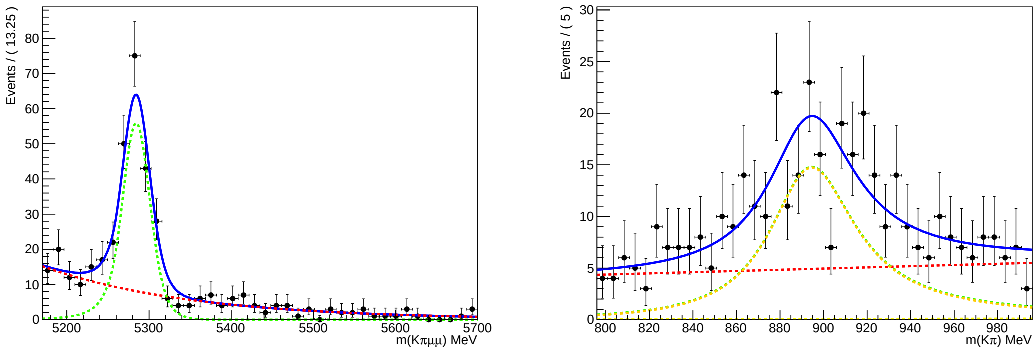

Figure 62: Results of the mass fit to $m(K^+\pi^-\mu^+\mu^-)$ mass and $m(K^+\pi^-)$ in $7.0 < q^2 < 8.0$ GeV$^2/c^4$. The red component is the background, the green component is the sum of the P and S-wave, the dark yellow component is the P-wave and the lighter yellow component the S-wave.

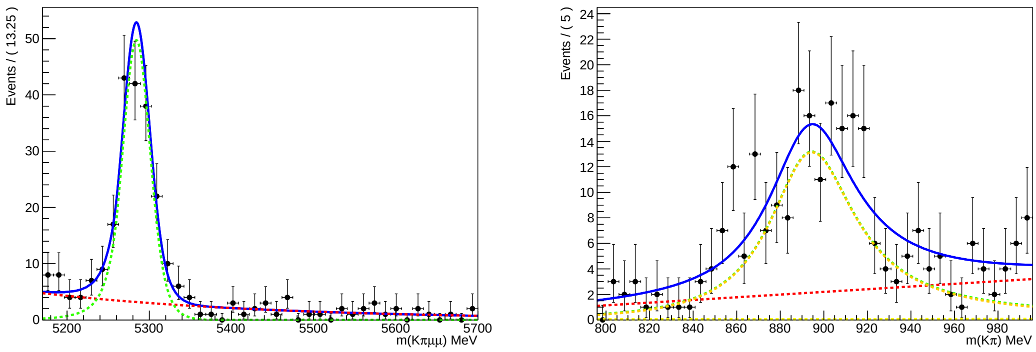

Figure 63: Results of the mass fit to $m(K^+\pi^-\mu^+\mu^-)$ mass and $m(K^+\pi^-)$ in $11.0 < q^2 < 11.75$ GeV$^2/c^4$. The red component is the background, the green component is the sum of the P and S-wave, the dark yellow component is the P-wave and the lighter yellow component the S-wave.

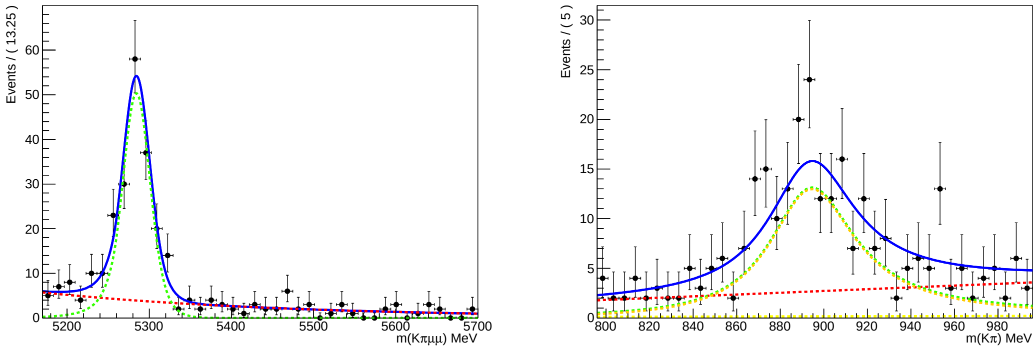

Figure 64: Results of the mass fit to $m(K^+\pi^-\mu^+\mu^-)$ mass and $m(K^+\pi^-)$ in $11.75 < q^2 < 12.5$ GeV^2/c^4. The red component is the background, the green component is the sum of the P and S-wave, the dark yellow component is the P-wave and the lighter yellow component the S-wave.

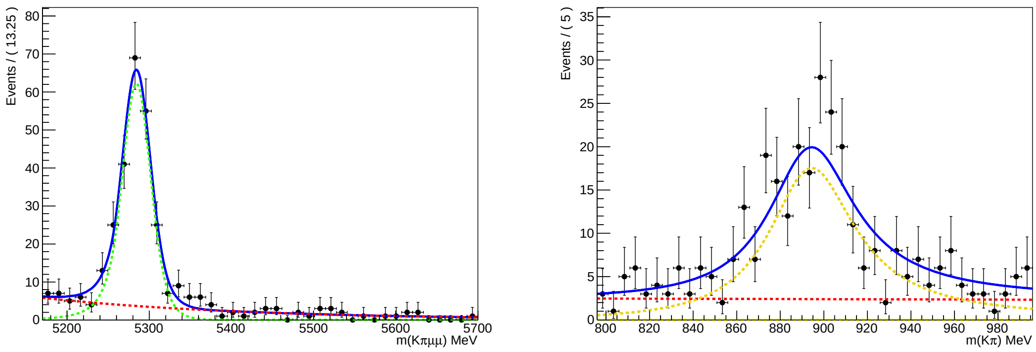

Figure 65: Results of the mass fit to $m(K^+\pi^-\mu^+\mu^-)$ mass and $m(K^+\pi^-)$ in $15.0 < q^2 < 16.0$ GeV^2/c^4. The red component is the background, the green component is the sum of the P and S-wave, the dark yellow component is the P-wave and the lighter yellow component the S-wave.

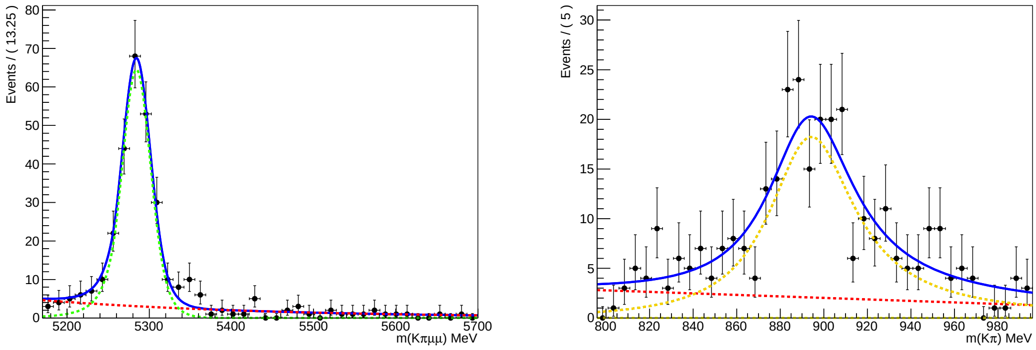

Figure 66: Results of the mass fit to $m(K^+\pi^-\mu^+\mu^-)$ mass and $m(K^+\pi^-)$ in $16.0 < q^2 < 17.0\ \mathrm{GeV}^2/c^4$. The red component is the background, the green component is the sum of the P and S-wave, the dark yellow component is the P-wave and the lighter yellow component the S-wave.

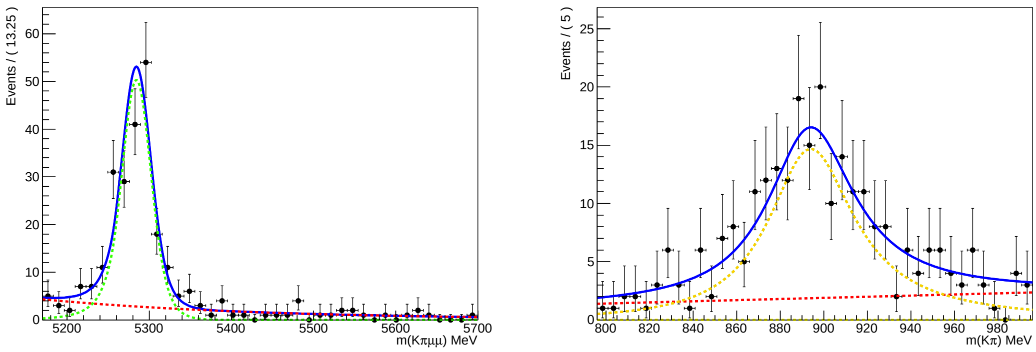

Figure 67: Results of the mass fit to $m(K^+\pi^-\mu^+\mu^-)$ mass and $m(K^+\pi^-)$ in $17.0 < q^2 < 18.0\ \mathrm{GeV}^2/c^4$. The red component is the background, the green component is the sum of the P and S-wave, the dark yellow component is the P-wave and the lighter yellow component the S-wave.

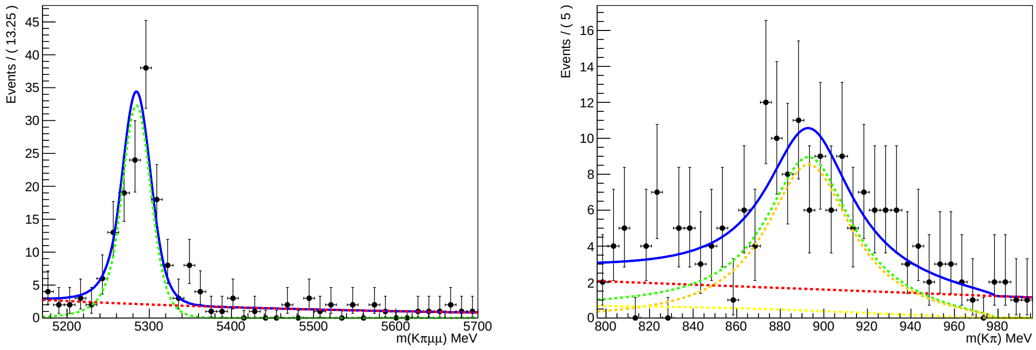

Figure 68: Results of the mass fit to $m(K^+\pi^-\mu^+\mu^-)$ mass and $m(K^+\pi^-)$ in $18.0 < q^2 < 19.0\ \mathrm{GeV}^2/c^4$. The red component is the background, the green component is the sum of the P and S-wave, the dark yellow component is the P-wave and the lighter yellow component the S-wave.

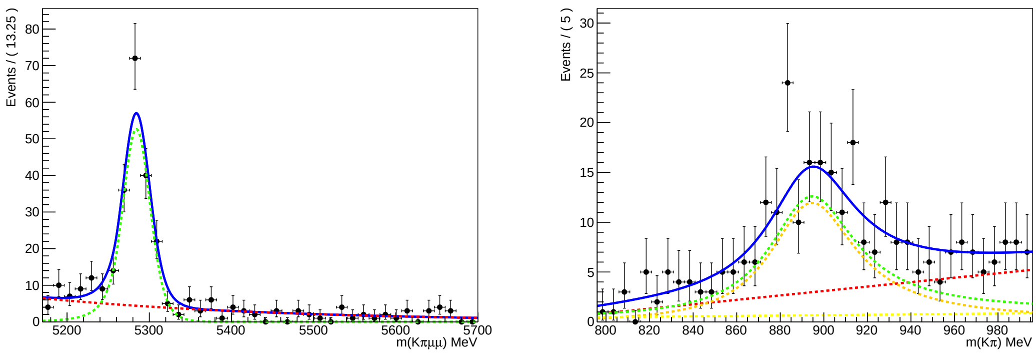

Figure 69: Results of the mass fit to $m(K^+\pi^-\mu^+\mu^-)$ mass and $m(K^+\pi^-)$ in $1.1 < q^2 < 2.5\ \mathrm{GeV}^2/c^4$. The red component is the background, the green component is the sum of the P and S-wave, the dark yellow component is the P-wave and the lighter yellow component the S-wave.

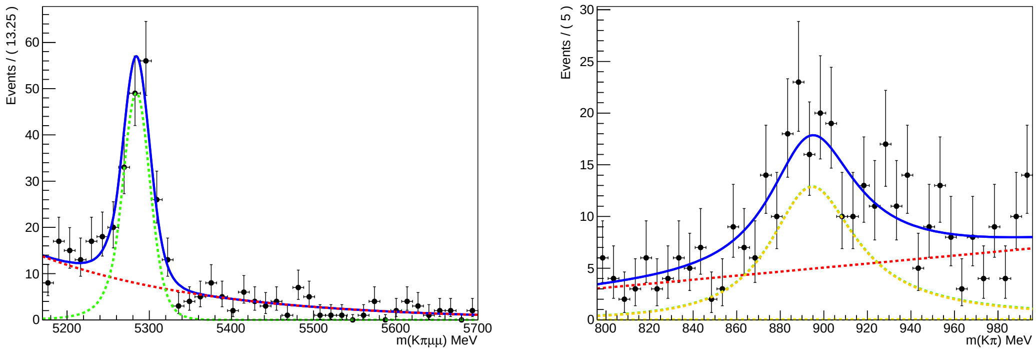

Figure 70: Results of the mass fit to $m(K^+\pi^-\mu^+\mu^-)$ mass and $m(K^+\pi^-)$ in $2.5 < q^2 < 4.0\ \mathrm{GeV}^2/c^4$. The red component is the background, the green component is the sum of the P and S-wave, the dark yellow component is the P-wave and the lighter yellow component the S-wave.

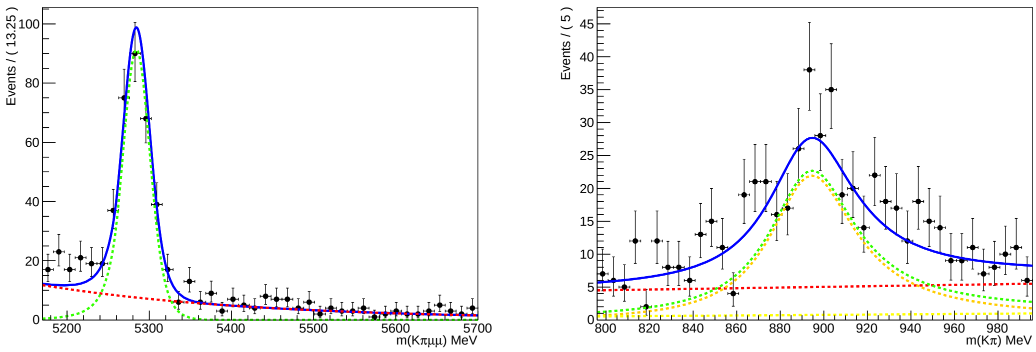

Figure 71: Results of the mass fit to $m(K^+\pi^-\mu^+\mu^-)$ mass and $m(K^+\pi^-)$ in $4.0 < q^2 < 6.0\ \mathrm{GeV}^2/c^4$. The red component is the background, the green component is the sum of the P and S-wave, the dark yellow component is the P-wave and the lighter yellow component the S-wave.

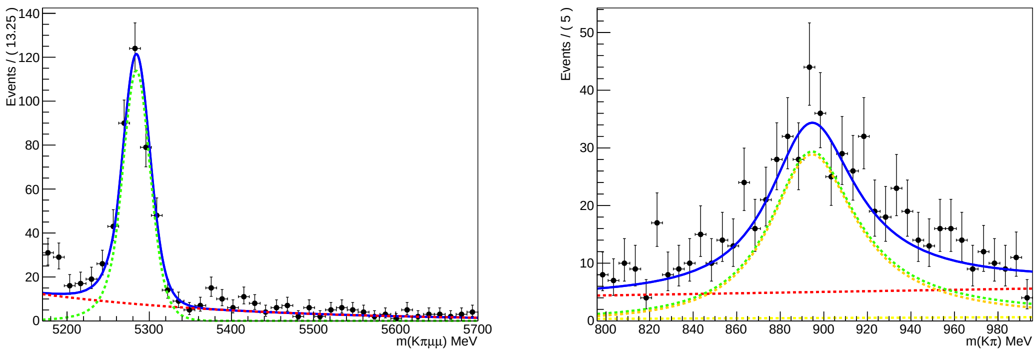

Figure 72: Results of the mass fit to $m(K^+\pi^-\mu^+\mu^-)$ mass and $m(K^+\pi^-)$ in $6.0 < q^2 < 8.0\ \mathrm{GeV}^2/c^4$. The red component is the background, the green component is the sum of the P and S-wave, the dark yellow component is the P-wave and the lighter yellow component the S-wave.

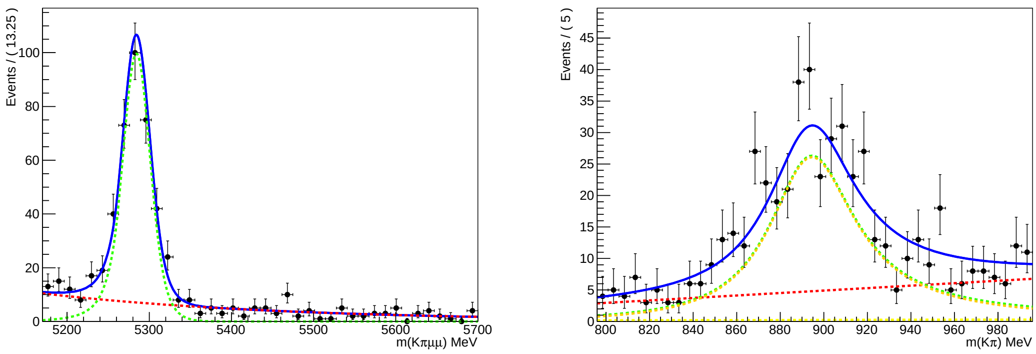

Figure 73: Results of the mass fit to $m(K^+\pi^-\mu^+\mu^-)$ mass and $m(K^+\pi^-)$ in $11.0 < q^2 < 12.5\ \mathrm{GeV}^2/c^4$. The red component is the background, the green component is the sum of the P and S-wave, the dark yellow component is the P-wave and the lighter yellow component the S-wave.

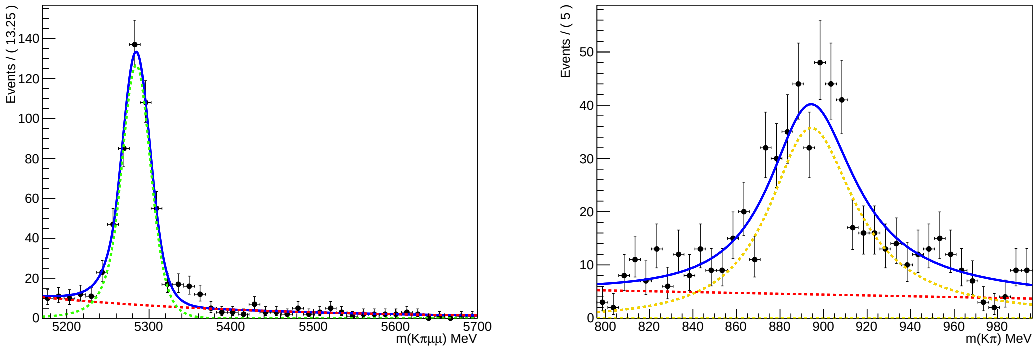

Figure 74: Results of the mass fit to $m(K^+\pi^-\mu^+\mu^-)$ mass and $m(K^+\pi^-)$ in $15.0 < q^2 < 17.0$ GeV^2/c^4. The red component is the background, the green component is the sum of the P and S-wave, the dark yellow component is the P-wave and the lighter yellow component the S-wave.

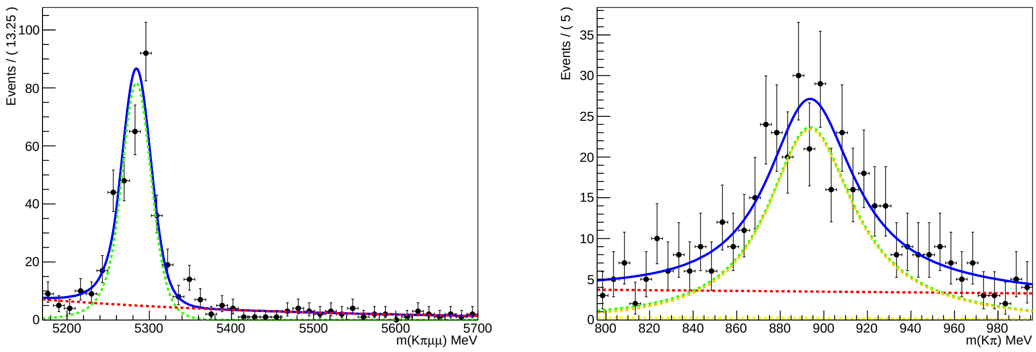

Figure 75: Results of the mass fit to $m(K^+\pi^-\mu^+\mu^-)$ mass and $m(K^+\pi^-)$ in $17.0 < q^2 < 19.0$ GeV^2/c^4. The red component is the background, the green component is the sum of the P and S-wave, the dark yellow component is the P-wave and the lighter yellow component the S-wave.

Table 35: Results of method of moments in terms of the S_i basis.

	F_{L}	S_3	S_4	S_5	A_{FB}	S_7	S_8	S_9	S_{6s}	S_{6c}
$0.1 < q^2 < 0.98$	$0.242^{+0.058}_{-0.056}$	$-0.014^{+0.059}_{-0.06}$	$0.039^{+0.091}_{-0.09}$	$0.129^{+0.068}_{-0.066}$	$-0.138^{+0.095}_{-0.092}$	$0.038^{+0.063}_{-0.062}$	$0.063^{+0.079}_{-0.08}$	$-0.113^{+0.061}_{-0.063}$	$-0.148^{+0.13}_{-0.124}$	$-0.098^{+0.132}_{-0.134}$
$1.1 < q^2 < 2.0$	$0.768^{+0.141}_{-0.13}$	$0.065^{+0.137}_{-0.127}$	$0.127^{+0.19}_{-0.18}$	$0.286^{+0.168}_{-0.172}$	$-0.333^{+0.115}_{-0.13}$	$-0.293^{+0.18}_{-0.176}$	$-0.114^{+0.185}_{-0.196}$	$-0.11^{+0.14}_{-0.138}$	$-0.345^{+0.13}_{-0.138}$	$-0.01^{+0.223}_{-0.212}$
$2.0 < q^2 < 3.0$	$0.69^{+0.113}_{-0.082}$	$0.006^{+0.1}_{-0.1}$	$-0.339^{+0.115}_{-0.14}$	$0.206^{+0.131}_{-0.115}$	$-0.158^{+0.08}_{-0.09}$	$-0.252^{+0.127}_{-0.151}$	$-0.176^{+0.149}_{-0.165}$	$-0.0^{+0.1}_{-0.102}$	$-0.152^{+0.12}_{-0.119}$	$-0.239^{+0.268}_{-0.263}$
$3.0 < q^2 < 4.0$	$0.873^{+0.154}_{-0.105}$	$0.078^{+0.131}_{-0.122}$	$-0.046^{+0.193}_{-0.196}$	$-0.11^{+0.163}_{-0.169}$	$-0.041^{+0.091}_{-0.091}$	$0.171^{+0.175}_{-0.158}$	$0.097^{+0.189}_{-0.184}$	$-0.203^{+0.112}_{-0.132}$	$-0.046^{+0.129}_{-0.135}$	$-0.031^{+0.359}_{-0.337}$
$4.0 < q^2 < 5.0$	$0.899^{+0.106}_{-0.104}$	$0.2^{+0.101}_{-0.097}$	$-0.148^{+0.154}_{-0.154}$	$-0.306^{+0.138}_{-0.141}$	$0.052^{+0.08}_{-0.08}$	$-0.082^{+0.129}_{-0.128}$	$0.107^{+0.144}_{-0.146}$	$0.181^{+0.105}_{-0.099}$	$-0.052^{+0.122}_{-0.12}$	$0.485^{+0.309}_{-0.317}$
$5.0 < q^2 < 6.0$	$0.644^{+0.13}_{-0.121}$	$-0.122^{+0.119}_{-0.126}$	$-0.273^{+0.174}_{-0.184}$	$-0.095^{+0.137}_{-0.142}$	$0.057^{+0.094}_{-0.09}$	$0.038^{+0.135}_{-0.135}$	$-0.037^{+0.16}_{-0.159}$	$-0.08^{+0.117}_{-0.12}$	$-0.053^{+0.118}_{-0.115}$	$0.447^{+0.328}_{-0.333}$
$6.0 < q^2 < 7.0$	$0.644^{+0.089}_{-0.084}$	$-0.069^{+0.089}_{-0.091}$	$-0.311^{+0.111}_{-0.118}$	$-0.339^{+0.108}_{-0.114}$	$0.058^{+0.064}_{-0.063}$	$0.009^{+0.123}_{-0.124}$	$0.08^{+0.131}_{-0.129}$	$0.061^{+0.091}_{-0.091}$	$0.022^{+0.1}_{-0.101}$	$0.219^{+0.249}_{-0.25}$
$7.0 < q^2 < 8.0$	$0.609^{+0.103}_{-0.082}$	$-0.054^{+0.097}_{-0.099}$	$-0.236^{+0.116}_{-0.136}$	$-0.386^{+0.105}_{-0.135}$	$0.241^{+0.08}_{-0.062}$	$-0.094^{+0.123}_{-0.13}$	$-0.295^{+0.119}_{-0.139}$	$0.03^{+0.1}_{-0.098}$	$0.254^{+0.097}_{-0.098}$	$0.249^{+0.209}_{-0.208}$
$11.0 < q^2 < 11.75$	$0.502^{+0.09}_{-0.082}$	$-0.217^{+0.077}_{-0.09}$	$-0.252^{+0.095}_{-0.113}$	$-0.235^{+0.095}_{-0.115}$	$0.37^{+0.076}_{-0.054}$	$-0.11^{+0.108}_{-0.114}$	$-0.079^{+0.12}_{-0.122}$	$-0.084^{+0.097}_{-0.102}$	$0.467^{+0.099}_{-0.097}$	$0.082^{+0.22}_{-0.223}$
$11.75 < q^2 < 12.5$	$0.734^{+0.107}_{-0.094}$	$-0.157^{+0.09}_{-0.098}$	$-0.309^{+0.099}_{-0.111}$	$-0.366^{+0.096}_{-0.112}$	$0.293^{+0.064}_{-0.052}$	$-0.212^{+0.11}_{-0.118}$	$-0.09^{+0.108}_{-0.111}$	$0.03^{+0.093}_{-0.091}$	$0.278^{+0.101}_{-0.099}$	$0.392^{+0.293}_{-0.294}$
$15.0 < q^2 < 16.0$	$0.385^{+0.067}_{-0.066}$	$-0.06^{+0.085}_{-0.088}$	$-0.321^{+0.082}_{-0.099}$	$-0.36^{+0.074}_{-0.092}$	$0.396^{+0.068}_{-0.047}$	$0.04^{+0.092}_{-0.089}$	$-0.057^{+0.093}_{-0.095}$	$-0.054^{+0.083}_{-0.087}$	$0.596^{+0.081}_{-0.083}$	$-0.273^{+0.164}_{-0.161}$
$16.0 < q^2 < 17.0$	$0.295^{+0.058}_{-0.062}$	$-0.25^{+0.079}_{-0.092}$	$-0.246^{+0.083}_{-0.096}$	$-0.254^{+0.069}_{-0.081}$	$0.451^{+0.071}_{-0.048}$	$0.144^{+0.091}_{-0.085}$	$0.055^{+0.09}_{-0.088}$	$-0.014^{+0.084}_{-0.086}$	$0.63^{+0.078}_{-0.079}$	$-0.112^{+0.127}_{-0.129}$
$17.0 < q^2 < 18.0$	$0.363^{+0.073}_{-0.072}$	$-0.099^{+0.091}_{-0.092}$	$-0.229^{+0.09}_{-0.096}$	$-0.305^{+0.081}_{-0.088}$	$0.274^{+0.069}_{-0.061}$	$0.022^{+0.094}_{-0.093}$	$-0.007^{+0.098}_{-0.098}$	$-0.09^{+0.092}_{-0.095}$	$0.415^{+0.095}_{-0.093}$	$-0.195^{+0.169}_{-0.17}$
$18.0 < q^2 < 19.0$	$0.421^{+0.1}_{-0.1}$	$-0.131^{+0.128}_{-0.13}$	$-0.607^{+0.153}_{-0.17}$	$-0.534^{+0.131}_{-0.15}$	$0.354^{+0.111}_{-0.099}$	$0.058^{+0.123}_{-0.124}$	$0.149^{+0.139}_{-0.138}$	$-0.079^{+0.122}_{-0.121}$	$0.367^{+0.127}_{-0.124}$	$0.187^{+0.201}_{-0.207}$
$15.0 < q^2 < 19.0$	$0.357^{+0.035}_{-0.035}$	$-0.135^{+0.046}_{-0.05}$	$-0.314^{+0.046}_{-0.054}$	$-0.335^{+0.041}_{-0.047}$	$0.367^{+0.037}_{-0.029}$	$0.066^{+0.049}_{-0.046}$	$0.024^{+0.05}_{-0.048}$	$-0.056^{+0.046}_{-0.047}$	$0.521^{+0.045}_{-0.047}$	$-0.125^{+0.082}_{-0.084}$
$1.1 < q^2 < 2.5$	$0.75^{+0.097}_{-0.095}$	$0.03^{+0.095}_{-0.092}$	$-0.037^{+0.132}_{-0.125}$	$0.266^{+0.119}_{-0.116}$	$-0.254^{+0.08}_{-0.085}$	$-0.33^{+0.127}_{-0.131}$	$-0.163^{+0.14}_{-0.15}$	$-0.066^{+0.096}_{-0.094}$	$-0.239^{+0.102}_{-0.103}$	$-0.196^{+0.2}_{-0.203}$
$2.5 < q^2 < 4.0$	$0.785^{+0.115}_{-0.08}$	$0.055^{+0.099}_{-0.094}$	$-0.207^{+0.134}_{-0.147}$	$-0.007^{+0.125}_{-0.125}$	$-0.087^{+0.073}_{-0.076}$	$0.062^{+0.129}_{-0.125}$	$0.02^{+0.141}_{-0.141}$	$-0.128^{+0.091}_{-0.102}$	$-0.107^{+0.107}_{-0.108}$	$-0.03^{+0.275}_{-0.258}$
$4.0 < q^2 < 6.0$	$0.742^{+0.083}_{-0.07}$	$0.042^{+0.072}_{-0.07}$	$-0.186^{+0.105}_{-0.113}$	$-0.188^{+0.089}_{-0.097}$	$0.049^{+0.057}_{-0.055}$	$-0.032^{+0.087}_{-0.088}$	$0.042^{+0.103}_{-0.1}$	$0.049^{+0.073}_{-0.071}$	$-0.054^{+0.085}_{-0.084}$	$0.465^{+0.229}_{-0.233}$
$6.0 < q^2 < 8.0$	$0.612^{+0.065}_{-0.059}$	$-0.069^{+0.065}_{-0.066}$	$-0.274^{+0.08}_{-0.088}$	$-0.359^{+0.075}_{-0.084}$	$0.151^{+0.048}_{-0.044}$	$-0.05^{+0.086}_{-0.088}$	$-0.115^{+0.089}_{-0.091}$	$0.048^{+0.066}_{-0.065}$	$0.149^{+0.07}_{-0.07}$	$0.211^{+0.165}_{-0.163}$
$11.0 < q^2 < 12.5$	$0.621^{+0.069}_{-0.063}$	$-0.186^{+0.06}_{-0.065}$	$-0.281^{+0.069}_{-0.078}$	$-0.302^{+0.069}_{-0.077}$	$0.331^{+0.048}_{-0.039}$	$-0.163^{+0.077}_{-0.08}$	$-0.085^{+0.08}_{-0.081}$	$-0.026^{+0.067}_{-0.066}$	$0.369^{+0.071}_{-0.069}$	$0.241^{+0.186}_{-0.186}$
$15.0 < q^2 < 17.0$	$0.339^{+0.044}_{-0.045}$	$-0.156^{+0.058}_{-0.063}$	$-0.282^{+0.058}_{-0.067}$	$-0.306^{+0.051}_{-0.06}$	$0.425^{+0.047}_{-0.035}$	$0.092^{+0.064}_{-0.061}$	$0.001^{+0.064}_{-0.064}$	$-0.034^{+0.058}_{-0.06}$	$0.613^{+0.057}_{-0.057}$	$-0.187^{+0.103}_{-0.102}$
$17.0 < q^2 < 19.0$	$0.383^{+0.057}_{-0.057}$	$-0.108^{+0.072}_{-0.075}$	$-0.365^{+0.075}_{-0.086}$	$-0.384^{+0.067}_{-0.079}$	$0.297^{+0.06}_{-0.05}$	$0.032^{+0.074}_{-0.072}$	$0.057^{+0.079}_{-0.078}$	$-0.089^{+0.071}_{-0.074}$	$0.395^{+0.075}_{-0.075}$	$-0.042^{+0.131}_{-0.132}$

Table 36: Results of method of moments in terms of the A_i basis.

	A_3	A_4	A_5	$A(A_{\mathrm{FB}})$	A_7	A_8	A_9	A_{6s}	A_{6c}
$0.1 < q^2 < 0.98$	$-0.04^{+0.059}_{-0.061}$	$-0.047^{+0.09}_{-0.092}$	$-0.008^{+0.066}_{-0.066}$	$0.125^{+0.096}_{-0.095}$	$0.112^{+0.064}_{-0.062}$	$0.021^{+0.08}_{-0.08}$	$0.043^{+0.062}_{-0.062}$	$0.202^{+0.127}_{-0.128}$	$-0.183^{+0.131}_{-0.126}$
$1.1 < q^2 < 2.0$	$-0.134^{+0.126}_{-0.136}$	$0.283^{+0.191}_{-0.181}$	$-0.11^{+0.166}_{-0.176}$	$0.16^{+0.121}_{-0.116}$	$-0.193^{+0.167}_{-0.2}$	$0.13^{+0.203}_{-0.18}$	$-0.126^{+0.136}_{-0.153}$	$0.142^{+0.137}_{-0.133}$	$0.1^{+0.213}_{-0.22}$
$2.0 < q^2 < 3.0$	$-0.018^{+0.101}_{-0.1}$	$0.261^{+0.146}_{-0.123}$	$0.028^{+0.124}_{-0.12}$	$0.058^{+0.091}_{-0.083}$	$-0.162^{+0.13}_{-0.144}$	$-0.06^{+0.152}_{-0.161}$	$0.013^{+0.102}_{-0.101}$	$0.016^{+0.121}_{-0.12}$	$0.242^{+0.258}_{-0.259}$
$3.0 < q^2 < 4.0$	$-0.118^{+0.12}_{-0.132}$	$0.002^{+0.194}_{-0.196}$	$0.015^{+0.167}_{-0.168}$	$-0.035^{+0.091}_{-0.094}$	$-0.004^{+0.165}_{-0.162}$	$0.005^{+0.188}_{-0.185}$	$-0.129^{+0.115}_{-0.125}$	$-0.138^{+0.133}_{-0.128}$	$0.37^{+0.356}_{-0.379}$
$4.0 < q^2 < 5.0$	$-0.064^{+0.098}_{-0.098}$	$0.076^{+0.155}_{-0.154}$	$0.051^{+0.143}_{-0.142}$	$-0.064^{+0.08}_{-0.08}$	$-0.146^{+0.13}_{-0.13}$	$0.183^{+0.15}_{-0.146}$	$0.16^{+0.103}_{-0.1}$	$0.058^{+0.12}_{-0.122}$	$-0.575^{+0.318}_{-0.316}$
$5.0 < q^2 < 6.0$	$-0.076^{+0.119}_{-0.122}$	$-0.457^{+0.174}_{-0.187}$	$-0.011^{+0.139}_{-0.139}$	$0.087^{+0.093}_{-0.091}$	$0.058^{+0.135}_{-0.135}$	$-0.195^{+0.156}_{-0.167}$	$-0.001^{+0.118}_{-0.12}$	$0.029^{+0.118}_{-0.117}$	$0.243^{+0.34}_{-0.338}$
$6.0 < q^2 < 7.0$	$-0.073^{+0.089}_{-0.091}$	$-0.104^{+0.121}_{-0.12}$	$0.04^{+0.117}_{-0.116}$	$0.047^{+0.065}_{-0.062}$	$0.181^{+0.125}_{-0.122}$	$0.004^{+0.131}_{-0.13}$	$0.125^{+0.092}_{-0.09}$	$-0.012^{+0.101}_{-0.1}$	$0.3^{+0.258}_{-0.26}$
$7.0 < q^2 < 8.0$	$0.168^{+0.104}_{-0.093}$	$0.058^{+0.132}_{-0.127}$	$0.084^{+0.122}_{-0.117}$	$0.075^{+0.072}_{-0.066}$	$0.064^{+0.129}_{-0.125}$	$0.078^{+0.131}_{-0.127}$	$0.195^{+0.108}_{-0.093}$	$0.131^{+0.097}_{-0.098}$	$-0.131^{+0.21}_{-0.208}$
$11.0 < q^2 < 11.75$	$0.124^{+0.09}_{-0.083}$	$-0.058^{+0.101}_{-0.105}$	$-0.042^{+0.102}_{-0.106}$	$0.012^{+0.068}_{-0.067}$	$-0.064^{+0.11}_{-0.113}$	$0.072^{+0.123}_{-0.121}$	$-0.082^{+0.097}_{-0.102}$	$0.067^{+0.098}_{-0.097}$	$-0.206^{+0.219}_{-0.219}$
$11.75 < q^2 < 12.5$	$0.124^{+0.096}_{-0.09}$	$-0.242^{+0.102}_{-0.112}$	$0.097^{+0.105}_{-0.102}$	$-0.074^{+0.057}_{-0.061}$	$0.144^{+0.116}_{-0.11}$	$-0.017^{+0.112}_{-0.107}$	$-0.014^{+0.092}_{-0.092}$	$-0.107^{+0.098}_{-0.1}$	$0.05^{+0.299}_{-0.296}$
$15.0 < q^2 < 16.0$	$-0.108^{+0.085}_{-0.091}$	$0.059^{+0.094}_{-0.091}$	$0.039^{+0.087}_{-0.085}$	$-0.088^{+0.057}_{-0.061}$	$-0.124^{+0.087}_{-0.094}$	$0.087^{+0.095}_{-0.092}$	$0.145^{+0.089}_{-0.082}$	$-0.163^{+0.088}_{-0.086}$	$0.181^{+0.163}_{-0.163}$
$16.0 < q^2 < 17.0$	$0.016^{+0.087}_{-0.087}$	$-0.11^{+0.087}_{-0.093}$	$-0.138^{+0.073}_{-0.079}$	$-0.026^{+0.059}_{-0.061}$	$-0.081^{+0.087}_{-0.092}$	$0.013^{+0.089}_{-0.089}$	$0.058^{+0.086}_{-0.084}$	$-0.044^{+0.085}_{-0.086}$	$0.036^{+0.128}_{-0.128}$
$17.0 < q^2 < 18.0$	$-0.145^{+0.09}_{-0.094}$	$-0.071^{+0.093}_{-0.095}$	$-0.02^{+0.085}_{-0.086}$	$-0.082^{+0.065}_{-0.068}$	$-0.025^{+0.093}_{-0.094}$	$0.131^{+0.1}_{-0.097}$	$0.116^{+0.095}_{-0.092}$	$-0.108^{+0.099}_{-0.099}$	$-0.004^{+0.173}_{-0.172}$
$18.0 < q^2 < 19.0$	$0.05^{+0.133}_{-0.129}$	$-0.12^{+0.155}_{-0.162}$	$0.186^{+0.134}_{-0.131}$	$-0.125^{+0.099}_{-0.104}$	$0.022^{+0.125}_{-0.122}$	$-0.029^{+0.14}_{-0.138}$	$-0.147^{+0.121}_{-0.128}$	$-0.112^{+0.127}_{-0.128}$	$-0.138^{+0.202}_{-0.204}$
$15.0 < q^2 < 19.0$	$-0.053^{+0.047}_{-0.048}$	$-0.049^{+0.049}_{-0.052}$	$-0.01^{+0.044}_{-0.044}$	$-0.072^{+0.034}_{-0.033}$	$-0.062^{+0.048}_{-0.049}$	$0.056^{+0.05}_{-0.049}$	$0.065^{+0.048}_{-0.045}$	$-0.106^{+0.05}_{-0.048}$	$0.042^{+0.084}_{-0.082}$
$1.1 < q^2 < 2.5$	$-0.045^{+0.093}_{-0.093}$	$0.348^{+0.138}_{-0.126}$	$-0.078^{+0.116}_{-0.117}$	$0.078^{+0.082}_{-0.082}$	$-0.187^{+0.123}_{-0.136}$	$0.052^{+0.144}_{-0.143}$	$0.004^{+0.093}_{-0.099}$	$0.014^{+0.105}_{-0.102}$	$0.301^{+0.192}_{-0.204}$
$2.5 < q^2 < 4.0$	$-0.117^{+0.092}_{-0.101}$	$0.017^{+0.142}_{-0.141}$	$0.049^{+0.127}_{-0.124}$	$0.039^{+0.077}_{-0.074}$	$-0.059^{+0.126}_{-0.127}$	$-0.032^{+0.14}_{-0.143}$	$-0.137^{+0.091}_{-0.101}$	$0.002^{+0.109}_{-0.105}$	$0.197^{+0.269}_{-0.283}$
$4.0 < q^2 < 6.0$	$-0.067^{+0.07}_{-0.072}$	$-0.164^{+0.106}_{-0.112}$	$0.018^{+0.094}_{-0.093}$	$0.01^{+0.056}_{-0.056}$	$-0.044^{+0.086}_{-0.088}$	$0.008^{+0.101}_{-0.101}$	$0.074^{+0.073}_{-0.071}$	$0.047^{+0.084}_{-0.085}$	$-0.135^{+0.237}_{-0.234}$
$6.0 < q^2 < 8.0$	$0.046^{+0.066}_{-0.066}$	$-0.023^{+0.088}_{-0.087}$	$0.055^{+0.084}_{-0.081}$	$0.06^{+0.047}_{-0.046}$	$0.115^{+0.088}_{-0.085}$	$0.04^{+0.09}_{-0.09}$	$0.163^{+0.068}_{-0.064}$	$0.057^{+0.071}_{-0.07}$	$0.093^{+0.166}_{-0.169}$
$11.0 < q^2 < 12.5$	$0.124^{+0.065}_{-0.061}$	$-0.152^{+0.072}_{-0.076}$	$0.029^{+0.073}_{-0.072}$	$-0.032^{+0.043}_{-0.045}$	$0.043^{+0.08}_{-0.078}$	$0.026^{+0.082}_{-0.08}$	$-0.047^{+0.066}_{-0.068}$	$-0.023^{+0.069}_{-0.07}$	$-0.074^{+0.188}_{-0.187}$
$15.0 < q^2 < 17.0$	$-0.043^{+0.061}_{-0.062}$	$-0.027^{+0.064}_{-0.064}$	$-0.054^{+0.055}_{-0.058}$	$-0.055^{+0.041}_{-0.043}$	$-0.102^{+0.061}_{-0.065}$	$0.049^{+0.065}_{-0.063}$	$0.101^{+0.061}_{-0.058}$	$-0.101^{+0.061}_{-0.061}$	$0.107^{+0.103}_{-0.104}$
$17.0 < q^2 < 19.0$	$-0.068^{+0.073}_{-0.075}$	$-0.079^{+0.08}_{-0.083}$	$0.051^{+0.073}_{-0.071}$	$-0.097^{+0.054}_{-0.057}$	$-0.007^{+0.073}_{-0.073}$	$0.067^{+0.08}_{-0.079}$	$0.017^{+0.073}_{-0.073}$	$-0.113^{+0.078}_{-0.078}$	$-0.047^{+0.131}_{-0.132}$

Table 37: Results of method of moments in terms of the P_i basis.

	F_{L}	$P1$	$P2$	$P3$	$P4$	$P5$	$P6$	$P8$
$0.1 < q^2 < 0.98$	$0.242^{+0.058}_{-0.056}$	$-0.038^{+0.157}_{-0.158}$	$-0.119^{+0.08}_{-0.081}$	$0.147^{+0.086}_{-0.08}$	$0.086^{+0.221}_{-0.209}$	$0.3^{+0.171}_{-0.152}$	$0.086^{+0.152}_{-0.145}$	$0.143^{+0.195}_{-0.184}$
$1.1 < q^2 < 2.0$	$0.768^{+0.141}_{-0.13}$	$0.439^{+1.916}_{-1.013}$	$-0.667^{+0.149}_{-1.939}$	$0.363^{+1.088}_{-0.506}$	$0.266^{+0.648}_{-0.406}$	$0.606^{+0.769}_{-0.326}$	$-0.632^{+0.347}_{-0.753}$	$-0.244^{+0.433}_{-0.645}$
$2.0 < q^2 < 3.0$	$0.69^{+0.113}_{-0.082}$	$0.055^{+0.677}_{-0.756}$	$-0.323^{+0.147}_{-0.316}$	$0.005^{+0.362}_{-0.364}$	$-0.765^{+0.271}_{-0.359}$	$0.461^{+0.313}_{-0.256}$	$-0.549^{+0.276}_{-0.393}$	$-0.393^{+0.332}_{-0.388}$
$3.0 < q^2 < 4.0$	$0.873^{+0.154}_{-0.105}$	$0.421^{+18.351}_{-1.19}$	$-0.117^{+0.485}_{-4.435}$	$0.905^{+17.506}_{-0.258}$	$-0.134^{+0.81}_{-1.343}$	$-0.295^{+0.508}_{-7.112}$	$0.449^{+19.043}_{-0.397}$	$0.303^{+1.394}_{-0.719}$
$4.0 < q^2 < 5.0$	$0.899^{+0.106}_{-0.104}$	$2.296^{+17.706}_{--0.694}$	$0.174^{+3.034}_{-0.376}$	$-0.801^{+0.221}_{-17.419}$	$-0.415^{+0.438}_{-1.911}$	$-0.799^{+0.266}_{-18.192}$	$-0.215^{+0.397}_{-1.243}$	$0.293^{+1.522}_{-0.441}$
$5.0 < q^2 < 6.0$	$0.644^{+0.13}_{-0.121}$	$-0.54^{+0.521}_{-1.1}$	$0.089^{+0.227}_{-0.155}$	$0.178^{+0.465}_{-0.286}$	$-0.561^{+0.345}_{-0.465}$	$-0.197^{+0.287}_{-0.334}$	$0.074^{+0.309}_{-0.288}$	$-0.068^{+0.338}_{-0.372}$
$6.0 < q^2 < 7.0$	$0.644^{+0.089}_{-0.084}$	$-0.353^{+0.469}_{-0.602}$	$0.104^{+0.136}_{-0.115}$	$-0.161^{+0.246}_{-0.291}$	$-0.641^{+0.222}_{-0.294}$	$-0.713^{+0.228}_{-0.268}$	$0.017^{+0.267}_{-0.261}$	$0.162^{+0.289}_{-0.267}$
$7.0 < q^2 < 8.0$	$0.609^{+0.103}_{-0.082}$	$-0.284^{+0.513}_{-0.548}$	$0.393^{+0.231}_{-0.093}$	$-0.063^{+0.244}_{-0.298}$	$-0.503^{+0.253}_{-0.288}$	$-0.808^{+0.226}_{-0.303}$	$-0.201^{+0.261}_{-0.274}$	$-0.623^{+0.255}_{-0.295}$
$11.0 < q^2 < 11.75$	$0.502^{+0.09}_{-0.082}$	$-0.869^{+0.304}_{-0.408}$	$0.494^{+0.134}_{-0.071}$	$0.166^{+0.221}_{-0.192}$	$-0.522^{+0.203}_{-0.222}$	$-0.485^{+0.203}_{-0.224}$	$-0.233^{+0.227}_{-0.224}$	$-0.159^{+0.241}_{-0.25}$
$11.75 < q^2 < 12.5$	$0.734^{+0.107}_{-0.094}$	$-1.002^{+0.502}_{-1.36}$	$0.637^{+0.599}_{-0.1}$	$-0.105^{+0.349}_{-0.42}$	$-0.701^{+0.215}_{-0.342}$	$-0.827^{+0.205}_{-0.357}$	$-0.473^{+0.233}_{-0.344}$	$-0.211^{+0.255}_{-0.274}$
$15.0 < q^2 < 16.0$	$0.385^{+0.067}_{-0.066}$	$-0.199^{+0.28}_{-0.285}$	$0.433^{+0.074}_{-0.054}$	$0.087^{+0.144}_{-0.135}$	$-0.673^{+0.178}_{-0.199}$	$-0.758^{+0.165}_{-0.179}$	$0.083^{+0.189}_{-0.187}$	$-0.12^{+0.192}_{-0.198}$
$16.0 < q^2 < 17.0$	$0.295^{+0.058}_{-0.062}$	$-0.726^{+0.239}_{-0.241}$	$0.43^{+0.063}_{-0.049}$	$0.019^{+0.122}_{-0.119}$	$-0.552^{+0.191}_{-0.213}$	$-0.567^{+0.157}_{-0.186}$	$0.328^{+0.192}_{-0.195}$	$0.122^{+0.199}_{-0.196}$
$17.0 < q^2 < 18.0$	$0.363^{+0.073}_{-0.072}$	$-0.313^{+0.286}_{-0.293}$	$0.288^{+0.075}_{-0.064}$	$0.144^{+0.149}_{-0.147}$	$-0.486^{+0.19}_{-0.2}$	$-0.646^{+0.176}_{-0.19}$	$0.047^{+0.198}_{-0.197}$	$-0.006^{+0.199}_{-0.215}$
$18.0 < q^2 < 19.0$	$0.421^{+0.1}_{-0.1}$	$-0.45^{+0.44}_{-0.447}$	$0.393^{+0.159}_{-0.1}$	$0.134^{+0.219}_{-0.208}$	$-1.221^{+0.28}_{-0.388}$	$-1.07^{+0.237}_{-0.349}$	$0.128^{+0.246}_{-0.265}$	$0.3^{+0.297}_{-0.276}$
$15.0 < q^2 < 19.0$	$0.357^{+0.035}_{-0.035}$	$-0.424^{+0.139}_{-0.15}$	$0.385^{+0.035}_{-0.036}$	$0.089^{+0.071}_{-0.072}$	$-0.663^{+0.102}_{-0.105}$	$-0.709^{+0.093}_{-0.09}$	$0.14^{+0.101}_{-0.1}$	$0.049^{+0.106}_{-0.102}$
$1.1 < q^2 < 2.5$	$0.75^{+0.097}_{-0.095}$	$0.227^{+0.86}_{-0.764}$	$-0.547^{+0.13}_{-0.64}$	$0.234^{+0.468}_{-0.361}$	$-0.082^{+0.313}_{-0.318}$	$0.586^{+0.386}_{-0.237}$	$-0.714^{+0.244}_{-0.459}$	$-0.363^{+0.309}_{-0.414}$
$2.5 < q^2 < 4.0$	$0.785^{+0.115}_{-0.08}$	$0.399^{+1.507}_{-0.817}$	$-0.227^{+0.179}_{-0.492}$	$0.483^{+1.106}_{-0.306}$	$-0.511^{+0.321}_{-0.505}$	$-0.02^{+0.344}_{-0.348}$	$0.155^{+0.378}_{-0.327}$	$0.057^{+0.381}_{-0.397}$
$4.0 < q^2 < 6.0$	$0.742^{+0.083}_{-0.07}$	$0.282^{+0.698}_{-0.513}$	$0.114^{+0.193}_{-0.132}$	$-0.16^{+0.25}_{-0.377}$	$-0.431^{+0.241}_{-0.287}$	$-0.43^{+0.201}_{-0.265}$	$-0.071^{+0.199}_{-0.218}$	$0.094^{+0.25}_{-0.232}$
$6.0 < q^2 < 8.0$	$0.612^{+0.065}_{-0.059}$	$-0.349^{+0.328}_{-0.371}$	$0.256^{+0.103}_{-0.072}$	$-0.119^{+0.165}_{-0.187}$	$-0.572^{+0.173}_{-0.183}$	$-0.745^{+0.162}_{-0.18}$	$-0.103^{+0.18}_{-0.181}$	$-0.241^{+0.186}_{-0.187}$
$11.0 < q^2 < 12.5$	$0.621^{+0.069}_{-0.063}$	$-0.954^{+0.293}_{-0.439}$	$0.564^{+0.16}_{-0.069}$	$0.061^{+0.192}_{-0.168}$	$-0.588^{+0.147}_{-0.162}$	$-0.63^{+0.144}_{-0.166}$	$-0.342^{+0.161}_{-0.168}$	$-0.177^{+0.168}_{-0.169}$
$15.0 < q^2 < 17.0$	$0.339^{+0.044}_{-0.045}$	$-0.478^{+0.179}_{-0.186}$	$0.433^{+0.046}_{-0.038}$	$0.052^{+0.092}_{-0.089}$	$-0.607^{+0.132}_{-0.138}$	$-0.658^{+0.116}_{-0.122}$	$0.197^{+0.132}_{-0.133}$	$0.002^{+0.135}_{-0.137}$
$17.0 < q^2 < 19.0$	$0.383^{+0.057}_{-0.057}$	$-0.359^{+0.242}_{-0.235}$	$0.323^{+0.067}_{-0.056}$	$0.145^{+0.121}_{-0.117}$	$-0.762^{+0.16}_{-0.172}$	$-0.796^{+0.14}_{-0.166}$	$0.066^{+0.153}_{-0.15}$	$0.117^{+0.164}_{-0.162}$

9.3 Comparison of results from likelihood fit and method of moments

A comparison between the results of the likelihood fit (including the FC) and the moments (including the interval from the bootstrapping) is provided for the S_i and the A_i observables in Figs. 76 and 77. Systematic uncertainties have been included for both the likelihood fit and the method of moments. The difference between the observables is consistent with expectation, given the typical differences between the two estimators ($\sim 50\%$ of the statistical uncertainty in toys).

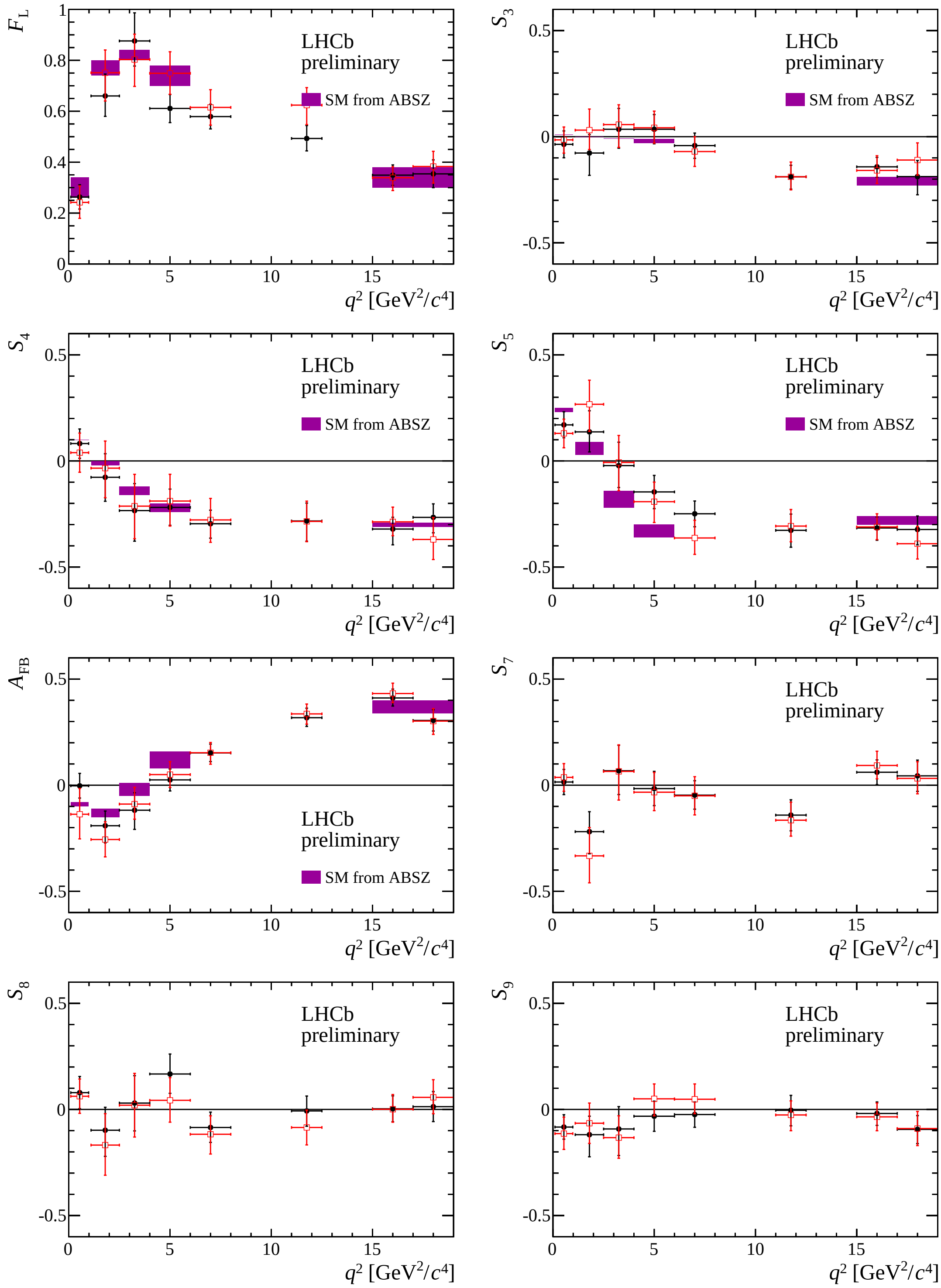

Figure 76: Comparison of the results from the likelihood fit (black closed markers) to the method of moments (red open markers) in the $2\,\mathrm{GeV}^2/c^4$ binning scheme for the S_i observables.

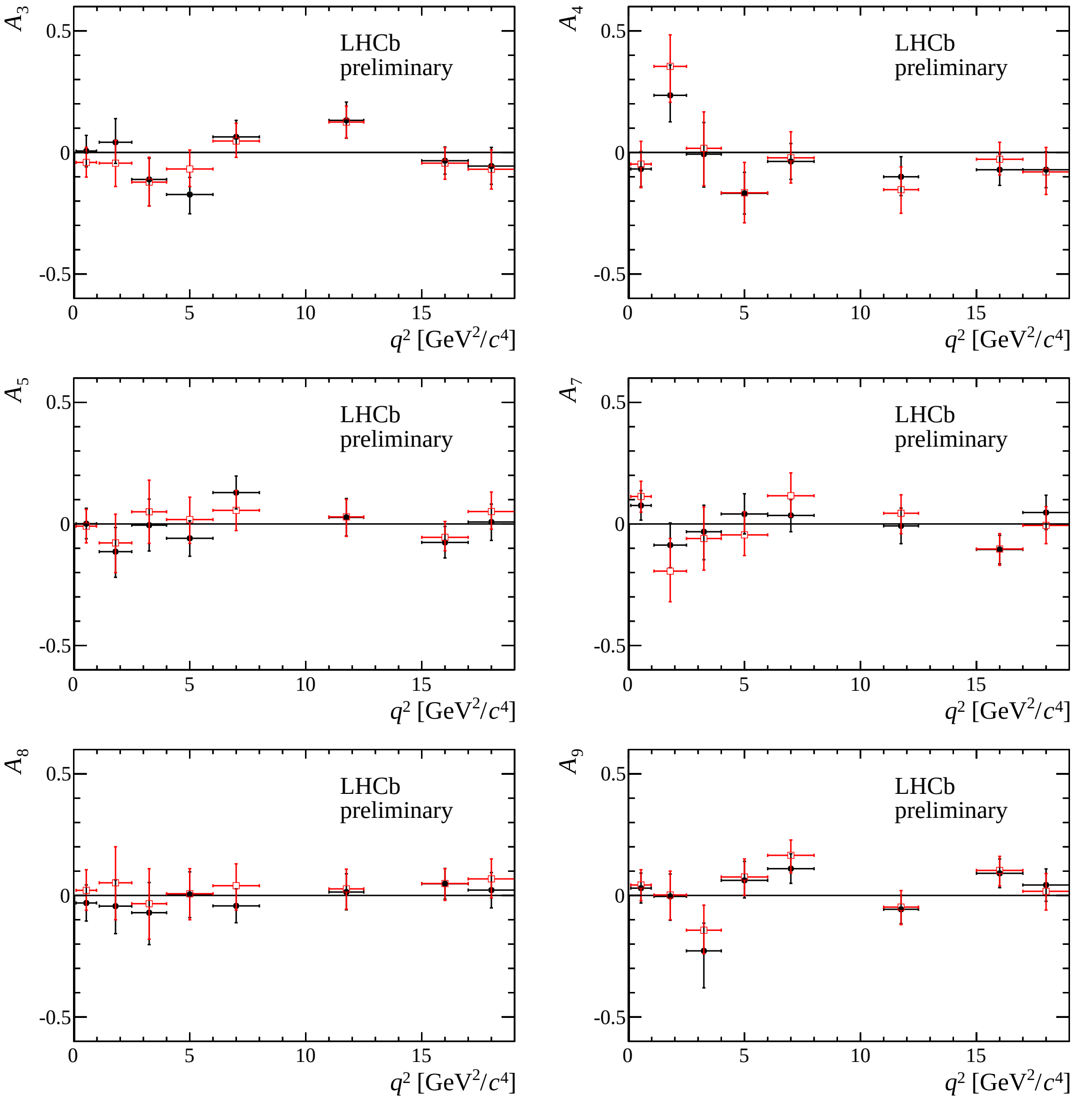

Figure 77: Comparison of the results from the likelihood fit (black closed markers) to the method of moments (red open markers) in the 2 GeV$^2/c^4$ binning scheme for the A_i observables..

9.4 Results of the fits for the amplitudes

9.4.1 Direct fit to the data

The resulting projections of the pdf and the data are shown in Figs. 78 and 79, integrated accross the full B^0 mass region and 50 MeV/c^2 around the nominal B^0 mass respectively. In order to ensure the fit converges at the global minimum, the fit is repeated fifty times from a randomised starting point sampled from a Gaussian distribution centered at the SM value with a width of $\pm 500\%$ of the SM value, and the lowest likelihood point is selected. A good description of the data is observed.

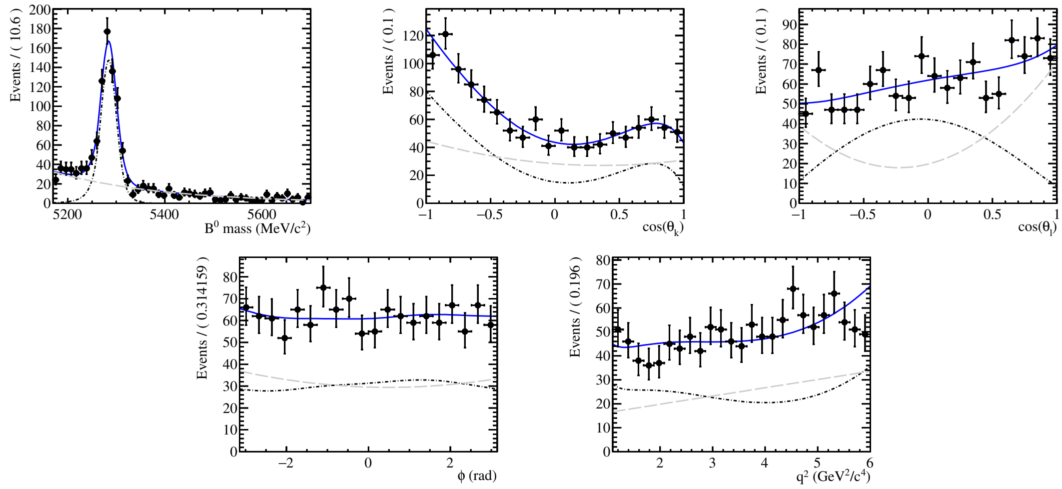

Figure 78: Mass and angular projections of the results of the fit to $B^0 \to \mu^+\mu^- K^{*0}$ data.

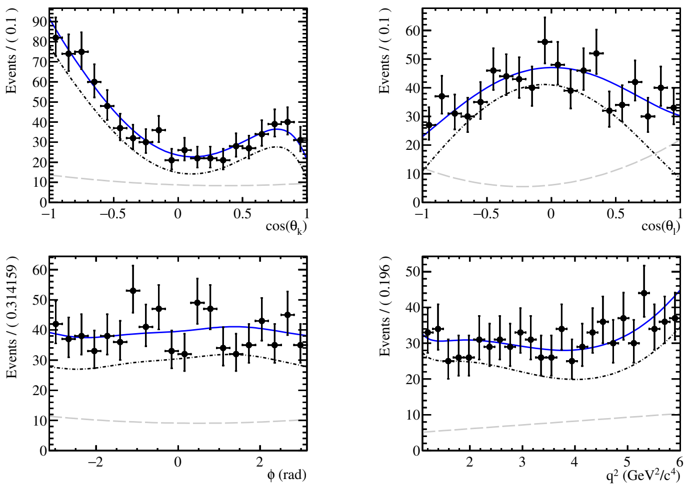

Figure 79: Mass and angular projections of the results of the fit to $B^0 \to \mu^+\mu^- K^{*0}$ data, 50 MeV/c^2 around the nominal B^0 mass.

9.4.2 One dimensional profile likelihoods

As briefly mentioned in Sec. 6.4.11, the result of the fit to the amplitude coefficients in the data is unfortunately such that one cannot simply provide a best-fit point and an error matrix of the amplitude coefficients. Figures 80 and 81 show the one-dimensional likelihood profiles of the amplitude coefficients in the fit to the data. For each scanning point, the fit is repeated fifty times as mentioned above, and the lowest likelihood point is selected. It is clear that the exact symmetry $A_i \to -A_i$ described in Sec. **??** is apparent. The black and red points correspond to cases where the fit landed at the original or the symmetric solution respectively. This separation is exact for the left handed amplitudes, by requiring that $\mathrm{Re}(A_0^L)$ is negative (positive). For the right-handed amplitudes the separation can be performed by requiring that $\mathrm{Re}(A_\parallel^R)$ is negative (positive) at $q^2 = 2\ \mathrm{GeV}^2/c^4$. However for the right-handed amplitudes this separation is not exact.

The left-handed amplitudes exhibit a parabolic profile. The right-handed ones however appear more problematic. Specifically, $\mathrm{Im}(A_\parallel^R)$ is clearly non-parabolic and $\mathrm{Re}(A_\perp^R)$ appears to have a set of "horns" which signify the presence of a local minimum 0.8 likelihood units away from the minimum. This will become more apparent in the following section. Given the shape of the 1D profile likelihoods it is evident that a simple coveriance matrix is not sufficient in order to convey the full information of the amplitude fit.

9.4.3 Bootstrapping the data

The Bootstrapping technique [34] can be employed to determine the intervals of measured quantities when an analytic description is insufficient. Two dimensional histograms of the distributions of the amplitudes vs q^2, from fits of 11.5K bootstraps of the data, are shown in Fig. 82. Each fit is repeated 50 times by randomizing the starting point 500% around the SM values. The $A_i \to -A_i$ degeneracy is broken by requiring that the resulting amplitudes from the fit satisfy $\mathrm{Re}(A_0^L) < 0$ and $\phi(A_\parallel^R) < 1.57$ at $q^2 = 2\ \mathrm{GeV}^2/c^4$. It is evident that a second solution exists for $\mathrm{Re}(A_\perp^R)$ and $\mathrm{Re}(A_\perp^R)$. This second solution is consistent with the "horn" feature observed in the 1D profiles of $\mathrm{Re}(A_\perp^R)$ (see Fig. 81). We can conclude therefore that this second solution corresponds to a local minimum 0.8 NLL units from the minimum of the original LHCb dataset. The closeness of these two solutions means that they cannot be separated and therefore if the bootstraps are used to quote an interval, the spread of the boostraps including both solutions will be considered.

In principle intervals could be provided for the amplitude coefficients, however the presence of the exact symmetry $A_i \to -A_i$, makes the determination of whether the coverage is correct difficult. However the angular observables (S_i) are invariant under this exact symmetry. Therefore testing the coverage of the bootraps for the observables S_i is indeed possible.

The bootstrap coverage is tested by generating 1000 signal and background toy datasets using the model obtained from the best fit to the LHCb data. Each toy dataset is bootstrapped 200 times. A fit is then performed to each bootstrapped dataset of each generated toy dataset. Each fit is repeated fifty times with a randomized starting point as

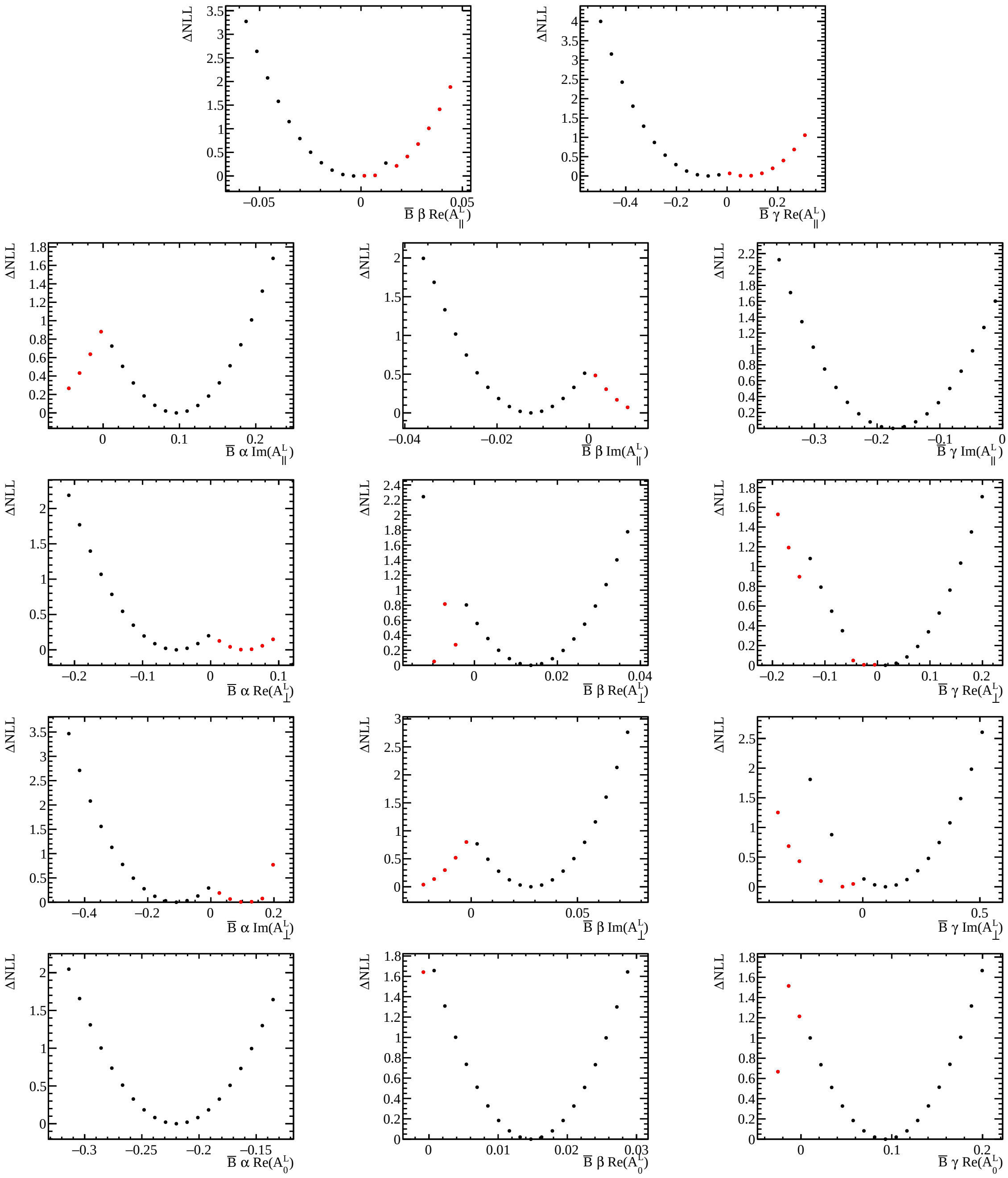

Figure 80: One dimensional profile likelihoods of left handed $\overline{B}^0$ amplitude coefficients from a fit to the data. The black (red) points correspond to cases where the fit landed at a nominal (symmetric) point under $A_i \to -A_i$. For more details please see the text.

discussed in Sec. 9.4.1 and the fit with the lowest NLL is kept. This results in a total of 10M fits.

For each toy dataset the interval on an observable is constructed by calculating the

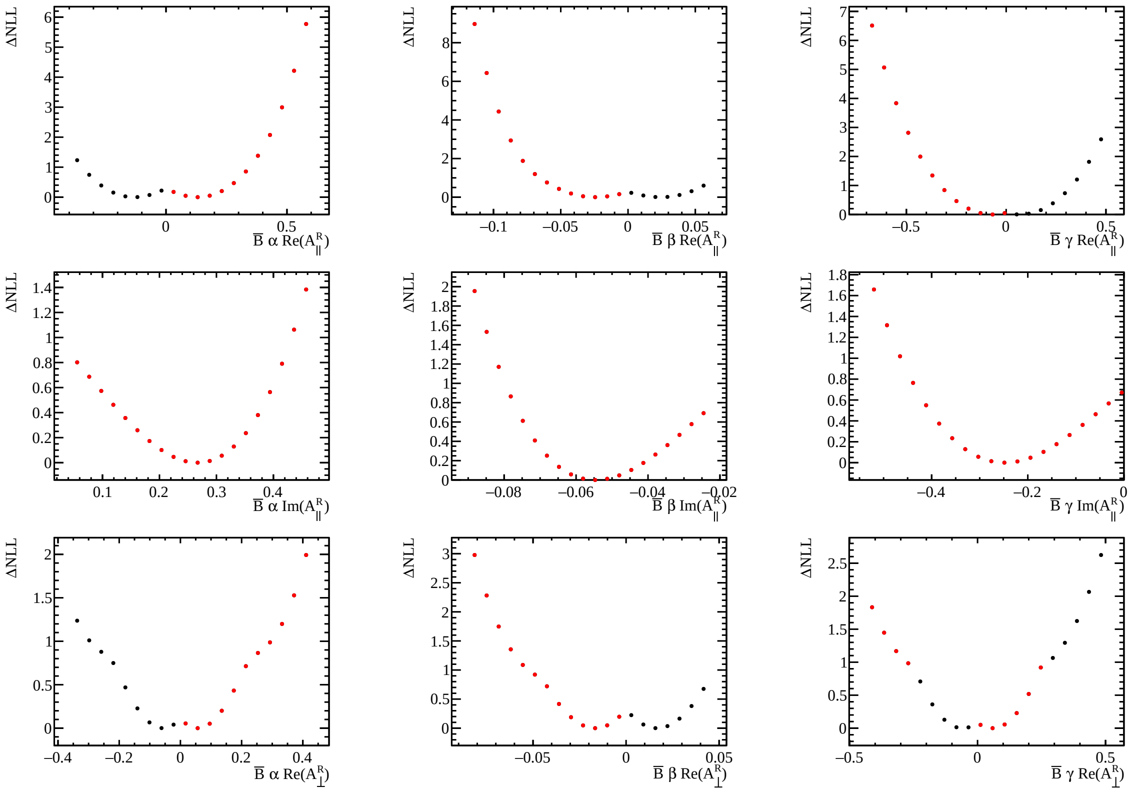

Figure 81: One dimensional profile likelihoods of right handed $\overline{B}^0$ amplitude coefficients from a fit to the data. The black (red) points correspond to cases where the fit landed at a nominal (symmetric) point under $A_i \to -A_i$. For more details please see the text.

S_is out of the amplitude coefficients. The 16th and 84th percentiles of the bootstraps for each toy, of the S_i observables at six points in q^2, are then computed. If these intervals contain the values of the observables, used in the generation of the toys, 68% of the time then the coverage of the bootstrap technique is correct at the 1 σ level. The traditional method of requiring the pull to be a normal distribution is insufficient as the observables are non-gaussianly distributed both int the toys and in the bootstraps of the toys.

Tables 38 to 45 show the coverage of the bootstrap method. Overall the coverage at the 1 σ level is correct. However there are some exeptions for S_8 and S_9 which are not understood. This motivates the use of the bootstrap method to obtain the coverage for S_4, S_5 and S_{6s} as well as their corresponding zero-crossing points.

9.4.4 Results on observables using bootstraps

The results of S_4, S_5 and S_{6s} as a function of q^2 are shown in Fig. 83. The intervals are determined from the bootstraps by calculating the 16th and 84th percentiles of the distributions at each q^2 point. The solid line corresponds to the best fit point of the original dataset and the dashed line to the median of the distribution of the bootstraps.

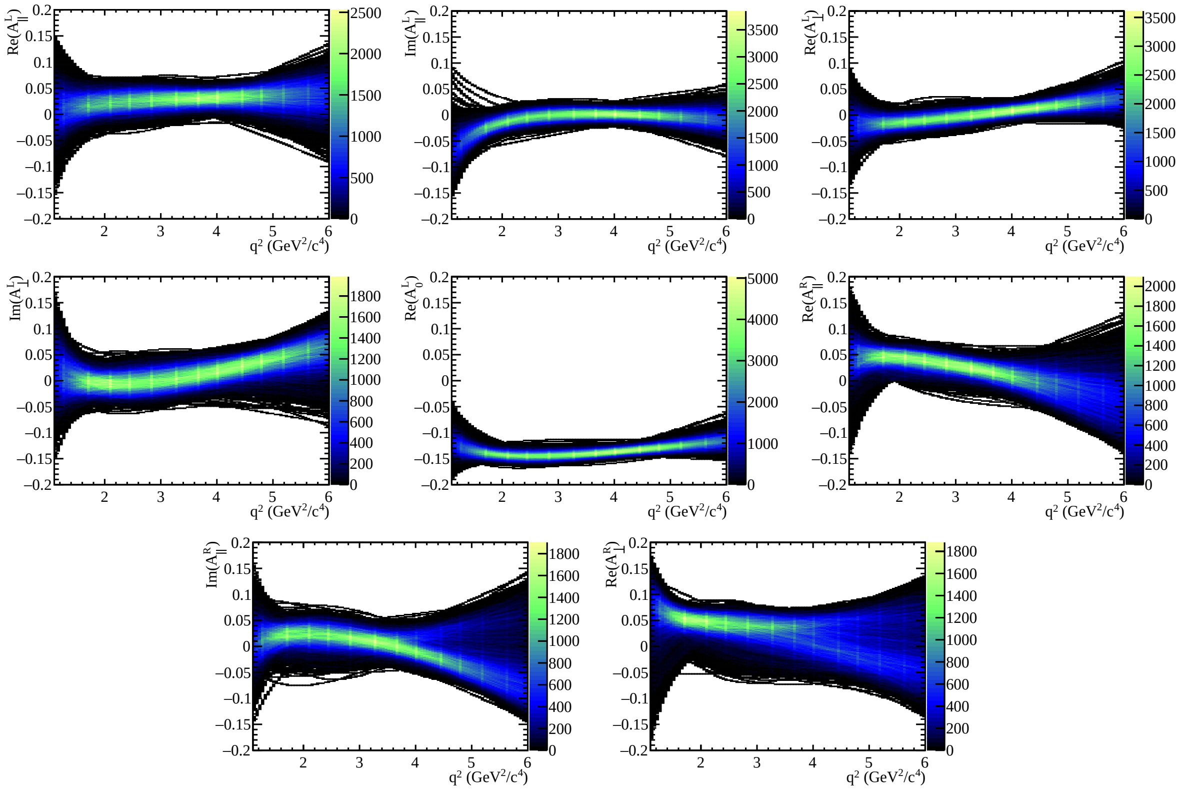

Figure 82: Distribution of amplitudes as a function of q^2 as obtained by bootstrapping the data 11.5K times and fitting it each time. The shadow seen at the high q^2 region of $\mathrm{Re}(A_{\perp}^{R})$ and $\mathrm{Im}(A_{\parallel}^{R})$ corresponds to the presence of the local minimum present in the likelihood of the original LHCb dataset.

Systematic uncertainties are included, however their effect is negligible. These figures are intended for publication but only for aesthetic purposes, as their correlations will

q^2 value (GeV^2/c^4)	Frac. 68% of boots
	S_{1c}
1.104	$0.650 \pm 0.041(toys) \pm 0.021(boot.)$
2.000	$0.695 \pm 0.043(toys) \pm 0.015(boot.)$
3.000	$0.577 \pm 0.039(toys) \pm 0.013(boot.)$
4.000	$0.585 \pm 0.039(toys) \pm 0.023(boot.)$
5.000	$0.621 \pm 0.040(toys) \pm 0.013(boot.)$
6.000	$0.666 \pm 0.042(toys) \pm 0.023(boot.)$

Table 38: Bootstrap coverage of S_{1c}

q^2 value (GeV^2/c^4)	Frac. 68% of boots
	S_3
1.104	$0.650 \pm 0.041(toys) \pm 0.016(boot.)$
2.000	$0.715 \pm 0.043(toys) \pm 0.018(boot.)$
3.000	$0.671 \pm 0.042(toys) \pm 0.018(boot.)$
4.000	$0.778 \pm 0.045(toys) \pm 0.010(boot.)$
5.000	$0.736 \pm 0.044(toys) \pm 0.003(boot.)$
6.000	$0.715 \pm 0.043(toys) \pm 0.023(boot.)$

Table 39: Bootstrap coverage of S_3

q^2 value (GeV^2/c^4)	Frac. 68% of boots
	S_4
1.104	$0.658 \pm 0.041(toys) \pm 0.005(boot.)$
2.000	$0.728 \pm 0.044(toys) \pm 0.013(boot.)$
3.000	$0.627 \pm 0.040(toys) \pm 0.018(boot.)$
4.000	$0.590 \pm 0.039(toys) \pm 0.031(boot.)$
5.000	$0.705 \pm 0.043(toys) \pm 0.023(boot.)$
6.000	$0.713 \pm 0.043(toys) \pm 0.010(boot.)$

Table 40: Bootstrap coverage of S_4

not be provided. However we plan to provide results of the zero-crossing points of these observables as will be discussed in the next section.

q^2 value (GeV^2/c^4)	Frac. 68% of boots
	S_5
1.104	$0.705 \pm 0.043(toys) \pm 0.013(boot.)$
2.000	$0.658 \pm 0.041(toys) \pm 0.015(boot.)$
3.000	$0.679 \pm 0.042(toys) \pm 0.013(boot.)$
4.000	$0.689 \pm 0.042(toys) \pm 0.010(boot.)$
5.000	$0.708 \pm 0.043(toys) \pm 0.013(boot.)$
6.000	$0.676 \pm 0.042(toys) \pm 0.016(boot.)$

Table 41: Bootstrap coverage of S_5

q^2 value (GeV^2/c^4)	Frac. 68% of boots
	S_{6s}
1.104	$0.663 \pm 0.042(toys) \pm 0.013(boot.)$
2.000	$0.598 \pm 0.040(toys) \pm 0.034(boot.)$
3.000	$0.658 \pm 0.041(toys) \pm 0.010(boot.)$
4.000	$0.731 \pm 0.044(toys) \pm 0.015(boot.)$
5.000	$0.715 \pm 0.043(toys) \pm 0.013(boot.)$
6.000	$0.728 \pm 0.044(toys) \pm 0.018(boot.)$

Table 42: Bootstrap coverage of S_{6s}

q^2 value (GeV^2/c^4)	Frac. 68% of boots
	S_7
1.104	$0.582 \pm 0.039(toys) \pm 0.029(boot.)$
2.000	$0.723 \pm 0.043(toys) \pm 0.016(boot.)$
3.000	$0.692 \pm 0.043(toys) \pm 0.005(boot.)$
4.000	$0.661 \pm 0.042(toys) \pm 0.005(boot.)$
5.000	$0.674 \pm 0.042(toys) \pm 0.005(boot.)$
6.000	$0.705 \pm 0.043(toys) \pm 0.003(boot.)$

Table 43: Bootstrap coverage of S_7

9.4.5 Zero-Crossing Point measurements

The expression of the observables as a function of q^2 enables the analytic determination of the point at which the obervable crosses zero. Given the amplitude ansatz and the fact

q^2 value (GeV^2/c^4)	Frac. 68% of boots
	S_8
1.104	$0.648 \pm 0.041(toys) \pm 0.016(boot.)$
2.000	$0.671 \pm 0.042(toys) \pm 0.047(boot.)$
3.000	$0.731 \pm 0.044(toys) \pm 0.018(boot.)$
4.000	$0.595 \pm 0.039(toys) \pm 0.021(boot.)$
5.000	$\mathbf{0.535 \pm 0.037(toys) \pm 0.039(boot.)}$
6.000	$0.554 \pm 0.038(toys) \pm 0.050(boot.)$

Table 44: Bootstrap coverage of S_8

q^2 value (GeV^2/c^4)	Frac. 68% of boots
	S_9
1.104	$0.721 \pm 0.043(toys) \pm 0.010(boot.)$
2.000	$\mathbf{0.520 \pm 0.037(toys) \pm 0.016(boot.)}$
3.000	$0.728 \pm 0.044(toys) \pm 0.013(boot.)$
4.000	$\mathbf{0.548 \pm 0.038(toys) \pm 0.018(boot.)}$
5.000	$0.747 \pm 0.044(toys) \pm 0.018(boot.)$
6.000	$0.661 \pm 0.042(toys) \pm 0.016(boot.)$

Table 45: Bootstrap coverage of S_9

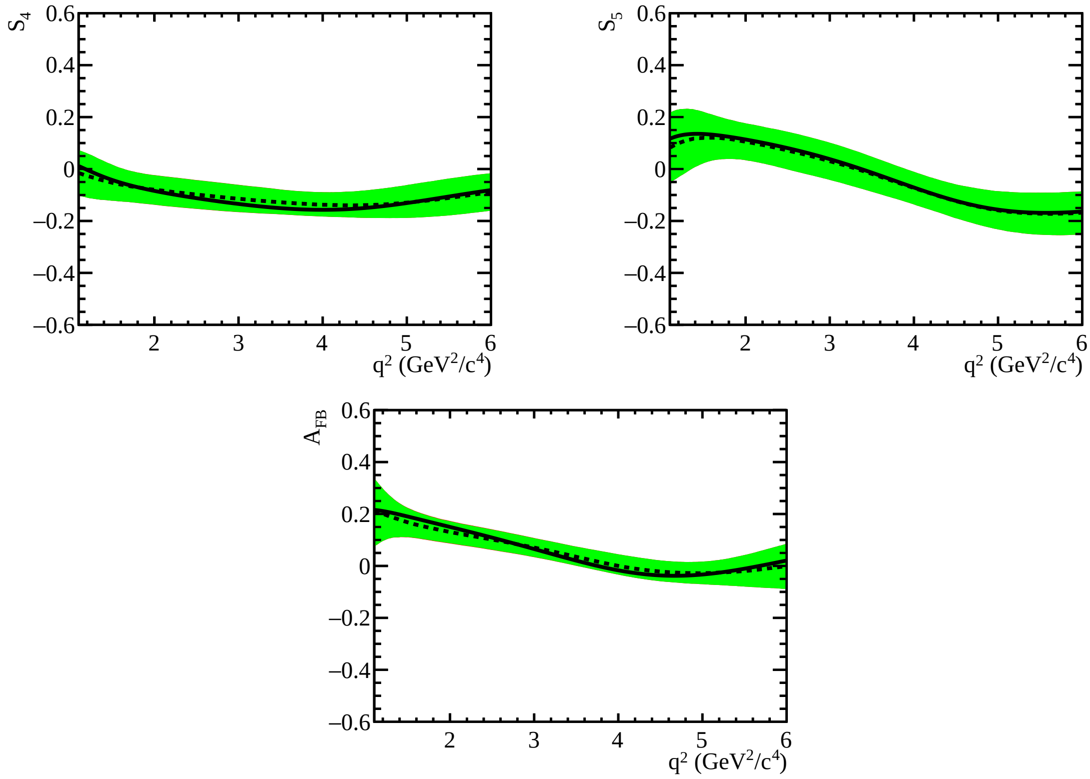

Figure 83: Results of the amplitudes fits for S_4, S_5 and A_{FB}. The solid line is the result of the fit to the data and the dashed line is the median of the distribution of the bootstraps. The green band corresponds to the 16th and 84th percentile obtained from bootstrapping the data. Systematic uncertainties have been added in quadrature (red band) however their effect is negligible

that the numerator of the S_i observables are bilinear combinations of the amplitudes, the determination of the ZCP reduces to solving a quartic equation. The sign of the slope in the viscinity of the ZCP helps to choose the solutions which are expected given theory and experimental measurements in the q^2 range in question.

The q^2 parametrisation of the amplitudes is known not to hold below ~ 1 GeV$^2/c^4$ due to the presence of the ϕ resonance and also the effect the muon mass has on the symmetries of the angular distribution. In addition, the choice to only fit up to 6 GeV$^2/c^4$ in q^2 restricts the range of ZCPs that can be quoted to the range $1.1 - 6.0$ GeV$^2/c^4$.

The bootstrap technique is chosen in order to quote the 68% interval of the ZCPs. In order to guarantee the correct statistical coverage of the bootstraps, the ZCP will only be given for S_4, S_5 and $A_{FB}(S_{6s})$. Out of these observables only the ZCP with the correctly-signed slope in the viscinity of the ZCP will be quoted. If a ZCP is such that a well defined 68% interval cannot be quoted, the point in q^2 above which 5% of the bootstraps lie, will be quoted.

Figure 84 shows the distributions the ZCPs with the correctly signed slope for observables S_4 S_5 and A_{FB}. The fraction of bootstraps where there is correctly-signed ZCP within the q^2 range between 1.1 and 6.0 GeV$^2/c^4$ is $\sim 10\%$. This fraction is accounted for when estimating the 16th and 84th percentiles of the bootstraps distributions, by randomly assigning half of these 10% bootstraps to plus-infinity and the other half to minus-infinity.

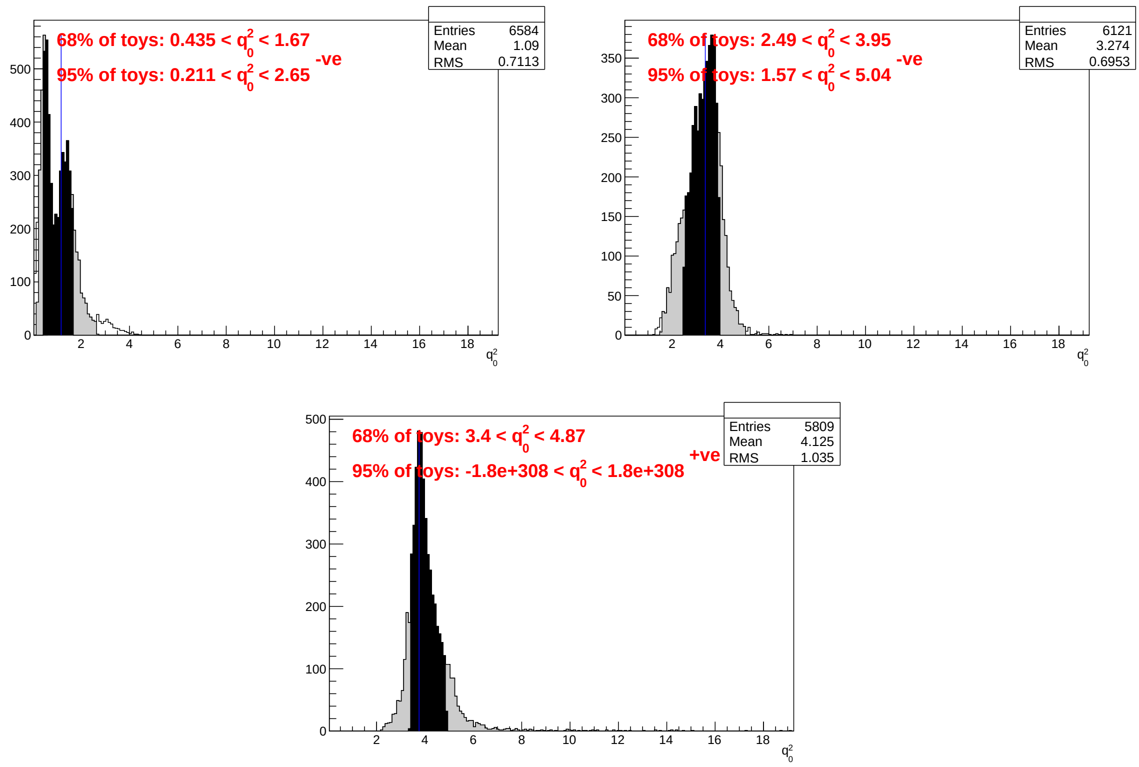

Figure 84: Distributions of the ZCPs with the correctly signed slope for observables S_4 (left) S_5 (right) and S_{6s} (bottom) from the bootstraps.

For S_4, a 68% interval cannot be defined within 1.1 and 6 GeV$^2/c^4$. However 5% of

Observable	interval (GeV^2/c^4)	syst. unc.
S_4	< 2.65 at 95%	0.01
S_5	$(2.49, 3.95)$	0.02
S_{6s}	$(3.4, 4.87)$	0.13

Table 46: Summary of intervals of the ZCP from bootstraps. For S_4 a lower limit is quoted.

bootstraps have a ZCP above 2.65 GeV^2/c^4. Therefore this upper q^2 limit will be quoted. The summary of all the intervals along with the systematic uncertainty is shown in Tab. 46.

10 Systematic uncertainties

The main systematic effects that need to be evaluated by all three angular analysis methods are related to the acceptance correction. Here, the statistical uncertainty of the acceptance correction from simulation as well as possible differences between simulation and data need to be considered. In addition, possible biases from pollution by peaking backgrounds and the background parametrization need to be determined.

The strategy for determining the aforementioned systematic uncertainties involves using high statistics toy data generated by varying the parameters in question (e.g acceptance or background parameters) and fitting/counting back these datasets using both the nominal and systematically varied models. The spread of the variation of the parameter of interest is then taken as the systematic uncertainty on that parameter.

10.1 Systematics for observable fits

10.1.1 Statistical uncertainty of the four-dimensional acceptance

The four-dimensional acceptance described in Sec. 8 relies on the determination of Legendre coefficients from a sample of simulated $B^0 \to K^{*0}\mu^+\mu^-$ phase-space events. To determine the effect of the limited size of the simulated sample, the covariance matrix of the coefficients is determined alongside their numerical values. High statistics toy studies are then performed, where events are generated with an acceptance that is varied according to the (inverse) covariance matrix. These simulated events are then fit using both the varied and the nominal acceptance. Fig. 85 gives the distributions for 500 toy experiments for the q^2 bin in the range $0.1 < q^2 < 1.0\,\mathrm{GeV}^2/c^4$. The observed deviations of the parameters are fit using Gaussian functions. The distributions are centered around 0, their widths are used as systematic uncertainties due to the statistical uncertainty of the acceptance. Tab. 47 gives the resulting systematic uncertainties for all q^2 bins. They are negligible compared to the expected statistical uncertainties.

10.1.2 Differences between data and simulation

The determination of the acceptance relies on accurate simulation of the signal decay $B^0 \to K^{*0}\mu^+\mu^-$. The control decay $B^0 \to J/\psi\, K^{*0}$ is used to cross-check if distributions in data are reproduced properly. Ref. [13] describes the procedure used to correct the unsatisfactory simulation of the transverse momentum of the signal B^0, as well as the B^0 vertex χ^2 and the track multiplicity in the event. The effect of these corrections on the acceptance is evaluated by redetermining the acceptance correction without the reweighting. Toy studies are performed to evaluate the effect on the observables. The results are given in Tabs. 48, 49 and 50. All deviations seen are negligible.

In addition, there are small differences for the kinematic variables of the B^0 daughter particles. Fig. 86 shows the (transverse) momentum for the signal kaon and pion for both truth-matched simulated events as well as $B^0 \to J/\psi\, K^{*0}$ events from data. The distributions for data are extracted using the *sWeighting* technique. To minimize the influence of pollution from an S-wave component which is not simulated in data, the window for invariant mass of the $K^+\pi^-$ system is reduced from the nominal $\pm 100\,\mathrm{MeV}/c^2$ to $\pm 20\,\mathrm{MeV}/c^2$. From the two-dimensional distributions of K^+ and π^- in data and simulation a correction factor is determined. This correction factor, depending on the particles momentum and transverse momentum is given in shown in Fig. 87. The systematic uncertainty from the modeling of the signal decay is then evaluated using toy studies where the acceptance is redetermined using the reweightings. Tabs. 51 and 52 give the resulting systematic uncertainties for the reweighting of both kaon and pion. While the reweighting of the kaon has a negligible effect, there is an, albeit small, systematic uncertainty for the reweighting of the pion.

10.1.3 Fixing of q^2 for four-dimensional acceptance

For the $2\,\mathrm{GeV}^2/c^4$ bins, the efficiency is included in the PDF in the fit, since a weighted fit of the data is less stable for the small statistics in these narrow bins[5]. The PDF used to

[5] The unfolding can be used for the larger q^2 bins $1 < q^2 < 6\,\mathrm{GeV}^2/c^4$ and $15 < q^2 < 19\,\mathrm{GeV}^2/c^4$.

Figure 85: Distributions of deviations of observables from toy experiment for the first q^2 bin in the range $0.1 < q^2 < 1.0\,\mathrm{GeV}^2/c^4$. Events are generated with an acceptance varied according to its statistical uncertainty and fit back using the nominal acceptance.

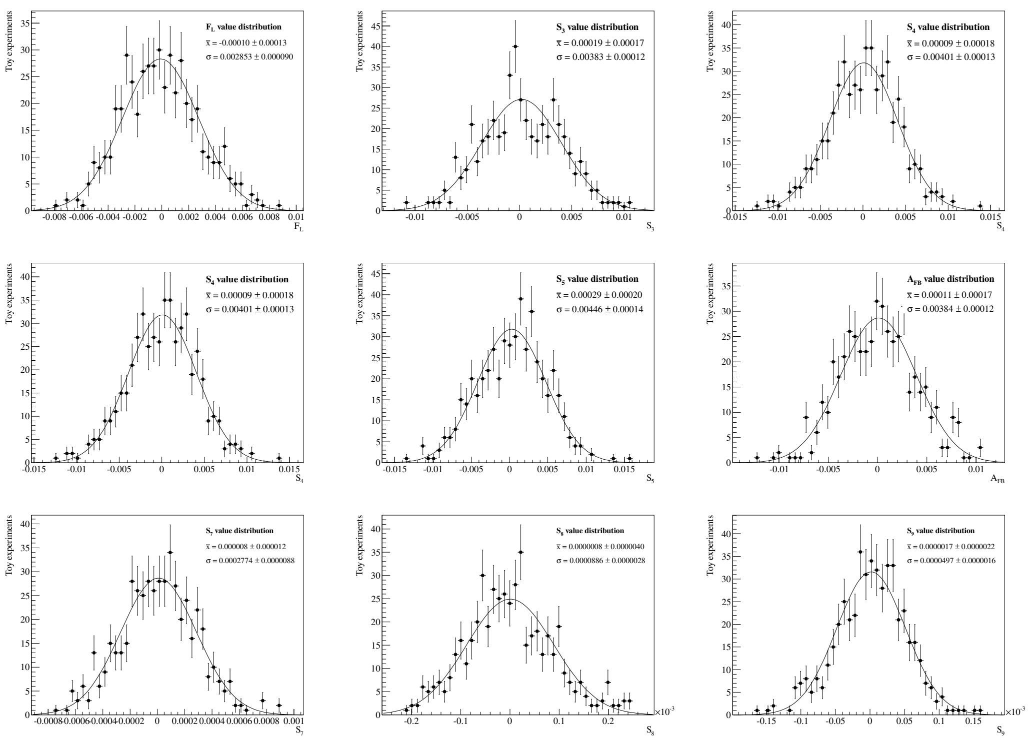

Table 47: Systematic uncertainties due to the statistical uncertainty on the four-dimensional acceptance. Ranges of q^2 bins are given in GeV^2/c^4.

$0.1 < q^2 < 1.0$		$1.0 < q^2 < 2.5$		$2.5 < q^2 < 4.0$		$4.0 < q^2 < 6.0$		$6.0 < q^2 < 8.0$	
param.	$\sigma_{\text{syst.}}$	param.	$\sigma_{\text{syst.}}$	param.	$\sigma_{\text{syst.}}$	param.	$\sigma_{\text{syst.}}$	param.	$\sigma_{\text{syst.}}$
F_L	0.0029	F_L	0.0018	F_L	0.0013	F_L	0.0012	F_L	0.0013
S_3	0.0038	S_3	0.0015	S_3	0.0012	S_3	0.0012	S_3	0.0013
S_4	0.0040	S_4	0.0025	S_4	0.0018	S_4	0.0015	S_4	0.0012
S_5	0.0045	S_5	0.0026	S_5	0.0022	S_5	0.0018	S_5	0.0018
A_{FB}	0.0038	A_{FB}	0.0013	A_{FB}	0.0009	A_{FB}	0.0008	A_{FB}	0.0009
S_7	0.0003	S_7	0.0002	S_7	0.0001	S_7	0.0001	S_7	0.0001
S_8	0.0001	S_8	0.0001	S_8	0.0001	S_8	0.0000	S_8	0.0000
S_9	0.0000	S_9	0.0001	S_9	0.0000	S_9	0.0000	S_9	0.0000

$15.0 < q^2 < 17.0$		$17.0 < q^2 < 19.0$		$11.0 < q^2 < 12.5$		$1.1 < q^2 < 6.0$		$15.0 < q^2 < 19.0$	
param.	$\sigma_{\text{syst.}}$	param.	$\sigma_{\text{syst.}}$	param.	$\sigma_{\text{syst.}}$	param.	$\sigma_{\text{syst.}}$	param.	$\sigma_{\text{syst.}}$
F_L	0.0025	F_L	0.0044	F_L	0.0017	F_L	0.0012	F_L	0.0029
S_3	0.0030	S_3	0.0067	S_3	0.0017	S_3	0.0011	S_3	0.0039
S_4	0.0021	S_4	0.0037	S_4	0.0012	S_4	0.0016	S_4	0.0023
S_5	0.0028	S_5	0.0046	S_5	0.0019	S_5	0.0018	S_5	0.0031
A_{FB}	0.0020	A_{FB}	0.0037	A_{FB}	0.0012	A_{FB}	0.0007	A_{FB}	0.0022
S_7	0.0000	S_7	0.0000	S_7	0.0000	S_7	0.0001	S_7	0.0001
S_8	0.0000	S_8	0.0000	S_8	0.0000	S_8	0.0001	S_8	0.0001
S_9	0.0000	S_9	0.0000	S_9	0.0000	S_9	0.0000	S_9	0.0000

fit the observables is in itself not q^2 dependent, therefore the four-dimensional efficiency is evaluated for a fixed q^2. The nominal setting is to use the mean of the q^2 bin to determine the efficiency used for the specific bin. To evaluate a possible systematic bias from this choice, toy experiments are used to determine the deviation for the observables seen for fixing q^2 for the mean of the bin, q^2_{mean}, as well as $q^2_{\text{mean}} \pm \frac{3}{4}\Delta q^2$, where the q^2 bin is given by $[q^2_{\text{mean}} - \Delta q^2, q^2_{\text{mean}} + \Delta q^2]$. The largest deviation is taken as systematic uncertainty and given in Tab. 53 for all observables and q^2 bins. While this approach likely overestimates the systematic effect, the resulting systematic uncertainties are small compared to the expected statistical errors.

10.1.4 Higher order acceptance model

There is some choice in the maximum order of the Legendre polynomials used to model the four-dimensional acceptance. While higher orders generaly will be able to describe details in the acceptance better, more coefficients also will lead to higher computational requirements. An additional potential drawback of higher order polynomials are oscillations at the borders of the intervals (Runge phenomenon). Therefore the lowest order of polynomials that describes the acceptance sufficiently well should be chosen. A higher order parametrisation is used to determine a systematic uncertainty of this choice.

Figure 86: Distribution of p and p_T for (up) K^+ and (down) π^- for *sWeighted* $B^0 \to J/\psi\, K^{*0}$ candidates from data (black) and truthmatched $B^0 \to J/\psi\, K^{*0}$ decays from simulation (red).

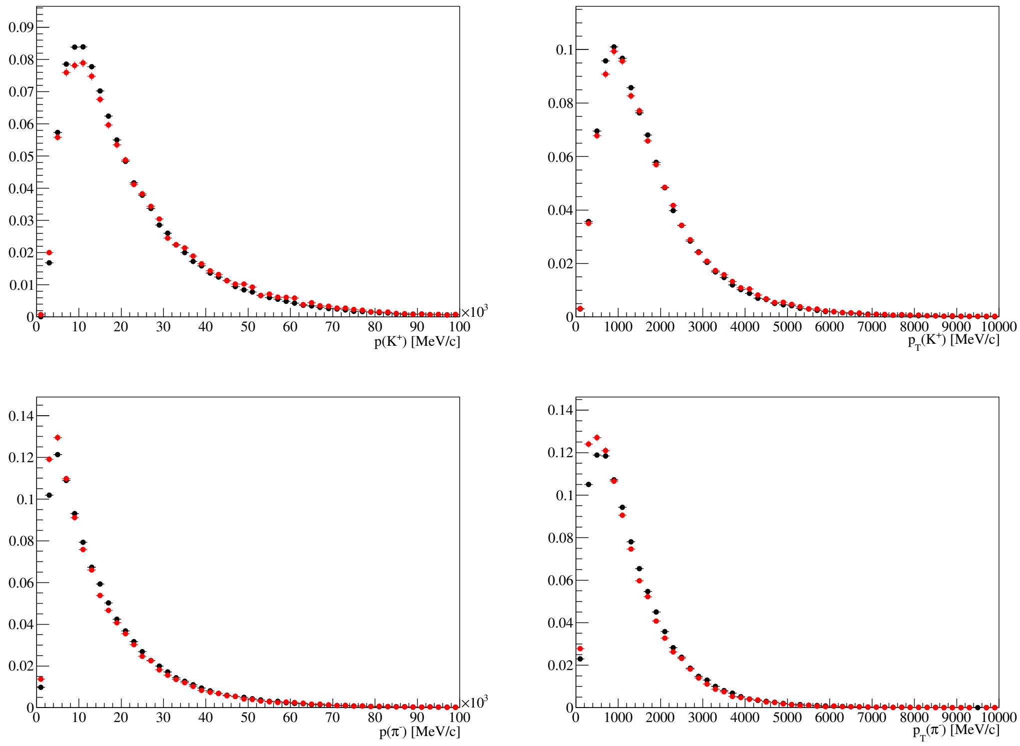

The nominal choice is to include Legendre polynomials of order four and lower for $\cos\theta_l$, order five for $\cos\theta_K$ and q^2, and order six for the angle ϕ as described in Sec. 8.2. In addition, the acceptance is assumed to be even in ϕ resulting in only non-zero coefficients of even order for these polynomials. The projections of the four-dimensional acceptance determined with these settings show very good description of the angles $\cos\theta_l$ and ϕ (See Fig. 44). Small deviations are observed for low q^2 and large $\cos\theta_K$. To estimate the effect of these imperfections on the angular observables, we determine an acceptance including higer order polynomials for the description of $\cos\theta_K$ and q^2, choosing a maximal order of seven for both. Table 54 gives the result of the angular fit of the control decay $B^0 \to J/\psi\, K^{*0}$ using this higher order acceptance and for comparison the nominal result. No deviation of a size sigificant for the angular analysis of the signal decay is seen. This gives again confidence in the choice of the acceptance desciption.

To determine the systematic uncertainties properly, high statistics toys are performed, where events are generated using the higher order acceptance model and fit with the nominal one. The resulting deviations are given in Tab. 55, they are negligible for all bins.

Figure 87: Correction factor for simulated events depending on p and p_T for (left) K^+ and (right) π^-.

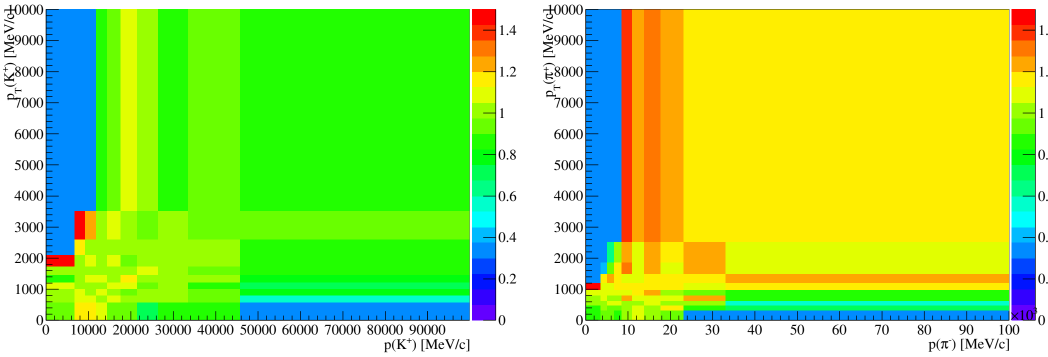

Table 48: Systematic uncertainties from neglecting the explicit reweighting of the B^0 p_{T}. Ranges of q^2 bins are given in GeV^2/c^4.

$0.1 < q^2 < 1.0$		$1.0 < q^2 < 2.5$		$2.5 < q^2 < 4.0$		$4.0 < q^2 < 6.0$		$6.0 < q^2 < 8.0$	
param.	$\sigma_{\text{syst.}}$	param.	$\sigma_{\text{syst.}}$	param.	$\sigma_{\text{syst.}}$	param.	$\sigma_{\text{syst.}}$	param.	$\sigma_{\text{syst.}}$
F_L	0.0009	F_L	0.0028	F_L	0.0027	F_L	0.0032	F_L	0.0039
S_3	0.0002	S_3	0.0000	S_3	0.0001	S_3	0.0001	S_3	0.0001
S_4	0.0003	S_4	0.0002	S_4	0.0005	S_4	0.0004	S_4	0.0001
S_5	0.0004	S_5	0.0005	S_5	0.0001	S_5	0.0005	S_5	0.0005
A_{FB}	0.0003	A_{FB}	0.0014	A_{FB}	0.0009	A_{FB}	0.0005	A_{FB}	0.0016
S_7	0.0000	S_7	0.0000	S_7	0.0001	S_7	0.0000	S_7	0.0000
S_8	0.0001	S_8	0.0000	S_8	0.0001	S_8	0.0000	S_8	0.0000
S_9	0.0000	S_9	0.0000	S_9	0.0000	S_9	0.0000	S_9	0.0000

$15.0 < q^2 < 17.0$		$17.0 < q^2 < 19.0$		$11.0 < q^2 < 12.5$		$1.1 < q^2 < 6.0$		$15.0 < q^2 < 19.0$	
param.	$\sigma_{\text{syst.}}$	param.	$\sigma_{\text{syst.}}$	param.	$\sigma_{\text{syst.}}$	param.	$\sigma_{\text{syst.}}$	param.	$\sigma_{\text{syst.}}$
F_L	0.0032	F_L	0.0024	F_L	0.0046	F_L	0.0032	F_L	0.0029
S_3	0.0001	S_3	0.0005	S_3	0.0005	S_3	0.0000	S_3	0.0002
S_4	0.0001	S_4	0.0005	S_4	0.0006	S_4	0.0002	S_4	0.0003
S_5	0.0005	S_5	0.0003	S_5	0.0009	S_5	0.0001	S_5	0.0004
A_{FB}	0.0017	A_{FB}	0.0011	A_{FB}	0.0028	A_{FB}	0.0005	A_{FB}	0.0015
S_7	0.0000	S_7	0.0000	S_7	0.0000	S_7	0.0000	S_7	0.0000
S_8	0.0000	S_8	0.0000	S_8	0.0000	S_8	0.0000	S_8	0.0000
S_9	0.0000	S_9	0.0000	S_9	0.0000	S_9	0.0000	S_9	0.0000

Table 49: Systematic uncertainties form neglecting the explicit reweighting of the B^0 vertex χ^2. Ranges of q^2 bins are given in GeV^2/c^4.

$0.1 < q^2 < 1.0$		$1.0 < q^2 < 2.5$		$2.5 < q^2 < 4.0$		$4.0 < q^2 < 6.0$		$6.0 < q^2 < 8.0$	
param.	$\sigma_{\text{syst.}}$	param.	$\sigma_{\text{syst.}}$	param.	$\sigma_{\text{syst.}}$	param.	$\sigma_{\text{syst.}}$	param.	$\sigma_{\text{syst.}}$
F_L	0.0019	F_L	0.0004	F_L	0.0005	F_L	0.0004	F_L	0.0004
S_3	0.0001	S_3	0.0001	S_3	0.0001	S_3	0.0001	S_3	0.0000
S_4	0.0019	S_4	0.0001	S_4	0.0003	S_4	0.0002	S_4	0.0001
S_5	0.0004	S_5	0.0006	S_5	0.0004	S_5	0.0000	S_5	0.0001
A_{FB}	0.0019	A_{FB}	0.0003	A_{FB}	0.0001	A_{FB}	0.0001	A_{FB}	0.0002
S_7	0.0002	S_7	0.0000	S_7	0.0000	S_7	0.0000	S_7	0.0000
S_8	0.0000	S_8	0.0000	S_8	0.0000	S_8	0.0000	S_8	0.0000
S_9	0.0001	S_9	0.0000	S_9	0.0000	S_9	0.0000	S_9	0.0000

$15.0 < q^2 < 17.0$		$17.0 < q^2 < 19.0$		$11.0 < q^2 < 12.5$		$1.1 < q^2 < 6.0$		$15.0 < q^2 < 19.0$	
param.	$\sigma_{\text{syst.}}$	param.	$\sigma_{\text{syst.}}$	param.	$\sigma_{\text{syst.}}$	param.	$\sigma_{\text{syst.}}$	param.	$\sigma_{\text{syst.}}$
F_L	0.0010	F_L	0.0013	F_L	0.0010	F_L	0.0005	F_L	0.0011
S_3	0.0002	S_3	0.0007	S_3	0.0000	S_3	0.0001	S_3	0.0004
S_4	0.0003	S_4	0.0004	S_4	0.0001	S_4	0.0003	S_4	0.0003
S_5	0.0004	S_5	0.0002	S_5	0.0001	S_5	0.0003	S_5	0.0003
A_{FB}	0.0004	A_{FB}	0.0002	A_{FB}	0.0006	A_{FB}	0.0000	A_{FB}	0.0003
S_7	0.0000	S_7	0.0000	S_7	0.0000	S_7	0.0000	S_7	0.0000
S_8	0.0000	S_8	0.0000	S_8	0.0000	S_8	0.0000	S_8	0.0000
S_9	0.0000	S_9	0.0000	S_9	0.0000	S_9	0.0000	S_9	0.0000

10.1.5 Peaking backgrounds

Several peaking backgrounds are able to mimic the signal decay. An overview is given in Tab. 56 taken from [13], where the peaking background processes are discussed in more detail. To determine the effect of neglecting the peaking backgrounds in the angular analysis, high statistics toy studies are performed. In addition to the signal and combinatorial background component, peaking background events are added according to their expected fraction. The deviation of the fitted angular observables from their nominal values when neglecting these peaking background events in the fit are then taken as systematic uncertainties.

The distributions of the peaking background events in reconstructed B^0 mass, decay angles and q^2 are taken from data. To select these peaking background events, specific selections are applied. The explicit vetoes against the peaking backgrounds are removed and the criteria listed in Tab. 57 are applied instead. Since the nominal BDT used to suppress combinatorial background includes particle identification criteria, the nominal BDT cut is removed. Instead, a new BDT, trained without particle identification criteria, is applied to remove combinatorial backgrounds.

The selected peaking backgrounds $\Lambda_b^0 \to pK\mu^+\mu^-$, $B_s^0 \to \phi\mu^+\mu^-$ and $B^0 \to \pi^+\pi^-\mu^+\mu^-$, as well as $K\pi$ swapped $B^0 \to K^{*0}\mu^+\mu^-$ events, are given in Fig. 88. Here, the standard

Table 50: Systematic uncertainties form neglecting the explicit reweighting of the track multiplicity. Ranges of q^2 bins are given in GeV^2/c^4.

$0.1 < q^2 < 1.0$		$1.0 < q^2 < 2.5$		$2.5 < q^2 < 4.0$		$4.0 < q^2 < 6.0$		$6.0 < q^2 < 8.0$	
param.	$\sigma_{\mathrm{syst.}}$	param.	$\sigma_{\mathrm{syst.}}$	param.	$\sigma_{\mathrm{syst.}}$	param.	$\sigma_{\mathrm{syst.}}$	param.	$\sigma_{\mathrm{syst.}}$
F_L	0.0010	F_L	0.0002	F_L	0.0003	F_L	0.0004	F_L	0.0007
S_3	0.0000	S_3	0.0002	S_3	0.0002	S_3	0.0000	S_3	0.0001
S_4	0.0005	S_4	0.0010	S_4	0.0010	S_4	0.0008	S_4	0.0006
S_5	0.0003	S_5	0.0003	S_5	0.0001	S_5	0.0001	S_5	0.0001
A_{FB}	0.0022	A_{FB}	0.0000	A_{FB}	0.0005	A_{FB}	0.0006	A_{FB}	0.0006
S_7	0.0001	S_7	0.0000	S_7	0.0000	S_7	0.0000	S_7	0.0000
S_8	0.0002	S_8	0.0000	S_8	0.0000	S_8	0.0000	S_8	0.0000
S_9	0.0000	S_9	0.0000	S_9	0.0000	S_9	0.0000	S_9	0.0000

$15.0 < q^2 < 17.0$		$17.0 < q^2 < 19.0$		$11.0 < q^2 < 12.5$		$1.1 < q^2 < 6.0$		$15.0 < q^2 < 19.0$	
param.	$\sigma_{\mathrm{syst.}}$	param.	$\sigma_{\mathrm{syst.}}$	param.	$\sigma_{\mathrm{syst.}}$	param.	$\sigma_{\mathrm{syst.}}$	param.	$\sigma_{\mathrm{syst.}}$
F_L	0.0010	F_L	0.0015	F_L	0.0003	F_L	0.0000	F_L	0.0003
S_3	0.0001	S_3	0.0001	S_3	0.0007	S_3	0.0002	S_3	0.0002
S_4	0.0002	S_4	0.0009	S_4	0.0003	S_4	0.0011	S_4	0.0003
S_5	0.0004	S_5	0.0001	S_5	0.0005	S_5	0.0003	S_5	0.0002
A_{FB}	0.0006	A_{FB}	0.0016	A_{FB}	0.0002	A_{FB}	0.0004	A_{FB}	0.0005
S_7	0.0000	S_7	0.0000	S_7	0.0000	S_7	0.0000	S_7	0.0000
S_8	0.0000	S_8	0.0000	S_8	0.0000	S_8	0.0000	S_8	0.0000
S_9	0.0000	S_9	0.0000	S_9	0.0000	S_9	0.0000	S_9	0.0000

charmonium vetoes are applied. In addition, Fig. 89 gives the corresponding high statistics charmonium modes $\Lambda_b^0 \to J/\psi\, pK$, $B_s^0 \to J/\psi\, \phi$, $B^0 \to J/\psi\, \pi^+\pi^-$ and $B^0 \to J/\psi\, K^{*0}$ swaps, where q^2 is in the range $[8, 11]\,\mathrm{GeV}^2/c^4$. The selected peaking background yields are 109 ($\Lambda_b^0 \to pK\mu^+\mu^-$), 156 ($B_s^0 \to \phi\mu^+\mu^-$) and 92 ($B^0 \to \pi^+\pi^-\mu^+\mu^-$) events. As expected, the charmonium decays have much larger yields with $9,000$ ($\Lambda_b^0 \to J/\psi\, pK$), $24,100$ ($B_s^0 \to J/\psi\, \phi$) and $9,000$ ($B^0 \to J/\psi\, \pi^+\pi^-$) events.

Two different methods are employed to determine the angular distributions of the peaking background events. The first is to simply sample events randomly from the high statistics $b \to J/\psi\, X$ decays, using the q^2 distribution of the corresponding rare modes to determine the fraction of background events expected in the different q^2 bins. The second approach is to use a kernel density method to describe the distributions, using only the

Figure 88: Selected (first row) $\Lambda_b^0 \to pK\mu^+\mu^-$, (second row) $B_s^0 \to \phi\mu^+\mu^-$ and (third row) $B^0 \to \pi^+\pi^-\mu^+\mu^-$ peaking background events, as well as (fourth row) $B^0 \to K^{*0}\mu^+\mu^-$ swaps. The left column gives the reconstructed mass of the b hadron, the right column the reconstructed mass of the final state hadron.

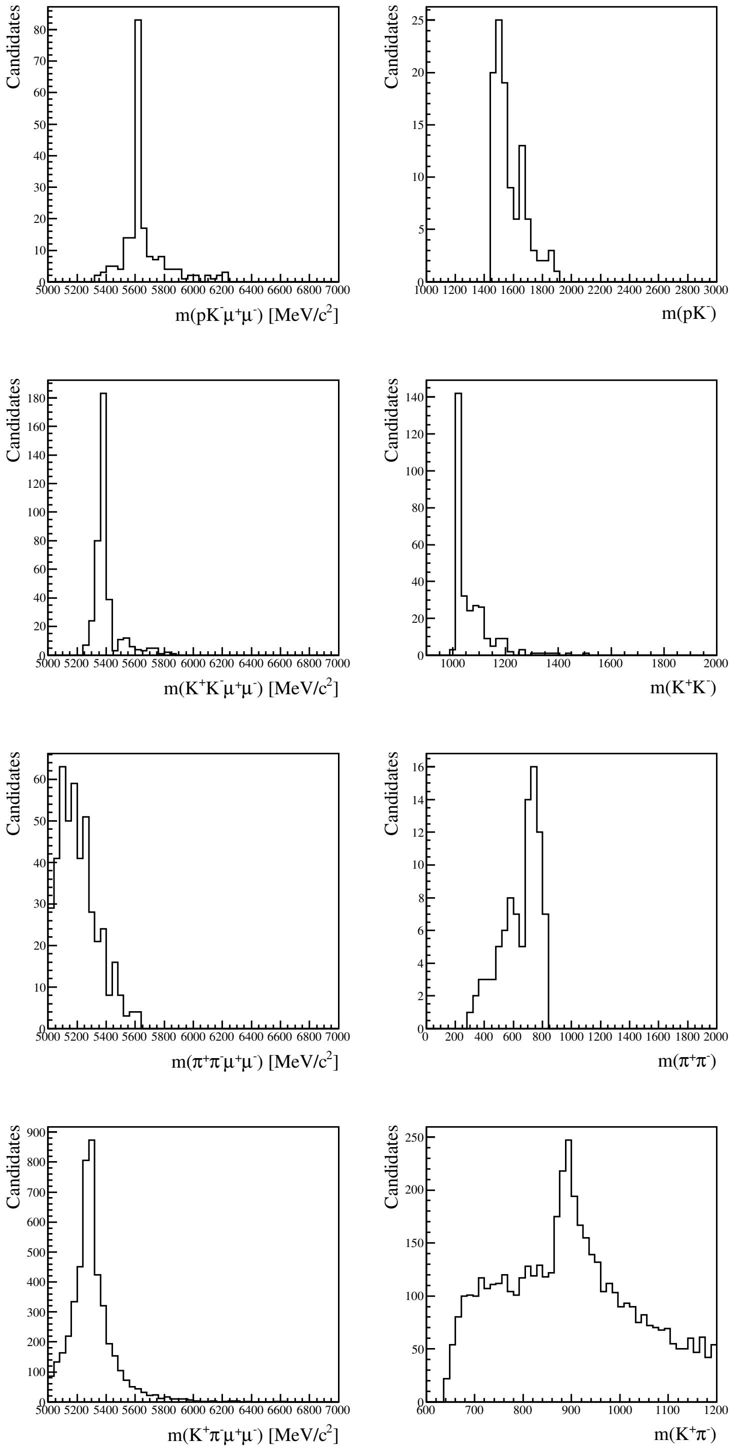

Figure 89: Selected (first row) $\Lambda_b^0 \to J/\psi\, pK$, (second row) $B_s^0 \to J/\psi\, \phi$ and (third row) $B^0 \to J/\psi\, \pi^+\pi^-$ peaking background events, as well as (fourth row) $B^0 \to J/\psi\, K^{*0}$ swaps. The left column gives the reconstructed mass of the b hadron, the right column the reconstructed mass of the final state hadron.

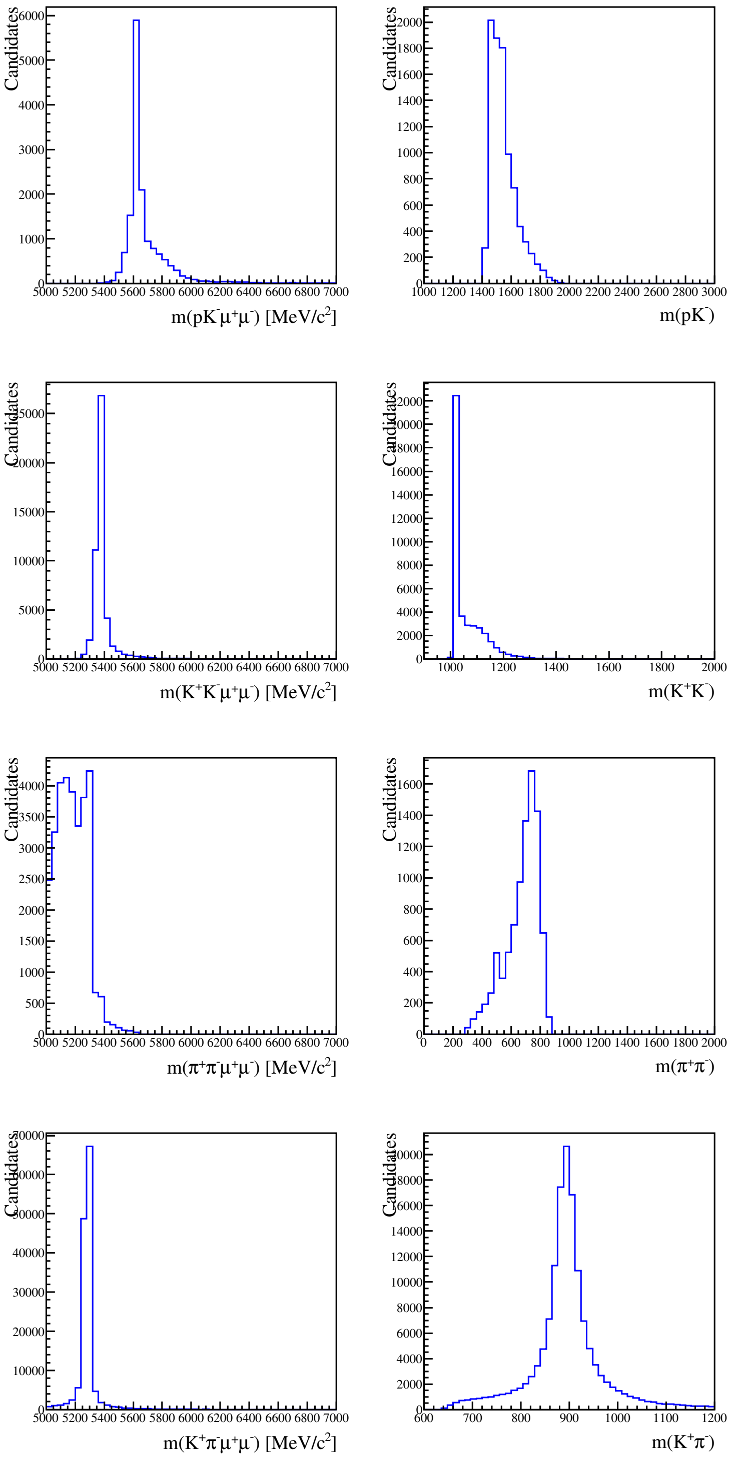

Table 51: Systematic uncertainties from reweighting depending on pion p and p_{T}. Ranges of q^2 bins are given in GeV^2/c^4.

$0.1 < q^2 < 1.0$		$1.0 < q^2 < 2.5$		$2.5 < q^2 < 4.0$		$4.0 < q^2 < 6.0$		$6.0 < q^2 < 8.0$	
param.	$\sigma_{\text{syst.}}$	param.	$\sigma_{\text{syst.}}$	param.	$\sigma_{\text{syst.}}$	param.	$\sigma_{\text{syst.}}$	param.	$\sigma_{\text{syst.}}$
F_L	0.0139	F_L	0.0149	F_L	0.0118	F_L	0.0126	F_L	0.0130
S_3	0.0010	S_3	0.0002	S_3	0.0005	S_3	0.0011	S_3	0.0014
S_4	0.0005	S_4	0.0017	S_4	0.0007	S_4	0.0021	S_4	0.0020
S_5	0.0030	S_5	0.0006	S_5	0.0017	S_5	0.0020	S_5	0.0010
A_{FB}	0.0003	A_{FB}	0.0077	A_{FB}	0.0043	A_{FB}	0.0020	A_{FB}	0.0058
S_7	0.0003	S_7	0.0001	S_7	0.0003	S_7	0.0002	S_7	0.0001
S_8	0.0000	S_8	0.0001	S_8	0.0002	S_8	0.0002	S_8	0.0001
S_9	0.0001	S_9	0.0001	S_9	0.0002	S_9	0.0002	S_9	0.0001

$15.0 < q^2 < 17.0$		$17.0 < q^2 < 19.0$		$11.0 < q^2 < 12.5$		$1.1 < q^2 < 6.0$		$15.0 < q^2 < 19.0$	
param.	$\sigma_{\text{syst.}}$	param.	$\sigma_{\text{syst.}}$	param.	$\sigma_{\text{syst.}}$	param.	$\sigma_{\text{syst.}}$	param.	$\sigma_{\text{syst.}}$
F_L	0.0059	F_L	0.0021	F_L	0.0108	F_L	0.0139	F_L	0.0040
S_3	0.0020	S_3	0.0019	S_3	0.0015	S_3	0.0004	S_3	0.0021
S_4	0.0006	S_4	0.0010	S_4	0.0002	S_4	0.0001	S_4	0.0009
S_5	0.0018	S_5	0.0011	S_5	0.0016	S_5	0.0011	S_5	0.0015
A_{FB}	0.0031	A_{FB}	0.0005	A_{FB}	0.0066	A_{FB}	0.0023	A_{FB}	0.0017
S_7	0.0000	S_7	0.0000	S_7	0.0000	S_7	0.0002	S_7	0.0000
S_8	0.0000	S_8	0.0000	S_8	0.0000	S_8	0.0001	S_8	0.0000
S_9	0.0000	S_9	0.0000	S_9	0.0000	S_9	0.0001	S_9	0.0000

low statistics $b \to X\mu^+\mu^-$ modes. This method uses Gaussian kernels according to

$$\begin{aligned}\mathcal{P}_{\text{peaking}}(m_{K\pi\mu\mu}, \cos\theta_l, \cos\theta_K, \phi) = \frac{1}{N} \sum_{\text{events } i=1}^{N} & \frac{1}{\sqrt{2\pi}^4 \sigma(\cos\theta_l)\sigma(\cos\theta_K)\sigma(\phi)\sigma(m_{K\pi\mu\mu})} \\ & \times \exp\left[-\frac{(m_{K\pi\mu\mu} - m_{K\pi\mu\mu,i})^2}{2\sigma^2(m_{K\pi\mu\mu})} - \frac{(\cos\theta_l - \cos\theta_{l,i})^2}{2\sigma^2(\cos\theta_l)}\right] \\ & \times \exp\left[-\frac{(\cos\theta_K - \cos\theta_{K,i})^2}{2\sigma^2(\cos\theta_K)} - \frac{(\phi - \phi_i)^2}{2\sigma^2(\phi)}\right], \end{aligned} \tag{110}$$

where $\sigma(\cos\theta_l) = \sigma(\cos\theta_K) = 0.2$, $\sigma(\phi) = \pi/5\,\text{rad}$ and $\sigma(m_{K\pi\mu\mu}) = 10.6\,\text{MeV}/c^2$. Events near the borders of the $\cos\theta_l$ and $\cos\theta_K$ distributions are handled by folding back the PDF. Fig. 90 shows the angular distributions for $b \to X\mu^+\mu^-$ decays in black. Overlayed are the angular distributions of the $b \to J/\psi X$ decays in blue and the results from the kernel method in red. The results from the kernel method follow the data smoothly, the angular distributions from the charmonium modes seem to be statistically compatible with the rare decays. The most interesting feature is certainly the $\cos\theta_K$ dependence of the $B_s^0 \to \phi\mu^+\mu^-$ and $B_s^0 \to J/\psi\,\phi$ decays which strongly peak towards $\cos\theta_K = -1$. This is due to the mass of the ϕ resonance being just above the K^+K^- threshold.

Figure 90: The decay angles (left) $\cos\theta_l$, (middle) $\cos\theta_K$, and (right) ϕ for (black) $b \to X\mu^+\mu^-$ decays, (blue) $b \to J/\psi X$ decays, and (red) from the kernel method described in the text. The three peaking backgrounds studied are (first row) $\Lambda_b^0 \to pK\mu^+\mu^-$, (second row) $B_s^0 \to \phi\mu^+\mu^-$, (third row) $B^0 \to \pi^+\pi^-\mu^+\mu^-$ and (fourth row) $B^0 \to K^+\pi^-\mu^+\mu^-$ swaps.

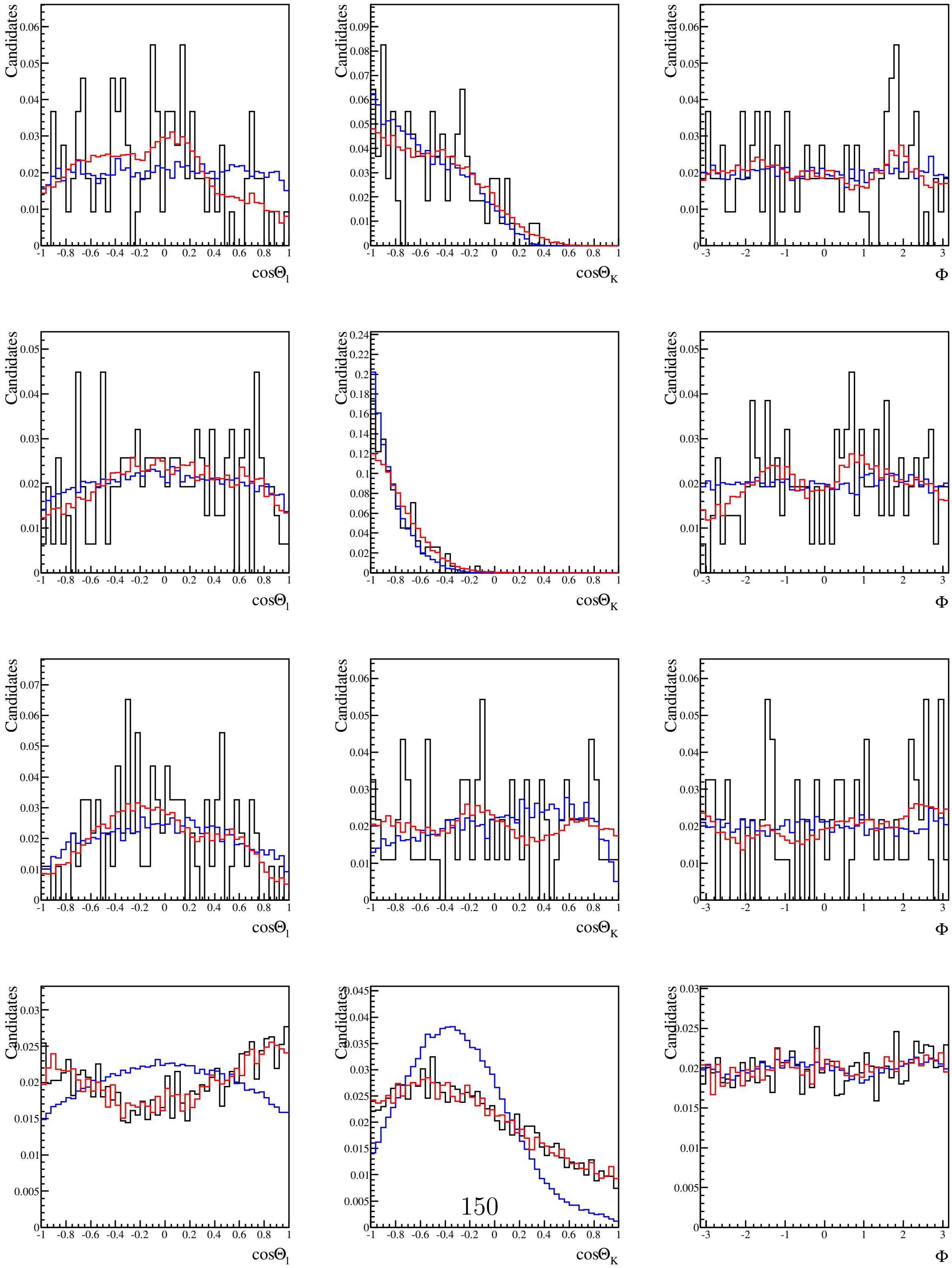

Table 52: Systematic uncertainties from reweighting depending on kaon p and p_{T}. Ranges of q^2 bins are given in GeV^2/c^4.

param.	$0.1 < q^2 < 1.0$ $\sigma_{\text{syst.}}$	param.	$1.0 < q^2 < 2.5$ $\sigma_{\text{syst.}}$	param.	$2.5 < q^2 < 4.0$ $\sigma_{\text{syst.}}$	param.	$4.0 < q^2 < 6.0$ $\sigma_{\text{syst.}}$	param.	$6.0 < q^2 < 8.0$ $\sigma_{\text{syst.}}$
F_L	0.0035	F_L	0.0006	F_L	0.0001	F_L	0.0004	F_L	0.0008
S_3	0.0010	S_3	0.0002	S_3	0.0001	S_3	0.0001	S_3	0.0002
S_4	0.0003	S_4	0.0006	S_4	0.0010	S_4	0.0010	S_4	0.0008
S_5	0.0010	S_5	0.0004	S_5	0.0000	S_5	0.0004	S_5	0.0004
A_{FB}	0.0008	A_{FB}	0.0004	A_{FB}	0.0001	A_{FB}	0.0001	A_{FB}	0.0001
S_7	0.0002	S_7	0.0000	S_7	0.0000	S_7	0.0000	S_7	0.0000
S_8	0.0001	S_8	0.0000	S_8	0.0000	S_8	0.0000	S_8	0.0000
S_9	0.0001	S_9	0.0000	S_9	0.0000	S_9	0.0000	S_9	0.0000

param.	$15.0 < q^2 < 17.0$ $\sigma_{\text{syst.}}$	param.	$17.0 < q^2 < 19.0$ $\sigma_{\text{syst.}}$	param.	$11.0 < q^2 < 12.5$ $\sigma_{\text{syst.}}$	param.	$1.1 < q^2 < 6.0$ $\sigma_{\text{syst.}}$	param.	$15.0 < q^2 < 19.0$ $\sigma_{\text{syst.}}$
F_L	0.0008	F_L	0.0002	F_L	0.0012	F_L	0.0000	F_L	0.0003
S_3	0.0002	S_3	0.0006	S_3	0.0001	S_3	0.0000	S_3	0.0004
S_4	0.0000	S_4	0.0001	S_4	0.0002	S_4	0.0013	S_4	0.0000
S_5	0.0000	S_5	0.0002	S_5	0.0002	S_5	0.0000	S_5	0.0001
A_{FB}	0.0005	A_{FB}	0.0001	A_{FB}	0.0008	A_{FB}	0.0001	A_{FB}	0.0003
S_7	0.0000	S_7	0.0000	S_7	0.0000	S_7	0.0000	S_7	0.0000
S_8	0.0000	S_8	0.0000	S_8	0.0000	S_8	0.0000	S_8	0.0000
S_9	0.0000	S_9	0.0000	S_9	0.0000	S_9	0.0000	S_9	0.0000

In addition to the peaking backgrounds from misidentified $\Lambda_b^0 \to pK\mu^+\mu^-$, $B_s^0 \to K^+K^-\mu^+\mu^-$ and $B^0 \to K^+\pi^-\mu^+\mu^-$ decays, 2% of $B^0 \to K^+\pi^-_{\text{rnd}}\mu^+\mu^-$ decays originating from $B^0 \to K^{*0}\mu^+\mu^-$ decays, where the π^- was replaced by a random pion in the event. The distributions of this background source are modelled using $B^0 \to K^{*+}(\to K^+\pi^0)\mu^+\mu^-$ decays.

The resulting deviations from high statistics toys containing the appropriate fraction of $\Lambda_b^0 \to pK\mu^+\mu^-$, $B_s^0 \to K^+K^-\mu^+\mu^-$ and $B^0 \to K^+\pi^-\mu^+\mu^-$, as well as $B^0 \to K^+\pi^-_{\text{rnd}}\mu^+\mu^-$ peaking background events sampled from the charmonium decays are given in the Tab. 58. The corresponding results from the kernel method are given in Tab. 59.

10.1.6 Angular background modeling

The nominal background parametrisation uses Chebyshev polynomials of second order and lower to describe the decay angles. To estimate the systematic effect of this choice of angular background model, the high mass sideband ($m_{K\pi\mu\mu} \in [5355, 5700]\,\mathrm{MeV}/c^2$) is fit with Chebyshev polynomials of forth order and lower instead. To have enough combinatorial background events to fit the Chebyshev coefficients, the BDT requirement is removed for the fit. Fig. 91 shows the fitted angular distributions in bins of q^2. To determine the systematic effect of only fitting the background with polynomials of order

Table 53: Systematic uncertainties from fixing q^2 of the four-dimensional acceptance. Ranges of q^2 bins are given in GeV^2/c^4.

$0.1 < q^2 < 1.0$		$1.0 < q^2 < 2.5$		$2.5 < q^2 < 4.0$		$4.0 < q^2 < 6.0$		$6.0 < q^2 < 8.0$	
param.	$\sigma_{\text{syst.}}$	param.	$\sigma_{\text{syst.}}$	param.	$\sigma_{\text{syst.}}$	param.	$\sigma_{\text{syst.}}$	param.	$\sigma_{\text{syst.}}$
F_L	0.0025	F_L	0.0088	F_L	0.0089	F_L	0.0089	F_L	0.0043
S_3	0.0014	S_3	0.0005	S_3	0.0002	S_3	0.0005	S_3	0.0003
S_4	0.0037	S_4	0.0029	S_4	0.0002	S_4	0.0009	S_4	0.0001
S_5	0.0014	S_5	0.0005	S_5	0.0019	S_5	0.0020	S_5	0.0004
A_{FB}	0.0028	A_{FB}	0.0043	A_{FB}	0.0034	A_{FB}	0.0013	A_{FB}	0.0020
S_7	0.0001	S_7	0.0001	S_7	0.0002	S_7	0.0002	S_7	0.0001
S_8	0.0003	S_8	0.0001	S_8	0.0002	S_8	0.0000	S_8	0.0001
S_9	0.0000	S_9	0.0000	S_9	0.0001	S_9	0.0001	S_9	0.0001

$15.0 < q^2 < 17.0$		$17.0 < q^2 < 19.0$		$11.0 < q^2 < 12.5$	
param.	$\sigma_{\text{syst.}}$	param.	$\sigma_{\text{syst.}}$	param.	$\sigma_{\text{syst.}}$
F_L	0.0034	F_L	0.0226	F_L	0.0013
S_3	0.0033	S_3	0.0102	S_3	0.0009
S_4	0.0030	S_4	0.0062	S_4	0.0005
S_5	0.0024	S_5	0.0044	S_5	0.0005
A_{FB}	0.0014	A_{FB}	0.0063	A_{FB}	0.0009
S_7	0.0002	S_7	0.0000	S_7	0.0001
S_8	0.0002	S_8	0.0000	S_8	0.0002
S_9	0.0001	S_9	0.0000	S_9	0.0000

Table 54: Results from the angular fit of the control decay $B^0 \to J/\psi\, K^{*0}$ using (left) the higher order acceptance description detailed in Sec. 10.1.4 and (right) the nominal acceptance correction.

parameter	higher order result	parameter	nominal result
S_{1s}	0.330 ± 0.001	S_1^s	0.331 ± 0.001
S_3	0.001 ± 0.002	S_3	0.000 ± 0.002
S_4	-0.274 ± 0.002	S_4	-0.276 ± 0.002
S_5	-0.005 ± 0.002	S_5	-0.002 ± 0.002
S_{6s}	0.002 ± 0.002	S_6^s	0.002 ± 0.002
S_7	0.001 ± 0.002	S_7	0.001 ± 0.002
S_8	-0.050 ± 0.002	S_8	-0.050 ± 0.002
S_9	-0.085 ± 0.002	S_9	-0.087 ± 0.002
F_S	0.073 ± 0.003	F_S	0.083 ± 0.003
S_{S1}	-0.235 ± 0.003	S_{S1}	-0.229 ± 0.003
S_{S2}	0.002 ± 0.002	S_{S2}	0.001 ± 0.002
S_{S3}	0.001 ± 0.002	S_{S3}	0.003 ± 0.002
S_{S4}	0.001 ± 0.002	S_{S4}	0.001 ± 0.002
S_{S5}	-0.065 ± 0.002	S_{S5}	-0.065 ± 0.002

Table 55: The effect of using a the nominal instead of a higher order acceptance model.

$0.1 < q^2 < 1.0$		$1.0 < q^2 < 2.5$		$2.5 < q^2 < 4.0$		$4.0 < q^2 < 6.0$		$6.0 < q^2 < 8.0$	
param.	$\sigma_{\text{syst.}}$	param.	$\sigma_{\text{syst.}}$	param.	$\sigma_{\text{syst.}}$	param.	$\sigma_{\text{syst.}}$	param.	$\sigma_{\text{syst.}}$
F_L	0.0037	F_L	0.0108	F_L	0.0022	F_L	0.0033	F_L	0.0034
S_3	0.0007	S_3	0.0015	S_3	0.0003	S_3	0.0003	S_3	0.0010
S_4	0.0042	S_4	0.0007	S_4	0.0017	S_4	0.0015	S_4	0.0014
S_5	0.0162	S_5	0.0065	S_5	0.0025	S_5	0.0020	S_5	0.0021
A_{FB}	0.0004	A_{FB}	0.0020	A_{FB}	0.0000	A_{FB}	0.0011	A_{FB}	0.0021
S_7	0.0036	S_7	0.0030	S_7	0.0005	S_7	0.0001	S_7	0.0009
S_8	0.0003	S_8	0.0030	S_8	0.0009	S_8	0.0006	S_8	0.0013
S_9	0.0017	S_9	0.0013	S_9	0.0012	S_9	0.0008	S_9	0.0020

$15.0 < q^2 < 17.0$		$17.0 < q^2 < 19.0$		$11.0 < q^2 < 12.5$		$1.1 < q^2 < 6.0$		$15.0 < q^2 < 19.0$	
param.	$\sigma_{\text{syst.}}$	param.	$\sigma_{\text{syst.}}$	param.	$\sigma_{\text{syst.}}$	param.	$\sigma_{\text{syst.}}$	param.	$\sigma_{\text{syst.}}$
F_L	0.0018	F_L	0.0084	F_L	0.0032	F_L	0.0001	F_L	0.0003
S_3	0.0013	S_3	0.0025	S_3	0.0005	S_3	0.0000	S_3	0.0010
S_4	0.0009	S_4	0.0002	S_4	0.0003	S_4	0.0006	S_4	0.0002
S_5	0.0022	S_5	0.0031	S_5	0.0028	S_5	0.0001	S_5	0.0002
A_{FB}	0.0004	A_{FB}	0.0059	A_{FB}	0.0018	A_{FB}	0.0001	A_{FB}	0.0004
S_7	0.0016	S_7	0.0112	S_7	0.0014	S_7	0.0014	S_7	0.0050
S_8	0.0018	S_8	0.0027	S_8	0.0023	S_8	0.0011	S_8	0.0003
S_9	0.0024	S_9	0.0015	S_9	0.0008	S_9	0.0007	S_9	0.0002

Table 56: Estimated yields, and percentage relative to estimated signal yield, of peaking background events before and after the vetoes. The dominant uncertainty contributing to these numbers is in $\sigma_{b\bar{b}}$ and the estimate of $\mathcal{B}(\Lambda_b^0 \to \Lambda^*(1520)^0\mu^+\mu^-)$.

	after preselection, before vetoes		after vetoes and selection	
Channel	Estimated events	% signal	Estimated events	% signal
$\Lambda_b^0 \to \Lambda^*(1520)^0\mu^+\mu^-$	$(1.0 \pm 0.5) \times 10^3$	19 ± 8	51 ± 25	1.0 ± 0.4
$\Lambda_b^0 \to pK^-\mu^+\mu^-$	$(1.0 \pm 0.5) \times 10^2$	1.9 ± 0.8	5.7 ± 2.8	0.11 ± 0.05
$B^+ \to K^+\mu^+\mu^-$	28 ± 7	0.55 ± 0.06	1.6 ± 0.5	0.031 ± 0.006
$B_s^0 \to \phi\mu^+\mu^-$	$(3.2 \pm 1.3) \times 10^2$	6.2 ± 2.1	17 ± 7	0.33 ± 0.12
signal swaps	$(3.6 \pm 0.9) \times 10^2$	6.9 ± 0.6	33 ± 9	0.64 ± 0.06
$B^0 \to J/\psi K^{*0}$ swaps	$(1.3 \pm 0.4) \times 10^2$	2.6 ± 0.4	2.7 ± 2.8	0.05 ± 0.05
$B^0 \to J/\psi K^{*0}$	70 ± 22	1.35 ± 0.28	59 ± 19	1.14 ± 0.26
$B^+ \to K^{*+}\mu^+\mu^-$	0	0	0	0

two and lower, high statistics toy MC is used. The toy MC is generated using the forth order angular backgorund description using the nominal signal fraction. Then the toys are fitted once with the fourth order and one with the second order angular backgorund description. The observed difference is taken as systematic uncertainty and is given in

Table 57: Particle identification criteria and mass ranges to explicitly select specific peaking backgrounds.

mode	selection criteria
$\Lambda_b^0 \to pK\mu^+\mu^-$	$\texttt{ProbNNk}(K) > 0.3$
	$\texttt{ProbNNp}(\pi) > 0.3$
	$\lvert m_{pK\mu\mu} - m_{\Lambda_b^0}\rvert < 50\,\mathrm{MeV}/c^2$
$B_s^0 \to \phi\mu^+\mu^-$	$\texttt{ProbNNk}(K,\pi) > 0.3$
	$\lvert m_{KK} - m_{\phi}\rvert < 20\,\mathrm{MeV}/c^2$
	$\lvert m_{KK\mu\mu} - m_{B_s^0}\rvert < 50\,\mathrm{MeV}/c^2$
$B^0 \to \pi^+\pi^-\mu^+\mu^-$	$\texttt{ProbNNpi}(K,\pi) > 0.3$
	$\texttt{ProbNNk}(K,\pi) < 0.1$
	$\lvert m_{\pi\pi\mu\mu} - m_{B^0}\rvert < 50\,\mathrm{MeV}/c^2$

Table 58: Deviations from the nominal observables due to the peaking backgrounds. The background events have been sampled from the corresponding charmonium mode.

$0.1 < q^2 < 1.0$		$1.0 < q^2 < 2.5$		$2.5 < q^2 < 4.0$		$4.0 < q^2 < 6.0$		$6.0 < q^2 < 8.0$	
param.	$\sigma_{\text{syst.}}$	param.	$\sigma_{\text{syst.}}$	param.	$\sigma_{\text{syst.}}$	param.	$\sigma_{\text{syst.}}$	param.	$\sigma_{\text{syst.}}$
F_L	0.0047	F_L	0.0018	F_L	0.0006	F_L	0.0006	F_L	0.0001
S_3	0.0023	S_3	0.0008	S_3	0.0010	S_3	0.0036	S_3	0.0100
S_4	0.0028	S_4	0.0012	S_4	0.0037	S_4	0.0034	S_4	0.0019
S_5	0.0028	S_5	0.0032	S_5	0.0007	S_5	0.0018	S_5	0.0005
A_{FB}	0.0062	A_{FB}	0.0075	A_{FB}	0.0018	A_{FB}	0.0001	A_{FB}	0.0022
S_7	0.0038	S_7	0.0002	S_7	0.0050	S_7	0.0031	S_7	0.0001
S_8	0.0020	S_8	0.0034	S_8	0.0048	S_8	0.0019	S_8	0.0057
S_9	0.0030	S_9	0.0024	S_9	0.0060	S_9	0.0014	S_9	0.0016

$15.0 < q^2 < 17.0$		$17.0 < q^2 < 19.0$		$11.0 < q^2 < 12.5$		$1.1 < q^2 < 6.0$		$15.0 < q^2 < 19.0$	
param.	$\sigma_{\text{syst.}}$	param.	$\sigma_{\text{syst.}}$	param.	$\sigma_{\text{syst.}}$	param.	$\sigma_{\text{syst.}}$	param.	$\sigma_{\text{syst.}}$
F_L	0.0030	F_L	0.0020	F_L	0.0018	F_L	0.0055	F_L	0.0046
S_3	0.0018	S_3	0.0029	S_3	0.0000	S_3	0.0032	S_3	0.0050
S_4	0.0018	S_4	0.0029	S_4	0.0080	S_4	0.0012	S_4	0.0037
S_5	0.0014	S_5	0.0019	S_5	0.0058	S_5	0.0041	S_5	0.0032
A_{FB}	0.0014	A_{FB}	0.0032	A_{FB}	0.0013	A_{FB}	0.0058	A_{FB}	0.0056
S_7	0.0050	S_7	0.0037	S_7	0.0047	S_7	0.0005	S_7	0.0025
S_8	0.0013	S_8	0.0043	S_8	0.0034	S_8	0.0042	S_8	0.0014
S_9	0.0009	S_9	0.0004	S_9	0.0051	S_9	0.0021	S_9	0.0012

Tab. 60. The systematic effect is negligible.

Figure 91: The angular distribution of combinatorial background events in the high mass sideband ($m_{K\pi\mu\mu} \in [5355, 5700]\,\mathrm{MeV}/c^2$).

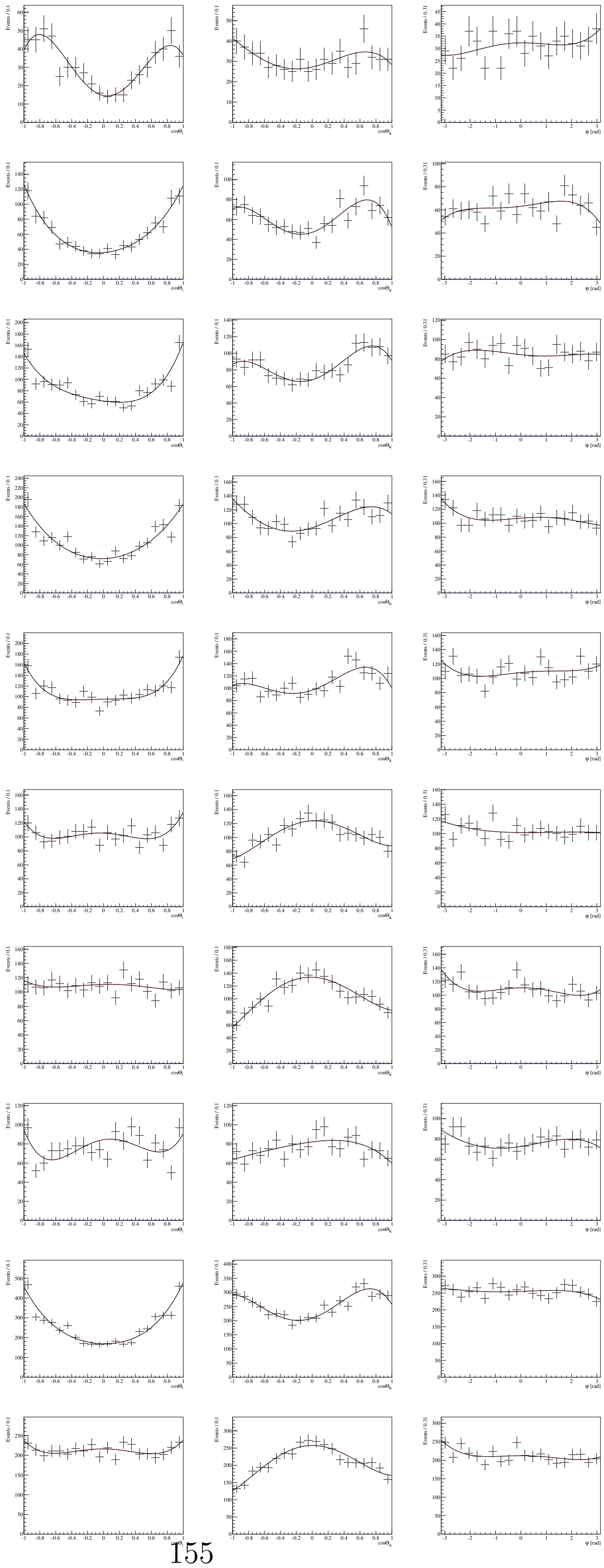

$0.1 < q^2 < 0.98\,\mathrm{GeV}^2/c^4$:

$1.1 < q^2 < 2.5\,\mathrm{GeV}^2/c^4$:

$2.5 < q^2 < 4.0\,\mathrm{GeV}^2/c^4$:

$4.0 < q^2 < 6.0\,\mathrm{GeV}^2/c^4$:

$6.0 < q^2 < 8.0\,\mathrm{GeV}^2/c^4$:

$15.0 < q^2 < 17.0\,\mathrm{GeV}^2/c^4$:

$17.0 < q^2 < 19.0\,\mathrm{GeV}^2/c^4$:

$11.0 < q^2 < 12.5\,\mathrm{GeV}^2/c^4$:

$1.1 < q^2 < 6.0\,\mathrm{GeV}^2/c^4$:

$15.0 < q^2 < 19.0\,\mathrm{GeV}^2/c^4$:

Table 59: Deviations from the nominal observables due to the peaking backgrounds. The background events have been generated using the kernel method described in the text.

$0.1 < q^2 < 1.0$		$1.0 < q^2 < 2.5$		$2.5 < q^2 < 4.0$		$4.0 < q^2 < 6.0$		$6.0 < q^2 < 8.0$	
param.	$\sigma_{\text{syst.}}$	param.	$\sigma_{\text{syst.}}$	param.	$\sigma_{\text{syst.}}$	param.	$\sigma_{\text{syst.}}$	param.	$\sigma_{\text{syst.}}$
F_L	0.0064	F_L	0.0035	F_L	0.0024	F_L	0.0041	F_L	0.0023
S_3	0.0015	S_3	0.0029	S_3	0.0048	S_3	0.0050	S_3	0.0064
S_4	0.0039	S_4	0.0001	S_4	0.0052	S_4	0.0069	S_4	0.0097
S_5	0.0040	S_5	0.0040	S_5	0.0051	S_5	0.0085	S_5	0.0082
A_{FB}	0.0031	A_{FB}	0.0005	A_{FB}	0.0033	A_{FB}	0.0013	A_{FB}	0.0040
S_7	0.0011	S_7	0.0011	S_7	0.0017	S_7	0.0037	S_7	0.0009
S_8	0.0066	S_8	0.0005	S_8	0.0032	S_8	0.0032	S_8	0.0026
S_9	0.0014	S_9	0.0042	S_9	0.0052	S_9	0.0009	S_9	0.0011

$15.0 < q^2 < 17.0$		$17.0 < q^2 < 19.0$		$11.0 < q^2 < 12.5$		$1.1 < q^2 < 6.0$		$15.0 < q^2 < 19.0$	
param.	$\sigma_{\text{syst.}}$	param.	$\sigma_{\text{syst.}}$	param.	$\sigma_{\text{syst.}}$	param.	$\sigma_{\text{syst.}}$	param.	$\sigma_{\text{syst.}}$
F_L	0.0034	F_L	0.0037	F_L	0.0017	F_L	0.0063	F_L	0.0027
S_3	0.0015	S_3	0.0049	S_3	0.0031	S_3	0.0005	S_3	0.0038
S_4	0.0049	S_4	0.0061	S_4	0.0047	S_4	0.0009	S_4	0.0020
S_5	0.0068	S_5	0.0038	S_5	0.0033	S_5	0.0010	S_5	0.0008
A_{FB}	0.0054	A_{FB}	0.0074	A_{FB}	0.0022	A_{FB}	0.0034	A_{FB}	0.0055
S_7	0.0014	S_7	0.0010	S_7	0.0016	S_7	0.0055	S_7	0.0002
S_8	0.0025	S_8	0.0033	S_8	0.0042	S_8	0.0066	S_8	0.0003
S_9	0.0034	S_9	0.0033	S_9	0.0032	S_9	0.0037	S_9	0.0012

10.1.7 Signal mass modeling

The signal mass peak is modelled using the sum of two Crystal Ball functions with common mean and tail parameters and different widths. The nominal signal mass shape parameters are determined from the control decay $B^0 \to J/\psi K^{*0}$ and fixed in the nominal fit of the signal decay. To determine the systematic effect of this choice of signal mass model, a double Gaussian is used as alternative model. The parameters of the double Gaussian are determined from a fit to $B^0 \to J/\psi K^{*0}$ events. High statistics toy MC is then generated using the double Gaussian mass model and fitted twice, once using the double Gaussian and once using the nominal Crystal Ball parametrisation. The observed difference is given in Tab. 61 and used as systematic uncertainty.

10.1.8 $m_{K\pi}$ related systematic uncertainties

The nominal fit used the $m_{K\pi}$ distribution to constrain F_S as described in Sec. 6.2.12. Three possible sources of systematic uncertainties connected to the $m_{K\pi}$ distribution are studied: The parametrisation of the S-wave component, the parametrisation of the background in $m_{K\pi}$, and the effect of an $m_{K\pi}$ dependent efficiency which is neglected in the nominal fit.

Table 60: Systematic effect due to the angular background modeling.

$0.1 < q^2 < 1.0$		$1.0 < q^2 < 2.5$		$2.5 < q^2 < 4.0$		$4.0 < q^2 < 6.0$		$6.0 < q^2 < 8.0$	
param.	$\sigma_{\text{syst.}}$	param.	$\sigma_{\text{syst.}}$	param.	$\sigma_{\text{syst.}}$	param.	$\sigma_{\text{syst.}}$	param.	$\sigma_{\text{syst.}}$
F_L	0.0003	F_L	0.0033	F_L	0.0013	F_L	0.0010	F_L	0.0012
S_3	0.0010	S_3	0.0031	S_3	0.0024	S_3	0.0022	S_3	0.0039
S_4	0.0007	S_4	0.0004	S_4	0.0003	S_4	0.0010	S_4	0.0016
S_5	0.0002	S_5	0.0010	S_5	0.0010	S_5	0.0010	S_5	0.0034
A_{FB}	0.0001	A_{FB}	0.0009	A_{FB}	0.0014	A_{FB}	0.0005	A_{FB}	0.0008
S_7	0.0001	S_7	0.0005	S_7	0.0002	S_7	0.0002	S_7	0.0003
S_8	0.0000	S_8	0.0004	S_8	0.0002	S_8	0.0002	S_8	0.0001
S_9	0.0006	S_9	0.0013	S_9	0.0019	S_9	0.0033	S_9	0.0018

$15.0 < q^2 < 17.0$		$17.0 < q^2 < 19.0$		$11.0 < q^2 < 12.5$		$1.1 < q^2 < 6.0$		$15.0 < q^2 < 19.0$	
param.	$\sigma_{\text{syst.}}$	param.	$\sigma_{\text{syst.}}$	param.	$\sigma_{\text{syst.}}$	param.	$\sigma_{\text{syst.}}$	param.	$\sigma_{\text{syst.}}$
F_L	0.0011	F_L	0.0003	F_L	0.0007	F_L	0.0021	F_L	0.0005
S_3	0.0002	S_3	0.0059	S_3	0.0011	S_3	0.0010	S_3	0.0008
S_4	0.0012	S_4	0.0002	S_4	0.0014	S_4	0.0017	S_4	0.0015
S_5	0.0005	S_5	0.0001	S_5	0.0024	S_5	0.0005	S_5	0.0010
A_{FB}	0.0002	A_{FB}	0.0002	A_{FB}	0.0021	A_{FB}	0.0013	A_{FB}	0.0000
S_7	0.0000	S_7	0.0001	S_7	0.0003	S_7	0.0002	S_7	0.0001
S_8	0.0000	S_8	0.0002	S_8	0.0002	S_8	0.0001	S_8	0.0000
S_9	0.0004	S_9	0.0018	S_9	0.0034	S_9	0.0004	S_9	0.0007

To evaluate the systematic uncertainty due to using the LASS shape as nominal model for the S-wave contribution, the effect of using the ISOBAR model instead is evaluated. The ISOBAR model consists of the sum of two amplitudes modelling the f_{800} and the $K_0^{*0}(1430)$,

$$\mathcal{A}_{\text{ISOBAR}}(m_{K\pi}) = |r_{f_{800}}|e^{i\arg\delta_{f_{800}}}\mathcal{A}_{f_{800}}(m_{K\pi}) + (1-|r_{f_{800}}|)\mathcal{A}_{K_0^{*0}(1430)}(m_{K\pi}),$$

where $\mathcal{A}_{f_{800}}(m_{K\pi})$ and $\mathcal{A}_{K_0^{*0}(1430)}(m_{K\pi})$ are Breit-Wigner amplitudes as in Eq. 37. The masses and widths of the resonances are set to $m(f_{800}) = 682\,\text{MeV}/c^2$ and $\Gamma(f_{800}) = 547\,\text{MeV}/c^2$ for the f_{800} contribution and $m(K_0^{*0}(1430)) = 1.425\,\text{GeV}/c^2$ and $\Gamma(K_0^{*0}(1430)) = 0.270\,\text{GeV}/c^2$ for the $K_0^{*0}(1430)$ [40]. The parameters $|r_{800}|$ and δ_{800} are determined from a fit to the $m_{K\pi\mu\mu}$ and $m_{K\pi}$ distributions of $B^0 \to J/\psi\, K^{*0}$ decays. High statistics toy Monte Carlo generated using the ISOBAR model and fit twice, once using the ISOBAR, and once the nominal LASS model. The observed deviations for the angular observables are used as systematic uncertainties and given in Tab. 62.

To evaluate the systematic uncertainty due to the background parametrisation of $m_{K\pi}$ a first order Chebyshev polynomial is compared to a fourth order parametrisation. The fourth order coefficients are determined from $B^0 \to J/\psi\, K^{*0}$. High statistics toy Monte Carlo is generated using the fourth order parametrisation and fit using both the fourth order and the nominal first order parametrisation. The observed deviations for the angular observables are used as systematic uncertainties and given in Tab. 63.

Table 61: Systematic effect of the signal mass model.

$0.1 < q^2 < 1.0$		$1.0 < q^2 < 2.5$		$2.5 < q^2 < 4.0$		$4.0 < q^2 < 6.0$		$6.0 < q^2 < 8.0$	
param.	$\sigma_{\text{syst.}}$	param.	$\sigma_{\text{syst.}}$	param.	$\sigma_{\text{syst.}}$	param.	$\sigma_{\text{syst.}}$	param.	$\sigma_{\text{syst.}}$
F_L	0.0009	F_L	0.0021	F_L	0.0022	F_L	0.0013	F_L	0.0006
S_3	0.0001	S_3	0.0001	S_3	0.0003	S_3	0.0004	S_3	0.0006
S_4	0.0000	S_4	0.0001	S_4	0.0003	S_4	0.0004	S_4	0.0006
S_5	0.0008	S_5	0.0006	S_5	0.0007	S_5	0.0013	S_5	0.0019
A_{FB}	0.0005	A_{FB}	0.0011	A_{FB}	0.0003	A_{FB}	0.0007	A_{FB}	0.0011
S_7	0.0000	S_7	0.0005	S_7	0.0001	S_7	0.0001	S_7	0.0002
S_8	0.0000	S_8	0.0001	S_8	0.0000	S_8	0.0001	S_8	0.0002
S_9	0.0000	S_9	0.0001	S_9	0.0002	S_9	0.0004	S_9	0.0002

$15.0 < q^2 < 17.0$		$17.0 < q^2 < 19.0$		$11.0 < q^2 < 12.5$		$1.1 < q^2 < 6.0$		$15.0 < q^2 < 19.0$	
param.	$\sigma_{\text{syst.}}$	param.	$\sigma_{\text{syst.}}$	param.	$\sigma_{\text{syst.}}$	param.	$\sigma_{\text{syst.}}$	param.	$\sigma_{\text{syst.}}$
F_L	0.0013	F_L	0.0022	F_L	0.0011	F_L	0.0017	F_L	0.0017
S_3	0.0039	S_3	0.0072	S_3	0.0014	S_3	0.0001	S_3	0.0037
S_4	0.0003	S_4	0.0011	S_4	0.0005	S_4	0.0003	S_4	0.0005
S_5	0.0019	S_5	0.0020	S_5	0.0019	S_5	0.0005	S_5	0.0019
A_{FB}	0.0023	A_{FB}	0.0034	A_{FB}	0.0019	A_{FB}	0.0001	A_{FB}	0.0027
S_7	0.0000	S_7	0.0003	S_7	0.0000	S_7	0.0003	S_7	0.0000
S_8	0.0001	S_8	0.0000	S_8	0.0000	S_8	0.0002	S_8	0.0000
S_9	0.0001	S_9	0.0001	S_9	0.0000	S_9	0.0001	S_9	0.0001

For the nominal fit the efficiency over the $m_{K\pi}$ range of the angular analysis, $[795.9, 995.9]\,\text{MeV}/c^2$, is assumed to be flat. The systematic effect of this assumption is quantified using high statistics toy Monte Carlo, including an additional $m_{K\pi}$ dependent efficiency. This efficiency is parametrised using a linearly rising or falling function with a variation of $\pm 5\%$ at the borders of the $m_{K\pi}$ mass range. The additional efficiency is applied on top of the usual four-dimensional efficiency described in Sec. 8.2. The angular observables are then determined using the nominal fit, and the largest deviations from the generated values are taken as systematic uncertainties and given in Tab. 64.

10.1.9 Production asymmetry

The production of B^0 and $\overline{B}^0$ mesons is known to be asymmetric at the LHC, due to the non-charge symmetric initial state in *pp* collision. The production asymmetry $\mathcal{A}_{\text{prod}}$, defined as

$$\mathcal{A}_{\text{prod}} = \frac{N(\overline{B}^0) - N(B^0)}{N(\overline{B}^0) - N(B^0)},$$

Table 62: Systematic deviations due to using the ISOBAR model instead of the nominal LASS description of the S-wave.

$0.1 < q^2 < 1.0$		$1.0 < q^2 < 2.5$		$2.5 < q^2 < 4.0$		$4.0 < q^2 < 6.0$		$6.0 < q^2 < 8.0$	
param.	$\sigma_{\text{syst.}}$	param.	$\sigma_{\text{syst.}}$	param.	$\sigma_{\text{syst.}}$	param.	$\sigma_{\text{syst.}}$	param.	$\sigma_{\text{syst.}}$
F_L	0.0002	F_L	0.0004	F_L	0.0004	F_L	0.0002	F_L	0.0001
S_3	0.0000	S_3	0.0000	S_3	0.0000	S_3	0.0000	S_3	0.0000
S_4	0.0001	S_4	0.0000	S_4	0.0001	S_4	0.0001	S_4	0.0002
S_5	0.0004	S_5	0.0002	S_5	0.0002	S_5	0.0004	S_5	0.0004
A_{FB}	0.0001	A_{FB}	0.0001	A_{FB}	0.0000	A_{FB}	0.0000	A_{FB}	0.0001
S_7	0.0000	S_7	0.0001	S_7	0.0000	S_7	0.0000	S_7	0.0000
S_8	0.0000	S_8	0.0000	S_8	0.0000	S_8	0.0000	S_8	0.0000
S_9	0.0000	S_9	0.0000	S_9	0.0000	S_9	0.0000	S_9	0.0000

$15.0 < q^2 < 17.0$		$17.0 < q^2 < 19.0$		$11.0 < q^2 < 12.5$		$1.1 < q^2 < 6.0$		$15.0 < q^2 < 19.0$	
param.	$\sigma_{\text{syst.}}$	param.	$\sigma_{\text{syst.}}$	param.	$\sigma_{\text{syst.}}$	param.	$\sigma_{\text{syst.}}$	param.	$\sigma_{\text{syst.}}$
F_L	0.0003	F_L	0.0010	F_L	0.0001	F_L	0.0003	F_L	0.0003
S_3	0.0007	S_3	0.0035	S_3	0.0001	S_3	0.0000	S_3	0.0011
S_4	0.0006	S_4	0.0024	S_4	0.0002	S_4	0.0001	S_4	0.0009
S_5	0.0010	S_5	0.0026	S_5	0.0005	S_5	0.0002	S_5	0.0013
A_{FB}	0.0008	A_{FB}	0.0024	A_{FB}	0.0003	A_{FB}	0.0000	A_{FB}	0.0011
S_7	0.0000	S_7	0.0000	S_7	0.0000	S_7	0.0000	S_7	0.0000
S_8	0.0000	S_8	0.0000	S_8	0.0000	S_8	0.0000	S_8	0.0000
S_9	0.0000	S_9	0.0000	S_9	0.0000	S_9	0.0000	S_9	0.0000

is measured to be $(-0.35 \pm 0.76 \pm 0.28)\%$ [43]. This affects both the measured *CP* asymmetries and the *CP*-averaged observables, according to

$$\begin{aligned} A_i^{\text{meas}} &= A_i - S_i(\kappa \mathcal{A}_{\text{prod}}), \\ S_i^{\text{meas}} &= S_i - A_i(\kappa \mathcal{A}_{\text{prod}}), \end{aligned}$$

where κ is a dilution factor due to $B^0 - \overline{B}^0$ mixing. For B^0 mixing, κ is calculated via

$$\kappa = \frac{\int_0^\infty \epsilon(t) e^{-\Gamma t} \cos(\Delta m_d t) \mathrm{d}t}{\int_0^\infty \epsilon(t) e^{-\Gamma t} \mathrm{d}t},$$

with $\Gamma = 1/\tau_d = 1/1.519\,\mathrm{ps}^{-1}$ and the mixing frequency $\Delta m_d = 0.510\,\mathrm{ps}^{-1}$ [40]. The decay time dependent efficiency $\epsilon(t)$ is given in Fig. 92. The calculation results in a factor of $\kappa = 35.2\%$.

Table 63: Systematic uncertainties due to the $m_{K\pi}$ parametrisation of background events.

$0.1 < q^2 < 1.0$		$1.0 < q^2 < 2.5$		$2.5 < q^2 < 4.0$		$4.0 < q^2 < 6.0$		$6.0 < q^2 < 8.0$	
param.	$\sigma_{\text{syst.}}$	param.	$\sigma_{\text{syst.}}$	param.	$\sigma_{\text{syst.}}$	param.	$\sigma_{\text{syst.}}$	param.	$\sigma_{\text{syst.}}$
F_L	0.0004	F_L	0.0024	F_L	0.0050	F_L	0.0035	F_L	0.0016
S_3	0.0000	S_3	0.0000	S_3	0.0002	S_3	0.0003	S_3	0.0005
S_4	0.0003	S_4	0.0002	S_4	0.0011	S_4	0.0020	S_4	0.0019
S_5	0.0009	S_5	0.0011	S_5	0.0024	S_5	0.0047	S_5	0.0047
A_{FB}	0.0003	A_{FB}	0.0009	A_{FB}	0.0006	A_{FB}	0.0006	A_{FB}	0.0014
S_7	0.0001	S_7	0.0003	S_7	0.0005	S_7	0.0004	S_7	0.0003
S_8	0.0000	S_8	0.0001	S_8	0.0001	S_8	0.0001	S_8	0.0001
S_9	0.0000	S_9	0.0000	S_9	0.0001	S_9	0.0000	S_9	0.0000

$15.0 < q^2 < 17.0$		$17.0 < q^2 < 19.0$		$11.0 < q^2 < 12.5$		$1.1 < q^2 < 6.0$		$15.0 < q^2 < 19.0$	
param.	$\sigma_{\text{syst.}}$	param.	$\sigma_{\text{syst.}}$	param.	$\sigma_{\text{syst.}}$	param.	$\sigma_{\text{syst.}}$	param.	$\sigma_{\text{syst.}}$
F_L	0.0006	F_L	0.0004	F_L	0.0006	F_L	0.0042	F_L	0.0013
S_3	0.0013	S_3	0.0015	S_3	0.0012	S_3	0.0001	S_3	0.0042
S_4	0.0012	S_4	0.0010	S_4	0.0021	S_4	0.0013	S_4	0.0035
S_5	0.0018	S_5	0.0011	S_5	0.0044	S_5	0.0026	S_5	0.0048
A_{FB}	0.0015	A_{FB}	0.0010	A_{FB}	0.0027	A_{FB}	0.0004	A_{FB}	0.0042
S_7	0.0000	S_7	0.0000	S_7	0.0000	S_7	0.0006	S_7	0.0000
S_8	0.0000	S_8	0.0000	S_8	0.0000	S_8	0.0001	S_8	0.0000
S_9	0.0000	S_9	0.0000	S_9	0.0000	S_9	0.0000	S_9	0.0000

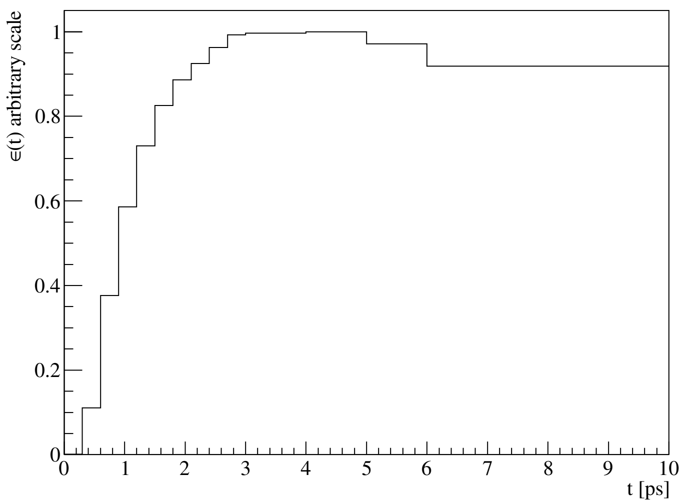

Figure 92: The decay time dependent selection efficiency $\epsilon(t)$.

Table 64: Systematic uncertainties due to the assumption of flat efficiency in $m_{K\pi}$.

param.	$0.1 < q^2 < 1.0$ $\sigma_{\text{syst.}}$	$1.0 < q^2 < 2.5$ $\sigma_{\text{syst.}}$	$2.5 < q^2 < 4.0$ $\sigma_{\text{syst.}}$	$4.0 < q^2 < 6.0$ $\sigma_{\text{syst.}}$	$6.0 < q^2 < 8.0$ $\sigma_{\text{syst.}}$
F_L	0.0007	0.0022	0.0010	0.0033	0.0031
S_3	0.0008	0.0006	0.0034	0.0028	0.0016
S_4	0.0025	0.0003	0.0023	0.0002	0.0030
S_5	0.0011	0.0029	0.0025	0.0012	0.0054
A_{FB}	0.0005	0.0006	0.0031	0.0012	0.0019
S_7	0.0019	0.0009	0.0020	0.0023	0.0023
S_8	0.0033	0.0008	0.0033	0.0031	0.0018
S_9	0.0009	0.0003	0.0025	0.0016	0.0034

param.	$15.0 < q^2 < 17.0$ $\sigma_{\text{syst.}}$	$17.0 < q^2 < 19.0$ $\sigma_{\text{syst.}}$	$11.0 < q^2 < 12.5$ $\sigma_{\text{syst.}}$	$1.1 < q^2 < 6.0$ $\sigma_{\text{syst.}}$	$15.0 < q^2 < 19.0$ $\sigma_{\text{syst.}}$
F_L	0.0020	0.0008	0.0006	0.0001	0.0016
S_3	0.0017	0.0015	0.0013	0.0017	0.0034
S_4	0.0009	0.0014	0.0013	0.0027	0.0036
S_5	0.0012	0.0009	0.0023	0.0002	0.0060
A_{FB}	0.0007	0.0013	0.0005	0.0018	0.0036
S_7	0.0010	0.0056	0.0017	0.0007	0.0031
S_8	0.0010	0.0007	0.0020	0.0041	0.0026
S_9	0.0013	0.0020	0.0019	0.0021	0.0008

10.1.10 Detection asymmetry

Similarly to the production asymmetry, the measurement can also be affected by the $K^+\pi^-$ detection asymmetry

$$\mathcal{A}_{\text{det}} = \frac{\epsilon(K^+\pi^-) - \epsilon(K^-\pi^+)}{\epsilon(K^+\pi^-) + \epsilon(K^-\pi^+)},$$

according to

$$\begin{aligned} A_i^{\text{meas}} &= A_i - S_i\mathcal{A}_{\text{det}}, \\ S_i^{\text{meas}} &= S_i - A_i\mathcal{A}_{\text{det}}. \end{aligned}$$

The $K^+\pi^-$ detection asymmetry is known to be driven by the kaon detection asymmetry, which is momentum dependent. The kaon detection asymmetry, in bins of kaon momentum, is given in Tab. 65, which is taken from Ref. [44] and was used in Ref. [45]. Since the momentum spectra for the hadrons depend on q^2, the detection asymmetry is determined for all q^2 bins, and given in Tab. 65.

10.1.11 Summary of systematic uncertainties

Tables 66, 67, 68, 69 and 70 give an overview of the systematic uncertainties for the observables in bins of q^2. The different systematic sources and their constribution to the

Table 65: (Left) kaon detection asymmetry, depending on kaon momentum. (Right) resulting $K^+\pi^-$ detection asymmetry $\mathcal{A}_{\text{det}}$ for the different q^2 bins.

$p(K)$ [GeV/c]	$\mathcal{A}_{\text{det}}$ [%]
$0 < p(K) < 10$	-1.37 ± 0.11
$10 < p(K) < 17.5$	-1.2 ± 0.10
$17.5 < p(K) < 22.5$	-1.15 ± 0.11
$22.5 < p(K) < 30$	-1.09 ± 0.12
$30 < p(K) < 50$	-0.88 ± 0.16
$50 < p(K) < 70$	-0.71 ± 0.29
$70 < p(K) < 100$	-0.33 ± 0.30
$100 < p(K) < 150$	0.18 ± 0.45

q^2 bin [GeV$^2/c^4$]	$\mathcal{A}_{\text{det}}$ [%]
$0.1 < q^2 < 0.98$	-0.010
$1.1 < q^2 < 2.5$	-0.011
$2.5 < q^2 < 4.0$	-0.011
$4.0 < q^2 < 6.0$	-0.011
$6.0 < q^2 < 8.0$	-0.011
$11.0 < q^2 < 12.5$	-0.011
$15.0 < q^2 < 17.0$	-0.012
$17.0 < q^2 < 19.0$	-0.012
$1.1 < q^2 < 6.0$	-0.011
$15.0 < q^2 < 19.0$	-0.012

total systematic uncertainty are shown. The total systematic uncertainty is calculated as quadratic sum of the individual contributions. The statistical uncertainty from a fit of the data, evaluated using `HESSE`, is given as well for comparison.

The Tables 71, 72, 73, 74 and 75 give the corresponding systematic uncertainties for the $P_i^{(\prime)}$ basis. Tables 76, 77, 78, 79 and 80 give the systematic uncertainties for the *CP* asymmetries A_i.

Table 66: Summary of systematic uncertainties for the CP-averaged observables S_i in the q^2 bins $1.1 < q^2 < 6.0\,\mathrm{GeV}^2/c^4$ and $15.0 < q^2 < 19.0\,\mathrm{GeV}^2/c^4$.

				$1.1 < q^2 < 6.0\,\mathrm{GeV}^2/c^4$				
σ	F_{L}	S_3	S_4	S_5	A_{FB}	S_7	S_8	S_9
$\sigma_{\mathrm{stat.}}$	0.0307	0.0375	0.0497	0.0457	0.0294	0.0460	0.0500	0.0405
π reweighting	0.0139	0.0004	0.0001	0.0011	0.0023	0.0002	0.0001	0.0001
K reweighting	0.0000	0.0000	0.0013	0.0000	0.0001	0.0000	0.0000	0.0000
$p_{\mathrm{T}}(B^0)$ reweighting	0.0032	0.0000	0.0002	0.0001	0.0005	0.0000	0.0000	0.0000
$\chi^2_{\mathrm{Vtx.}}$ reweighting	0.0005	0.0001	0.0003	0.0003	0.0000	0.0000	0.0000	0.0000
N_{tracks} reweighting	0.0000	0.0002	0.0011	0.0003	0.0004	0.0000	0.0000	0.0000
higher order acc.	0.0001	0.0000	0.0006	0.0001	0.0001	0.0014	0.0011	0.0007
$\epsilon(q^2)$	0.0000	0.0000	0.0000	0.0000	0.0000	0.0000	0.0000	0.0000
peaking bkg.	0.0063	0.0032	0.0012	0.0041	0.0058	0.0055	0.0066	0.0037
angular bkg. model	0.0021	0.0010	0.0017	0.0005	0.0013	0.0002	0.0001	0.0004
sig. mass	0.0017	0.0001	0.0003	0.0005	0.0001	0.0003	0.0002	0.0001
$m_{K\pi}$ isobar	0.0003	0.0000	0.0001	0.0002	0.0000	0.0000	0.0000	0.0000
$m_{K\pi}$ bkg.	0.0042	0.0001	0.0013	0.0026	0.0004	0.0006	0.0001	0.0000
$m_{K\pi}$ eff.	0.0001	0.0017	0.0027	0.0002	0.0018	0.0007	0.0041	0.0021
acc. stat.	0.0012	0.0011	0.0016	0.0018	0.0007	0.0001	0.0001	0.0000
$\mathcal{A}_{\mathrm{det}}$	0.0000	0.0008	0.0001	0.0005	0.0002	0.0005	0.0005	0.0004
$\mathcal{A}_{\mathrm{prod}}$	0.0000	0.0001	0.0000	0.0001	0.0000	0.0001	0.0001	0.0000
$\sigma_{\mathrm{syst.}}$	0.0165	0.0040	0.0044	0.0054	0.0067	0.0058	0.0079	0.0043

				$15.0 < q^2 < 19.0\,\mathrm{GeV}^2/c^4$				
σ	F_{L}	S_3	S_4	S_5	A_{FB}	S_7	S_8	S_9
$\sigma_{\mathrm{stat.}}$	0.0267	0.0335	0.0364	0.0349	0.0279	0.0414	0.0425	0.0402
π reweighting	0.0040	0.0021	0.0009	0.0015	0.0017	0.0000	0.0000	0.0000
K reweighting	0.0003	0.0004	0.0000	0.0001	0.0003	0.0000	0.0000	0.0000
$p_{\mathrm{T}}(B^0)$ reweighting	0.0029	0.0002	0.0003	0.0004	0.0015	0.0000	0.0000	0.0000
$\chi^2_{\mathrm{Vtx.}}$ reweighting	0.0011	0.0004	0.0003	0.0003	0.0003	0.0000	0.0000	0.0000
N_{tracks} reweighting	0.0003	0.0002	0.0003	0.0002	0.0005	0.0000	0.0000	0.0000
higher order acc.	0.0003	0.0010	0.0002	0.0002	0.0004	0.0050	0.0003	0.0002
$\epsilon(q^2)$	0.0000	0.0000	0.0000	0.0000	0.0000	0.0000	0.0000	0.0000
peaking bkg.	0.0046	0.0050	0.0037	0.0032	0.0056	0.0025	0.0014	0.0012
angular bkg. model	0.0005	0.0008	0.0015	0.0010	0.0000	0.0001	0.0000	0.0007
sig. mass	0.0017	0.0037	0.0005	0.0019	0.0027	0.0000	0.0000	0.0001
$m_{K\pi}$ isobar	0.0003	0.0011	0.0009	0.0013	0.0011	0.0000	0.0000	0.0000
$m_{K\pi}$ bkg.	0.0013	0.0042	0.0035	0.0048	0.0042	0.0000	0.0000	0.0000
$m_{K\pi}$ eff.	0.0016	0.0034	0.0036	0.0060	0.0036	0.0031	0.0026	0.0008
acc. stat.	0.0029	0.0039	0.0023	0.0031	0.0022	0.0001	0.0001	0.0000
$\mathcal{A}_{\mathrm{det}}$	0.0000	0.0004	0.0009	0.0004	0.0013	0.0005	0.0003	0.0007
$\mathcal{A}_{\mathrm{prod}}$	0.0000	0.0000	0.0001	0.0000	0.0001	0.0000	0.0000	0.0001
$\sigma_{\mathrm{syst.}}$	0.0079	0.0095	0.0071	0.0094	0.0090	0.0065	0.0030	0.0018

Table 67: Summary of systematic uncertainties for the CP-averaged observables S_i in the q^2 bins $0.1 < q^2 < 0.98\,\mathrm{GeV}^2/c^4$ and $1.1 < q^2 < 2.5\,\mathrm{GeV}^2/c^4$.

	$0.1 < q^2 < 0.98\,\mathrm{GeV}^2/c^4$							
σ	F_{L}	S_3	S_4	S_5	A_{FB}	S_7	S_8	S_9
$\sigma_{\mathrm{stat.}}$	0.0436	0.0608	0.0658	0.0569	0.0563	0.0580	0.0738	0.0576
π reweighting	0.0139	0.0010	0.0005	0.0030	0.0003	0.0003	0.0000	0.0001
K reweighting	0.0035	0.0010	0.0003	0.0010	0.0008	0.0002	0.0001	0.0001
$p_{\mathrm{T}}(B^0)$ reweighting	0.0009	0.0002	0.0003	0.0004	0.0003	0.0000	0.0001	0.0000
$\chi^2_{\mathrm{Vtx.}}$ reweighting	0.0019	0.0001	0.0019	0.0004	0.0019	0.0002	0.0000	0.0001
N_{tracks} reweighting	0.0010	0.0000	0.0005	0.0003	0.0022	0.0001	0.0002	0.0000
higher order acc.	0.0037	0.0007	0.0042	0.0162	0.0004	0.0036	0.0003	0.0017
$\epsilon(q^2)$	0.0025	0.0014	0.0037	0.0014	0.0028	0.0001	0.0003	0.0000
peaking bkg.	0.0064	0.0023	0.0039	0.0040	0.0062	0.0038	0.0066	0.0030
angular bkg. model	0.0003	0.0010	0.0007	0.0002	0.0001	0.0001	0.0000	0.0006
sig. mass	0.0009	0.0001	0.0000	0.0008	0.0005	0.0000	0.0000	0.0000
$m_{K\pi}$ isobar	0.0002	0.0000	0.0001	0.0004	0.0001	0.0000	0.0000	0.0000
$m_{K\pi}$ bkg.	0.0004	0.0000	0.0003	0.0009	0.0003	0.0001	0.0000	0.0000
$m_{K\pi}$ eff.	0.0007	0.0008	0.0025	0.0011	0.0005	0.0019	0.0033	0.0009
acc. stat.	0.0029	0.0038	0.0040	0.0045	0.0038	0.0003	0.0001	0.0000
$\mathcal{A}_{\mathrm{det}}$	0.0000	0.0001	0.0007	0.0000	0.0013	0.0008	0.0003	0.0003
$\mathcal{A}_{\mathrm{prod}}$	0.0000	0.0000	0.0001	0.0000	0.0001	0.0001	0.0000	0.0000
$\sigma_{\mathrm{syst.}}$	0.0168	0.0051	0.0086	0.0177	0.0085	0.0057	0.0074	0.0036

	$1.1 < q^2 < 2.5\,\mathrm{GeV}^2/c^4$							
σ	F_{L}	S_3	S_4	S_5	A_{FB}	S_7	S_8	S_9
$\sigma_{\mathrm{stat.}}$	0.0679	0.0744	0.0939	0.0872	0.0596	0.0883	0.0977	0.0741
π reweighting	0.0149	0.0002	0.0017	0.0006	0.0077	0.0001	0.0001	0.0001
K reweighting	0.0006	0.0002	0.0006	0.0004	0.0004	0.0000	0.0000	0.0000
$p_{\mathrm{T}}(B^0)$ reweighting	0.0028	0.0000	0.0002	0.0005	0.0014	0.0000	0.0000	0.0000
$\chi^2_{\mathrm{Vtx.}}$ reweighting	0.0004	0.0001	0.0001	0.0006	0.0003	0.0000	0.0000	0.0000
N_{tracks} reweighting	0.0002	0.0002	0.0010	0.0003	0.0000	0.0000	0.0000	0.0000
higher order acc.	0.0108	0.0015	0.0007	0.0065	0.0020	0.0030	0.0030	0.0013
$\epsilon(q^2)$	0.0088	0.0005	0.0029	0.0005	0.0043	0.0001	0.0001	0.0000
peaking bkg.	0.0035	0.0029	0.0012	0.0040	0.0075	0.0011	0.0034	0.0042
angular bkg. model	0.0033	0.0031	0.0004	0.0010	0.0009	0.0005	0.0004	0.0013
sig. mass	0.0021	0.0001	0.0001	0.0006	0.0011	0.0005	0.0001	0.0001
$m_{K\pi}$ isobar	0.0004	0.0000	0.0000	0.0002	0.0001	0.0001	0.0000	0.0000
$m_{K\pi}$ bkg.	0.0024	0.0000	0.0002	0.0011	0.0009	0.0003	0.0001	0.0000
$m_{K\pi}$ eff.	0.0022	0.0006	0.0003	0.0029	0.0006	0.0009	0.0008	0.0003
acc. stat.	0.0018	0.0015	0.0025	0.0026	0.0013	0.0002	0.0001	0.0001
$\mathcal{A}_{\mathrm{det}}$	0.0000	0.0004	0.0025	0.0012	0.0004	0.0009	0.0005	0.0000
$\mathcal{A}_{\mathrm{prod}}$	0.0000	0.0001	0.0003	0.0001	0.0000	0.0001	0.0001	0.0000
$\sigma_{\mathrm{syst.}}$	0.0216	0.0049	0.0052	0.0089	0.0121	0.0036	0.0047	0.0047

Table 68: Summary of systematic uncertainties for the CP-averaged observables S_i in the q^2 bins $2.5 < q^2 < 4.0\,\mathrm{GeV}^2/c^4$ and $4.0 < q^2 < 6.0\,\mathrm{GeV}^2/c^4$.

	$2.5 < q^2 < 4.0\,\mathrm{GeV}^2/c^4$							
σ	F_{L}	S_3	S_4	S_5	A_{FB}	S_7	S_8	S_9
$\sigma_{\mathrm{stat.}}$	0.0857	0.0694	0.1162	0.0952	0.0661	0.1017	0.1124	0.0847
π reweighting	0.0118	0.0005	0.0007	0.0017	0.0043	0.0003	0.0002	0.0002
K reweighting	0.0001	0.0001	0.0010	0.0000	0.0001	0.0000	0.0000	0.0000
$p_{\mathrm{T}}(B^0)$ reweighting	0.0027	0.0001	0.0005	0.0001	0.0009	0.0001	0.0001	0.0000
$\chi^2_{\mathrm{Vtx.}}$ reweighting	0.0005	0.0001	0.0003	0.0004	0.0001	0.0000	0.0000	0.0000
N_{tracks} reweighting	0.0003	0.0002	0.0010	0.0001	0.0005	0.0000	0.0000	0.0000
higher order acc.	0.0022	0.0003	0.0017	0.0025	0.0000	0.0005	0.0009	0.0012
$\epsilon(q^2)$	0.0089	0.0002	0.0002	0.0019	0.0034	0.0002	0.0002	0.0001
peaking bkg.	0.0024	0.0048	0.0052	0.0051	0.0033	0.0050	0.0048	0.0060
angular bkg. model	0.0013	0.0024	0.0003	0.0010	0.0014	0.0002	0.0002	0.0019
sig. mass	0.0022	0.0003	0.0003	0.0007	0.0003	0.0001	0.0000	0.0002
$m_{K\pi}$ isobar	0.0004	0.0000	0.0001	0.0002	0.0000	0.0000	0.0000	0.0000
$m_{K\pi}$ bkg.	0.0050	0.0002	0.0011	0.0024	0.0006	0.0005	0.0001	0.0001
$m_{K\pi}$ eff.	0.0010	0.0034	0.0023	0.0025	0.0031	0.0020	0.0033	0.0025
acc. stat.	0.0013	0.0012	0.0018	0.0022	0.0009	0.0001	0.0001	0.0000
$\mathcal{A}_{\mathrm{det}}$	0.0000	0.0012	0.0001	0.0001	0.0002	0.0003	0.0008	0.0024
$\mathcal{A}_{\mathrm{prod}}$	0.0000	0.0001	0.0000	0.0000	0.0000	0.0000	0.0001	0.0003
$\sigma_{\mathrm{syst.}}$	0.0165	0.0066	0.0065	0.0076	0.0074	0.0055	0.0059	0.0073

	$4.0 < q^2 < 6.0\,\mathrm{GeV}^2/c^4$							
σ	F_{L}	S_3	S_4	S_5	A_{FB}	S_7	S_8	S_9
$\sigma_{\mathrm{stat.}}$	0.0513	0.0646	0.0802	0.0747	0.0493	0.0785	0.0878	0.0674
π reweighting	0.0126	0.0011	0.0021	0.0020	0.0020	0.0002	0.0002	0.0002
K reweighting	0.0004	0.0001	0.0010	0.0004	0.0001	0.0000	0.0000	0.0000
$p_{\mathrm{T}}(B^0)$ reweighting	0.0032	0.0001	0.0004	0.0005	0.0005	0.0000	0.0000	0.0000
$\chi^2_{\mathrm{Vtx.}}$ reweighting	0.0004	0.0001	0.0002	0.0000	0.0001	0.0000	0.0000	0.0000
N_{tracks} reweighting	0.0004	0.0000	0.0008	0.0001	0.0006	0.0000	0.0000	0.0000
higher order acc.	0.0033	0.0003	0.0015	0.0020	0.0011	0.0001	0.0006	0.0008
$\epsilon(q^2)$	0.0089	0.0005	0.0009	0.0020	0.0013	0.0002	0.0000	0.0001
peaking bkg.	0.0041	0.0050	0.0069	0.0085	0.0013	0.0037	0.0032	0.0014
angular bkg. model	0.0010	0.0022	0.0010	0.0010	0.0005	0.0002	0.0002	0.0033
sig. mass	0.0013	0.0004	0.0004	0.0013	0.0007	0.0001	0.0001	0.0004
$m_{K\pi}$ isobar	0.0002	0.0000	0.0001	0.0004	0.0000	0.0000	0.0000	0.0000
$m_{K\pi}$ bkg.	0.0035	0.0003	0.0020	0.0047	0.0006	0.0004	0.0001	0.0000
$m_{K\pi}$ eff.	0.0033	0.0028	0.0002	0.0012	0.0012	0.0023	0.0031	0.0016
acc. stat.	0.0012	0.0012	0.0015	0.0018	0.0008	0.0001	0.0000	0.0000
$\mathcal{A}_{\mathrm{det}}$	0.0000	0.0018	0.0018	0.0006	0.0002	0.0004	0.0000	0.0007
$\mathcal{A}_{\mathrm{prod}}$	0.0000	0.0002	0.0002	0.0001	0.0000	0.0001	0.0000	0.0001
$\sigma_{\mathrm{syst.}}$	0.0174	0.0067	0.0082	0.0107	0.0035	0.0044	0.0045	0.0041

Table 69: Summary of systematic uncertainties for the CP-averaged observables S_i in the q^2 bins $6.0 < q^2 < 8.0\,\mathrm{GeV}^2/c^4$ and $11.0 < q^2 < 12.5\,\mathrm{GeV}^2/c^4$.

				$6.0 < q^2 < 8.0\,\mathrm{GeV}^2/c^4$				
σ	F_{L}	S_3	S_4	S_5	A_{FB}	S_7	S_8	S_9
$\sigma_{\mathrm{stat.}}$	0.0442	0.0551	0.0606	0.0574	0.0390	0.0647	0.0682	0.0571
π reweighting	0.0130	0.0014	0.0020	0.0010	0.0058	0.0001	0.0001	0.0001
K reweighting	0.0008	0.0002	0.0008	0.0004	0.0001	0.0000	0.0000	0.0000
$p_{\mathrm{T}}(B^0)$ reweighting	0.0039	0.0001	0.0001	0.0005	0.0016	0.0000	0.0000	0.0000
$\chi^2_{\mathrm{Vtx.}}$ reweighting	0.0004	0.0000	0.0001	0.0001	0.0002	0.0000	0.0000	0.0000
N_{tracks} reweighting	0.0007	0.0001	0.0006	0.0001	0.0006	0.0000	0.0000	0.0000
higher order acc.	0.0034	0.0010	0.0014	0.0021	0.0021	0.0009	0.0013	0.0020
$\epsilon(q^2)$	0.0043	0.0003	0.0001	0.0004	0.0020	0.0001	0.0001	0.0001
peaking bkg.	0.0023	0.0100	0.0097	0.0082	0.0040	0.0009	0.0057	0.0016
angular bkg. model	0.0012	0.0039	0.0016	0.0034	0.0008	0.0003	0.0001	0.0018
sig. mass	0.0006	0.0006	0.0006	0.0019	0.0011	0.0002	0.0002	0.0002
$m_{K\pi}$ isobar	0.0001	0.0000	0.0002	0.0004	0.0001	0.0000	0.0000	0.0000
$m_{K\pi}$ bkg.	0.0016	0.0005	0.0019	0.0047	0.0014	0.0003	0.0001	0.0000
$m_{K\pi}$ eff.	0.0031	0.0016	0.0030	0.0054	0.0019	0.0023	0.0018	0.0034
acc. stat.	0.0013	0.0013	0.0012	0.0018	0.0009	0.0001	0.0000	0.0000
$\mathcal{A}_{\mathrm{det}}$	0.0000	0.0007	0.0004	0.0014	0.0005	0.0004	0.0005	0.0012
$\mathcal{A}_{\mathrm{prod}}$	0.0000	0.0001	0.0000	0.0002	0.0001	0.0000	0.0001	0.0001
$\sigma_{\mathrm{syst.}}$	0.0153	0.0111	0.0109	0.0120	0.0083	0.0027	0.0061	0.0048

				$11.0 < q^2 < 12.5\,\mathrm{GeV}^2/c^4$				
σ	F_{L}	S_3	S_4	S_5	A_{FB}	S_7	S_8	S_9
$\sigma_{\mathrm{stat.}}$	0.0420	0.0434	0.0676	0.0613	0.0363	0.0689	0.0636	0.0581
π reweighting	0.0108	0.0015	0.0002	0.0016	0.0066	0.0000	0.0000	0.0000
K reweighting	0.0012	0.0001	0.0002	0.0002	0.0008	0.0000	0.0000	0.0000
$p_{\mathrm{T}}(B^0)$ reweighting	0.0046	0.0005	0.0006	0.0009	0.0028	0.0000	0.0000	0.0000
$\chi^2_{\mathrm{Vtx.}}$ reweighting	0.0010	0.0000	0.0001	0.0001	0.0006	0.0000	0.0000	0.0000
N_{tracks} reweighting	0.0003	0.0007	0.0003	0.0005	0.0002	0.0000	0.0000	0.0000
higher order acc.	0.0032	0.0005	0.0003	0.0028	0.0018	0.0014	0.0023	0.0008
$\epsilon(q^2)$	0.0013	0.0009	0.0005	0.0005	0.0009	0.0001	0.0002	0.0000
peaking bkg.	0.0018	0.0031	0.0080	0.0058	0.0022	0.0047	0.0042	0.0051
angular bkg. model	0.0007	0.0011	0.0014	0.0024	0.0021	0.0003	0.0002	0.0034
sig. mass	0.0011	0.0014	0.0005	0.0019	0.0019	0.0000	0.0000	0.0000
$m_{K\pi}$ isobar	0.0001	0.0001	0.0002	0.0005	0.0003	0.0000	0.0000	0.0000
$m_{K\pi}$ bkg.	0.0006	0.0012	0.0021	0.0044	0.0027	0.0000	0.0000	0.0000
$m_{K\pi}$ eff.	0.0006	0.0013	0.0013	0.0023	0.0005	0.0017	0.0020	0.0019
acc. stat.	0.0017	0.0017	0.0012	0.0019	0.0012	0.0000	0.0000	0.0000
$\mathcal{A}_{\mathrm{det}}$	0.0000	0.0015	0.0011	0.0003	0.0003	0.0001	0.0002	0.0006
$\mathcal{A}_{\mathrm{prod}}$	0.0000	0.0002	0.0001	0.0000	0.0000	0.0000	0.0000	0.0001
$\sigma_{\mathrm{syst.}}$	0.0126	0.0050	0.0087	0.0092	0.0089	0.0052	0.0052	0.0065

Table 70: Summary of systematic uncertainties for the CP-averaged observables S_i in the q^2 bins $15.0 < q^2 < 17.0\,\mathrm{GeV}^2/c^4$ and $17.0 < q^2 < 19.0\,\mathrm{GeV}^2/c^4$.

				$15.0 < q^2 < 17.0\,\mathrm{GeV}^2/c^4$				
σ	F_{L}	S_3	S_4	S_5	A_{FB}	S_7	S_8	S_9
$\sigma_{\mathrm{stat.}}$	0.0371	0.0402	0.0475	0.0469	0.0351	0.0547	0.0552	0.0501
π reweighting	0.0059	0.0020	0.0006	0.0018	0.0031	0.0000	0.0000	0.0000
K reweighting	0.0008	0.0002	0.0000	0.0000	0.0005	0.0000	0.0000	0.0000
$p_{\mathrm{T}}(B^0)$ reweighting	0.0032	0.0001	0.0001	0.0005	0.0017	0.0000	0.0000	0.0000
$\chi^2_{\mathrm{Vtx.}}$ reweighting	0.0010	0.0002	0.0003	0.0004	0.0004	0.0000	0.0000	0.0000
N_{tracks} reweighting	0.0010	0.0001	0.0002	0.0004	0.0006	0.0000	0.0000	0.0000
higher order acc.	0.0018	0.0013	0.0009	0.0022	0.0004	0.0016	0.0018	0.0024
$\epsilon(q^2)$	0.0034	0.0033	0.0030	0.0024	0.0014	0.0002	0.0002	0.0001
peaking bkg.	0.0034	0.0018	0.0049	0.0068	0.0054	0.0050	0.0025	0.0034
angular bkg. model	0.0011	0.0002	0.0012	0.0005	0.0002	0.0000	0.0000	0.0004
sig. mass	0.0013	0.0039	0.0003	0.0019	0.0023	0.0000	0.0001	0.0001
$m_{K\pi}$ isobar	0.0003	0.0007	0.0006	0.0010	0.0008	0.0000	0.0000	0.0000
$m_{K\pi}$ bkg.	0.0006	0.0013	0.0012	0.0018	0.0015	0.0000	0.0000	0.0000
$m_{K\pi}$ eff.	0.0020	0.0017	0.0009	0.0012	0.0007	0.0010	0.0010	0.0013
acc. stat.	0.0025	0.0030	0.0021	0.0028	0.0020	0.0000	0.0000	0.0000
$\mathcal{A}_{\mathrm{det}}$	0.0000	0.0004	0.0008	0.0009	0.0010	0.0012	0.0006	0.0011
$\mathcal{A}_{\mathrm{prod}}$	0.0000	0.0000	0.0001	0.0001	0.0001	0.0001	0.0001	0.0001
$\sigma_{\mathrm{syst.}}$	0.0093	0.0071	0.0066	0.0089	0.0076	0.0055	0.0033	0.0045

				$17.0 < q^2 < 19.0\,\mathrm{GeV}^2/c^4$				
σ	F_{L}	S_3	S_4	S_5	A_{FB}	S_7	S_8	S_9
$\sigma_{\mathrm{stat.}}$	0.0453	0.0642	0.0538	0.0527	0.0445	0.0682	0.0656	0.0576
π reweighting	0.0021	0.0019	0.0010	0.0011	0.0005	0.0000	0.0000	0.0000
K reweighting	0.0002	0.0006	0.0001	0.0002	0.0001	0.0000	0.0000	0.0000
$p_{\mathrm{T}}(B^0)$ reweighting	0.0024	0.0005	0.0005	0.0003	0.0011	0.0000	0.0000	0.0000
$\chi^2_{\mathrm{Vtx.}}$ reweighting	0.0013	0.0007	0.0004	0.0002	0.0002	0.0000	0.0000	0.0000
N_{tracks} reweighting	0.0015	0.0001	0.0009	0.0001	0.0016	0.0000	0.0000	0.0000
higher order acc.	0.0084	0.0025	0.0002	0.0031	0.0059	0.0112	0.0027	0.0015
$\epsilon(q^2)$	0.0226	0.0102	0.0062	0.0044	0.0063	0.0000	0.0000	0.0000
peaking bkg.	0.0037	0.0049	0.0061	0.0038	0.0074	0.0037	0.0043	0.0033
angular bkg. model	0.0003	0.0059	0.0002	0.0001	0.0002	0.0001	0.0002	0.0018
sig. mass	0.0022	0.0072	0.0011	0.0020	0.0034	0.0003	0.0000	0.0001
$m_{K\pi}$ isobar	0.0010	0.0035	0.0024	0.0026	0.0024	0.0000	0.0000	0.0000
$m_{K\pi}$ bkg.	0.0004	0.0015	0.0010	0.0011	0.0010	0.0000	0.0000	0.0000
$m_{K\pi}$ eff.	0.0008	0.0015	0.0014	0.0009	0.0013	0.0056	0.0007	0.0020
acc. stat.	0.0044	0.0067	0.0037	0.0046	0.0037	0.0000	0.0000	0.0000
$\mathcal{A}_{\mathrm{det}}$	0.0000	0.0007	0.0009	0.0001	0.0016	0.0006	0.0003	0.0005
$\mathcal{A}_{\mathrm{prod}}$	0.0000	0.0001	0.0001	0.0000	0.0002	0.0001	0.0000	0.0001
$\sigma_{\mathrm{syst.}}$	0.0252	0.0170	0.0102	0.0089	0.0130	0.0131	0.0051	0.0045

Table 71: Summary of systematic uncertainties for the $P_i^{(\prime)}$ in the q^2 bins $1.1 < q^2 < 6.0\,\mathrm{GeV}^2/c^4$ and $15.0 < q^2 < 19.0\,\mathrm{GeV}^2/c^4$.

	$1.1 < q^2 < 6.0\,\mathrm{GeV}^2/c^4$						
σ	P_1	P_2	P_3	P_4	P_5	P_6	P_8
$\sigma_{\mathrm{stat.}}$	0.2418	0.0643	0.1307	0.1074	0.0987	0.0997	0.1081
π reweighting	0.0016	0.0008	0.0003	0.0040	0.0034	0.0009	0.0002
K reweighting	0.0004	0.0002	0.0001	0.0029	0.0001	0.0000	0.0000
$p_{\mathrm{T}}(B^0)$ reweighting	0.0004	0.0002	0.0001	0.0004	0.0014	0.0002	0.0000
$\chi^2_{\mathrm{Vtx.}}$ reweighting	0.0010	0.0001	0.0000	0.0005	0.0004	0.0001	0.0000
N_{tracks} reweighting	0.0014	0.0010	0.0000	0.0025	0.0006	0.0000	0.0000
higher order acc.	0.0007	0.0000	0.0026	0.0013	0.0000	0.0031	0.0030
$\epsilon(q^2)$	0.0000	0.0000	0.0000	0.0000	0.0000	0.0000	0.0000
peaking bkg.	0.0426	0.0076	0.0149	0.0076	0.0104	0.0199	0.0084
angular bkg. model	0.0022	0.0052	0.0019	0.0034	0.0002	0.0005	0.0005
sig. mass	0.0019	0.0020	0.0002	0.0010	0.0021	0.0006	0.0001
$m_{K\pi}$ isobar	0.0001	0.0002	0.0000	0.0003	0.0005	0.0001	0.0000
$m_{K\pi}$ bkg.	0.0021	0.0027	0.0002	0.0037	0.0065	0.0016	0.0002
$m_{K\pi}$ eff.	0.0029	0.0007	0.0061	0.0035	0.0003	0.0035	0.0019
acc. stat.	0.0081	0.0018	0.0001	0.0036	0.0044	0.0002	0.0001
$\mathcal{A}_{\mathrm{det}}$	0.0049	0.0003	0.0011	0.0003	0.0010	0.0010	0.0011
$\mathcal{A}_{\mathrm{prod}}$	0.0006	0.0000	0.0001	0.0000	0.0001	0.0001	0.0001
$\sigma_{\mathrm{syst.}}$	0.0440	0.0100	0.0165	0.0119	0.0138	0.0205	0.0092

	$15.0 < q^2 < 19.0\,\mathrm{GeV}^2/c^4$						
σ	P_1	P_2	P_3	P_4	P_5	P_6	P_8
$\sigma_{\mathrm{stat.}}$	0.1006	0.0264	0.0611	0.0769	0.0743	0.0872	0.0896
π reweighting	0.0031	0.0008	0.0000	0.0001	0.0012	0.0000	0.0000
K reweighting	0.0016	0.0001	0.0000	0.0002	0.0004	0.0000	0.0000
$p_{\mathrm{T}}(B^0)$ reweighting	0.0031	0.0003	0.0000	0.0018	0.0006	0.0000	0.0000
$\chi^2_{\mathrm{Vtx.}}$ reweighting	0.0003	0.0004	0.0000	0.0002	0.0001	0.0000	0.0000
N_{tracks} reweighting	0.0008	0.0004	0.0000	0.0005	0.0005	0.0000	0.0000
higher order acc.	0.0036	0.0002	0.0002	0.0008	0.0003	0.0099	0.0005
$\epsilon(q^2)$	0.0000	0.0000	0.0000	0.0000	0.0000	0.0000	0.0000
peaking bkg.	0.0120	0.0077	0.0047	0.0035	0.0093	0.0047	0.0075
angular bkg. model	0.0016	0.0004	0.0015	0.0035	0.0021	0.0002	0.0001
sig. mass	0.0094	0.0022	0.0003	0.0018	0.0046	0.0000	0.0003
$m_{K\pi}$ isobar	0.0031	0.0009	0.0000	0.0022	0.0030	0.0000	0.0000
$m_{K\pi}$ bkg.	0.0134	0.0040	0.0000	0.0092	0.0127	0.0001	0.0000
$m_{K\pi}$ eff.	0.0120	0.0033	0.0013	0.0081	0.0086	0.0028	0.0018
acc. stat.	0.0111	0.0013	0.0001	0.0049	0.0066	0.0002	0.0002
$\mathcal{A}_{\mathrm{det}}$	0.0013	0.0010	0.0011	0.0020	0.0009	0.0010	0.0006
$\mathcal{A}_{\mathrm{prod}}$	0.0001	0.0001	0.0001	0.0002	0.0001	0.0001	0.0001
$\sigma_{\mathrm{syst.}}$	0.0270	0.0098	0.0052	0.0147	0.0201	0.0114	0.0077

Table 72: Summary of systematic uncertainties for the $P_i^{(\prime)}$ in the q^2 bins $0.1 < q^2 < 0.98\,\mathrm{GeV}^2/c^4$ and $1.1 < q^2 < 2.5\,\mathrm{GeV}^2/c^4$.

	$0.1 < q^2 < 0.98\,\mathrm{GeV}^2/c^4$						
σ	P_1	P_2	P_3	P_4	P_5	P_6	P_8
$\sigma_{\mathrm{stat.}}$	0.1649	0.0510	0.0780	0.1498	0.1302	0.1317	0.1673
π reweighting	0.0027	0.0017	0.0001	0.0055	0.0036	0.0003	0.0001
K reweighting	0.0028	0.0009	0.0000	0.0011	0.0002	0.0003	0.0002
$p_{\mathrm{T}}(B^0)$ reweighting	0.0005	0.0004	0.0000	0.0009	0.0001	0.0000	0.0001
$\chi^2_{\mathrm{Vtx.}}$ reweighting	0.0004	0.0015	0.0000	0.0014	0.0002	0.0004	0.0001
N_{tracks} reweighting	0.0000	0.0017	0.0000	0.0019	0.0001	0.0001	0.0002
higher order acc.	0.0025	0.0009	0.0021	0.0118	0.0435	0.0079	0.0007
$\epsilon(q^2)$	0.0038	0.0024	0.0000	0.0093	0.0031	0.0004	0.0007
peaking bkg.	0.0057	0.0041	0.0044	0.0127	0.0249	0.0114	0.0052
angular bkg. model	0.0028	0.0000	0.0006	0.0018	0.0008	0.0002	0.0000
sig. mass	0.0007	0.0000	0.0002	0.0005	0.0029	0.0002	0.0001
$m_{K\pi}$ isobar	0.0000	0.0001	0.0000	0.0004	0.0012	0.0001	0.0000
$m_{K\pi}$ bkg.	0.0000	0.0001	0.0000	0.0005	0.0015	0.0001	0.0000
$m_{K\pi}$ eff.	0.0037	0.0022	0.0043	0.0026	0.0021	0.0042	0.0041
acc. stat.	0.0101	0.0035	0.0001	0.0097	0.0119	0.0008	0.0002
$\mathcal{A}_{\mathrm{det}}$	0.0002	0.0009	0.0004	0.0016	0.0000	0.0018	0.0007
$\mathcal{A}_{\mathrm{prod}}$	0.0000	0.0001	0.0001	0.0002	0.0000	0.0002	0.0001
$\sigma_{\mathrm{syst.}}$	0.0139	0.0070	0.0065	0.0231	0.0519	0.0147	0.0067

	$1.1 < q^2 < 2.5\,\mathrm{GeV}^2/c^4$						
σ	P_1	P_2	P_3	P_4	P_5	P_6	P_8
$\sigma_{\mathrm{stat.}}$	0.4388	0.1330	0.2237	0.1982	0.1858	0.1891	0.2071
π reweighting	0.0014	0.0035	0.0003	0.0032	0.0047	0.0009	0.0001
K reweighting	0.0012	0.0001	0.0001	0.0015	0.0010	0.0000	0.0000
$p_{\mathrm{T}}(B^0)$ reweighting	0.0000	0.0008	0.0000	0.0005	0.0004	0.0002	0.0000
$\chi^2_{\mathrm{Vtx.}}$ reweighting	0.0004	0.0001	0.0001	0.0003	0.0014	0.0000	0.0000
N_{tracks} reweighting	0.0013	0.0003	0.0001	0.0023	0.0007	0.0000	0.0000
higher order acc.	0.0103	0.0104	0.0046	0.0027	0.0170	0.0054	0.0069
$\epsilon(q^2)$	0.0032	0.0026	0.0001	0.0052	0.0029	0.0008	0.0003
peaking bkg.	0.0224	0.0214	0.0118	0.0175	0.0100	0.0093	0.0175
angular bkg. model	0.0233	0.0062	0.0042	0.0008	0.0013	0.0010	0.0004
sig. mass	0.0013	0.0059	0.0003	0.0005	0.0022	0.0005	0.0004
$m_{K\pi}$ isobar	0.0000	0.0009	0.0000	0.0001	0.0005	0.0002	0.0000
$m_{K\pi}$ bkg.	0.0004	0.0060	0.0000	0.0006	0.0032	0.0010	0.0002
$m_{K\pi}$ eff.	0.0143	0.0056	0.0071	0.0034	0.0074	0.0039	0.0143
acc. stat.	0.0098	0.0020	0.0002	0.0054	0.0060	0.0004	0.0002
$\mathcal{A}_{\mathrm{det}}$	0.0026	0.0006	0.0001	0.0052	0.0026	0.0019	0.0010
$\mathcal{A}_{\mathrm{prod}}$	0.0003	0.0001	0.0000	0.0006	0.0003	0.0002	0.0001
$\sigma_{\mathrm{syst.}}$	0.0384	0.0270	0.0151	0.0207	0.0232	0.0117	0.0237

Table 73: Summary of systematic uncertainties for the $P_i^{(\prime)}$ in the q^2 bins $2.5 < q^2 < 4.0\,\mathrm{GeV}^2/c^4$ and $4.0 < q^2 < 6.0\,\mathrm{GeV}^2/c^4$.

	$2.5 < q^2 < 4.0\,\mathrm{GeV}^2/c^4$						
σ	P_1	P_2	P_3	P_4	P_5	P_6	P_8
$\sigma_{\mathrm{stat.}}$	1.1432	0.5744	0.8633	0.4373	0.2902	0.3215	0.3429
π reweighting	0.0031	0.0013	0.0006	0.0047	0.0042	0.0013	0.0001
K reweighting	0.0007	0.0004	0.0001	0.0026	0.0000	0.0001	0.0001
$p_{\mathrm{T}}(B^0)$ reweighting	0.0004	0.0004	0.0001	0.0001	0.0021	0.0003	0.0000
$\chi^2_{\mathrm{Vtx.}}$ reweighting	0.0012	0.0003	0.0000	0.0006	0.0007	0.0001	0.0000
N_{tracks} reweighting	0.0023	0.0012	0.0001	0.0027	0.0006	0.0000	0.0000
higher order acc.	0.0022	0.0028	0.0056	0.0030	0.0077	0.0015	0.0021
$\epsilon(q^2)$	0.0001	0.0006	0.0004	0.0044	0.0013	0.0010	0.0005
peaking bkg.	0.0009	0.0103	0.0186	0.0214	0.0151	0.0111	0.0248
angular bkg. model	0.0248	0.0027	0.0090	0.0003	0.0022	0.0004	0.0003
sig. mass	0.0017	0.0046	0.0017	0.0022	0.0037	0.0009	0.0004
$m_{K\pi}$ isobar	0.0002	0.0006	0.0000	0.0004	0.0007	0.0002	0.0001
$m_{K\pi}$ bkg.	0.0023	0.0081	0.0004	0.0051	0.0091	0.0022	0.0007
$m_{K\pi}$ eff.	0.0292	0.0042	0.0086	0.0021	0.0083	0.0056	0.0029
acc. stat.	0.0117	0.0023	0.0002	0.0046	0.0054	0.0004	0.0002
$\mathcal{A}_{\mathrm{det}}$	0.0192	0.0009	0.0197	0.0002	0.0002	0.0011	0.0023
$\mathcal{A}_{\mathrm{prod}}$	0.0022	0.0001	0.0023	0.0000	0.0000	0.0001	0.0003
$\sigma_{\mathrm{syst.}}$	0.0448	0.0154	0.0305	0.0241	0.0226	0.0129	0.0252

	$4.0 < q^2 < 6.0\,\mathrm{GeV}^2/c^4$						
σ	P_1	P_2	P_3	P_4	P_5	P_6	P_8
$\sigma_{\mathrm{stat.}}$	0.3327	0.0844	0.1737	0.1642	0.1528	0.1613	0.1808
π reweighting	0.0060	0.0040	0.0004	0.0021	0.0073	0.0006	0.0000
K reweighting	0.0006	0.0006	0.0000	0.0025	0.0006	0.0000	0.0000
$p_{\mathrm{T}}(B^0)$ reweighting	0.0001	0.0011	0.0001	0.0007	0.0017	0.0002	0.0000
$\chi^2_{\mathrm{Vtx.}}$ reweighting	0.0008	0.0000	0.0000	0.0003	0.0004	0.0000	0.0000
N_{tracks} reweighting	0.0002	0.0013	0.0000	0.0016	0.0002	0.0000	0.0000
higher order acc.	0.0025	0.0051	0.0031	0.0051	0.0074	0.0001	0.0013
$\epsilon(q^2)$	0.0020	0.0030	0.0003	0.0023	0.0032	0.0005	0.0004
peaking bkg.	0.0108	0.0017	0.0104	0.0152	0.0136	0.0068	0.0093
angular bkg. model	0.0184	0.0005	0.0124	0.0014	0.0011	0.0006	0.0008
sig. mass	0.0028	0.0002	0.0009	0.0016	0.0037	0.0001	0.0002
$m_{K\pi}$ isobar	0.0003	0.0003	0.0000	0.0005	0.0011	0.0001	0.0000
$m_{K\pi}$ bkg.	0.0033	0.0040	0.0001	0.0060	0.0137	0.0011	0.0004
$m_{K\pi}$ eff.	0.0068	0.0057	0.0164	0.0072	0.0035	0.0024	0.0011
acc. stat.	0.0098	0.0020	0.0001	0.0031	0.0044	0.0002	0.0001
$\mathcal{A}_{\mathrm{det}}$	0.0094	0.0003	0.0017	0.0036	0.0013	0.0009	0.0001
$\mathcal{A}_{\mathrm{prod}}$	0.0011	0.0000	0.0002	0.0004	0.0001	0.0001	0.0000
$\sigma_{\mathrm{syst.}}$	0.0274	0.0105	0.0233	0.0198	0.0233	0.0074	0.0095

Table 74: Summary of systematic uncertainties for the $P_i^{(\prime)}$ in the q^2 bins $6.0 < q^2 < 8.0\,\mathrm{GeV}^2/c^4$ and $11.0 < q^2 < 12.5\,\mathrm{GeV}^2/c^4$.

	$6.0 < q^2 < 8.0\,\mathrm{GeV}^2/c^4$						
σ	P_1	P_2	P_3	P_4	P_5	P_6	P_8
$\sigma_{\mathrm{stat.}}$	0.2626	0.0593	0.1362	0.1227	0.1164	0.1312	0.1383
π reweighting	0.0053	0.0034	0.0004	0.0002	0.0052	0.0003	0.0001
K reweighting	0.0013	0.0006	0.0000	0.0019	0.0005	0.0000	0.0000
$p_{\mathrm{T}}(B^0)$ reweighting	0.0000	0.0011	0.0001	0.0009	0.0010	0.0001	0.0000
$\chi^2_{\mathrm{Vtx.}}$ reweighting	0.0002	0.0000	0.0000	0.0002	0.0004	0.0000	0.0000
N_{tracks} reweighting	0.0001	0.0004	0.0000	0.0010	0.0002	0.0000	0.0000
higher order acc.	0.0048	0.0003	0.0056	0.0018	0.0063	0.0018	0.0027
$\epsilon(q^2)$	0.0009	0.0009	0.0001	0.0011	0.0015	0.0002	0.0002
peaking bkg.	0.0132	0.0094	0.0083	0.0074	0.0155	0.0108	0.0045
angular bkg. model	0.0164	0.0001	0.0061	0.0022	0.0058	0.0006	0.0003
sig. mass	0.0029	0.0031	0.0004	0.0010	0.0041	0.0006	0.0000
$m_{K\pi}$ isobar	0.0002	0.0004	0.0000	0.0004	0.0010	0.0001	0.0000
$m_{K\pi}$ bkg.	0.0029	0.0048	0.0002	0.0050	0.0121	0.0007	0.0004
$m_{K\pi}$ eff.	0.0061	0.0046	0.0056	0.0006	0.0083	0.0022	0.0037
acc. stat.	0.0073	0.0011	0.0001	0.0025	0.0038	0.0002	0.0001
$\mathcal{A}_{\mathrm{det}}$	0.0033	0.0006	0.0028	0.0008	0.0028	0.0008	0.0009
$\mathcal{A}_{\mathrm{prod}}$	0.0004	0.0001	0.0003	0.0001	0.0003	0.0001	0.0001
$\sigma_{\mathrm{syst.}}$	0.0248	0.0126	0.0133	0.0101	0.0244	0.0113	0.0065

	$11.0 < q^2 < 12.5\,\mathrm{GeV}^2/c^4$						
σ	P_1	P_2	P_3	P_4	P_5	P_6	P_8
$\sigma_{\mathrm{stat.}}$	0.2808	0.0384	0.1152	0.1271	0.1162	0.1385	0.1285
π reweighting	0.0012	0.0012	0.0000	0.0021	0.0005	0.0000	0.0000
K reweighting	0.0007	0.0001	0.0000	0.0003	0.0001	0.0000	0.0000
$p_{\mathrm{T}}(B^0)$ reweighting	0.0000	0.0005	0.0000	0.0003	0.0005	0.0000	0.0000
$\chi^2_{\mathrm{Vtx.}}$ reweighting	0.0003	0.0001	0.0000	0.0003	0.0004	0.0000	0.0000
N_{tracks} reweighting	0.0025	0.0001	0.0000	0.0005	0.0009	0.0000	0.0000
higher order acc.	0.0005	0.0005	0.0013	0.0001	0.0047	0.0028	0.0047
$\epsilon(q^2)$	0.0035	0.0000	0.0001	0.0013	0.0015	0.0002	0.0002
peaking bkg.	0.0082	0.0014	0.0075	0.0127	0.0091	0.0055	0.0016
angular bkg. model	0.0040	0.0032	0.0058	0.0030	0.0049	0.0004	0.0005
sig. mass	0.0049	0.0013	0.0000	0.0007	0.0039	0.0001	0.0002
$m_{K\pi}$ isobar	0.0005	0.0003	0.0000	0.0005	0.0011	0.0000	0.0000
$m_{K\pi}$ bkg.	0.0033	0.0022	0.0001	0.0036	0.0077	0.0000	0.0000
$m_{K\pi}$ eff.	0.0051	0.0018	0.0026	0.0013	0.0028	0.0025	0.0008
acc. stat.	0.0057	0.0005	0.0000	0.0024	0.0038	0.0000	0.0000
$\mathcal{A}_{\mathrm{det}}$	0.0059	0.0003	0.0013	0.0023	0.0006	0.0002	0.0003
$\mathcal{A}_{\mathrm{prod}}$	0.0006	0.0000	0.0001	0.0002	0.0001	0.0000	0.0000
$\sigma_{\mathrm{syst.}}$	0.0152	0.0049	0.0100	0.0143	0.0151	0.0067	0.0050

Table 75: Summary of systematic uncertainties for the $P_i^{(\prime)}$ in the q^2 bins $15.0 < q^2 < 17.0\,\mathrm{GeV}^2/c^4$ and $17.0 < q^2 < 19.0\,\mathrm{GeV}^2/c^4$.

			$15.0 < q^2 < 17.0\,\mathrm{GeV}^2/c^4$				
σ	P_1	P_2	P_3	P_4	P_5	P_6	P_8
$\sigma_{\mathrm{stat.}}$	0.1196	0.0316	0.0768	0.0994	0.1012	0.1149	0.1158
π reweighting	0.0023	0.0008	0.0000	0.0010	0.0010	0.0000	0.0000
K reweighting	0.0013	0.0000	0.0000	0.0002	0.0003	0.0000	0.0000
$p_{\mathrm{T}}(B^0)$ reweighting	0.0018	0.0004	0.0000	0.0011	0.0005	0.0000	0.0000
$\chi^2_{\mathrm{Vtx.}}$ reweighting	0.0000	0.0002	0.0000	0.0001	0.0003	0.0000	0.0000
N_{tracks} reweighting	0.0003	0.0001	0.0000	0.0001	0.0003	0.0000	0.0000
higher order acc.	0.0028	0.0008	0.0036	0.0013	0.0037	0.0034	0.0038
$\epsilon(q^2)$	0.0078	0.0008	0.0000	0.0046	0.0029	0.0002	0.0001
peaking bkg.	0.0031	0.0042	0.0039	0.0123	0.0128	0.0042	0.0018
angular bkg. model	0.0004	0.0005	0.0011	0.0033	0.0021	0.0000	0.0000
sig. mass	0.0113	0.0015	0.0005	0.0012	0.0044	0.0000	0.0002
$m_{K\pi}$ isobar	0.0020	0.0006	0.0000	0.0014	0.0022	0.0000	0.0000
$m_{K\pi}$ bkg.	0.0049	0.0015	0.0000	0.0036	0.0055	0.0000	0.0000
$m_{K\pi}$ eff.	0.0018	0.0016	0.0016	0.0056	0.0035	0.0025	0.0027
acc. stat.	0.0091	0.0010	0.0000	0.0043	0.0063	0.0000	0.0000
$\mathcal{A}_{\mathrm{det}}$	0.0012	0.0008	0.0017	0.0018	0.0019	0.0026	0.0012
$\mathcal{A}_{\mathrm{prod}}$	0.0001	0.0001	0.0002	0.0002	0.0002	0.0003	0.0001
$\sigma_{\mathrm{syst.}}$	0.0182	0.0054	0.0059	0.0160	0.0174	0.0065	0.0051

			$17.0 < q^2 < 19.0\,\mathrm{GeV}^2/c^4$				
σ	P_1	P_2	P_3	P_4	P_5	P_6	P_8
$\sigma_{\mathrm{stat.}}$	0.2002	0.0436	0.0890	0.1148	0.1127	0.1424	0.1371
π reweighting	0.0038	0.0007	0.0000	0.0011	0.0014	0.0000	0.0000
K reweighting	0.0016	0.0002	0.0000	0.0002	0.0004	0.0000	0.0000
$p_{\mathrm{T}}(B^0)$ reweighting	0.0040	0.0002	0.0000	0.0024	0.0005	0.0000	0.0000
$\chi^2_{\mathrm{Vtx.}}$ reweighting	0.0007	0.0005	0.0000	0.0002	0.0001	0.0000	0.0000
N_{tracks} reweighting	0.0019	0.0008	0.0000	0.0011	0.0009	0.0000	0.0000
higher order acc.	0.0012	0.0014	0.0022	0.0039	0.0031	0.0238	0.0058
$\epsilon(q^2)$	0.0079	0.0056	0.0001	0.0016	0.0016	0.0002	0.0002
peaking bkg.	0.0104	0.0016	0.0063	0.0094	0.0084	0.0081	0.0036
angular bkg. model	0.0162	0.0004	0.0028	0.0003	0.0001	0.0001	0.0003
sig. mass	0.0193	0.0020	0.0002	0.0036	0.0054	0.0003	0.0001
$m_{K\pi}$ isobar	0.0095	0.0019	0.0000	0.0055	0.0059	0.0001	0.0000
$m_{K\pi}$ bkg.	0.0070	0.0014	0.0000	0.0041	0.0044	0.0000	0.0000
$m_{K\pi}$ eff.	0.0031	0.0007	0.0031	0.0039	0.0043	0.0006	0.0058
acc. stat.	0.0195	0.0025	0.0000	0.0080	0.0097	0.0001	0.0001
$\mathcal{A}_{\mathrm{det}}$	0.0021	0.0012	0.0008	0.0018	0.0002	0.0012	0.0006
$\mathcal{A}_{\mathrm{prod}}$	0.0002	0.0001	0.0001	0.0002	0.0000	0.0001	0.0001
$\sigma_{\mathrm{syst.}}$	0.0371	0.0074	0.0079	0.0161	0.0168	0.0252	0.0090

Table 76: Summary of systematic uncertainties for the CP asymmetries A_i in the q^2 bins $1.1 < q^2 < 6.0\,\mathrm{GeV}^2/c^4$ and $15.0 < q^2 < 19.0\,\mathrm{GeV}^2/c^4$.

$1.1 < q^2 < 6.0\,\mathrm{GeV}^2/c^4$							
σ	A_3	A_4	A_5	A_6	A_7	A_8	A_9
$\sigma_{\mathrm{stat.}}$	0.0375	0.0497	0.0457	0.0294	0.0460	0.0500	0.0405
π reweighting	0.0004	0.0001	0.0011	0.0031	0.0002	0.0001	0.0001
K reweighting	0.0000	0.0013	0.0000	0.0001	0.0000	0.0000	0.0000
$p_{\mathrm{T}}(B^0)$ reweighting	0.0000	0.0002	0.0001	0.0007	0.0000	0.0000	0.0000
$\chi^2_{\mathrm{Vtx.}}$ reweighting	0.0001	0.0003	0.0003	0.0000	0.0000	0.0000	0.0000
N_{tracks} reweighting	0.0002	0.0011	0.0003	0.0005	0.0000	0.0000	0.0000
higher order acc.	0.0000	0.0006	0.0001	0.0001	0.0014	0.0011	0.0007
$\epsilon(q^2)$	0.0000	0.0000	0.0000	0.0000	0.0000	0.0000	0.0000
peaking bkg.	0.0032	0.0012	0.0041	0.0078	0.0055	0.0066	0.0037
angular bkg. model	0.0010	0.0017	0.0005	0.0018	0.0002	0.0001	0.0004
sig. mass	0.0001	0.0003	0.0005	0.0001	0.0003	0.0002	0.0001
$m_{K\pi}$ isobar	0.0000	0.0001	0.0002	0.0000	0.0000	0.0000	0.0000
$m_{K\pi}$ bkg.	0.0001	0.0013	0.0026	0.0006	0.0006	0.0001	0.0000
$m_{K\pi}$ eff.	0.0017	0.0027	0.0002	0.0023	0.0007	0.0041	0.0021
acc. stat.	0.0011	0.0016	0.0018	0.0010	0.0001	0.0001	0.0000
$\mathcal{A}_{\mathrm{det}}$	0.0001	0.0016	0.0002	0.0011	0.0008	0.0003	0.0007
$\mathcal{A}_{\mathrm{prod}}$	0.0000	0.0002	0.0000	0.0001	0.0001	0.0000	0.0001
$\sigma_{\mathrm{syst.}}$	0.0039	0.0047	0.0054	0.0090	0.0058	0.0078	0.0044

$15.0 < q^2 < 19.0\,\mathrm{GeV}^2/c^4$							
σ	A_3	A_4	A_5	A_6	A_7	A_8	A_9
$\sigma_{\mathrm{stat.}}$	0.0335	0.0364	0.0349	0.0279	0.0414	0.0425	0.0402
π reweighting	0.0021	0.0009	0.0015	0.0023	0.0000	0.0000	0.0000
K reweighting	0.0004	0.0000	0.0001	0.0004	0.0000	0.0000	0.0000
$p_{\mathrm{T}}(B^0)$ reweighting	0.0002	0.0003	0.0004	0.0019	0.0000	0.0000	0.0000
$\chi^2_{\mathrm{Vtx.}}$ reweighting	0.0004	0.0003	0.0003	0.0004	0.0000	0.0000	0.0000
N_{tracks} reweighting	0.0002	0.0003	0.0002	0.0007	0.0000	0.0000	0.0000
higher order acc.	0.0010	0.0002	0.0002	0.0006	0.0050	0.0003	0.0002
$\epsilon(q^2)$	0.0000	0.0000	0.0000	0.0000	0.0000	0.0000	0.0000
peaking bkg.	0.0050	0.0037	0.0032	0.0074	0.0025	0.0014	0.0012
angular bkg. model	0.0008	0.0015	0.0010	0.0000	0.0001	0.0000	0.0007
sig. mass	0.0037	0.0005	0.0019	0.0036	0.0000	0.0000	0.0001
$m_{K\pi}$ isobar	0.0011	0.0009	0.0013	0.0015	0.0000	0.0000	0.0000
$m_{K\pi}$ bkg.	0.0042	0.0035	0.0048	0.0056	0.0000	0.0000	0.0000
$m_{K\pi}$ eff.	0.0034	0.0036	0.0060	0.0047	0.0031	0.0026	0.0008
acc. stat.	0.0039	0.0023	0.0031	0.0030	0.0001	0.0001	0.0000
$\mathcal{A}_{\mathrm{det}}$	0.0020	0.0034	0.0039	0.0057	0.0006	0.0003	0.0006
$\mathcal{A}_{\mathrm{prod}}$	0.0002	0.0003	0.0004	0.0006	0.0001	0.0000	0.0001
$\sigma_{\mathrm{syst.}}$	0.0097	0.0078	0.0102	0.0132	0.0065	0.0030	0.0018

Table 77: Summary of systematic uncertainties for the CP asymmetries A_i in the q^2 bins $0.1 < q^2 < 0.98\,\mathrm{GeV}^2/c^4$ and $1.1 < q^2 < 2.5\,\mathrm{GeV}^2/c^4$.

	$0.1 < q^2 < 0.98\,\mathrm{GeV}^2/c^4$						
σ	A_3	A_4	A_5	A_6	A_7	A_8	A_9
$\sigma_{\mathrm{stat.}}$	0.0608	0.0658	0.0569	0.0563	0.0580	0.0738	0.0576
π reweighting	0.0010	0.0005	0.0030	0.0005	0.0003	0.0000	0.0001
K reweighting	0.0010	0.0003	0.0010	0.0011	0.0002	0.0001	0.0001
$p_{\mathrm{T}}(B^0)$ reweighting	0.0002	0.0003	0.0004	0.0004	0.0000	0.0001	0.0000
$\chi^2_{\mathrm{Vtx.}}$ reweighting	0.0001	0.0019	0.0004	0.0025	0.0002	0.0000	0.0001
N_{tracks} reweighting	0.0000	0.0005	0.0003	0.0029	0.0001	0.0002	0.0000
higher order acc.	0.0007	0.0042	0.0162	0.0005	0.0036	0.0003	0.0017
$\epsilon(q^2)$	0.0014	0.0037	0.0014	0.0037	0.0001	0.0003	0.0000
peaking bkg.	0.0023	0.0039	0.0040	0.0082	0.0038	0.0066	0.0030
angular bkg. model	0.0010	0.0007	0.0002	0.0001	0.0001	0.0000	0.0006
sig. mass	0.0001	0.0000	0.0008	0.0007	0.0000	0.0000	0.0000
$m_{K\pi}$ isobar	0.0000	0.0001	0.0004	0.0002	0.0000	0.0000	0.0000
$m_{K\pi}$ bkg.	0.0000	0.0003	0.0009	0.0004	0.0001	0.0000	0.0000
$m_{K\pi}$ eff.	0.0008	0.0025	0.0011	0.0007	0.0019	0.0033	0.0009
acc. stat.	0.0038	0.0040	0.0045	0.0051	0.0003	0.0001	0.0000
$\mathcal{A}_{\mathrm{det}}$	0.0004	0.0008	0.0018	0.0000	0.0002	0.0008	0.0009
$\mathcal{A}_{\mathrm{prod}}$	0.0000	0.0001	0.0002	0.0000	0.0000	0.0001	0.0001
$\sigma_{\mathrm{syst.}}$	0.0051	0.0086	0.0178	0.0112	0.0056	0.0074	0.0037

	$1.1 < q^2 < 2.5\,\mathrm{GeV}^2/c^4$						
σ	A_3	A_4	A_5	A_6	A_7	A_8	A_9
$\sigma_{\mathrm{stat.}}$	0.0744	0.0939	0.0872	0.0596	0.0883	0.0977	0.0741
π reweighting	0.0002	0.0017	0.0006	0.0103	0.0001	0.0001	0.0001
K reweighting	0.0002	0.0006	0.0004	0.0005	0.0000	0.0000	0.0000
$p_{\mathrm{T}}(B^0)$ reweighting	0.0000	0.0002	0.0005	0.0018	0.0000	0.0000	0.0000
$\chi^2_{\mathrm{Vtx.}}$ reweighting	0.0001	0.0001	0.0006	0.0004	0.0000	0.0000	0.0000
N_{tracks} reweighting	0.0002	0.0010	0.0003	0.0001	0.0000	0.0000	0.0000
higher order acc.	0.0015	0.0007	0.0065	0.0027	0.0030	0.0030	0.0013
$\epsilon(q^2)$	0.0005	0.0029	0.0005	0.0057	0.0001	0.0001	0.0000
peaking bkg.	0.0029	0.0012	0.0040	0.0100	0.0011	0.0034	0.0042
angular bkg. model	0.0031	0.0004	0.0010	0.0011	0.0005	0.0004	0.0013
sig. mass	0.0001	0.0001	0.0006	0.0014	0.0005	0.0001	0.0001
$m_{K\pi}$ isobar	0.0000	0.0000	0.0002	0.0002	0.0001	0.0000	0.0000
$m_{K\pi}$ bkg.	0.0000	0.0002	0.0011	0.0012	0.0003	0.0001	0.0000
$m_{K\pi}$ eff.	0.0006	0.0003	0.0029	0.0008	0.0009	0.0008	0.0003
acc. stat.	0.0015	0.0025	0.0026	0.0017	0.0002	0.0001	0.0001
$\mathcal{A}_{\mathrm{det}}$	0.0008	0.0008	0.0014	0.0027	0.0023	0.0010	0.0013
$\mathcal{A}_{\mathrm{prod}}$	0.0001	0.0001	0.0002	0.0003	0.0003	0.0001	0.0001
$\sigma_{\mathrm{syst.}}$	0.0049	0.0046	0.0089	0.0163	0.0042	0.0048	0.0048

Table 78: Summary of systematic uncertainties for the CP asymmetries A_i in the q^2 bins $2.5 < q^2 < 4.0\,\mathrm{GeV}^2/c^4$ and $4.0 < q^2 < 6.0\,\mathrm{GeV}^2/c^4$.

			$2.5 < q^2 < 4.0\,\mathrm{GeV}^2/c^4$				
σ	A_3	A_4	A_5	A_6	A_7	A_8	A_9
$\sigma_{\mathrm{stat.}}$	0.0694	0.1162	0.0952	0.0661	0.1017	0.1124	0.0847
π reweighting	0.0005	0.0007	0.0017	0.0057	0.0003	0.0002	0.0002
K reweighting	0.0001	0.0010	0.0000	0.0001	0.0000	0.0000	0.0000
$p_{\mathrm{T}}(B^0)$ reweighting	0.0001	0.0005	0.0001	0.0013	0.0001	0.0001	0.0000
$\chi^2_{\mathrm{Vtx.}}$ reweighting	0.0001	0.0003	0.0004	0.0001	0.0000	0.0000	0.0000
N_{tracks} reweighting	0.0002	0.0010	0.0001	0.0006	0.0000	0.0000	0.0000
higher order acc.	0.0003	0.0017	0.0025	0.0000	0.0005	0.0009	0.0012
$\epsilon(q^2)$	0.0002	0.0002	0.0019	0.0045	0.0002	0.0002	0.0001
peaking bkg.	0.0048	0.0052	0.0051	0.0044	0.0050	0.0048	0.0060
angular bkg. model	0.0024	0.0003	0.0010	0.0019	0.0002	0.0002	0.0019
sig. mass	0.0003	0.0003	0.0007	0.0003	0.0001	0.0000	0.0002
$m_{K\pi}$ isobar	0.0000	0.0001	0.0002	0.0001	0.0000	0.0000	0.0000
$m_{K\pi}$ bkg.	0.0002	0.0011	0.0024	0.0008	0.0005	0.0001	0.0001
$m_{K\pi}$ eff.	0.0034	0.0023	0.0025	0.0042	0.0020	0.0033	0.0025
acc. stat.	0.0012	0.0018	0.0022	0.0012	0.0001	0.0001	0.0000
$\mathcal{A}_{\mathrm{det}}$	0.0004	0.0025	0.0002	0.0017	0.0007	0.0003	0.0010
$\mathcal{A}_{\mathrm{prod}}$	0.0000	0.0003	0.0000	0.0002	0.0001	0.0000	0.0001
$\sigma_{\mathrm{syst.}}$	0.0065	0.0070	0.0076	0.0100	0.0055	0.0059	0.0070

			$4.0 < q^2 < 6.0\,\mathrm{GeV}^2/c^4$				
σ	A_3	A_4	A_5	A_6	A_7	A_8	A_9
$\sigma_{\mathrm{stat.}}$	0.0646	0.0802	0.0747	0.0493	0.0785	0.0878	0.0674
π reweighting	0.0011	0.0021	0.0020	0.0027	0.0002	0.0002	0.0002
K reweighting	0.0001	0.0010	0.0004	0.0002	0.0000	0.0000	0.0000
$p_{\mathrm{T}}(B^0)$ reweighting	0.0001	0.0004	0.0005	0.0006	0.0000	0.0000	0.0000
$\chi^2_{\mathrm{Vtx.}}$ reweighting	0.0001	0.0002	0.0000	0.0002	0.0000	0.0000	0.0000
N_{tracks} reweighting	0.0000	0.0008	0.0001	0.0008	0.0000	0.0000	0.0000
higher order acc.	0.0003	0.0015	0.0020	0.0015	0.0001	0.0006	0.0008
$\epsilon(q^2)$	0.0005	0.0009	0.0020	0.0017	0.0002	0.0000	0.0001
peaking bkg.	0.0050	0.0069	0.0085	0.0017	0.0037	0.0032	0.0014
angular bkg. model	0.0022	0.0010	0.0010	0.0006	0.0002	0.0002	0.0033
sig. mass	0.0004	0.0004	0.0013	0.0009	0.0001	0.0001	0.0004
$m_{K\pi}$ isobar	0.0000	0.0001	0.0004	0.0001	0.0000	0.0000	0.0000
$m_{K\pi}$ bkg.	0.0003	0.0020	0.0047	0.0008	0.0004	0.0001	0.0000
$m_{K\pi}$ eff.	0.0028	0.0002	0.0012	0.0015	0.0023	0.0031	0.0016
acc. stat.	0.0012	0.0015	0.0018	0.0011	0.0001	0.0000	0.0000
$\mathcal{A}_{\mathrm{det}}$	0.0004	0.0023	0.0015	0.0003	0.0002	0.0018	0.0003
$\mathcal{A}_{\mathrm{prod}}$	0.0000	0.0003	0.0002	0.0000	0.0000	0.0002	0.0000
$\sigma_{\mathrm{syst.}}$	0.0064	0.0083	0.0108	0.0047	0.0044	0.0048	0.0041

Table 79: Summary of systematic uncertainties for the CP asymmetries A_i in the q^2 bins $6.0 < q^2 < 8.0\,\mathrm{GeV}^2/c^4$ and $11.0 < q^2 < 12.5\,\mathrm{GeV}^2/c^4$.

$6.0 < q^2 < 8.0\,\mathrm{GeV}^2/c^4$							
σ	A_3	A_4	A_5	A_6	A_7	A_8	A_9
$\sigma_{\mathrm{stat.}}$	0.0551	0.0606	0.0574	0.0390	0.0647	0.0682	0.0571
π reweighting	0.0014	0.0020	0.0010	0.0077	0.0001	0.0001	0.0001
K reweighting	0.0002	0.0008	0.0004	0.0002	0.0000	0.0000	0.0000
$p_{\mathrm{T}}(B^0)$ reweighting	0.0001	0.0001	0.0005	0.0022	0.0000	0.0000	0.0000
$\chi^2_{\mathrm{Vtx.}}$ reweighting	0.0000	0.0001	0.0001	0.0003	0.0000	0.0000	0.0000
N_{tracks} reweighting	0.0001	0.0006	0.0001	0.0008	0.0000	0.0000	0.0000
higher order acc.	0.0010	0.0014	0.0021	0.0028	0.0009	0.0013	0.0020
$\epsilon(q^2)$	0.0003	0.0001	0.0004	0.0027	0.0001	0.0001	0.0001
peaking bkg.	0.0100	0.0097	0.0082	0.0053	0.0009	0.0057	0.0016
angular bkg. model	0.0039	0.0016	0.0034	0.0010	0.0003	0.0001	0.0018
sig. mass	0.0006	0.0006	0.0019	0.0015	0.0002	0.0002	0.0002
$m_{K\pi}$ isobar	0.0000	0.0002	0.0004	0.0002	0.0000	0.0000	0.0000
$m_{K\pi}$ bkg.	0.0005	0.0019	0.0047	0.0018	0.0003	0.0001	0.0000
$m_{K\pi}$ eff.	0.0016	0.0030	0.0054	0.0025	0.0023	0.0018	0.0034
acc. stat.	0.0013	0.0012	0.0018	0.0012	0.0001	0.0000	0.0000
$\mathcal{A}_{\mathrm{det}}$	0.0005	0.0032	0.0027	0.0022	0.0005	0.0009	0.0003
$\mathcal{A}_{\mathrm{prod}}$	0.0001	0.0004	0.0003	0.0002	0.0001	0.0001	0.0000
$\sigma_{\mathrm{syst.}}$	0.0111	0.0113	0.0123	0.0113	0.0027	0.0062	0.0047

$11.0 < q^2 < 12.5\,\mathrm{GeV}^2/c^4$							
σ	A_3	A_4	A_5	A_6	A_7	A_8	A_9
$\sigma_{\mathrm{stat.}}$	0.0434	0.0676	0.0613	0.0363	0.0689	0.0636	0.0581
π reweighting	0.0015	0.0002	0.0016	0.0088	0.0000	0.0000	0.0000
K reweighting	0.0001	0.0002	0.0002	0.0010	0.0000	0.0000	0.0000
$p_{\mathrm{T}}(B^0)$ reweighting	0.0005	0.0006	0.0009	0.0038	0.0000	0.0000	0.0000
$\chi^2_{\mathrm{Vtx.}}$ reweighting	0.0000	0.0001	0.0001	0.0009	0.0000	0.0000	0.0000
N_{tracks} reweighting	0.0007	0.0003	0.0005	0.0002	0.0000	0.0000	0.0000
higher order acc.	0.0005	0.0003	0.0028	0.0024	0.0014	0.0023	0.0008
$\epsilon(q^2)$	0.0009	0.0005	0.0005	0.0012	0.0001	0.0002	0.0000
peaking bkg.	0.0031	0.0080	0.0058	0.0030	0.0047	0.0042	0.0051
angular bkg. model	0.0011	0.0014	0.0024	0.0028	0.0003	0.0002	0.0034
sig. mass	0.0014	0.0005	0.0019	0.0025	0.0000	0.0000	0.0000
$m_{K\pi}$ isobar	0.0001	0.0002	0.0005	0.0004	0.0000	0.0000	0.0000
$m_{K\pi}$ bkg.	0.0012	0.0021	0.0044	0.0037	0.0000	0.0000	0.0000
$m_{K\pi}$ eff.	0.0013	0.0013	0.0023	0.0007	0.0017	0.0020	0.0019
acc. stat.	0.0017	0.0012	0.0019	0.0016	0.0000	0.0000	0.0000
$\mathcal{A}_{\mathrm{det}}$	0.0021	0.0032	0.0037	0.0048	0.0016	0.0001	0.0000
$\mathcal{A}_{\mathrm{prod}}$	0.0002	0.0003	0.0004	0.0005	0.0002	0.0000	0.0000
$\sigma_{\mathrm{syst.}}$	0.0052	0.0092	0.0099	0.0128	0.0055	0.0052	0.0065

Table 80: Summary of systematic uncertainties for the CP asymmetries A_i in the q^2 bins $15.0 < q^2 < 17.0\,\mathrm{GeV}^2/c^4$ and $17.0 < q^2 < 19.0\,\mathrm{GeV}^2/c^4$.

$15.0 < q^2 < 17.0\,\mathrm{GeV}^2/c^4$							
σ	A_3	A_4	A_5	A_6	A_7	A_8	A_9
$\sigma_{\mathrm{stat.}}$	0.0402	0.0475	0.0469	0.0351	0.0547	0.0552	0.0501
π reweighting	0.0020	0.0006	0.0018	0.0042	0.0000	0.0000	0.0000
K reweighting	0.0002	0.0000	0.0000	0.0007	0.0000	0.0000	0.0000
$p_{\mathrm{T}}(B^0)$ reweighting	0.0001	0.0001	0.0005	0.0023	0.0000	0.0000	0.0000
$\chi^2_{\mathrm{Vtx.}}$ reweighting	0.0002	0.0003	0.0004	0.0006	0.0000	0.0000	0.0000
N_{tracks} reweighting	0.0001	0.0002	0.0004	0.0007	0.0000	0.0000	0.0000
higher order acc.	0.0013	0.0009	0.0022	0.0005	0.0016	0.0018	0.0024
$\epsilon(q^2)$	0.0033	0.0030	0.0024	0.0019	0.0002	0.0002	0.0001
peaking bkg.	0.0018	0.0049	0.0068	0.0072	0.0050	0.0025	0.0034
angular bkg. model	0.0002	0.0012	0.0005	0.0003	0.0000	0.0000	0.0004
sig. mass	0.0039	0.0003	0.0019	0.0031	0.0000	0.0001	0.0001
$m_{K\pi}$ isobar	0.0007	0.0006	0.0010	0.0010	0.0000	0.0000	0.0000
$m_{K\pi}$ bkg.	0.0013	0.0012	0.0018	0.0020	0.0000	0.0000	0.0000
$m_{K\pi}$ eff.	0.0017	0.0009	0.0012	0.0009	0.0010	0.0010	0.0013
acc. stat.	0.0030	0.0021	0.0028	0.0026	0.0000	0.0000	0.0000
$\mathcal{A}_{\mathrm{det}}$	0.0017	0.0038	0.0037	0.0065	0.0007	0.0000	0.0002
$\mathcal{A}_{\mathrm{prod}}$	0.0002	0.0004	0.0004	0.0007	0.0001	0.0000	0.0000
$\sigma_{\mathrm{syst.}}$	0.0072	0.0076	0.0096	0.0120	0.0054	0.0032	0.0043

$17.0 < q^2 < 19.0\,\mathrm{GeV}^2/c^4$							
σ	A_3	A_4	A_5	A_6	A_7	A_8	A_9
$\sigma_{\mathrm{stat.}}$	0.0642	0.0538	0.0527	0.0445	0.0682	0.0656	0.0576
π reweighting	0.0019	0.0010	0.0011	0.0006	0.0000	0.0000	0.0000
K reweighting	0.0006	0.0001	0.0002	0.0001	0.0000	0.0000	0.0000
$p_{\mathrm{T}}(B^0)$ reweighting	0.0005	0.0005	0.0003	0.0015	0.0000	0.0000	0.0000
$\chi^2_{\mathrm{Vtx.}}$ reweighting	0.0007	0.0004	0.0002	0.0002	0.0000	0.0000	0.0000
N_{tracks} reweighting	0.0001	0.0009	0.0001	0.0021	0.0000	0.0000	0.0000
higher order acc.	0.0025	0.0002	0.0031	0.0079	0.0112	0.0027	0.0015
$\epsilon(q^2)$	0.0102	0.0062	0.0044	0.0084	0.0000	0.0000	0.0000
peaking bkg.	0.0049	0.0061	0.0038	0.0098	0.0037	0.0043	0.0033
angular bkg. model	0.0059	0.0002	0.0001	0.0003	0.0001	0.0002	0.0018
sig. mass	0.0072	0.0011	0.0020	0.0045	0.0003	0.0000	0.0001
$m_{K\pi}$ isobar	0.0035	0.0024	0.0026	0.0032	0.0000	0.0000	0.0000
$m_{K\pi}$ bkg.	0.0015	0.0010	0.0011	0.0013	0.0000	0.0000	0.0000
$m_{K\pi}$ eff.	0.0015	0.0014	0.0009	0.0018	0.0056	0.0007	0.0020
acc. stat.	0.0067	0.0037	0.0046	0.0049	0.0000	0.0000	0.0000
$\mathcal{A}_{\mathrm{det}}$	0.0023	0.0032	0.0039	0.0050	0.0005	0.0002	0.0011
$\mathcal{A}_{\mathrm{prod}}$	0.0002	0.0003	0.0004	0.0005	0.0001	0.0000	0.0001
$\sigma_{\mathrm{syst.}}$	0.0171	0.0106	0.0097	0.0179	0.0131	0.0051	0.0046

10.2 Systematics for the method of moments

For the method of moments a similar strategy as the one described for the likelihood fit (Sec. 10.1.1) is used to evaluate the systematics. The same procudere is used to determine the systematic uncertainty on the observables S_i, A_i and P_i. The following sources of systematic uncertainty are evaluated for the moments:

- Statistical uncertainty of the four-dimensional acceptance
- Difference between data and simulation
- Higher order acceptance model
- Peaking backgrounds
- Signal mass modelling
- $m_{K\pi}$ invariant mass model

10.2.1 Statistical uncertainty of the four-dimensional acceptance

In order to evaluate the systematics due to the limited knowledge of the acceptance, the same procedure described in Sec. 10.1 is applied. We have generated 500 pseudo-experiments, varying the acceptance according with its statistical uncertainty and fit back with the nominal acceptance correction. The distribution of the fit results is shown in Fig 93 for the last q^2-bin, where the statistical uncertainty on the acceptance is largest.. Numerical results for all q^2 bins are summarized in Tables 81, 83 and 82.

Table 81: Systematic uncertainties due to the statistical uncertainty on the four-dimensional acceptance on the S_i observables. Ranges of q^2 bins are given in GeV^2/c^4.

q^2	F_{L}	S_3	S_4	S_5	A_{FB}	S_7	S_8	S_9	S_{6s}	S_{6c}
$0.1 < q^2 < 0.98$	0.0002	0.0004	0.0003	0.0003	0.0002	0.0003	0.0003	0.0004	0.0001	0.0
$1.1 < q^2 < 2.0$	0.0004	0.0003	0.0006	0.0007	0.0003	0.0004	0.0004	0.0002	0.0001	0.0
$2.0 < q^2 < 3.0$	0.0004	0.0004	0.0005	0.0006	0.0002	0.0005	0.0005	0.0003	0.0	0.0
$3.0 < q^2 < 4.0$	0.0003	0.0003	0.0003	0.0004	0.0002	0.0004	0.0004	0.0003	0.0001	0.0
$4.0 < q^2 < 5.0$	0.0002	0.0002	0.0003	0.0004	0.0002	0.0003	0.0002	0.0003	0.0	0.0
$5.0 < q^2 < 6.0$	0.0003	0.0002	0.0004	0.0004	0.0002	0.0003	0.0002	0.0002	0.0001	0.0
$6.0 < q^2 < 7.0$	0.0002	0.0002	0.0003	0.0003	0.0002	0.0003	0.0002	0.0002	0.0	0.0
$7.0 < q^2 < 8.0$	0.0003	0.0002	0.0003	0.0002	0.0002	0.0003	0.0002	0.0001	0.0	0.0
$11.0 < q^2 < 11.75$	0.0002	0.0001	0.0002	0.0002	0.0002	0.0001	0.0001	0.0001	0.0	0.0
$11.75 < q^2 < 12.5$	0.0002	0.0002	0.0002	0.0002	0.0003	0.0001	0.0001	0.0001	0.0001	0.0
$15.0 < q^2 < 16.0$	0.0003	0.0003	0.0004	0.0003	0.0004	0.0002	0.0002	0.0002	0.0001	0.0
$16.0 < q^2 < 17.0$	0.0003	0.0003	0.0004	0.0003	0.0004	0.0002	0.0002	0.0002	0.0001	0.0
$17.0 < q^2 < 18.0$	0.0004	0.0004	0.0004	0.0004	0.0004	0.0003	0.0002	0.0003	0.0001	0.0
$18.0 < q^2 < 19.0$	0.0011	0.0006	0.0007	0.0005	0.001	0.0005	0.0004	0.0005	0.0002	0.0001
$15.0 < q^2 < 19.0$	0.0003	0.0002	0.0003	0.0002	0.0003	0.0001	0.0001	0.0001	0.0001	0.0
$1.1 < q^2 < 2.5$	0.0003	0.0003	0.0005	0.0005	0.0002	0.0003	0.0003	0.0003	0.0001	0.0
$2.5 < q^2 < 4.0$	0.0002	0.0002	0.0003	0.0003	0.0002	0.0003	0.0004	0.0002	0.0	0.0
$4.0 < q^2 < 6.0$	0.0002	0.0002	0.0002	0.0003	0.0002	0.0002	0.0002	0.0002	0.0	0.0
$6.0 < q^2 < 8.0$	0.0002	0.0002	0.0002	0.0002	0.0001	0.0002	0.0002	0.0001	0.0	0.0
$11.0 < q^2 < 12.5$	0.0002	0.0001	0.0002	0.0002	0.0002	0.0001	0.0001	0.0001	0.0001	0.0
$15.0 < q^2 < 17.0$	0.0003	0.0002	0.0004	0.0003	0.0003	0.0001	0.0001	0.0001	0.0001	0.0
$17.0 < q^2 < 19.0$	0.0005	0.0004	0.0004	0.0003	0.0005	0.0002	0.0002	0.0002	0.0001	0.0

Table 82: Systematic uncertainties due to the statistical uncertainty on the four-dimensional acceptance on the P_i observables. Ranges of q^2 bins are given in GeV^2/c^4.

q^2	F_{L}	P_1	P_2	P_3	P_4'	P_5'	P_6'	P_8
$0.1 < q^2 < 0.98$	0.0002	0.0009	0.0002	0.0005	0.0011	0.001	0.0011	0.0009
$1.1 < q^2 < 2.0$	0.0004	0.0014	0.0005	0.0006	0.0012	0.0013	0.0007	0.0008
$2.0 < q^2 < 3.0$	0.0004	0.0028	0.0005	0.0013	0.001	0.0014	0.0011	0.001
$3.0 < q^2 < 4.0$	0.0003	0.0022	0.0006	0.0011	0.0008	0.0009	0.001	0.001
$4.0 < q^2 < 5.0$	0.0002	0.0016	0.0005	0.0008	0.0007	0.0009	0.0006	0.0005
$5.0 < q^2 < 6.0$	0.0003	0.0013	0.0005	0.0006	0.0007	0.0008	0.0006	0.0005
$6.0 < q^2 < 7.0$	0.0002	0.0008	0.0003	0.0004	0.0006	0.0006	0.0005	0.0005
$7.0 < q^2 < 8.0$	0.0003	0.001	0.0003	0.0002	0.0005	0.0005	0.0006	0.0004
$11.0 < q^2 < 11.75$	0.0002	0.0005	0.0001	0.0002	0.0004	0.0003	0.0002	0.0002
$11.75 < q^2 < 12.5$	0.0002	0.0005	0.0002	0.0002	0.0005	0.0004	0.0002	0.0002
$15.0 < q^2 < 16.0$	0.0003	0.0008	0.0003	0.0003	0.0008	0.0007	0.0005	0.0004
$16.0 < q^2 < 17.0$	0.0003	0.0009	0.0003	0.0002	0.0009	0.0007	0.0004	0.0003
$17.0 < q^2 < 18.0$	0.0004	0.0011	0.0004	0.0005	0.0008	0.0008	0.0006	0.0004
$18.0 < q^2 < 19.0$	0.0011	0.0023	0.0009	0.0007	0.0015	0.0012	0.001	0.0009
$15.0 < q^2 < 19.0$	0.0003	0.0007	0.0002	0.0002	0.0006	0.0005	0.0003	0.0002
$1.1 < q^2 < 2.5$	0.0003	0.0015	0.0004	0.0007	0.001	0.0011	0.0007	0.0007
$2.5 < q^2 < 4.0$	0.0002	0.0019	0.0005	0.0009	0.0006	0.0008	0.0008	0.0008
$4.0 < q^2 < 6.0$	0.0002	0.0011	0.0004	0.0005	0.0005	0.0006	0.0004	0.0004
$6.0 < q^2 < 8.0$	0.0002	0.0007	0.0002	0.0002	0.0004	0.0004	0.0004	0.0003
$11.0 < q^2 < 12.5$	0.0002	0.0004	0.0001	0.0001	0.0004	0.0003	0.0002	0.0001
$15.0 < q^2 < 17.0$	0.0003	0.0007	0.0002	0.0002	0.0007	0.0006	0.0003	0.0003
$17.0 < q^2 < 19.0$	0.0005	0.0012	0.0005	0.0003	0.0009	0.0007	0.0005	0.0004

10.2.2 Difference between data and simulation

The acceptance is determined as a function of the three angles $\theta_\ell, \theta_K, \phi$ and q^2. This approach relies on having a good agreement between data and Monte-Carlo for what concerns detector description and B-meson production mechanism. The control channel $B^0 \to J/\psi K^{*0}$ is used to evaluate the data/MC agreement. Known data/MC discrepancies are corrected for, as described in Ref. [13]. These discrepancies are in the following observables: the transverse momentum of the signal B^0, as well as the B^0 vertex χ^2 and the track multiplicity in the event. The effect of these corrections on the acceptance is evaluated by redetermining the acceptance correction without the reweighting. Toy studies are performed to evaluate the effect on the observables. These effects are negligibly small and are shown in Tables 90, 91, 92 for the vertex χ^2 reweight, Tab. 93, 94 and 95 for the B-meson momentum reweight. The systematic uncertainty due to the reweighting for the track multiplicity is shown in Tab. 96, 98 and **??**.

In addition, small differences in the momentum and transverse momentum of the daughter of the B-meson is observed. The distributions for data are extracted using the *sWeighting* technique. To minimize the influence of pollution from an S-wave component which is not simulated in data, the window for invariant mass of the $K^+\pi^-$ system is reduced from the nominal $\pm 100\,\mathrm{MeV}/c^2$ to $\pm 20\,\mathrm{MeV}/c^2$. From the two-dimensional

Table 83: Systematic uncertainties due to the statistical uncertainty on the four-dimensional acceptance on the A_i observables. Ranges of q^2 bins are given in GeV^2/c^4.

q^2	A_3	A_4	A_5	$A(A_{\mathrm{FB}})$	A_7	A_8	A_9	A_{6s}	A_{6c}
$0.1 < q^2 < 0.98$	0.0004	0.0003	0.0003	0.0002	0.0003	0.0003	0.0004	0.0001	0.0
$1.1 < q^2 < 2.0$	0.0003	0.0006	0.0007	0.0003	0.0004	0.0004	0.0002	0.0001	0.0
$2.0 < q^2 < 3.0$	0.0004	0.0005	0.0006	0.0002	0.0005	0.0005	0.0003	0.0	0.0
$3.0 < q^2 < 4.0$	0.0003	0.0003	0.0004	0.0002	0.0004	0.0004	0.0003	0.0001	0.0
$4.0 < q^2 < 5.0$	0.0002	0.0003	0.0004	0.0002	0.0003	0.0002	0.0003	0.0	0.0
$5.0 < q^2 < 6.0$	0.0002	0.0004	0.0004	0.0002	0.0003	0.0002	0.0002	0.0001	0.0
$6.0 < q^2 < 7.0$	0.0002	0.0003	0.0003	0.0002	0.0003	0.0002	0.0002	0.0	0.0
$7.0 < q^2 < 8.0$	0.0002	0.0003	0.0002	0.0002	0.0003	0.0002	0.0001	0.0	0.0
$11.0 < q^2 < 11.75$	0.0001	0.0002	0.0002	0.0002	0.0001	0.0001	0.0001	0.0	0.0
$11.75 < q^2 < 12.5$	0.0002	0.0002	0.0002	0.0003	0.0001	0.0001	0.0001	0.0001	0.0
$15.0 < q^2 < 16.0$	0.0003	0.0004	0.0003	0.0004	0.0002	0.0002	0.0002	0.0001	0.0
$16.0 < q^2 < 17.0$	0.0003	0.0004	0.0003	0.0004	0.0002	0.0002	0.0002	0.0001	0.0
$17.0 < q^2 < 18.0$	0.0004	0.0004	0.0004	0.0004	0.0003	0.0002	0.0003	0.0001	0.0
$18.0 < q^2 < 19.0$	0.0006	0.0007	0.0005	0.001	0.0005	0.0004	0.0005	0.0002	0.0001
$15.0 < q^2 < 19.0$	0.0002	0.0003	0.0002	0.0003	0.0001	0.0001	0.0001	0.0001	0.0
$1.1 < q^2 < 2.5$	0.0003	0.0005	0.0005	0.0002	0.0003	0.0003	0.0003	0.0001	0.0
$2.5 < q^2 < 4.0$	0.0002	0.0003	0.0003	0.0002	0.0003	0.0004	0.0002	0.0	0.0
$4.0 < q^2 < 6.0$	0.0002	0.0002	0.0003	0.0002	0.0002	0.0002	0.0002	0.0	0.0
$6.0 < q^2 < 8.0$	0.0002	0.0002	0.0002	0.0001	0.0002	0.0002	0.0001	0.0	0.0
$11.0 < q^2 < 12.5$	0.0001	0.0002	0.0002	0.0002	0.0001	0.0001	0.0001	0.0001	0.0
$15.0 < q^2 < 17.0$	0.0002	0.0004	0.0003	0.0003	0.0001	0.0001	0.0001	0.0001	0.0
$17.0 < q^2 < 19.0$	0.0004	0.0004	0.0003	0.0005	0.0002	0.0002	0.0002	0.0001	0.0

distributions of K^+ and π^- in data and simulation a correction factor is determined. This correction factor, depending on the particles momentum and transverse momentum is given in shown in Fig. 87. The systematic uncertainty from the modeling of the signal decay is then evaluated using toy studies where the acceptance is redetermined using the reweightings. The systematics uncertainty for the pion and kaon momentum reweighting are shown in Tables 84, 85, 86, 87, 88 and 89.

10.2.3 Higher order acceptance model

As discussed in Sec. 10.1.4, the systematic uncertainty due to the maximum order of the Legendre polynomials used to model the four-dimensional acceptance are studied by including higer order polynomials for the description of $\cos\theta_K$ and q^2, choosing a maximal order of seven for both. High statistics toys are performed, where events are generated using the higher order acceptance model and fit with the nominal one. Since a high order acceptance is used to weight than to reject events, we find in the toys a small numbers of events with very high weight. Event with large weight are instead not present in the dataset. We therefore remove these few events with large weights and they are not considered in the toys. The bias obtained when the low order acceptance is used to generate and the high order acceptance is used to weight, is assigned as systematics. The resulting deviations are given in Tab. 99 - 101, they are negligible for all bins.

Figure 93: Distributions of deviations of observables from toy experiment for the first q^2 bin in the last q^2 bin. Events are generated with an acceptance varied according to its statistical uncertainty and fit back using the nominal acceptance.

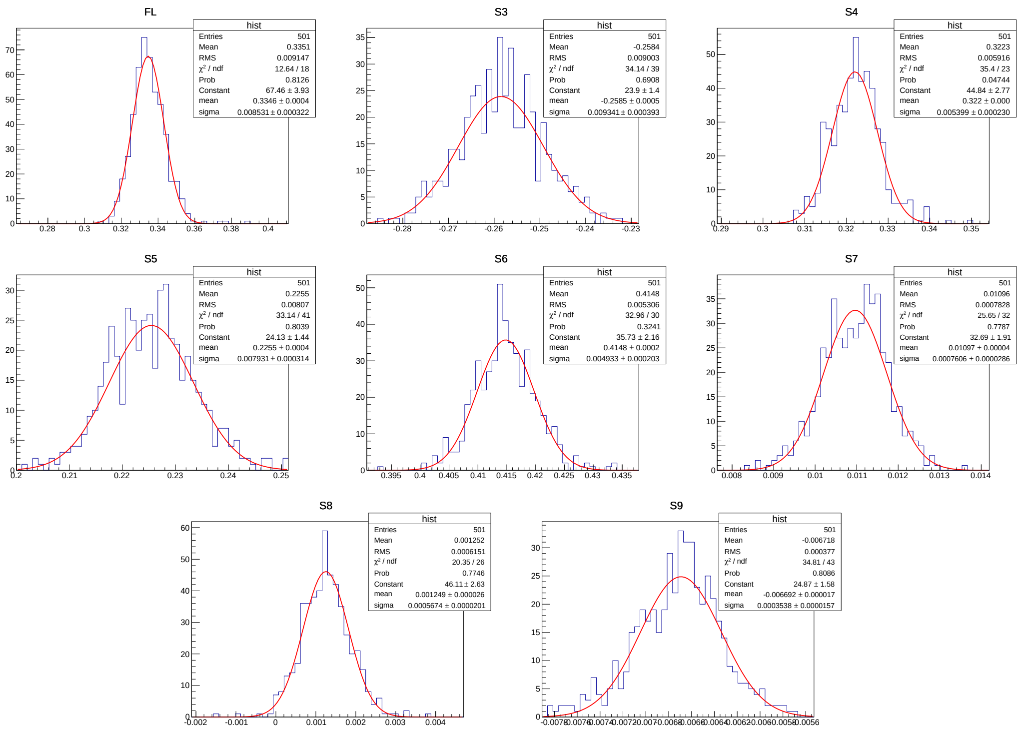

Table 84: Systematic uncertainties from reweighting depending on kaon p and p_{T} on the S_i observables. Ranges of q^2 bins are given in GeV^2/c^4.

q^2	F_{L}	S_3	S_4	S_5	A_{FB}	S_7	S_8	S_9	S_{6s}	S_{6c}
$0.1 < q^2 < 0.98$	0.0006	0.0012	0.0033	0.0003	0.0112	0.0008	0.0017	0.0002	0.0025	0.0008
$1.1 < q^2 < 2.0$	0.003	0.0002	0.0117	0.0019	0.002	0.0001	0.0001	0.0001	0.0006	0.0003
$2.0 < q^2 < 3.0$	0.0027	0.0001	0.0182	0.0012	0.0011	0.0001	0.0002	0.0001	0.0004	0.0003
$3.0 < q^2 < 4.0$	0.0029	0.0009	0.02	0.0007	0.0001	0.0001	0.0001	0.0001	0.0001	0.0001
$4.0 < q^2 < 5.0$	0.0028	0.0014	0.0205	0.0003	0.001	0.0001	0.0002	0.0001	0.0003	0.0002
$5.0 < q^2 < 6.0$	0.0026	0.0018	0.0211	0.0004	0.0018	0.0001	0.0002	0.0001	0.0005	0.0003
$6.0 < q^2 < 7.0$	0.0026	0.0021	0.0229	0.0011	0.0028	0.0001	0.0002	0.0001	0.0008	0.0004
$7.0 < q^2 < 8.0$	0.0027	0.0023	0.0259	0.0019	0.0038	0.0001	0.0002	0.0001	0.001	0.0005
$11.0 < q^2 < 11.75$	0.0034	0.0035	0.0279	0.0055	0.0057	0.0001	0.0001	0.0001	0.0013	0.0004
$11.75 < q^2 < 12.5$	0.0036	0.0036	0.025	0.0053	0.0053	0.0001	0.0001	0.0001	0.0012	0.0004
$15.0 < q^2 < 16.0$	0.0034	0.0011	0.0025	0.0003	0.0009	0.0001	0.0001	0.0001	0.0002	0.0001
$16.0 < q^2 < 17.0$	0.0032	0.0002	0.0119	0.0026	0.0005	0.0001	0.0001	0.0001	0.0001	0.0001
$17.0 < q^2 < 18.0$	0.0034	0.0011	0.0197	0.0052	0.0002	0.0001	0.0001	0.0001	0.0001	0.0001
$18.0 < q^2 < 19.0$	0.0054	0.0018	0.0256	0.0051	0.006	0.0001	0.0003	0.0002	0.0012	0.0003
$17.0 < q^2 < 19.0$	0.0042	0.0014	0.022	0.0051	0.0025	0.0001	0.0001	0.0001	0.0005	0.0001
$1.1 < q^2 < 2.5$	0.0029	0.0002	0.0134	0.0017	0.0018	0.0001	0.0001	0.0001	0.0005	0.0003
$2.5 < q^2 < 4.0$	0.0028	0.0007	0.0199	0.0008	0.0002	0.0001	0.0002	0.0001	0.0001	0.0001
$4.0 < q^2 < 6.0$	0.0027	0.0016	0.0208	0.0001	0.0015	0.0001	0.0002	0.0001	0.0004	0.0002
$6.0 < q^2 < 8.0$	0.0027	0.0022	0.0245	0.0016	0.0033	0.0001	0.0002	0.0001	0.0009	0.0005
$11.0 < q^2 < 12.5$	0.0035	0.0036	0.0264	0.0054	0.0055	0.0001	0.0001	0.0001	0.0012	0.0004
$15.0 < q^2 < 17.0$	0.0033	0.0005	0.007	0.0011	0.0003	0.0001	0.0001	0.0001	0.0001	0.0001
$17.0 < q^2 < 19.0$	0.0042	0.0014	0.022	0.0051	0.0025	0.0001	0.0001	0.0001	0.0005	0.0001

Table 85: Systematic uncertainties from reweighting depending on kaon p and p_{T} on the P_i observables. Ranges of q^2 bins are given in GeV^2/c^4.

q^2	F_{L}	P_1	P_2	P_3	P_4'	P_5'	P_6'	P_8'
$0.1 < q^2 < 0.98$	0.0006	0.003	0.0097	0.0003	0.0075	0.0012	0.0019	0.004
$1.1 < q^2 < 2.0$	0.003	0.0012	0.0005	0.0001	0.0249	0.0032	0.0001	0.0003
$2.0 < q^2 < 3.0$	0.0027	0.0013	0.0022	0.0002	0.0439	0.0033	0.0003	0.0006
$3.0 < q^2 < 4.0$	0.0029	0.0087	0.0028	0.0004	0.048	0.0044	0.0006	0.0005
$4.0 < q^2 < 5.0$	0.0028	0.0127	0.0018	0.0005	0.0466	0.0035	0.0005	0.0006
$5.0 < q^2 < 6.0$	0.0026	0.0133	0.0018	0.0005	0.0453	0.0014	0.0004	0.0004
$6.0 < q^2 < 7.0$	0.0026	0.0131	0.0028	0.0003	0.0477	0.0007	0.0004	0.0006
$7.0 < q^2 < 8.0$	0.0027	0.0126	0.0036	0.0003	0.0526	0.0028	0.0003	0.0005
$11.0 < q^2 < 11.75$	0.0034	0.0135	0.0038	0.0001	0.0571	0.0121	0.0001	0.0001
$11.75 < q^2 < 12.5$	0.0036	0.0138	0.0032	0.0001	0.0512	0.0117	0.0001	0.0002
$15.0 < q^2 < 16.0$	0.0034	0.0055	0.0015	0.0001	0.0039	0.0022	0.0001	0.0002
$16.0 < q^2 < 17.0$	0.0032	0.0017	0.0026	0.0001	0.0237	0.004	0.0001	0.0001
$17.0 < q^2 < 18.0$	0.0034	0.0004	0.0019	0.0001	0.04	0.0094	0.0001	0.0002
$18.0 < q^2 < 19.0$	0.0054	0.001	0.0036	0.0002	0.0516	0.009	0.0002	0.0006
$17.0 < q^2 < 19.0$	0.0042	0.0002	0.0003	0.0002	0.0446	0.0091	0.0002	0.0001
$1.1 < q^2 < 2.5$	0.0029	0.0011	0.0001	0.0001	0.0293	0.0031	0.0001	0.0003
$2.5 < q^2 < 4.0$	0.0028	0.0065	0.0029	0.0003	0.0479	0.0039	0.0005	0.0006
$4.0 < q^2 < 6.0$	0.0027	0.0131	0.0018	0.0005	0.0458	0.0023	0.0005	0.0005
$6.0 < q^2 < 8.0$	0.0027	0.0128	0.0033	0.0003	0.0502	0.0018	0.0003	0.0005
$11.0 < q^2 < 12.5$	0.0035	0.0137	0.0035	0.0001	0.0542	0.0119	0.0001	0.0001
$15.0 < q^2 < 17.0$	0.0033	0.0038	0.002	0.0001	0.0133	0.0007	0.0001	0.0001
$17.0 < q^2 < 19.0$	0.0042	0.0002	0.0003	0.0002	0.0446	0.0091	0.0002	0.0001

Table 86: Systematic uncertainties from reweighting depending on kaon p and p_{T} on the A_i observables. Ranges of q^2 bins are given in GeV^2/c^4.

q^2	A_3	A_4	A_5	$A(A_{\mathrm{FB}})$	A_7	A_8	A_9	A_{6s}	A_{6c}
$0.1 < q^2 < 0.98$	0.0012	0.0033	0.0003	0.0112	0.0008	0.0017	0.0002	0.0025	0.0008
$1.1 < q^2 < 2.0$	0.0002	0.0117	0.0019	0.002	0.0001	0.0001	0.0001	0.0006	0.0003
$2.0 < q^2 < 3.0$	0.0001	0.0182	0.0012	0.0011	0.0001	0.0002	0.0001	0.0004	0.0003
$3.0 < q^2 < 4.0$	0.0009	0.02	0.0007	0.0001	0.0001	0.0001	0.0001	0.0001	0.0001
$4.0 < q^2 < 5.0$	0.0014	0.0205	0.0003	0.001	0.0001	0.0002	0.0001	0.0003	0.0002
$5.0 < q^2 < 6.0$	0.0018	0.0211	0.0004	0.0018	0.0001	0.0002	0.0001	0.0005	0.0003
$6.0 < q^2 < 7.0$	0.0021	0.0229	0.0011	0.0028	0.0001	0.0002	0.0001	0.0008	0.0004
$7.0 < q^2 < 8.0$	0.0023	0.0259	0.0019	0.0038	0.0001	0.0002	0.0001	0.001	0.0005
$11.0 < q^2 < 11.75$	0.0035	0.0279	0.0055	0.0057	0.0001	0.0001	0.0001	0.0013	0.0004
$11.75 < q^2 < 12.5$	0.0036	0.025	0.0053	0.0053	0.0001	0.0001	0.0001	0.0012	0.0004
$15.0 < q^2 < 16.0$	0.0011	0.0025	0.0003	0.0009	0.0001	0.0001	0.0001	0.0002	0.0001
$16.0 < q^2 < 17.0$	0.0002	0.0119	0.0026	0.0005	0.0001	0.0001	0.0001	0.0001	0.0001
$17.0 < q^2 < 18.0$	0.0011	0.0197	0.0052	0.0002	0.0001	0.0001	0.0001	0.0001	0.0001
$18.0 < q^2 < 19.0$	0.0018	0.0256	0.0051	0.006	0.0001	0.0003	0.0002	0.0012	0.0003
$17.0 < q^2 < 19.0$	0.0014	0.022	0.0051	0.0025	0.0001	0.0001	0.0001	0.0005	0.0001
$1.1 < q^2 < 2.5$	0.0002	0.0134	0.0017	0.0018	0.0001	0.0001	0.0001	0.0005	0.0003
$2.5 < q^2 < 4.0$	0.0007	0.0199	0.0008	0.0002	0.0001	0.0002	0.0001	0.0001	0.0001
$4.0 < q^2 < 6.0$	0.0016	0.0208	0.0001	0.0015	0.0001	0.0002	0.0001	0.0004	0.0002
$6.0 < q^2 < 8.0$	0.0022	0.0245	0.0016	0.0033	0.0001	0.0002	0.0001	0.0009	0.0005
$11.0 < q^2 < 12.5$	0.0036	0.0264	0.0054	0.0055	0.0001	0.0001	0.0001	0.0012	0.0004
$15.0 < q^2 < 17.0$	0.0005	0.007	0.0011	0.0003	0.0001	0.0001	0.0001	0.0001	0.0001
$17.0 < q^2 < 19.0$	0.0014	0.022	0.0051	0.0025	0.0001	0.0001	0.0001	0.0005	0.0001

Table 87: Systematic uncertainties from reweighting depending on pion p and p_{T} for the S_i observables. Ranges of q^2 bins are given in GeV^2/c^4.

q^2	F_{L}	S_3	S_4	S_5	A_{FB}	S_7	S_8	S_9	S_{6s}	S_{6c}
$0.1 < q^2 < 0.98$	0.0131	0.0011	0.0008	0.0031	0.0058	0.0006	0.0033	0.0005	0.0013	0.0004
$1.1 < q^2 < 2.0$	0.0232	0.0002	0.0124	0.0029	0.0086	0.0002	0.0001	0.0001	0.002	0.0007
$2.0 < q^2 < 3.0$	0.0215	0.0003	0.0202	0.0024	0.0063	0.0004	0.0002	0.0001	0.0015	0.0006
$3.0 < q^2 < 4.0$	0.0211	0.0007	0.0225	0.0004	0.0019	0.0001	0.0001	0.0002	0.0005	0.0002
$4.0 < q^2 < 5.0$	0.0209	0.001	0.0239	0.0012	0.0023	0.0001	0.0001	0.0001	0.0006	0.0003
$5.0 < q^2 < 6.0$	0.0211	0.0009	0.024	0.0024	0.0052	0.0001	0.0001	0.0001	0.0013	0.0006
$6.0 < q^2 < 7.0$	0.0209	0.0011	0.0256	0.0026	0.0075	0.0002	0.0003	0.0003	0.0018	0.0007
$7.0 < q^2 < 8.0$	0.0203	0.0013	0.0285	0.003	0.0092	0.0004	0.0005	0.0002	0.0022	0.0009
$11.0 < q^2 < 11.75$	0.0178	0.0017	0.0285	0.0039	0.0106	0.0003	0.0001	0.0001	0.0023	0.0006
$11.75 < q^2 < 12.5$	0.017	0.0016	0.0251	0.0038	0.0099	0.0003	0.0003	0.0001	0.0021	0.0006
$15.0 < q^2 < 16.0$	0.011	0.0027	0.0043	0.0018	0.0035	0.0001	0.0001	0.0001	0.0007	0.0001
$16.0 < q^2 < 17.0$	0.0089	0.0047	0.0141	0.0047	0.0014	0.0002	0.0001	0.0001	0.0003	0.0001
$17.0 < q^2 < 18.0$	0.0071	0.006	0.0216	0.007	0.0011	0.0001	0.0001	0.0001	0.0002	0.0001
$18.0 < q^2 < 19.0$	0.0061	0.0063	0.0269	0.0062	0.0056	0.0001	0.0003	0.0003	0.0012	0.0003
$15.0 < q^2 < 19.0$	0.0086	0.0042	0.0149	0.004	0.0031	0.0001	0.0001	0.0001	0.0006	0.0001
$1.1 < q^2 < 2.5$	0.0229	0.0002	0.0144	0.0032	0.0082	0.0002	0.0001	0.0001	0.002	0.0007
$2.5 < q^2 < 4.0$	0.0211	0.0004	0.0223	0.0008	0.003	0.0003	0.0001	0.0002	0.0007	0.0003
$4.0 < q^2 < 6.0$	0.021	0.001	0.0239	0.0018	0.0038	0.0001	0.0001	0.0001	0.001	0.0004
$6.0 < q^2 < 8.0$	0.0206	0.0012	0.0271	0.0028	0.0084	0.0003	0.0004	0.0002	0.002	0.0008
$11.0 < q^2 < 12.5$	0.0174	0.0016	0.0268	0.0038	0.0102	0.0001	0.0002	0.0001	0.0022	0.0006
$15.0 < q^2 < 17.0$	0.01	0.0036	0.009	0.0031	0.0025	0.0001	0.0001	0.0001	0.0005	0.0001
$17.0 < q^2 < 19.0$	0.0067	0.006	0.0237	0.0065	0.0031	0.0001	0.0001	0.0001	0.0006	0.0001

Table 88: Systematic uncertainties from reweighting depending on pion p and p_{T} for the P_i observables. Ranges of q^2 bins are given in GeV^2/c^4.

q^2	F_{L}	P_1	P_2	P_3	P_4'	P_5'	P_6'	P_8'
$0.1 < q^2 < 0.98$	0.0131	0.003	0.0037	0.0007	0.0019	0.0026	0.0024	0.0075
$1.1 < q^2 < 2.0$	0.0232	0.0015	0.0099	0.0003	0.0282	0.0001	0.001	0.0003
$2.0 < q^2 < 3.0$	0.0215	0.0001	0.0283	0.0001	0.0464	0.0087	0.0024	0.0002
$3.0 < q^2 < 4.0$	0.0211	0.0072	0.0138	0.0012	0.0447	0.0208	0.003	0.0009
$4.0 < q^2 < 5.0$	0.0209	0.0148	0.0024	0.0014	0.0445	0.0199	0.0026	0.0014
$5.0 < q^2 < 6.0$	0.0211	0.0121	0.0081	0.0012	0.0431	0.0136	0.0013	0.0006
$6.0 < q^2 < 7.0$	0.0209	0.0119	0.0079	0.0006	0.047	0.0089	0.0006	0.001
$7.0 < q^2 < 8.0$	0.0203	0.0105	0.006	0.0002	0.0537	0.0037	0.0001	0.0013
$11.0 < q^2 < 11.75$	0.0178	0.0123	0.0024	0.0001	0.0603	0.0123	0.0006	0.0002
$11.75 < q^2 < 12.5$	0.017	0.0123	0.0026	0.0002	0.0533	0.012	0.0007	0.0006
$15.0 < q^2 < 16.0$	0.011	0.0015	0.0042	0.0001	0.0051	0.0013	0.0002	0.0001
$16.0 < q^2 < 17.0$	0.0089	0.0079	0.0045	0.0001	0.0259	0.0056	0.0004	0.0002
$17.0 < q^2 < 18.0$	0.0071	0.0117	0.0032	0.0001	0.0423	0.0116	0.0003	0.0001
$18.0 < q^2 < 19.0$	0.0061	0.0119	0.0028	0.0005	0.0539	0.0111	0.0002	0.0006
$15.0 < q^2 < 19.0$	0.0086	0.0058	0.0023	0.0001	0.0277	0.0046	0.0001	0.0001
$1.1 < q^2 < 2.5$	0.0229	0.0012	0.0137	0.0001	0.0329	0.001	0.0014	0.0001
$2.5 < q^2 < 4.0$	0.0211	0.0047	0.0184	0.0006	0.0461	0.018	0.0026	0.001
$4.0 < q^2 < 6.0$	0.021	0.0133	0.0062	0.0013	0.0436	0.0165	0.0018	0.0009
$6.0 < q^2 < 8.0$	0.0206	0.0111	0.007	0.0004	0.0505	0.0061	0.0002	0.0012
$11.0 < q^2 < 12.5$	0.0174	0.0123	0.0025	0.0002	0.0568	0.0122	0.0001	0.0004
$15.0 < q^2 < 17.0$	0.01	0.0043	0.0043	0.0001	0.015	0.0018	0.0001	0.0001
$17.0 < q^2 < 19.0$	0.0067	0.0113	0.0005	0.0002	0.0469	0.011	0.0001	0.0002

Table 89: Systematic uncertainties from reweighting depending on pion p and p_{T} for the A_i observables. Ranges of q^2 bins are given in GeV^2/c^4.

q^2	A_3	A_4	A_5	$A(A_{\mathrm{FB}})$	A_7	A_8	A_9	A_{6s}	A_{6c}
$0.1 < q^2 < 0.98$	0.0011	0.0008	0.0031	0.0058	0.0006	0.0033	0.0005	0.0013	0.0004
$1.1 < q^2 < 2.0$	0.0002	0.0124	0.0029	0.0086	0.0002	0.0001	0.0001	0.002	0.0007
$2.0 < q^2 < 3.0$	0.0003	0.0202	0.0024	0.0063	0.0004	0.0002	0.0001	0.0015	0.0006
$3.0 < q^2 < 4.0$	0.0007	0.0225	0.0004	0.0019	0.0001	0.0001	0.0002	0.0005	0.0002
$4.0 < q^2 < 5.0$	0.001	0.0239	0.0012	0.0023	0.0001	0.0001	0.0001	0.0006	0.0003
$5.0 < q^2 < 6.0$	0.0009	0.024	0.0024	0.0052	0.0001	0.0001	0.0001	0.0013	0.0006
$6.0 < q^2 < 7.0$	0.0011	0.0256	0.0026	0.0075	0.0002	0.0003	0.0003	0.0018	0.0007
$7.0 < q^2 < 8.0$	0.0013	0.0285	0.003	0.0092	0.0004	0.0005	0.0002	0.0022	0.0009
$11.0 < q^2 < 11.75$	0.0017	0.0285	0.0039	0.0106	0.0003	0.0001	0.0001	0.0023	0.0006
$11.75 < q^2 < 12.5$	0.0016	0.0251	0.0038	0.0099	0.0003	0.0003	0.0001	0.0021	0.0006
$15.0 < q^2 < 16.0$	0.0027	0.0043	0.0018	0.0035	0.0001	0.0001	0.0001	0.0007	0.0001
$16.0 < q^2 < 17.0$	0.0047	0.0141	0.0047	0.0014	0.0002	0.0001	0.0001	0.0003	0.0001
$17.0 < q^2 < 18.0$	0.006	0.0216	0.007	0.0011	0.0001	0.0001	0.0001	0.0002	0.0001
$18.0 < q^2 < 19.0$	0.0063	0.0269	0.0062	0.0056	0.0001	0.0003	0.0003	0.0012	0.0003
$15.0 < q^2 < 19.0$	0.0042	0.0149	0.004	0.0031	0.0001	0.0001	0.0001	0.0006	0.0001
$1.1 < q^2 < 2.5$	0.0002	0.0144	0.0032	0.0082	0.0002	0.0001	0.0001	0.002	0.0007
$2.5 < q^2 < 4.0$	0.0004	0.0223	0.0008	0.003	0.0003	0.0001	0.0002	0.0007	0.0003
$4.0 < q^2 < 6.0$	0.001	0.0239	0.0018	0.0038	0.0001	0.0001	0.0001	0.001	0.0004
$6.0 < q^2 < 8.0$	0.0012	0.0271	0.0028	0.0084	0.0003	0.0004	0.0002	0.002	0.0008
$11.0 < q^2 < 12.5$	0.0016	0.0268	0.0038	0.0102	0.0001	0.0002	0.0001	0.0022	0.0006
$15.0 < q^2 < 17.0$	0.0036	0.009	0.0031	0.0025	0.0001	0.0001	0.0001	0.0005	0.0001
$17.0 < q^2 < 19.0$	0.006	0.0237	0.0065	0.0031	0.0001	0.0001	0.0001	0.0006	0.0001

Table 90: Systematic uncertainties form neglecting the explicit reweighting of the B^0 vertex χ^2 for S_i observables. Ranges of q^2 bins are given in GeV^2/c^4.

q^2	F_L	S_3	S_4	S_5	A_FB	S_7	S_8	S_9	S_{6s}	S_{6c}
$0.1 < q^2 < 0.98$	0.0062	0.0016	0.0016	0.005	0.0704	0.002	0.0006	0.0423	0.0151	0.0039
$1.1 < q^2 < 2.0$	0.0009	0.0003	0.0117	0.003	0.0014	0.0003	0.0003	0.0006	0.0005	0.0003
$2.0 < q^2 < 3.0$	0.0012	0.0003	0.0181	0.0027	0.0006	0.0003	0.0003	0.0006	0.0003	0.0003
$3.0 < q^2 < 4.0$	0.0016	0.0006	0.0198	0.0017	0.0002	0.0003	0.0003	0.0014	0.0001	0.0001
$4.0 < q^2 < 5.0$	0.0012	0.0012	0.02	0.0007	0.0008	0.0003	0.0003	0.0019	0.0002	0.0001
$5.0 < q^2 < 6.0$	0.0007	0.0017	0.0206	0.0005	0.0013	0.0003	0.0003	0.002	0.0004	0.0003
$6.0 < q^2 < 7.0$	0.0006	0.002	0.0224	0.0015	0.002	0.0003	0.0003	0.0022	0.0006	0.0004
$7.0 < q^2 < 8.0$	0.0009	0.0022	0.0255	0.0023	0.0028	0.0003	0.0003	0.0027	0.0008	0.0004
$11.0 < q^2 < 11.75$	0.0026	0.0028	0.0278	0.0057	0.0045	0.0003	0.0003	0.0042	0.001	0.0003
$11.75 < q^2 < 12.5$	0.003	0.0029	0.0248	0.0054	0.0043	0.0003	0.0003	0.0035	0.001	0.0003
$15.0 < q^2 < 16.0$	0.0033	0.0005	0.0025	0.0004	0.0007	0.0003	0.0003	0.0005	0.0002	0.0001
$16.0 < q^2 < 17.0$	0.0035	0.0009	0.012	0.0028	0.0003	0.0003	0.0003	0.001	0.0001	0.0
$17.0 < q^2 < 18.0$	0.0047	0.0023	0.0198	0.0062	0.0006	0.0003	0.0003	0.0003	0.0001	0.0
$18.0 < q^2 < 19.0$	0.007	0.0039	0.0256	0.0075	0.006	0.0003	0.0003	0.0026	0.0013	0.0003
$15.0 < q^2 < 19.0$	0.0028	0.0099	0.003	0.0021	0.0008	0.0126	0.0088	0.014	0.0002	0.0001
$1.1 < q^2 < 2.5$	0.001	0.0003	0.0133	0.0029	0.0012	0.0003	0.0003	0.0003	0.0004	0.0003
$2.5 < q^2 < 4.0$	0.0015	0.0004	0.0196	0.0019	0.0002	0.0003	0.0003	0.0012	0.0001	0.0001
$4.0 < q^2 < 6.0$	0.001	0.0015	0.0203	0.0003	0.0011	0.0003	0.0003	0.0019	0.0003	0.0002
$6.0 < q^2 < 8.0$	0.0008	0.0021	0.024	0.0019	0.0024	0.0003	0.0003	0.0025	0.0007	0.0004
$11.0 < q^2 < 12.5$	0.0028	0.0029	0.0263	0.0056	0.0044	0.0003	0.0003	0.0039	0.001	0.0003
$15.0 < q^2 < 17.0$	0.0034	0.0003	0.007	0.0011	0.0002	0.0003	0.0003	0.0007	0.0001	0.0
$17.0 < q^2 < 19.0$	0.0056	0.0029	0.0221	0.0067	0.0027	0.0003	0.0003	0.0009	0.0006	0.0002

Table 91: Systematic uncertainties form neglecting the explicit reweighting of the B^0 vertex χ^2 for the P_i observables. Ranges of q^2 bins are given in GeV^2/c^4.

q^2	F_{L}	P_1	P_2	P_3	P_4'	P_5'	P_6'	P_8'
$0.1 < q^2 < 0.98$	0.0062	0.0042	0.0614	0.0008	0.0058	0.0068	0.0052	0.0173
$1.1 < q^2 < 2.0$	0.0009	0.0002	0.0018	0.0001	0.0246	0.006	0.0001	0.0004
$2.0 < q^2 < 3.0$	0.0012	0.0008	0.0008	0.0002	0.0436	0.0067	0.0001	0.0006
$3.0 < q^2 < 4.0$	0.0016	0.006	0.0022	0.0002	0.048	0.0056	0.0004	0.0004
$4.0 < q^2 < 5.0$	0.0012	0.0105	0.0019	0.0003	0.0463	0.0028	0.0003	0.0005
$5.0 < q^2 < 6.0$	0.0007	0.0123	0.0023	0.0004	0.0451	0.0004	0.0003	0.0004
$6.0 < q^2 < 7.0$	0.0006	0.0122	0.0033	0.0002	0.0473	0.0027	0.0003	0.0005
$7.0 < q^2 < 8.0$	0.0009	0.0115	0.0039	0.0003	0.0522	0.0043	0.0002	0.0004
$11.0 < q^2 < 11.75$	0.0026	0.0108	0.0031	0.0001	0.0567	0.0123	0.0001	0.0001
$11.75 < q^2 < 12.5$	0.003	0.011	0.0025	0.0001	0.0508	0.0118	0.0001	0.0001
$15.0 < q^2 < 16.0$	0.0033	0.0036	0.0016	0.0001	0.0041	0.0024	0.0001	0.0001
$16.0 < q^2 < 17.0$	0.0035	0.0001	0.0027	0.0001	0.0238	0.0042	0.0001	0.0001
$17.0 < q^2 < 18.0$	0.0047	0.0026	0.0022	0.0001	0.0397	0.011	0.0002	0.0002
$18.0 < q^2 < 19.0$	0.007	0.0034	0.0028	0.0003	0.0507	0.0135	0.0001	0.0006
$15.0 < q^2 < 19.0$	0.0028	0.0248	0.0007	0.0183	0.01	0.0081	0.0297	0.0208
$1.1 < q^2 < 2.5$	0.001	0.0005	0.0014	0.0001	0.029	0.0061	0.0001	0.0004
$2.5 < q^2 < 4.0$	0.0015	0.004	0.0021	0.0003	0.0478	0.0058	0.0003	0.0005
$4.0 < q^2 < 6.0$	0.001	0.0115	0.002	0.0004	0.0456	0.0011	0.0003	0.0004
$6.0 < q^2 < 8.0$	0.0008	0.0118	0.0037	0.0003	0.0498	0.0035	0.0003	0.0004
$11.0 < q^2 < 12.5$	0.0028	0.0109	0.0028	0.0001	0.0537	0.012	0.0001	0.0001
$15.0 < q^2 < 17.0$	0.0034	0.0019	0.0021	0.0001	0.0134	0.0007	0.0001	0.0001
$17.0 < q^2 < 19.0$	0.0056	0.003	0.0003	0.0002	0.044	0.0119	0.0001	0.0001

Table 92: Systematic uncertainties form neglecting the explicit reweighting of the B^0 vertex χ^2 for the A_i observables. Ranges of q^2 bins are given in GeV^2/c^4.

q^2	A_3	A_4	A_5	$A(A_{\mathrm{FB}})$	A_7	A_8	A_9	A_{6s}	A_{6c}
$0.1 < q^2 < 0.98$	0.0016	0.0016	0.005	0.0704	0.002	0.0072	0.0006	0.0151	0.0039
$1.1 < q^2 < 2.0$	0.0001	0.0117	0.003	0.0014	0.0001	0.0002	0.0001	0.0005	0.0003
$2.0 < q^2 < 3.0$	0.0001	0.0181	0.0027	0.0006	0.0001	0.0002	0.0001	0.0003	0.0003
$3.0 < q^2 < 4.0$	0.0006	0.0198	0.0017	0.0002	0.0001	0.0001	0.0001	0.0001	0.0001
$4.0 < q^2 < 5.0$	0.0012	0.02	0.0007	0.0008	0.0001	0.0002	0.0001	0.0002	0.0001
$5.0 < q^2 < 6.0$	0.0017	0.0206	0.0005	0.0013	0.0001	0.0002	0.0001	0.0004	0.0003
$6.0 < q^2 < 7.0$	0.002	0.0224	0.0015	0.002	0.0001	0.0002	0.0001	0.0006	0.0004
$7.0 < q^2 < 8.0$	0.0022	0.0255	0.0023	0.0028	0.0001	0.0002	0.0001	0.0008	0.0004
$11.0 < q^2 < 11.75$	0.0028	0.0278	0.0057	0.0045	0.0001	0.0001	0.0001	0.001	0.0003
$11.75 < q^2 < 12.5$	0.0029	0.0248	0.0054	0.0043	0.0001	0.0001	0.0001	0.001	0.0003
$15.0 < q^2 < 16.0$	0.0005	0.0025	0.0004	0.0007	0.0001	0.0001	0.0001	0.0001	0.0001
$16.0 < q^2 < 17.0$	0.0009	0.012	0.0028	0.0003	0.0001	0.0001	0.0001	0.0001	0.0001
$17.0 < q^2 < 18.0$	0.0023	0.0198	0.0062	0.0006	0.0001	0.0001	0.0001	0.0001	0.0001
$18.0 < q^2 < 19.0$	0.0039	0.0256	0.0075	0.006	0.0001	0.0003	0.0002	0.0013	0.0003
$15.0 < q^2 < 19.0$	0.0099	0.003	0.0021	0.0008	0.0126	0.0088	0.014	0.0002	0.0001
$1.1 < q^2 < 2.5$	0.0001	0.0133	0.0029	0.0012	0.0001	0.0002	0.0001	0.0004	0.0003
$2.5 < q^2 < 4.0$	0.0004	0.0196	0.0019	0.0001	0.0001	0.0002	0.0001	0.0001	0.0001
$4.0 < q^2 < 6.0$	0.0015	0.0203	0.0001	0.0011	0.0001	0.0002	0.0001	0.0003	0.0002
$6.0 < q^2 < 8.0$	0.0021	0.024	0.0019	0.0024	0.0001	0.0002	0.0001	0.0007	0.0004
$11.0 < q^2 < 12.5$	0.0029	0.0263	0.0056	0.0044	0.0001	0.0001	0.0001	0.001	0.0003
$15.0 < q^2 < 17.0$	0.0001	0.007	0.0011	0.0002	0.0001	0.0001	0.0001	0.0001	0.0001
$17.0 < q^2 < 19.0$	0.0029	0.0221	0.0067	0.0027	0.0001	0.0001	0.0001	0.0006	0.0001

Table 93: Systematic uncertainties from neglecting the explicit reweighting of the B^0 p_{T} for the S_i observables. Ranges of q^2 bins are given in GeV^2/c^4.

q^2	F_{L}	S_3	S_4	S_5	A_{FB}	S_7	S_8	S_9	S_{6s}	S_{6c}
$0.1 < q^2 < 0.98$	0.0077	0.0006	0.0016	0.0026	0.003	0.001	0.0007	0.0003	0.0007	0.0003
$1.1 < q^2 < 2.0$	0.006	0.0002	0.0118	0.0018	0.0011	0.0001	0.0002	0.0001	0.0004	0.0003
$2.0 < q^2 < 3.0$	0.0065	0.0001	0.0178	0.0025	0.0002	0.0002	0.0003	0.0001	0.0001	0.0002
$3.0 < q^2 < 4.0$	0.0059	0.0004	0.0193	0.0026	0.0006	0.0002	0.0002	0.0001	0.0001	0.0001
$4.0 < q^2 < 5.0$	0.0059	0.0007	0.0194	0.0021	0.0006	0.0002	0.0002	0.0001	0.0002	0.0001
$5.0 < q^2 < 6.0$	0.0063	0.001	0.02	0.0012	0.0004	0.0001	0.0002	0.0001	0.0002	0.0002
$6.0 < q^2 < 7.0$	0.0065	0.0012	0.0218	0.0001	0.0005	0.0002	0.0002	0.0001	0.0003	0.0003
$7.0 < q^2 < 8.0$	0.0064	0.0014	0.0248	0.0011	0.0008	0.0002	0.0001	0.0001	0.0003	0.0003
$11.0 < q^2 < 11.75$	0.0054	0.0028	0.0276	0.0059	0.0011	0.0001	0.0001	0.0001	0.0003	0.0001
$11.75 < q^2 < 12.5$	0.0049	0.0027	0.0248	0.0056	0.0008	0.0001	0.0001	0.0001	0.0002	0.0001
$15.0 < q^2 < 16.0$	0.0031	0.0008	0.0021	0.0005	0.0025	0.0001	0.0001	0.0001	0.0005	0.0001
$16.0 < q^2 < 17.0$	0.0026	0.0025	0.0117	0.0027	0.0033	0.0001	0.0001	0.0001	0.0007	0.0002
$17.0 < q^2 < 18.0$	0.0014	0.0039	0.0199	0.0056	0.0021	0.0001	0.0001	0.0001	0.0005	0.0001
$18.0 < q^2 < 19.0$	0.001	0.005	0.0264	0.0063	0.004	0.0001	0.0003	0.0001	0.0008	0.0002
$15.0 < q^2 < 19.0$	0.0019	0.0028	0.0128	0.0031	0.0018	0.0001	0.0001	0.0001	0.0004	0.0001
$1.1 < q^2 < 2.5$	0.0063	0.0002	0.0134	0.0019	0.0007	0.0002	0.0002	0.0001	0.0003	0.0003
$2.5 < q^2 < 4.0$	0.006	0.0003	0.0192	0.0025	0.0005	0.0002	0.0003	0.0001	0.0001	0.0001
$4.0 < q^2 < 6.0$	0.0061	0.0009	0.0197	0.0017	0.0005	0.0002	0.0002	0.0001	0.0002	0.0002
$6.0 < q^2 < 8.0$	0.0064	0.0013	0.0234	0.0005	0.0006	0.0002	0.0002	0.0001	0.0003	0.0003
$11.0 < q^2 < 12.5$	0.0051	0.0027	0.0262	0.0057	0.0009	0.0001	0.0001	0.0001	0.0003	0.0001
$15.0 < q^2 < 17.0$	0.0029	0.0016	0.0067	0.001	0.0028	0.0001	0.0001	0.0001	0.0006	0.0002
$17.0 < q^2 < 19.0$	0.0004	0.0044	0.0225	0.006	0.0001	0.0001	0.0001	0.0001	0.0001	0.0001

Table 94: Systematic uncertainties from neglecting the explicit reweighting of the B^0 p_{T} for the P_i observables. Ranges of q^2 bins are given in GeV^2/c^4.

q^2	F_{L}	P_1	P_2	P_3	P_4'	P_5'	P_6'	P_8'
$0.1 < q^2 < 0.98$	0.0077	0.0016	0.0018	0.0004	0.0064	0.0002	0.0031	0.0017
$1.1 < q^2 < 2.0$	0.006	0.0013	0.0087	0.0002	0.0244	0.0052	0.0001	0.0004
$2.0 < q^2 < 3.0$	0.0065	0.0001	0.0126	0.0003	0.0439	0.0052	0.0005	0.0005
$3.0 < q^2 < 4.0$	0.0059	0.0039	0.0031	0.0001	0.0503	0.0014	0.0003	0.0003
$4.0 < q^2 < 5.0$	0.0059	0.0043	0.0039	0.0001	0.0485	0.0008	0.0001	0.0002
$5.0 < q^2 < 6.0$	0.0063	0.0056	0.0065	0.0001	0.0469	0.0025	0.0001	0.0003
$6.0 < q^2 < 7.0$	0.0065	0.0056	0.0077	0.0003	0.0483	0.0039	0.0001	0.0004
$7.0 < q^2 < 8.0$	0.0064	0.0063	0.008	0.0004	0.0525	0.0049	0.0002	0.0002
$11.0 < q^2 < 11.75$	0.0054	0.0076	0.0055	0.0001	0.0551	0.0103	0.0001	0.0001
$11.75 < q^2 < 12.5$	0.0049	0.0074	0.0049	0.0001	0.0495	0.0098	0.0002	0.0001
$15.0 < q^2 < 16.0$	0.0031	0.0044	0.0004	0.0001	0.0055	0.0005	0.0001	0.0002
$16.0 < q^2 < 17.0$	0.0026	0.0093	0.0016	0.0001	0.0258	0.0069	0.0001	0.0001
$17.0 < q^2 < 18.0$	0.0014	0.0129	0.0013	0.0001	0.0429	0.0126	0.0002	0.0002
$18.0 < q^2 < 19.0$	0.001	0.0138	0.0035	0.0002	0.0555	0.0129	0.0001	0.0006
$15.0 < q^2 < 19.0$	0.0019	0.01	0.0006	0.0001	0.0278	0.0073	0.0001	0.0001
$1.1 < q^2 < 2.5$	0.0063	0.001	0.0098	0.0001	0.0286	0.0057	0.0001	0.0004
$2.5 < q^2 < 4.0$	0.006	0.0027	0.0055	0.0003	0.0496	0.0022	0.0003	0.0004
$4.0 < q^2 < 6.0$	0.0061	0.005	0.0055	0.0001	0.0476	0.0017	0.0001	0.0002
$6.0 < q^2 < 8.0$	0.0064	0.006	0.0079	0.0003	0.0504	0.0044	0.0002	0.0003
$11.0 < q^2 < 12.5$	0.0051	0.0075	0.0052	0.0001	0.0523	0.0101	0.0001	0.0001
$15.0 < q^2 < 17.0$	0.0029	0.0068	0.001	0.0001	0.0151	0.0035	0.0001	0.0001
$17.0 < q^2 < 19.0$	0.0004	0.0137	0.0004	0.0001	0.0478	0.0129	0.0001	0.0001

Table 95: Systematic uncertainties from neglecting the explicit reweighting of the B^0 p_{T} for the A_i observables. Ranges of q^2 bins are given in GeV^2/c^4.

q^2	A_3	A_4	A_5	$A(A_{\mathrm{FB}})$	A_7	A_8	A_9	A_{6s}	A_{6c}
$0.1 < q^2 < 0.98$	0.0006	0.0016	0.0026	0.003	0.001	0.0007	0.0003	0.0007	0.0003
$1.1 < q^2 < 2.0$	0.0002	0.0118	0.0018	0.0011	0.0001	0.0002	0.0001	0.0004	0.0003
$2.0 < q^2 < 3.0$	0.0001	0.0178	0.0025	0.0002	0.0002	0.0003	0.0001	0.0001	0.0002
$3.0 < q^2 < 4.0$	0.0004	0.0193	0.0026	0.0006	0.0002	0.0002	0.0001	0.0001	0.0001
$4.0 < q^2 < 5.0$	0.0007	0.0194	0.0021	0.0006	0.0002	0.0002	0.0001	0.0002	0.0001
$5.0 < q^2 < 6.0$	0.001	0.02	0.0012	0.0004	0.0001	0.0002	0.0001	0.0002	0.0002
$6.0 < q^2 < 7.0$	0.0012	0.0218	0.0001	0.0005	0.0002	0.0002	0.0001	0.0003	0.0003
$7.0 < q^2 < 8.0$	0.0014	0.0248	0.0011	0.0008	0.0002	0.0001	0.0001	0.0003	0.0003
$11.0 < q^2 < 11.75$	0.0028	0.0276	0.0059	0.0011	0.0001	0.0001	0.0001	0.0003	0.0001
$11.75 < q^2 < 12.5$	0.0027	0.0248	0.0056	0.0008	0.0001	0.0001	0.0001	0.0002	0.0001
$15.0 < q^2 < 16.0$	0.0008	0.0021	0.0005	0.0025	0.0001	0.0001	0.0001	0.0005	0.0001
$16.0 < q^2 < 17.0$	0.0025	0.0117	0.0027	0.0033	0.0001	0.0001	0.0001	0.0007	0.0002
$17.0 < q^2 < 18.0$	0.0039	0.0199	0.0056	0.0021	0.0001	0.0001	0.0001	0.0005	0.0001
$18.0 < q^2 < 19.0$	0.005	0.0264	0.0063	0.004	0.0001	0.0003	0.0001	0.0008	0.0002
$15.0 < q^2 < 19.0$	0.0028	0.0128	0.0031	0.0018	0.0001	0.0001	0.0001	0.0004	0.0001
$1.1 < q^2 < 2.5$	0.0002	0.0134	0.0019	0.0007	0.0002	0.0002	0.0001	0.0003	0.0003
$2.5 < q^2 < 4.0$	0.0003	0.0192	0.0025	0.0005	0.0002	0.0003	0.0001	0.0001	0.0001
$4.0 < q^2 < 6.0$	0.0009	0.0197	0.0017	0.0005	0.0002	0.0002	0.0001	0.0002	0.0002
$6.0 < q^2 < 8.0$	0.0013	0.0234	0.0005	0.0006	0.0002	0.0002	0.0001	0.0003	0.0003
$11.0 < q^2 < 12.5$	0.0027	0.0262	0.0057	0.0009	0.0001	0.0001	0.0001	0.0003	0.0001
$15.0 < q^2 < 17.0$	0.0016	0.0067	0.001	0.0028	0.0001	0.0001	0.0001	0.0006	0.0002
$17.0 < q^2 < 19.0$	0.0044	0.0225	0.006	0.0001	0.0001	0.0001	0.0001	0.0001	0.0001

Table 96: Systematic uncertainties form neglecting the explicit reweighting of the track multiplicity on the S_i observables. Ranges of q^2 bins are given in GeV^2/c^4.

q^2	F_{L}	S_3	S_4	S_5	A_{FB}	S_7	S_8	S_9	S_{6s}	S_{6c}
$0.1 < q^2 < 0.98$	0.0192	0.0003	0.012	0.0027	0.0036	0.0016	0.0045	0.0001	0.0019	0.0019
$1.1 < q^2 < 2.0$	0.0003	0.0008	0.0115	0.003	0.0018	0.0001	0.0002	0.0001	0.0005	0.0003
$2.0 < q^2 < 3.0$	0.0012	0.0005	0.018	0.0023	0.0005	0.0001	0.0003	0.0001	0.0003	0.0002
$3.0 < q^2 < 4.0$	0.0004	0.0007	0.0197	0.0017	0.0003	0.0001	0.0002	0.0001	0.0001	0.0001
$4.0 < q^2 < 5.0$	0.0001	0.0009	0.0199	0.0011	0.0008	0.0001	0.0002	0.0001	0.0002	0.0001
$5.0 < q^2 < 6.0$	0.0004	0.0011	0.0206	0.0002	0.0014	0.0001	0.0002	0.0001	0.0004	0.0003
$6.0 < q^2 < 7.0$	0.0005	0.0015	0.0224	0.0008	0.0021	0.0001	0.0002	0.0001	0.0006	0.0004
$7.0 < q^2 < 8.0$	0.0006	0.0019	0.0254	0.0018	0.0029	0.0001	0.0002	0.0001	0.0008	0.0004
$11.0 < q^2 < 11.75$	0.0005	0.0045	0.0278	0.0061	0.0042	0.0001	0.0001	0.0001	0.001	0.0003
$11.75 < q^2 < 12.5$	0.0009	0.0046	0.025	0.0059	0.004	0.0001	0.0001	0.0001	0.0009	0.0003
$15.0 < q^2 < 16.0$	0.003	0.0007	0.0021	0.0004	0.0011	0.0001	0.0001	0.0001	0.0002	0.0001
$16.0 < q^2 < 17.0$	0.0031	0.0012	0.0118	0.0028	0.0001	0.0001	0.0001	0.0001	0.0001	0.0001
$17.0 < q^2 < 18.0$	0.0028	0.0028	0.02	0.0057	0.0001	0.0001	0.0001	0.0001	0.0001	0.0001
$18.0 < q^2 < 19.0$	0.0019	0.0037	0.0259	0.0063	0.004	0.0001	0.0003	0.0001	0.0008	0.0002
$15.0 < q^2 < 19.0$	0.0028	0.0013	0.0128	0.003	0.001	0.0001	0.0001	0.0001	0.0002	0.0001
$1.1 < q^2 < 2.5$	0.0006	0.0007	0.0132	0.0028	0.0015	0.0001	0.0002	0.0001	0.0005	0.0003
$2.5 < q^2 < 4.0$	0.0006	0.0006	0.0195	0.0018	0.0001	0.0001	0.0002	0.0001	0.0001	0.0001
$4.0 < q^2 < 6.0$	0.0003	0.001	0.0202	0.0006	0.0011	0.0001	0.0002	0.0001	0.0003	0.0002
$6.0 < q^2 < 8.0$	0.0006	0.0017	0.024	0.0013	0.0025	0.0001	0.0002	0.0001	0.0007	0.0004
$11.0 < q^2 < 12.5$	0.0007	0.0045	0.0264	0.006	0.0041	0.0001	0.0001	0.0001	0.0009	0.0003
$15.0 < q^2 < 17.0$	0.003	0.0002	0.0067	0.0011	0.0005	0.0001	0.0001	0.0001	0.0001	0.0001
$17.0 < q^2 < 19.0$	0.0024	0.0031	0.0223	0.006	0.0015	0.0001	0.0001	0.0001	0.0003	0.0001

Table 97: Systematic uncertainties form neglecting the explicit reweighting of the track multiplicity on the P_i observables. Ranges of q^2 bins are given in GeV^2/c^4.

q^2	$F_{\rm L}$	P_1	P_2	P_3	P_4'	P_5'	P_6'	P_8'
$0.1 < q^2 < 0.98$	0.0192	0.0009	0.0011	0.0001	0.0228	0.0101	0.0023	0.0108
$1.1 < q^2 < 2.0$	0.0003	0.0047	0.0038	0.0001	0.0241	0.0064	0.0001	0.0003
$2.0 < q^2 < 3.0$	0.0012	0.0046	0.004	0.0003	0.0437	0.0055	0.0001	0.0006
$3.0 < q^2 < 4.0$	0.0004	0.0069	0.0005	0.0003	0.0487	0.0038	0.0003	0.0004
$4.0 < q^2 < 5.0$	0.0001	0.0072	0.0023	0.0004	0.0466	0.0027	0.0002	0.0004
$5.0 < q^2 < 6.0$	0.0004	0.008	0.0028	0.0004	0.0452	0.0008	0.0002	0.0004
$6.0 < q^2 < 7.0$	0.0005	0.0088	0.0037	0.0002	0.0474	0.0014	0.0003	0.0004
$7.0 < q^2 < 8.0$	0.0006	0.0101	0.0044	0.0003	0.0522	0.0035	0.0002	0.0004
$11.0 < q^2 < 11.75$	0.0005	0.0156	0.0044	0.0001	0.0565	0.0125	0.0001	0.0001
$11.75 < q^2 < 12.5$	0.0009	0.0161	0.0039	0.0001	0.0508	0.0121	0.0001	0.0001
$15.0 < q^2 < 16.0$	0.003	0.0042	0.001	0.0001	0.0033	0.0022	0.0001	0.0001
$16.0 < q^2 < 17.0$	0.0031	0.0014	0.0021	0.0001	0.0235	0.0044	0.0001	0.0001
$17.0 < q^2 < 18.0$	0.0028	0.0059	0.0017	0.0001	0.041	0.0108	0.0001	0.0002
$18.0 < q^2 < 19.0$	0.0019	0.0089	0.0032	0.0002	0.054	0.0127	0.0001	0.0007
$15.0 < q^2 < 19.0$	0.0028	0.0017	0.0007	0.0001	0.0258	0.005	0.0001	0.0001
$1.1 < q^2 < 2.5$	0.0006	0.0047	0.0039	0.0001	0.0286	0.0063	0.0001	0.0004
$2.5 < q^2 < 4.0$	0.0006	0.0061	0.0005	0.0004	0.0483	0.004	0.0001	0.0005
$4.0 < q^2 < 6.0$	0.0003	0.0077	0.0026	0.0004	0.0458	0.0017	0.0002	0.0004
$6.0 < q^2 < 8.0$	0.0006	0.0095	0.0041	0.0003	0.0498	0.0025	0.0003	0.0004
$11.0 < q^2 < 12.5$	0.0007	0.0159	0.0042	0.0001	0.0536	0.0123	0.0001	0.0001
$15.0 < q^2 < 17.0$	0.003	0.0015	0.0015	0.0001	0.0129	0.0009	0.0001	0.0001
$17.0 < q^2 < 19.0$	0.0024	0.007	0.0002	0.0001	0.0461	0.0116	0.0001	0.0002

Table 98: Systematic uncertainties form neglecting the explicit reweighting of the track multiplicity on the A_i observables. Ranges of q^2 bins are given in GeV^2/c^4.

q^2	A_3	A_4	A_5	$A(A_{\text{FB}})$	A_7	A_8	A_9	A_{6s}	A_{6c}
$0.1 < q^2 < 0.98$	0.0003	0.012	0.0027	0.0036	0.0016	0.0045	0.0001	0.0019	0.0019
$1.1 < q^2 < 2.0$	0.0008	0.0115	0.003	0.0018	0.0001	0.0002	0.0001	0.0005	0.0003
$2.0 < q^2 < 3.0$	0.0005	0.018	0.0023	0.0005	0.0001	0.0003	0.0001	0.0003	0.0002
$3.0 < q^2 < 4.0$	0.0007	0.0197	0.0017	0.0003	0.0001	0.0002	0.0001	0.0001	0.0001
$4.0 < q^2 < 5.0$	0.0009	0.0199	0.0011	0.0008	0.0001	0.0002	0.0001	0.0002	0.0001
$5.0 < q^2 < 6.0$	0.0011	0.0206	0.0002	0.0014	0.0001	0.0002	0.0001	0.0004	0.0003
$6.0 < q^2 < 7.0$	0.0015	0.0224	0.0008	0.0021	0.0001	0.0002	0.0001	0.0006	0.0004
$7.0 < q^2 < 8.0$	0.0019	0.0254	0.0018	0.0029	0.0001	0.0002	0.0001	0.0008	0.0004
$11.0 < q^2 < 11.75$	0.0045	0.0278	0.0061	0.0042	0.0001	0.0001	0.0001	0.001	0.0003
$11.75 < q^2 < 12.5$	0.0046	0.025	0.0059	0.004	0.0001	0.0001	0.0001	0.0009	0.0003
$15.0 < q^2 < 16.0$	0.0007	0.0021	0.0004	0.0011	0.0001	0.0001	0.0001	0.0002	0.0001
$16.0 < q^2 < 17.0$	0.0012	0.0118	0.0028	0.0001	0.0001	0.0001	0.0001	0.0001	0.0001
$17.0 < q^2 < 18.0$	0.0028	0.02	0.0057	0.0001	0.0001	0.0001	0.0001	0.0001	0.0001
$18.0 < q^2 < 19.0$	0.0037	0.0259	0.0063	0.004	0.0001	0.0003	0.0001	0.0008	0.0002
$15.0 < q^2 < 19.0$	0.0013	0.0128	0.003	0.001	0.0001	0.0001	0.0001	0.0002	0.0001
$1.1 < q^2 < 2.5$	0.0007	0.0132	0.0028	0.0015	0.0001	0.0002	0.0001	0.0005	0.0003
$2.5 < q^2 < 4.0$	0.0006	0.0195	0.0018	0.0001	0.0001	0.0002	0.0001	0.0001	0.0001
$4.0 < q^2 < 6.0$	0.001	0.0202	0.0006	0.0011	0.0001	0.0002	0.0001	0.0003	0.0002
$6.0 < q^2 < 8.0$	0.0017	0.024	0.0013	0.0025	0.0001	0.0002	0.0001	0.0007	0.0004
$11.0 < q^2 < 12.5$	0.0045	0.0264	0.006	0.0041	0.0001	0.0001	0.0001	0.0009	0.0003
$15.0 < q^2 < 17.0$	0.0002	0.0067	0.0011	0.0005	0.0001	0.0001	0.0001	0.0001	0.0001
$17.0 < q^2 < 19.0$	0.0031	0.0223	0.006	0.0015	0.0001	0.0001	0.0001	0.0003	0.0001

Table 99: The effect of using a the nominal instead of a higher order acceptance model on the S_i observables.

q^2	F_{L}	S3	S4	S5	A_{FB}	S7	S8	S9	S_{6s}	S_{6c}
$0.1 < q^2 < 0.98$	0.0022	0.0056	0.0002	0.0075	0.0051	0.0078	0.0001	0.0032	0.0011	0.0003
$1.1 < q^2 < 2.0$	0.0048	0.0018	0.0014	0.0049	0.0063	0.0041	0.0047	0.0003	0.0014	0.0004
$2.0 < q^2 < 3.0$	0.0005	0.0001	0.0003	0.0051	0.0035	0.0016	0.0002	0.0023	0.0008	0.0003
$3.0 < q^2 < 4.0$	0.0003	0.0011	0.0009	0.0017	0.0001	0.0016	0.0013	0.002	0.0001	0.0001
$4.0 < q^2 < 5.0$	0.0029	0.0003	0.0001	0.0014	0.0004	0.001	0.0002	0.0009	0.0001	0.0001
$5.0 < q^2 < 6.0$	0.0066	0.0012	0.0005	0.0027	0.0011	0.0015	0.0015	0.0003	0.0002	0.0001
$6.0 < q^2 < 7.0$	0.0082	0.002	0.0009	0.0025	0.0023	0.0033	0.0019	0.0001	0.0005	0.0002
$7.0 < q^2 < 8.0$	0.0065	0.0015	0.0005	0.0011	0.0028	0.0029	0.0016	0.0006	0.0006	0.0002
$11.0 < q^2 < 11.75$	0.0031	0.0029	0.0007	0.0038	0.0021	0.0017	0.0029	0.0028	0.0005	0.0001
$11.75 < q^2 < 12.5$	0.0008	0.0021	0.0004	0.002	0.0016	0.0003	0.0029	0.0019	0.0004	0.0001
$15.0 < q^2 < 16.0$	0.0033	0.0035	0.0016	0.0045	0.0028	0.0005	0.004	0.004	0.0006	0.0001
$16.0 < q^2 < 17.0$	0.0057	0.0001	0.0008	0.0011	0.0008	0.0048	0.0043	0.0034	0.0002	0.0001
$17.0 < q^2 < 18.0$	0.012	0.0048	0.0025	0.0061	0.0046	0.0097	0.0002	0.0012	0.001	0.0002
$18.0 < q^2 < 19.0$	0.002	0.0023	0.0006	0.0026	0.0001	0.0049	0.0091	0.0059	0.0001	0.0001
$15.0 < q^2 < 19.0$	0.0037	0.0002	0.0002	0.0002	0.0006	0.0043	0.0012	0.0016	0.0001	0.0001
$1.1 < q^2 < 2.5$	0.0037	0.0014	0.0011	0.0051	0.0059	0.0037	0.0035	0.0009	0.0013	0.0004
$2.5 < q^2 < 4.0$	0.0003	0.0008	0.0007	0.0024	0.0009	0.0009	0.0011	0.0022	0.0002	0.0001
$4.0 < q^2 < 6.0$	0.0049	0.0005	0.0003	0.0021	0.0008	0.0003	0.0009	0.0006	0.0001	0.0001
$6.0 < q^2 < 8.0$	0.0074	0.0018	0.0007	0.0018	0.0027	0.0031	0.0017	0.0003	0.0006	0.0002
$11.0 < q^2 < 12.5$	0.0019	0.0025	0.0005	0.0029	0.0018	0.001	0.0029	0.0024	0.0004	0.0001
$15.0 < q^2 < 17.0$	0.001	0.0019	0.0012	0.0018	0.0011	0.0021	0.0041	0.0037	0.0002	0.0001
$17.0 < q^2 < 19.0$	0.0081	0.0036	0.0013	0.0025	0.003	0.0078	0.0034	0.0016	0.0007	0.0002

Table 100: The effect of using a the nominal instead of a higher order acceptance model on the P_i observables.

q^2	F_L	P_1	P_2	P_3	P_4'	P_5'	P_6'	P_8'
$0.1 < q^2 < 0.98$	0.0022	0.0142	0.0041	0.0041	0.0013	0.0159	0.0191	0.0001
$1.1 < q^2 < 2.0$	0.0048	0.0088	0.0064	0.0007	0.0031	0.0106	0.0082	0.0095
$2.0 < q^2 < 3.0$	0.0005	0.0007	0.0074	0.0077	0.0005	0.0111	0.0036	0.0005
$3.0 < q^2 < 4.0$	0.0003	0.0079	0.0004	0.0072	0.002	0.004	0.0036	0.0029
$4.0 < q^2 < 5.0$	0.0029	0.0022	0.0001	0.003	0.0011	0.0047	0.0024	0.0005
$5.0 < q^2 < 6.0$	0.0066	0.0055	0.0021	0.001	0.0008	0.0088	0.0029	0.0032
$6.0 < q^2 < 7.0$	0.0082	0.0086	0.0025	0.0001	0.0002	0.0079	0.0065	0.0038
$7.0 < q^2 < 8.0$	0.0065	0.006	0.0012	0.0013	0.0002	0.0036	0.0058	0.0032
$11.0 < q^2 < 11.75$	0.0031	0.0085	0.0001	0.0046	0.0006	0.0064	0.0035	0.006
$11.75 < q^2 < 12.5$	0.0008	0.0067	0.0011	0.0032	0.0006	0.0037	0.0005	0.0059
$15.0 < q^2 < 16.0$	0.0033	0.0089	0.0006	0.0061	0.0022	0.0077	0.001	0.0084
$16.0 < q^2 < 17.0$	0.0057	0.0042	0.0029	0.0052	0.0041	0.0004	0.0102	0.0089
$17.0 < q^2 < 18.0$	0.012	0.0035	0.0024	0.0018	0.0004	0.0073	0.0204	0.0005
$18.0 < q^2 < 19.0$	0.002	0.0044	0.0008	0.0088	0.0023	0.0063	0.0104	0.0193
$15.0 < q^2 < 19.0$	0.0037	0.0025	0.0017	0.0025	0.0021	0.0022	0.0091	0.0025
$1.1 < q^2 < 2.5$	0.0037	0.0073	0.0069	0.0023	0.0023	0.011	0.0074	0.0073
$2.5 < q^2 < 4.0$	0.0003	0.006	0.0024	0.0078	0.0015	0.0055	0.002	0.0025
$4.0 < q^2 < 6.0$	0.0049	0.0021	0.0008	0.0019	0.001	0.007	0.0004	0.0019
$6.0 < q^2 < 8.0$	0.0074	0.0072	0.0018	0.0007	0.0002	0.0055	0.0061	0.0035
$11.0 < q^2 < 12.5$	0.0019	0.0076	0.0006	0.0039	0.0006	0.0051	0.002	0.0059
$15.0 < q^2 < 17.0$	0.001	0.0065	0.0017	0.0057	0.003	0.0043	0.0043	0.0086
$17.0 < q^2 < 19.0$	0.0081	0.0028	0.0012	0.0024	0.0013	0.0018	0.0165	0.0072

Table 101: The effect of using a the nominal instead of a higher order acceptance model on the A_i observables.

q^2	A_3	A_4	A_5	$A(A_{\mathrm{FB}})$	A_7	A_8	A_9	A_{6s}	A_{6c}
$0.1 < q^2 < 0.98$	0.0056	0.0002	0.0075	0.0051	0.0078	0.0001	0.0032	0.0011	0.0003
$1.1 < q^2 < 2.0$	0.0018	0.0014	0.0049	0.0063	0.0041	0.0047	0.0003	0.0014	0.0004
$2.0 < q^2 < 3.0$	0.0001	0.0003	0.0051	0.0035	0.0016	0.0002	0.0023	0.0008	0.0003
$3.0 < q^2 < 4.0$	0.0011	0.0009	0.0017	0.0001	0.0016	0.0013	0.002	0.0001	0.0001
$4.0 < q^2 < 5.0$	0.0003	0.0001	0.0014	0.0004	0.001	0.0002	0.0009	0.0001	0.0001
$5.0 < q^2 < 6.0$	0.0012	0.0005	0.0027	0.0011	0.0015	0.0015	0.0003	0.0002	0.0001
$6.0 < q^2 < 7.0$	0.002	0.0009	0.0025	0.0023	0.0033	0.0019	0.0001	0.0005	0.0002
$7.0 < q^2 < 8.0$	0.0015	0.0005	0.0011	0.0028	0.0029	0.0016	0.0006	0.0006	0.0002
$11.0 < q^2 < 11.75$	0.0029	0.0007	0.0038	0.0021	0.0017	0.0029	0.0028	0.0005	0.0001
$11.75 < q^2 < 12.5$	0.0021	0.0004	0.002	0.0016	0.0003	0.0029	0.0019	0.0004	0.0001
$15.0 < q^2 < 16.0$	0.0035	0.0016	0.0045	0.0028	0.0005	0.004	0.004	0.0006	0.0001
$16.0 < q^2 < 17.0$	0.0001	0.0008	0.0011	0.0008	0.0048	0.0043	0.0034	0.0002	0.0001
$17.0 < q^2 < 18.0$	0.0048	0.0025	0.0061	0.0046	0.0097	0.0002	0.0012	0.001	0.0002
$18.0 < q^2 < 19.0$	0.0023	0.0006	0.0026	0.0001	0.0049	0.0091	0.0059	0.0001	0.0001
$15.0 < q^2 < 19.0$	0.0002	0.0002	0.0002	0.0006	0.0043	0.0012	0.0016	0.0001	0.0001
$1.1 < q^2 < 2.5$	0.0014	0.0011	0.0051	0.0059	0.0037	0.0035	0.0009	0.0013	0.0004
$2.5 < q^2 < 4.0$	0.0008	0.0007	0.0024	0.0009	0.0009	0.0011	0.0022	0.0002	0.0001
$4.0 < q^2 < 6.0$	0.0005	0.0003	0.0021	0.0008	0.0003	0.0009	0.0006	0.0001	0.0001
$6.0 < q^2 < 8.0$	0.0018	0.0007	0.0018	0.0027	0.0031	0.0017	0.0003	0.0006	0.0002
$11.0 < q^2 < 12.5$	0.0025	0.0005	0.0029	0.0018	0.001	0.0029	0.0024	0.0004	0.0001
$15.0 < q^2 < 17.0$	0.0019	0.0012	0.0018	0.0011	0.0021	0.0041	0.0037	0.0002	0.0001
$17.0 < q^2 < 19.0$	0.0036	0.0013	0.0025	0.003	0.0078	0.0034	0.0016	0.0007	0.0002

10.2.4 Peaking backgrounds

Peaking background systematics are determined in the same way as for the observables 10.1. An overview of the peaking background is given in Tab 56. High statistics toy studies are performed where the various peaking background components are generated, in addition to the signa and the combinatorial background. The sample so generated is then fitted ignoring the peaking background and the bias is taken as a systematic uncertainty. The summary of the numerical results is given in Tab. 102, 103 and 104.

Table 102: The effect of inclusion of peaking backgrounds on the S_i observables.

q^2	F_{L}	S_3	S_4	S_5	A_{FB}	S_7	S_8	S_9	S_{6s}	S_{6c}
$0.1 < q^2 < 0.98$	0.0053	0.0037	0.0075	0.0022	0.0012	0.0004	0.0006	0.0007	0.0026	0.0008
$1.1 < q^2 < 2.0$	0.0042	0.0068	0.0018	0.0048	0.0028	0.0007	0.002	0.0003	0.0065	0.0023
$2.0 < q^2 < 3.0$	0.0044	0.0073	0.0011	0.0038	0.0014	0.0007	0.0057	0.0018	0.0033	0.0012
$3.0 < q^2 < 4.0$	0.0056	0.0075	0.0023	0.001	0.001	0.0011	0.0015	0.0004	0.0003	0.0002
$4.0 < q^2 < 5.0$	0.0066	0.0069	0.002	0.0012	0.0025	0.0007	0.0027	0.0005	0.0006	0.0002
$5.0 < q^2 < 6.0$	0.0078	0.0081	0.0015	0.001	0.0012	0.0007	0.002	0.0007	0.0025	0.0007
$6.0 < q^2 < 7.0$	0.0084	0.001	0.0011	0.0065	0.0023	0.001	0.0004	0.001	0.005	0.0014
$7.0 < q^2 < 8.0$	0.0091	0.0012	0.0012	0.0051	0.0034	0.0006	0.0011	0.0009	0.0075	0.0021
$11.0 < q^2 < 11.75$	0.0098	0.0017	0.0022	0.0016	0.0058	0.0002	0.0007	0.0002	0.0012	0.0031
$11.75 < q^2 < 12.5$	0.0011	0.0019	0.0019	0.0014	0.0061	0.0018	0.0004	0.0005	0.0013	0.0034
$15.0 < q^2 < 16.0$	0.0013	0.0032	0.001	0.0011	0.0068	0.0016	0.0002	0.0004	0.0015	0.0038
$16.0 < q^2 < 17.0$	0.0012	0.0038	0.01	0.0063	0.0062	0.0001	0.0001	0.0004	0.0013	0.0034
$17.0 < q^2 < 18.0$	0.0011	0.0045	0.0023	0.0033	0.0048	0.0001	0.0004	0.0007	0.001	0.0027
$18.0 < q^2 < 19.0$	0.0067	0.0056	0.0034	0.0018	0.002	0.0007	0.0007	0.0009	0.0044	0.0012
$15.0 < q^2 < 19.0$	0.0011	0.0042	0.0013	0.0003	0.0056	0.0008	0.0001	0.0006	0.0012	0.0032
$1.1 < q^2 < 2.5$	0.0042	0.0064	0.0005	0.0039	0.0025	0.0009	0.0016	0.0005	0.0058	0.002
$2.5 < q^2 < 4.0$	0.0053	0.008	0.0021	0.001	0.0041	0.0013	0.0002	0.0013	0.001	0.0004
$4.0 < q^2 < 6.0$	0.0073	0.0074	0.0017	0.0012	0.0081	0.0007	0.0003	0.0002	0.0018	0.0005
$6.0 < q^2 < 8.0$	0.0088	0.0011	0.0012	0.0059	0.0029	0.0008	0.0005	0.001	0.0064	0.0018
$11.0 < q^2 < 12.5$	0.001	0.0018	0.002	0.0015	0.0059	0.001	0.0005	0.0004	0.0013	0.0032
$15.0 < q^2 < 17.0$	0.0012	0.0035	0.0052	0.0084	0.0065	0.0007	0.0001	0.0004	0.0014	0.0036
$17.0 < q^2 < 19.0$	0.0091	0.005	0.0027	0.0097	0.0038	0.0005	0.0001	0.0008	0.0083	0.0022

Table 103: The effect of inclusion of peaking backgrounds on the P_i observables.

q^2	F_{L}	P_1	P_2	P_3	P'_4	P'_5	P'_6	P'_8
$0.1 < q^2 < 0.98$	0.0053	0.0095	0.0013	0.0005	0.0056	0.0071	0.008	0.0014
$1.1 < q^2 < 2.0$	0.0042	0.0026	0.0073	0.001	0.0055	0.0046	0.0005	0.0046
$2.0 < q^2 < 3.0$	0.0044	0.0041	0.0077	0.0078	0.0026	0.0046	0.0014	0.0012
$3.0 < q^2 < 4.0$	0.0056	0.005	0.0025	0.0032	0.0064	0.0016	0.0047	0.0049
$4.0 < q^2 < 5.0$	0.0066	0.004	0.0078	0.0053	0.006	0.0066	0.0051	0.0055
$5.0 < q^2 < 6.0$	0.0078	0.0049	0.0023	0.007	0.0047	0.0064	0.004	0.0049
$6.0 < q^2 < 7.0$	0.0084	0.0047	0.0025	0.0001	0.0033	0.0056	0.0005	0.0002
$7.0 < q^2 < 8.0$	0.0091	0.005	0.0022	0.0002	0.0029	0.0021	0.0007	0.0026
$11.0 < q^2 < 11.75$	0.0098	0.0077	0.0099	0.0009	0.0091	0.0026	0.0004	0.0014
$11.75 < q^2 < 12.5$	0.0011	0.0088	0.0013	0.0009	0.0001	0.0033	0.0033	0.0006
$15.0 < q^2 < 16.0$	0.0013	0.0015	0.0015	0.0011	0.0086	0.0081	0.0038	0.0029
$16.0 < q^2 < 17.0$	0.0012	0.0017	0.0013	0.0028	0.0011	0.0085	0.0043	0.0018
$17.0 < q^2 < 18.0$	0.0011	0.002	0.0012	0.0007	0.0013	0.0081	0.0017	0.0004
$18.0 < q^2 < 19.0$	0.0067	0.0022	0.0086	0.0005	0.0013	0.0073	0.0003	0.0037
$15.0 < q^2 < 19.0$	0.0011	0.0019	0.0099	0.0012	0.0011	0.0082	0.0029	0.0009
$1.1 < q^2 < 2.5$	0.0042	0.0029	0.0076	0.001	0.0005	0.0027	0.0035	0.0027
$2.5 < q^2 < 4.0$	0.0053	0.0045	0.0041	0.0066	0.0056	0.0033	0.0006	0.0014
$4.0 < q^2 < 6.0$	0.0073	0.0045	0.0015	0.006	0.0053	0.0063	0.0046	0.0001
$6.0 < q^2 < 8.0$	0.0088	0.0049	0.0023	0.0001	0.0031	0.0016	0.0006	0.0015
$11.0 < q^2 < 12.5$	0.001	0.0082	0.0011	0.0001	0.0045	0.003	0.0019	0.001
$15.0 < q^2 < 17.0$	0.0012	0.0016	0.0014	0.002	0.0098	0.0083	0.0039	0.0008
$17.0 < q^2 < 19.0$	0.0091	0.0021	0.0086	0.0001	0.0013	0.0078	0.0009	0.0012

Table 104: The effect of inclusion of peaking backgrounds on the A_i observables.

q^2	A_3	A_4	A_5	$A(A_{\mathrm{FB}})$	A_7	A_8	A_9	A_{6s}	A_{6c}
$0.1 < q^2 < 0.98$	0.0026	0.001	0.0024	0.0076	0.0029	0.0072	0.0081	0.0017	0.0054
$1.1 < q^2 < 2.0$	0.0012	0.0075	0.0018	0.002	0.0035	0.0062	0.0098	0.0044	0.0014
$2.0 < q^2 < 3.0$	0.0013	0.0048	0.0035	0.0015	0.0019	0.0058	0.0065	0.0034	0.001
$3.0 < q^2 < 4.0$	0.0072	0.0013	0.0021	0.0057	0.0026	0.0021	0.0019	0.0013	0.0039
$4.0 < q^2 < 5.0$	0.0045	0.0019	0.0031	0.0039	0.0028	0.0011	0.008	0.0089	0.003
$5.0 < q^2 < 6.0$	0.0018	0.002	0.0037	0.0012	0.0023	0.0068	0.0022	0.0027	0.0083
$6.0 < q^2 < 7.0$	0.0056	0.0024	0.0044	0.002	0.0028	0.0022	0.0054	0.0045	0.0014
$7.0 < q^2 < 8.0$	0.001	0.0023	0.0045	0.0024	0.0014	0.0014	0.0026	0.0053	0.0017
$11.0 < q^2 < 11.75$	0.0017	0.0022	0.0016	0.0058	0.0002	0.0007	0.0002	0.0012	0.0031
$11.75 < q^2 < 12.5$	0.0019	0.0019	0.0014	0.0061	0.0018	0.0004	0.0005	0.0013	0.0034
$15.0 < q^2 < 16.0$	0.0013	0.003	0.0036	0.0043	0.0035	0.0018	0.005	0.0097	0.0031
$16.0 < q^2 < 17.0$	0.0015	0.003	0.0033	0.0042	0.0022	0.0011	0.0013	0.0096	0.0031
$17.0 < q^2 < 18.0$	0.002	0.0031	0.0028	0.0039	0.0001	0.0035	0.006	0.0089	0.0029
$18.0 < q^2 < 19.0$	0.0026	0.0032	0.0023	0.003	0.0024	0.0015	0.0018	0.0069	0.0023
$15.0 < q^2 < 19.0$	0.0018	0.003	0.0031	0.004	0.0039	0.004	0.0066	0.009	0.0029
$1.1 < q^2 < 2.5$	0.0042	0.0043	0.0013	0.0019	0.0039	0.0021	0.0056	0.0042	0.0013
$2.5 < q^2 < 4.0$	0.0086	0.0011	0.0017	0.0083	0.0014	0.0013	0.0018	0.0018	0.0056
$4.0 < q^2 < 6.0$	0.0012	0.002	0.0034	0.0082	0.0025	0.004	0.0015	0.0018	0.0057
$6.0 < q^2 < 8.0$	0.0032	0.0024	0.0044	0.0022	0.0021	0.0018	0.0039	0.0049	0.0016
$11.0 < q^2 < 12.5$	0.0018	0.002	0.0015	0.0059	0.001	0.0005	0.0004	0.0013	0.0032
$15.0 < q^2 < 17.0$	0.0014	0.003	0.0035	0.0043	0.0012	0.0041	0.0089	0.0097	0.0031
$17.0 < q^2 < 19.0$	0.0023	0.0031	0.0026	0.0036	0.0093	0.0037	0.003	0.0081	0.0026

10.2.5 Signal mass modelling

As already discussed in Sec. 10.1, to determine the systematic effect of this choice of signal mass model, a double Gaussian is used as alternative model. The parameters of the double Gaussian are determined from a fit to $B^0 \to J/\psi K^{*0}$ events. High statistics toy MC is then generated using the double Gaussian mass model and fitted twice, once using the double Gaussian and once using the nominal Crystal Ball parametrisation. The observed difference is used as systematic uncertainty and given in Tab. 105, 106 and 107.

Table 105: Systematic effect of the signal mass model for the S_i observables.

q^2	$F_{\rm L}$	S_3	S_4	S_5	$A_{\rm FB}$	S_7	S_8	S_9	S_{6s}	S_{6c}
$0.1 < q^2 < 0.98$	0.0011	0.0028	0.0001	0.0037	0.0025	0.0039	0.0001	0.0016	0.0006	0.0002
$1.1 < q^2 < 2.0$	0.0024	0.0009	0.0007	0.0025	0.0032	0.002	0.0023	0.0001	0.0007	0.0002
$2.0 < q^2 < 3.0$	0.0002	0.0001	0.0001	0.0025	0.0018	0.0008	0.0001	0.0011	0.0004	0.0001
$3.0 < q^2 < 4.0$	0.0001	0.0006	0.0005	0.0009	0.0001	0.0008	0.0007	0.001	0.0001	0.0001
$4.0 < q^2 < 5.0$	0.0015	0.0001	0.0001	0.0007	0.0002	0.0005	0.0001	0.0005	0.0001	0.0001
$5.0 < q^2 < 6.0$	0.0033	0.0006	0.0002	0.0014	0.0005	0.0007	0.0007	0.0001	0.0001	0.0001
$6.0 < q^2 < 7.0$	0.0041	0.001	0.0004	0.0013	0.0012	0.0016	0.0009	0.0001	0.0003	0.0001
$7.0 < q^2 < 8.0$	0.0033	0.0008	0.0002	0.0006	0.0014	0.0015	0.0008	0.0003	0.0003	0.0001
$11.0 < q^2 < 11.75$	0.0015	0.0015	0.0003	0.0019	0.0011	0.0008	0.0015	0.0014	0.0002	0.0001
$11.75 < q^2 < 12.5$	0.0004	0.0011	0.0002	0.001	0.0008	0.0001	0.0014	0.001	0.0002	0.0001
$15.0 < q^2 < 16.0$	0.0016	0.0018	0.0008	0.0022	0.0014	0.0002	0.002	0.002	0.0003	0.0001
$16.0 < q^2 < 17.0$	0.0029	0.0001	0.0004	0.0006	0.0004	0.0024	0.0021	0.0017	0.0001	0.0001
$17.0 < q^2 < 18.0$	0.006	0.0024	0.0012	0.003	0.0023	0.0048	0.0001	0.0006	0.0005	0.0001
$18.0 < q^2 < 19.0$	0.001	0.0011	0.0003	0.0013	0.0001	0.0024	0.0045	0.003	0.0001	0.0001
$15.0 < q^2 < 19.0$	0.0019	0.0001	0.0001	0.0001	0.0003	0.0022	0.0006	0.0008	0.0001	0.0001
$1.1 < q^2 < 2.5$	0.0019	0.0007	0.0005	0.0026	0.0029	0.0018	0.0018	0.0004	0.0007	0.0002
$2.5 < q^2 < 4.0$	0.0002	0.0004	0.0003	0.0012	0.0005	0.0004	0.0006	0.0011	0.0001	0.0001
$4.0 < q^2 < 6.0$	0.0024	0.0002	0.0001	0.001	0.0004	0.0001	0.0004	0.0003	0.0001	0.0001
$6.0 < q^2 < 8.0$	0.0037	0.0009	0.0003	0.0009	0.0013	0.0015	0.0009	0.0001	0.0003	0.0001
$11.0 < q^2 < 12.5$	0.001	0.0013	0.0003	0.0014	0.0009	0.0005	0.0014	0.0012	0.0002	0.0001
$15.0 < q^2 < 17.0$	0.0005	0.0009	0.0006	0.0009	0.0005	0.001	0.0021	0.0018	0.0001	0.0001
$17.0 < q^2 < 19.0$	0.004	0.0018	0.0007	0.0012	0.0015	0.0039	0.0017	0.0008	0.0003	0.0001

10.2.6 Systematic uncertainty on $m(K^+\pi^-)$ lineshape

The $m_{K\pi}$ invariant mass distribution is used in the small $1\,\mathrm{GeV}^2/c^4$ to determine the S-wave fraction F_S. The $m_{K\pi}$ mass model is parametrized with the LASS model. The uncertainty on the using the ISOBAR model instead of LASS has been evaluated in Sec. 10.1.8 and found negligibly small.

Table 106: Systematic effect of the signal mass model for the P_i observables.

q^2	F_{L}	P_1	P_2	P_3	P'_4	P'_5	P'_6	P'_8
$0.1 < q^2 < 0.98$	0.0011	0.0071	0.0021	0.002	0.0006	0.008	0.0096	0.0001
$1.1 < q^2 < 2.0$	0.0024	0.0044	0.0032	0.0003	0.0015	0.0053	0.0041	0.0047
$2.0 < q^2 < 3.0$	0.0002	0.0003	0.0037	0.0038	0.0003	0.0056	0.0018	0.0002
$3.0 < q^2 < 4.0$	0.0001	0.0039	0.0002	0.0036	0.001	0.002	0.0018	0.0015
$4.0 < q^2 < 5.0$	0.0015	0.0011	0.0001	0.0015	0.0005	0.0024	0.0012	0.0003
$5.0 < q^2 < 6.0$	0.0033	0.0028	0.0011	0.0005	0.0004	0.0044	0.0014	0.0016
$6.0 < q^2 < 7.0$	0.0041	0.0043	0.0012	0.0001	0.0001	0.004	0.0032	0.0019
$7.0 < q^2 < 8.0$	0.0033	0.003	0.0006	0.0006	0.0001	0.0018	0.0029	0.0016
$11.0 < q^2 < 11.75$	0.0015	0.0043	0.0001	0.0023	0.0003	0.0032	0.0017	0.003
$11.75 < q^2 < 12.5$	0.0004	0.0033	0.0006	0.0016	0.0003	0.0018	0.0003	0.0029
$15.0 < q^2 < 16.0$	0.0016	0.0044	0.0003	0.003	0.0011	0.0038	0.0005	0.0042
$16.0 < q^2 < 17.0$	0.0029	0.0021	0.0015	0.0026	0.002	0.0002	0.0051	0.0045
$17.0 < q^2 < 18.0$	0.006	0.0018	0.0012	0.0009	0.0002	0.0037	0.0102	0.0003
$18.0 < q^2 < 19.0$	0.001	0.0022	0.0004	0.0044	0.0012	0.0031	0.0052	0.0097
$15.0 < q^2 < 19.0$	0.0019	0.0012	0.0008	0.0012	0.001	0.0011	0.0045	0.0012
$1.1 < q^2 < 2.5$	0.0019	0.0037	0.0035	0.0011	0.0012	0.0055	0.0037	0.0036
$2.5 < q^2 < 4.0$	0.0002	0.003	0.0012	0.0039	0.0007	0.0027	0.001	0.0013
$4.0 < q^2 < 6.0$	0.0024	0.001	0.0004	0.001	0.0005	0.0035	0.0002	0.001
$6.0 < q^2 < 8.0$	0.0037	0.0036	0.0009	0.0003	0.0001	0.0028	0.0031	0.0017
$11.0 < q^2 < 12.5$	0.001	0.0038	0.0003	0.0019	0.0003	0.0025	0.001	0.003
$15.0 < q^2 < 17.0$	0.0005	0.0032	0.0009	0.0028	0.0015	0.0021	0.0022	0.0043
$17.0 < q^2 < 19.0$	0.004	0.0014	0.0006	0.0012	0.0006	0.0009	0.0082	0.0036

10.2.7 Systematic uncertainty from production and detection asymmetries

The observables S_i and A_i are sensitive to production and detection asymmetries according to

$$\begin{aligned} A_i^{\text{measured}} &= A_i - S_i\mathcal{A}_{\text{det.}} - S_i(\kappa\mathcal{A}_{\text{prod.}}), \\ S_i^{\text{measured}} &= S_i - A_i\mathcal{A}_{\text{det.}} - A_i(\kappa\mathcal{A}_{\text{prod.}}), \end{aligned}$$

where, as described in details in Sec. 10.1.9, κ is a dilution factor due to $B^0 - \overline{B}^0$ mixing and is estimated to be $\kappa = 35.2\%$. The uncertainty due to production and detection asymmetries is negligibly small, as can be seen in Tables 108, 109 and 110.

10.2.8 Summary on systematic uncertainties

The various systematic uncertainties are summed in quadrature in order to get the total systematic uncertainties in each q^2-bin. The total systematic uncertainties are shown in Tab. 111, 112 and 113. They are always small with respect to the statistical uncertainty.

Table 107: Systematic effect of the signal mass model for the A_i observables.

q^2	A_3	A_4	A_5	$A(A_{\rm FB})$	A_7	A_8	A_9	A_{6s}	A_{6c}
$0.1 < q^2 < 0.98$	0.0028	0.0001	0.0037	0.0025	0.0039	0.0001	0.0016	0.0006	0.0002
$1.1 < q^2 < 2.0$	0.0009	0.0007	0.0025	0.0032	0.002	0.0023	0.0001	0.0007	0.0002
$2.0 < q^2 < 3.0$	0.0001	0.0001	0.0025	0.0018	0.0008	0.0001	0.0011	0.0004	0.0001
$3.0 < q^2 < 4.0$	0.0006	0.0005	0.0009	0.0001	0.0008	0.0007	0.001	0.0001	0.0001
$4.0 < q^2 < 5.0$	0.0001	0.0001	0.0007	0.0002	0.0005	0.0001	0.0005	0.0001	0.0001
$5.0 < q^2 < 6.0$	0.0006	0.0002	0.0014	0.0005	0.0007	0.0007	0.0001	0.0001	0.0001
$6.0 < q^2 < 7.0$	0.001	0.0004	0.0013	0.0012	0.0016	0.0009	0.0001	0.0003	0.0001
$7.0 < q^2 < 8.0$	0.0008	0.0002	0.0006	0.0014	0.0015	0.0008	0.0003	0.0003	0.0001
$11.0 < q^2 < 11.75$	0.0015	0.0003	0.0019	0.0011	0.0008	0.0015	0.0014	0.0002	0.0001
$11.75 < q^2 < 12.5$	0.0011	0.0002	0.001	0.0008	0.0001	0.0014	0.001	0.0002	0.0001
$15.0 < q^2 < 16.0$	0.0018	0.0008	0.0022	0.0014	0.0002	0.002	0.002	0.0003	0.0001
$16.0 < q^2 < 17.0$	0.0001	0.0004	0.0006	0.0004	0.0024	0.0021	0.0017	0.0001	0.0001
$17.0 < q^2 < 18.0$	0.0024	0.0012	0.003	0.0023	0.0048	0.0001	0.0006	0.0005	0.0001
$18.0 < q^2 < 19.0$	0.0011	0.0003	0.0013	0.0001	0.0024	0.0045	0.003	0.0001	0.0001
$15.0 < q^2 < 19.0$	0.0001	0.0001	0.0001	0.0003	0.0022	0.0006	0.0008	0.0001	0.0001
$1.1 < q^2 < 2.5$	0.0007	0.0005	0.0026	0.0029	0.0018	0.0018	0.0004	0.0007	0.0002
$2.5 < q^2 < 4.0$	0.0004	0.0003	0.0012	0.0005	0.0004	0.0006	0.0011	0.0001	0.0001
$4.0 < q^2 < 6.0$	0.0002	0.0001	0.001	0.0004	0.0001	0.0004	0.0003	0.0001	0.0001
$6.0 < q^2 < 8.0$	0.0009	0.0003	0.0009	0.0013	0.0015	0.0009	0.0001	0.0003	0.0001
$11.0 < q^2 < 12.5$	0.0013	0.0003	0.0014	0.0009	0.0005	0.0014	0.0012	0.0002	0.0001
$15.0 < q^2 < 17.0$	0.0009	0.0006	0.0009	0.0005	0.001	0.0021	0.0018	0.0001	0.0001
$17.0 < q^2 < 19.0$	0.0018	0.0007	0.0012	0.0015	0.0039	0.0017	0.0008	0.0003	0.0001

Table 108: Systematic effect the detector and production assymetry for the S_i observables.

q^2	F_{L}	S_3	S_4	S_5	A_{FB}	S_7	S_8	S_9	S_{6s}	S_{6c}
$0.1 < q^2 < 0.98$	0.0	0.0	0.0001	0.0003	0.0001	0.0	0.0	0.0	0.0	0.0
$1.1 < q^2 < 2.0$	0.0	0.0	0.0001	0.0002	0.0003	0.0001	0.0	0.0	0.0001	0.0
$2.0 < q^2 < 3.0$	0.0	0.0	0.0001	0.0	0.0002	0.0001	0.0	0.0	0.0	0.0
$3.0 < q^2 < 4.0$	0.0	0.0	0.0002	0.0003	0.0001	0.0	0.0	0.0	0.0	0.0
$4.0 < q^2 < 5.0$	0.0	0.0	0.0002	0.0004	0.0	0.0	0.0	0.0	0.0	0.0
$5.0 < q^2 < 6.0$	0.0	0.0	0.0003	0.0005	0.0002	0.0	0.0	0.0	0.0	0.0
$6.0 < q^2 < 7.0$	0.0	0.0	0.0003	0.0006	0.0003	0.0	0.0	0.0	0.0001	0.0
$7.0 < q^2 < 8.0$	0.0	0.0	0.0003	0.0006	0.0003	0.0	0.0	0.0	0.0001	0.0
$11.0 < q^2 < 11.75$	0.0	0.0001	0.0004	0.0006	0.0006	0.0	0.0	0.0	0.0001	0.0
$11.75 < q^2 < 12.5$	0.0	0.0001	0.0004	0.0006	0.0006	0.0	0.0	0.0	0.0001	0.0
$15.0 < q^2 < 16.0$	0.0	0.0002	0.0004	0.0005	0.0006	0.0	0.0	0.0	0.0001	0.0
$16.0 < q^2 < 17.0$	0.0	0.0002	0.0004	0.0005	0.0006	0.0	0.0	0.0	0.0001	0.0
$17.0 < q^2 < 18.0$	0.0	0.0003	0.0004	0.0004	0.0005	0.0	0.0	0.0	0.0001	0.0
$18.0 < q^2 < 19.0$	0.0	0.0004	0.0004	0.0003	0.0004	0.0	0.0	0.0	0.0001	0.0
$15.0 < q^2 < 19.0$	0.0	0.0002	0.0004	0.0004	0.0005	0.0	0.0	0.0	0.0001	0.0
$1.1 < q^2 < 2.5$	0.0	0.0	0.0	0.0002	0.0003	0.0001	0.0	0.0	0.0001	0.0
$2.5 < q^2 < 4.0$	0.0	0.0	0.0001	0.0002	0.0001	0.0	0.0	0.0	0.0	0.0
$4.0 < q^2 < 6.0$	0.0	0.0	0.0003	0.0005	0.0001	0.0	0.0	0.0	0.0	0.0
$6.0 < q^2 < 8.0$	0.0	0.0	0.0003	0.0006	0.0003	0.0	0.0	0.0	0.0001	0.0
$11.0 < q^2 < 12.5$	0.0	0.0001	0.0004	0.0006	0.0006	0.0	0.0	0.0	0.0001	0.0
$15.0 < q^2 < 17.0$	0.0	0.0002	0.0004	0.0005	0.0006	0.0	0.0	0.0	0.0001	0.0
$17.0 < q^2 < 19.0$	0.0	0.0003	0.0004	0.0004	0.0005	0.0	0.0	0.0	0.0001	0.0

Table 109: Systematic effect the detector and production assymetry for the P_i observables.

q^2	F_{L}	P_1	P_2	P_3	P_4'	P_5'	P_6'	P_8'
$0.1 < q^2 < 0.98$	0.0	0.0	0.0001	0.0	0.0003	0.0008	0.0001	0.0
$1.1 < q^2 < 2.0$	0.0	0.0	0.0004	0.0	0.0002	0.0005	0.0001	0.0
$2.0 < q^2 < 3.0$	0.0	0.0	0.0005	0.0	0.0001	0.0001	0.0001	0.0
$3.0 < q^2 < 4.0$	0.0	0.0	0.0002	0.0	0.0004	0.0006	0.0001	0.0
$4.0 < q^2 < 5.0$	0.0	0.0001	0.0001	0.0	0.0005	0.0009	0.0001	0.0
$5.0 < q^2 < 6.0$	0.0	0.0001	0.0003	0.0	0.0006	0.0011	0.0001	0.0
$6.0 < q^2 < 7.0$	0.0	0.0001	0.0004	0.0	0.0007	0.0012	0.0001	0.0
$7.0 < q^2 < 8.0$	0.0	0.0001	0.0005	0.0	0.0007	0.0012	0.0001	0.0
$11.0 < q^2 < 11.75$	0.0	0.0003	0.0006	0.0	0.0007	0.0012	0.0	0.0
$11.75 < q^2 < 12.5$	0.0	0.0003	0.0006	0.0	0.0007	0.0012	0.0	0.0
$15.0 < q^2 < 16.0$	0.0	0.0005	0.0006	0.0	0.0008	0.001	0.0	0.0
$16.0 < q^2 < 17.0$	0.0	0.0006	0.0006	0.0	0.0008	0.001	0.0	0.0
$17.0 < q^2 < 18.0$	0.0	0.0008	0.0005	0.0	0.0009	0.0008	0.0	0.0
$18.0 < q^2 < 19.0$	0.0	0.0011	0.0004	0.0	0.0009	0.0006	0.0	0.0
$15.0 < q^2 < 19.0$	0.0	0.0007	0.0006	0.0	0.0008	0.0009	0.0	0.0
$1.1 < q^2 < 2.5$	0.0	0.0	0.0005	0.0	0.0001	0.0004	0.0001	0.0
$2.5 < q^2 < 4.0$	0.0	0.0	0.0003	0.0	0.0003	0.0005	0.0001	0.0
$4.0 < q^2 < 6.0$	0.0	0.0001	0.0002	0.0	0.0006	0.001	0.0001	0.0
$6.0 < q^2 < 8.0$	0.0	0.0001	0.0005	0.0	0.0007	0.0012	0.0001	0.0
$11.0 < q^2 < 12.5$	0.0	0.0003	0.0006	0.0	0.0007	0.0012	0.0	0.0
$15.0 < q^2 < 17.0$	0.0	0.0006	0.0006	0.0	0.0008	0.001	0.0	0.0
$17.0 < q^2 < 19.0$	0.0	0.0009	0.0005	0.0	0.0009	0.0008	0.0	0.0

Table 110: Systematic effect the detector and production assymetry for the A_i observables.

q^2	A_3	A_4	A_5	$A(A_{\mathrm{FB}})$	A_7	A_8	A_9	A_{6s}	A_{6c}
$0.1 < q^2 < 0.98$	0.0	0.0001	0.0003	0.0001	0.0	0.0	0.0	0.0	0.0
$1.1 < q^2 < 2.0$	0.0	0.0001	0.0002	0.0003	0.0001	0.0	0.0	0.0001	0.0
$2.0 < q^2 < 3.0$	0.0	0.0001	0.0	0.0002	0.0001	0.0	0.0	0.0	0.0
$3.0 < q^2 < 4.0$	0.0	0.0002	0.0003	0.0001	0.0	0.0	0.0	0.0	0.0
$4.0 < q^2 < 5.0$	0.0	0.0002	0.0004	0.0	0.0	0.0	0.0	0.0	0.0
$5.0 < q^2 < 6.0$	0.0	0.0003	0.0005	0.0002	0.0	0.0	0.0	0.0	0.0
$6.0 < q^2 < 7.0$	0.0	0.0003	0.0006	0.0003	0.0	0.0	0.0	0.0001	0.0
$7.0 < q^2 < 8.0$	0.0	0.0003	0.0006	0.0003	0.0	0.0	0.0	0.0001	0.0
$11.0 < q^2 < 11.75$	0.0001	0.0004	0.0006	0.0006	0.0	0.0	0.0	0.0001	0.0
$11.75 < q^2 < 12.5$	0.0001	0.0004	0.0006	0.0006	0.0	0.0	0.0	0.0001	0.0
$15.0 < q^2 < 16.0$	0.0002	0.0004	0.0005	0.0006	0.0	0.0	0.0	0.0001	0.0
$16.0 < q^2 < 17.0$	0.0002	0.0004	0.0005	0.0006	0.0	0.0	0.0	0.0001	0.0
$17.0 < q^2 < 18.0$	0.0003	0.0004	0.0004	0.0005	0.0	0.0	0.0	0.0001	0.0
$18.0 < q^2 < 19.0$	0.0004	0.0004	0.0003	0.0004	0.0	0.0	0.0	0.0001	0.0
$15.0 < q^2 < 19.0$	0.0002	0.0004	0.0004	0.0005	0.0	0.0	0.0	0.0001	0.0
$1.1 < q^2 < 2.5$	0.0	0.0	0.0002	0.0003	0.0001	0.0	0.0	0.0001	0.0
$2.5 < q^2 < 4.0$	0.0	0.0001	0.0002	0.0001	0.0	0.0	0.0	0.0	0.0
$4.0 < q^2 < 6.0$	0.0	0.0003	0.0005	0.0001	0.0	0.0	0.0	0.0	0.0
$6.0 < q^2 < 8.0$	0.0	0.0003	0.0006	0.0003	0.0	0.0	0.0	0.0001	0.0
$11.0 < q^2 < 12.5$	0.0001	0.0004	0.0006	0.0006	0.0	0.0	0.0	0.0001	0.0
$15.0 < q^2 < 17.0$	0.0002	0.0004	0.0005	0.0006	0.0	0.0	0.0	0.0001	0.0
$17.0 < q^2 < 19.0$	0.0003	0.0004	0.0004	0.0005	0.0	0.0	0.0	0.0001	0.0

Table 111: Total systematic effect for the S_i observables.

q^2	F_L	S_3	S_4	S_5	A_{FB}	S_7	S_8	S_9	S_{6s}	S_{6c}
$0.1 < q^2 < 0.98$	0.0259	0.0077	0.0147	0.0111	0.0719	0.0092	0.0093	0.0038	0.0158	0.0045
$1.1 < q^2 < 2.0$	0.0251	0.0071	0.0265	0.0093	0.0119	0.0047	0.0056	0.0005	0.007	0.0025
$2.0 < q^2 < 3.0$	0.0231	0.0073	0.0413	0.0086	0.0077	0.0021	0.0057	0.0032	0.0038	0.0014
$3.0 < q^2 < 4.0$	0.0228	0.0078	0.0455	0.0042	0.0023	0.0022	0.0022	0.0023	0.0006	0.0004
$4.0 < q^2 < 5.0$	0.0232	0.0073	0.0466	0.0035	0.0038	0.0014	0.0028	0.0012	0.001	0.0005
$5.0 < q^2 < 6.0$	0.0246	0.0087	0.0477	0.0042	0.0061	0.0019	0.0026	0.0008	0.003	0.001
$6.0 < q^2 < 7.0$	0.0253	0.0044	0.0517	0.0078	0.0092	0.0038	0.0022	0.0011	0.0055	0.0017
$7.0 < q^2 < 8.0$	0.0245	0.0047	0.0583	0.0071	0.0117	0.0034	0.0022	0.0011	0.008	0.0024
$11.0 < q^2 < 11.75$	0.0217	0.0081	0.0625	0.0131	0.0149	0.0019	0.0033	0.0031	0.0033	0.0032
$11.75 < q^2 < 12.5$	0.0184	0.0078	0.0558	0.012	0.0142	0.0019	0.0033	0.0022	0.0031	0.0035
$15.0 < q^2 < 16.0$	0.0133	0.006	0.0067	0.0055	0.0088	0.0017	0.0045	0.0045	0.0019	0.0038
$16.0 < q^2 < 17.0$	0.0127	0.0067	0.0294	0.0096	0.0072	0.0054	0.0048	0.0038	0.0016	0.0034
$17.0 < q^2 < 18.0$	0.0166	0.0107	0.0454	0.0154	0.0075	0.0108	0.0006	0.0016	0.0016	0.0027
$18.0 < q^2 < 19.0$	0.0131	0.0116	0.0585	0.0146	0.0118	0.0055	0.0102	0.0067	0.0051	0.0014
$15.0 < q^2 < 19.0$	0.0112	0.012	0.027	0.0068	0.0069	0.0135	0.0089	0.0142	0.0015	0.0032
$1.1 < q^2 < 2.5$	0.0246	0.0066	0.0303	0.009	0.0111	0.0042	0.0043	0.0012	0.0063	0.0023
$2.5 < q^2 < 4.0$	0.0228	0.0081	0.0451	0.0048	0.0052	0.0017	0.0014	0.0028	0.0013	0.0006
$4.0 < q^2 < 6.0$	0.0239	0.0079	0.0471	0.0036	0.0093	0.0008	0.0011	0.0008	0.0022	0.0008
$6.0 < q^2 < 8.0$	0.0249	0.0045	0.0551	0.0074	0.0105	0.0036	0.002	0.0011	0.0069	0.0021
$11.0 < q^2 < 12.5$	0.0189	0.0079	0.0591	0.0125	0.0146	0.0015	0.0033	0.0027	0.0032	0.0033
$15.0 < q^2 < 17.0$	0.0119	0.0057	0.0173	0.0095	0.0077	0.0024	0.0046	0.0041	0.0016	0.0036
$17.0 < q^2 < 19.0$	0.0162	0.0108	0.0505	0.0169	0.0072	0.0087	0.0038	0.002	0.0084	0.0022

Table 112: Total systematic effect for the P_i observables.

q^2	F_{L}	P_1	P_2	P_3	P_4'	P_5'	P_6'	P_8'
$0.1 < q^2 < 0.98$	0.0259	0.0196	0.0625	0.0048	0.0262	0.0229	0.0239	0.0222
$1.1 < q^2 < 2.0$	0.0251	0.0115	0.0172	0.0014	0.0569	0.0166	0.0093	0.0116
$2.0 < q^2 < 3.0$	0.0231	0.0069	0.0333	0.0117	0.0992	0.0191	0.005	0.002
$3.0 < q^2 < 4.0$	0.0228	0.0182	0.0148	0.0088	0.1075	0.0229	0.007	0.0061
$4.0 < q^2 < 5.0$	0.0232	0.0242	0.0097	0.0065	0.1042	0.0223	0.0063	0.0058
$5.0 < q^2 < 6.0$	0.0246	0.0252	0.0117	0.0073	0.1011	0.0183	0.0054	0.0061
$6.0 < q^2 < 7.0$	0.0253	0.0262	0.013	0.0009	0.1064	0.0147	0.0073	0.0045
$7.0 < q^2 < 8.0$	0.0245	0.0248	0.0125	0.0016	0.1177	0.0099	0.0066	0.0047
$11.0 < q^2 < 11.75$	0.0217	0.03	0.0133	0.0052	0.1282	0.0278	0.004	0.0069
$11.75 < q^2 < 12.5$	0.0184	0.0302	0.0081	0.0036	0.1143	0.0264	0.0035	0.0066
$15.0 < q^2 < 16.0$	0.0133	0.0136	0.0052	0.0069	0.0134	0.0126	0.004	0.0098
$16.0 < q^2 < 17.0$	0.0127	0.0135	0.0073	0.0064	0.0551	0.0144	0.0122	0.0101
$17.0 < q^2 < 18.0$	0.0166	0.0191	0.0057	0.0021	0.0922	0.0274	0.0229	0.0009
$18.0 < q^2 < 19.0$	0.0131	0.0215	0.0113	0.0099	0.1189	0.0286	0.0117	0.022
$15.0 < q^2 < 19.0$	0.0112	0.0277	0.0104	0.0186	0.0545	0.0159	0.0315	0.021
$1.1 < q^2 < 2.5$	0.0246	0.0102	0.0204	0.0028	0.0665	0.0168	0.0091	0.0086
$2.5 < q^2 < 4.0$	0.0228	0.0139	0.0202	0.011	0.1074	0.0211	0.0037	0.0036
$4.0 < q^2 < 6.0$	0.0239	0.0243	0.0093	0.0066	0.1023	0.0197	0.005	0.0025
$6.0 < q^2 < 8.0$	0.0249	0.0253	0.0127	0.0011	0.1122	0.011	0.0069	0.0044
$11.0 < q^2 < 12.5$	0.0189	0.0301	0.0085	0.0043	0.1212	0.027	0.0029	0.0067
$15.0 < q^2 < 17.0$	0.0119	0.0118	0.006	0.0066	0.0329	0.0106	0.0062	0.0097
$17.0 < q^2 < 19.0$	0.0162	0.0197	0.0087	0.0028	0.1027	0.0266	0.0185	0.0082

Table 113: Total systematic effect for the A_i observables.

q^2	A_3	A_4	A_5	$A(A_{\mathrm{FB}})$	A_7	A_8	A_9	A_{6s}	A_{6c}
$0.1 < q^2 < 0.98$	0.0072	0.0127	0.0112	0.0723	0.0096	0.0118	0.0089	0.0157	0.007
$1.1 < q^2 < 2.0$	0.0025	0.0275	0.0082	0.0118	0.0058	0.0081	0.0098	0.0052	0.0018
$2.0 < q^2 < 3.0$	0.0015	0.0416	0.0084	0.0077	0.0027	0.0058	0.007	0.0039	0.0013
$3.0 < q^2 < 4.0$	0.0074	0.0454	0.0046	0.0061	0.0032	0.0026	0.0029	0.0014	0.004
$4.0 < q^2 < 5.0$	0.0051	0.0466	0.0045	0.0048	0.003	0.0012	0.0081	0.0089	0.003
$5.0 < q^2 < 6.0$	0.0038	0.0477	0.0056	0.0061	0.0028	0.007	0.0022	0.0031	0.0084
$6.0 < q^2 < 7.0$	0.007	0.0517	0.0062	0.0091	0.0046	0.0031	0.0055	0.005	0.0018
$7.0 < q^2 < 8.0$	0.0046	0.0583	0.0067	0.0114	0.0036	0.0023	0.0027	0.006	0.0021
$11.0 < q^2 < 11.75$	0.0081	0.0625	0.0131	0.0149	0.0019	0.0033	0.0031	0.0033	0.0032
$11.75 < q^2 < 12.5$	0.0078	0.0558	0.012	0.0142	0.0019	0.0033	0.0022	0.0031	0.0035
$15.0 < q^2 < 16.0$	0.0052	0.0072	0.0065	0.007	0.0036	0.0048	0.0067	0.0097	0.0031
$16.0 < q^2 < 17.0$	0.0057	0.0278	0.008	0.0057	0.0058	0.0049	0.004	0.0097	0.0031
$17.0 < q^2 < 18.0$	0.0099	0.0454	0.0153	0.007	0.0108	0.0035	0.0062	0.009	0.0029
$18.0 < q^2 < 19.0$	0.0105	0.0585	0.0146	0.0121	0.006	0.0103	0.0069	0.0073	0.0023
$15.0 < q^2 < 19.0$	0.0113	0.0271	0.0075	0.0057	0.014	0.0098	0.0156	0.0091	0.0029
$1.1 < q^2 < 2.5$	0.0046	0.0306	0.0083	0.011	0.0057	0.0045	0.0057	0.0049	0.0017
$2.5 < q^2 < 4.0$	0.0088	0.045	0.005	0.0089	0.0018	0.0019	0.003	0.002	0.0057
$4.0 < q^2 < 6.0$	0.003	0.0472	0.0049	0.0093	0.0026	0.0041	0.0017	0.0022	0.0058
$6.0 < q^2 < 8.0$	0.0054	0.0551	0.0063	0.0104	0.0041	0.0027	0.004	0.0055	0.0019
$11.0 < q^2 < 12.5$	0.0079	0.0591	0.0125	0.0146	0.0015	0.0033	0.0027	0.0032	0.0033
$15.0 < q^2 < 17.0$	0.0047	0.0167	0.0055	0.0059	0.0026	0.0061	0.0098	0.0097	0.0031
$17.0 < q^2 < 19.0$	0.0098	0.0505	0.0141	0.0071	0.0128	0.0053	0.0035	0.0082	0.0027

10.3 Systematics for amplitude fits

The systematic uncertainties for the amplitude method are currently under investigation. Below we give an outline of systematic uncertainties specific for the amplitude fit.

10.3.1 Statistical uncertainty of the four-dimensional acceptance

The same procedure as described in Sec. 10.1.1, to estimate the systematic uncertainty arising form the statistical uncertainty in the acceptance correction. The effect of this systematic uncertainty on the observables in shown in Fig 94. The effect is negligible compared to the statistical uncertainty.

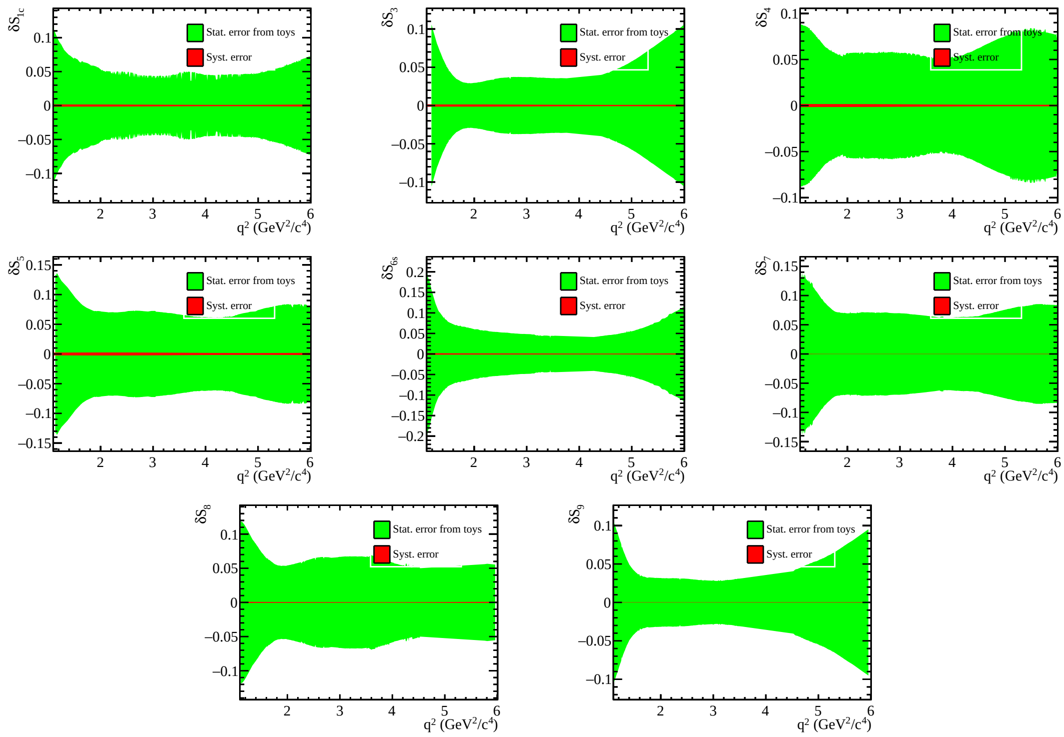

Figure 94: Systematic uncertainty on observables due to the statistical uncertainty of the four-dimensional acceptance correction.

10.3.2 Difference between data and simulation

As described in Sec. 10.1.2, the same procedure is used to estimate the systematic uncertainty due to the the ability of the simulation to model the Data. The effect of removing the corrections to the transverse momentum of the signal B^0, as well as the B^0 vertex χ^2 and the track multiplicity in the event, in terms of the observables is shown in Figs. 95, 96 and 97. The effect of this systematic uncertainty is negligible compared to the statistical uncertainty.

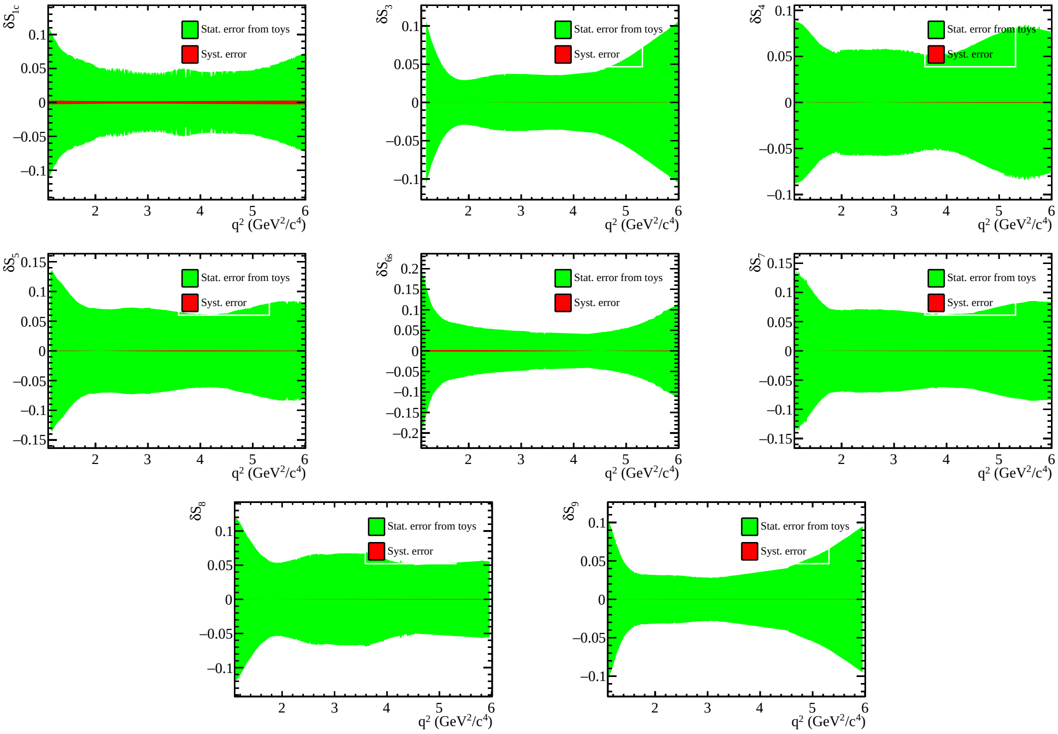

Figure 95: Systematic uncertainty on observables due to removing the reweighting of the transverse momentum of the signal B^0

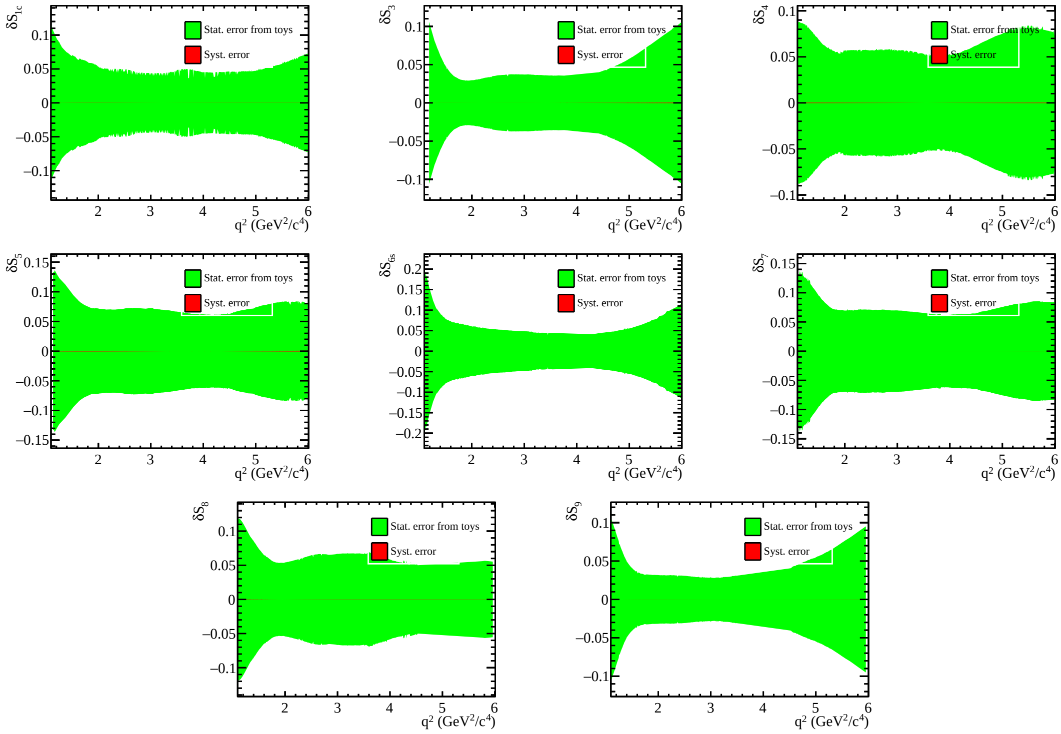

Figure 96: Systematic uncertainty on observables due to removing the reweighting of the vertex χ^2 of the signal B^0

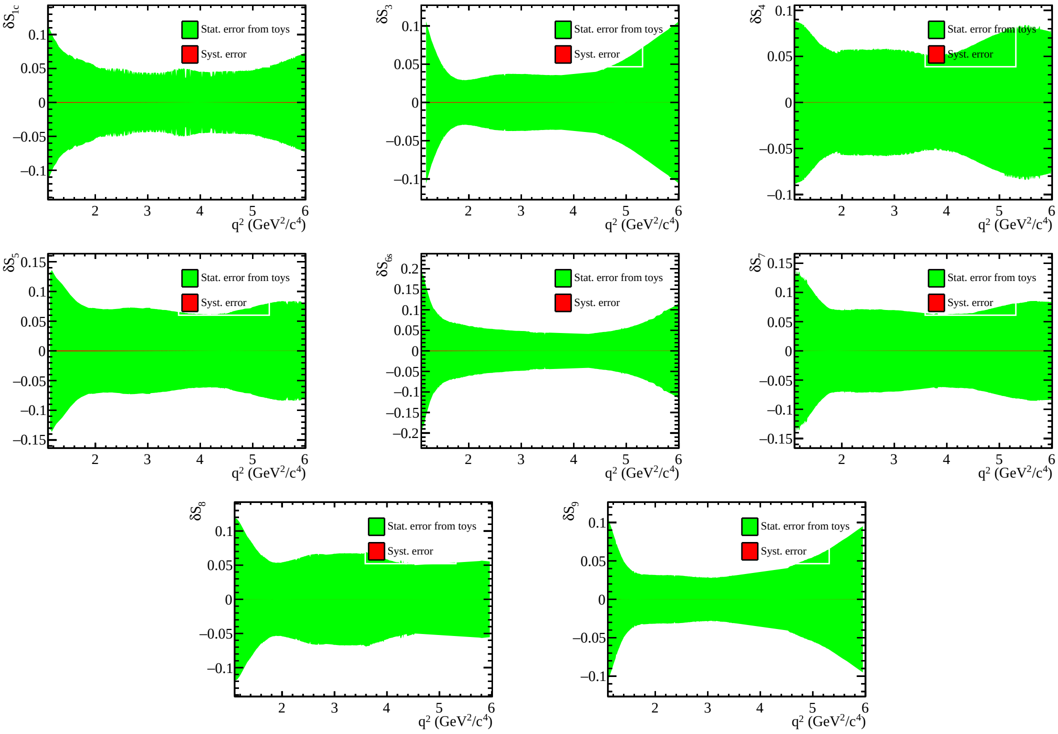

Figure 97: Systematic uncertainty on observables due to removing the reweighting of the track multiplicity of the event.

As with the fit to the observables, a systematic uncertainty for the residual Data-MC disagreement is obtained by reweighting in p, p_T of the Kaon and the Pion by comparing truth matched simulated events to $B^0 \to J/\psi\, K^{*0}$ data, as discussed in Sec. 10.1.2. The effect that the residual kinematic reweightings have on the observables are shown in Figures 98 and 99 for the Pion and Kaon momentum reweighting respectively.

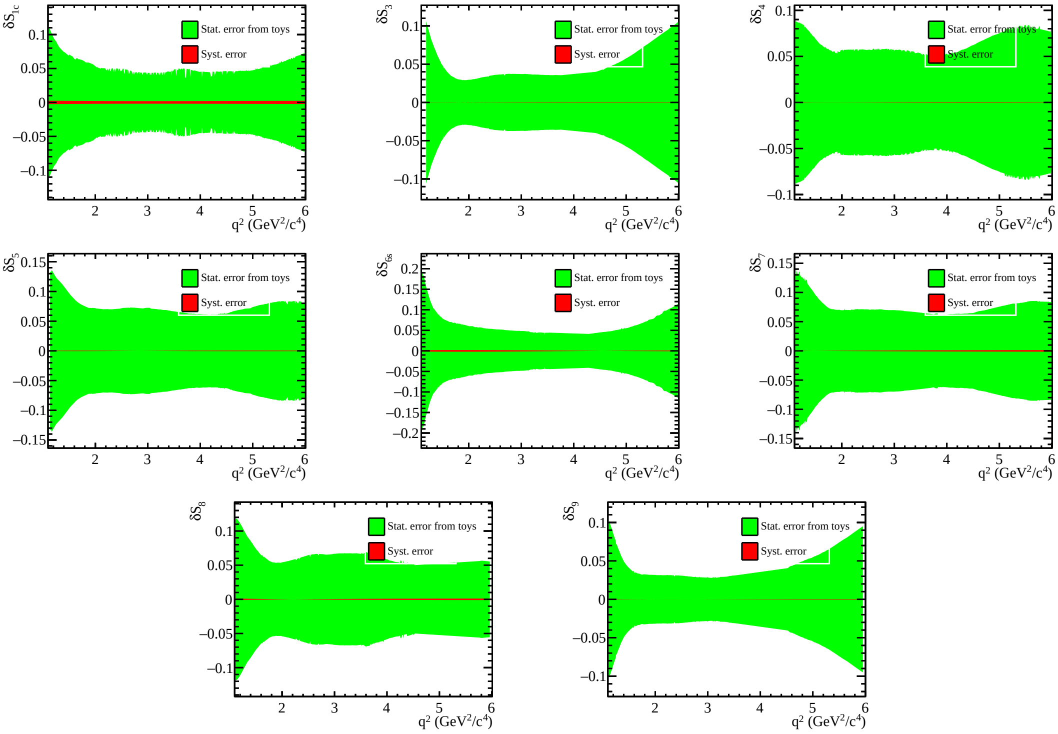

Figure 98: Systematic uncertainty on observables due to residual correction to the Kaon kinematics.

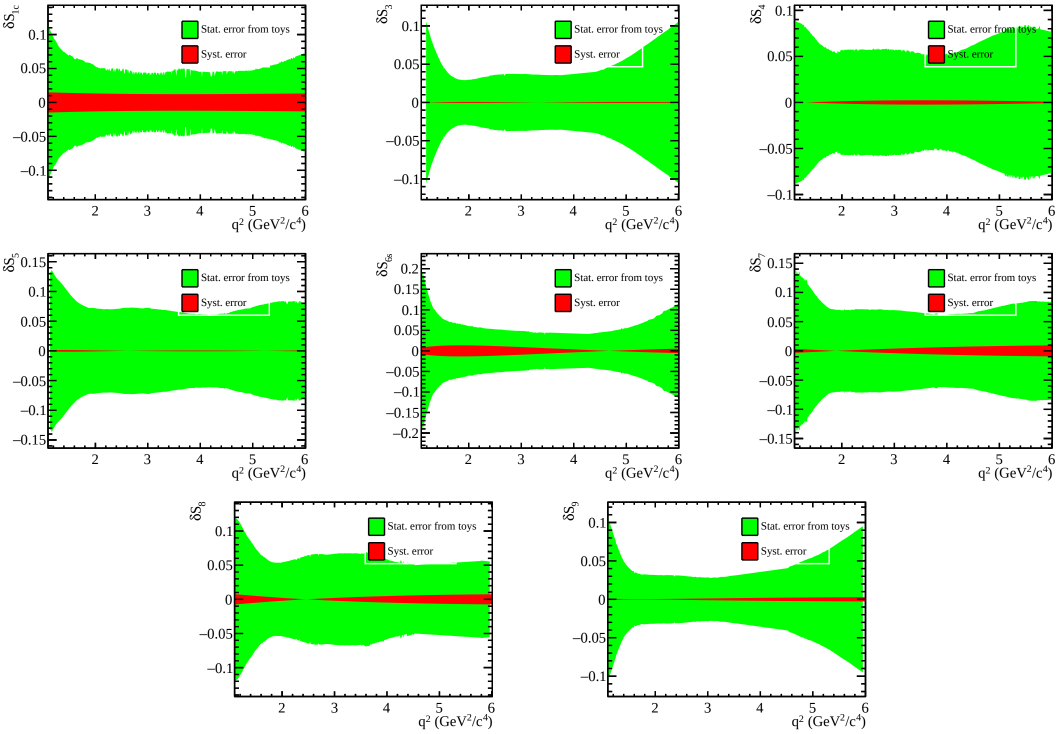

Figure 99: Systematic uncertainty on observables due to residual correction to the Pion kinematics.

Although the effect for the reweighting of the kaon kinematics is negligible compared to the statistical uncertainty, the pion kinematic reweighting introduces a systematic uncertainty up to 20% of the statistical. It is instructive to see the effect of this systematic uncertainty at the level of the amplitudes and derive a systematic for the amplitude coefficients. Figure 100 shows the systematic uncertainty due to the reweighting of the pion kinematics at the amplitude level.

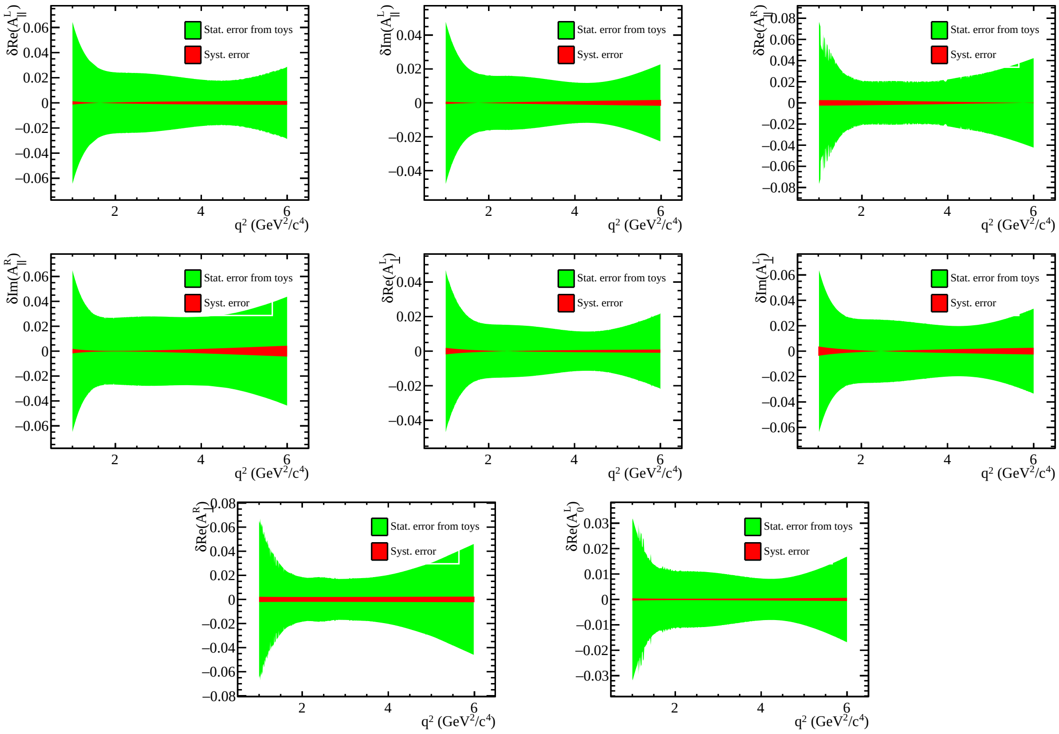

Figure 100: Systematic uncertainty on the $\overline{B}^0$ P-wave amplitudes due to residual correction to the Pion kinematics.

In order to obtain a systematic uncertainty in terms of the amplitude coefficients, the systematic uncertainty as a function of q^2 for each amplitude is fit using three parameter ansatz $\delta\alpha + \delta\beta q^2 + \gamma/q^2$. These $\delta\alpha$, $\delta\beta$ and $\delta\gamma$ can then be added in quadrature to the statistical uncertainty of the amplitude coefficients. Figure 101 shows the results of the three parameter ansatz fit to the q^2 dependent systematic uncertainty of all the $\overline{B}^0$ amplitudes. In some cases the resulting fit is not an exact match, however it is sufficient in order to obtain a good estimate of the systematic uncertainty in terms of the amplitude coefficients. The motivation behind this approach for obtaining the systematic uncertainty of the amplitude coefficients is due to the large correlation between the coefficients of a single amplitude (eg. see Fig. 32). This large correlation does not allow to simply take the difference of the amplitude coefficients directly from the resulting nominal and systematically varied fit.

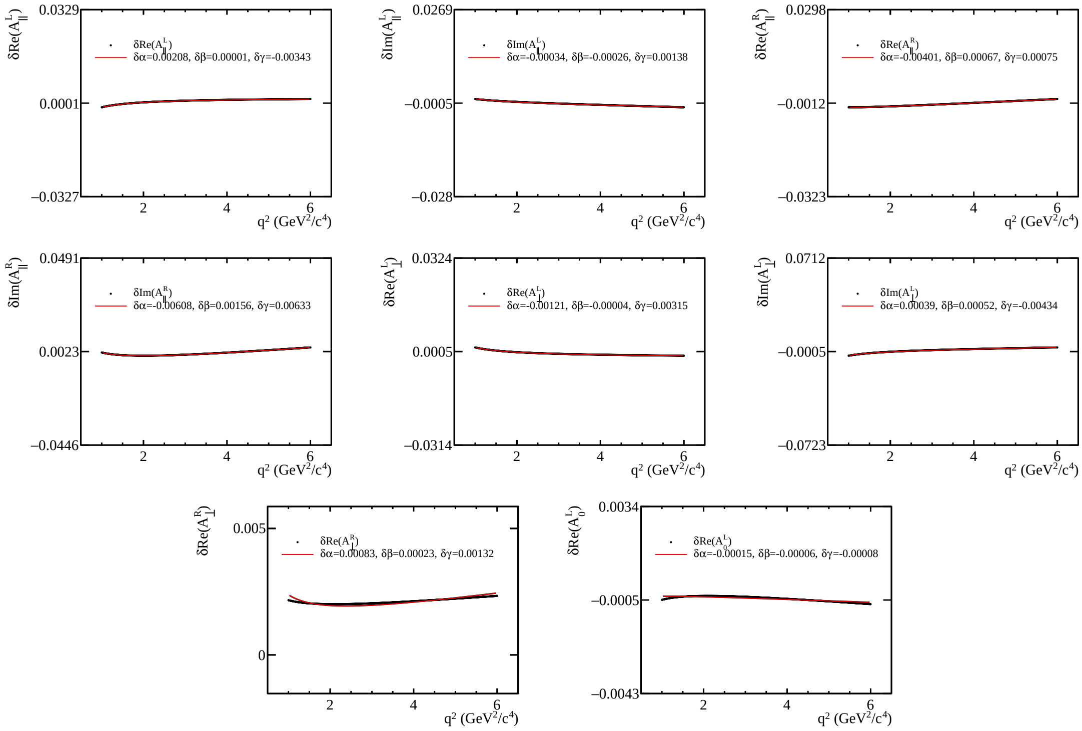

Figure 101: Systematic uncertainty on the $\overline{B}^0$ P-wave amplitudes due to the residual correction to the Pion kinematics. The q^2 dependence of the systematic uncertainty is fit back using the ansatz $\delta\alpha + \delta\beta q^2 + \delta\gamma/q^2$, in order to translate the uncertainty of the amplitude in terms of the amplitude coefficients.

10.3.3 Higher order acceptance model

Section 10.1.4 discusses the effect of the choice of the maximum order of the coefficients of the Legendre polynomial used to parametrise the four dimensional acceptance correction. Using the same treatment as the fits to the observables, the effect of this systematic is evaluated from amplitude fits to simulated toy data. The effect on the observables calculated from the fits to the amplitudes is shown in Fig. 102.

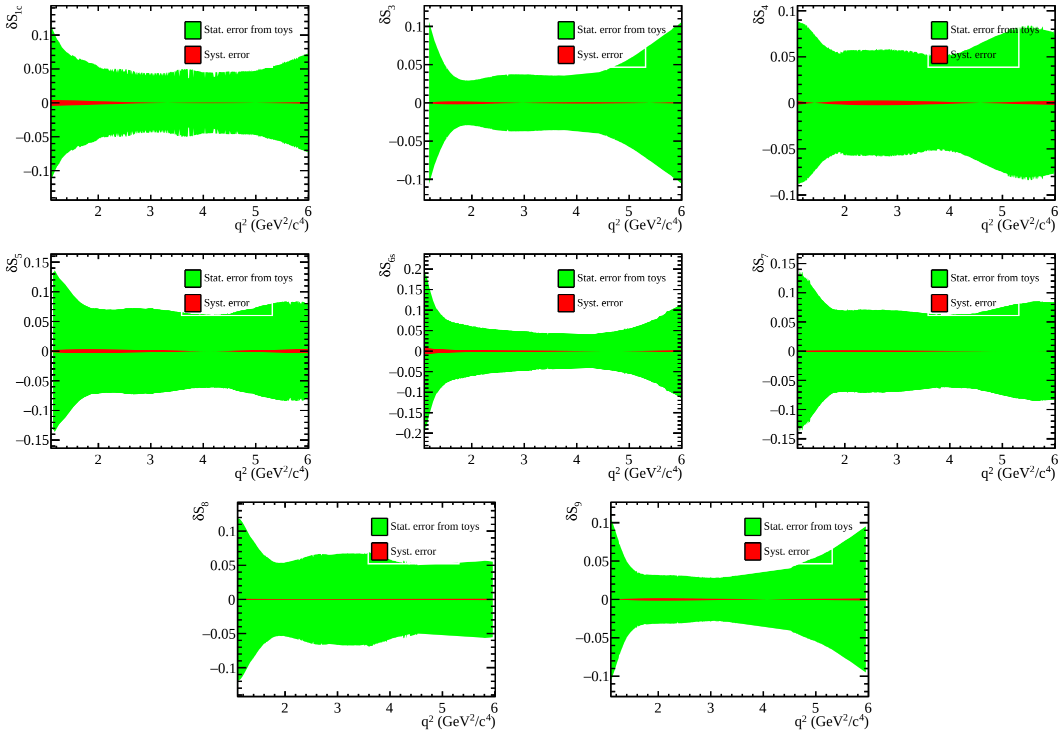

Figure 102: Systematic uncertainty on observables due to choice of the order of the Legendre polynomials used to parametrise the acceptance correction.

The effect of this systematic uncertainty is negligible compared to the statistical precision.

10.3.4 Uncertainty due to the combinatorial background model choice

The combinatorial background is parametrised using a product of four Chebychev polynomial distributions each up to second order as discussed in Sec. 6.4.8. The choice of this model was made by looking at the upper mass sideband data ($5350 < m_B < 5700$) that pass all selections, with $1.1 < q^2 < 6\ \mathrm{GeV}^2/c^4$ but with a slightly looser BDT in order to improve the statistical precision of the background model. Figure 103 shows the results of the fits to the four separate Chebychev polynomials. An equally valid parametrisation can be obtained using fourth order polynomials in $\cos\theta_\ell$ and $\cos\theta_K$, and third order in q^2. The second order parametrisation of the ϕ angle is sufficiently good not to motivate a higher order parametrisation. Figure 104 shows the variant combinatorial background model used to assess the systematic uncertainty.

The uncertainty due to the choice of the combinatorial background parametrisation on the amplitudes and observables, is assessed by generating high statistics toys according to the parametrisation of Fig. 104, and fitting back either with the same order or with the nominal one. The resulting differences on the amplitudes and therefore on the observables, between the two fits, give the systematic uncertainty. This is the same procedure as that

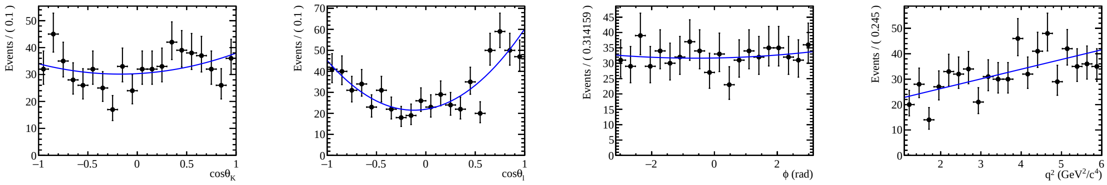

Figure 103: Fits to upper mass sideband data ($5350 < m_B < 5700$) that pass all selections, with $1 < q^2 < 6$ GeV$^2/c^4$. The blue distributions are Chebychev polynomials of second order in the angles and first order in q^2.

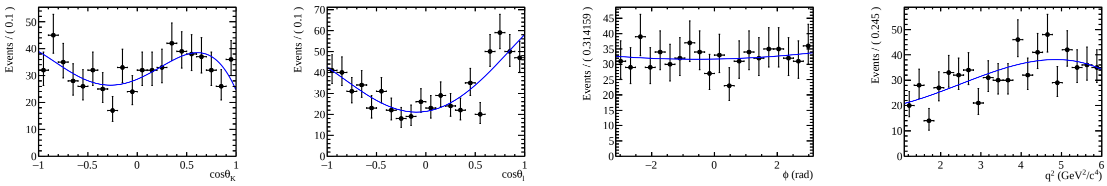

Figure 104: Fits to upper mass sideband data ($5350 < m_B < 5700$) that pass all selections, with $1 < q^2 < 6$ GeV$^2/c^4$. The blue distributions are Chebychev polynomials of fourth order in the angles and third order in q^2.

described in Sec. 10.1.6, with the addition of a q^2 dimension. The difference of the fits in terms of observables is shown in Fig. 105.

10.3.5 Uncertainty due to the $m_{K\pi}$ model choice

As the angular distribution is sensitive to bilinear combinations of the amplitudes, and the fit is performed over the bin of $796 < m_{K\pi} < 996$ MeV/c, fitting for the amplitudes would introduce a bias due to this $m_{K\pi}$ averaged result. In order to avoid this bias we adopt a model for the $m_{K\pi}$ dependence of the amplitudes and integrate over it as discussed in Sec. 6.4.6. Different $m_{K\pi}$ models result in different values for the integrals of the $m_{K\pi}$ dependence as shown in Tab. 29. The size of the dependence on the choice of the $m_{K\pi}$ model is assessed by comparing the values of the observables obtained from a fit to the amplitudes in $B^0 \to J/\psi K^{*0}$ events, using either an Isobar or a LASS parametrisation for the S-wave $m_{K\pi}$ shape. Table 114 summarises the different values obtained for $796 < m_{K\pi} < 996$ MeV/c^2. Accounting for the factor 1000 more signal candidates in $B^0 \to J/\psi K^{*0}$ (combining B^0 and $\overline{B}^0$ candidates) compared to the rare mode for $1 < q^2 < 6$ GeV/c^2 (separate for B^0 and $\overline{B}^0$) , the differences observed are at the level of 10% of the statistical uncertainty of the rare mode. The largest difference is seen for S_{S5}, however all S-wave terms are not parameters of interest and will be treated as nuisance parameters. It also must be noted that the systematic uncertainty due to the modelling of the $m_{K\pi}$ line-shape is insufficient to account for differences between fits to amplitudes and observables for S_4 and S_{S2}. As mentioned earlier however these differences are well below the statistical precision of the rare mode.

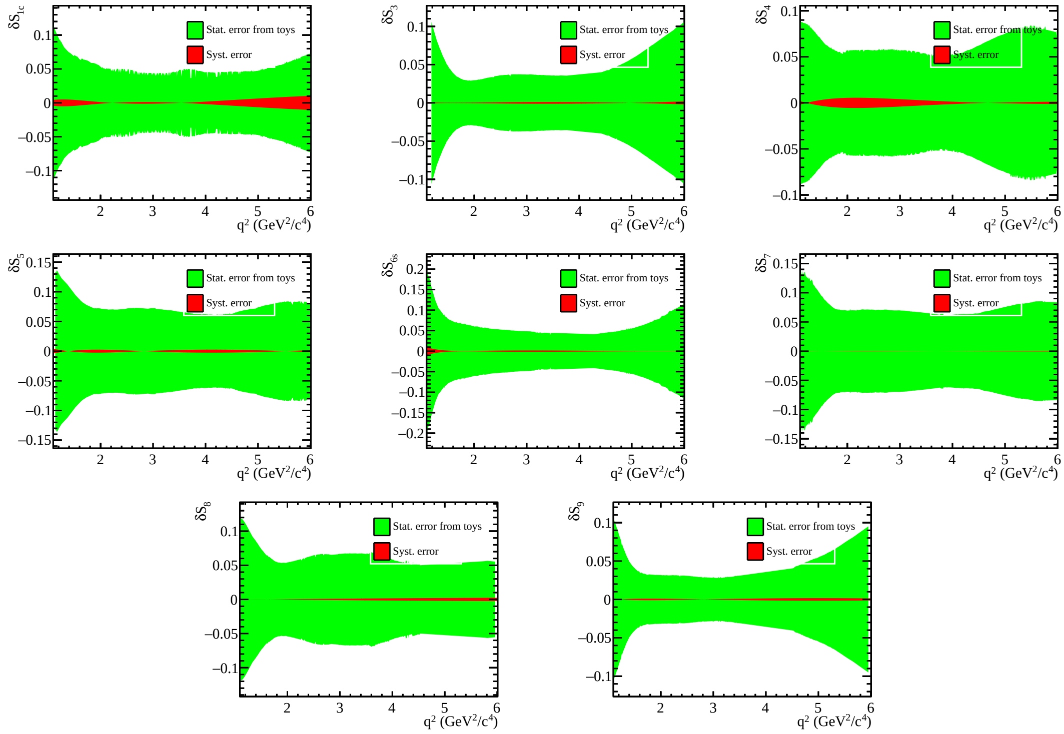

Figure 105: Systematic uncertainty on observables due to choice of the combinatorial background parametrisation as discussed in the main text.

10.3.6 Uncertainty due to residual peaking backgrounds

The systematic uncertainty due to the effect of residual peaking backgrounds follows the treatment of 10.1. Figure 106 shows 1D projections of the model used to describe the dominant peaking background components obtained from signal depleted/peaking enriched rare decay data. The high statistics toys where injected with these peaking backgrounds at a level dictated in Tab. 56.

The effect of the sum of the peaking background contributions to the observables is shown in Fig. 107. Their effect is found to be far below the statistical uncertainty.

Table 114: Comparison between the Isobar and LASS parametrisation when integrating over $m_{K\pi}$ in fits for $B^0 \to J/\psi K^{*0}$ for $m_{K\pi} \in [796, 996]\,\mathrm{MeV}/c^2$, using the full available data set corresponding to $3\,\mathrm{fb}^{-1}$. The last column shows the difference as a fraction of the expected statistical uncertainty in the rare mode for $1 < q^2 < 6\ \mathrm{GeV}/c^2$.

parameter	$m_{K\pi} \in [796, 996]\,\mathrm{MeV}/c^2$		
	Isobar	LASS	frac. of stat.
S_1^s	0.3318 ± 0.0009	0.3290 ± 0.0010	9%
S_3	-0.0154 ± 0.0015	-0.0133 ± 0.0016	4%
S_4	-0.2528 ± 0.0009	-0.2490 ± 0.0009	12%
S_5	-0.0026 ± 0.0018	-0.0017 ± 0.0019	1%
S_6^s	0.0041 ± 0.0015	0.0018 ± 0.0015	5%
S_7	-0.0027 ± 0.0019	0.0007 ± 0.0019	5%
S_8	-0.0560 ± 0.0017	-0.0496 ± 0.0017	12%
S_9	-0.0888 ± 0.0015	-0.0921 ± 0.0016	7%
F_S	0.0777 ± 0.0023	0.0846 ± 0.0024	9%
S_{S1}	-0.284 ± 0.0019	-0.287 ± 0.0019	0%
S_{S2}	0.021 ± 0.0021	0.020 ± 0.002	0%
S_{S3}	0.002 ± 0.0021	0.002 ± 0.002	0%
S_{S4}	-0.002 ± 0.0020	0.001 ± 0.002	4%
S_{S5}	-0.051 ± 0.0020	-0.040 ± 0.002	15%

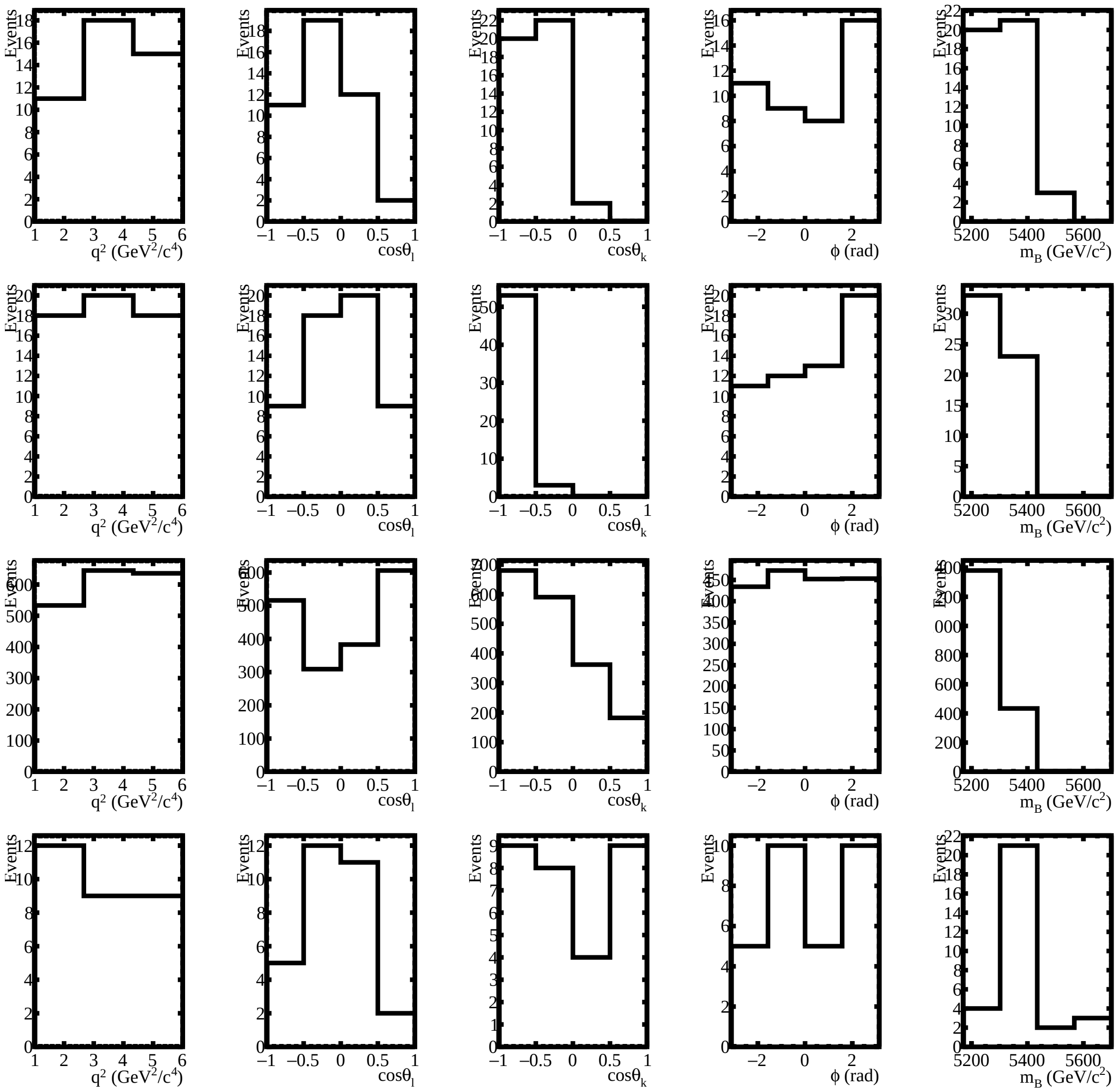

Figure 106: Projections of the models used in the generation of the toys containing the dominant peaking backgrounds. From top to bottom: $\Lambda_b \to pK\mu^+\mu^-$, $B_s \to \phi\mu^+\mu^-$, $B^0 \to K^{*0}\mu^+\mu^-$ with $K \leftrightarrow \pi$ swaps, $B \to \pi\pi\mu^+\mu^-$.

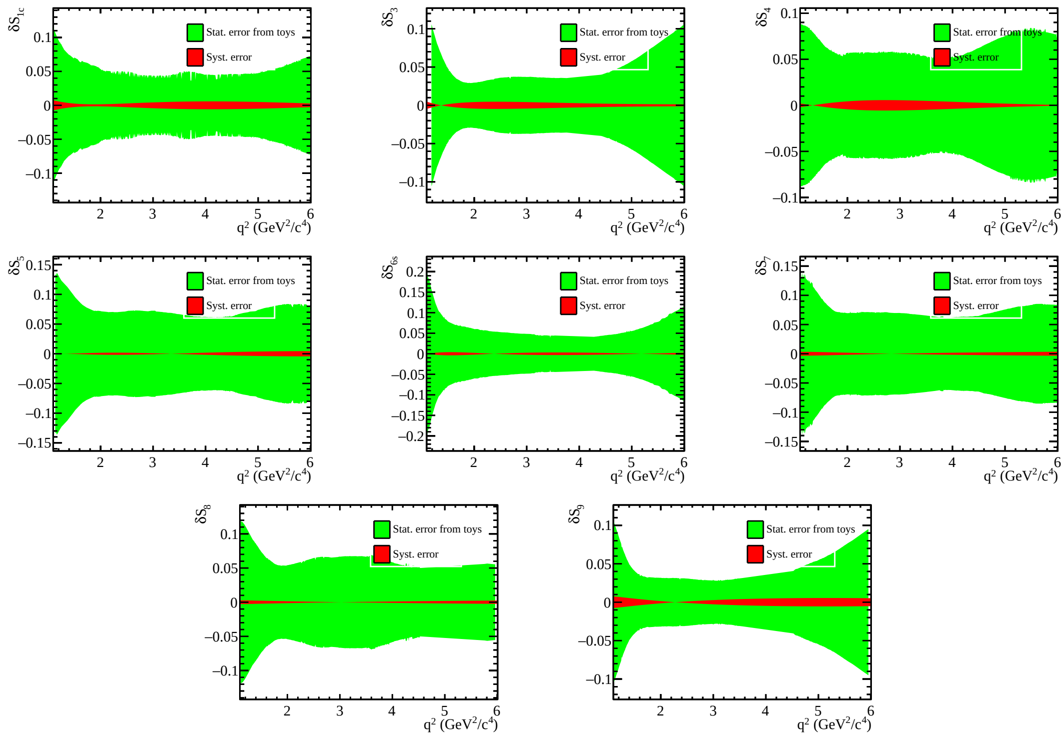

Figure 107: Systematic uncertainty on observables due to the residual peaking backgrounds.

11 Compatibility with the Standard Model

The EOS software package [14] is used to determine the level of compatibility of the data with the SM. It provides predictions for the observables integrated over the q^2 bins used in the analysis. A χ^2 fit is performed to the CP-averaged angular observables F_{L}, A_{FB} and S_3–S_9 obtained from the likelihood fit to the data in the bins $0.1 < q^2 < 0.98\,\mathrm{GeV}^2/c^4$, $1.1 < q^2 < 2.5\,\mathrm{GeV}^2/c^4$, $2.5 < q^2 < 4.0\,\mathrm{GeV}^2/c^4$, $4.0 < q^2 < 6.0\,\mathrm{GeV}^2/c^4$, $6.0 < q^2 < 8.0\,\mathrm{GeV}^2/c^4$ and $15 < q^2 < 19\,\mathrm{GeV}^2/c^4$. Previous analyses have shown that a discrepancy in P_5' can be accounted for by modifying only the real part of the vector coupling strength of the decay. This coupling strength is conventionally denoted $\mathrm{Re}(\mathcal{C}_9)$. In this fit, the correlations between the different observables are accounted for and the floating parameters are $\mathrm{Re}(\mathcal{C}_9)$ and a number of nuisance parameters motivated by Ref. [7]. The nuisance parameters include the form-factor and CKM parameters, as well as parameters describing possible sub-leading ($1/m_b$ suppressed) corrections to the amplitudes. The nuisance parameters are included with Gaussian constraints, taken from Ref. [7]. The best-fit point results in a value of $\mathrm{Re}(\mathcal{C}_9)$ shifted by $\Delta\mathrm{Re}(\mathcal{C}_9) = -1.04 \pm 0.25$ from the SM (see Fig. 108). Using the difference in χ^2 between the SM and best-fit points, the significance of this shift corresponds to $3.4\,\sigma$. As has been discussed in the literature [?, ?, ?, ?, ?, 5–11, 46], a shift in C_9 could be caused by a contribution from a new vector particle or could result from an underestimated hadronic effect.

To estimate the effect of the nuisance parameters on the significance of the shift of $\mathrm{Re}(\mathcal{C}_9)$, the widths of the Gaussian constraints on the form-factor parameters and the parameters encoding the sub-leading corrections are chosen to be twice (three times) their nominal size. The resulting significances for the shift $\Delta\mathrm{Re}(\mathcal{C}_9)$ are reduced to $2.9\,\sigma$ ($2.7\,\sigma$). In addition, fits of $\mathrm{Re}(\mathcal{C}_7)$ and $\mathrm{Re}(\mathcal{C}_{10})$ were performed. The resulting shift for $\mathrm{Re}(\mathcal{C}_{10})$ of $\Delta\mathrm{Re}(\mathcal{C}_{10}) = -1.77 \pm 0.63$ is excluded by the measured $B_s^0 \to \mu^+\mu^-$ branching fraction. A fit of $\mathrm{Re}(\mathcal{C}_7)$ only marginally improves the agreement with the data with a significance of $1.6\,\sigma$. It is also interesting to perform a fit using only the two large q^2 bins $1.1 < q^2 < 6.0\,\mathrm{GeV}^2/c^4$ and $15 < q^2 < 19\,\mathrm{GeV}^2/c^4$. In this case, the fit finds a best fit point of $\Delta\mathrm{Re}(\mathcal{C}_9) = -1.00 \pm 0.30$ with a significance of $2.7\,\sigma$. Finally, even though the basis of F_{L}, A_{FB} and S_3–S_9 is chosen to perform the above fits for the global significance, it is interesting to study the effect on the observable P_5'. Using `EOS` to predict the SM value of this observable results in $P_5'(4.0 < q^2 < 6.0\,\mathrm{GeV}^2/c^4)_{\mathrm{SM}} = -0.78^{+0.10}_{-0.09}$ and $P_5'(6.0 < q^2 < 8.0\,\mathrm{GeV}^2/c^4)_{\mathrm{SM}} = -0.89^{+0.11}_{-0.10}$. The values for the best fit point of $\Delta\mathrm{Re}(\mathcal{C}_9) = -1.04$ are $P_5'(4.0 < q^2 < 6.0\,\mathrm{GeV}^2/c^4)_{\Delta\mathcal{C}_9} = -0.49^{+0.11}_{-0.10}$ and $P_5'(6.0 < q^2 < 8.0\,\mathrm{GeV}^2/c^4)_{\Delta\mathcal{C}_9} = -0.70^{+0.11}_{-0.09}$ respectively, significantly improving the agreement with the values of $-0.300\,^{+0.160}_{-0.161} \pm 0.023$ and $-0.505\,^{+0.123}_{-0.121} \pm 0.024$ measured in data. The uncertainties on the predictions are determined by a variation of the nuisance parameters as illustrated in Fig. 109.

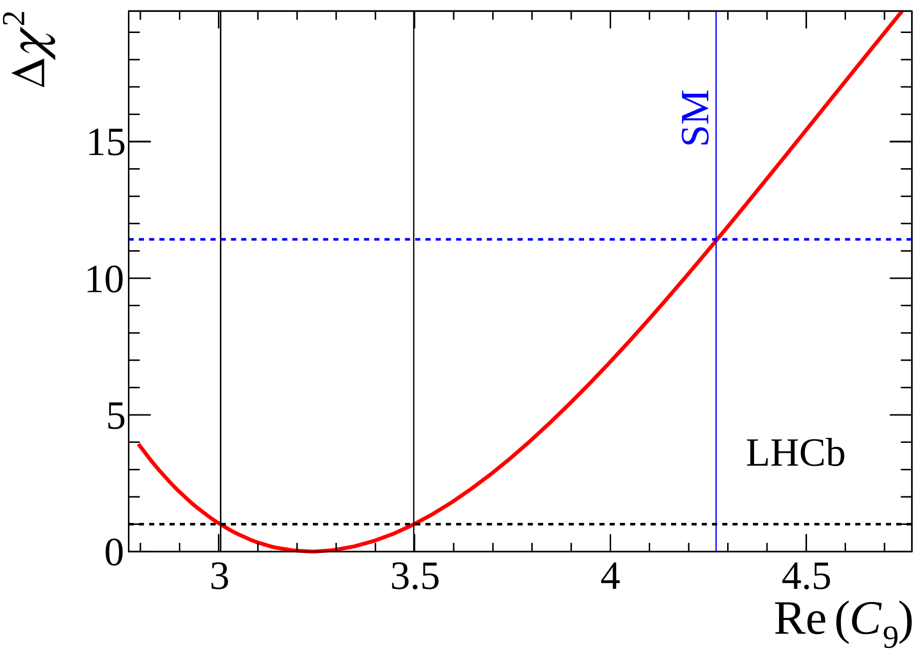

Figure 108: The $\Delta\chi^2$ distribution for the real part of the Wilson coefficient for the generalised vector-coupling strength, $\mathcal{C}_9$. The SM prediction is $\text{Re}(\mathcal{C}_9^{\text{SM}}) = 4.27$, the best fit point is found to be at $\Delta\text{Re}(\mathcal{C}_9) = -1.04$.

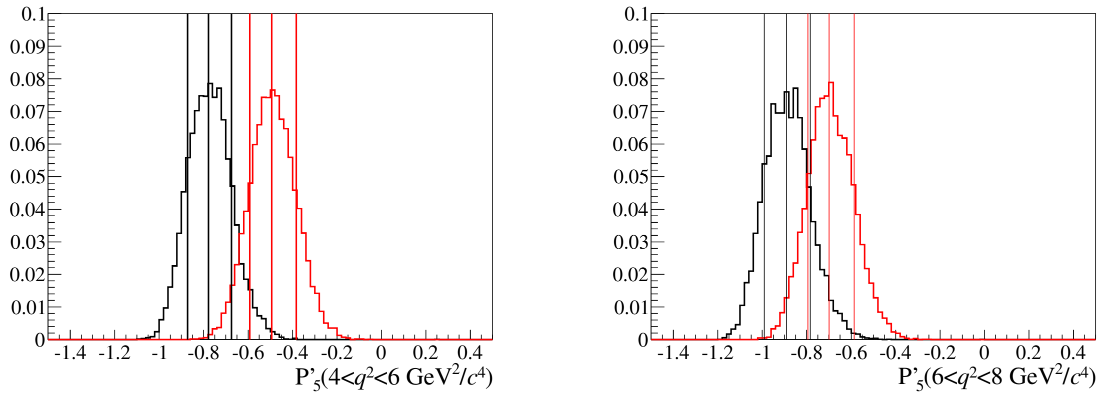

Figure 109: Predictions for the observable P_5' using `EOS` for (left) the bin $4.0 < q^2 < 6.0\,\text{GeV}^2/c^4$ and (right) the bin $6.0 < q^2 < 8.0\,\text{GeV}^2/c^4$. The black distribution is generated using the SM couplings and varying the nuisance parameters according to their uncertainties. The red distribution is generated using the best fit value of $\Delta\text{Re}(\mathcal{C}_9) = -1.04$.

12 Conclusions

The *CP*-averaged angular observables S_i from the likelihood fit and the method of moments are given in Tab. 32 and 35. Figure 76 shows the agreement of the methods in the wider q^2 binning. The measurement is statistically dominated for all bins and observables. Comparing the measurement with the SM predictions [46, 47], generally good agreement is observed. However, some tension is observed for S_5 in the q^2 bin $4.0 < q^2 < 6.0\,\mathrm{GeV}^2/c^4$, as well slight tensions for A_{FB} in the region $2.5 < q^2 < 6.0\,\mathrm{GeV}^2/c^4$. As explained in Sec. **??**, the determination of the $P_i^{(\prime)}$ observables from the method of moments is currently still under study. Table 34 gives the results from the likelihood fit. Of particular interest is of course the observable P_5', where a significant deviation from the SM prediction [10] is observed for the q^2 region $4.0 < q^2 < 8.0\,\mathrm{GeV}^2/c^4$. Table 115 gives the numerical values of the measurement and the SM prediction [10]. Using the more recent form KMPW factor calculations [48], the deviations correspond to $2.8\,\sigma$ and $3.0\,\sigma$ for the q^2 bins $4.0 < q^2 < 6.0\,\mathrm{GeV}^2/c^4$ and $6.0 < q^2 < 8.0\,\mathrm{GeV}^2/c^4$, respectively. Combining the two bins naively, by calculating the χ^2 probability for two degrees of freedom, this corresponds to a deviation of $3.6\,\sigma$[6]. It should be noted, that this combination neglects correlations of the theory prediction between the q^2 bins.

The *CP* asymmetries A_i are determined using both the likelihood fit and the method of moments and the results are given in Tab. 33 and 36. Again good agreement between the methods is observed when using identical binning, as shown in Fig. 77. All *CP* asymmetries A_i are compatible with the SM predictions, that are close to zero in the SM.

Table 115: Comparison of the measured P_5' with the SM prediction using two different form-factor sets, KMPW [48] and BZ [49]. According to the authors, the more recent KMPW calculations are to be preferred.

q^2 bin [GeV^2/c^4]	LHCb	Ref. [10] KMPW (σ)		Ref. [10] BZ (σ)	
$0.1 < q^2 < 0.98$	$0.387^{+0.132}_{-0.133} \pm 0.052$	$0.675^{+0.157}_{-0.191}$	(-1.2)	$0.678^{+0.033}_{-0.040}$	(-2.0)
$1.1 < q^2 < 2.5$	$0.289^{+0.220}_{-0.202} \pm 0.023$	$0.195^{+0.135}_{-0.167}$	(0.4)	$0.170^{+0.096}_{-0.117}$	(0.5)
$2.5 < q^2 < 4.0$	$-0.066^{+0.343}_{-0.364} \pm 0.023$	$-0.468^{+0.155}_{-0.169}$	(1.0)	$-0.492^{+0.104}_{-0.118}$	(1.1)
$4.0 < q^2 < 6.0$	$-0.300^{+0.158}_{-0.159} \pm 0.023$	$-0.816^{+0.097}_{-0.119}$	(2.8)	$-0.789^{+0.066}_{-0.081}$	(2.8)
$6.0 < q^2 < 8.0$	$-0.505^{+0.122}_{-0.122} \pm 0.024$	$-0.936^{+0.077}_{-0.102}$	(3.0)	$-0.882^{+0.049}_{-0.059}$	(2.8)

[6]The change from $3.7\,\sigma$ with respect to LHCb-CONF-2015-002 is due to the ten times larger number of Feldman-Cousins toys that changed the third digit of the statistical uncertainties and the change to the KMPW form factors.

Appendix

A Fitting for constant K^{*0} amplitudes

When averaging over the q^2 bin, the dataset is sensitive to

$$\langle J_i \rangle = \frac{\int (\mathrm{d}\Gamma/\mathrm{d}q^2) J_i(q^2) \mathrm{d}q^2}{\int (\mathrm{d}\Gamma/\mathrm{d}q^2) \mathrm{d}q^2} \tag{111}$$

where the $J_i(q^2)$ are combinations of $A_j(q^2)A_k^*(q^2)$. Unfortunately this makes fitting directly for the amplitudes difficult if the amplitudes vary widely over the q^2 bin used in the fit – it is not neccessarily possible to determine average amplitudes $\langle A_j \rangle$ that result in a consistent set of average $\langle J_i \rangle$. This effect is demonstrated in Fig. 110. A single signal only toy experiment, corresponding to approximately 1000 times the number of signal candidates in the data, is fitted in the range $1 < q^2 < q^2_{\mathrm{max}}$. As q^2_{max} increases the bias, defined as

$$\langle J_i \rangle_{\mathrm{SM}} - J_i(\langle A_j \rangle, \langle A_k^* \rangle) \quad , \tag{112}$$

is seen to increase. In the smallest bin of q^2 the amplitude is approximately constant and the bias becomes small. In wide bins of q^2, the amplitudes and the J_i vary rapidly over the q^2 bin and the bias is typically largest. The scale of the bias on $J_{3,4,8,9}$ is similar in size to the statistical uncertainty on the observable expected in the $3\,\mathrm{fb}^{-1}$ dataset. To avoid this potential source of bias, the q^2 parameterisation described in Sec. 6.4 is adopted for the analysis.

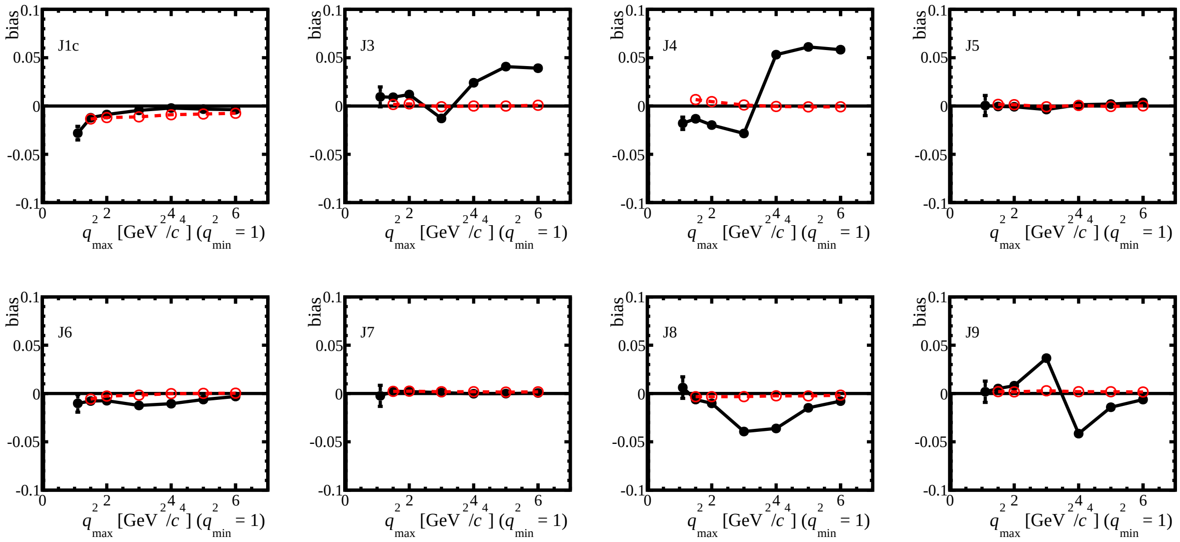

Figure 110: Bias on the angular obsevables calculated after fitting for constant amplitudes over a q^2 range $1 < q^2 < q^2_{\rm max}$. Large biases are seen as $q^2_{\rm max}$ increases. Small discrepancies in the first data point are due to lepton mass effects in the SM expectation used to determine the bias. The result of fitting the same dataset directly for the angular observables is also shown as the red-dashed line.

B CP-Asymmetries A_i from the observables fit

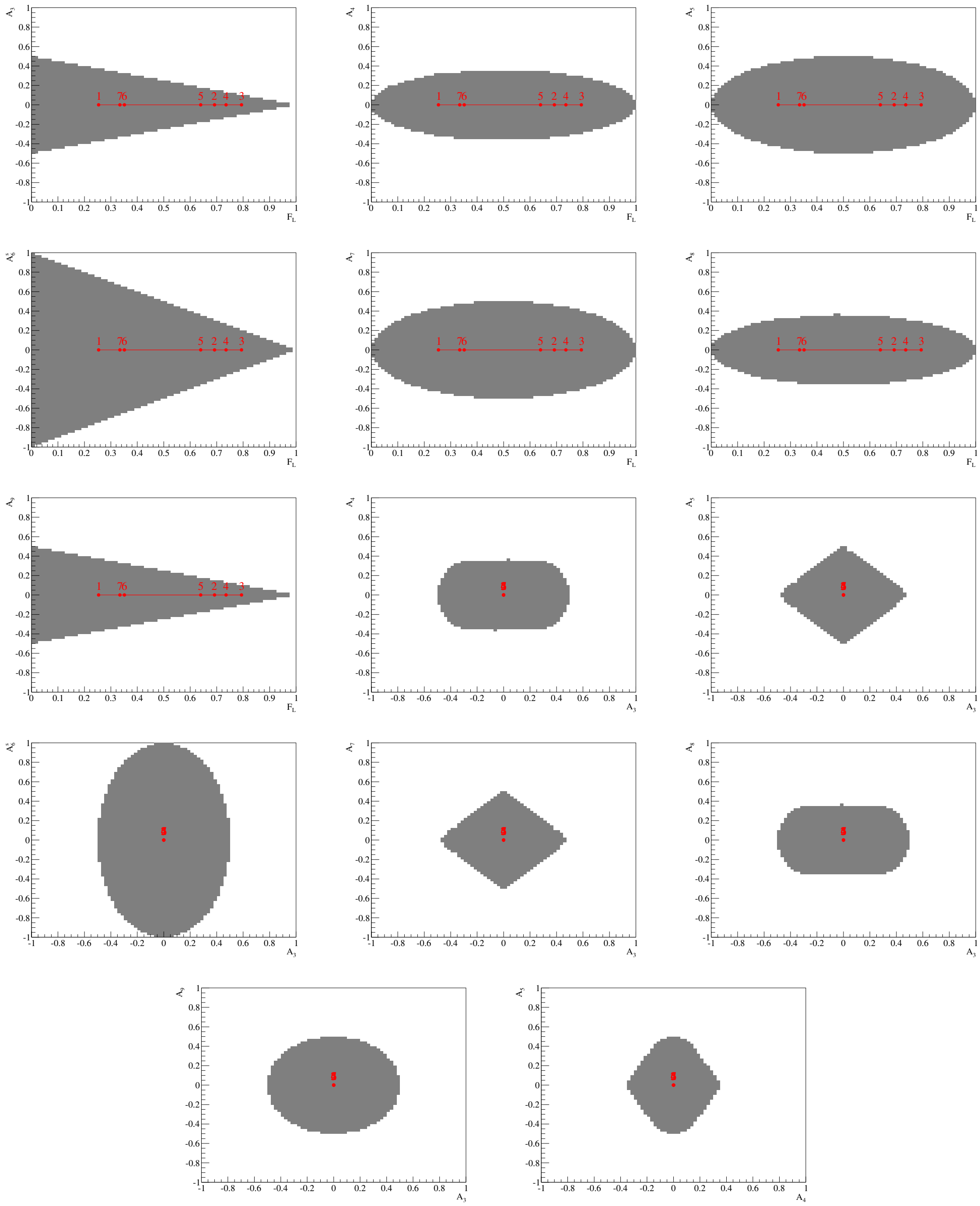

Figure 111: Projection of the allowed parameter range, where the PDF is positive everywhere, for different combinations of parameters. The SM values of the CP-asymmetries $A_{3,\ldots,9}$ are close to zero, further away from the physical parameter boundaries than the CP averaged observables S_i.

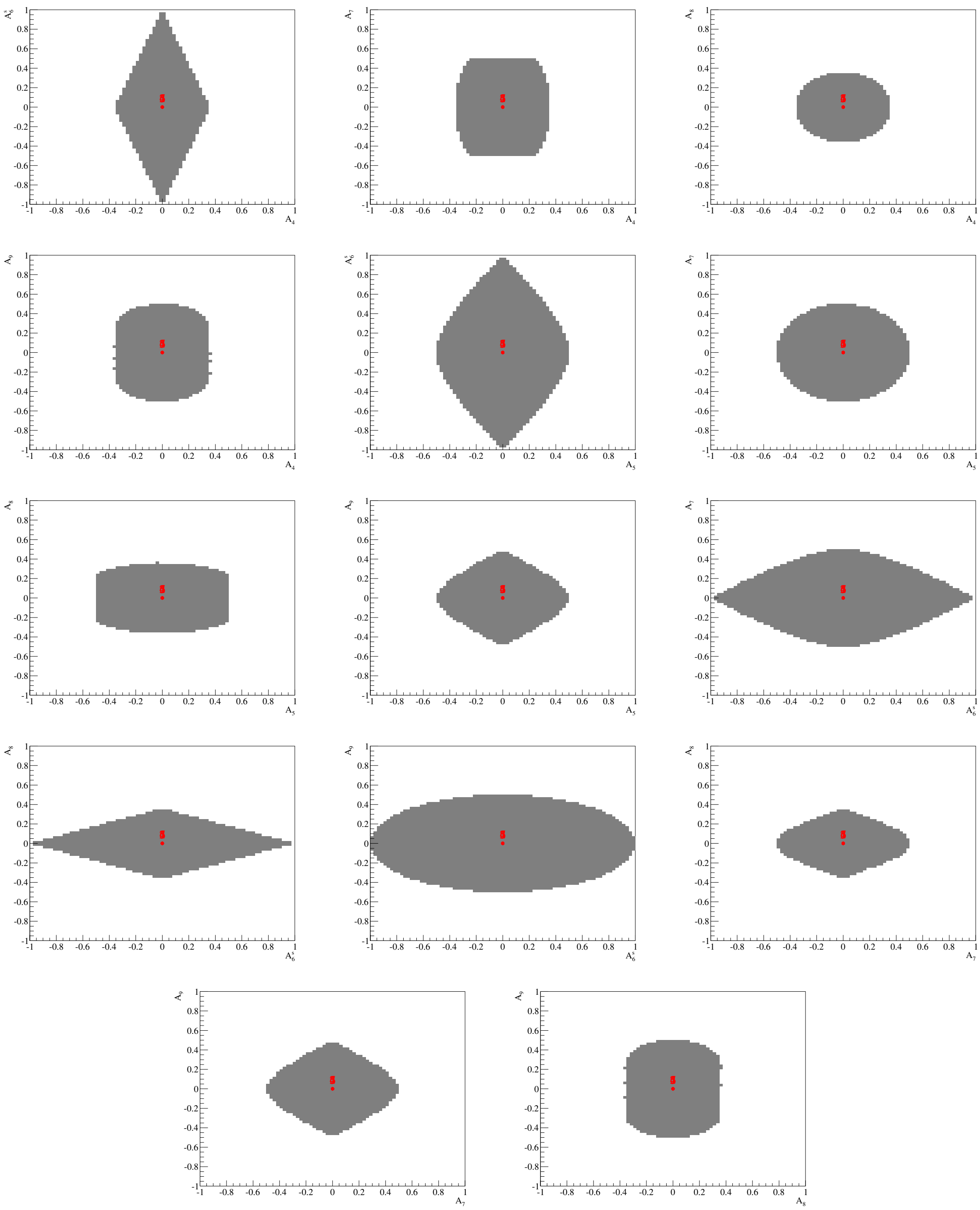

Figure 112: Projection of the allowed parameter range, where the PDF is positive everywhere, for different combinations of parameters. The SM values of the CP-asymmetries $A_{3,...,9}$ are close to zero, further away from the physical parameter boundaries than the CP averaged observables S_i.

Table 116: Results from pull studies on `EOS` toys in bins of q^2. A background component is included. The acceptance effect is included and is assumed to be constant over the q^2 bins.

	$0.1 < q^2 < 1.0\,\text{GeV}^2$		
	sensitivity	pull mean	pull width
S_1^s	0.030 ± 0.001	0.77 ± 0.03	1.05 ± 0.02
A_3	0.057 ± 0.001	-0.02 ± 0.03	1.01 ± 0.02
A_4	0.071 ± 0.002	-0.05 ± 0.03	1.08 ± 0.02
A_5	0.057 ± 0.001	-0.07 ± 0.03	1.04 ± 0.02
A_6^s	0.073 ± 0.002	-0.01 ± 0.03	1.02 ± 0.02
A_7	0.054 ± 0.001	0.02 ± 0.03	0.99 ± 0.02
A_8	0.067 ± 0.002	-0.01 ± 0.03	1.03 ± 0.02
A_9	0.056 ± 0.001	0.07 ± 0.03	1.00 ± 0.02

	$1.1 < q^2 < 2.5\,\text{GeV}^2$		
	sensitivity	pull mean	pull width
S_1^s	0.049 ± 0.001	-0.02 ± 0.03	1.04 ± 0.02
A_3	0.076 ± 0.002	0.02 ± 0.03	1.08 ± 0.02
A_4	0.101 ± 0.002	-0.00 ± 0.03	1.03 ± 0.02
A_5	0.086 ± 0.002	-0.01 ± 0.03	0.99 ± 0.02
A_6^s	0.083 ± 0.002	-0.02 ± 0.03	1.06 ± 0.02
A_7	0.093 ± 0.002	0.05 ± 0.03	1.07 ± 0.02
A_8	0.103 ± 0.002	-0.04 ± 0.03	1.04 ± 0.02
A_9	0.074 ± 0.002	-0.00 ± 0.03	1.05 ± 0.02

	$2.5 < q^2 < 4.0\,\text{GeV}^2$		
	sensitivity	pull mean	pull width
S_1^s	0.046 ± 0.001	-0.06 ± 0.03	1.03 ± 0.02
A_3	0.077 ± 0.002	0.01 ± 0.03	1.08 ± 0.02
A_4	0.103 ± 0.002	-0.03 ± 0.03	1.04 ± 0.02
A_5	0.097 ± 0.002	-0.00 ± 0.03	1.07 ± 0.02
A_6^s	0.074 ± 0.002	0.00 ± 0.03	1.05 ± 0.02
A_7	0.101 ± 0.002	0.06 ± 0.03	1.11 ± 0.02
A_8	0.107 ± 0.002	0.02 ± 0.03	1.10 ± 0.02
A_9	0.079 ± 0.002	-0.04 ± 0.04	1.11 ± 0.02

	$4.0 < q^2 < 6.0\,\text{GeV}^2$		
	sensitivity	pull mean	pull width
S_1^s	0.035 ± 0.001	-0.01 ± 0.03	0.97 ± 0.02
A_3	0.063 ± 0.001	-0.02 ± 0.03	1.05 ± 0.02
A_4	0.083 ± 0.002	-0.03 ± 0.03	1.07 ± 0.02
A_5	0.075 ± 0.002	0.01 ± 0.03	1.02 ± 0.02
A_6^s	0.057 ± 0.001	-0.03 ± 0.03	1.02 ± 0.02
A_7	0.074 ± 0.002	-0.00 ± 0.03	1.00 ± 0.02
A_8	0.081 ± 0.002	0.01 ± 0.03	1.06 ± 0.02
A_9	0.063 ± 0.001	0.02 ± 0.03	1.06 ± 0.02

	$6.0 < q^2 < 8.0\,\text{GeV}^2$		
	sensitivity	pull mean	pull width
S_1^s	0.035 ± 0.001	-0.14 ± 0.03	1.04 ± 0.02
A_3	0.061 ± 0.001	-0.01 ± 0.03	1.07 ± 0.02
A_4	0.073 ± 0.002	0.02 ± 0.03	1.04 ± 0.02
A_5	0.069 ± 0.002	-0.01 ± 0.03	1.03 ± 0.02
A_6^s	0.053 ± 0.001	-0.05 ± 0.03	1.00 ± 0.02
A_7	0.069 ± 0.002	-0.01 ± 0.03	1.03 ± 0.02
A_8	0.070 ± 0.002	0.00 ± 0.03	1.02 ± 0.02
A_9	0.060 ± 0.001	0.01 ± 0.03	1.05 ± 0.02

	$15.0 < q^2 < 17.0\,\text{GeV}^2$		
	sensitivity	pull mean	pull width
S_1^s	0.032 ± 0.001	-0.30 ± 0.03	1.03 ± 0.02
A_3	0.059 ± 0.001	0.03 ± 0.03	1.01 ± 0.02
A_4	0.069 ± 0.002	-0.06 ± 0.03	1.03 ± 0.02
A_5	0.066 ± 0.001	-0.01 ± 0.03	1.04 ± 0.02
A_6^s	0.056 ± 0.001	0.01 ± 0.03	1.03 ± 0.02
A_7	0.061 ± 0.001	-0.02 ± 0.03	1.02 ± 0.02
A_8	0.065 ± 0.001	-0.01 ± 0.03	1.03 ± 0.02
A_9	0.060 ± 0.001	0.02 ± 0.03	1.04 ± 0.02

	$17.0 < q^2 < 19.0\,\text{GeV}^2$		
	sensitivity	pull mean	pull width
S_1^s	0.041 ± 0.001	-0.08 ± 0.03	1.03 ± 0.02
A_3	0.078 ± 0.002	-0.05 ± 0.03	1.03 ± 0.02
A_4	0.086 ± 0.002	0.01 ± 0.03	1.02 ± 0.02
A_5	0.084 ± 0.002	0.03 ± 0.03	1.05 ± 0.02
A_6^s	0.075 ± 0.002	0.01 ± 0.03	1.02 ± 0.02
A_7	0.075 ± 0.002	0.04 ± 0.03	1.03 ± 0.02
A_8	0.088 ± 0.002	-0.00 ± 0.03	1.09 ± 0.02
A_9	0.078 ± 0.002	0.01 ± 0.03	1.06 ± 0.02

Table 117: Results from pull studies on toys including S-wave constribution in bins of q^2. A background component is included as well. The acceptance effect is included and is assumed to be constant over the q^2 bins.

	$0.1 < q^2 < 1.0\,\mathrm{GeV}^2$				$1.1 < q^2 < 2.5\,\mathrm{GeV}^2$		
	sensitivity	pull mean	pull width		sensitivity	pull mean	pull width
S_1^s	0.040 ± 0.001	-0.04 ± 0.03	0.97 ± 0.02	S_1^s	0.096 ± 0.002	-0.06 ± 0.03	1.01 ± 0.02
A_3	0.070 ± 0.002	0.03 ± 0.03	0.96 ± 0.02	A_3	0.110 ± 0.002	0.02 ± 0.03	1.06 ± 0.02
A_4	0.081 ± 0.002	-0.00 ± 0.03	0.98 ± 0.02	A_4	0.134 ± 0.003	0.10 ± 0.03	1.05 ± 0.02
A_5	0.070 ± 0.002	0.04 ± 0.03	0.99 ± 0.02	A_5	0.116 ± 0.003	0.04 ± 0.03	1.04 ± 0.02
A_{6s}	0.086 ± 0.002	-0.03 ± 0.03	1.02 ± 0.02	A_{6s}	0.117 ± 0.003	-0.00 ± 0.03	1.08 ± 0.02
A_7	0.066 ± 0.001	-0.05 ± 0.03	0.97 ± 0.02	A_7	0.119 ± 0.003	-0.02 ± 0.03	0.99 ± 0.02
A_8	0.080 ± 0.002	0.02 ± 0.03	0.98 ± 0.02	A_8	0.138 ± 0.003	-0.01 ± 0.03	1.06 ± 0.02
A_9	0.072 ± 0.002	-0.01 ± 0.03	0.97 ± 0.02	A_9	0.108 ± 0.002	-0.02 ± 0.03	1.05 ± 0.02
F_S	0.119 ± 0.003	0.11 ± 0.03	0.90 ± 0.02	F_S	0.143 ± 0.003	0.16 ± 0.03	1.06 ± 0.02
S_{S1}	0.094 ± 0.002	-0.03 ± 0.03	1.00 ± 0.02	S_{S1}	0.178 ± 0.004	0.02 ± 0.03	1.09 ± 0.02
S_{S2}	0.090 ± 0.002	-0.02 ± 0.03	1.02 ± 0.02	S_{S2}	0.131 ± 0.003	0.03 ± 0.04	1.12 ± 0.02
S_{S3}	0.078 ± 0.002	0.02 ± 0.03	1.05 ± 0.02	S_{S3}	0.114 ± 0.003	-0.03 ± 0.04	1.11 ± 0.02
S_{S4}	0.076 ± 0.002	0.02 ± 0.03	1.04 ± 0.02	S_{S4}	0.115 ± 0.003	0.04 ± 0.04	1.12 ± 0.03
S_{S5}	0.092 ± 0.002	0.03 ± 0.03	1.03 ± 0.02	S_{S5}	0.131 ± 0.003	-0.04 ± 0.04	1.11 ± 0.02

	$2.5 < q^2 < 4.0\,\mathrm{GeV}^2$				$4.0 < q^2 < 6.0\,\mathrm{GeV}^2$		
	sensitivity	pull mean	pull width		sensitivity	pull mean	pull width
S_1^s	0.107 ± 0.002	-0.11 ± 0.03	0.99 ± 0.02	S_1^s	0.050 ± 0.001	-0.07 ± 0.03	1.00 ± 0.02
A_3	0.116 ± 0.003	0.03 ± 0.03	1.07 ± 0.02	A_3	0.080 ± 0.002	0.02 ± 0.03	1.03 ± 0.02
A_4	0.137 ± 0.003	0.01 ± 0.03	1.05 ± 0.02	A_4	0.090 ± 0.002	0.02 ± 0.03	1.02 ± 0.02
A_5	0.121 ± 0.003	0.02 ± 0.03	1.03 ± 0.02	A_5	0.086 ± 0.002	-0.03 ± 0.03	1.01 ± 0.02
A_{6s}	0.121 ± 0.003	-0.03 ± 0.04	1.11 ± 0.02	A_{6s}	0.069 ± 0.002	0.03 ± 0.03	1.05 ± 0.02
A_7	0.129 ± 0.003	0.02 ± 0.03	1.06 ± 0.02	A_7	0.086 ± 0.002	0.04 ± 0.03	0.98 ± 0.02
A_8	0.133 ± 0.003	0.01 ± 0.03	1.04 ± 0.02	A_8	0.091 ± 0.002	-0.03 ± 0.03	1.01 ± 0.02
A_9	0.116 ± 0.003	0.01 ± 0.03	1.09 ± 0.02	A_9	0.079 ± 0.002	0.03 ± 0.03	1.02 ± 0.02
F_S	0.137 ± 0.003	0.12 ± 0.04	1.23 ± 0.03	F_S	0.102 ± 0.002	0.12 ± 0.03	0.98 ± 0.02
S_{S1}	0.181 ± 0.004	-0.05 ± 0.03	1.04 ± 0.02	S_{S1}	0.145 ± 0.003	0.00 ± 0.03	1.04 ± 0.02
S_{S2}	0.139 ± 0.003	0.01 ± 0.04	1.21 ± 0.03	S_{S2}	0.099 ± 0.002	-0.00 ± 0.04	1.13 ± 0.03
S_{S3}	0.125 ± 0.003	-0.02 ± 0.04	1.17 ± 0.03	S_{S3}	0.088 ± 0.002	-0.03 ± 0.03	1.08 ± 0.02
S_{S4}	0.121 ± 0.003	0.06 ± 0.04	1.15 ± 0.03	S_{S4}	0.093 ± 0.002	-0.04 ± 0.04	1.12 ± 0.03
S_{S5}	0.134 ± 0.003	0.08 ± 0.04	1.16 ± 0.03	S_{S5}	0.092 ± 0.002	-0.04 ± 0.03	1.04 ± 0.02

Table 118: Results from pull studies on toys including S-wave constribution in bins of q^2. A background component is included as well. The acceptance effect is included and is assumed to be constant over the q^2 bins.

	$6.0 < q^2 < 8.0\,\mathrm{GeV}^2$			$15.0 < q^2 < 17.0\,\mathrm{GeV}^2$		
	sensitivity	pull mean	pull width	sensitivity	pull mean	pull width
S_1^s	0.040 ± 0.001	0.01 ± 0.03	1.00 ± 0.02	0.035 ± 0.001	-0.06 ± 0.03	0.96 ± 0.02
A_3	0.070 ± 0.002	0.01 ± 0.03	1.00 ± 0.02	0.067 ± 0.001	0.07 ± 0.03	0.98 ± 0.02
A_4	0.081 ± 0.002	-0.06 ± 0.03	1.04 ± 0.02	0.067 ± 0.002	-0.01 ± 0.03	0.98 ± 0.02
A_5	0.074 ± 0.002	-0.10 ± 0.03	0.98 ± 0.02	0.065 ± 0.001	0.01 ± 0.03	0.99 ± 0.02
A_{6s}	0.058 ± 0.001	-0.00 ± 0.03	1.01 ± 0.02	0.061 ± 0.001	-0.02 ± 0.03	1.03 ± 0.02
A_7	0.078 ± 0.002	-0.01 ± 0.03	1.01 ± 0.02	0.071 ± 0.002	0.03 ± 0.03	1.03 ± 0.02
A_8	0.078 ± 0.002	0.04 ± 0.03	1.01 ± 0.02	0.072 ± 0.002	0.02 ± 0.03	1.01 ± 0.02
A_9	0.071 ± 0.002	-0.03 ± 0.03	1.01 ± 0.02	0.068 ± 0.002	0.05 ± 0.03	1.01 ± 0.02
F_S	0.091 ± 0.002	0.04 ± 0.03	0.94 ± 0.02	0.091 ± 0.002	0.07 ± 0.03	0.94 ± 0.02
S_{S1}	0.128 ± 0.003	-0.05 ± 0.03	1.04 ± 0.02	0.105 ± 0.002	0.03 ± 0.03	1.06 ± 0.02
S_{S2}	0.083 ± 0.002	0.07 ± 0.03	1.03 ± 0.02	0.078 ± 0.002	-0.04 ± 0.03	1.01 ± 0.02
S_{S3}	0.079 ± 0.002	0.03 ± 0.03	1.05 ± 0.02	0.074 ± 0.002	0.01 ± 0.03	1.03 ± 0.02
S_{S4}	0.077 ± 0.002	-0.02 ± 0.03	1.01 ± 0.02	0.077 ± 0.002	-0.03 ± 0.03	1.05 ± 0.02
S_{S5}	0.081 ± 0.002	-0.00 ± 0.03	1.01 ± 0.02	0.081 ± 0.002	0.00 ± 0.03	1.02 ± 0.02

	$17.0 < q^2 < 19.0\,\mathrm{GeV}^2$		
	sensitivity	pull mean	pull width
S_1^s	0.052 ± 0.001	-0.03 ± 0.03	1.01 ± 0.02
A_3	0.093 ± 0.002	0.05 ± 0.03	0.98 ± 0.02
A_4	0.097 ± 0.002	0.03 ± 0.03	1.03 ± 0.02
A_5	0.089 ± 0.002	-0.02 ± 0.03	1.00 ± 0.02
A_{6s}	0.088 ± 0.002	-0.01 ± 0.03	1.05 ± 0.02
A_7	0.092 ± 0.002	0.04 ± 0.03	0.98 ± 0.02
A_8	0.096 ± 0.002	0.01 ± 0.03	0.98 ± 0.02
A_9	0.097 ± 0.002	-0.03 ± 0.03	1.00 ± 0.02
F_S	0.120 ± 0.003	0.18 ± 0.03	0.90 ± 0.02
S_{S1}	0.127 ± 0.003	0.01 ± 0.03	1.02 ± 0.02
S_{S2}	0.108 ± 0.002	0.08 ± 0.03	1.07 ± 0.02
S_{S3}	0.098 ± 0.002	0.02 ± 0.03	1.06 ± 0.02
S_{S4}	0.093 ± 0.002	-0.00 ± 0.03	0.97 ± 0.02
S_{S5}	0.108 ± 0.002	-0.04 ± 0.03	1.03 ± 0.02

C Likelihood scans

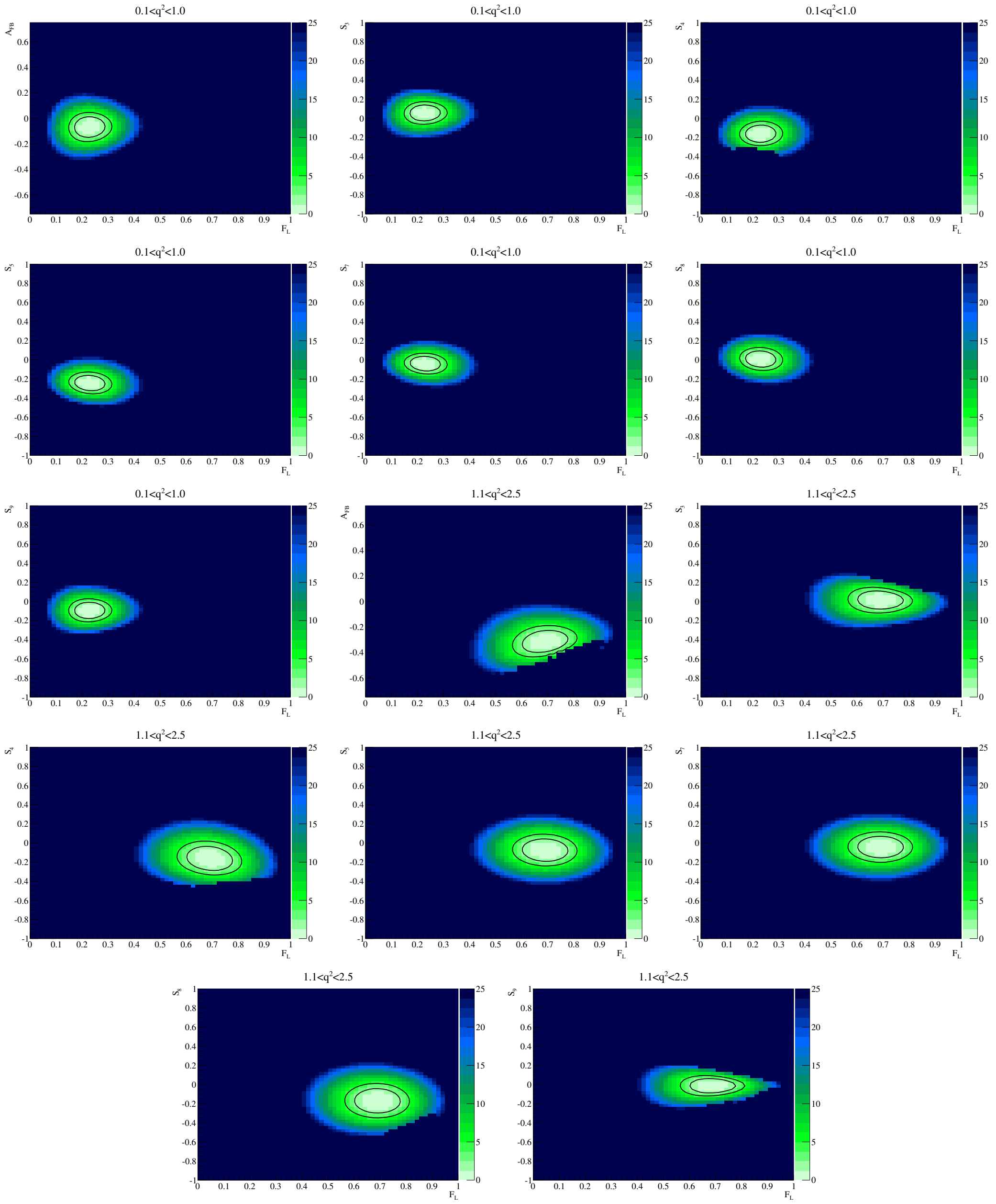

Figure 113: Two-dimensional profile likelihood scans for a single `EOS` toy in the two q^2 regions $0.1 < q^2 < 2.5\,\mathrm{GeV}^2/c^4$ and $2.5 < q^2 < 4.0\,\mathrm{GeV}^2/c^4$. The z-axis gives the negative logarithmic likelihood at the given parameter point, minimized with respect to all other parameters. The black contours give the 68.3% and 90% confidence regions. All combinations of F_L with the other observables are given.

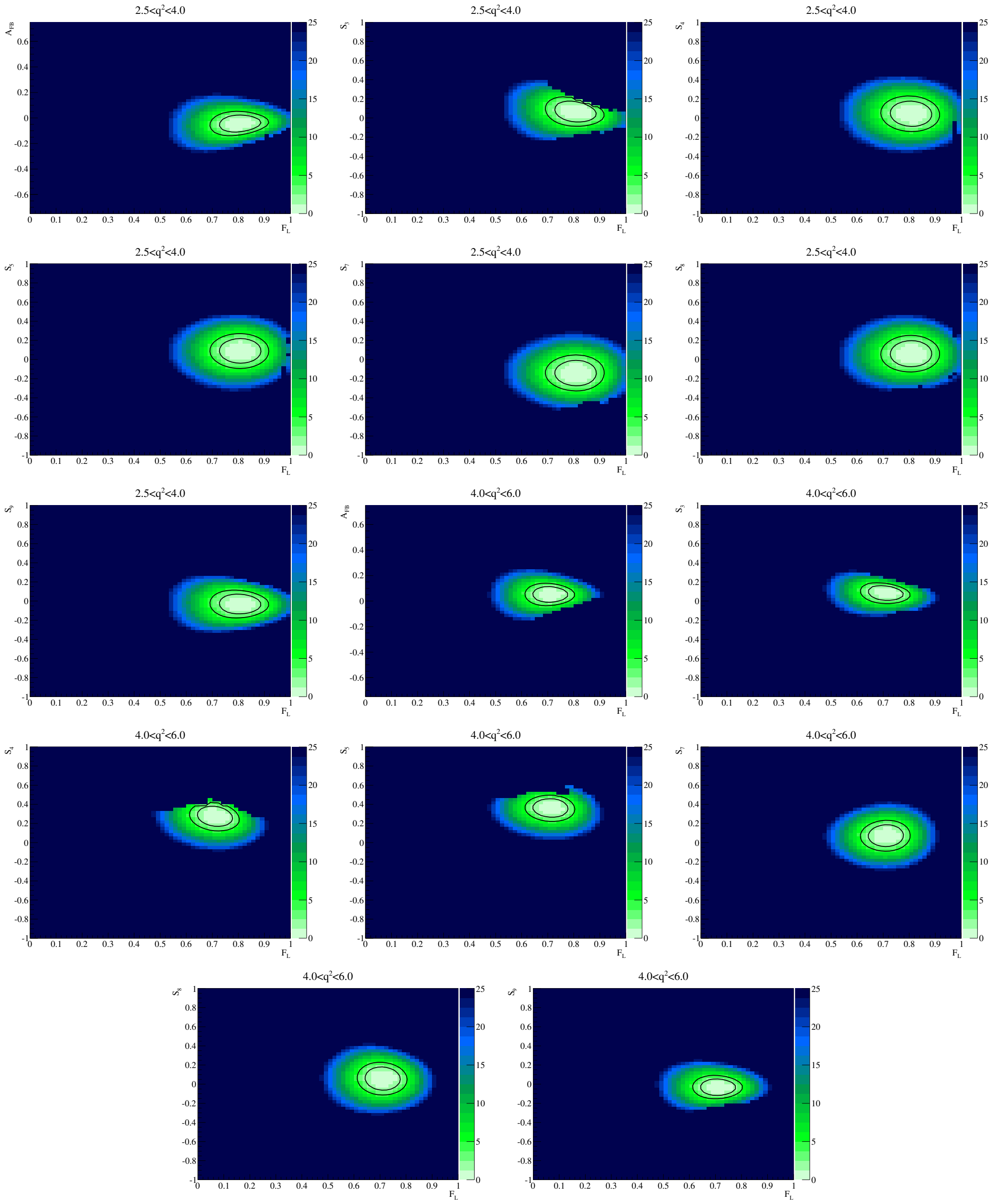

Figure 114: Two-dimensional profile likelihood scans for a single `EOS` toy in the two q^2 regions $2.5 < q^2 < 4.0\,\mathrm{GeV}^2/c^4$ and $4.0 < q^2 < 6.0\,\mathrm{GeV}^2/c^4$. The z-axis gives the negative logarithmic likelihood at the given parameter point, minimized with respect to all other parameters. The black contours give the 68.3% and 90% confidence regions. All combinations of F_L with the other observables are given.

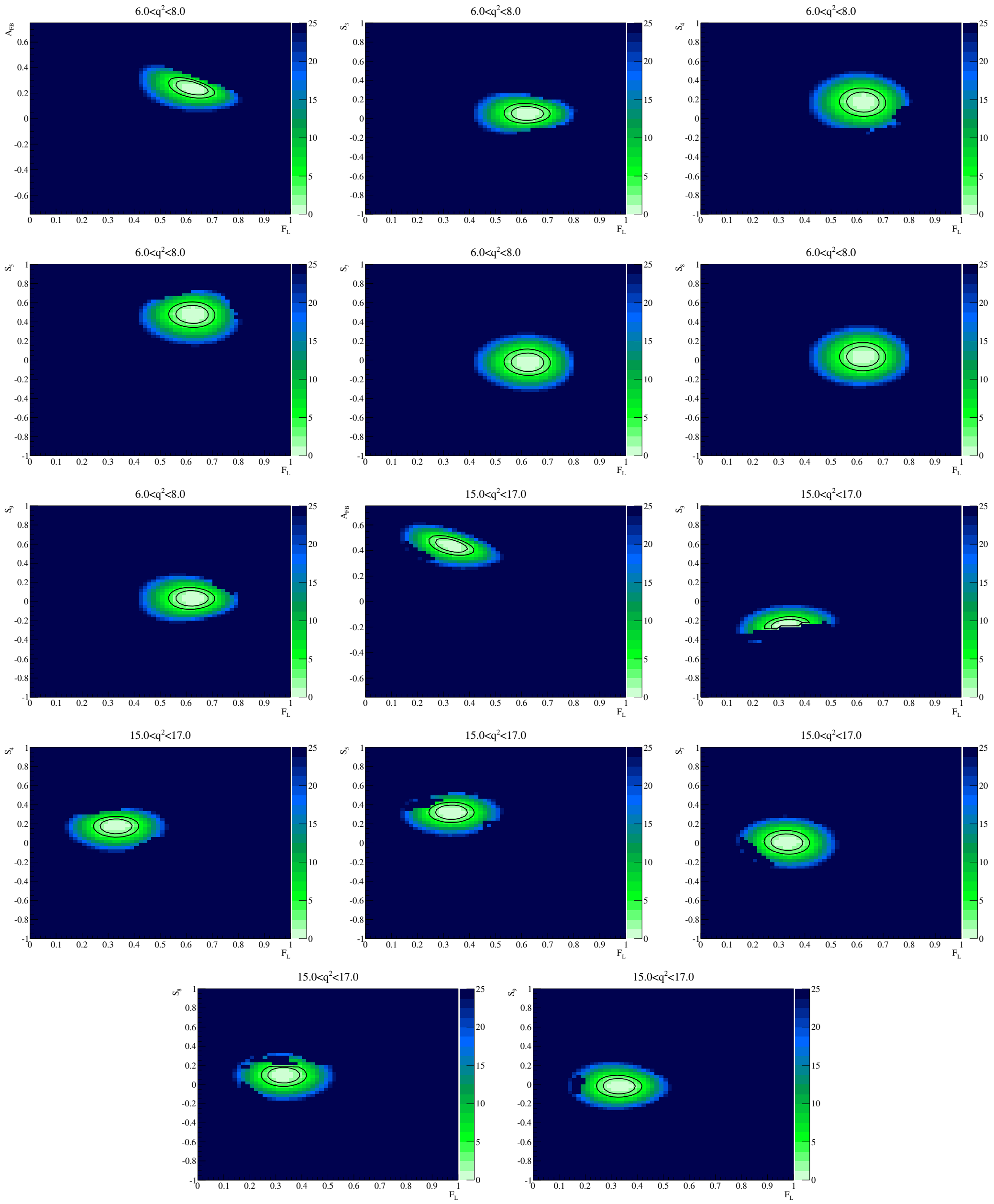

Figure 115: Two-dimensional likelihood scans for a single EOS toy in the two q^2 regions $6.0 < q^2 < 8.0\,\mathrm{GeV}^2/c^4$ and $15.0 < q^2 < 17.0\,\mathrm{GeV}^2/c^4$. All combinations of F_L with the other observables are given.

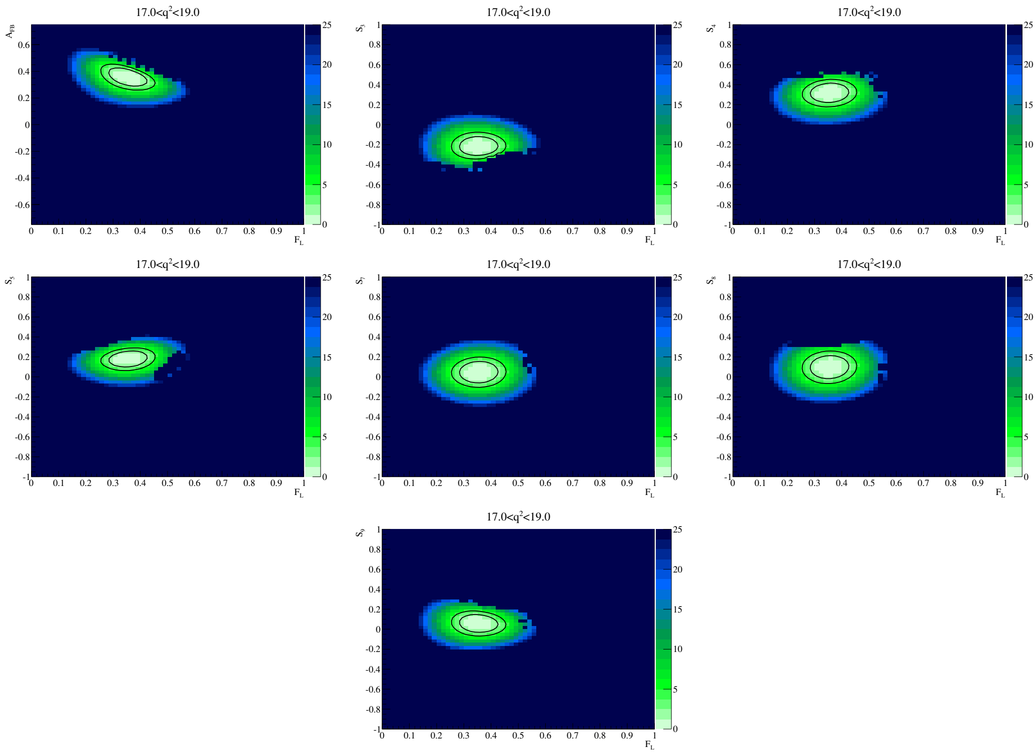

Figure 116: Two-dimensional likelihood scans for a single EOS toy in the q^2 region $17.0 < q^2 < 19.0\,\mathrm{GeV}^2/c^4$. All combinations of F_L with the other observables are given.

D Feldman-Cousins confidence intervals

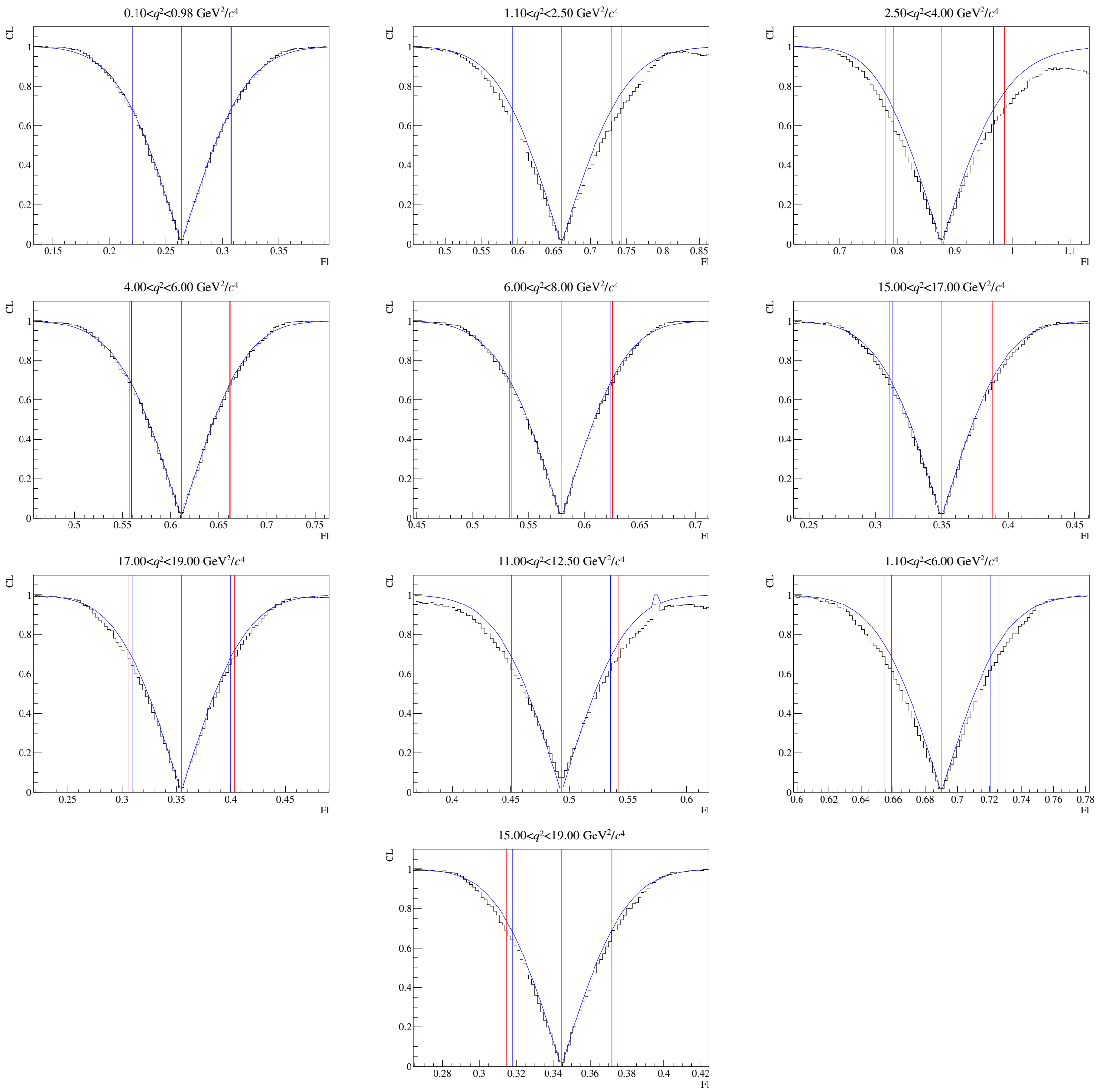

Figure 117: Feldman-Cousins scan for the angular observable F_{L}.

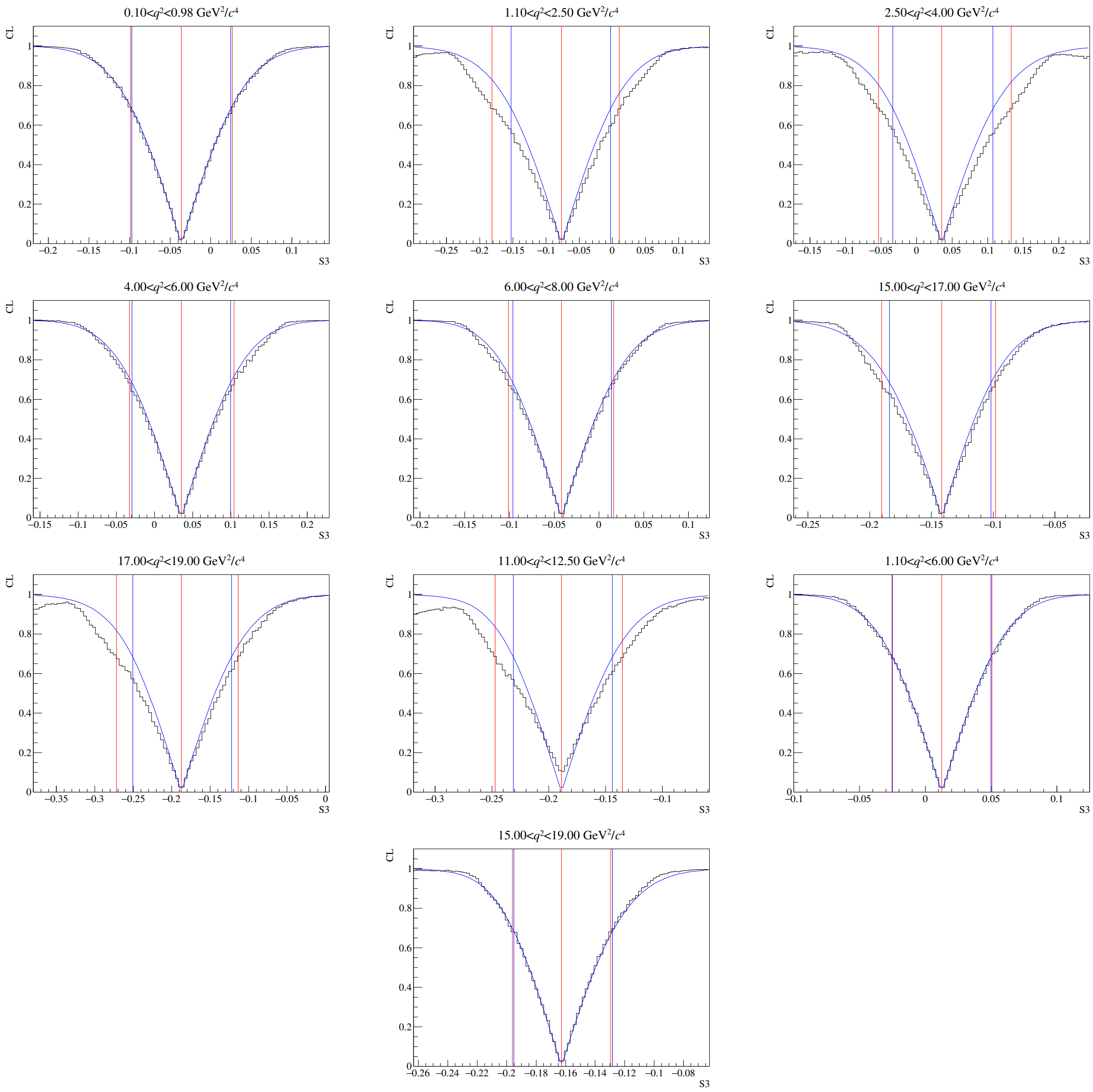

Figure 118: Feldman-Cousins scan for the angular observable S_3.

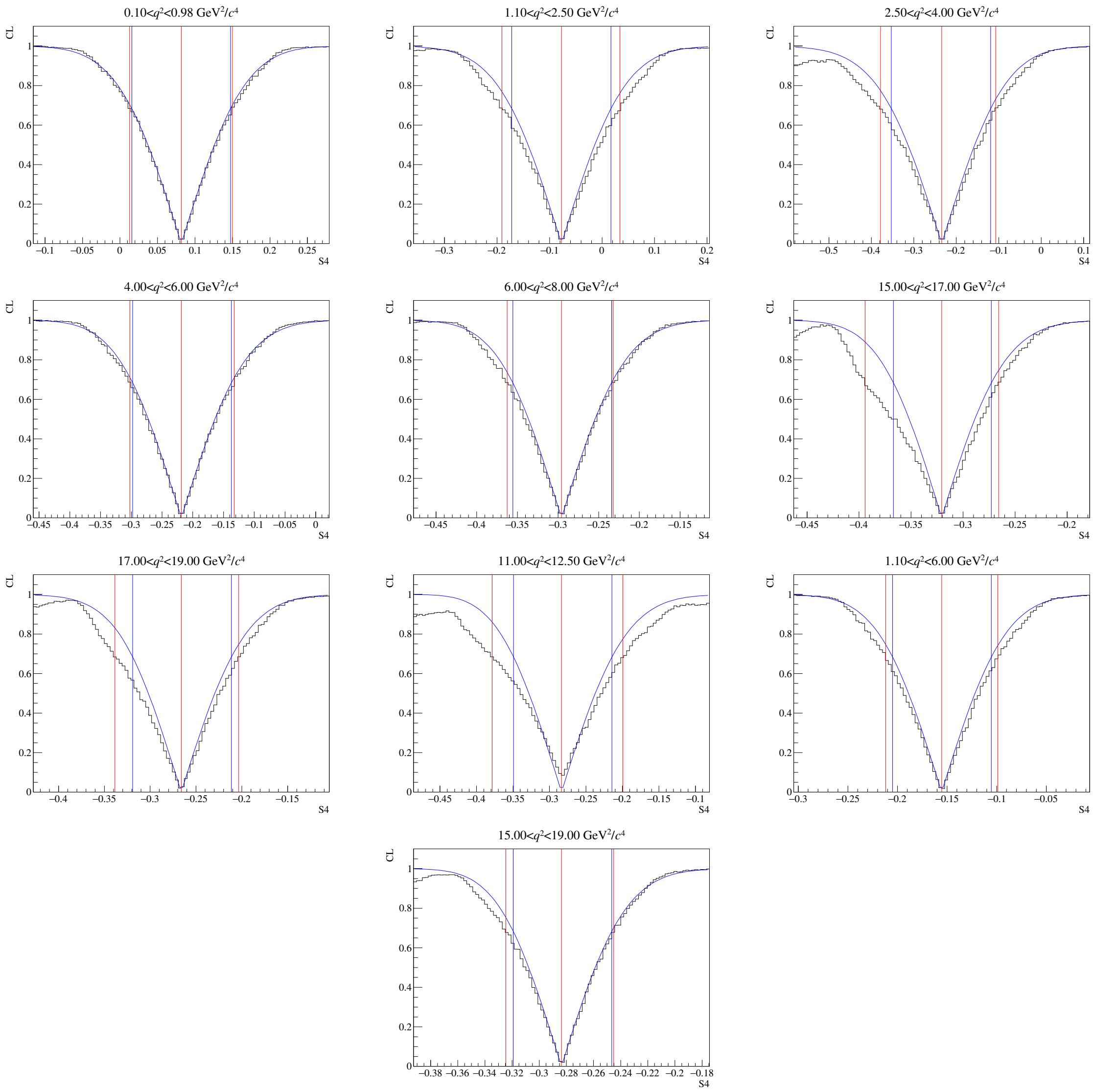

Figure 119: Feldman-Cousins scan for the angular observable S_4.

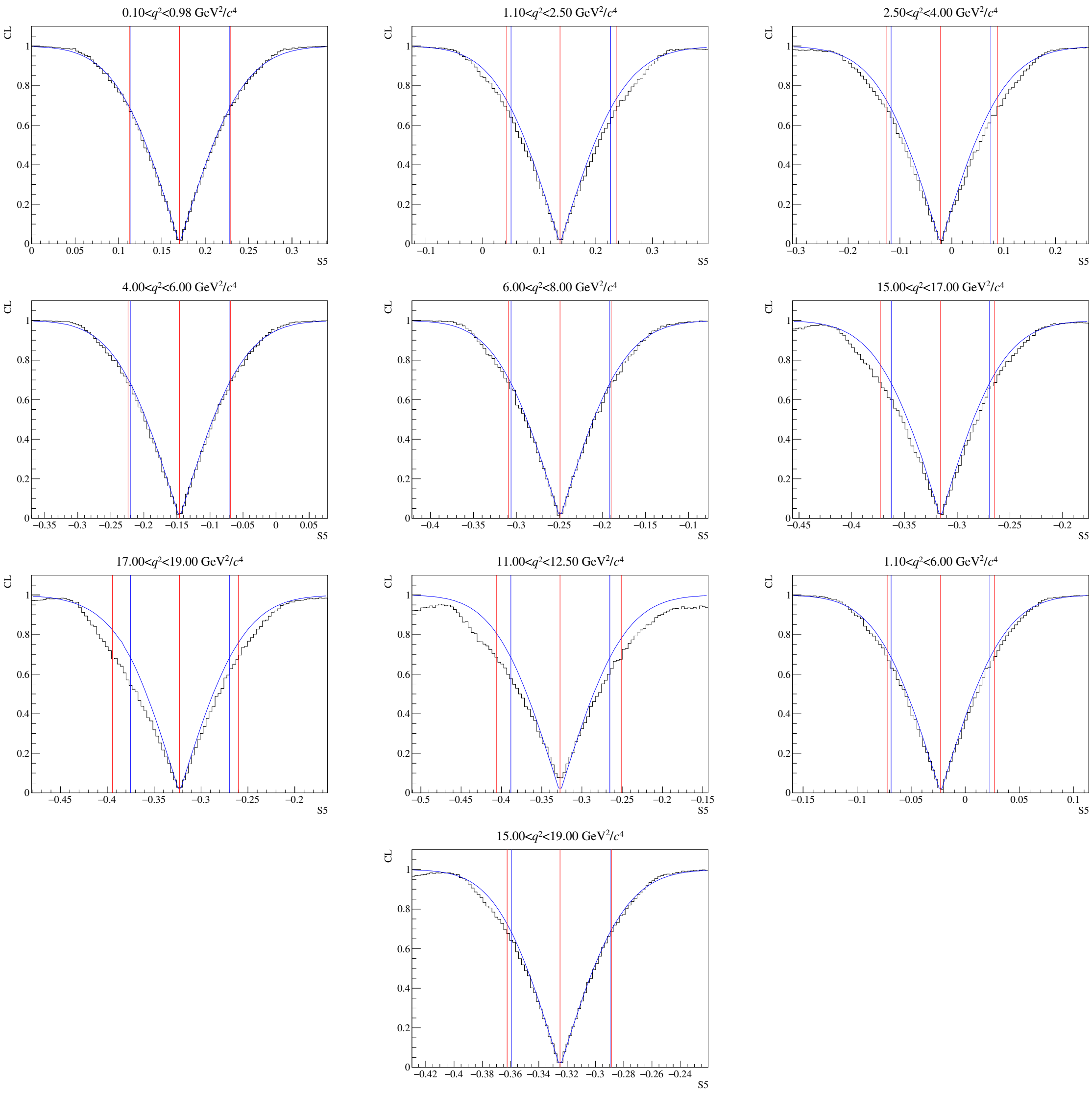

Figure 120: Feldman-Cousins scan for the angular observable S_5.

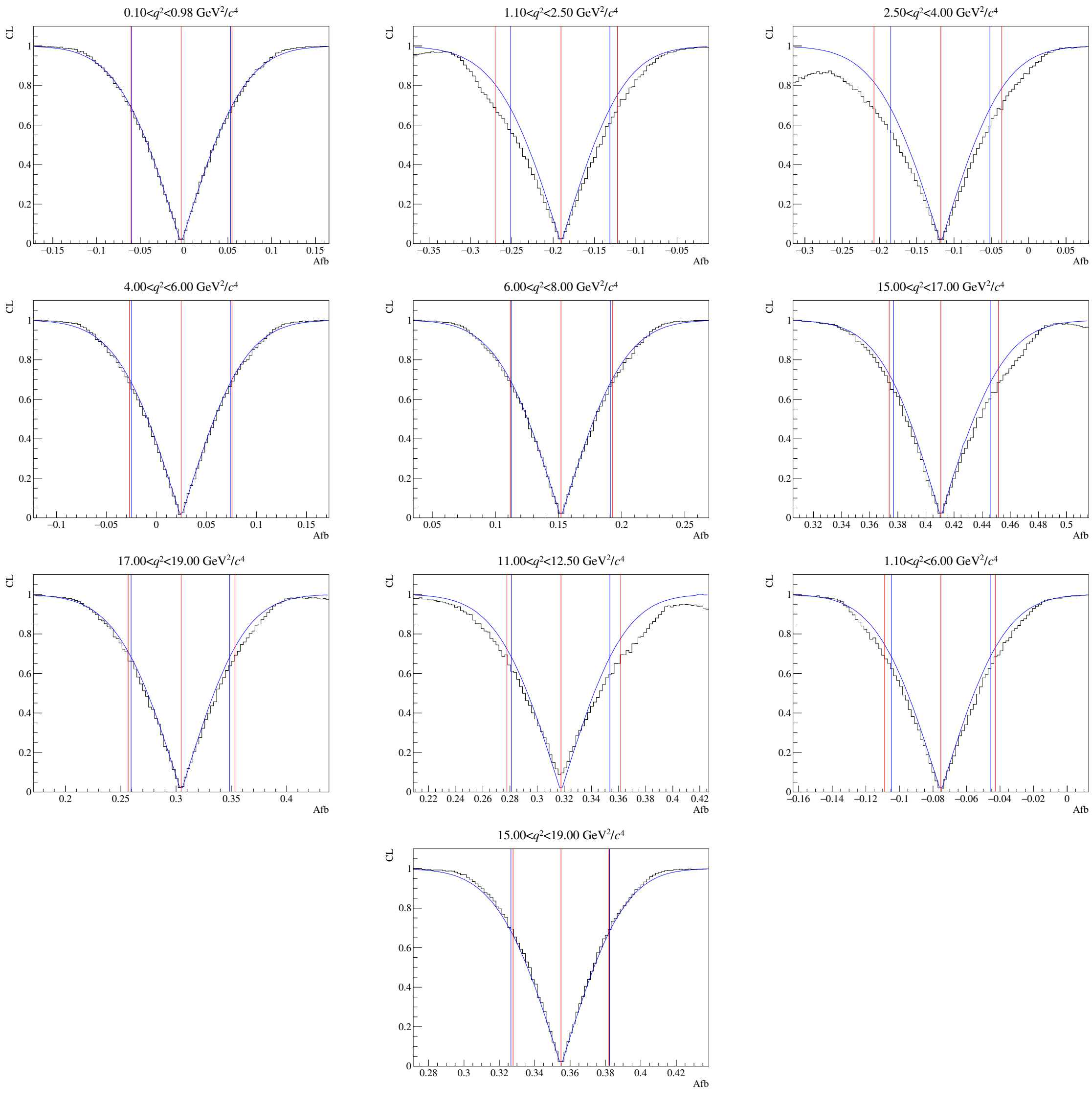

Figure 121: Feldman-Cousins scan for the angular observable A_{FB}.

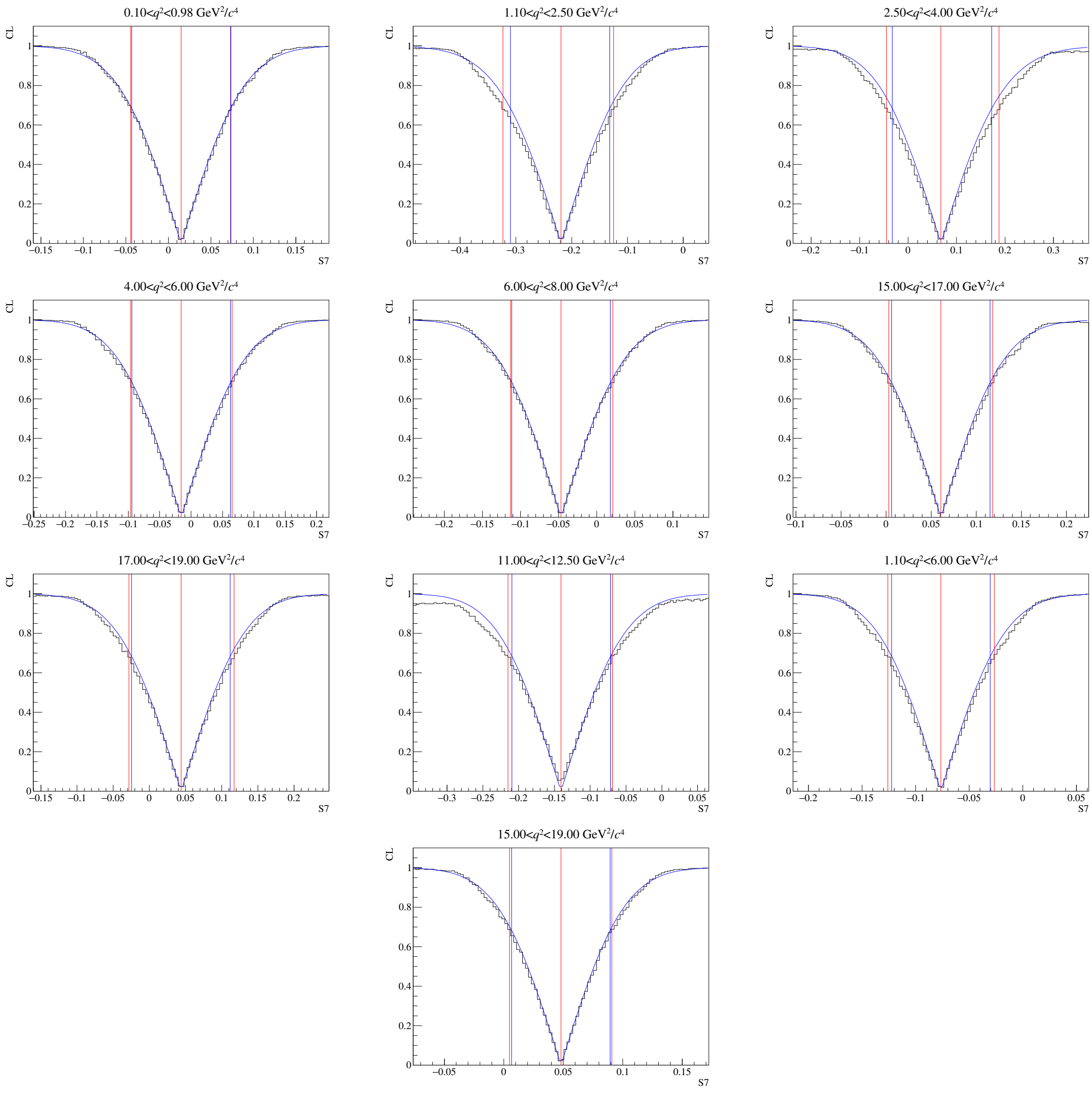

Figure 122: Feldman-Cousins scan for the angular observable S_7.

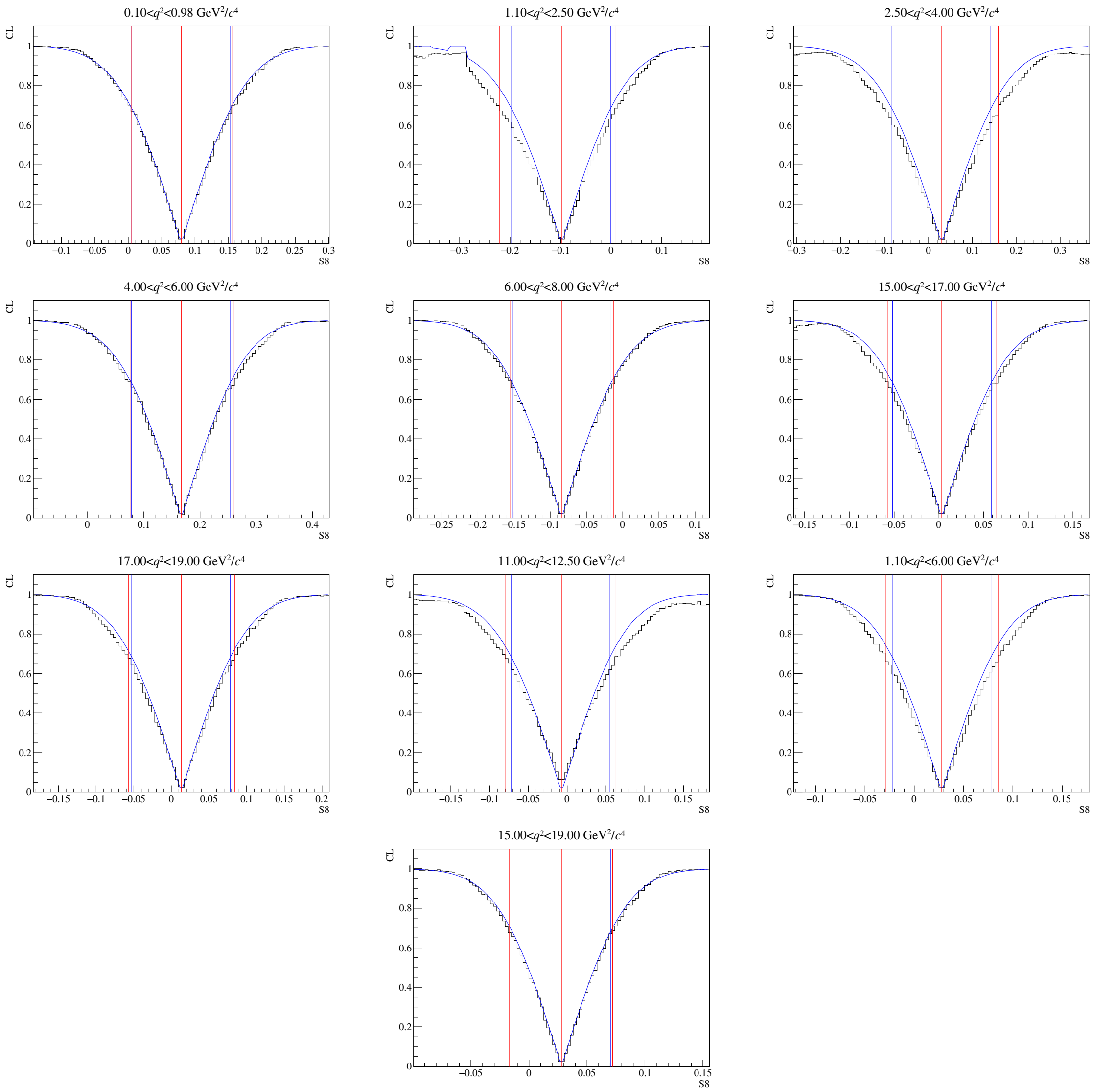

Figure 123: Feldman-Cousins scan for the angular observable S_8.

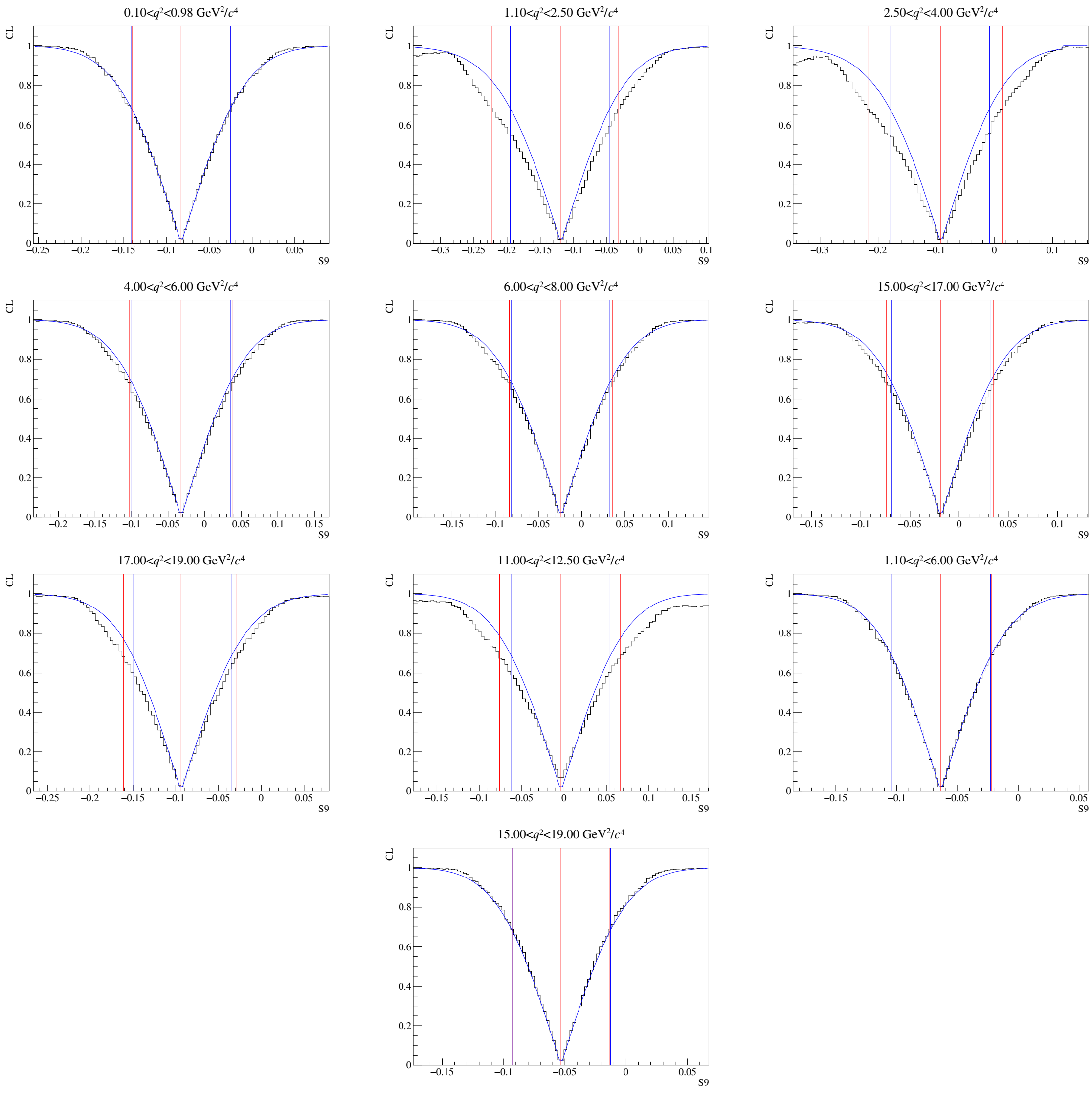

Figure 124: Feldman-Cousins scan for the angular observable S_9.

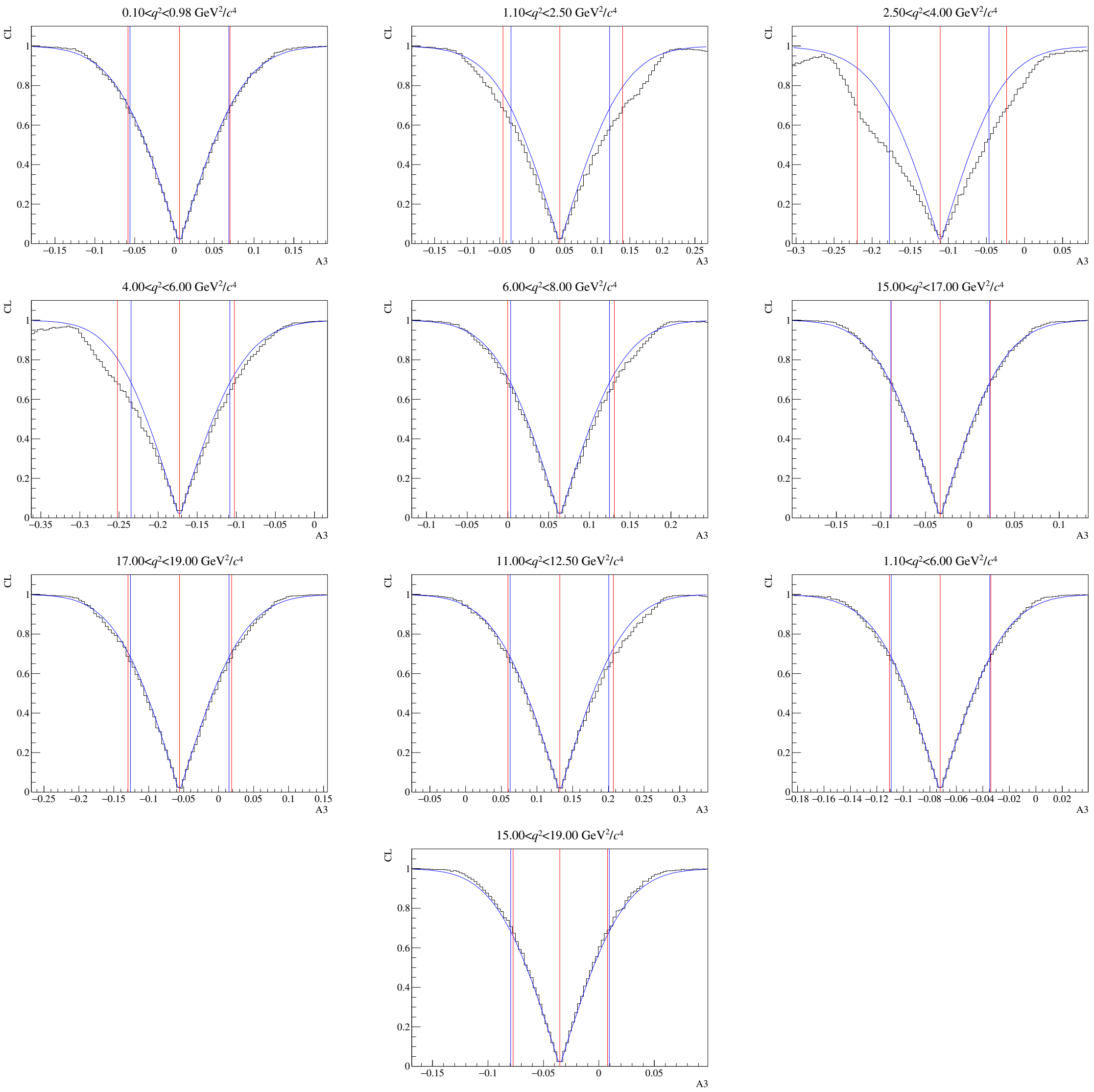

Figure 125: Feldman-Cousins scan for the angular observable A_3.

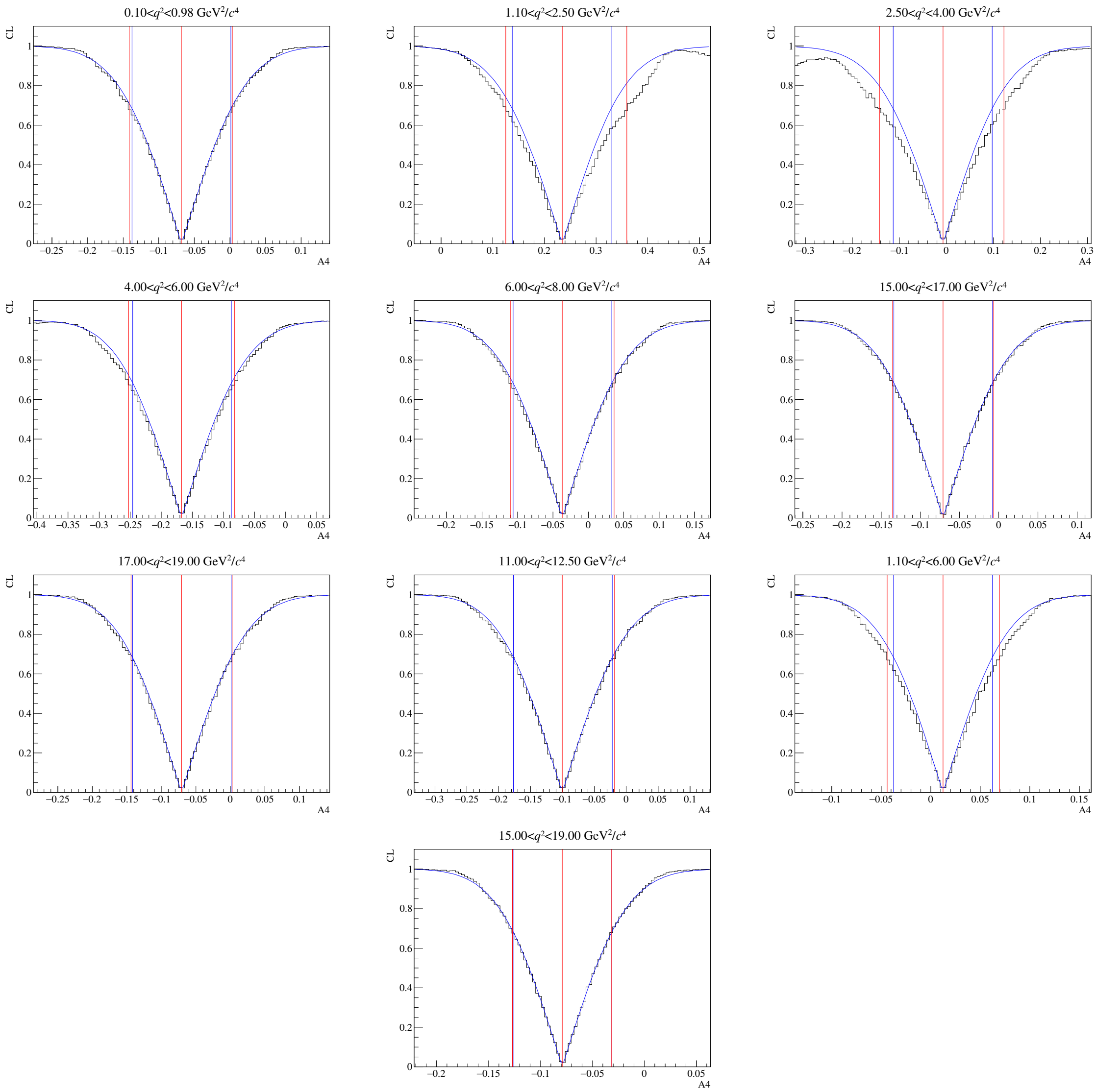

Figure 126: Feldman-Cousins scan for the angular observable A_4.

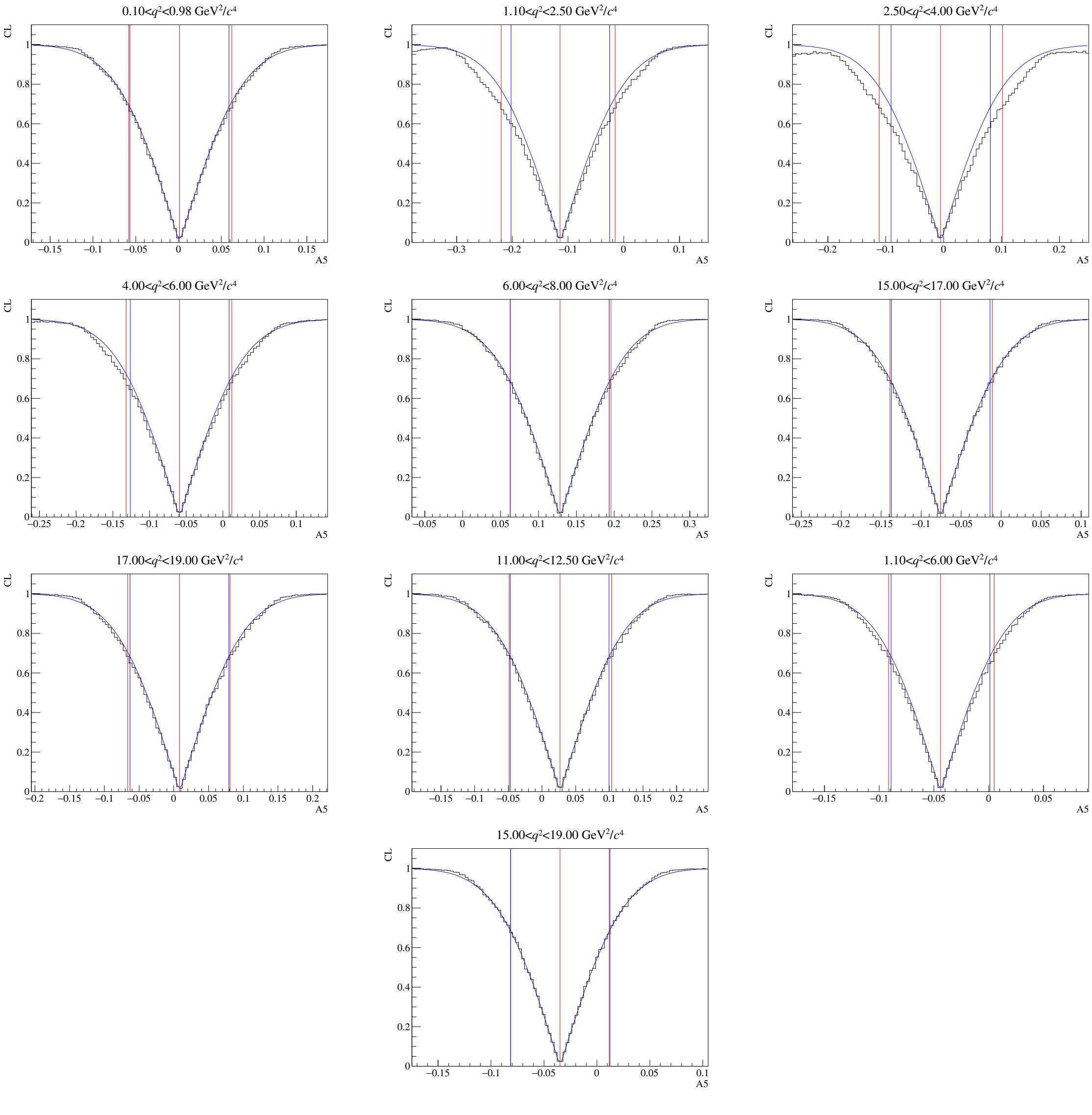

Figure 127: Feldman-Cousins scan for the angular observable A_5.

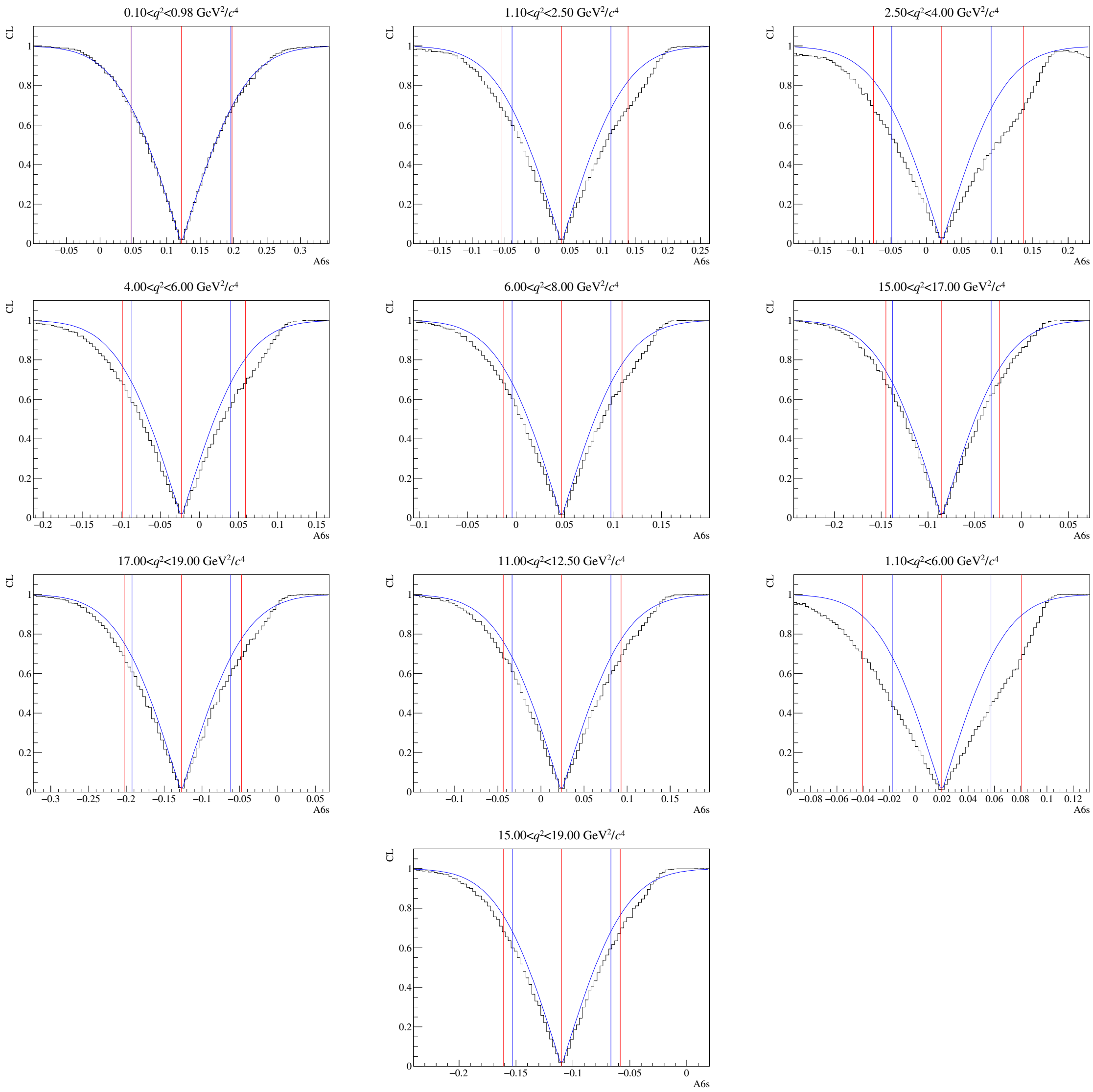

Figure 128: Feldman-Cousins scan for the angular observable A_6.

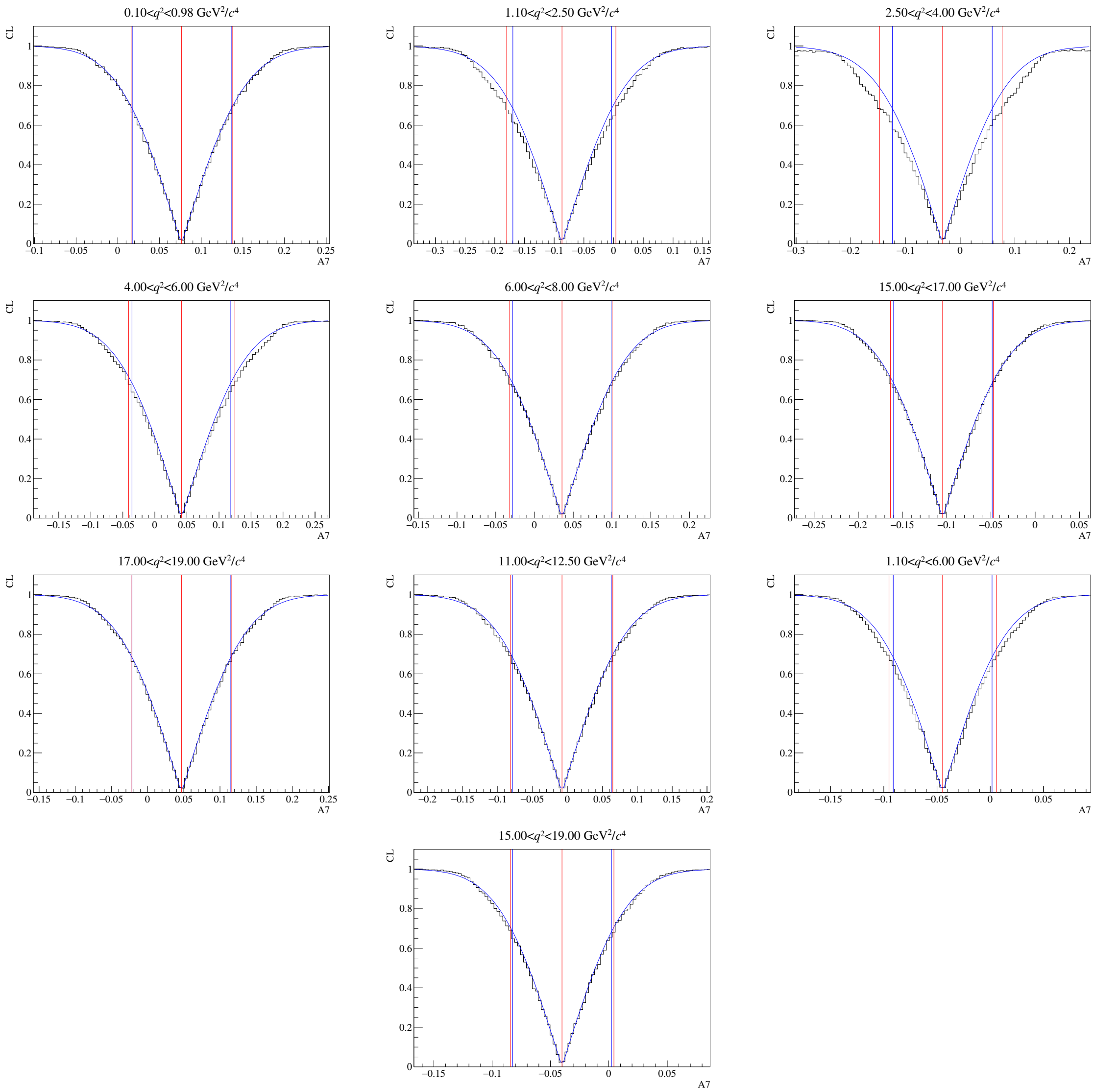

Figure 129: Feldman-Cousins scan for the angular observable A_7.

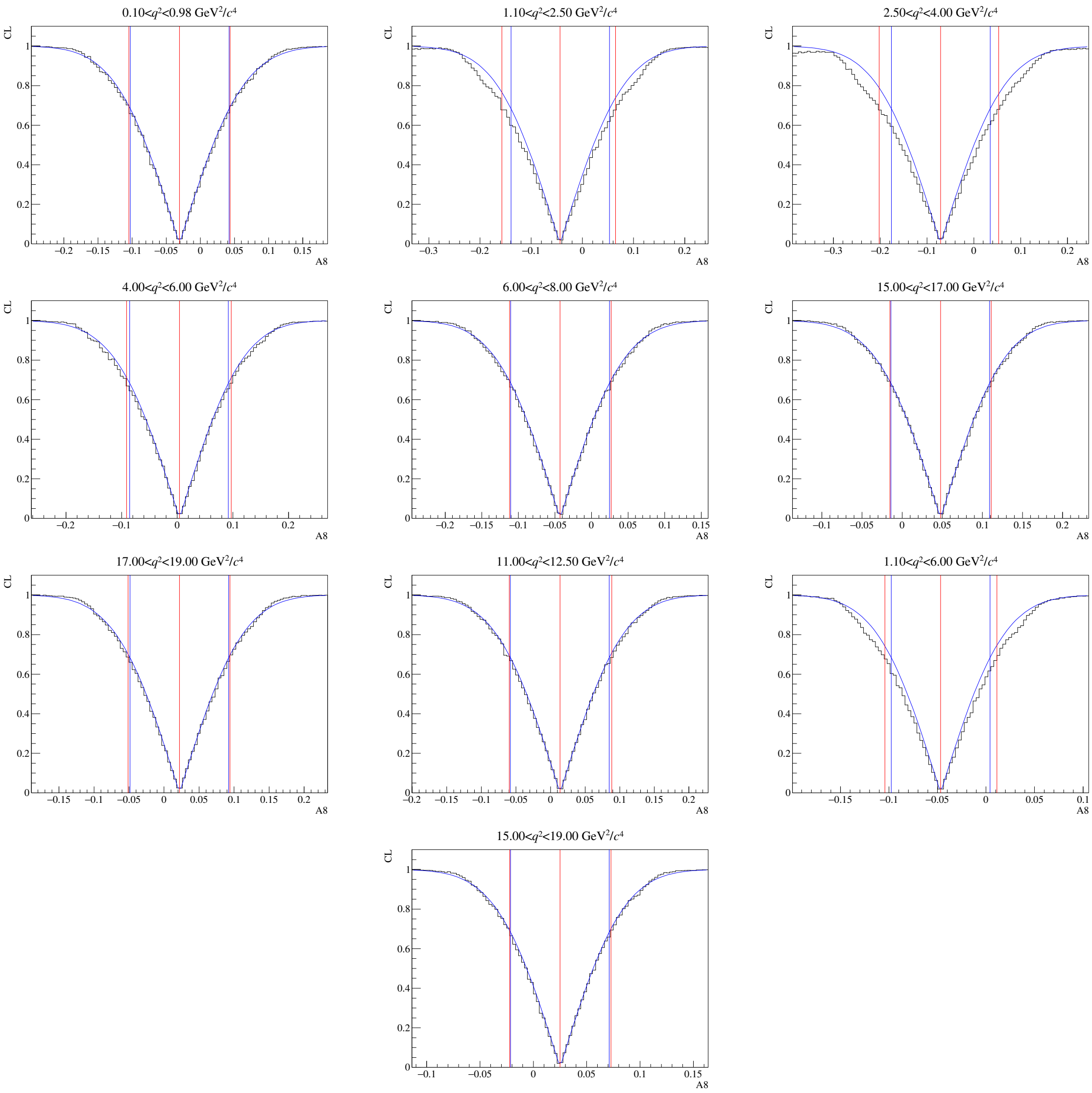

Figure 130: Feldman-Cousins scan for the angular observable A_8.

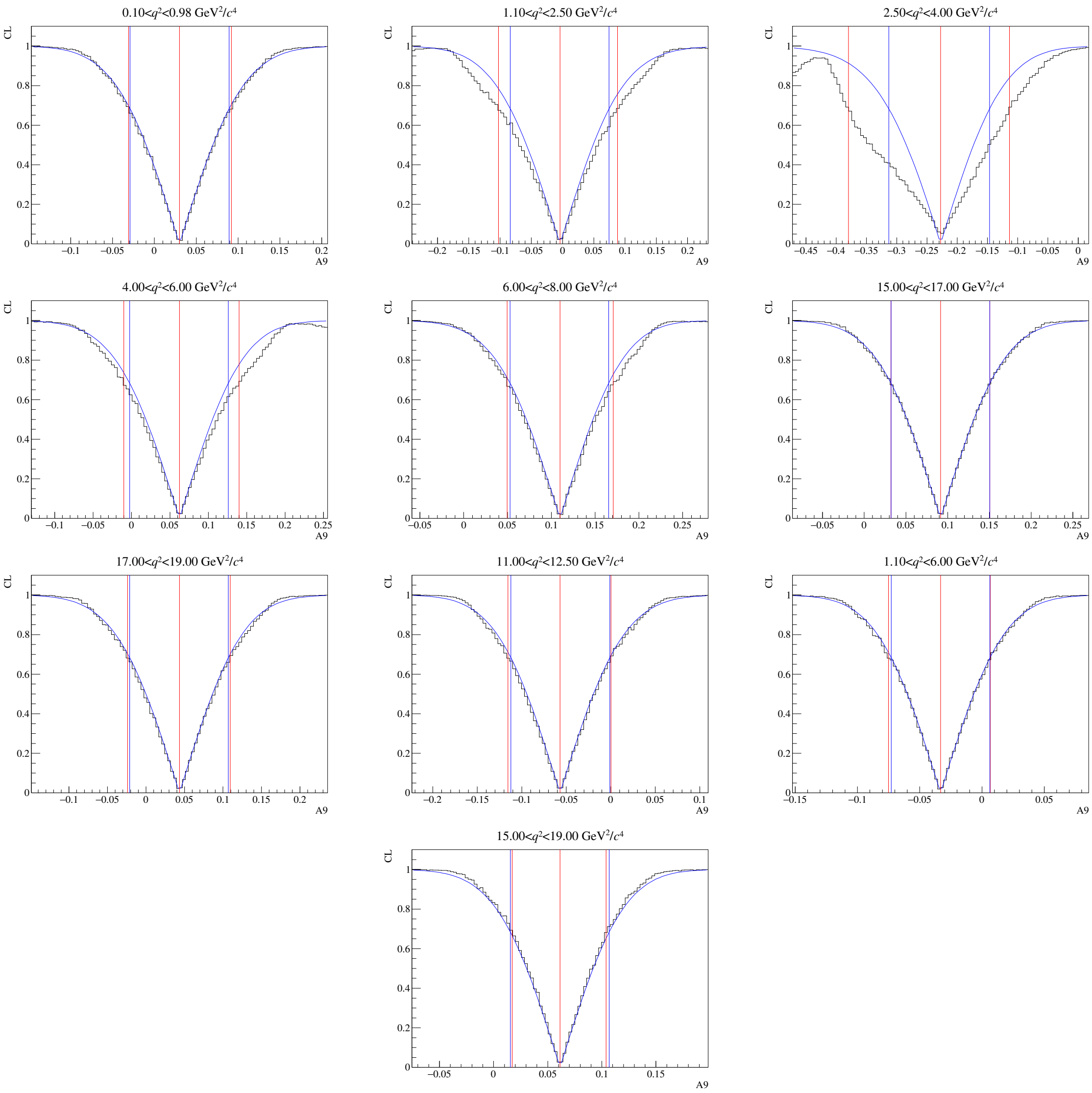

Figure 131: Feldman-Cousins scan for the angular observable A_9.

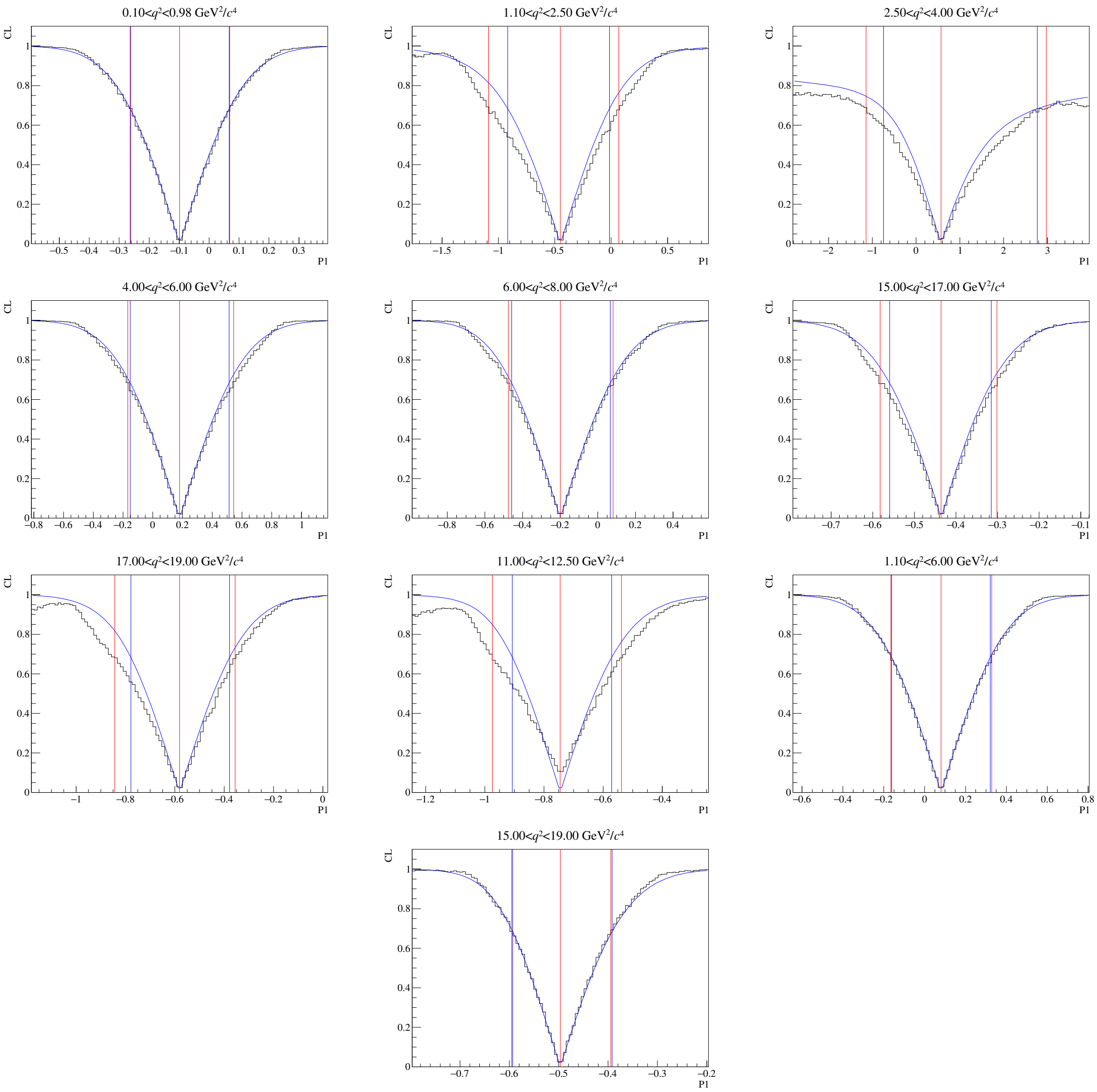

Figure 132: Feldman-Cousins scan for the angular observable P_1.

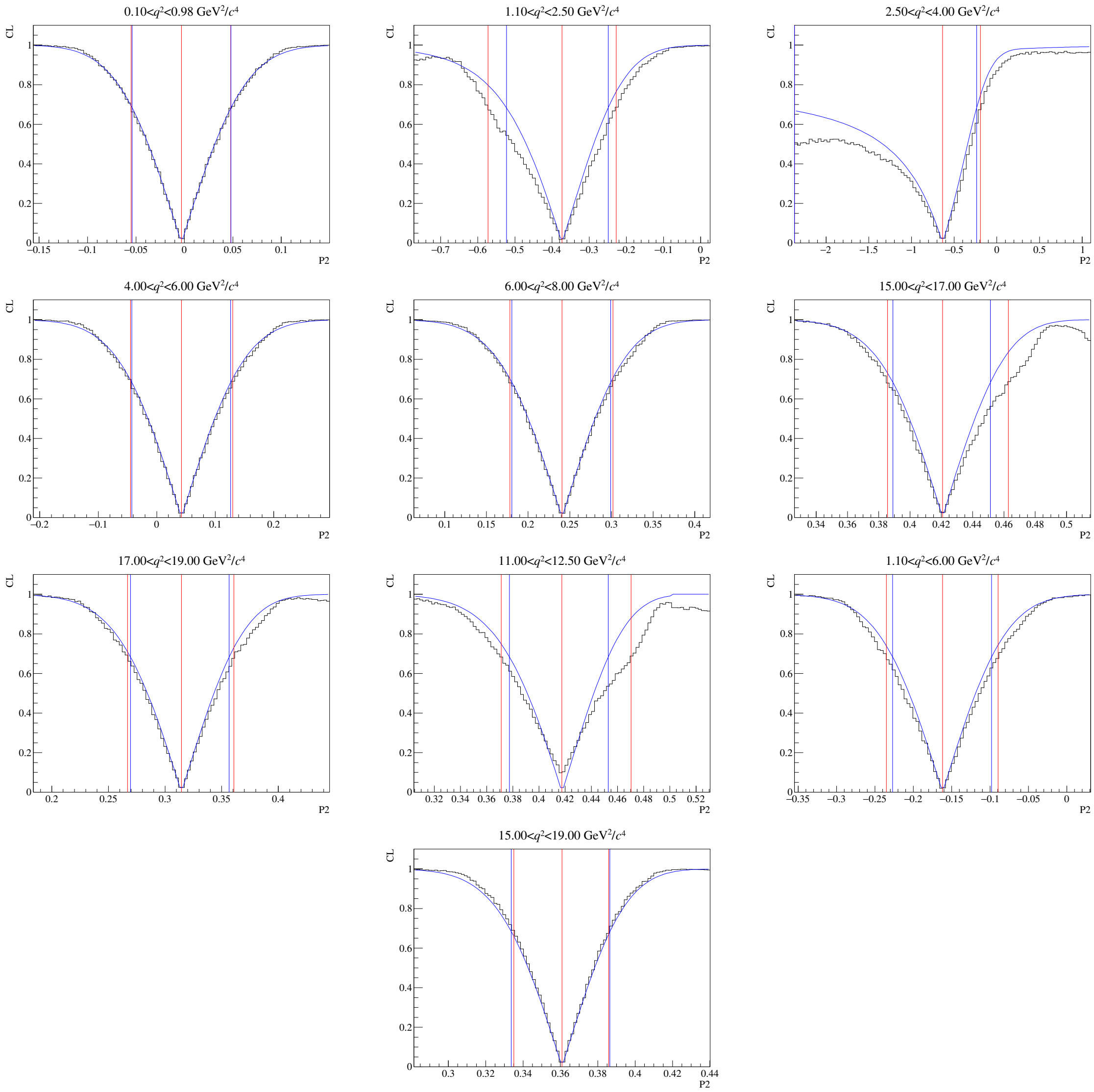

Figure 133: Feldman-Cousins scan for the angular observable P_2.

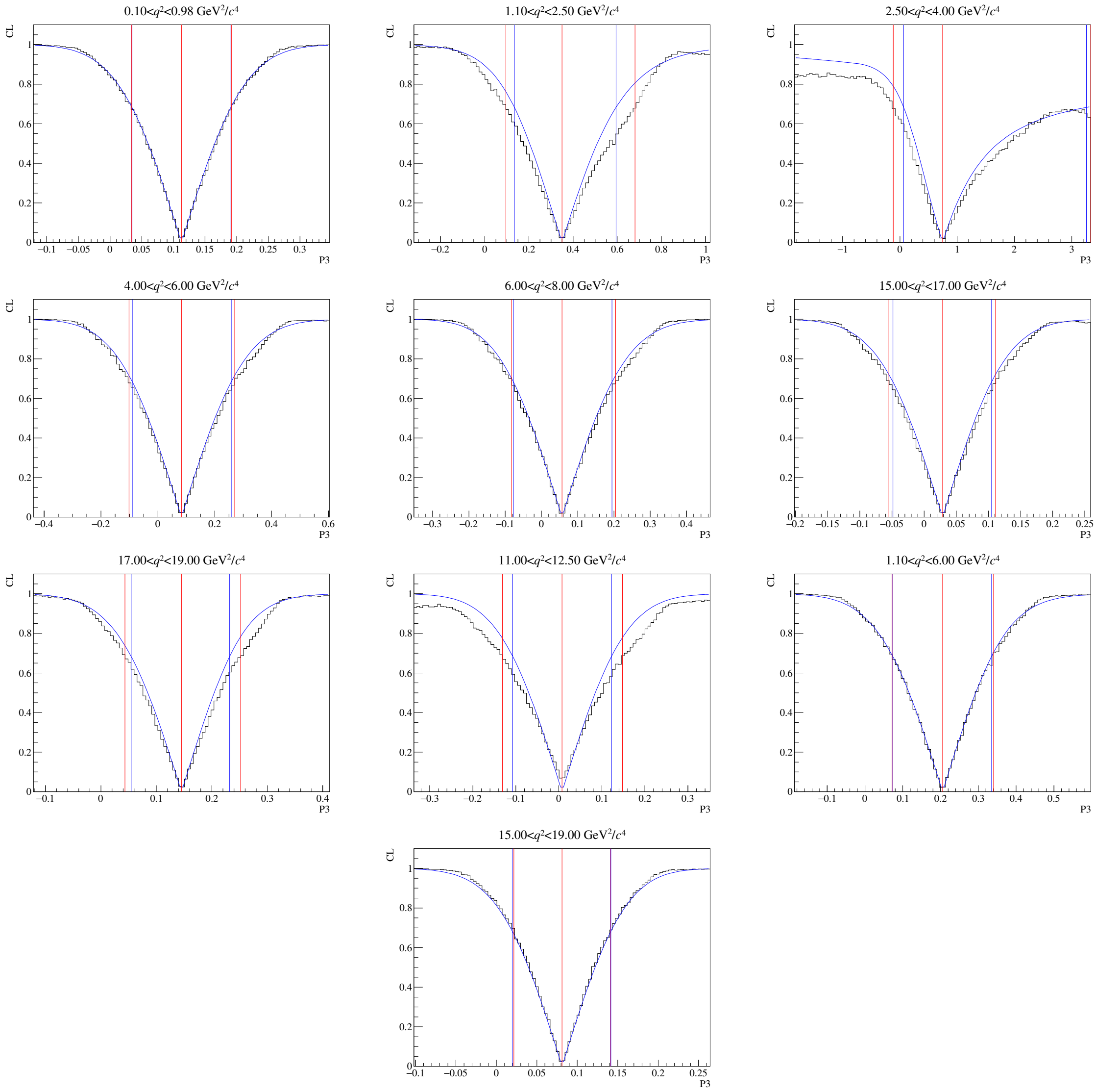

Figure 134: Feldman-Cousins scan for the angular observable P_3.

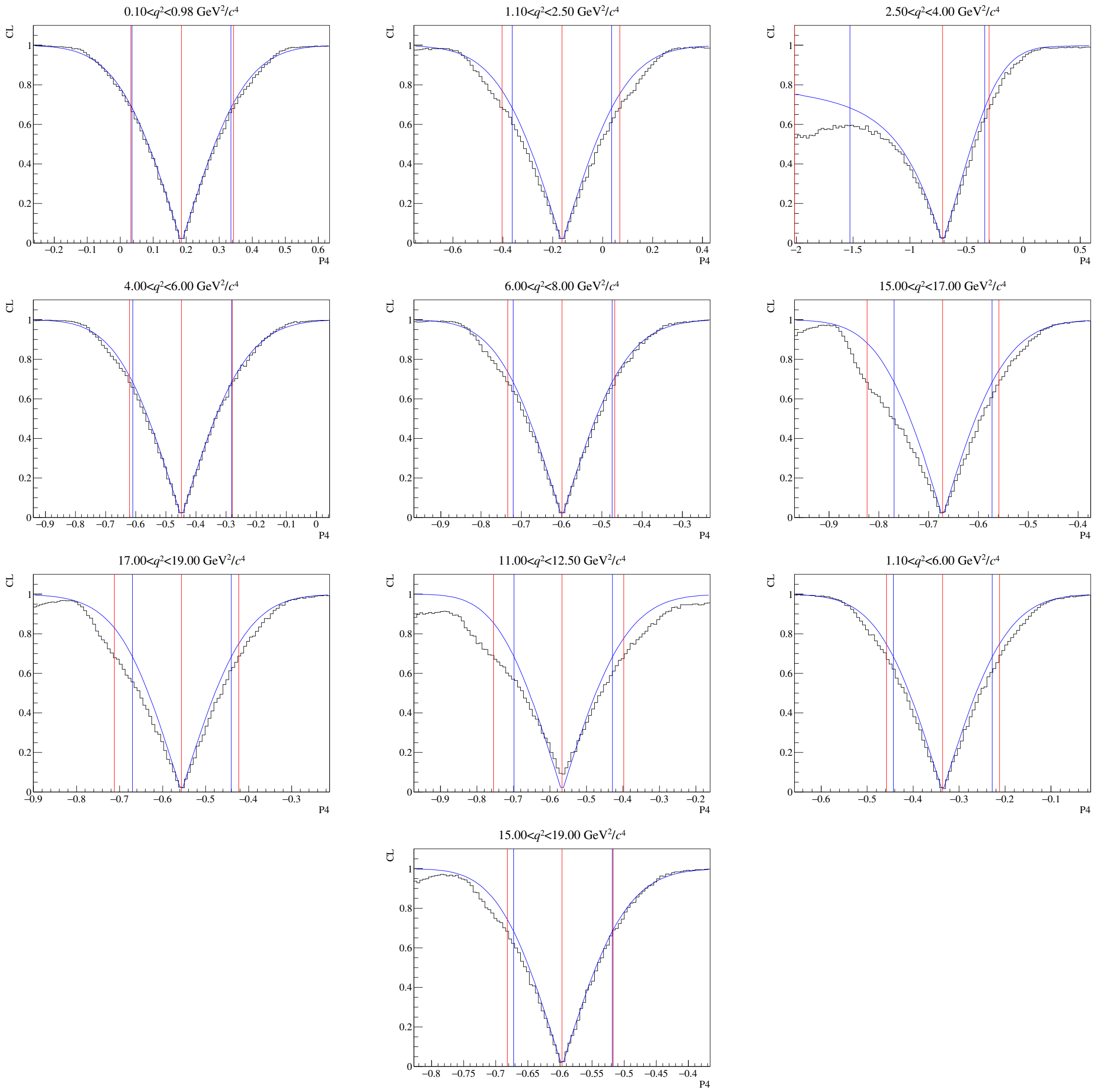

Figure 135: Feldman-Cousins scan for the angular observable P_4'.

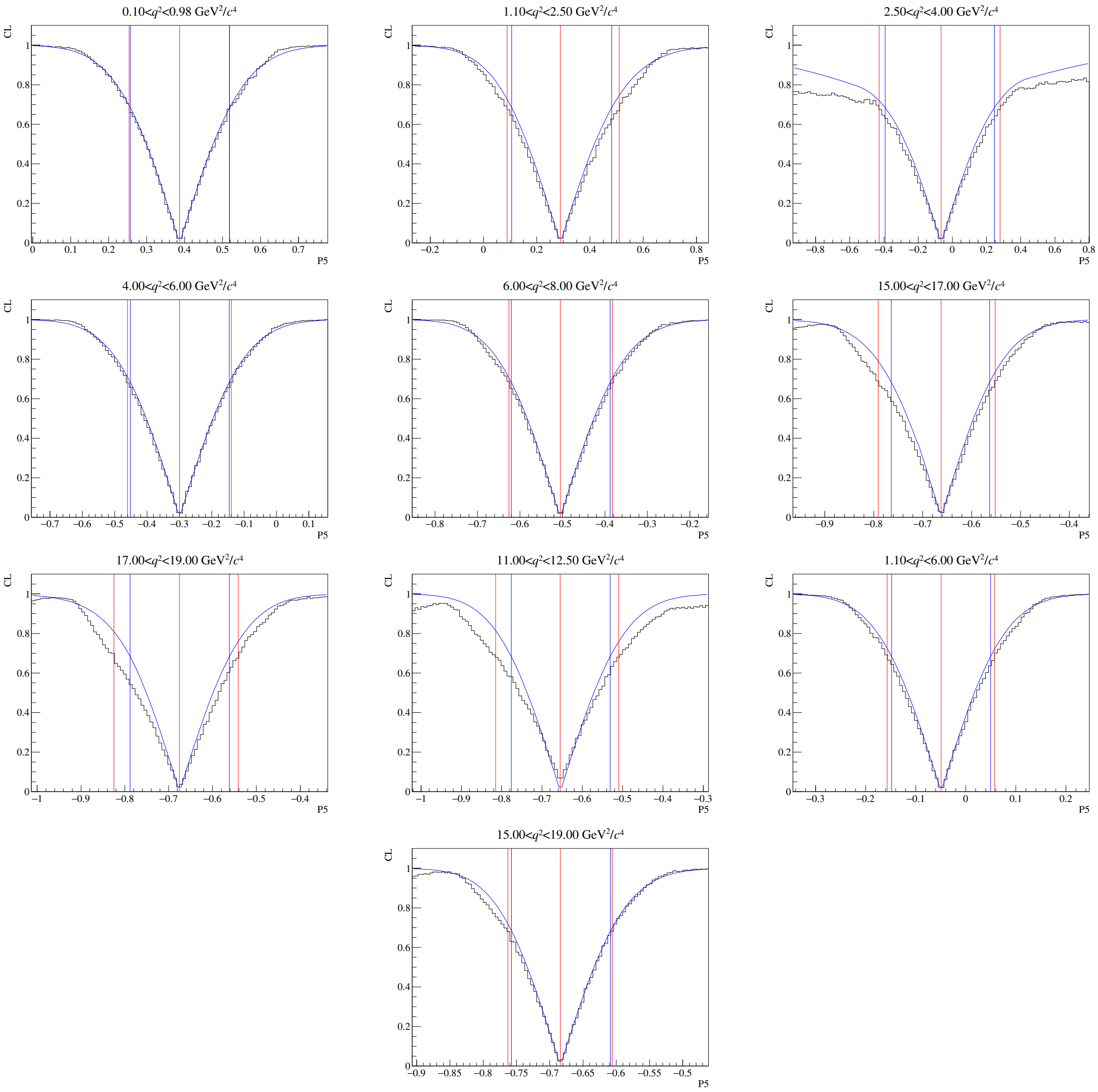

Figure 136: Feldman-Cousins scan for the angular observable P_5'.

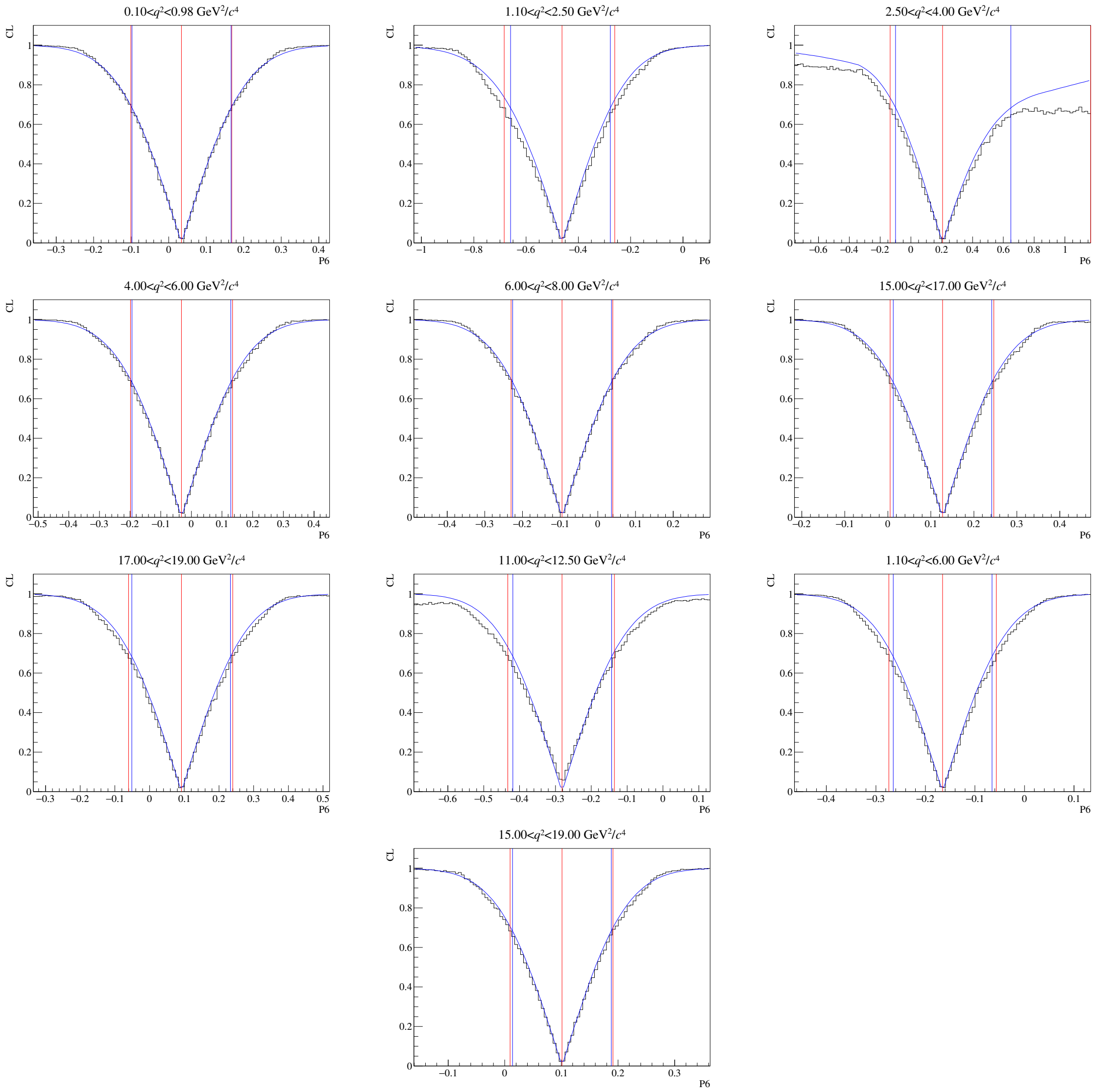

Figure 137: Feldman-Cousins scan for the angular observable P_6'.

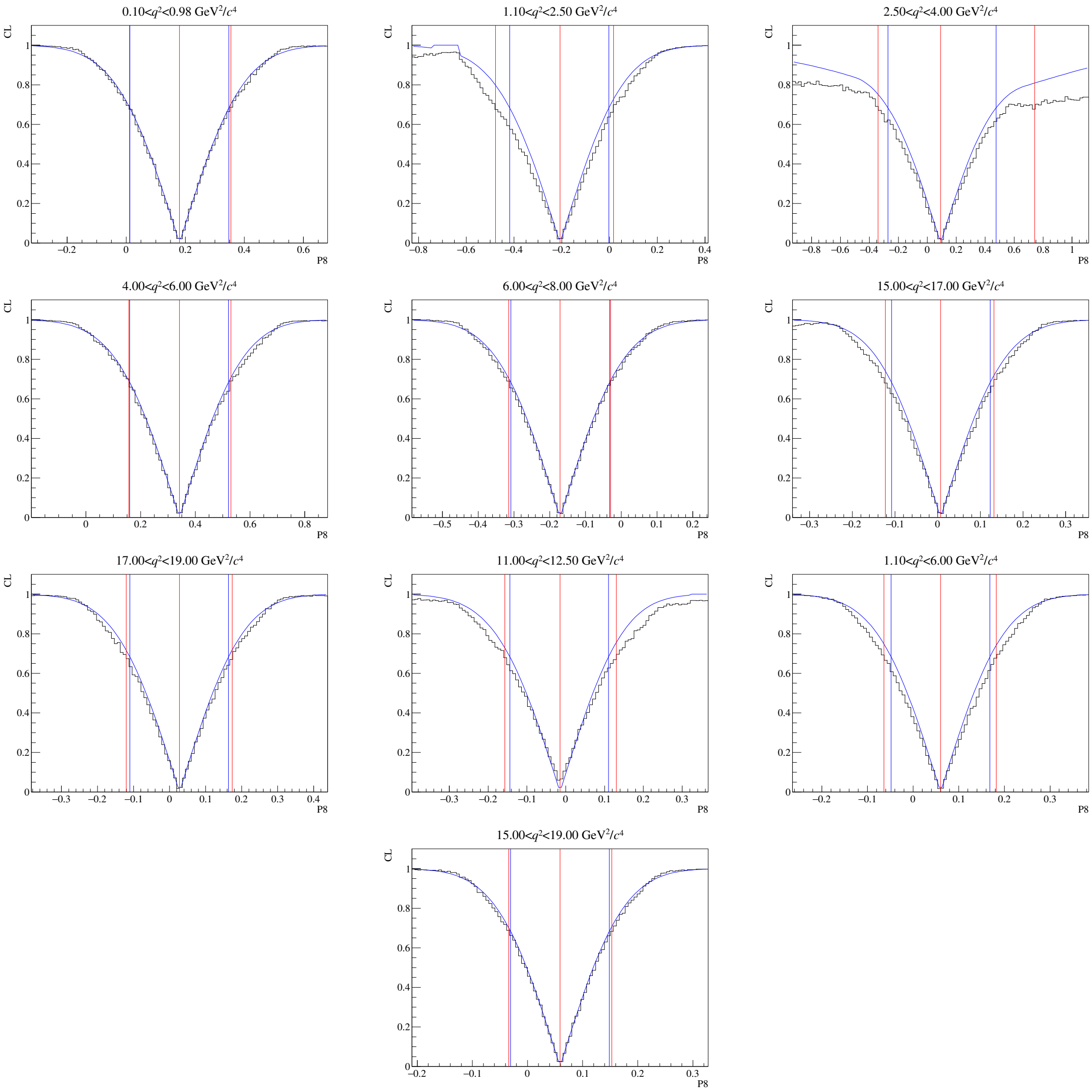

Figure 138: Feldman-Cousins scan for the angular observable P_8'.

E Correlations for the likelihood fit

Table 119: Correlations for the CP-averaged observables S_i.

$0.1 < q^2 < 0.98\,\mathrm{GeV}^2/c^4$

	F_{L}	S_3	S_4	S_5	A_{FB}	S_7	S_8	S_9
F_{L}	1.00	0.06	0.00	0.03	0.04	−0.02	0.07	0.08
S_3		1.00	0.01	0.10	−0.00	−0.07	−0.01	−0.03
S_4			1.00	0.08	0.11	−0.00	0.07	0.02
S_5				1.00	0.05	−0.01	0.00	0.04
A_{FB}					1.00	0.03	−0.07	0.02
S_7						1.00	0.01	0.11
S_8							1.00	0.02
S_9								1.00

$1.1 < q^2 < 2.5\,\mathrm{GeV}^2/c^4$

	F_{L}	S_3	S_4	S_5	A_{FB}	S_7	S_8	S_9
F_{L}	1.00	0.09	0.07	0.07	0.09	−0.05	−0.04	0.08
S_3		1.00	−0.04	0.04	0.01	0.13	0.09	0.12
S_4			1.00	−0.22	−0.01	−0.00	−0.05	0.03
S_5				1.00	−0.14	−0.11	−0.03	−0.21
A_{FB}					1.00	−0.03	−0.10	−0.11
S_7						1.00	−0.11	0.23
S_8							1.00	−0.04
S_9								1.00

$2.5 < q^2 < 4.0\,\mathrm{GeV}^2/c^4$

	F_{L}	S_3	S_4	S_5	A_{FB}	S_7	S_8	S_9
F_{L}	1.00	−0.13	−0.14	0.01	−0.03	0.10	−0.03	−0.01
S_3		1.00	−0.06	0.09	0.07	−0.02	0.01	−0.07
S_4			1.00	−0.19	−0.09	−0.05	0.12	0.07
S_5				1.00	−0.01	0.05	−0.02	0.10
A_{FB}					1.00	−0.01	−0.10	0.10
S_7						1.00	0.07	−0.05
S_8							1.00	−0.01
S_9								1.00

$4.0 < q^2 < 6.0\,\mathrm{GeV}^2/c^4$

	F_{L}	S_3	S_4	S_5	A_{FB}	S_7	S_8	S_9
F_{L}	1.00	−0.03	0.09	0.10	−0.05	−0.10	0.04	0.00
S_3		1.00	−0.04	−0.03	0.09	−0.10	−0.00	−0.12
S_4			1.00	0.10	−0.10	−0.02	−0.04	0.04
S_5				1.00	−0.06	−0.03	−0.01	−0.04
A_{FB}					1.00	0.03	0.07	−0.03
S_7						1.00	0.06	−0.15
S_8							1.00	0.03
S_9								1.00

$6.0 < q^2 < 8.0\,\mathrm{GeV}^2/c^4$

	F_{L}	S_3	S_4	S_5	A_{FB}	S_7	S_8	S_9
F_{L}	1.00	0.03	0.06	0.03	−0.31	−0.08	−0.01	−0.06
S_3		1.00	−0.16	−0.23	0.01	0.02	0.02	−0.07
S_4			1.00	−0.13	−0.12	−0.01	−0.11	0.01
S_5				1.00	−0.16	−0.14	−0.01	−0.04
A_{FB}					1.00	−0.01	0.04	0.02
S_7						1.00	0.10	−0.05
S_8							1.00	−0.10
S_9								1.00

$11.0 < q^2 < 12.5\,\mathrm{GeV}^2/c^4$

	F_{L}	S_3	S_4	S_5	A_{FB}	S_7	S_8	S_9
F_{L}	1.00	0.25	0.02	−0.02	−0.62	0.03	0.05	0.02
S_3		1.00	0.05	−0.35	−0.24	−0.04	0.06	−0.02
S_4			1.00	−0.02	0.06	−0.05	−0.12	−0.08
S_5				1.00	0.01	−0.04	−0.09	−0.24
A_{FB}					1.00	−0.01	−0.06	0.07
S_7						1.00	0.27	−0.19
S_8							1.00	−0.09
S_9								1.00

$15.0 < q^2 < 17.0\,\mathrm{GeV}^2/c^4$

	F_{L}	S_3	S_4	S_5	A_{FB}	S_7	S_8	S_9
F_{L}	1.00	0.26	−0.10	0.09	−0.50	−0.02	−0.06	0.14
S_3		1.00	−0.08	−0.03	−0.00	−0.04	−0.05	0.10
S_4			1.00	0.26	−0.16	−0.05	0.19	0.05
S_5				1.00	−0.20	0.12	−0.01	0.05
A_{FB}					1.00	0.05	−0.02	−0.08
S_7						1.00	0.25	−0.23
S_8							1.00	−0.11
S_9								1.00

$17.0 < q^2 < 19.0\,\mathrm{GeV}^2/c^4$

	F_{L}	S_3	S_4	S_5	A_{FB}	S_7	S_8	S_9
F_{L}	1.00	0.07	0.06	0.04	−0.35	0.07	0.07	0.08
S_3		1.00	−0.15	−0.39	−0.05	−0.06	−0.04	−0.07
S_4			1.00	0.10	−0.17	0.03	0.18	−0.04
S_5				1.00	−0.11	0.04	0.01	−0.00
A_{FB}					1.00	−0.02	−0.09	−0.03
S_7						1.00	0.34	−0.15
S_8							1.00	−0.11
S_9								1.00

$1.1 < q^2 < 6.0\,\mathrm{GeV}^2/c^4$

	F_{L}	S_3	S_4	S_5	A_{FB}	S_7	S_8	S_9
F_{L}	1.00	−0.04	0.05	0.03	0.05	−0.04	−0.01	0.08
S_3		1.00	−0.05	−0.00	0.05	0.01	0.01	−0.01
S_4			1.00	−0.05	−0.11	−0.02	−0.01	0.05
S_5				1.00	−0.07	−0.01	−0.02	−0.04
A_{FB}					1.00	0.02	−0.02	−0.04
S_7						1.00	0.04	−0.01
S_8							1.00	−0.03
S_9								1.00

$15.0 < q^2 < 19.0\,\mathrm{GeV}^2/c^4$

	F_{L}	S_3	S_4	S_5	A_{FB}	S_7	S_8	S_9
F_{L}	1.00	0.17	−0.03	−0.02	−0.39	0.01	−0.00	0.11
S_3		1.00	−0.15	−0.19	0.05	−0.02	−0.04	−0.02
S_4			1.00	0.06	−0.12	0.03	0.14	0.01
S_5				1.00	−0.12	0.12	0.04	0.02
A_{FB}					1.00	0.00	−0.02	−0.01
S_7						1.00	0.24	−0.19
S_8							1.00	−0.13
S_9								1.00

Table 120: Correlations for the CP asymmetries A_i.

$0.1 < q^2 < 0.98\,\mathrm{GeV}^2/c^4$

	F_L	A_3	A_4	A_5	A_6	A_7	A_8	A_9
F_L	1.00	−0.00	0.02	0.01	−0.07	−0.01	−0.01	−0.03
A_3		1.00	−0.04	−0.07	0.00	−0.03	0.02	−0.05
A_4			1.00	0.05	−0.08	0.02	0.09	−0.03
A_5				1.00	−0.04	0.08	0.03	0.02
A_6					1.00	−0.04	−0.07	0.01
A_7						1.00	0.00	−0.14
A_8							1.00	−0.01
A_9								1.00

$1.1 < q^2 < 2.5\,\mathrm{GeV}^2/c^4$

	F_L	A_3	A_4	A_5	A_6	A_7	A_8	A_9
F_L	1.00	0.07	−0.14	−0.06	−0.04	0.06	−0.04	−0.10
A_3		1.00	−0.05	−0.11	0.01	−0.04	0.05	−0.05
A_4			1.00	0.09	−0.26	0.03	−0.15	0.10
A_5				1.00	0.03	0.03	0.06	0.01
A_6					1.00	0.10	0.11	0.01
A_7						1.00	0.19	0.12
A_8							1.00	0.03
A_9								1.00

$2.5 < q^2 < 4.0\,\mathrm{GeV}^2/c^4$

	F_L	A_3	A_4	A_5	A_6	A_7	A_8	A_9
F_L	1.00	0.13	−0.04	0.07	0.10	−0.08	0.08	0.11
A_3		1.00	0.19	−0.00	−0.07	−0.03	0.09	0.11
A_4			1.00	0.21	−0.12	0.02	0.13	0.09
A_5				1.00	0.11	0.08	0.01	0.06
A_6					1.00	−0.05	−0.28	−0.05
A_7						1.00	0.31	−0.03
A_8							1.00	0.10
A_9								1.00

$4.0 < q^2 < 6.0\,\mathrm{GeV}^2/c^4$

	F_L	A_3	A_4	A_5	A_6	A_7	A_8	A_9
F_L	1.00	0.03	0.02	0.03	0.01	0.05	0.08	0.01
A_3		1.00	0.08	0.19	0.10	−0.16	0.06	−0.08
A_4			1.00	0.06	−0.01	−0.01	−0.01	−0.03
A_5				1.00	0.08	0.00	0.01	−0.12
A_6					1.00	−0.12	0.06	−0.05
A_7						1.00	0.05	−0.01
A_8							1.00	0.13
A_9								1.00

$6.0 < q^2 < 8.0\,\mathrm{GeV}^2/c^4$

	F_L	A_3	A_4	A_5	A_6	A_7	A_8	A_9
F_L	1.00	−0.07	−0.06	0.03	−0.03	−0.01	0.02	−0.15
A_3		1.00	0.08	0.12	−0.07	−0.01	0.01	−0.06
A_4			1.00	−0.07	0.08	0.01	−0.00	0.05
A_5				1.00	0.13	−0.03	0.01	0.01
A_6					1.00	0.02	0.05	−0.06
A_7						1.00	−0.11	0.12
A_8							1.00	0.06
A_9								1.00

$11.0 < q^2 < 12.5\,\mathrm{GeV}^2/c^4$

	F_L	A_3	A_4	A_5	A_6	A_7	A_8	A_9
F_L	1.00	−0.09	−0.01	0.00	−0.01	−0.02	0.01	0.06
A_3		1.00	0.05	0.19	0.02	−0.16	0.08	0.11
A_4			1.00	−0.26	0.20	−0.10	0.02	−0.01
A_5				1.00	0.11	−0.03	−0.06	0.04
A_6					1.00	−0.06	0.11	−0.02
A_7						1.00	−0.22	0.19
A_8							1.00	0.04
A_9								1.00

$15.0 < q^2 < 17.0\,\mathrm{GeV}^2/c^4$

	F_L	A_3	A_4	A_5	A_6	A_7	A_8	A_9
F_L	1.00	0.04	0.02	0.02	0.06	−0.07	0.04	−0.07
A_3		1.00	0.05	0.16	0.02	−0.00	−0.02	0.04
A_4			1.00	−0.25	0.16	−0.07	0.10	−0.01
A_5				1.00	0.12	0.09	−0.07	−0.07
A_6					1.00	−0.01	0.04	0.03
A_7						1.00	−0.17	0.11
A_8							1.00	0.08
A_9								1.00

$17.0 < q^2 < 19.0\,\mathrm{GeV}^2/c^4$

	F_L	A_3	A_4	A_5	A_6	A_7	A_8	A_9
F_L	1.00	−0.00	0.03	−0.00	0.09	−0.04	0.07	−0.03
A_3		1.00	0.14	0.18	−0.01	−0.07	−0.05	−0.06
A_4			1.00	−0.09	0.10	−0.11	0.04	−0.09
A_5				1.00	0.11	0.04	−0.11	−0.04
A_6					1.00	−0.01	−0.08	−0.08
A_7						1.00	−0.03	0.14
A_8							1.00	0.01
A_9								1.00

$1.1 < q^2 < 6.0\,\mathrm{GeV}^2/c^4$

	F_L	A_3	A_4	A_5	A_6	A_7	A_8	A_9
F_L	1.00	0.04	0.00	−0.00	−0.01	0.01	0.04	−0.01
A_3		1.00	0.05	0.04	0.04	−0.08	0.05	0.01
A_4			1.00	0.12	−0.09	−0.02	0.03	0.03
A_5				1.00	0.05	0.05	−0.01	0.01
A_6					1.00	−0.02	0.05	−0.03
A_7						1.00	0.18	0.00
A_8							1.00	0.06
A_9								1.00

$15.0 < q^2 < 19.0\,\mathrm{GeV}^2/c^4$

	F_L	A_3	A_4	A_5	A_6	A_7	A_8	A_9
F_L	1.00	0.02	0.01	−0.01	0.06	−0.04	0.04	−0.04
A_3		1.00	0.07	0.17	0.03	−0.02	−0.02	0.02
A_4			1.00	−0.19	0.13	−0.06	0.06	−0.03
A_5				1.00	0.11	0.06	−0.07	−0.05
A_6					1.00	−0.00	−0.01	−0.01
A_7						1.00	−0.11	0.13
A_8							1.00	0.05
A_9								1.00

Table 121: Correlations for the CP-averaged observables $P_i^{(\prime)}$.

$0.1 < q^2 < 0.98\,\mathrm{GeV}^2/c^4$

	F_L	P_1	P_2	P_3	P_4'	P_5'	P_6'	P_8'
F_L	1.00	0.02	0.03	0.00	−0.07	−0.12	−0.03	0.01
P_1		1.00	−0.00	0.04	0.01	0.09	−0.07	−0.02
P_2			1.00	−0.02	0.11	0.04	0.03	−0.08
P_3				1.00	−0.02	−0.04	−0.11	−0.01
P_4'					1.00	0.09	0.00	0.07
P_5'						1.00	−0.00	−0.00
P_6'							1.00	0.01
P_8'								1.00

$1.1 < q^2 < 2.5\,\mathrm{GeV}^2/c^4$

	F_L	P_1	P_2	P_3	P_4'	P_5'	P_6'	P_8'
F_L	1.00	−0.11	−0.48	0.23	0.03	0.15	−0.17	−0.09
P_1		1.00	0.06	−0.13	−0.05	0.01	0.15	0.11
P_2			1.00	−0.02	−0.03	−0.19	0.06	−0.04
P_3				1.00	−0.01	0.24	−0.26	0.01
P_4'					1.00	−0.22	−0.00	−0.05
P_5'						1.00	−0.13	−0.04
P_6'							1.00	−0.10
P_8'								1.00

$2.5 < q^2 < 4.0\,\mathrm{GeV}^2/c^4$

	F_L	P_1	P_2	P_3	P_4'	P_5'	P_6'	P_8'
F_L	1.00	0.23	−0.79	0.61	−0.60	−0.05	0.29	0.06
P_1		1.00	−0.14	0.19	−0.20	0.08	0.06	0.02
P_2			1.00	−0.53	0.43	0.04	−0.23	−0.11
P_3				1.00	−0.41	−0.11	0.21	0.04
P_4'					1.00	−0.12	−0.21	0.06
P_5'						1.00	0.03	−0.03
P_6'							1.00	0.08
P_8'								1.00

$4.0 < q^2 < 6.0\,\mathrm{GeV}^2/c^4$

	F_L	P_1	P_2	P_3	P_4'	P_5'	P_6'	P_8'
F_L	1.00	0.04	0.02	0.06	0.02	0.06	−0.10	0.09
P_1		1.00	0.09	0.12	−0.04	−0.03	−0.11	0.00
P_2			1.00	0.03	−0.09	−0.05	0.02	0.07
P_3				1.00	−0.04	0.04	0.14	−0.02
P_4'					1.00	0.10	−0.02	−0.04
P_5'						1.00	−0.03	−0.01
P_6'							1.00	0.06
P_8'								1.00

$6.0 < q^2 < 8.0\,\mathrm{GeV}^2/c^4$

	F_L	P_1	P_2	P_3	P_4'	P_5'	P_6'	P_8'
F_L	1.00	−0.05	0.11	0.11	−0.01	−0.03	−0.09	−0.03
P_1		1.00	0.02	0.06	−0.16	−0.23	0.03	0.02
P_2			1.00	0.01	−0.11	−0.16	−0.05	0.04
P_3				1.00	−0.01	0.03	0.05	0.10
P_4'					1.00	−0.13	−0.01	−0.11
P_5'						1.00	−0.13	−0.01
P_6'							1.00	0.10
P_8'								1.00

$11.0 < q^2 < 12.5\,\mathrm{GeV}^2/c^4$

	F_L	P_1	P_2	P_3	P_4'	P_5'	P_6'	P_8'
F_L	1.00	−0.12	0.13	−0.02	0.03	−0.02	0.03	0.05
P_1		1.00	−0.13	0.03	0.04	−0.35	−0.05	0.05
P_2			1.00	−0.12	0.10	−0.01	0.01	−0.04
P_3				1.00	0.08	0.24	0.19	0.09
P_4'					1.00	−0.02	−0.05	−0.12
P_5'						1.00	−0.04	−0.09
P_6'							1.00	0.27
P_8'								1.00

$15.0 < q^2 < 17.0\,\mathrm{GeV}^2/c^4$

	F_L	P_1	P_2	P_3	P_4'	P_5'	P_6'	P_8'
F_L	1.00	0.06	0.19	−0.12	0.07	0.25	−0.05	−0.07
P_1		1.00	0.16	−0.07	−0.06	−0.04	−0.04	−0.04
P_2			1.00	−0.01	−0.22	−0.12	0.04	−0.07
P_3				1.00	−0.07	−0.07	0.23	0.11
P_4'					1.00	0.28	−0.06	0.18
P_5'						1.00	0.10	−0.02
P_6'							1.00	0.25
P_8'								1.00

$17.0 < q^2 < 19.0\,\mathrm{GeV}^2/c^4$

	F_L	P_1	P_2	P_3	P_4'	P_5'	P_6'	P_8'
F_L	1.00	−0.14	0.14	0.03	0.20	0.21	0.05	0.07
P_1		1.00	−0.05	0.07	−0.18	−0.41	−0.07	−0.06
P_2			1.00	0.00	−0.13	−0.06	0.01	−0.05
P_3				1.00	0.05	0.01	0.16	0.12
P_4'					1.00	0.14	0.03	0.19
P_5'						1.00	0.05	0.02
P_6'							1.00	0.34
P_8'								1.00

$1.1 < q^2 < 6.0\,\mathrm{GeV}^2/c^4$

	F_L	P_1	P_2	P_3	P_4'	P_5'	P_6'	P_8'
F_L	1.00	−0.01	−0.20	0.07	−0.03	0.01	−0.08	0.00
P_1		1.00	0.05	0.00	−0.05	−0.00	0.01	0.01
P_2			1.00	0.03	−0.10	−0.07	0.04	−0.02
P_3				1.00	−0.05	0.04	0.00	0.03
P_4'					1.00	−0.05	−0.02	−0.01
P_5'						1.00	−0.01	−0.02
P_6'							1.00	0.04
P_8'								1.00

$15.0 < q^2 < 19.0\,\mathrm{GeV}^2/c^4$

	F_L	P_1	P_2	P_3	P_4'	P_5'	P_6'	P_8'
F_L	1.00	−0.03	0.14	−0.05	0.11	0.15	−0.01	−0.01
P_1		1.00	0.13	0.04	−0.14	−0.19	−0.02	−0.04
P_2			1.00	−0.05	−0.13	−0.11	0.01	−0.03
P_3				1.00	−0.02	−0.03	0.19	0.13
P_4'					1.00	0.08	0.03	0.14
P_5'						1.00	0.11	0.04
P_6'							1.00	0.24
P_8'								1.00

F Toy studies for the likelihood fit including $m_{K\pi}$ constraint

Table 122: Toy studies for the CP-averaged observables S_i.

	$0.1 < q^2 < 0.98\,\mathrm{GeV}^2/c^4$		
	sensitivity	pull mean	pull width
F_{L}	0.047 ± 0.001	0.04 ± 0.03	1.06 ± 0.03
S_3	0.066 ± 0.002	0.02 ± 0.03	1.05 ± 0.03
S_4	0.072 ± 0.002	-0.10 ± 0.03	1.00 ± 0.03
S_5	0.057 ± 0.002	-0.09 ± 0.03	0.92 ± 0.02
A_{FB}	0.058 ± 0.001	0.04 ± 0.03	1.00 ± 0.02
S_7	0.062 ± 0.002	0.07 ± 0.03	1.03 ± 0.03
S_8	0.071 ± 0.002	-0.06 ± 0.03	1.00 ± 0.03
S_9	0.065 ± 0.002	0.00 ± 0.03	1.00 ± 0.03
F_S	0.056 ± 0.002	0.03 ± 0.03	0.82 ± 0.02
S_{S1}	0.095 ± 0.003	0.01 ± 0.03	1.04 ± 0.03
S_{S2}	0.089 ± 0.002	-0.00 ± 0.03	0.99 ± 0.03
S_{S3}	0.075 ± 0.002	-0.03 ± 0.03	1.05 ± 0.03
S_{S4}	0.076 ± 0.002	-0.01 ± 0.03	1.02 ± 0.03
S_{S5}	0.096 ± 0.003	0.05 ± 0.03	1.01 ± 0.03

	$1.1 < q^2 < 2.5\,\mathrm{GeV}^2/c^4$		
	sensitivity	pull mean	pull width
F_{L}	0.077 ± 0.002	0.16 ± 0.03	1.04 ± 0.03
S_3	0.092 ± 0.002	0.06 ± 0.03	1.10 ± 0.03
S_4	0.125 ± 0.003	-0.03 ± 0.04	1.13 ± 0.03
S_5	0.104 ± 0.003	-0.05 ± 0.03	1.02 ± 0.02
A_{FB}	0.078 ± 0.002	-0.17 ± 0.04	1.11 ± 0.03
S_7	0.106 ± 0.003	-0.01 ± 0.03	1.07 ± 0.03
S_8	0.117 ± 0.003	-0.03 ± 0.04	1.10 ± 0.03
S_9	0.096 ± 0.003	0.01 ± 0.04	1.16 ± 0.03
F_S	0.099 ± 0.004	0.23 ± 0.02	0.76 ± 0.02
S_{S1}	0.167 ± 0.004	0.02 ± 0.03	1.06 ± 0.03
S_{S2}	0.135 ± 0.003	-0.01 ± 0.04	1.20 ± 0.03
S_{S3}	0.105 ± 0.003	-0.00 ± 0.03	1.08 ± 0.03
S_{S4}	0.101 ± 0.003	0.03 ± 0.03	1.01 ± 0.03
S_{S5}	0.130 ± 0.003	0.09 ± 0.04	1.16 ± 0.03

	$2.5 < q^2 < 4.0\,\mathrm{GeV}^2/c^4$		
	sensitivity	pull mean	pull width
F_{L}	0.080 ± 0.002	0.08 ± 0.03	0.92 ± 0.02
S_3	0.106 ± 0.003	-0.00 ± 0.04	1.12 ± 0.03
S_4	0.129 ± 0.003	0.05 ± 0.04	1.13 ± 0.03
S_5	0.110 ± 0.003	0.11 ± 0.03	1.01 ± 0.03
A_{FB}	0.073 ± 0.002	-0.13 ± 0.04	1.10 ± 0.03
S_7	0.116 ± 0.003	0.05 ± 0.03	1.05 ± 0.03
S_8	0.130 ± 0.003	-0.05 ± 0.04	1.10 ± 0.03
S_9	0.099 ± 0.003	0.03 ± 0.03	1.04 ± 0.03
F_S	0.118 ± 0.005	0.19 ± 0.03	0.83 ± 0.02
S_{S1}	0.182 ± 0.005	0.01 ± 0.03	1.03 ± 0.03
S_{S2}	0.134 ± 0.004	-0.04 ± 0.03	1.11 ± 0.03
S_{S3}	0.122 ± 0.003	0.00 ± 0.04	1.16 ± 0.03
S_{S4}	0.113 ± 0.003	-0.02 ± 0.03	1.08 ± 0.03
S_{S5}	0.129 ± 0.003	0.02 ± 0.03	1.07 ± 0.03

	$4.0 < q^2 < 6.0\,\mathrm{GeV}^2/c^4$		
	sensitivity	pull mean	pull width
F_{L}	0.056 ± 0.001	0.08 ± 0.03	1.00 ± 0.03
S_3	0.074 ± 0.002	-0.07 ± 0.03	1.04 ± 0.02
S_4	0.086 ± 0.002	0.06 ± 0.03	1.04 ± 0.03
S_5	0.082 ± 0.002	0.09 ± 0.03	0.98 ± 0.02
A_{FB}	0.048 ± 0.001	0.02 ± 0.03	1.03 ± 0.03
S_7	0.083 ± 0.002	0.03 ± 0.03	1.02 ± 0.03
S_8	0.088 ± 0.002	-0.06 ± 0.03	1.01 ± 0.03
S_9	0.073 ± 0.002	0.01 ± 0.03	1.03 ± 0.02
F_S	0.082 ± 0.003	0.17 ± 0.03	0.78 ± 0.02
S_{S1}	0.133 ± 0.003	-0.13 ± 0.03	0.97 ± 0.02
S_{S2}	0.084 ± 0.002	-0.03 ± 0.03	1.04 ± 0.03
S_{S3}	0.082 ± 0.002	-0.01 ± 0.03	1.02 ± 0.03
S_{S4}	0.079 ± 0.002	-0.03 ± 0.03	1.04 ± 0.03
S_{S5}	0.087 ± 0.002	-0.02 ± 0.03	0.99 ± 0.02

	$6.0 < q^2 < 8.0\,\mathrm{GeV}^2/c^4$		
	sensitivity	pull mean	pull width
F_{L}	0.052 ± 0.001	0.07 ± 0.03	1.03 ± 0.03
S_3	0.065 ± 0.002	-0.02 ± 0.03	1.05 ± 0.03
S_4	0.072 ± 0.002	0.07 ± 0.03	1.02 ± 0.03
S_5	0.073 ± 0.002	0.10 ± 0.03	0.91 ± 0.02
A_{FB}	0.044 ± 0.001	0.07 ± 0.03	0.98 ± 0.02
S_7	0.073 ± 0.002	-0.04 ± 0.03	1.01 ± 0.02
S_8	0.074 ± 0.002	-0.00 ± 0.03	1.04 ± 0.03
S_9	0.063 ± 0.002	0.04 ± 0.03	0.97 ± 0.02
F_S	0.076 ± 0.003	0.15 ± 0.03	0.81 ± 0.02
S_{S1}	0.122 ± 0.003	-0.02 ± 0.03	1.01 ± 0.03
S_{S2}	0.080 ± 0.002	0.01 ± 0.04	1.13 ± 0.03
S_{S3}	0.075 ± 0.002	0.03 ± 0.03	1.04 ± 0.02
S_{S4}	0.074 ± 0.002	-0.02 ± 0.03	0.98 ± 0.02
S_{S5}	0.079 ± 0.002	0.03 ± 0.03	1.04 ± 0.03

Table 123: Toy studies for the CP-averaged observables S_i.

$15.0 < q^2 < 17.0\,\mathrm{GeV}^2/c^4$	sensitivity	pull mean	pull width
F_{L}	0.043 ± 0.001	0.05 ± 0.03	1.00 ± 0.02
S_3	0.060 ± 0.002	-0.12 ± 0.03	1.07 ± 0.03
S_4	0.061 ± 0.002	0.18 ± 0.03	1.10 ± 0.03
S_5	0.056 ± 0.002	0.01 ± 0.03	0.96 ± 0.02
A_{FB}	0.040 ± 0.001	0.09 ± 0.03	1.01 ± 0.03
S_7	0.060 ± 0.002	0.06 ± 0.03	0.97 ± 0.02
S_8	0.065 ± 0.002	0.03 ± 0.03	1.07 ± 0.03
S_9	0.055 ± 0.001	0.05 ± 0.03	1.01 ± 0.02
F_S	0.059 ± 0.002	0.13 ± 0.03	0.86 ± 0.02
S_{S1}	0.089 ± 0.002	0.03 ± 0.03	1.00 ± 0.03
S_{S2}	0.070 ± 0.002	0.04 ± 0.04	1.15 ± 0.03
S_{S3}	0.064 ± 0.002	-0.01 ± 0.03	1.07 ± 0.03
S_{S4}	0.070 ± 0.002	0.07 ± 0.03	0.98 ± 0.02
S_{S5}	0.071 ± 0.002	0.01 ± 0.03	1.01 ± 0.02

$17.0 < q^2 < 19.0\,\mathrm{GeV}^2/c^4$	sensitivity	pull mean	pull width
F_{L}	0.051 ± 0.001	-0.01 ± 0.03	1.02 ± 0.02
S_3	0.074 ± 0.002	-0.10 ± 0.03	1.04 ± 0.03
S_4	0.079 ± 0.002	0.16 ± 0.03	1.09 ± 0.03
S_5	0.072 ± 0.002	-0.06 ± 0.03	0.99 ± 0.02
A_{FB}	0.054 ± 0.001	0.10 ± 0.03	1.02 ± 0.02
S_7	0.080 ± 0.002	-0.04 ± 0.03	1.01 ± 0.02
S_8	0.079 ± 0.002	-0.01 ± 0.03	1.01 ± 0.03
S_9	0.073 ± 0.002	-0.02 ± 0.03	1.01 ± 0.03
F_S	0.079 ± 0.003	0.16 ± 0.03	0.77 ± 0.02
S_{S1}	0.109 ± 0.003	0.03 ± 0.03	1.01 ± 0.02
S_{S2}	0.089 ± 0.002	-0.03 ± 0.04	1.12 ± 0.03
S_{S3}	0.078 ± 0.002	0.00 ± 0.03	1.09 ± 0.03
S_{S4}	0.092 ± 0.003	0.01 ± 0.03	1.00 ± 0.03
S_{S5}	0.097 ± 0.003	0.06 ± 0.03	1.03 ± 0.03

$11.0 < q^2 < 12.5\,\mathrm{GeV}^2/c^4$	sensitivity	pull mean	pull width
F_{L}	0.052 ± 0.001	0.10 ± 0.03	1.04 ± 0.03
S_3	0.068 ± 0.002	-0.00 ± 0.03	1.02 ± 0.03
S_4	0.073 ± 0.002	0.15 ± 0.03	1.09 ± 0.03
S_5	0.075 ± 0.002	0.05 ± 0.03	1.00 ± 0.02
A_{FB}	0.050 ± 0.001	0.15 ± 0.03	1.05 ± 0.03
S_7	0.075 ± 0.002	-0.02 ± 0.03	1.05 ± 0.03
S_8	0.073 ± 0.002	-0.01 ± 0.03	1.05 ± 0.03
S_9	0.070 ± 0.002	-0.00 ± 0.03	1.04 ± 0.03
F_S	0.077 ± 0.003	0.14 ± 0.03	0.78 ± 0.02
S_{S1}	0.118 ± 0.003	-0.01 ± 0.03	1.05 ± 0.03
S_{S2}	0.083 ± 0.002	0.05 ± 0.04	1.11 ± 0.03
S_{S3}	0.085 ± 0.002	-0.01 ± 0.03	1.10 ± 0.03
S_{S4}	0.084 ± 0.002	-0.11 ± 0.03	1.02 ± 0.03
S_{S5}	0.086 ± 0.002	-0.02 ± 0.03	1.07 ± 0.03

$1.1 < q^2 < 6.0\,\mathrm{GeV}^2/c^4$	sensitivity	pull mean	pull width
F_{L}	0.041 ± 0.001	0.00 ± 0.02	0.77 ± 0.02
S_3	0.048 ± 0.001	0.04 ± 0.03	0.97 ± 0.02
S_4	0.057 ± 0.001	-0.03 ± 0.03	0.94 ± 0.02
S_5	0.057 ± 0.002	-0.01 ± 0.03	0.96 ± 0.03
A_{FB}	0.035 ± 0.001	0.01 ± 0.03	0.97 ± 0.02
S_7	0.057 ± 0.002	-0.02 ± 0.03	1.00 ± 0.03
S_8	0.059 ± 0.002	0.05 ± 0.03	0.97 ± 0.02
S_9	0.043 ± 0.001	0.03 ± 0.03	0.95 ± 0.02
F_S	0.054 ± 0.002	0.03 ± 0.03	0.63 ± 0.02
S_{S1}	0.098 ± 0.002	-0.04 ± 0.03	1.02 ± 0.02
S_{S2}	0.055 ± 0.001	0.02 ± 0.03	0.94 ± 0.02
S_{S3}	0.053 ± 0.001	-0.03 ± 0.03	0.99 ± 0.03
S_{S4}	0.053 ± 0.001	-0.14 ± 0.03	0.95 ± 0.03
S_{S5}	0.060 ± 0.002	0.08 ± 0.03	0.98 ± 0.03

$15.0 < q^2 < 19.0\,\mathrm{GeV}^2/c^4$	sensitivity	pull mean	pull width
F_{L}	0.032 ± 0.001	-0.03 ± 0.03	1.08 ± 0.03
S_3	0.045 ± 0.001	0.07 ± 0.03	1.01 ± 0.03
S_4	0.044 ± 0.001	-0.04 ± 0.03	1.06 ± 0.03
S_5	0.043 ± 0.001	-0.11 ± 0.03	1.02 ± 0.03
A_{FB}	0.031 ± 0.001	-0.12 ± 0.03	1.00 ± 0.02
S_7	0.047 ± 0.001	-0.12 ± 0.03	0.96 ± 0.02
S_8	0.045 ± 0.001	-0.01 ± 0.03	0.94 ± 0.02
S_9	0.042 ± 0.001	0.01 ± 0.03	0.96 ± 0.02
F_S	0.043 ± 0.001	-0.20 ± 0.03	0.96 ± 0.02
S_{S1}	0.069 ± 0.002	-0.02 ± 0.03	1.01 ± 0.03
S_{S2}	0.046 ± 0.001	0.07 ± 0.03	0.98 ± 0.02
S_{S3}	0.048 ± 0.001	0.02 ± 0.03	1.01 ± 0.03
S_{S4}	0.055 ± 0.001	-0.01 ± 0.03	0.99 ± 0.03
S_{S5}	0.059 ± 0.002	0.02 ± 0.03	1.05 ± 0.03

Table 124: Toy studies for the CP asymmetries A_i.

	$0.1 < q^2 < 0.98\,\mathrm{GeV}^2/c^4$		
	sensitivity	pull mean	pull width
F_L	0.048 ± 0.001	0.04 ± 0.03	1.02 ± 0.03
A_3	0.067 ± 0.002	0.01 ± 0.03	1.05 ± 0.03
A_4	0.073 ± 0.002	0.00 ± 0.03	1.00 ± 0.02
A_5	0.064 ± 0.002	-0.06 ± 0.03	1.01 ± 0.03
A_{6s}	0.077 ± 0.002	-0.02 ± 0.03	0.97 ± 0.02
A_7	0.062 ± 0.002	-0.02 ± 0.03	1.00 ± 0.03
A_8	0.075 ± 0.002	0.08 ± 0.03	1.02 ± 0.03
A_9	0.064 ± 0.002	0.01 ± 0.03	1.01 ± 0.03
F_S	0.057 ± 0.002	0.01 ± 0.03	0.87 ± 0.02
S_{S1}	0.092 ± 0.002	0.00 ± 0.03	1.01 ± 0.02
S_{S2}	0.084 ± 0.002	0.05 ± 0.03	1.00 ± 0.03
S_{S3}	0.072 ± 0.002	0.04 ± 0.03	0.96 ± 0.02
S_{S4}	0.074 ± 0.002	0.01 ± 0.03	1.03 ± 0.03
S_{S5}	0.091 ± 0.002	-0.03 ± 0.03	1.03 ± 0.03

	$1.1 < q^2 < 2.5\,\mathrm{GeV}^2/c^4$		
	sensitivity	pull mean	pull width
F_L	0.071 ± 0.002	0.07 ± 0.03	0.98 ± 0.02
A_3	0.092 ± 0.003	0.03 ± 0.03	1.09 ± 0.03
A_4	0.119 ± 0.003	-0.03 ± 0.03	1.07 ± 0.02
A_5	0.095 ± 0.002	-0.02 ± 0.03	0.98 ± 0.02
A_{6s}	0.099 ± 0.003	0.08 ± 0.03	1.10 ± 0.03
A_7	0.103 ± 0.002	-0.05 ± 0.03	1.08 ± 0.03
A_8	0.115 ± 0.003	-0.00 ± 0.03	1.03 ± 0.03
A_9	0.093 ± 0.002	0.02 ± 0.04	1.11 ± 0.03
F_S	0.099 ± 0.004	0.16 ± 0.03	0.77 ± 0.02
S_{S1}	0.170 ± 0.004	-0.01 ± 0.03	1.06 ± 0.03
S_{S2}	0.127 ± 0.004	0.00 ± 0.03	1.08 ± 0.03
S_{S3}	0.105 ± 0.003	0.05 ± 0.03	1.04 ± 0.03
S_{S4}	0.104 ± 0.002	0.05 ± 0.04	1.11 ± 0.03
S_{S5}	0.123 ± 0.003	-0.05 ± 0.04	1.10 ± 0.03

	$2.5 < q^2 < 4.0\,\mathrm{GeV}^2/c^4$		
	sensitivity	pull mean	pull width
F_L	0.079 ± 0.002	0.09 ± 0.03	0.91 ± 0.02
A_3	0.100 ± 0.003	0.04 ± 0.03	1.09 ± 0.03
A_4	0.124 ± 0.003	-0.06 ± 0.03	1.07 ± 0.03
A_5	0.112 ± 0.003	-0.08 ± 0.03	1.03 ± 0.03
A_{6s}	0.103 ± 0.003	-0.04 ± 0.04	1.14 ± 0.03
A_7	0.114 ± 0.003	-0.00 ± 0.03	1.05 ± 0.03
A_8	0.129 ± 0.004	-0.07 ± 0.03	1.07 ± 0.03
A_9	0.099 ± 0.003	-0.00 ± 0.03	1.04 ± 0.03
F_S	0.121 ± 0.005	0.14 ± 0.02	0.81 ± 0.03
S_{S1}	0.190 ± 0.004	0.05 ± 0.03	1.06 ± 0.03
S_{S2}	0.138 ± 0.004	-0.01 ± 0.03	1.10 ± 0.03
S_{S3}	0.122 ± 0.003	0.03 ± 0.04	1.14 ± 0.03
S_{S4}	0.126 ± 0.004	-0.03 ± 0.04	1.13 ± 0.03
S_{S5}	0.132 ± 0.003	-0.04 ± 0.03	1.08 ± 0.03

	$4.0 < q^2 < 6.0\,\mathrm{GeV}^2/c^4$		
	sensitivity	pull mean	pull width
F_L	0.055 ± 0.001	0.02 ± 0.03	0.95 ± 0.02
A_3	0.074 ± 0.002	0.06 ± 0.03	1.06 ± 0.03
A_4	0.088 ± 0.002	-0.04 ± 0.03	1.01 ± 0.02
A_5	0.081 ± 0.002	-0.02 ± 0.03	0.99 ± 0.03
A_{6s}	0.064 ± 0.002	0.01 ± 0.03	1.04 ± 0.03
A_7	0.079 ± 0.002	0.05 ± 0.03	0.96 ± 0.02
A_8	0.090 ± 0.002	-0.04 ± 0.03	1.04 ± 0.03
A_9	0.075 ± 0.002	0.01 ± 0.03	1.02 ± 0.02
F_S	0.080 ± 0.003	0.19 ± 0.03	0.76 ± 0.02
S_{S1}	0.144 ± 0.004	0.00 ± 0.03	1.02 ± 0.02
S_{S2}	0.088 ± 0.002	0.06 ± 0.03	0.98 ± 0.02
S_{S3}	0.083 ± 0.002	0.08 ± 0.03	1.03 ± 0.02
S_{S4}	0.084 ± 0.002	0.06 ± 0.03	1.02 ± 0.03
S_{S5}	0.092 ± 0.002	0.02 ± 0.03	1.05 ± 0.03

	$6.0 < q^2 < 8.0\,\mathrm{GeV}^2/c^4$		
	sensitivity	pull mean	pull width
F_L	0.053 ± 0.001	0.07 ± 0.03	1.02 ± 0.03
A_3	0.066 ± 0.002	0.02 ± 0.03	0.99 ± 0.02
A_4	0.071 ± 0.002	-0.08 ± 0.03	0.97 ± 0.02
A_5	0.071 ± 0.002	-0.03 ± 0.03	1.03 ± 0.03
A_{6s}	0.059 ± 0.001	0.07 ± 0.03	1.04 ± 0.03
A_7	0.078 ± 0.002	-0.02 ± 0.03	1.04 ± 0.03
A_8	0.075 ± 0.002	0.05 ± 0.03	0.96 ± 0.03
A_9	0.068 ± 0.002	-0.05 ± 0.03	0.99 ± 0.02
F_S	0.076 ± 0.003	0.17 ± 0.03	0.78 ± 0.02
S_{S1}	0.123 ± 0.003	0.03 ± 0.03	1.00 ± 0.02
S_{S2}	0.088 ± 0.002	-0.01 ± 0.03	1.09 ± 0.03
S_{S3}	0.075 ± 0.002	-0.06 ± 0.03	1.01 ± 0.03
S_{S4}	0.080 ± 0.002	0.02 ± 0.03	1.03 ± 0.03
S_{S5}	0.084 ± 0.002	0.05 ± 0.03	1.04 ± 0.03

Table 125: Toy studies for the CP asymmetries A_i.

	$15.0 < q^2 < 17.0\,\mathrm{GeV}^2/c^4$		
	sensitivity	pull mean	pull width
F_L	0.045 ± 0.001	-0.04 ± 0.03	1.00 ± 0.02
A_3	0.061 ± 0.002	0.02 ± 0.03	0.98 ± 0.02
A_4	0.064 ± 0.002	-0.06 ± 0.03	0.99 ± 0.03
A_5	0.063 ± 0.002	0.00 ± 0.03	1.04 ± 0.02
A_{6s}	0.054 ± 0.001	-0.06 ± 0.03	0.96 ± 0.02
A_7	0.062 ± 0.002	0.04 ± 0.03	1.01 ± 0.03
A_8	0.066 ± 0.002	0.05 ± 0.03	0.99 ± 0.02
A_9	0.065 ± 0.002	-0.06 ± 0.03	1.04 ± 0.02
F_S	0.056 ± 0.002	0.07 ± 0.03	0.81 ± 0.02
S_{S1}	0.097 ± 0.003	0.01 ± 0.03	1.03 ± 0.03
S_{S2}	0.075 ± 0.002	0.01 ± 0.03	1.01 ± 0.02
S_{S3}	0.066 ± 0.002	0.01 ± 0.03	0.97 ± 0.02
S_{S4}	0.069 ± 0.002	0.00 ± 0.03	0.97 ± 0.03
S_{S5}	0.078 ± 0.002	-0.06 ± 0.03	1.01 ± 0.02

	$17.0 < q^2 < 19.0\,\mathrm{GeV}^2/c^4$		
	sensitivity	pull mean	pull width
F_L	0.055 ± 0.001	0.02 ± 0.03	1.04 ± 0.03
A_3	0.073 ± 0.002	0.04 ± 0.03	0.95 ± 0.02
A_4	0.081 ± 0.002	0.02 ± 0.03	0.99 ± 0.03
A_5	0.073 ± 0.002	0.02 ± 0.03	0.99 ± 0.02
A_{6s}	0.074 ± 0.002	-0.07 ± 0.03	1.01 ± 0.02
A_7	0.078 ± 0.002	0.02 ± 0.03	1.02 ± 0.03
A_8	0.084 ± 0.002	0.02 ± 0.03	1.02 ± 0.03
A_9	0.077 ± 0.002	0.03 ± 0.03	0.99 ± 0.02
F_S	0.077 ± 0.003	0.17 ± 0.03	0.79 ± 0.02
S_{S1}	0.120 ± 0.003	0.00 ± 0.03	1.05 ± 0.03
S_{S2}	0.094 ± 0.002	-0.01 ± 0.03	0.99 ± 0.02
S_{S3}	0.086 ± 0.002	-0.02 ± 0.03	1.02 ± 0.03
S_{S4}	0.097 ± 0.003	0.06 ± 0.03	1.07 ± 0.03
S_{S5}	0.101 ± 0.003	0.02 ± 0.03	1.05 ± 0.03

	$11.0 < q^2 < 12.5\,\mathrm{GeV}^2/c^4$		
	sensitivity	pull mean	pull width
F_L	0.050 ± 0.001	-0.04 ± 0.03	0.95 ± 0.02
A_3	0.073 ± 0.002	-0.04 ± 0.03	0.99 ± 0.02
A_4	0.080 ± 0.002	-0.07 ± 0.03	1.06 ± 0.03
A_5	0.076 ± 0.002	0.00 ± 0.03	1.02 ± 0.03
A_{6s}	0.065 ± 0.002	-0.05 ± 0.03	1.01 ± 0.03
A_7	0.073 ± 0.002	-0.02 ± 0.03	1.00 ± 0.03
A_8	0.077 ± 0.002	-0.04 ± 0.03	0.98 ± 0.03
A_9	0.072 ± 0.002	-0.03 ± 0.03	0.99 ± 0.02
F_S	0.073 ± 0.003	0.15 ± 0.03	0.78 ± 0.02
S_{S1}	0.124 ± 0.003	-0.03 ± 0.03	1.02 ± 0.02
S_{S2}	0.086 ± 0.002	0.06 ± 0.03	1.01 ± 0.03
S_{S3}	0.083 ± 0.002	-0.01 ± 0.03	1.04 ± 0.03
S_{S4}	0.087 ± 0.003	-0.00 ± 0.03	1.04 ± 0.03
S_{S5}	0.089 ± 0.002	-0.00 ± 0.03	0.99 ± 0.02

	$1.1 < q^2 < 6.0\,\mathrm{GeV}^2/c^4$		
	sensitivity	pull mean	pull width
F_L	0.042 ± 0.001	-0.00 ± 0.02	0.77 ± 0.02
A_3	0.046 ± 0.001	0.00 ± 0.03	0.96 ± 0.02
A_4	0.061 ± 0.002	-0.04 ± 0.03	1.04 ± 0.03
A_5	0.057 ± 0.001	-0.04 ± 0.03	1.04 ± 0.03
A_{6s}	0.044 ± 0.001	-0.04 ± 0.03	0.98 ± 0.02
A_7	0.058 ± 0.001	0.00 ± 0.03	1.03 ± 0.03
A_8	0.057 ± 0.001	0.05 ± 0.03	0.94 ± 0.02
A_9	0.049 ± 0.001	0.07 ± 0.03	1.05 ± 0.03
F_S	0.058 ± 0.002	0.09 ± 0.03	0.60 ± 0.02
S_{S1}	0.100 ± 0.003	0.01 ± 0.03	1.05 ± 0.03
S_{S2}	0.058 ± 0.002	-0.07 ± 0.03	0.99 ± 0.03
S_{S3}	0.054 ± 0.001	-0.07 ± 0.03	0.99 ± 0.03
S_{S4}	0.053 ± 0.001	-0.07 ± 0.03	0.97 ± 0.02
S_{S5}	0.061 ± 0.002	0.02 ± 0.03	1.01 ± 0.02

	$15.0 < q^2 < 19.0\,\mathrm{GeV}^2/c^4$		
	sensitivity	pull mean	pull width
F_L	0.032 ± 0.001	-0.00 ± 0.04	1.06 ± 0.03
A_3	0.048 ± 0.001	0.11 ± 0.03	0.95 ± 0.02
A_4	0.049 ± 0.001	0.04 ± 0.03	0.98 ± 0.03
A_5	0.047 ± 0.001	-0.05 ± 0.03	0.95 ± 0.02
A_{6s}	0.046 ± 0.001	-0.01 ± 0.03	1.04 ± 0.03
A_7	0.048 ± 0.001	0.01 ± 0.03	1.01 ± 0.03
A_8	0.050 ± 0.001	0.06 ± 0.03	0.95 ± 0.02
A_9	0.047 ± 0.001	0.01 ± 0.03	0.96 ± 0.02
F_S	0.045 ± 0.001	-0.13 ± 0.03	0.98 ± 0.03
S_{S1}	0.069 ± 0.002	-0.07 ± 0.03	0.91 ± 0.02
S_{S2}	0.061 ± 0.002	0.05 ± 0.03	1.02 ± 0.03
S_{S3}	0.054 ± 0.001	-0.03 ± 0.03	0.99 ± 0.03
S_{S4}	0.055 ± 0.002	-0.06 ± 0.03	0.99 ± 0.03
S_{S5}	0.061 ± 0.002	-0.03 ± 0.03	0.97 ± 0.02

Table 126: Toy studies for the less form-factor dependent observables $P_i^{(\prime)}$.

	$0.1 < q^2 < 0.98\,\mathrm{GeV}^2/c^4$		
	sensitivity	pull mean	pull width
F_L	0.046 ± 0.001	-0.01 ± 0.03	0.98 ± 0.02
P_1	0.173 ± 0.005	0.00 ± 0.03	1.04 ± 0.03
P_2	0.054 ± 0.001	0.02 ± 0.03	1.01 ± 0.03
P_3	0.082 ± 0.002	-0.06 ± 0.03	0.99 ± 0.03
P_4	0.178 ± 0.005	-0.06 ± 0.03	1.02 ± 0.03
P_5	0.147 ± 0.004	-0.05 ± 0.03	0.95 ± 0.03
P_6	0.144 ± 0.004	-0.07 ± 0.03	0.99 ± 0.03
P_8	0.180 ± 0.005	-0.01 ± 0.03	1.04 ± 0.03
F_S	0.055 ± 0.002	0.08 ± 0.03	0.84 ± 0.02
S_{S1}	0.087 ± 0.002	-0.05 ± 0.03	0.98 ± 0.03
S_{S2}	0.089 ± 0.002	0.02 ± 0.03	1.01 ± 0.03
S_{S3}	0.075 ± 0.002	0.03 ± 0.03	1.03 ± 0.03
S_{S4}	0.075 ± 0.002	-0.01 ± 0.03	1.02 ± 0.02
S_{S5}	0.092 ± 0.002	0.02 ± 0.03	1.02 ± 0.03

	$1.1 < q^2 < 2.5\,\mathrm{GeV}^2/c^4$		
	sensitivity	pull mean	pull width
F_L	0.067 ± 0.002	0.04 ± 0.03	0.96 ± 0.03
P_1	0.554 ± 0.014	-0.01 ± 0.03	1.02 ± 0.03
P_2	0.188 ± 0.008	0.08 ± 0.03	1.02 ± 0.03
P_3	0.312 ± 0.008	0.01 ± 0.03	1.07 ± 0.03
P_4	0.256 ± 0.006	-0.07 ± 0.04	1.09 ± 0.03
P_5	0.218 ± 0.006	-0.06 ± 0.03	0.99 ± 0.03
P_6	0.210 ± 0.005	0.03 ± 0.03	0.99 ± 0.02
P_8	0.258 ± 0.007	0.00 ± 0.04	1.11 ± 0.03
F_S	0.096 ± 0.004	0.07 ± 0.02	0.74 ± 0.02
S_{S1}	0.162 ± 0.004	0.06 ± 0.03	1.02 ± 0.03
S_{S2}	0.123 ± 0.003	0.01 ± 0.04	1.11 ± 0.03
S_{S3}	0.105 ± 0.003	0.03 ± 0.03	1.05 ± 0.03
S_{S4}	0.101 ± 0.003	0.03 ± 0.03	1.02 ± 0.03
S_{S5}	0.128 ± 0.003	-0.02 ± 0.03	1.06 ± 0.03

	$2.5 < q^2 < 4.0\,\mathrm{GeV}^2/c^4$		
	sensitivity	pull mean	pull width
F_L	0.070 ± 0.002	-0.01 ± 0.03	0.97 ± 0.02
P_1	0.939 ± 0.032	-0.00 ± 0.03	0.89 ± 0.02
P_2	0.255 ± 0.014	0.25 ± 0.03	0.89 ± 0.02
P_3	0.455 ± 0.016	-0.03 ± 0.03	0.85 ± 0.02
P_4	0.309 ± 0.009	-0.00 ± 0.03	0.99 ± 0.02
P_5	0.264 ± 0.007	0.01 ± 0.03	0.91 ± 0.02
P_6	0.288 ± 0.008	0.05 ± 0.03	1.01 ± 0.03
P_8	0.310 ± 0.009	-0.01 ± 0.03	1.03 ± 0.03
F_S	0.109 ± 0.004	0.03 ± 0.02	0.83 ± 0.02
S_{S1}	0.188 ± 0.005	0.07 ± 0.03	1.06 ± 0.03
S_{S2}	0.132 ± 0.004	0.01 ± 0.03	1.08 ± 0.03
S_{S3}	0.114 ± 0.003	-0.04 ± 0.03	1.09 ± 0.03
S_{S4}	0.107 ± 0.003	-0.07 ± 0.03	1.06 ± 0.03
S_{S5}	0.132 ± 0.003	-0.04 ± 0.04	1.15 ± 0.03

	$4.0 < q^2 < 6.0\,\mathrm{GeV}^2/c^4$		
	sensitivity	pull mean	pull width
F_L	0.054 ± 0.001	0.03 ± 0.03	1.04 ± 0.03
P_1	0.546 ± 0.016	-0.08 ± 0.03	1.01 ± 0.03
P_2	0.127 ± 0.004	-0.06 ± 0.03	0.96 ± 0.03
P_3	0.283 ± 0.009	-0.02 ± 0.03	1.01 ± 0.03
P_4	0.189 ± 0.005	0.13 ± 0.03	0.98 ± 0.03
P_5	0.205 ± 0.010	-0.14 ± 0.03	0.81 ± 0.02
P_6	0.199 ± 0.005	0.04 ± 0.03	1.05 ± 0.03
P_8	0.196 ± 0.005	-0.01 ± 0.03	1.05 ± 0.03
F_S	0.080 ± 0.003	0.17 ± 0.03	0.78 ± 0.02
S_{S1}	0.131 ± 0.004	-0.07 ± 0.03	0.95 ± 0.03
S_{S2}	0.085 ± 0.002	0.02 ± 0.03	0.99 ± 0.02
S_{S3}	0.079 ± 0.002	-0.04 ± 0.03	1.01 ± 0.02
S_{S4}	0.086 ± 0.003	0.02 ± 0.03	1.05 ± 0.03
S_{S5}	0.090 ± 0.002	-0.02 ± 0.03	1.01 ± 0.02

	$6.0 < q^2 < 8.0\,\mathrm{GeV}^2/c^4$		
	sensitivity	pull mean	pull width
F_L	0.049 ± 0.001	-0.03 ± 0.03	1.05 ± 0.03
P_1	0.339 ± 0.008	-0.07 ± 0.03	1.00 ± 0.02
P_2	0.085 ± 0.004	-0.14 ± 0.03	0.88 ± 0.02
P_3	0.182 ± 0.005	0.07 ± 0.03	1.00 ± 0.03
P_4	0.147 ± 0.004	0.06 ± 0.03	1.06 ± 0.03
P_5	0.178 ± 0.008	-0.25 ± 0.02	0.82 ± 0.02
P_6	0.148 ± 0.004	-0.02 ± 0.03	0.96 ± 0.03
P_8	0.151 ± 0.004	0.02 ± 0.03	1.00 ± 0.03
F_S	0.066 ± 0.002	0.02 ± 0.03	0.81 ± 0.02
S_{S1}	0.122 ± 0.003	0.01 ± 0.03	1.02 ± 0.03
S_{S2}	0.077 ± 0.002	0.07 ± 0.03	1.03 ± 0.03
S_{S3}	0.077 ± 0.002	0.01 ± 0.03	1.04 ± 0.03
S_{S4}	0.073 ± 0.002	0.06 ± 0.03	0.97 ± 0.02
S_{S5}	0.079 ± 0.002	-0.05 ± 0.03	1.03 ± 0.03

Table 127: Toy studies for the less form-factor dependent observables $P_i^{(\prime)}$.

	$15.0 < q^2 < 17.0\,\mathrm{GeV}^2/c^4$		
	sensitivity	pull mean	pull width
F_L	0.041 ± 0.001	-0.03 ± 0.03	0.99 ± 0.03
P_1	0.182 ± 0.005	-0.08 ± 0.03	1.07 ± 0.03
P_2	0.040 ± 0.002	0.03 ± 0.03	0.91 ± 0.02
P_3	0.087 ± 0.002	0.04 ± 0.03	1.00 ± 0.03
P_4	0.131 ± 0.004	0.10 ± 0.03	1.08 ± 0.03
P_5	0.124 ± 0.004	0.05 ± 0.03	0.95 ± 0.02
P_6	0.130 ± 0.003	-0.03 ± 0.03	1.01 ± 0.03
P_8	0.128 ± 0.003	0.02 ± 0.03	1.03 ± 0.03
F_S	0.059 ± 0.002	0.11 ± 0.03	0.88 ± 0.02
S_{S1}	0.087 ± 0.002	-0.01 ± 0.03	1.02 ± 0.03
S_{S2}	0.063 ± 0.002	-0.08 ± 0.03	1.03 ± 0.03
S_{S3}	0.062 ± 0.002	0.00 ± 0.03	1.02 ± 0.03
S_{S4}	0.067 ± 0.002	0.05 ± 0.03	0.94 ± 0.02
S_{S5}	0.071 ± 0.002	0.01 ± 0.03	0.98 ± 0.02

	$17.0 < q^2 < 19.0\,\mathrm{GeV}^2/c^4$		
	sensitivity	pull mean	pull width
F_L	0.049 ± 0.001	0.04 ± 0.03	0.97 ± 0.02
P_1	0.222 ± 0.006	-0.08 ± 0.03	1.00 ± 0.03
P_2	0.050 ± 0.001	0.12 ± 0.03	1.00 ± 0.02
P_3	0.109 ± 0.003	-0.00 ± 0.03	1.01 ± 0.03
P_4	0.158 ± 0.005	0.10 ± 0.03	0.98 ± 0.02
P_5	0.148 ± 0.004	0.04 ± 0.03	1.01 ± 0.03
P_6	0.175 ± 0.004	-0.01 ± 0.03	1.05 ± 0.03
P_8	0.184 ± 0.005	-0.02 ± 0.04	1.11 ± 0.03
F_S	0.075 ± 0.003	0.15 ± 0.03	0.74 ± 0.02
S_{S1}	0.112 ± 0.003	-0.04 ± 0.03	1.05 ± 0.03
S_{S2}	0.081 ± 0.002	0.06 ± 0.03	1.06 ± 0.03
S_{S3}	0.079 ± 0.002	-0.02 ± 0.03	1.10 ± 0.03
S_{S4}	0.091 ± 0.002	0.01 ± 0.03	1.01 ± 0.02
S_{S5}	0.095 ± 0.002	-0.01 ± 0.03	1.04 ± 0.03

	$11.0 < q^2 < 12.5\,\mathrm{GeV}^2/c^4$		
	sensitivity	pull mean	pull width
F_L	0.048 ± 0.001	0.01 ± 0.03	0.97 ± 0.03
P_1	0.245 ± 0.007	0.02 ± 0.03	1.04 ± 0.03
P_2	0.053 ± 0.002	-0.10 ± 0.03	0.93 ± 0.03
P_3	0.121 ± 0.003	-0.01 ± 0.03	1.04 ± 0.02
P_4	0.139 ± 0.004	-0.04 ± 0.03	1.03 ± 0.03
P_5	0.152 ± 0.007	-0.16 ± 0.03	0.83 ± 0.02
P_6	0.147 ± 0.004	-0.04 ± 0.03	0.99 ± 0.03
P_8	0.145 ± 0.004	0.00 ± 0.03	0.98 ± 0.02
F_S	0.069 ± 0.003	-0.06 ± 0.03	0.78 ± 0.02
S_{S1}	0.118 ± 0.003	-0.06 ± 0.03	1.03 ± 0.03
S_{S2}	0.084 ± 0.002	-0.06 ± 0.04	1.13 ± 0.03
S_{S3}	0.077 ± 0.002	-0.06 ± 0.03	1.05 ± 0.03
S_{S4}	0.082 ± 0.002	0.06 ± 0.03	0.97 ± 0.03
S_{S5}	0.080 ± 0.002	0.05 ± 0.03	1.00 ± 0.03

	$1.1 < q^2 < 6.0\,\mathrm{GeV}^2/c^4$		
	sensitivity	pull mean	pull width
F_L	0.040 ± 0.001	0.02 ± 0.02	0.73 ± 0.02
P_1	0.374 ± 0.009	0.04 ± 0.03	0.95 ± 0.02
P_2	0.086 ± 0.002	0.03 ± 0.03	0.88 ± 0.02
P_3	0.173 ± 0.005	-0.05 ± 0.03	0.88 ± 0.02
P_4	0.127 ± 0.003	0.02 ± 0.03	0.89 ± 0.02
P_5	0.125 ± 0.004	-0.00 ± 0.03	0.88 ± 0.02
P_6	0.129 ± 0.003	-0.03 ± 0.03	0.93 ± 0.02
P_8	0.145 ± 0.004	-0.08 ± 0.03	1.04 ± 0.02
F_S	0.054 ± 0.002	0.22 ± 0.02	0.42 ± 0.01
S_{S1}	0.095 ± 0.003	-0.02 ± 0.03	0.99 ± 0.03
S_{S2}	0.057 ± 0.002	-0.00 ± 0.03	0.99 ± 0.03
S_{S3}	0.058 ± 0.002	-0.03 ± 0.03	1.03 ± 0.03
S_{S4}	0.054 ± 0.001	0.01 ± 0.03	0.96 ± 0.02
S_{S5}	0.058 ± 0.001	-0.04 ± 0.03	0.99 ± 0.02

	$15.0 < q^2 < 19.0\,\mathrm{GeV}^2/c^4$		
	sensitivity	pull mean	pull width
F_L	0.031 ± 0.001	-0.02 ± 0.03	1.02 ± 0.03
P_1	0.135 ± 0.003	0.10 ± 0.03	0.97 ± 0.02
P_2	0.030 ± 0.001	-0.11 ± 0.03	1.03 ± 0.03
P_3	0.066 ± 0.002	-0.04 ± 0.03	0.99 ± 0.03
P_4	0.093 ± 0.002	0.02 ± 0.03	1.07 ± 0.03
P_5	0.088 ± 0.002	-0.06 ± 0.03	1.03 ± 0.03
P_6	0.104 ± 0.003	-0.01 ± 0.03	1.01 ± 0.03
P_8	0.098 ± 0.003	0.00 ± 0.03	1.00 ± 0.03
F_S	0.042 ± 0.001	-0.20 ± 0.03	0.90 ± 0.02
S_{S1}	0.068 ± 0.002	0.00 ± 0.03	1.02 ± 0.03
S_{S2}	0.050 ± 0.001	0.02 ± 0.03	1.05 ± 0.03
S_{S3}	0.048 ± 0.001	0.04 ± 0.03	1.04 ± 0.03
S_{S4}	0.053 ± 0.001	0.01 ± 0.03	0.98 ± 0.03
S_{S5}	0.054 ± 0.001	0.05 ± 0.03	0.97 ± 0.02

G Toy studies for the method of moments

In the following the pulls obtained for a the toy study for the method of moments are shown. These pulls are obtained including the detector acceptance and using the reweighting method to correct for it. No bias, apart for the known bias on F_L in the first bin, due to the non-vanishing lepton masses, is observed.

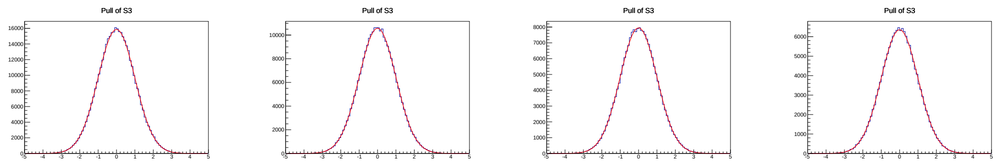

(a) Pull of S_3 with 100 events in toys. (b) Pull of S_3 with 150 events in toys. (c) Pull of S_3 with 200 events in toys. (d) Pull of S_3 with 250 events in toys.

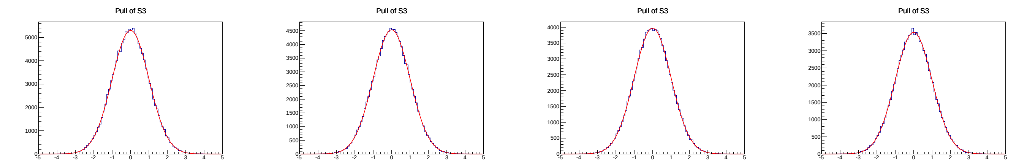

(e) Pull of S_3 with 300 events in toys. (f) Pull of S_3 with 350 events in toys. (g) Pull of S_3 with 400 events in toys. (h) Pull of S_3 with 450 events in toys.

Figure 139: Pull distributions for S_3 for different number of simulated events.

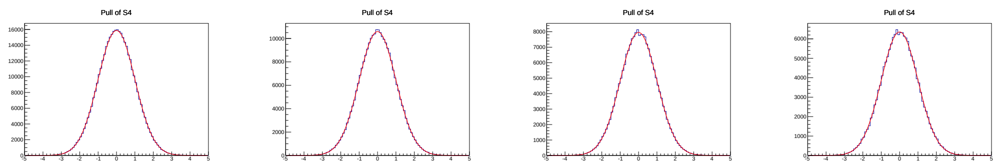

(a) Pull of S_4 with 100 events in toys. (b) Pull of S_4 with 150 events in toys. (c) Pull of S_4 with 200 events in toys. (d) Pull of S_4 with 250 events in toys.

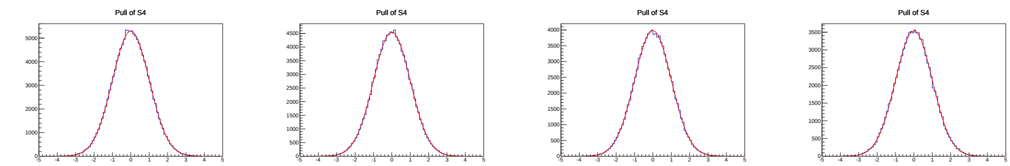

(e) Pull of S_4 with 300 events in toys. (f) Pull of S_4 with 350 events in toys. (g) Pull of S_4 with 400 events in toys. (h) Pull of S_4 with 450 events in toys.

Figure 140: Pull distributions for S_4 for different number of simulated events.

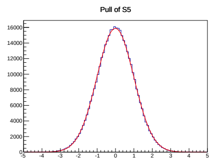

(a) Pull of S_5 with 100 events in toys.

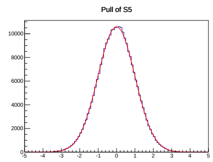

(b) Pull of S_5 with 150 events in toys.

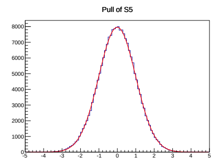

(c) Pull of S_5 with 200 events in toys.

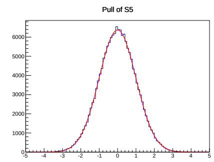

(d) Pull of S_5 with 250 events in toys.

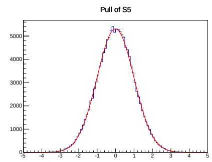

(e) Pull of S_5 with 300 events in toys.

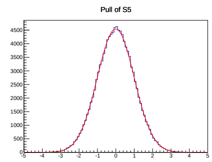

(f) Pull of S_5 with 350 events in toys.

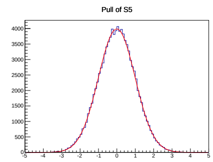

(g) Pull of S_5 with 400 events in toys.

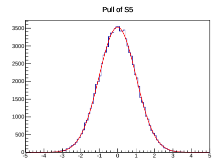

(h) Pull of S_5 with 450 events in toys.

Figure 141: Pull distributions for S_5 for different number of simulated events.

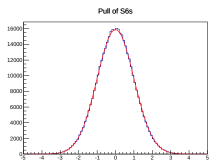

(a) Pull of S_6 with 100 events in toys.

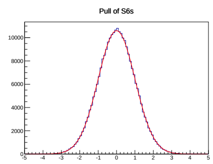

(b) Pull of S_6 with 150 events in toys.

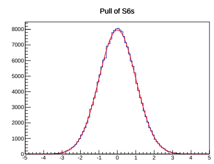

(c) Pull of S_6 with 200 events in toys.

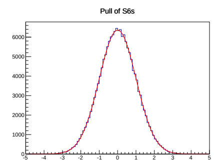

(d) Pull of S_6 with 250 events in toys.

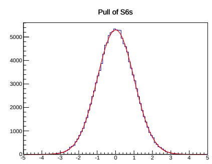

(e) Pull of S_6 with 300 events in toys.

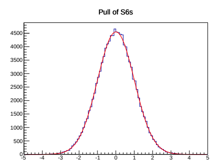

(f) Pull of S_6 with 350 events in toys.

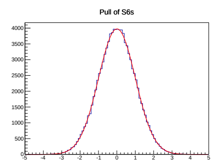

(g) Pull of S_6 with 400 events in toys.

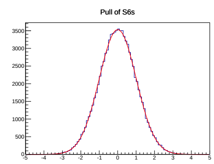

(h) Pull of S_6 with 450 events in toys.

Figure 142: Pull distributions for S_6 for different number of simulated events.

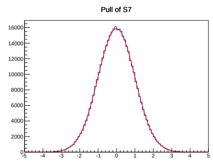

(a) Pull of S_7 with 100 events in toys.

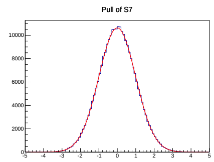

(b) Pull of S_7 with 150 events in toys.

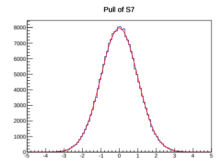

(c) Pull of S_7 with 200 events in toys.

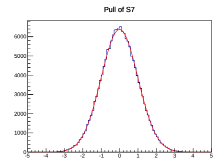

(d) Pull of S_7 with 250 events in toys.

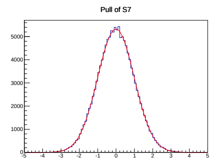

(e) Pull of S_7 with 300 events in toys.

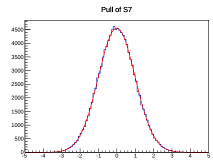

(f) Pull of S_7 with 350 events in toys.

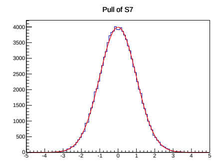

(g) Pull of S_7 with 400 events in toys.

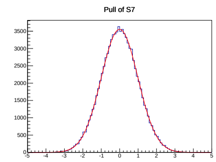

(h) Pull of S_7 with 450 events in toys.

Figure 143: Pull distributions for S_7 for different number of simulated events.

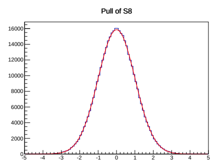

(a) Pull of S_8 with 100 events in toys.

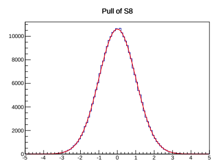

(b) Pull of S_8 with 150 events in toys.

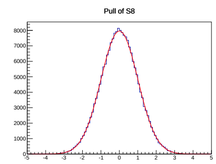

(c) Pull of S_8 with 200 events in toys.

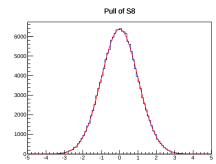

(d) Pull of S_8 with 250 events in toys.

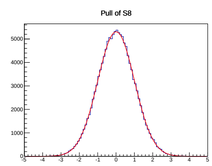

(e) Pull of S_8 with 300 events in toys.

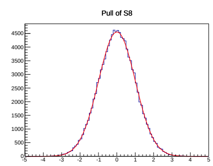

(f) Pull of S_8 with 350 events in toys.

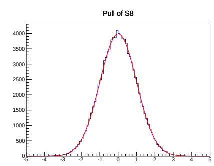

(g) Pull of S_8 with 400 events in toys.

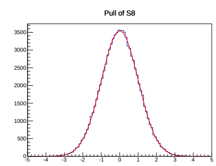

(h) Pull of S_8 with 450 events in toys.

Figure 144: Pull distributions for S_8 for different number of simulated events.

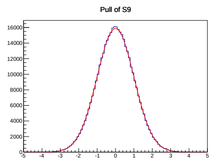

(a) Pull of S_9 with 100 events in toys.

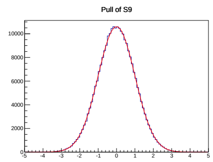

(b) Pull of S_9 with 150 events in toys.

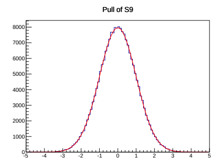

(c) Pull of S_9 with 200 events in toys.

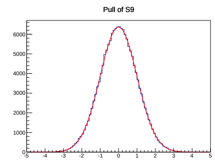

(d) Pull of S_9 with 250 events in toys.

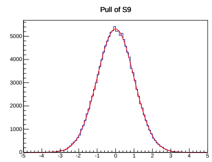

(e) Pull of S_9 with 300 events in toys.

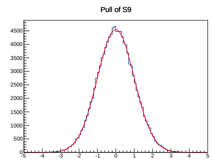

(f) Pull of S_9 with 350 events in toys.

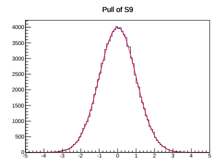

(g) Pull of S_9 with 400 events in toys.

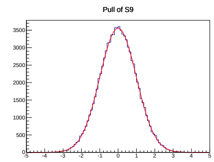

(h) Pull of S_9 with 450 events in toys.

Figure 145: Pull distributions for S_9 for different number of simulated events.

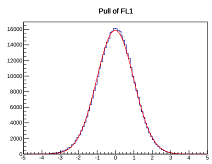

(a) Pull of F_l with 100 events in toys.

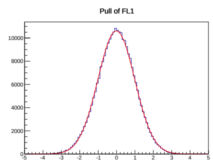

(b) Pull of F_l with 150 events in toys.

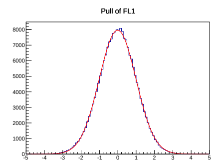

(c) Pull of F_l with 200 events in toys.

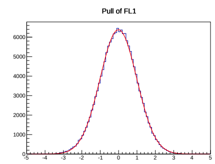

(d) Pull of F_l with 250 events in toys.

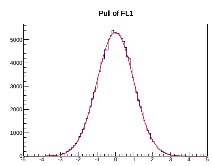

(e) Pull of F_l with 300 events in toys.

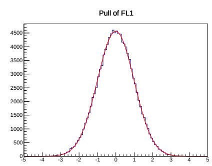

(f) Pull of F_l with 350 events in toys.

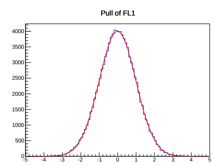

(g) Pull of F_l with 400 events in toys.

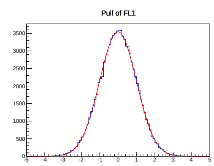

(h) Pull of F_l with 450 events in toys.

Figure 146: Pull distributions for F_l for different number of simulated events.

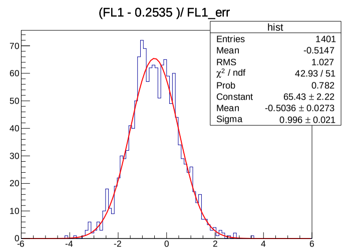

(a) Pull of F_l

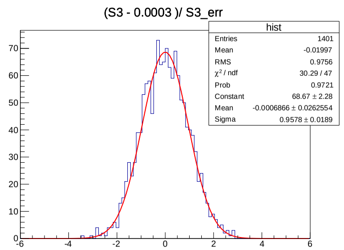

(b) Pull of S_3

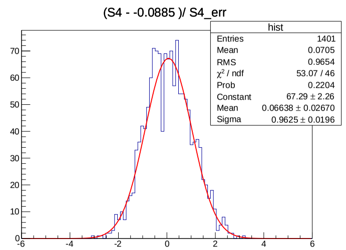

(c) Pull of S_4

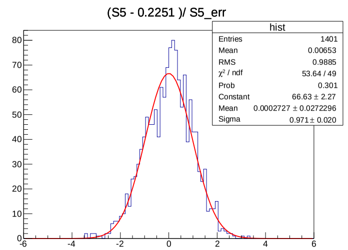

(d) Pull of S_5

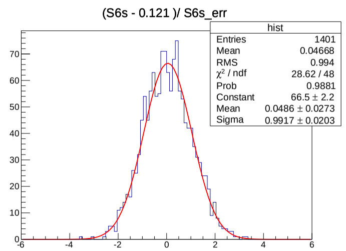

(e) Pull of S_{6s}

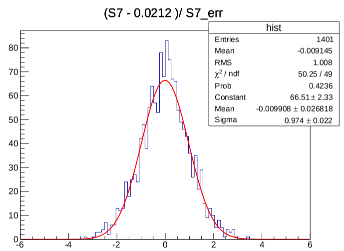

(f) Pull of S_7

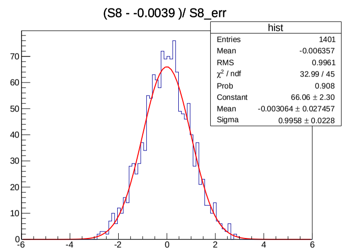

(g) Pull of S_8

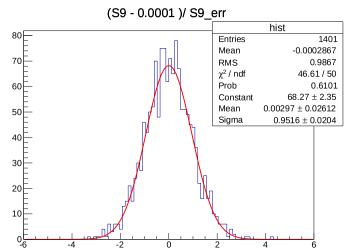

(h) Pull of S_9

Figure 147: Pull distributions for observables in $0.1 - 0.98\,\mathrm{GeV}^2$ q^2 bin.

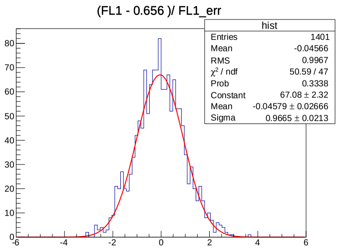

(a) Pull of F_l

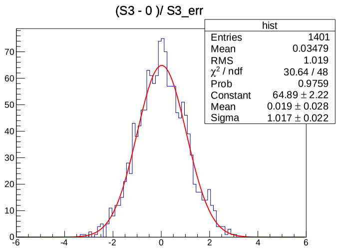

(b) Pull of S_3

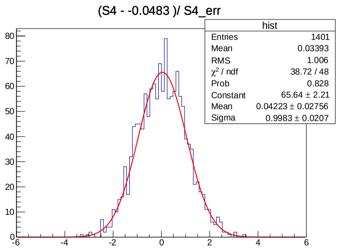

(c) Pull of S_4

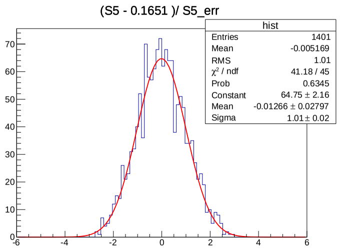

(d) Pull of S_5

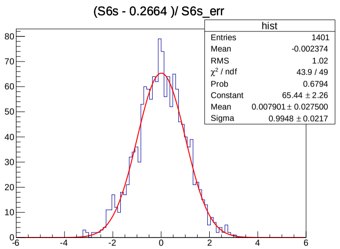

(e) Pull of S_{6s}

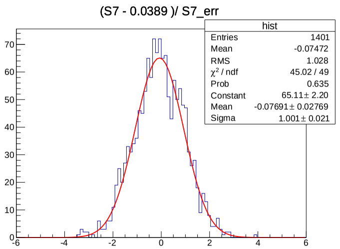

(f) Pull of S_7

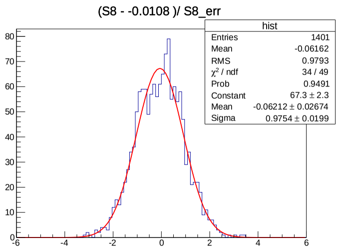

(g) Pull of S_8

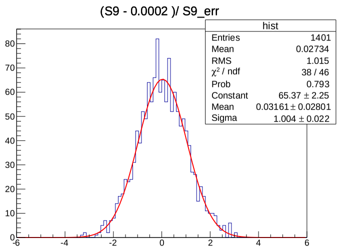

(h) Pull of S_9

Figure 148: Pull distributions for observables in $1.1 - 2.0\,\mathrm{GeV}^2$ q^2 bin.

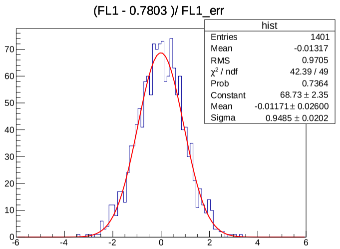

(a) Pull of F_l

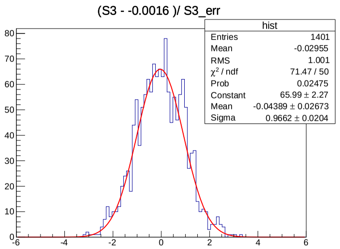

(b) Pull of S_3

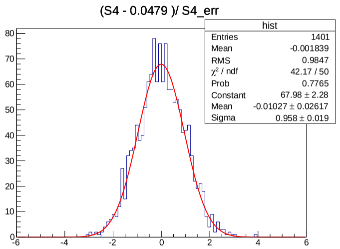

(c) Pull of S_4

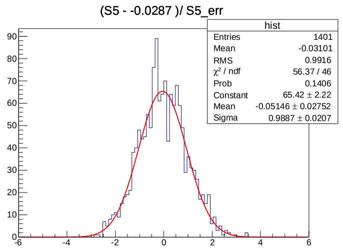

(d) Pull of S_5

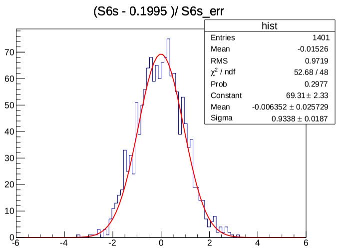

(e) Pull of S_{6s}

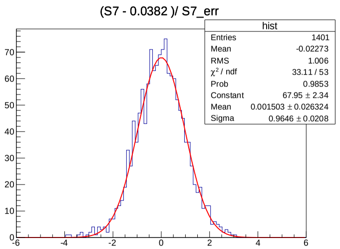

(f) Pull of S_7

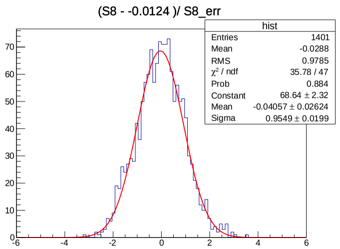

(g) Pull of S_8

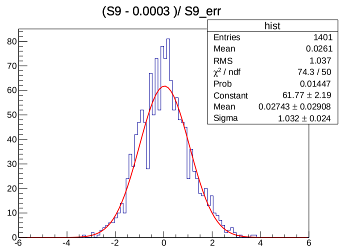

(h) Pull of S_9

Figure 149: Pull distributions for observables in $2.0 - 3.0\,\mathrm{GeV}^2$ q^2 bin.

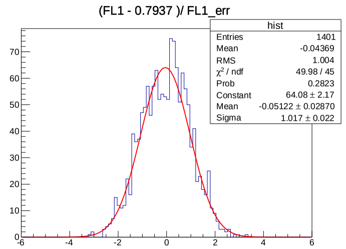

(a) Pull of F_l

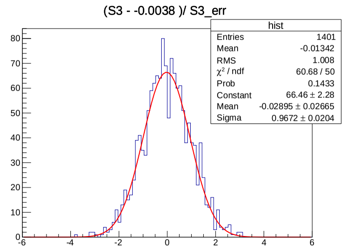

(b) Pull of S_3

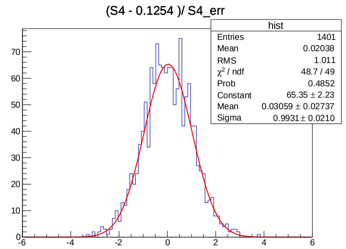

(c) Pull of S_4

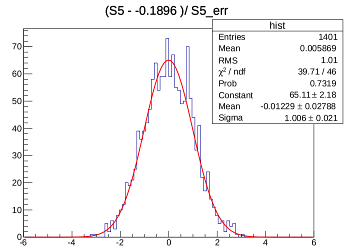

(d) Pull of S_5

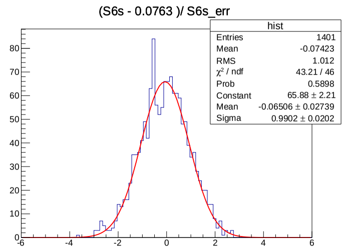

(e) Pull of S_{6s}

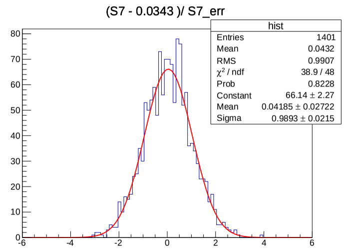

(f) Pull of S_7

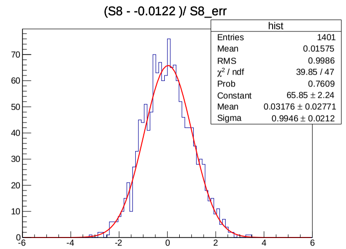

(g) Pull of S_8

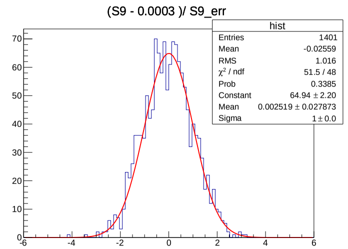

(h) Pull of S_9

Figure 150: Pull distributions for observables in $3.0 - 4.0\,\mathrm{GeV}^2$ q^2 bin.

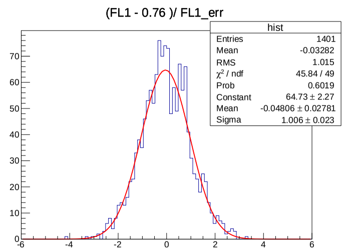

(a) Pull of F_l

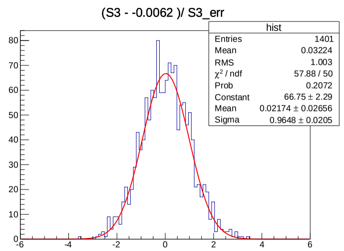

(b) Pull of S_3

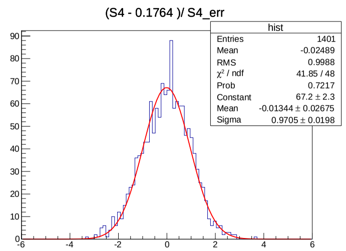

(c) Pull of S_4

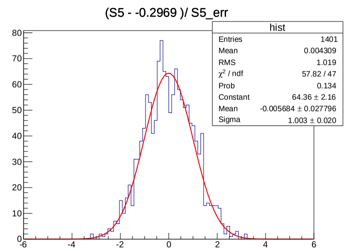

(d) Pull of S_5

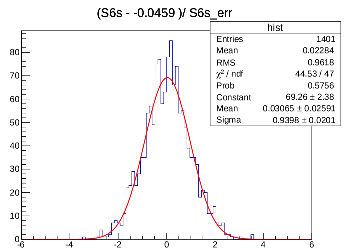

(e) Pull of S_{6s}

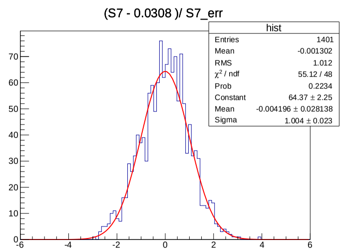

(f) Pull of S_7

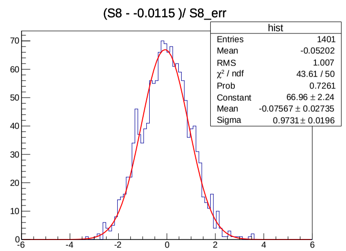

(g) Pull of S_8

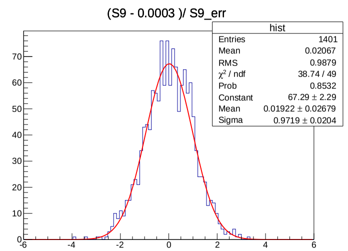

(h) Pull of S_9

Figure 151: Pull distributions for observables in $4.0 - 5.0\,\mathrm{GeV}^2$ q^2 bin.

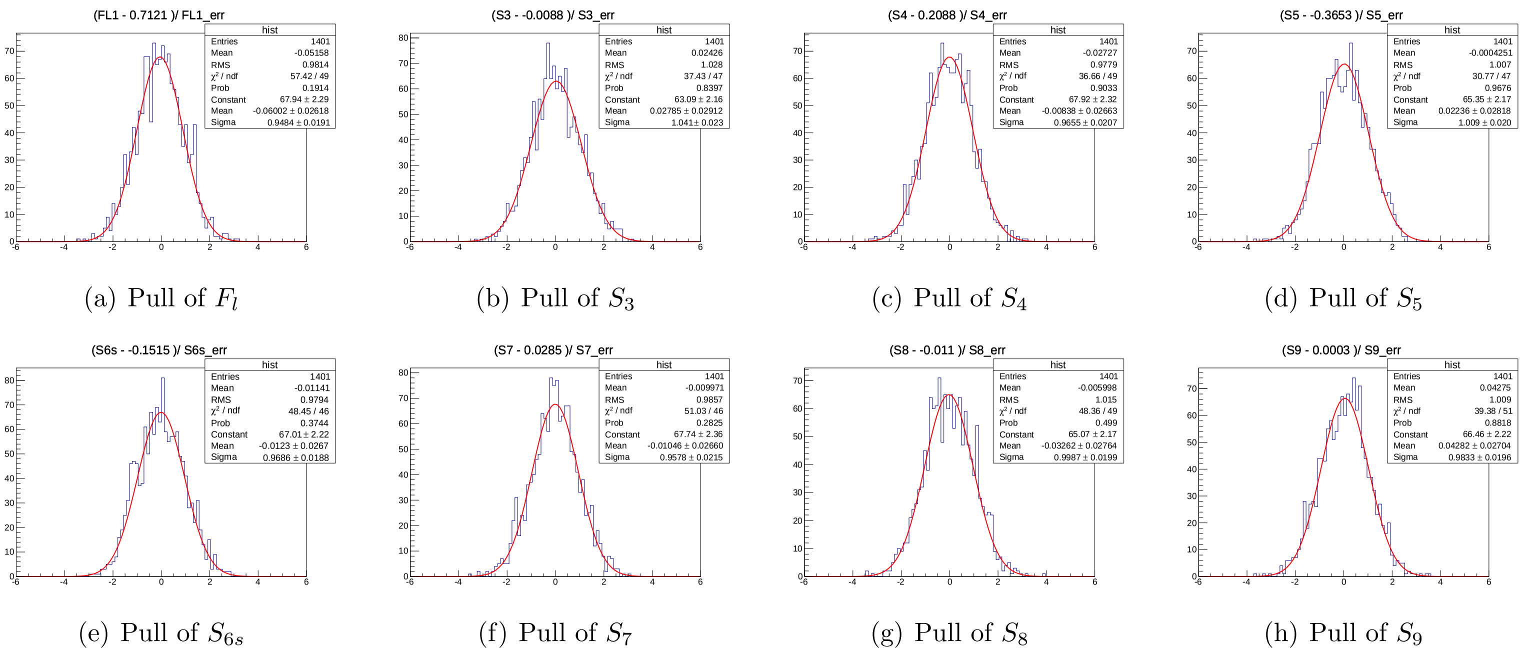

(a) Pull of F_l (b) Pull of S_3 (c) Pull of S_4 (d) Pull of S_5

(e) Pull of S_{6s} (f) Pull of S_7 (g) Pull of S_8 (h) Pull of S_9

Figure 152: Pull distributions for observables in $5.0 - 6.0\,\mathrm{GeV}^2$ q^2 bin.

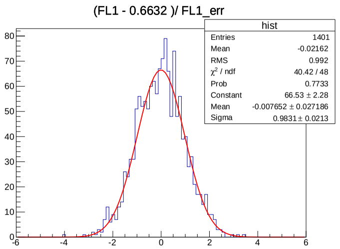

(a) Pull of F_l

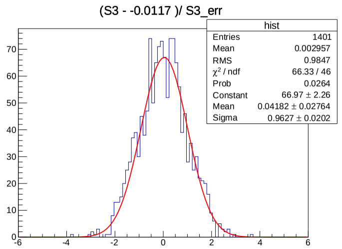

(b) Pull of S_3

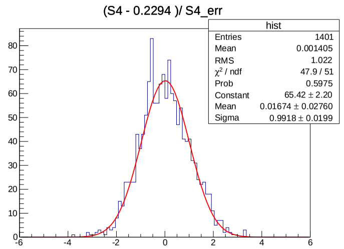

(c) Pull of S_4

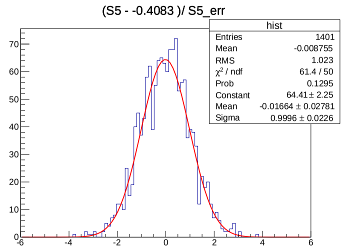

(d) Pull of S_5

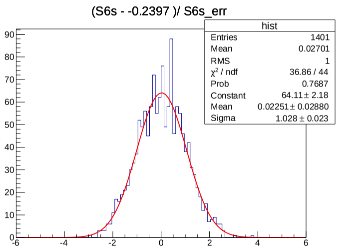

(e) Pull of S_{6s}

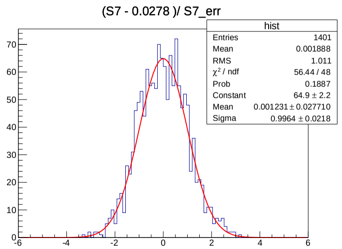

(f) Pull of S_7

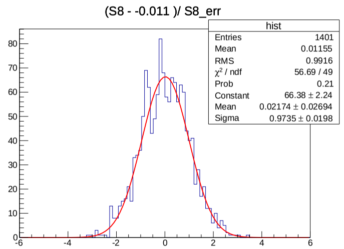

(g) Pull of S_8

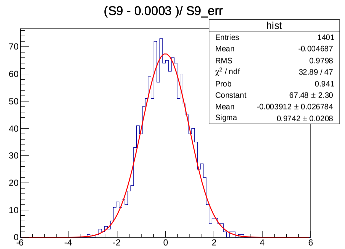

(h) Pull of S_9

Figure 153: Pull distributions for observables in $6.0 - 7.0\,\mathrm{GeV}^2$ q^2 bin.

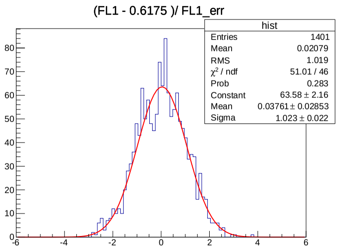

(a) Pull of F_l

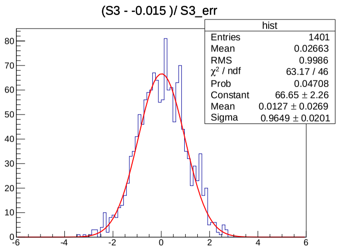

(b) Pull of S_3

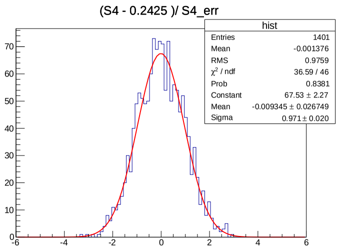

(c) Pull of S_4

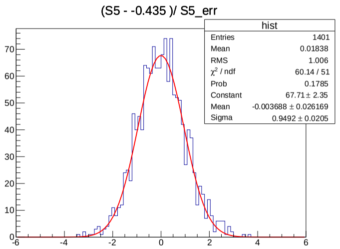

(d) Pull of S_5

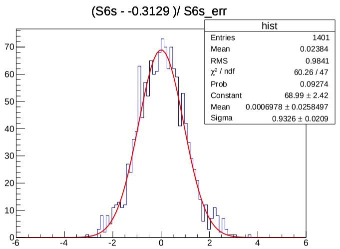

(e) Pull of S_{6s}

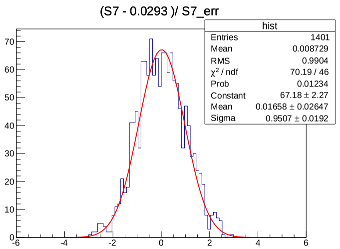

(f) Pull of S_7

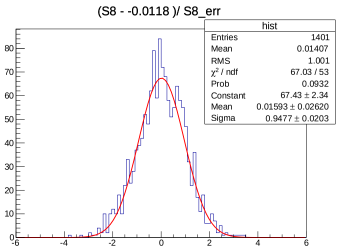

(g) Pull of S_8

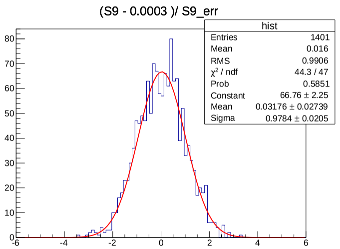

(h) Pull of S_9

Figure 154: Pull distributions for observables in $7.0 - 8.0\,\mathrm{GeV}^2$ q^2 bin.

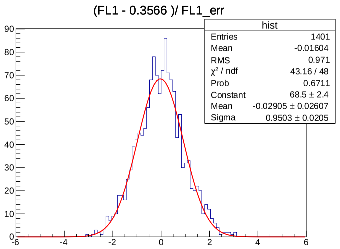

(a) Pull of F_l

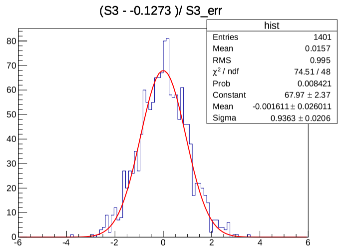

(b) Pull of S_3

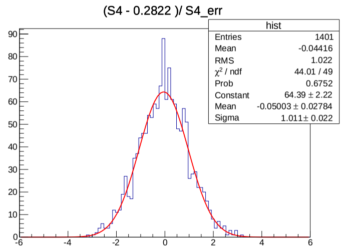

(c) Pull of S_4

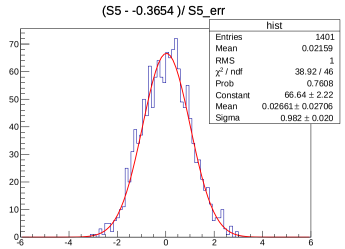

(d) Pull of S_5

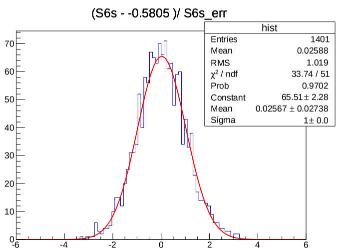

(e) Pull of S_{6s}

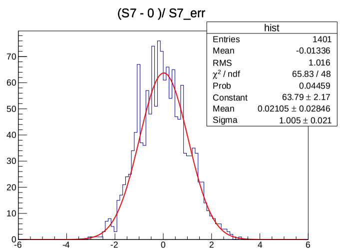

(f) Pull of S_7

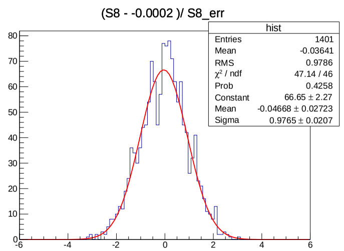

(g) Pull of S_8

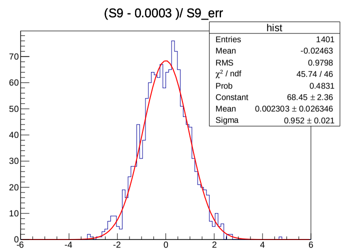

(h) Pull of S_9

Figure 155: Pull distributions for observables in $15.0 - 16.0\,\mathrm{GeV}^2$ q^2 bin.

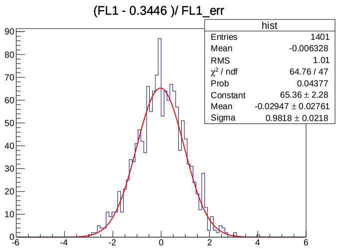

(a) Pull of F_l

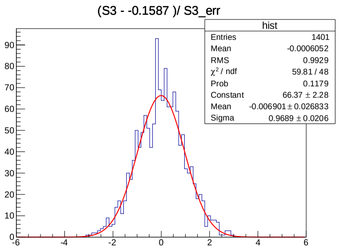

(b) Pull of S_3

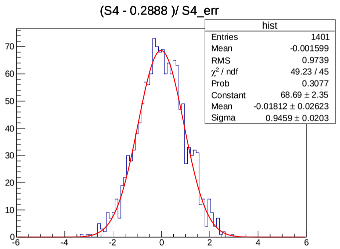

(c) Pull of S_4

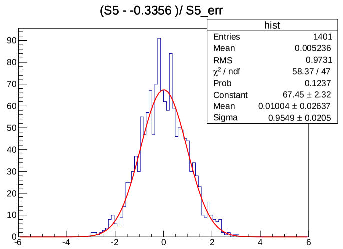

(d) Pull of S_5

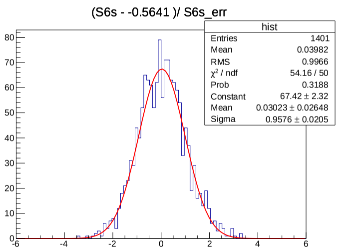

(e) Pull of S_{6s}

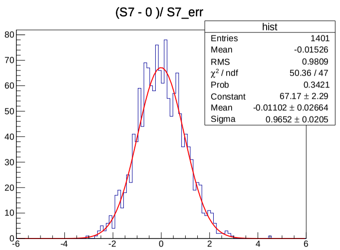

(f) Pull of S_7

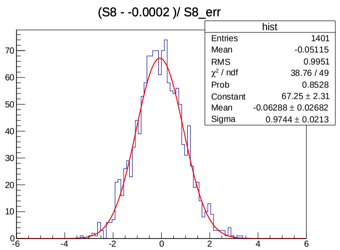

(g) Pull of S_8

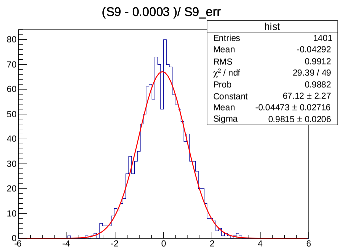

(h) Pull of S_9

Figure 156: Pull distributions for observables in $16.0 - 17.0\,\mathrm{GeV}^2$ q^2 bin.

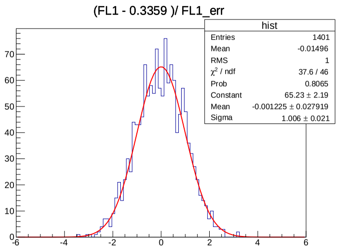

(a) Pull of F_l

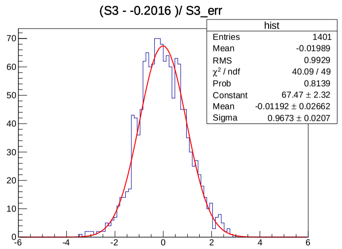

(b) Pull of S_3

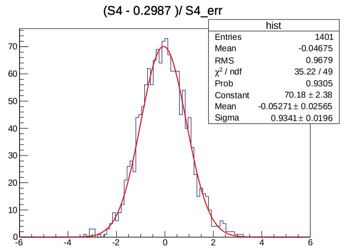

(c) Pull of S_4

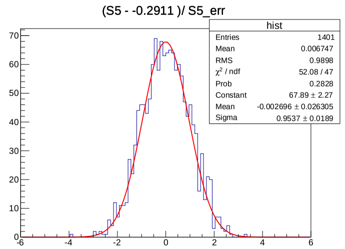

(d) Pull of S_5

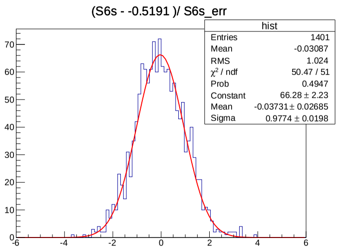

(e) Pull of S_{6s}

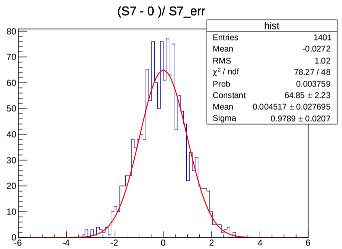

(f) Pull of S_7

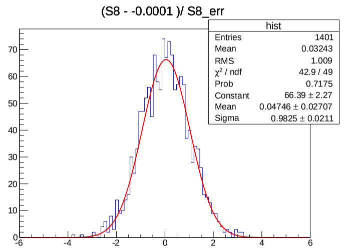

(g) Pull of S_8

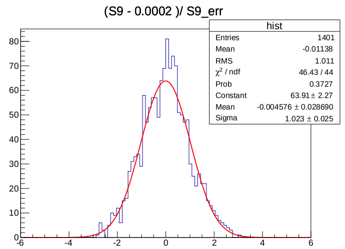

(h) Pull of S_9

Figure 157: Pull distributions for observables in $17.0 - 18.0\,\mathrm{GeV}^2$ q^2 bin.

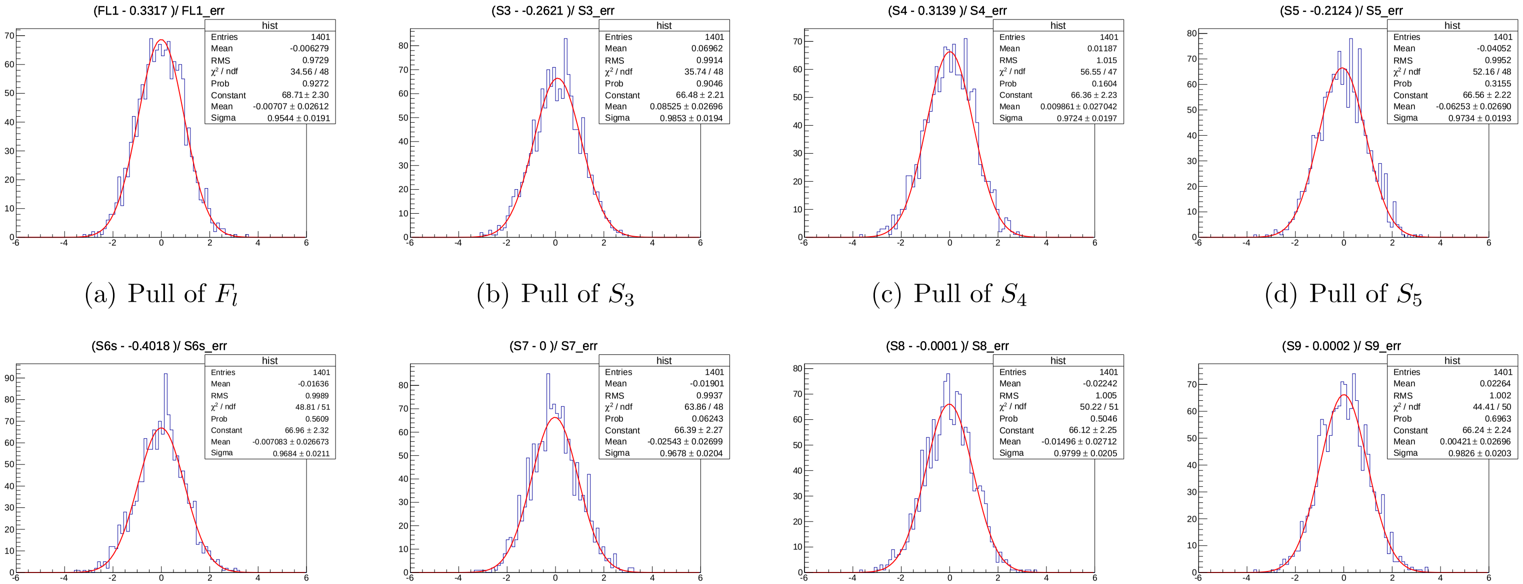

(a) Pull of F_l

(b) Pull of S_3

(c) Pull of S_4

(d) Pull of S_5

(e) Pull of S_{6s}

(f) Pull of S_7

(g) Pull of S_8

(h) Pull of S_9

Figure 158: Pull distributions for observables in $18.0 - 19.0\,\mathrm{GeV}^2$ q^2 bin.

H Factorisation of mass and decay angles for $B^0 \to J/\psi\, K^{*0}$

Figure 159: The three decay angles of $B^0 \to J/\psi\, K^{*0}$ decays in 8 bins of reconstructed B^0 mass. For the angle $\cos\theta_K$ a small difference is seen for the two outer B^0 mass bins.

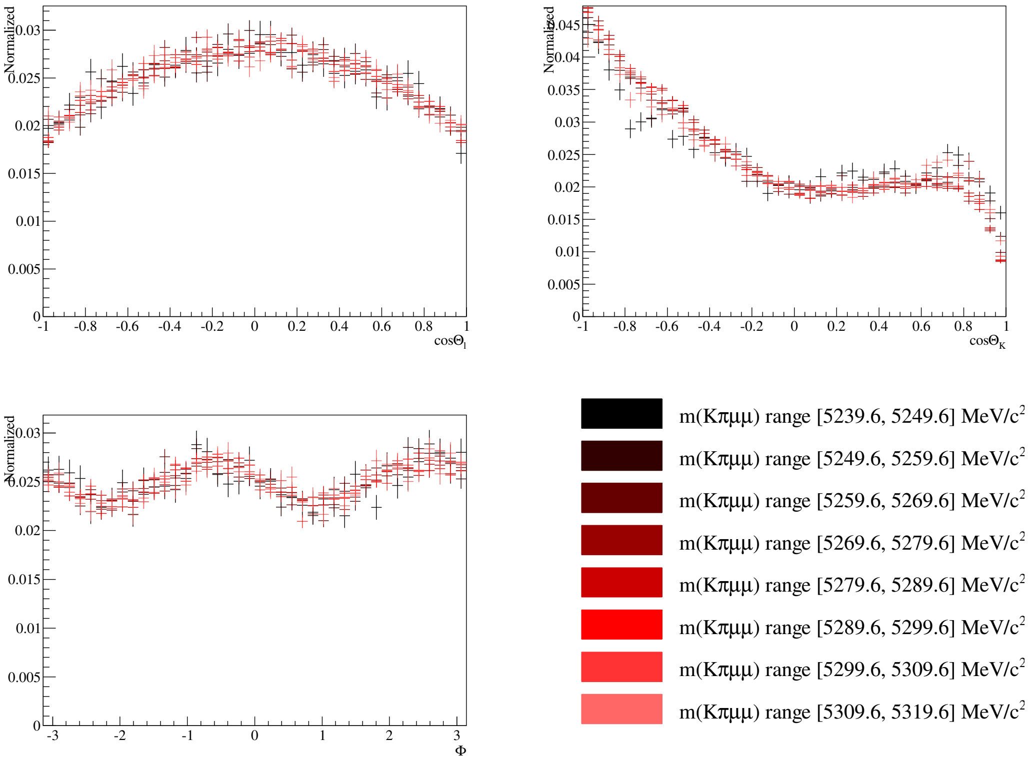

I Continuous symmetry transformations of the K^{*0} spin amplitudes

By defining a set of basis vectors [35]:

$$n_{\|} = \left(\begin{array}{c} A_{\|}^{L} \\ A_{\|}^{R*} \end{array} \right) , \; n_{\perp} = \left(\begin{array}{c} A_{\perp}^{L} \\ -A_{\perp}^{R*} \end{array} \right) , \; n_{0} = \left(\begin{array}{c} A_{0}^{L} \\ A_{0}^{R*} \end{array} \right), \tag{113}$$

the following continuous transformations of these basis vectors, and therefore of the amplitudes leave the angular distribution unchanged

$$n_i' = \left[\begin{array}{cc} e^{i\phi_L} & 0 \\ 0 & e^{-i\phi_R} \end{array} \right] \left[\begin{array}{cc} \cos\theta & -\sin\theta \\ \sin\theta & \cos\theta \end{array} \right] \left[\begin{array}{cc} \cosh i\omega & -\sinh i\omega \\ -\sinh i\omega & \cosh i\omega \end{array} \right] n_i \tag{114}$$

The components ϕ_L and ϕ_R are phase-rotations of the left- and right-handed amplitudes. These can be made separately for left- and right-handed amplitudes in the massless limit because no terms in the angular distribution mix left and right. The second and third matrices act as rotations between the left- and right- handed amplitudes and also leave the angular distribution unchanged.

The amplitudes in the improved fixed-basis exhibit a smooth behaviour in q^2 both in the SM as well as in a range of new physics models as discussed in Sec. 6.4.2. This was assessed by starting from Eq. 114, and expanded in terms of the amplitudes used in the basis-fixing. By inserting the values of the transformed and untransformed amplitudes on the left and right hand sides of Eq. 114 respectively for every point in q^2, the transformation parameters, ϕ_L, ϕ_R, θ and ω, where therefore obtained by numerically solving the system of four non-linear equations. With the values of these transformation parameters, the remaining amplitudes in the fixed-basis could then be determined.

Although not strictly relevant for this method, it is worth mentioning that given for the P-wave only case, $n_j = 11$ and $n_a = 12$, there should be three relations between the various J_i, yielding only eight independent J_i. The introduction of the S-wave terms does not bring in any new symmetry transformations.

It must be noted that the inclusion of the S-wave amplitudes in the fit does not introduce any new symmetries of the decay rate, or break any existing symmetry relations. As such, a fit to the simulated data can be performed following the treatment of Sec. 6.4.8 with the difference that the signal decay rate is given by Eq. 21 where the same q^2 ansatz as before is used to describe the S-wave amplitudes (see Eq. 91).

J Two dimensional amplitude parameter profile likelihoods

This list is still being populated

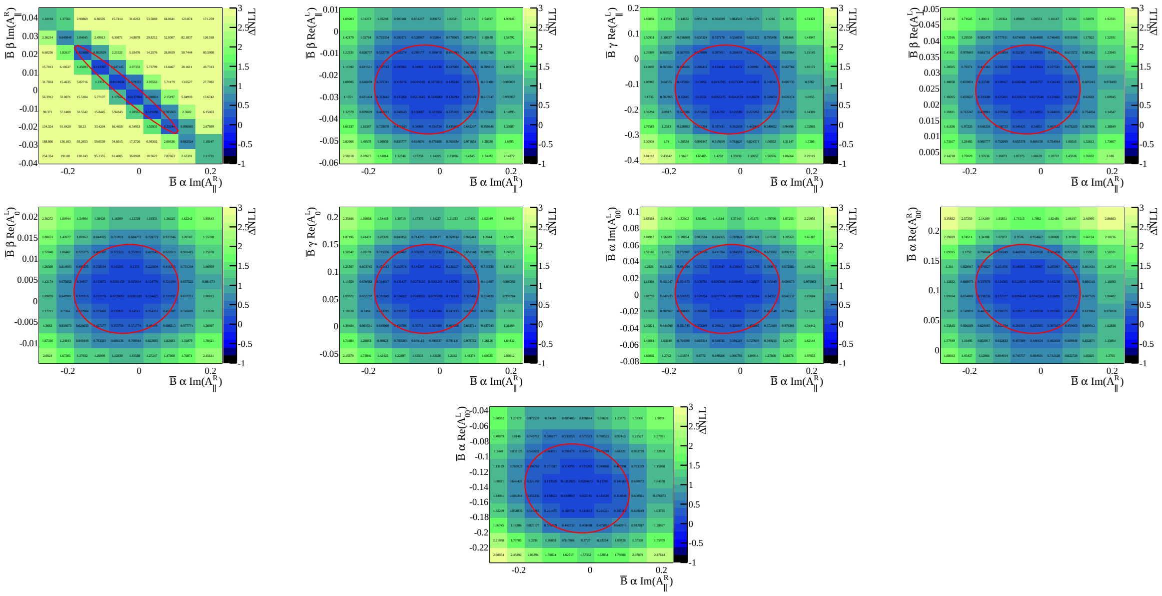

Figure 160: Two dimensional profile likelihoods of a of $Im(A_{\|}^{R})$ of $\bar{B}$ with other amplitude parameters. The ellipse corresponds to the one standard deviation value provided by HESSE. Values at -0.5 denote failed fits which need to be rerun with a different starting value.

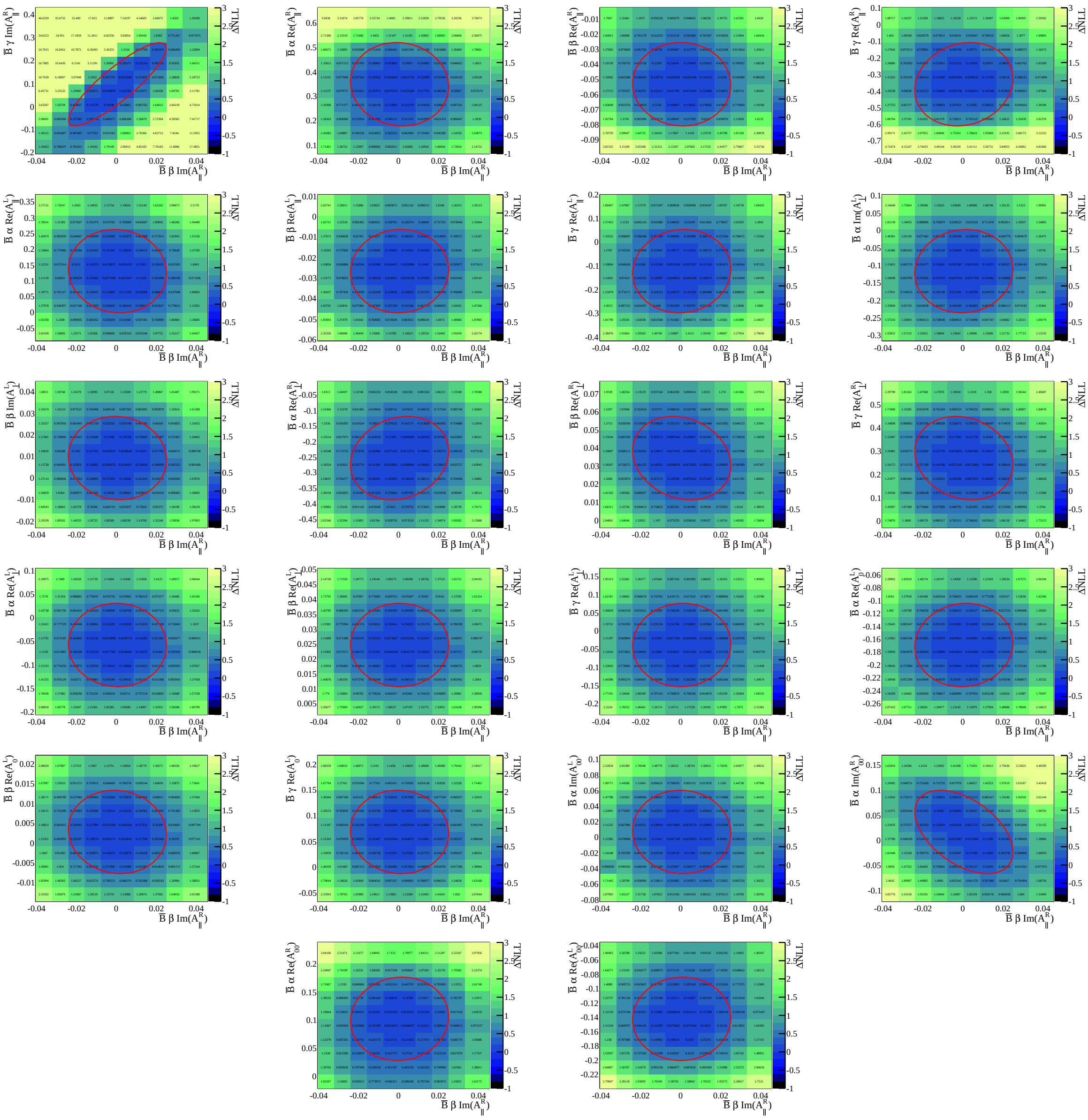

Figure 161: Two dimensional profile likelihoods of b of $Im(A_{\parallel}^{R})$ of $\bar{B}$ with other amplitude parameters. The ellipse corresponds to the one standard deviation value provided by HESSE. Values at -0.5 denote failed fits which need to be rerun with a different starting value.

1831

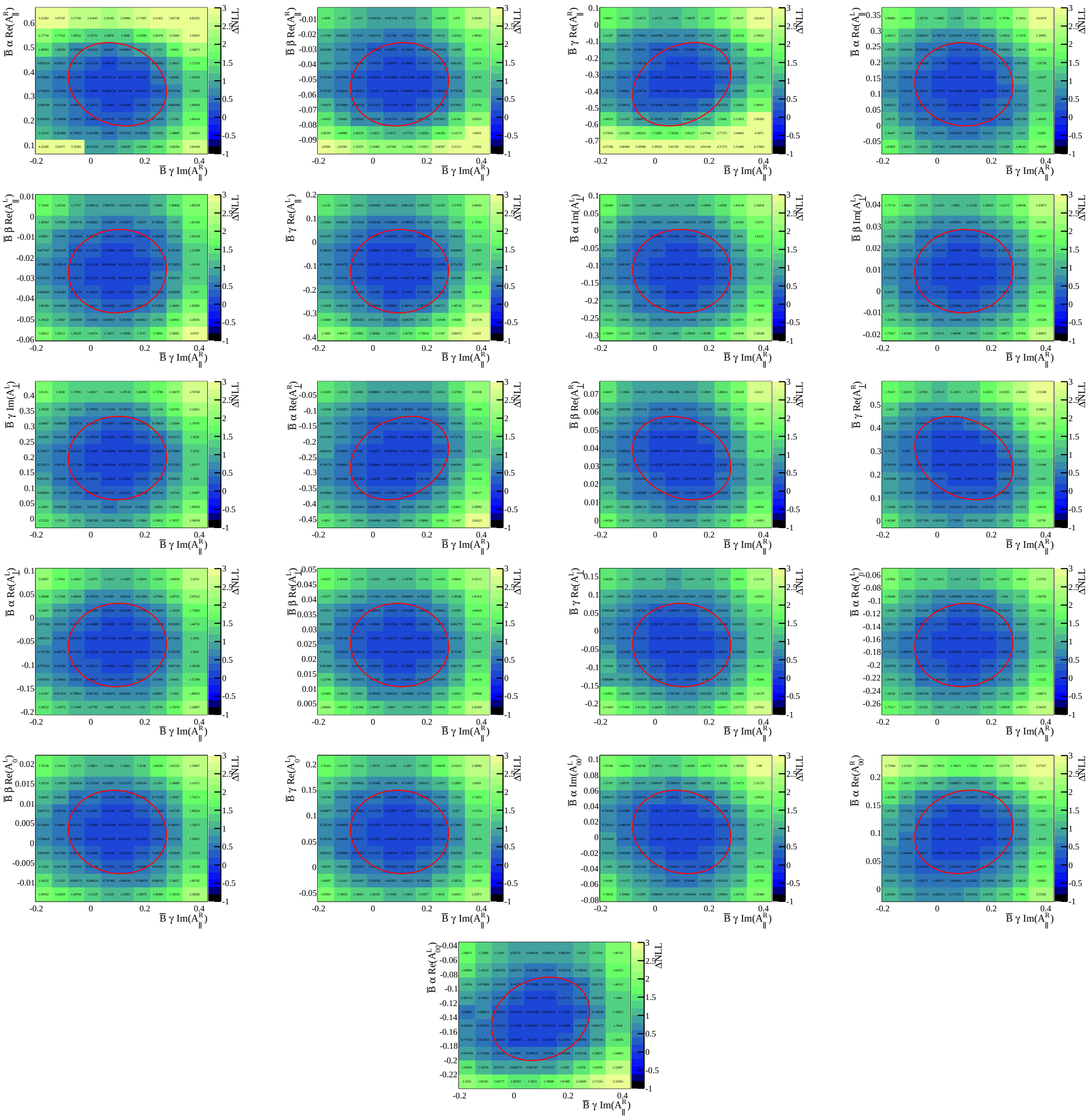

Figure 162: Two dimensional profile likelihoods of c of $Im(A_{\parallel}^{R})$ of $\bar{B}$ with other amplitude parameters. The ellipse corresponds to the one standard deviation value provided by HESSE. Values at -0.5 denote failed fits which need to be rerun with a different starting value.

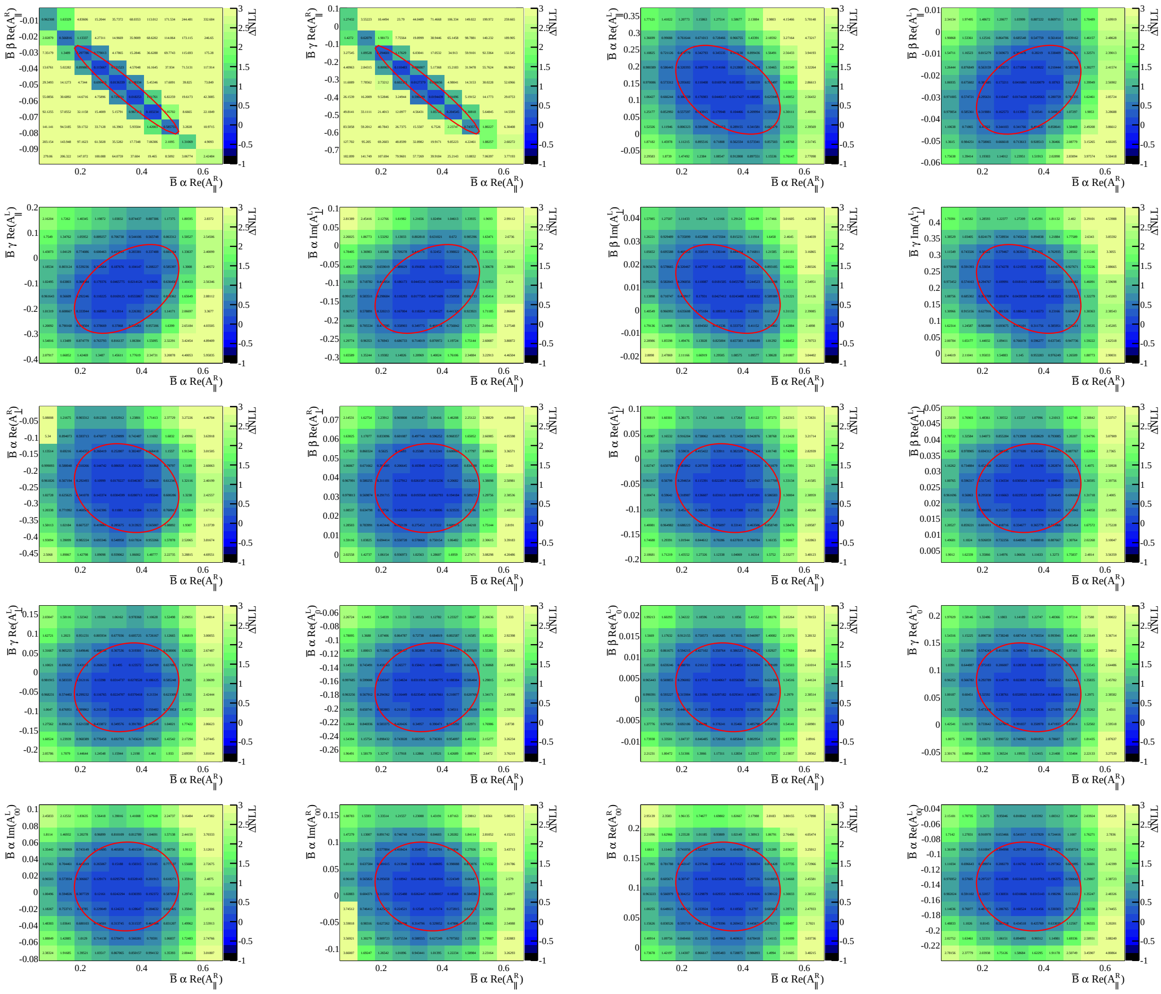

1832

Figure 163: Two dimensional profile likelihoods of a of $Re(A_{\parallel}^{R})$ of $\bar{B}$ with other amplitude parameters. The ellipse corresponds to the one standard deviation value provided by HESSE. Values at -0.5 denote failed fits which need to be rerun with a different starting value.

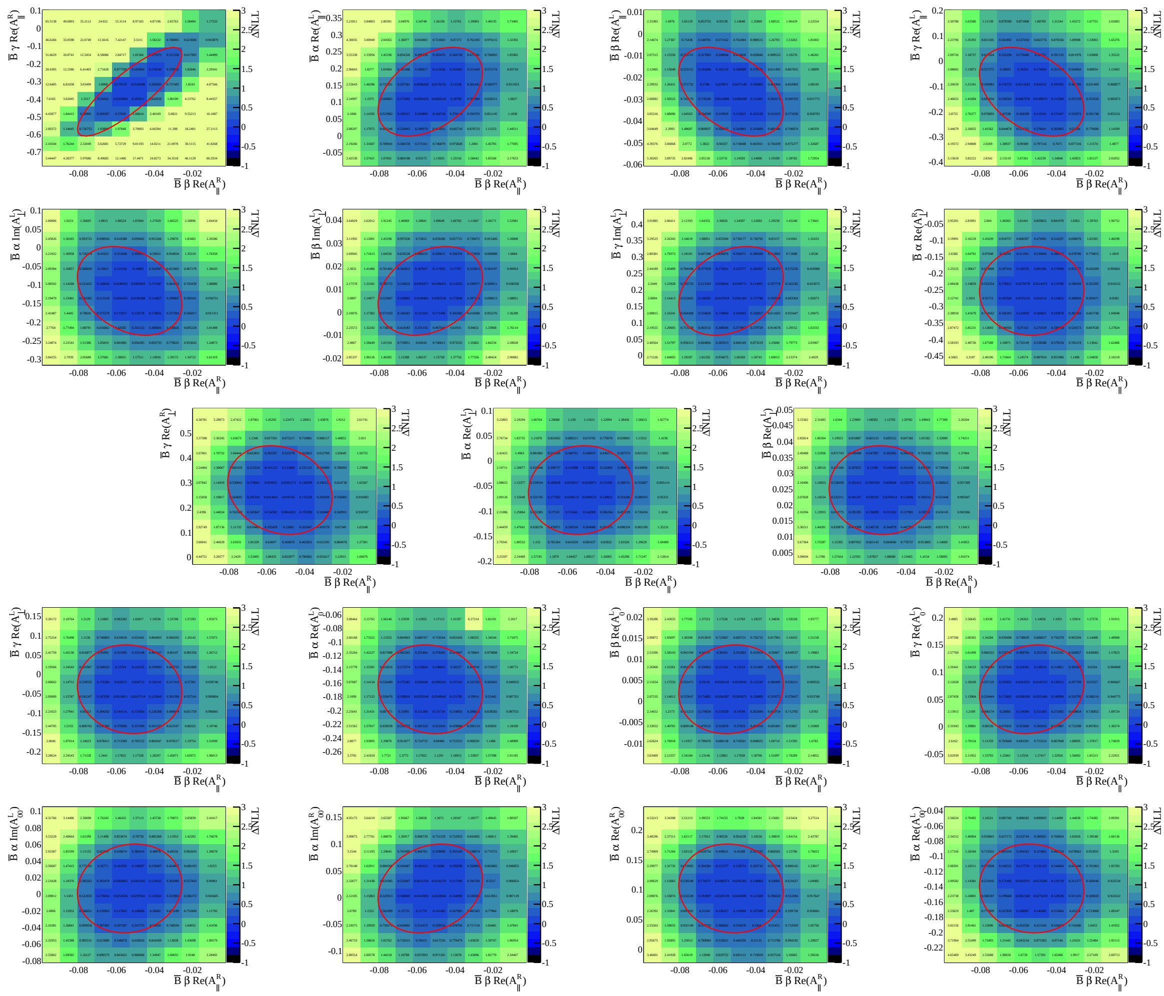

Figure 164: Two dimensional profile likelihoods of b of $Re(A_{\parallel}^{R})$ of $\bar{B}$ with other amplitude parameters. The ellipse corresponds to the one standard deviation value provided by HESSE. Values at -0.5 denote failed fits which need to be rerun with a different starting value.

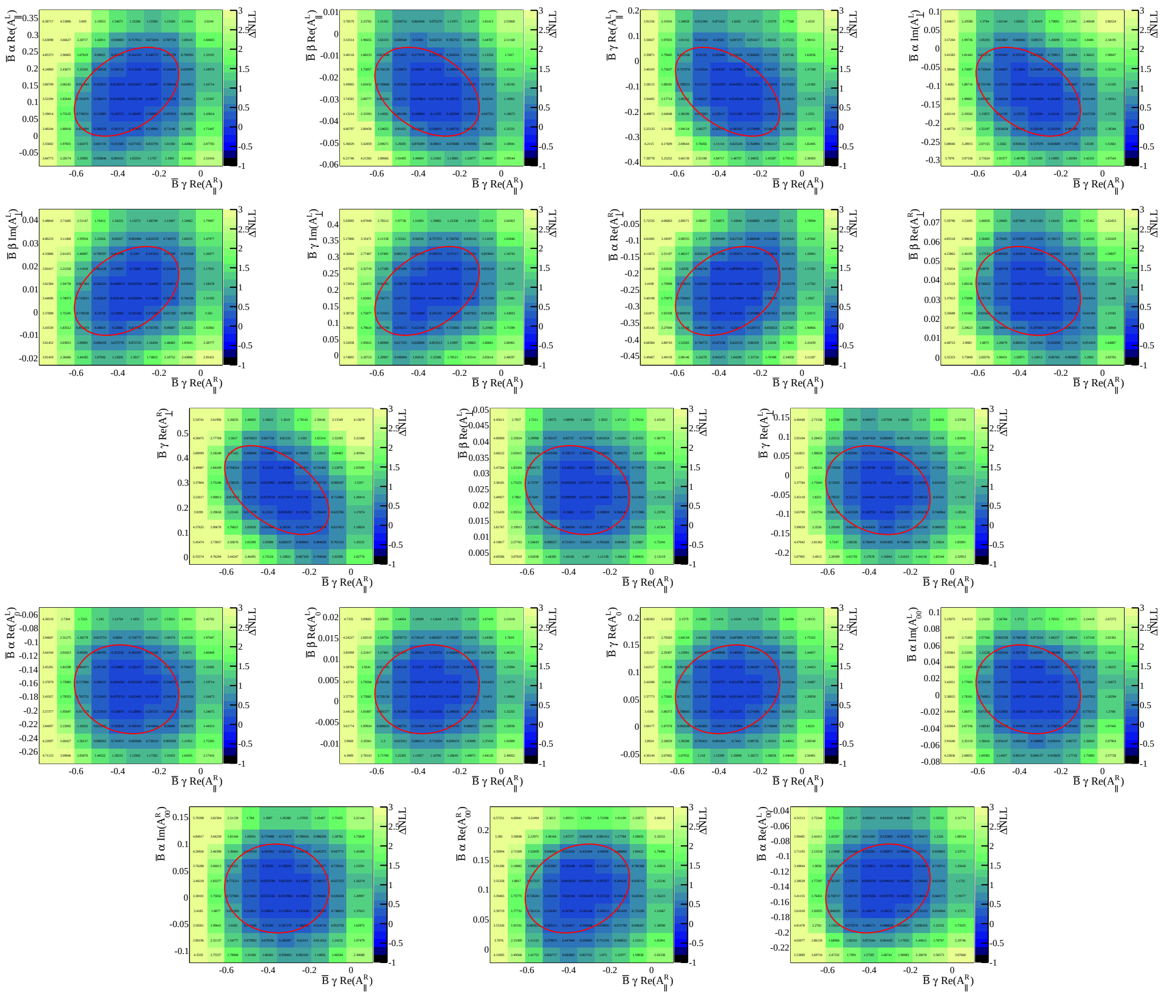

Figure 165: Two dimensional profile likelihoods of c of $Re(A_{\parallel}^{R})$ of $\bar{B}$ with other amplitude parameters. The ellipse corresponds to the one standard deviation value provided by HESSE. Values at -0.5 denote failed fits which need to be rerun with a different starting value.

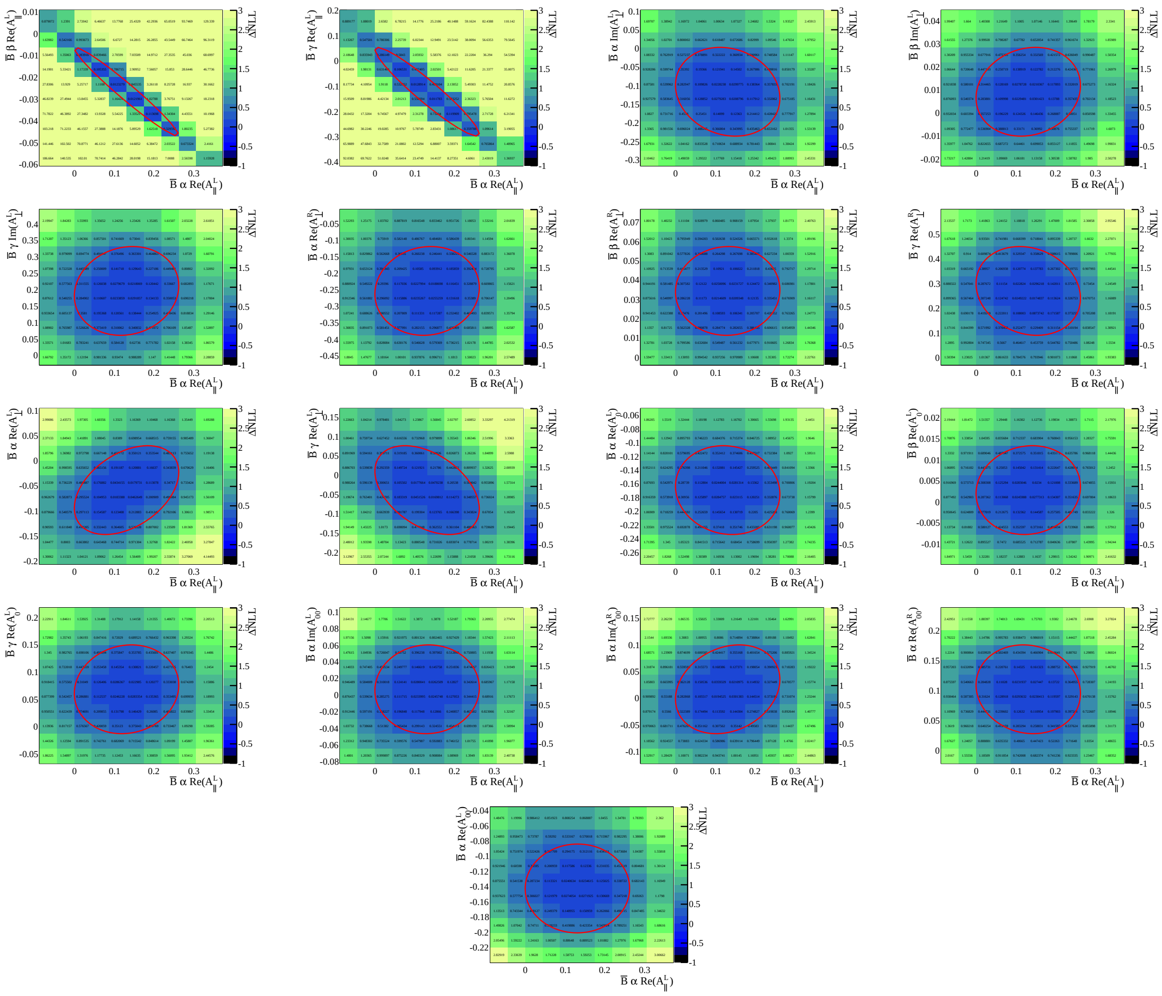

Figure 166: Two dimensional profile likelihoods of a of $Re(A_{\parallel}^{L})$ of $\bar{B}$ with other amplitude parameters. The ellipse corresponds to the one standard deviation value provided by HESSE. Values at -0.5 denote failed fits which need to be rerun with a different starting value.

1836

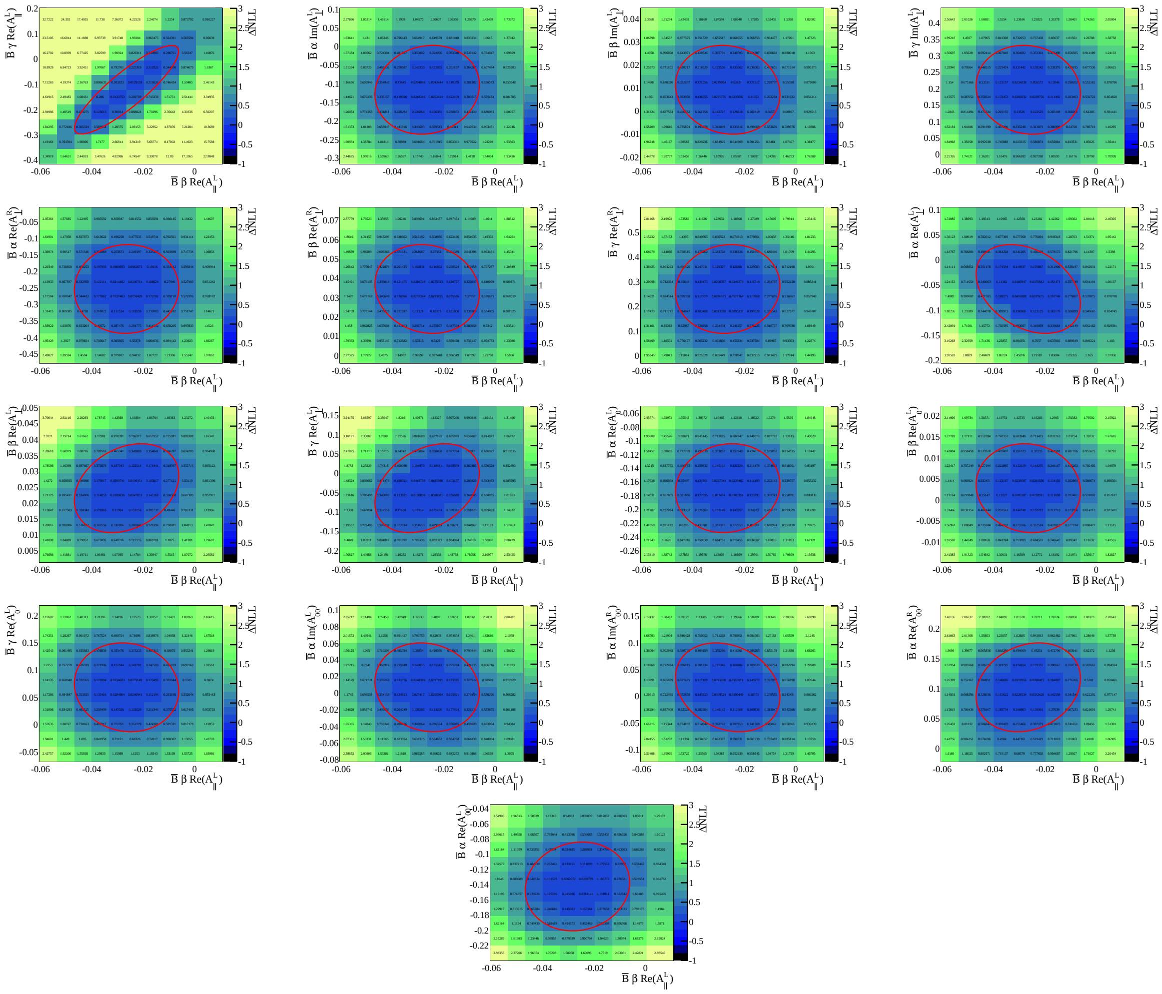

Figure 167: Two dimensional profile likelihoods of b of $Re(A_{\parallel}^{L})$ of $\bar{B}$ with other amplitude parameters. The ellipse corresponds to the one standard deviation value provided by HESSE. Values at -0.5 denote failed fits which need to be rerun with a different starting value.

1837

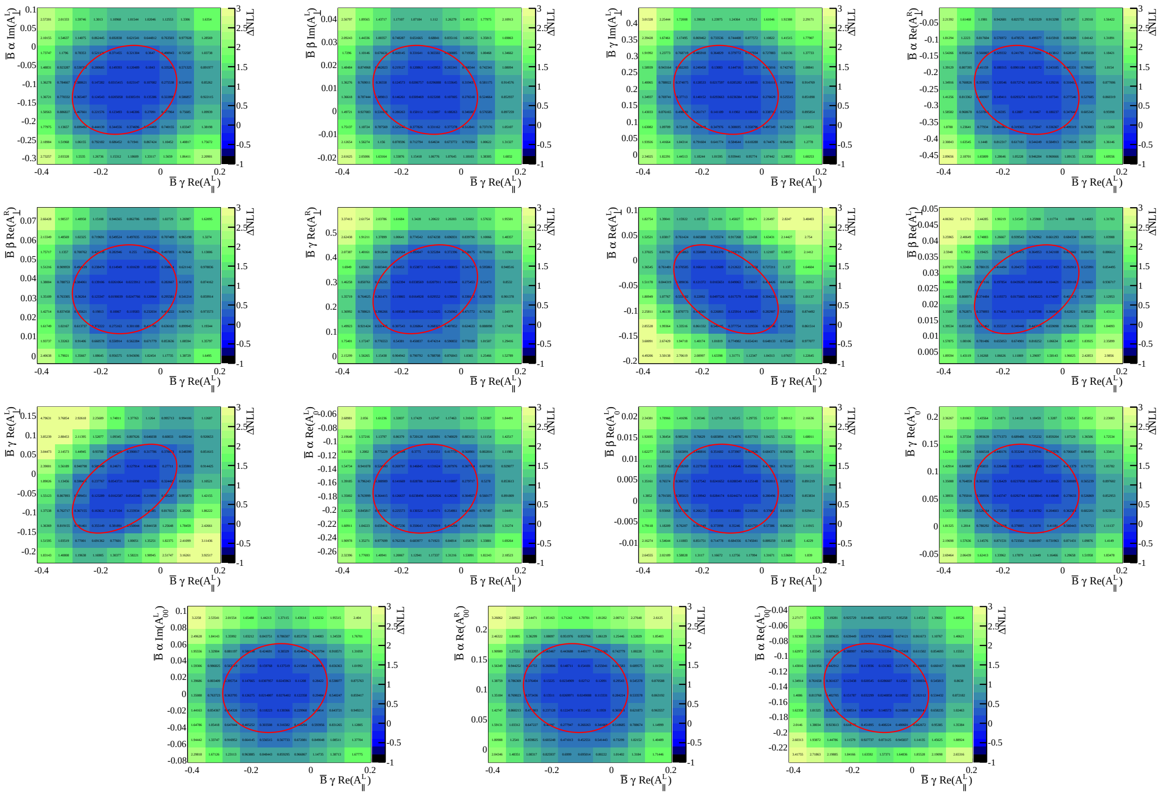

Figure 168: Two dimensional profile likelihoods of c of $Re(A_{\parallel}^{L})$ of $\bar{B}$ with other amplitude parameters. The ellipse corresponds to the one standard deviation value provided by HESSE. Values at -0.5 denote failed fits which need to be rerun with a different starting value.

1838

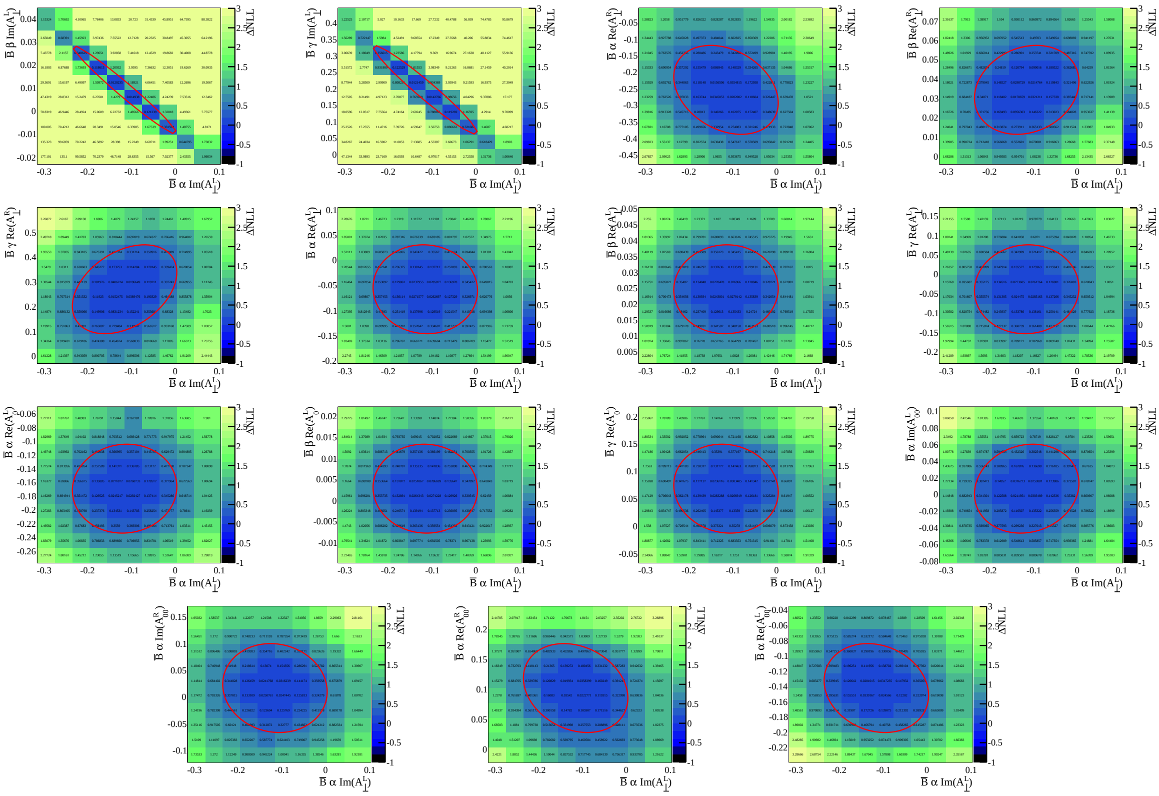

Figure 169: Two dimensional profile likelihoods of a of $Im(A_{\perp}^{L})$ of $\bar{B}$ with other amplitude parameters. The ellipse corresponds to the one standard deviation value provided by HESSE. Values at -0.5 denote failed fits which need to be rerun with a different starting value.

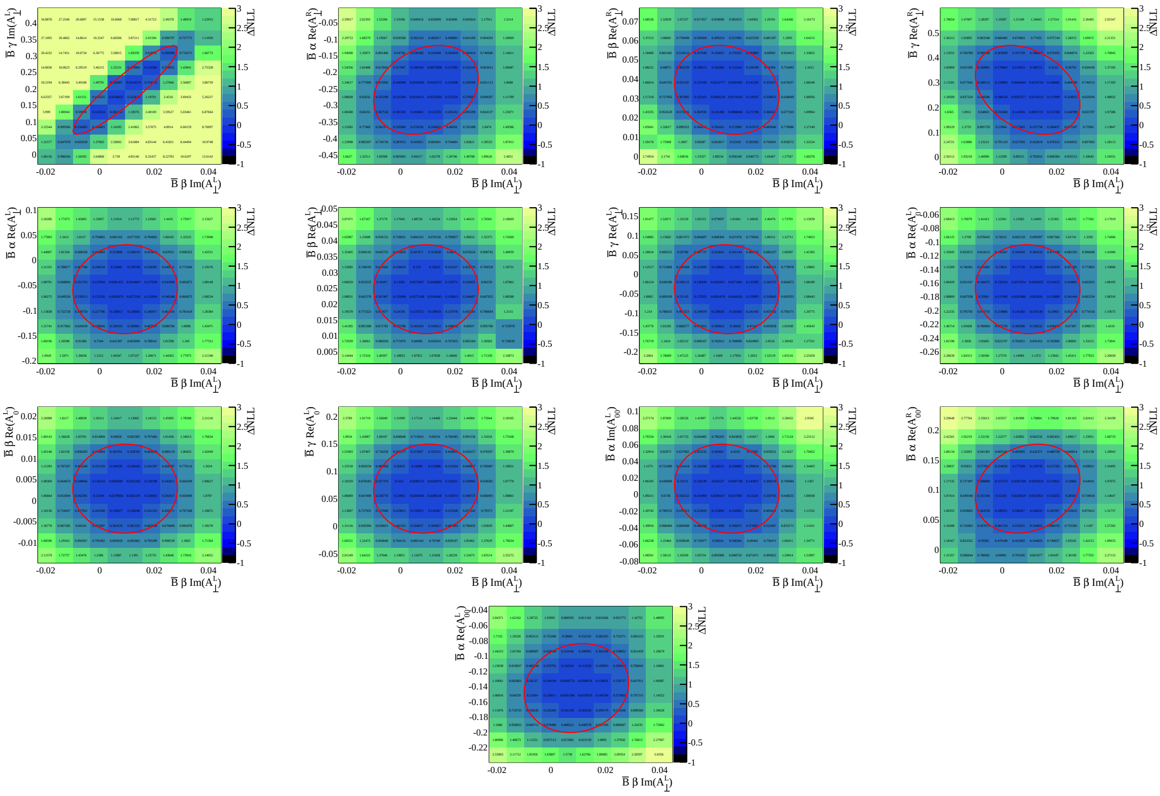

1839

Figure 170: Two dimensional profile likelihoods of b of $Im(A_{\perp}^{L})$ of $\bar{B}$ with other amplitude parameters. The ellipse corresponds to the one standard deviation value provided by HESSE. Values at -0.5 denote failed fits which need to be rerun with a different starting value.

1840

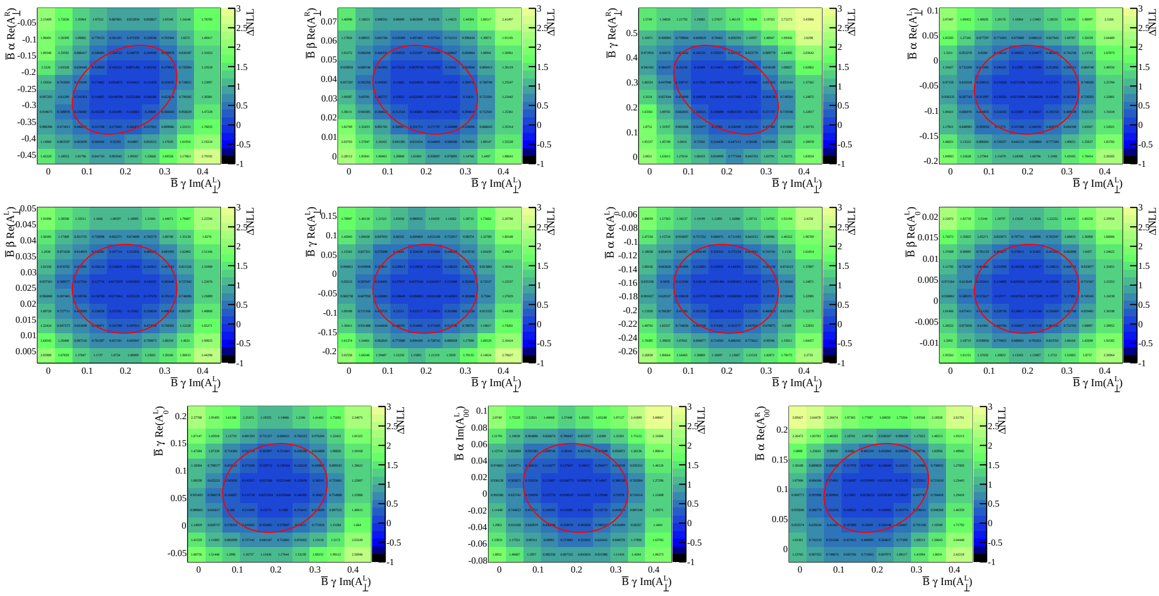

Figure 171: Two dimensional profile likelihoods of c of $Im(A_\perp^L)$ of $\bar{B}$ with other amplitude parameters. The ellipse corresponds to the one standard deviation value provided by HESSE. Values at -0.5 denote failed fits which need to be rerun with a different starting value.

1841

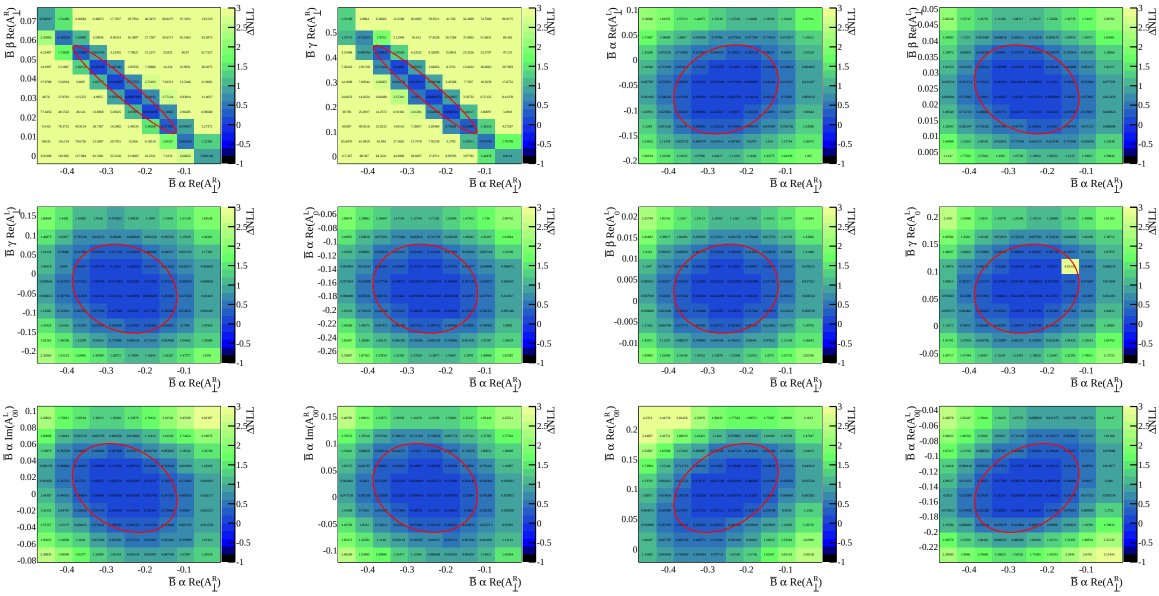

Figure 172: Two dimensional profile likelihoods of a of $Re(A_\perp^R)$ of $\bar{B}$ with other amplitude parameters. The ellipse corresponds to the one standard deviation value provided by HESSE. Values at -0.5 denote failed fits which need to be rerun with a different starting value.

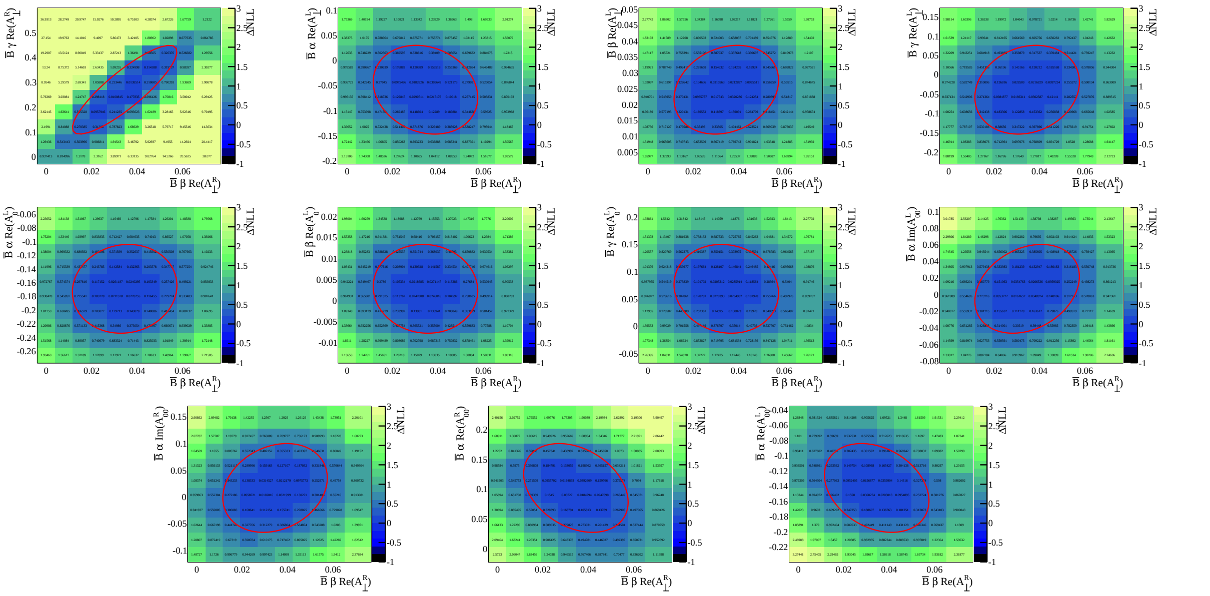

Figure 173: Two dimensional profile likelihoods of b of $Re(A_{\perp}^{R})$ of $\bar{B}$ with other amplitude parameters. The ellipse corresponds to the one standard deviation value provided by HESSE. Values at -0.5 denote failed fits which need to be rerun with a different starting value.

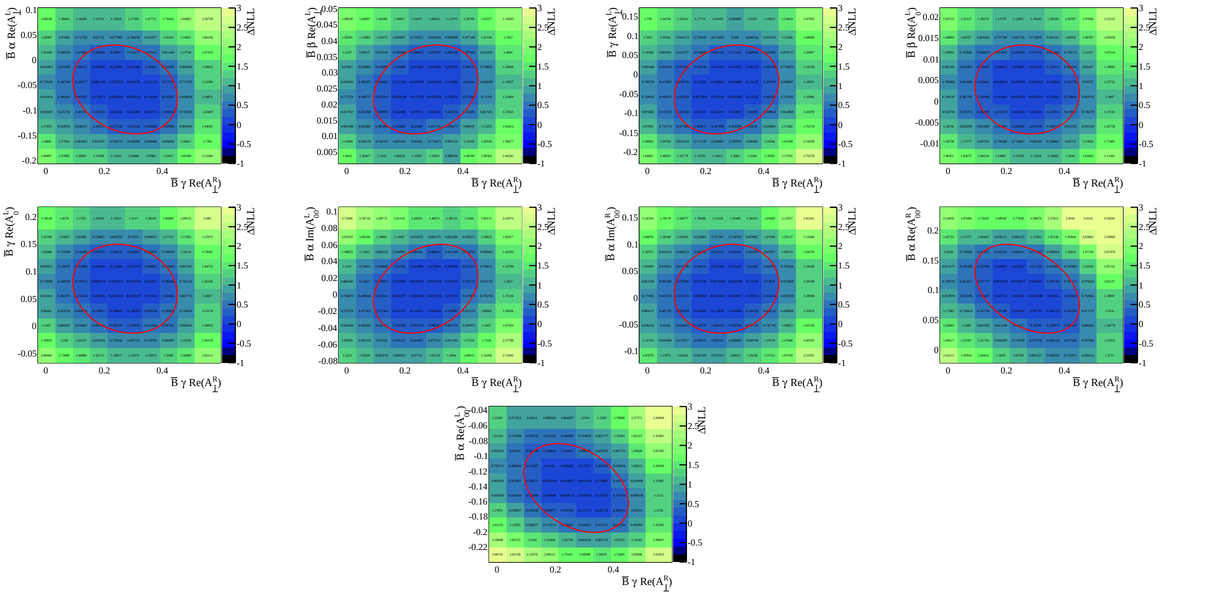

Figure 174: Two dimensional profile likelihoods of c of $Re(A_{\perp}^{R})$ of $\bar{B}$ with other amplitude parameters. The ellipse corresponds to the one standard deviation value provided by HESSE. Values at -0.5 denote failed fits which need to be rerun with a different starting value.

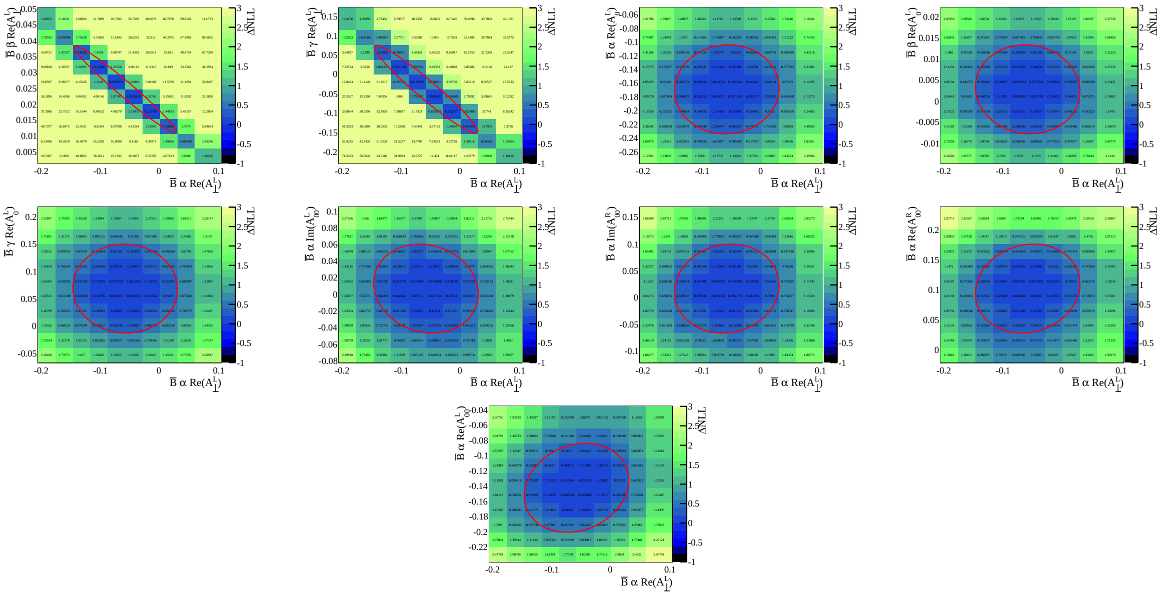

Figure 175: Two dimensional profile likelihoods of a of $Re(A_{\perp}^{L})$ of $\bar{B}$ with other amplitude parameters. The ellipse corresponds to the one standard deviation value provided by HESSE. Values at -0.5 denote failed fits which need to be rerun with a different starting value.

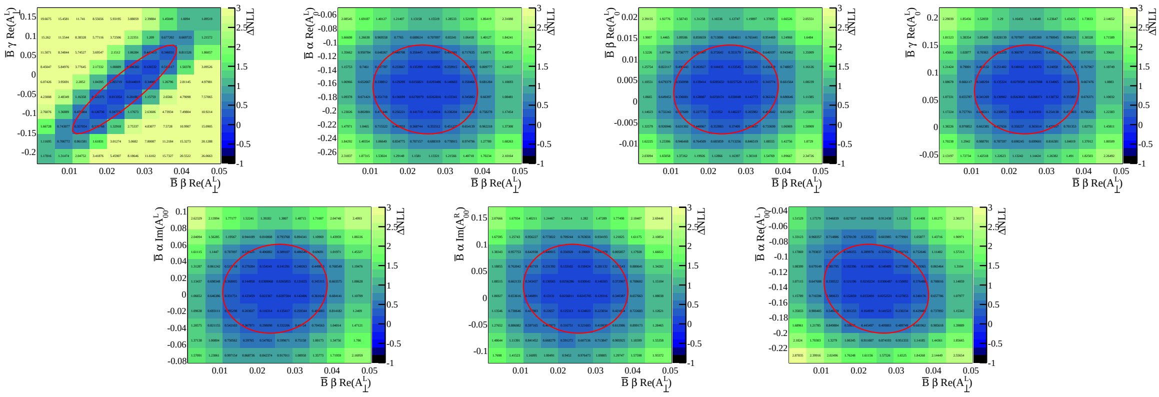

Figure 176: Two dimensional profile likelihoods of b of $Re(A_{\perp}^{L})$ of $\bar{B}$ with other amplitude parameters. The ellipse corresponds to the one standard deviation value provided by HESSE. Values at -0.5 denote failed fits which need to be rerun with a different starting value.

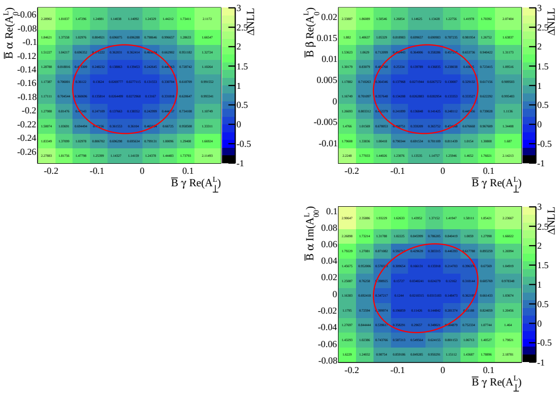

Figure 177: Two dimensional profile likelihoods of c of $Re(A_{\perp}^{L})$ of $\bar{B}$ with other amplitude parameters. The ellipse corresponds to the one standard deviation value provided by HESSE. Values at -0.5 denote failed fits which need to be rerun with a different starting value.

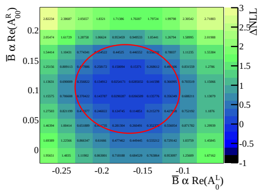

Figure 178: Two dimensional profile likelihoods of a of $Re(A_{0}^{L})$ of $\bar{B}$ with other amplitude parameters. The ellipse corresponds to the one standard deviation value provided by HESSE. Values at -0.5 denote failed fits which need to be rerun with a different starting value.

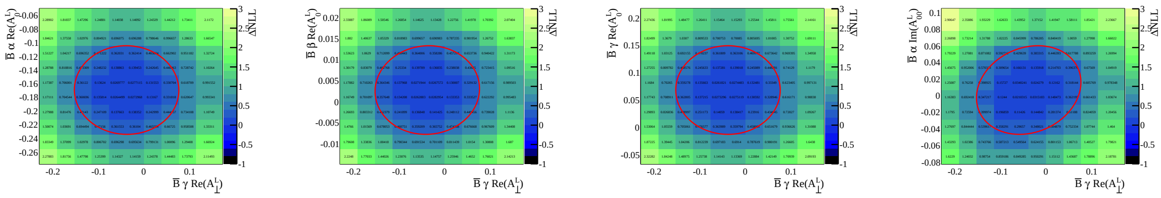

Figure 179: Two dimensional profile likelihoods of c of $Re(A_{\perp}^{L})$ of $\bar{B}$ with other amplitude parameters. The ellipse corresponds to the one standard deviation value provided by HESSE. Values at -0.5 denote failed fits which need to be rerun with a different starting value.

K Background factorisation

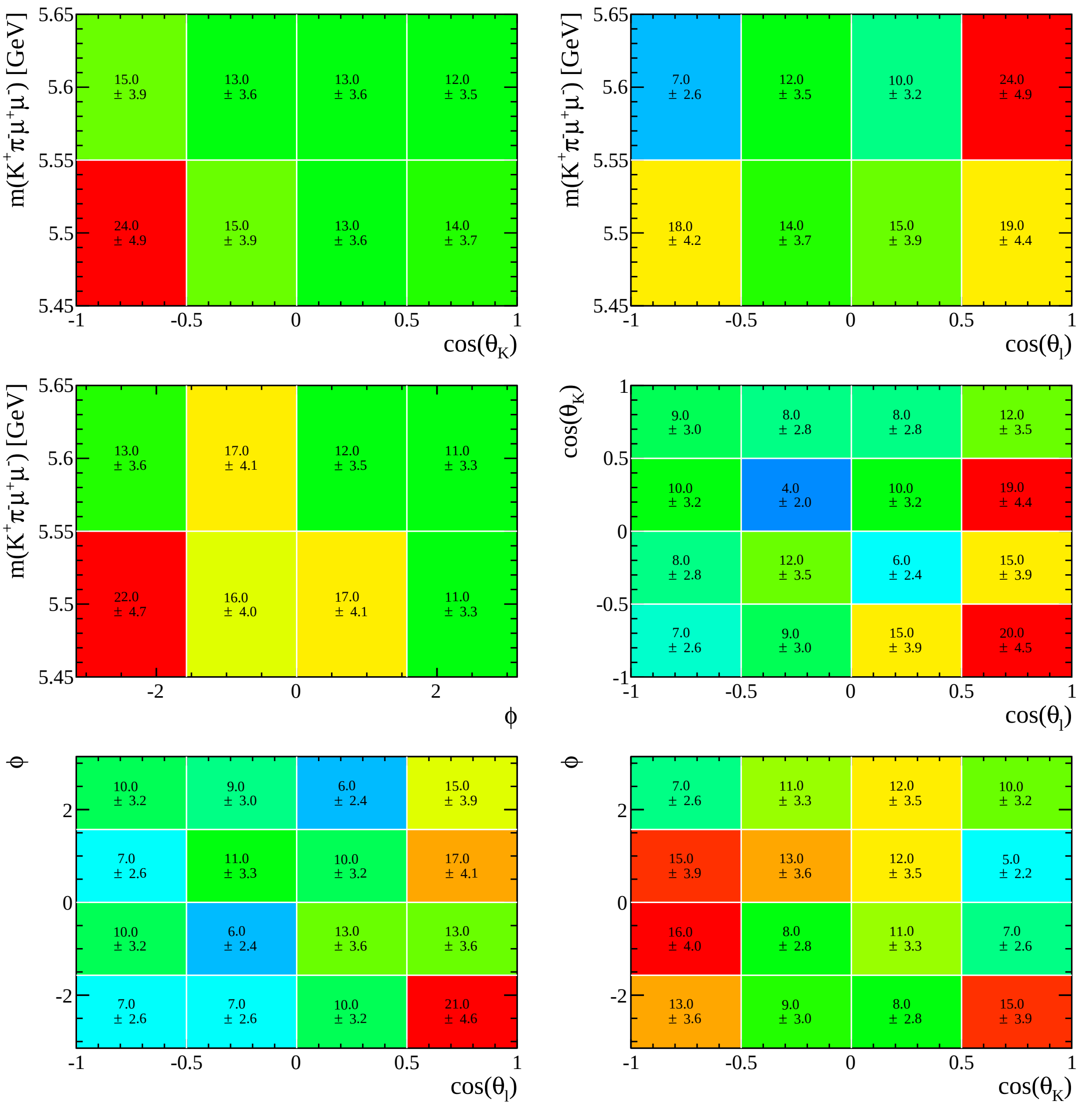

Figure 180: Distribution of events in the upper mass sideband $5450 < m(K^+\pi^-\mu^+\mu^-) < 5650\,\mathrm{MeV}/c^2$ for $1 < q^2 < 6\,\mathrm{GeV}^2/c^4$.

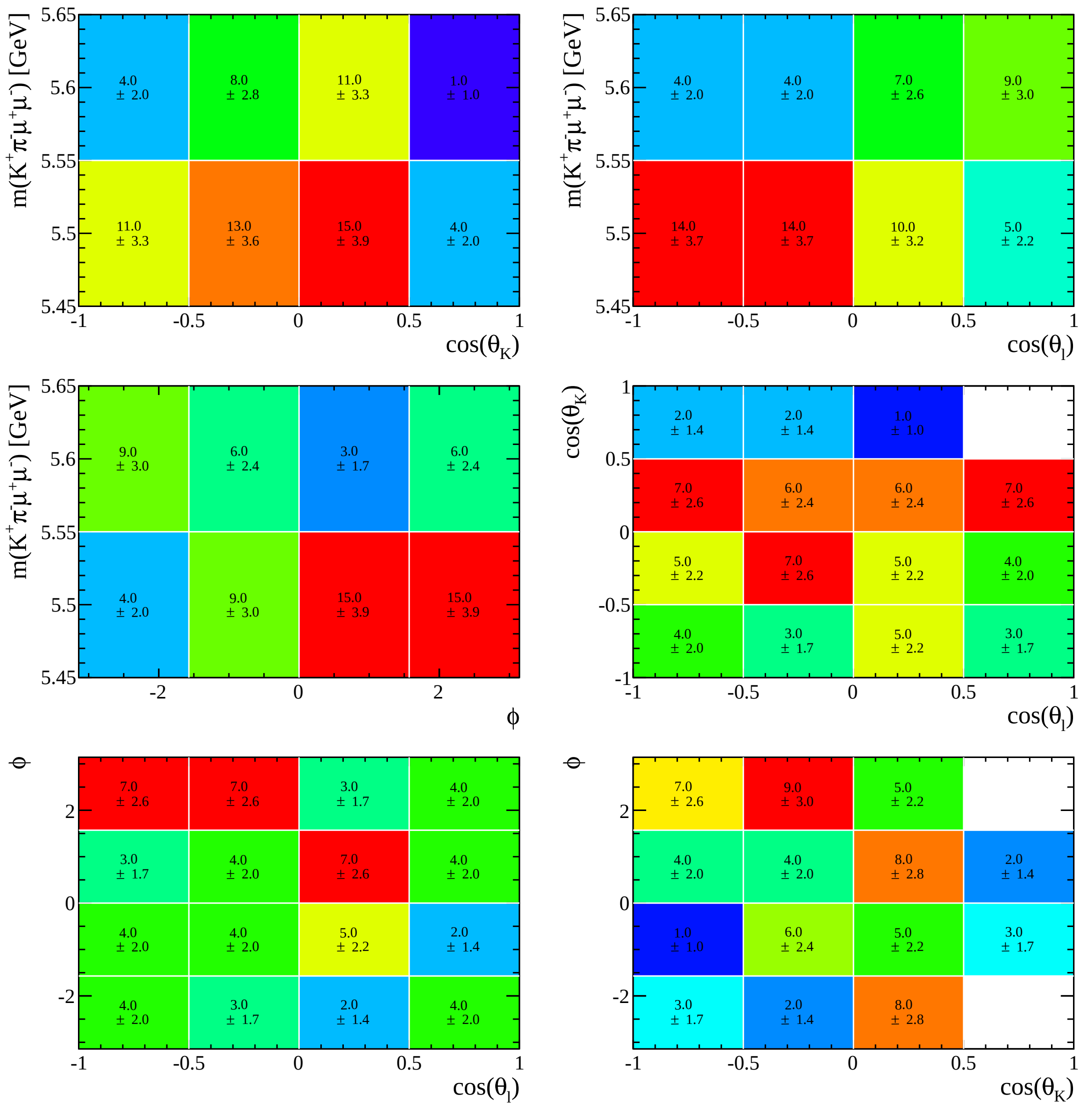

Figure 181: Distribution of events in the upper mass sideband $5450 < m(K^+\pi^-\mu^+\mu^-) < 5650\,\mathrm{MeV}/c^2$ for $15 < q^2 < 19\,\mathrm{GeV}^2/c^4$.

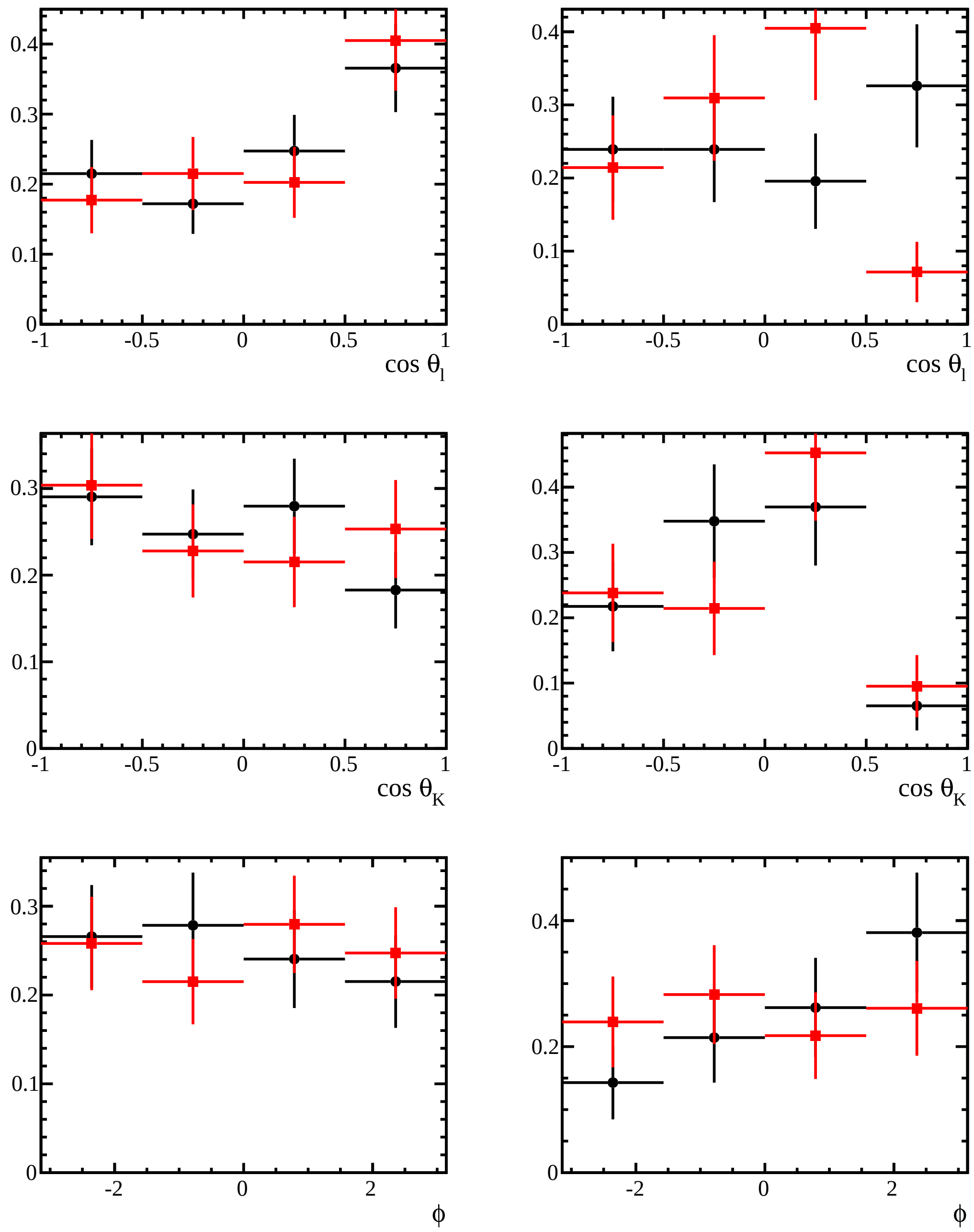

Figure 182: Distribution of events in the upper mass sideband showing that the angular distribution of events is consistent for different mass windows. The black points correspond to the range $5400 < m(K^+\pi^-\mu^+\mu^-) < 5500\,\mathrm{MeV}/c^2$. The red points correspond to the range $5500 < m(K^+\pi^-\mu^+\mu^-) < 5660\,\mathrm{MeV}/c^2$. The left-hand column corresponds to $1 < q^2 < 6\,\mathrm{GeV}^2/c^4$ and the right-hand column to $15 < q^2 < 19\,\mathrm{GeV}^2/c^4$.

L Results of Bootstrapping method for the method of moments

In the following we will show the distribution of the pseudo-experiment from bootstrapping the data. The 68% C.L. is also indicated for each observable.

Figure 183: Bootstraps distribution in $0.1 < q^2 < 0.98\,\mathrm{GeV}^2/c^4$ bin

1854

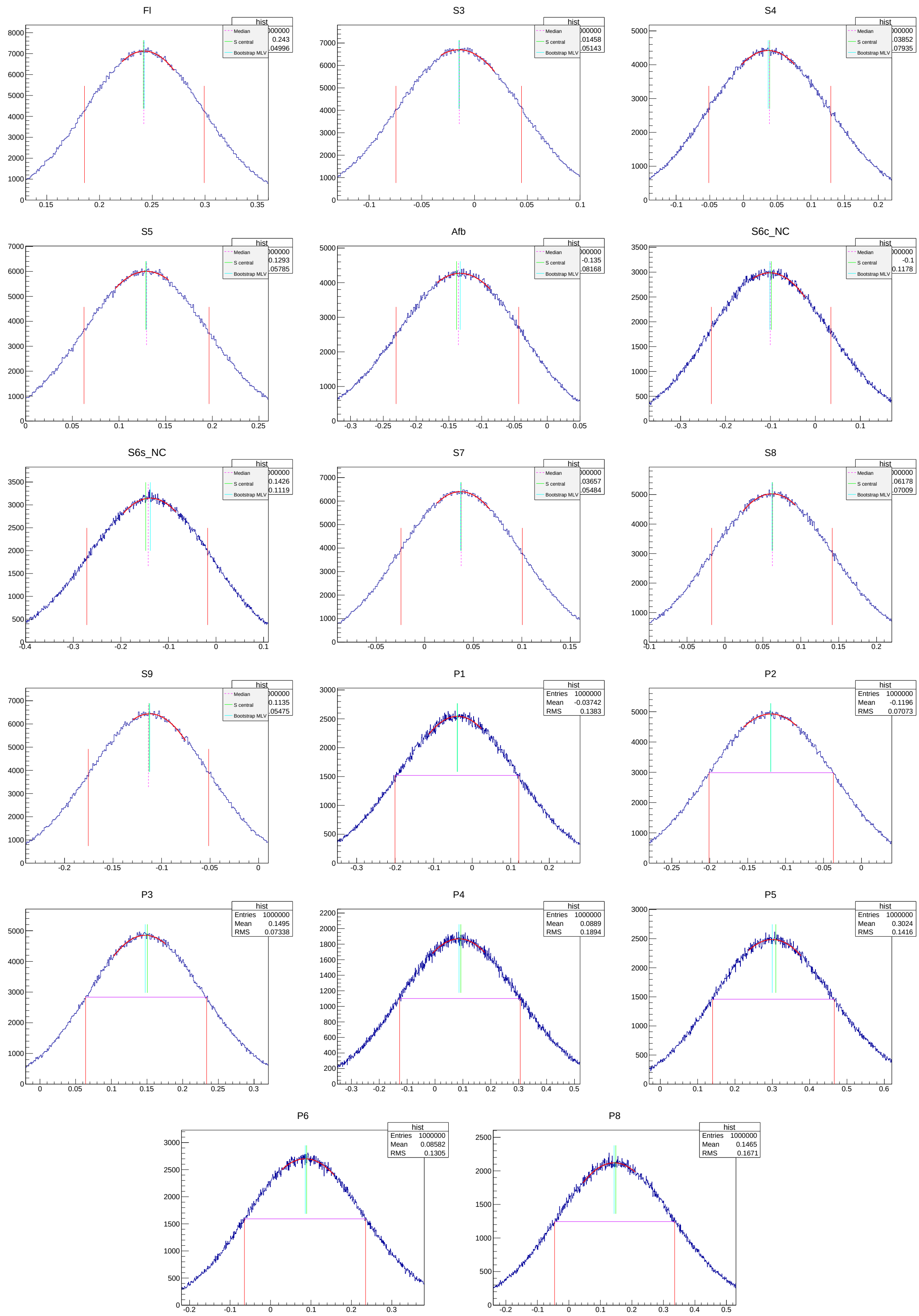

Figure 184: Bootstraps distribution in $1.1 < q^2 < 2.0\,\mathrm{GeV}^2/c^4$ bin

1855

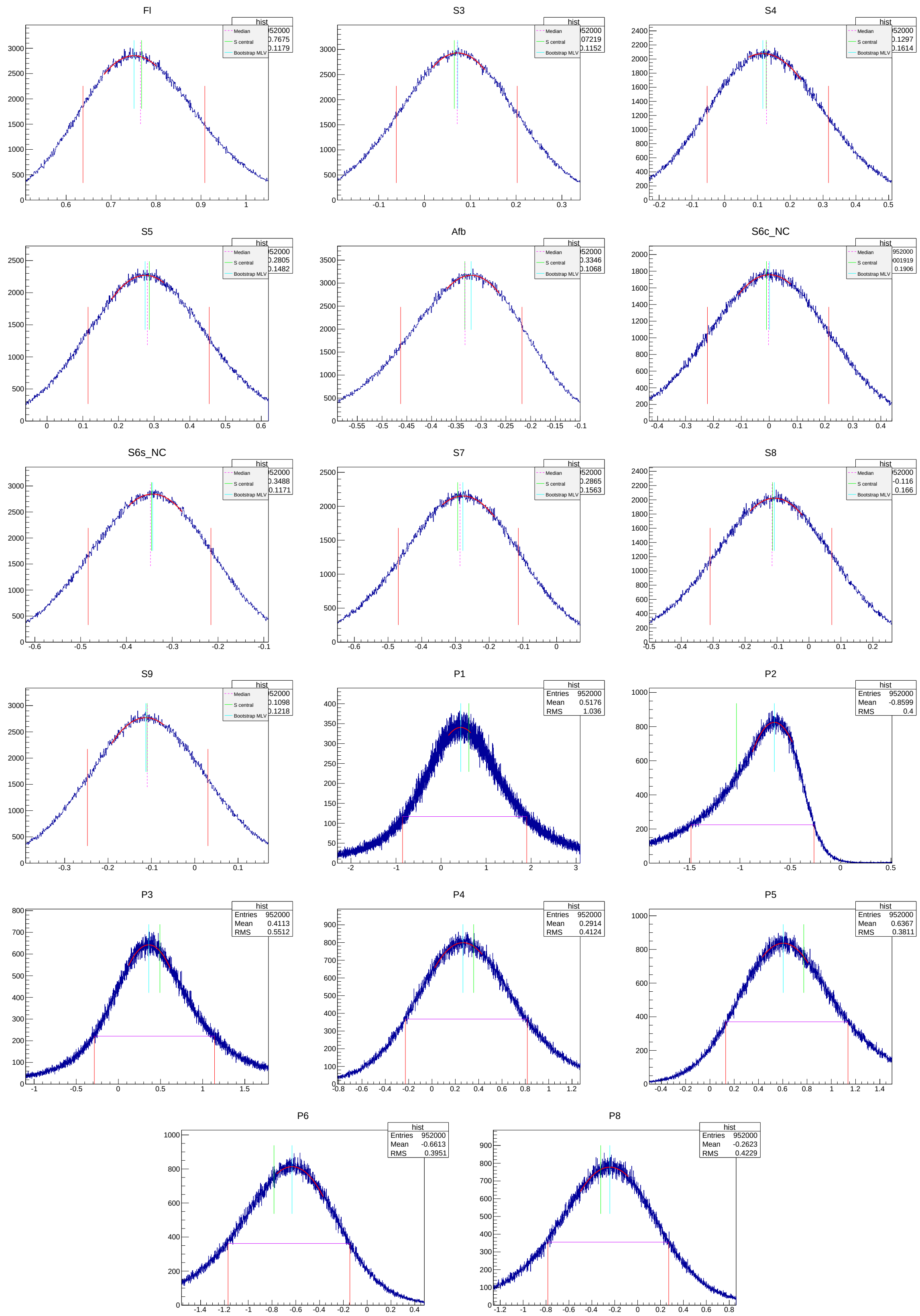

Figure 185: Bootstraps distribution in $2.0 < q^2 < 3.0\,\mathrm{GeV}^2/c^4$ bin

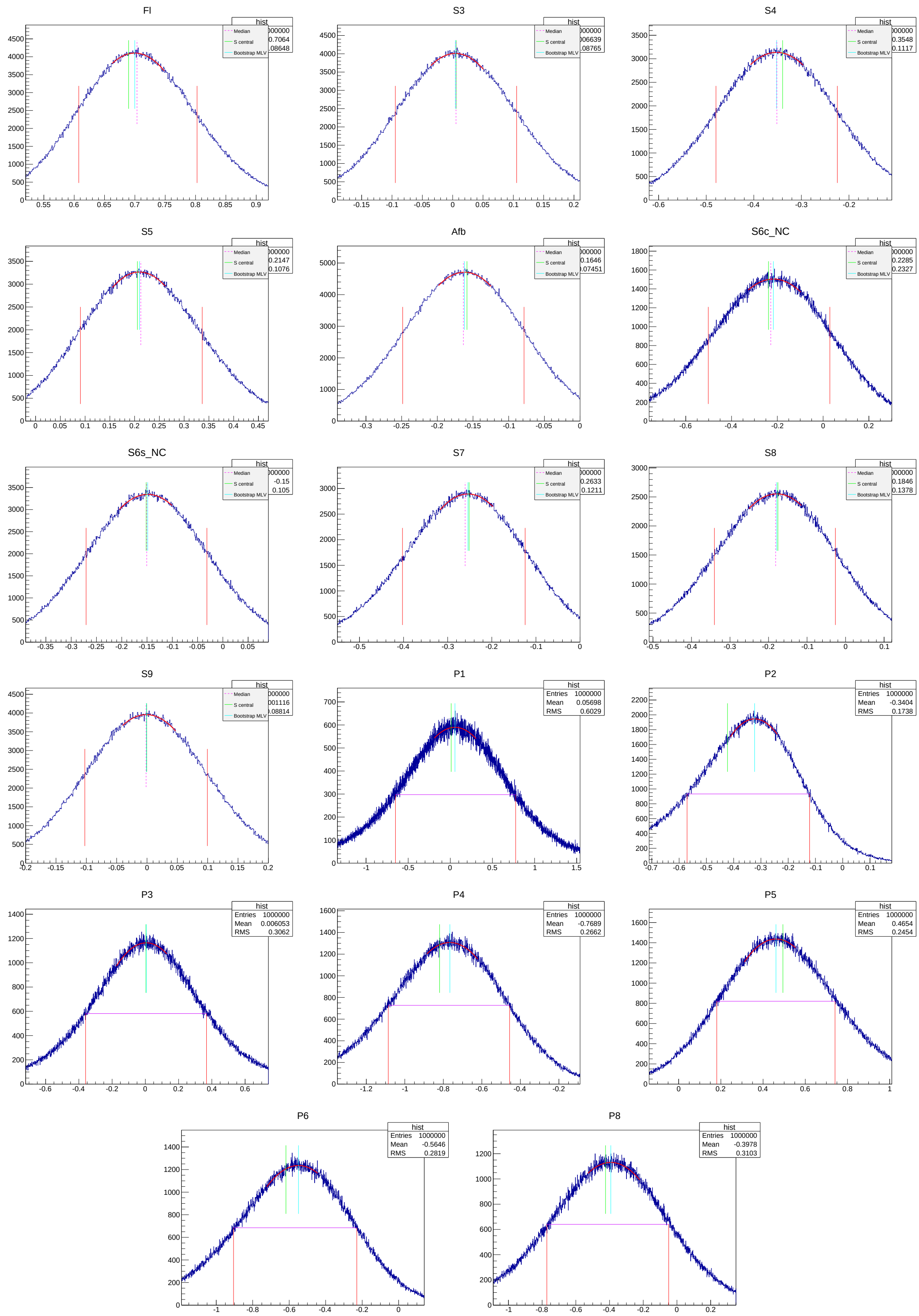

Figure 186: Bootstraps distribution in $3.0 < q^2 < 4.0\,\mathrm{GeV}^2/c^4$ bin

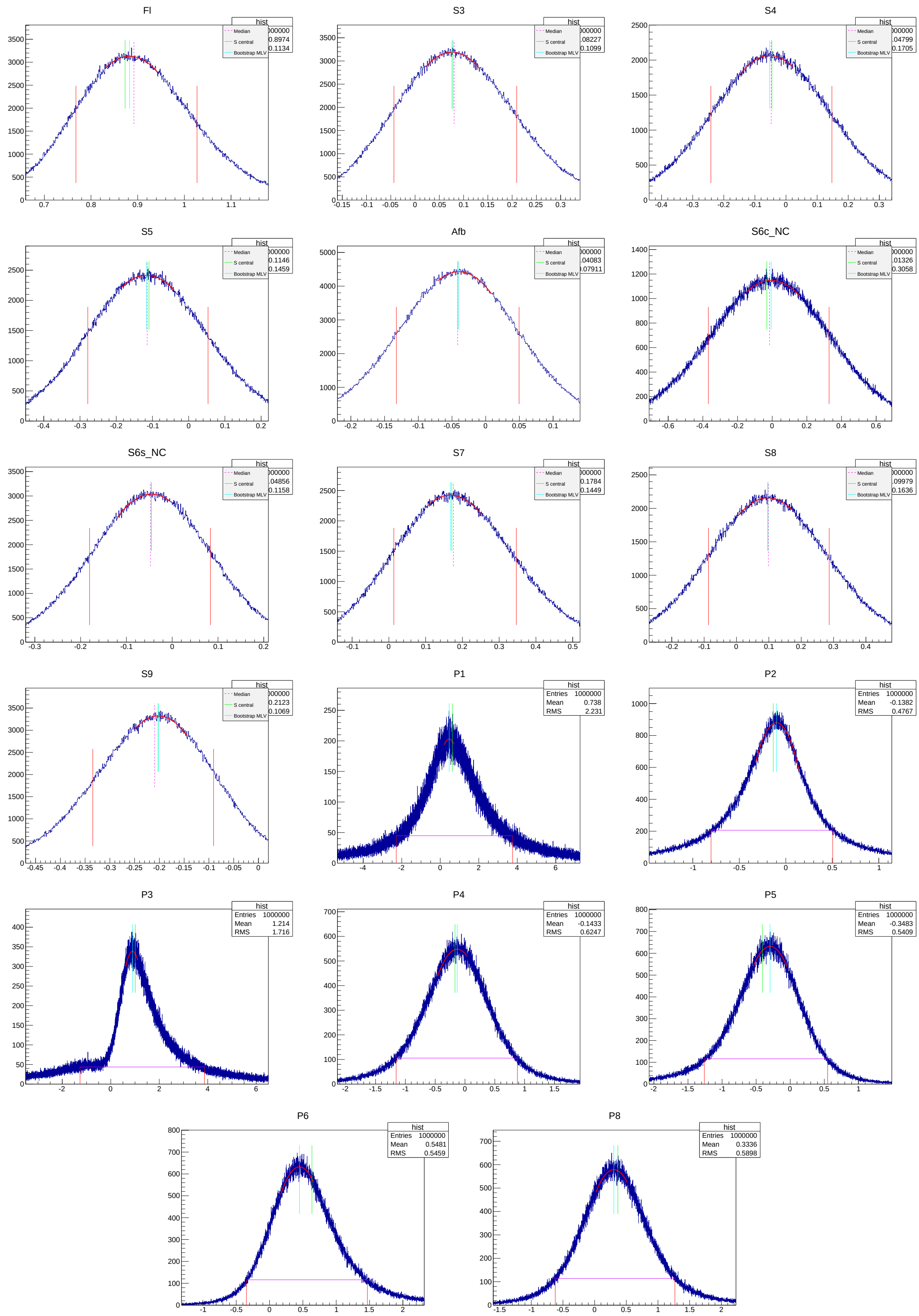

Figure 187: Bootstraps distribution in $4.0 < q^2 < 5.0\,\mathrm{GeV}^2/c^4$ bin

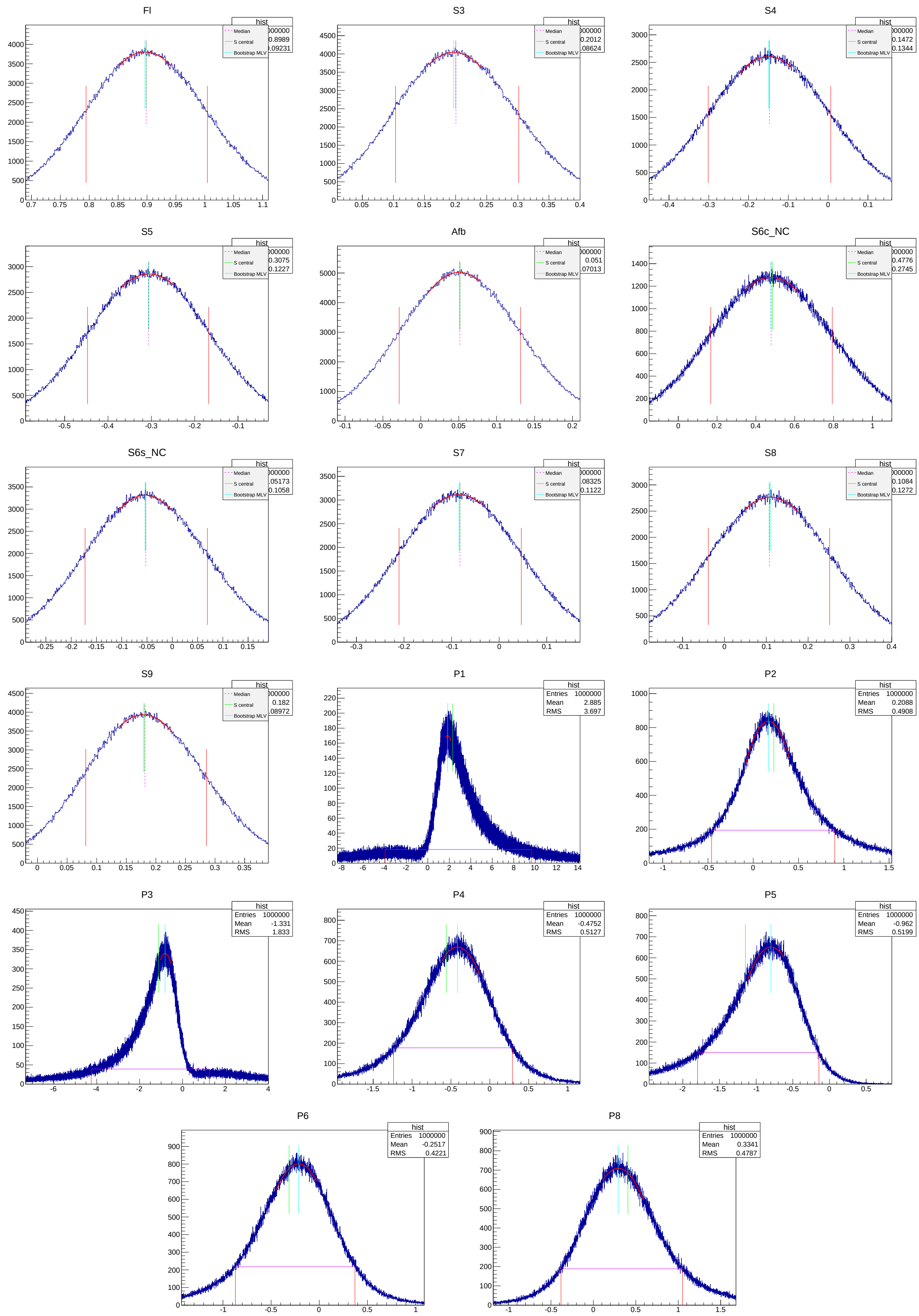

Figure 188: Bootstraps distribution in $5.0 < q^2 < 6.0\,\mathrm{GeV}^2/c^4$ bin

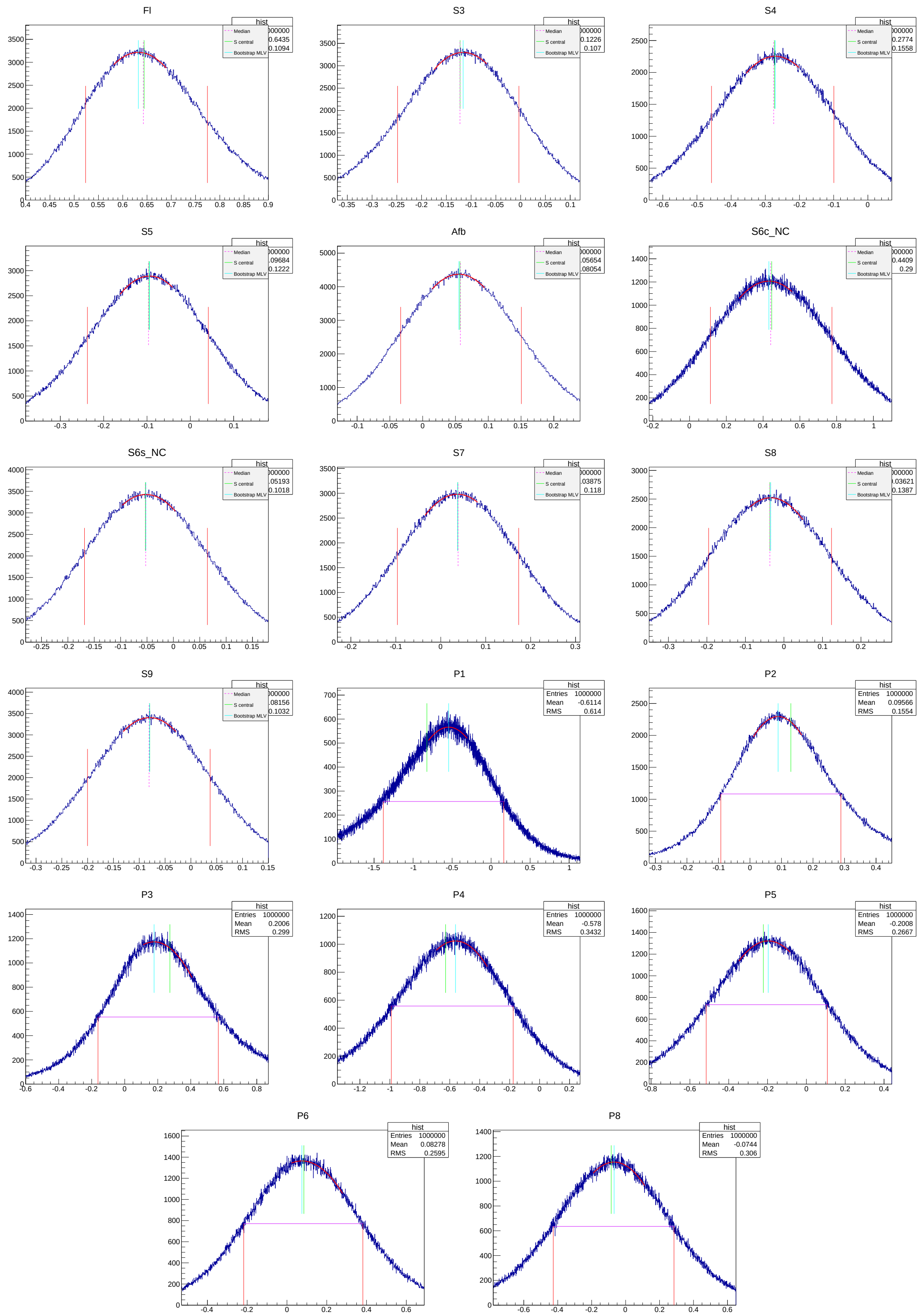

Figure 189: Bootstraps distribution in $6.0 < q^2 < 7.0\,\mathrm{GeV}^2/c^4$ bin

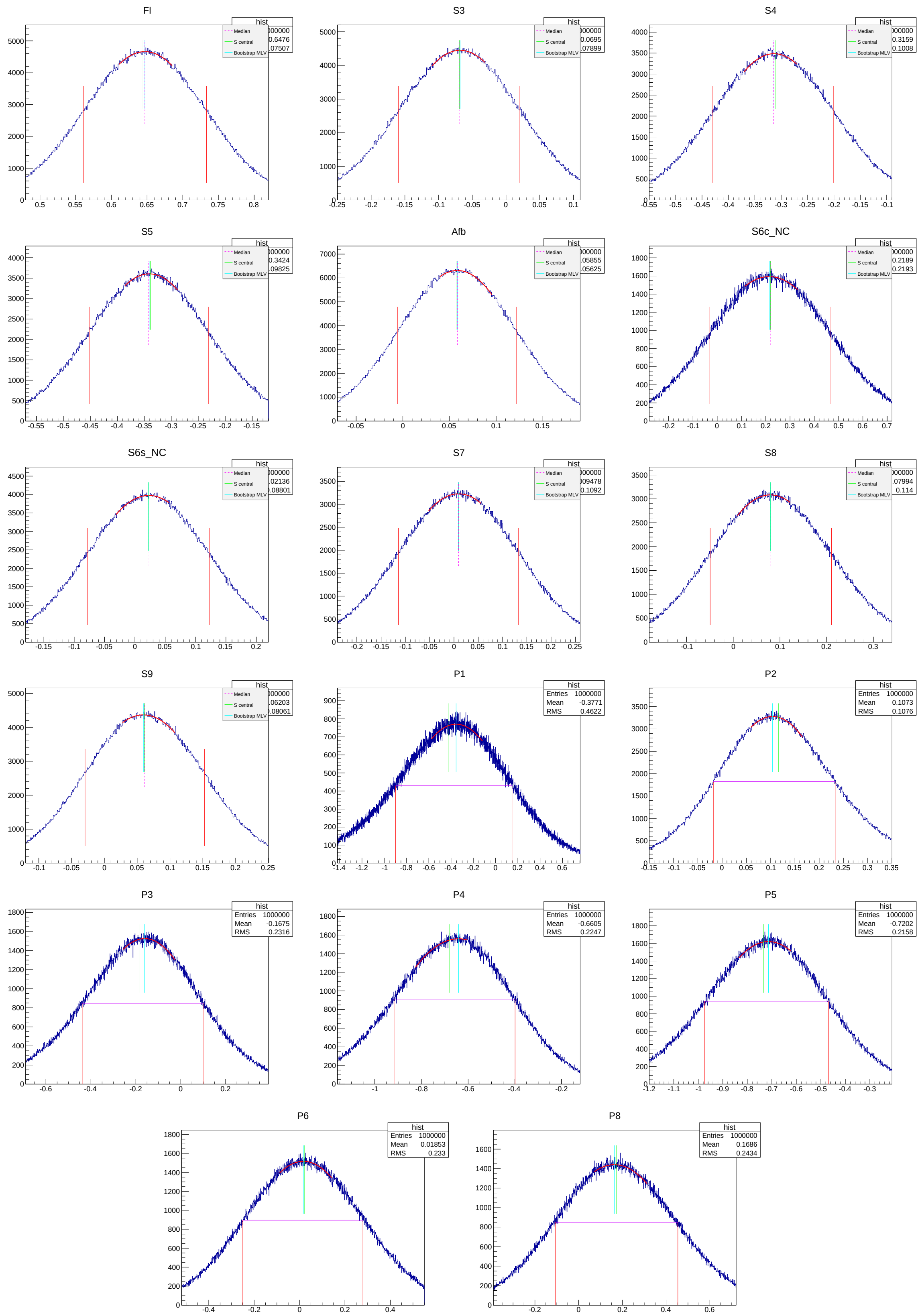

Figure 190: Bootstraps distribution in $7.0 < q^2 < 8.0\,\mathrm{GeV}^2/c^4$ bin

1861

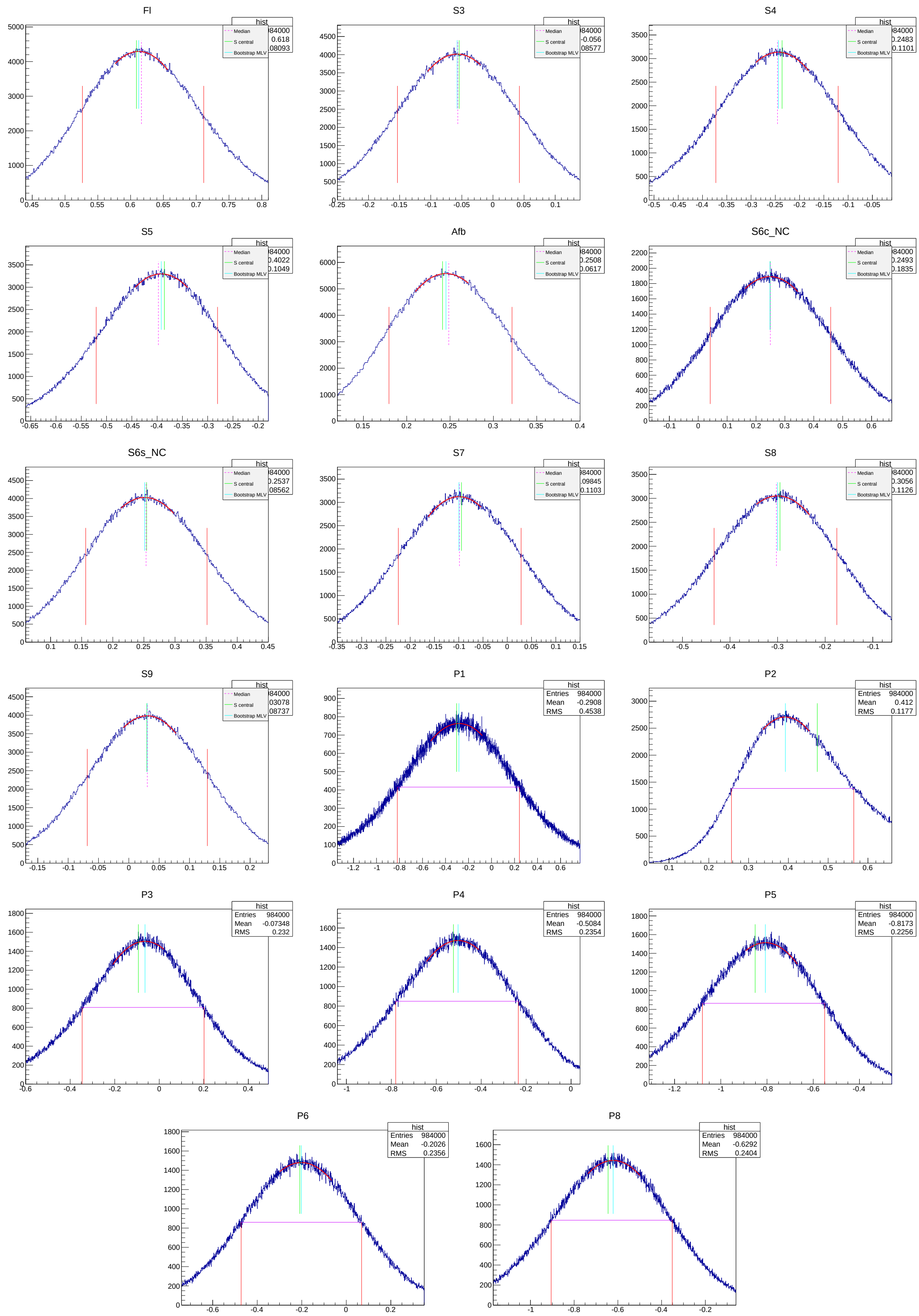

Figure 191: Bootstraps distribution in $11.0 < q^2 < 11.5\,\text{GeV}^2/c^4$ bin

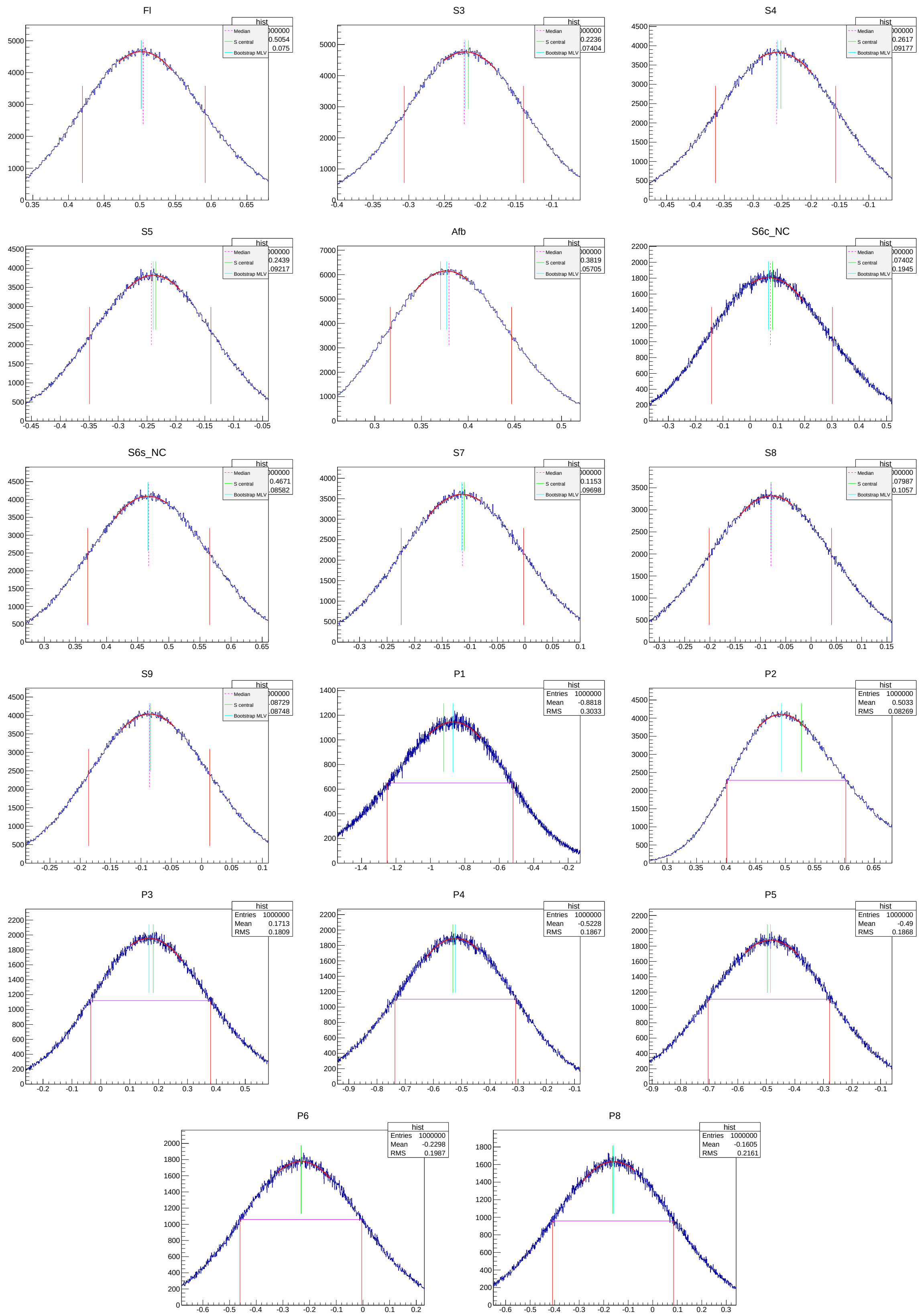

Figure 192: Bootstraps distribution in $11.75 < q^2 < 12.5\,\mathrm{GeV}^2/c^4$ bin

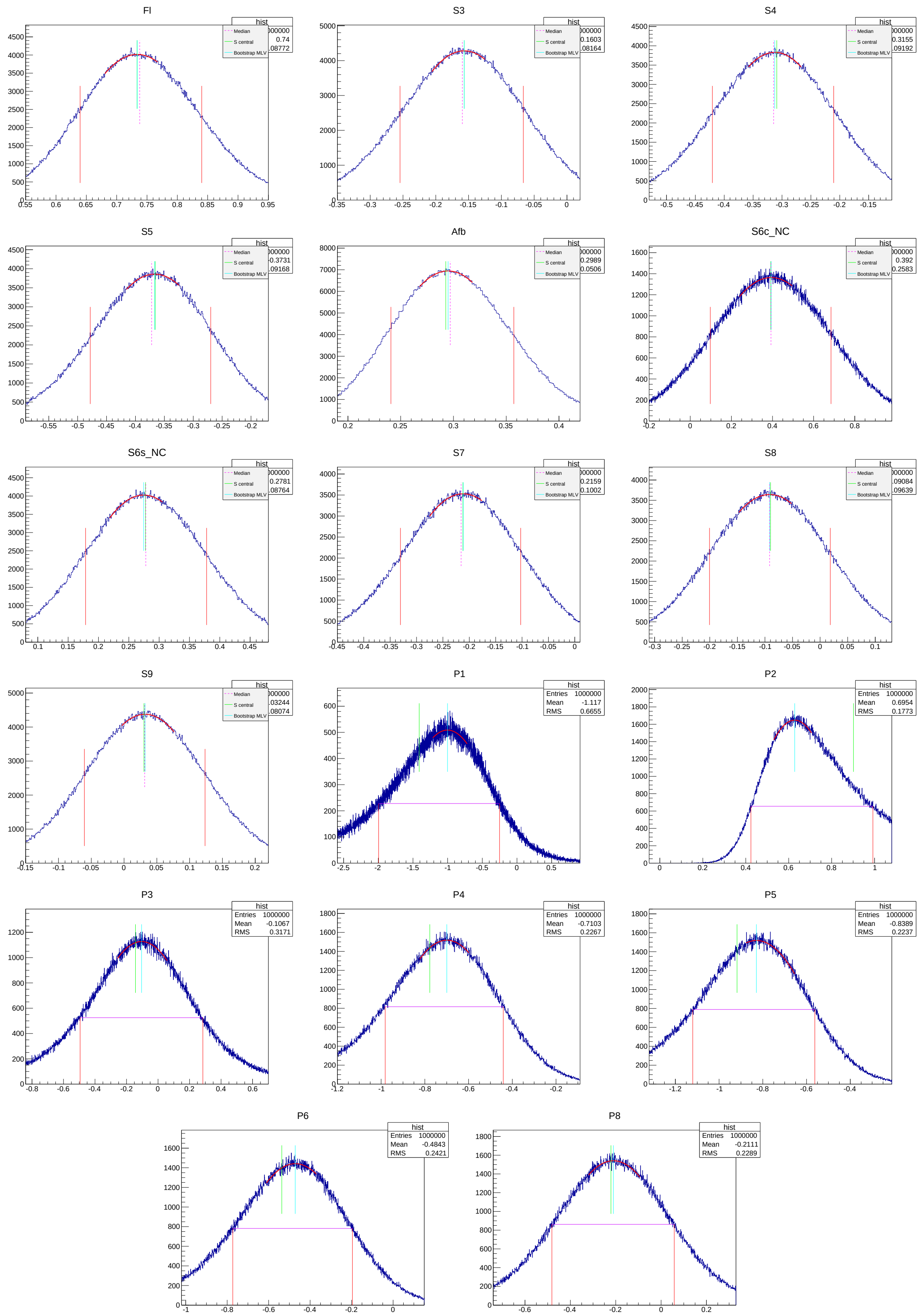

1863

Figure 193: Bootstraps distribution in $15.0 < q^2 < 16.0\,\mathrm{GeV}^2/c^4$ bin

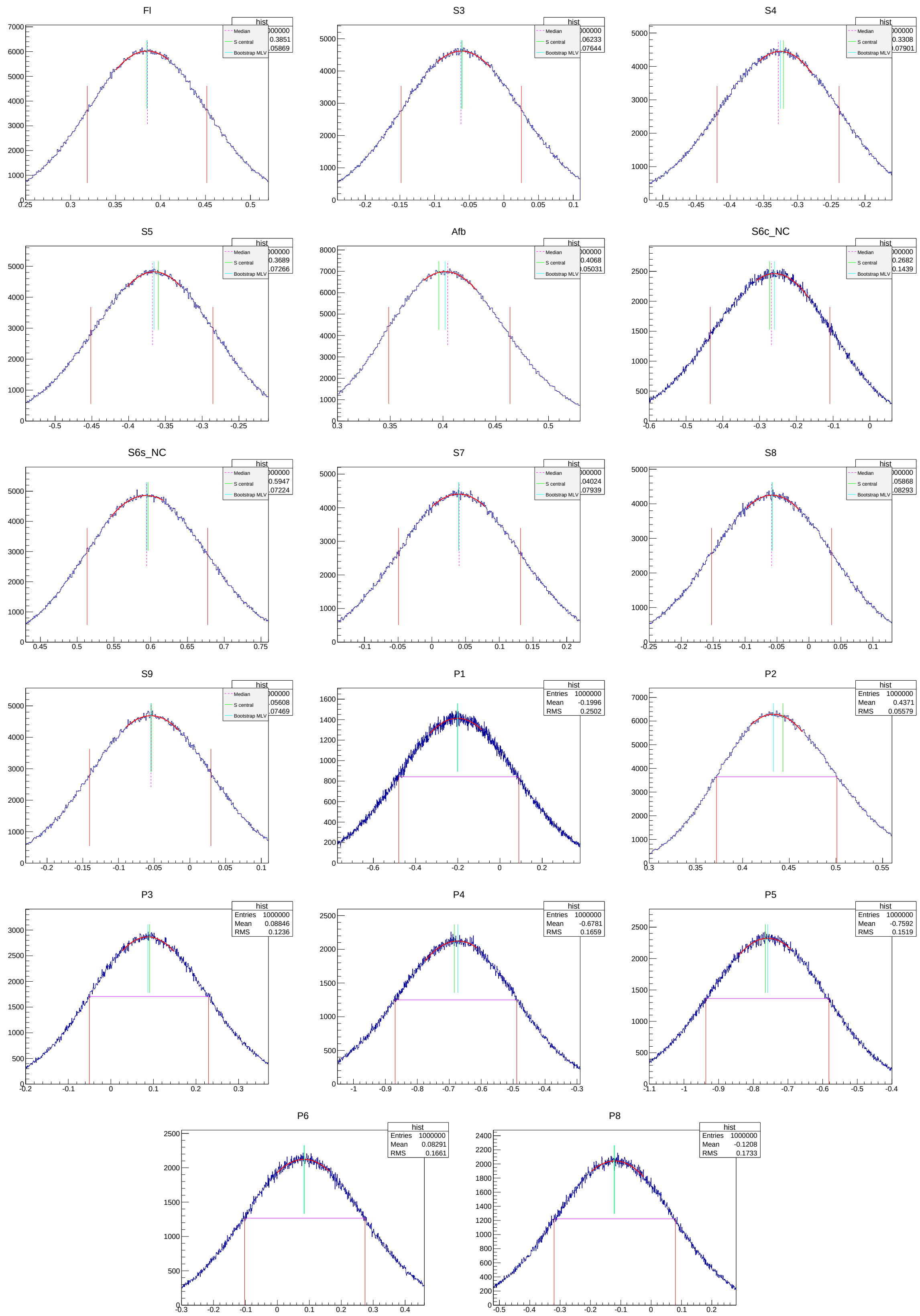

Figure 194: Bootstraps distribution in $16.0 < q^2 < 17.0\,\mathrm{GeV}^2/c^4$ bin

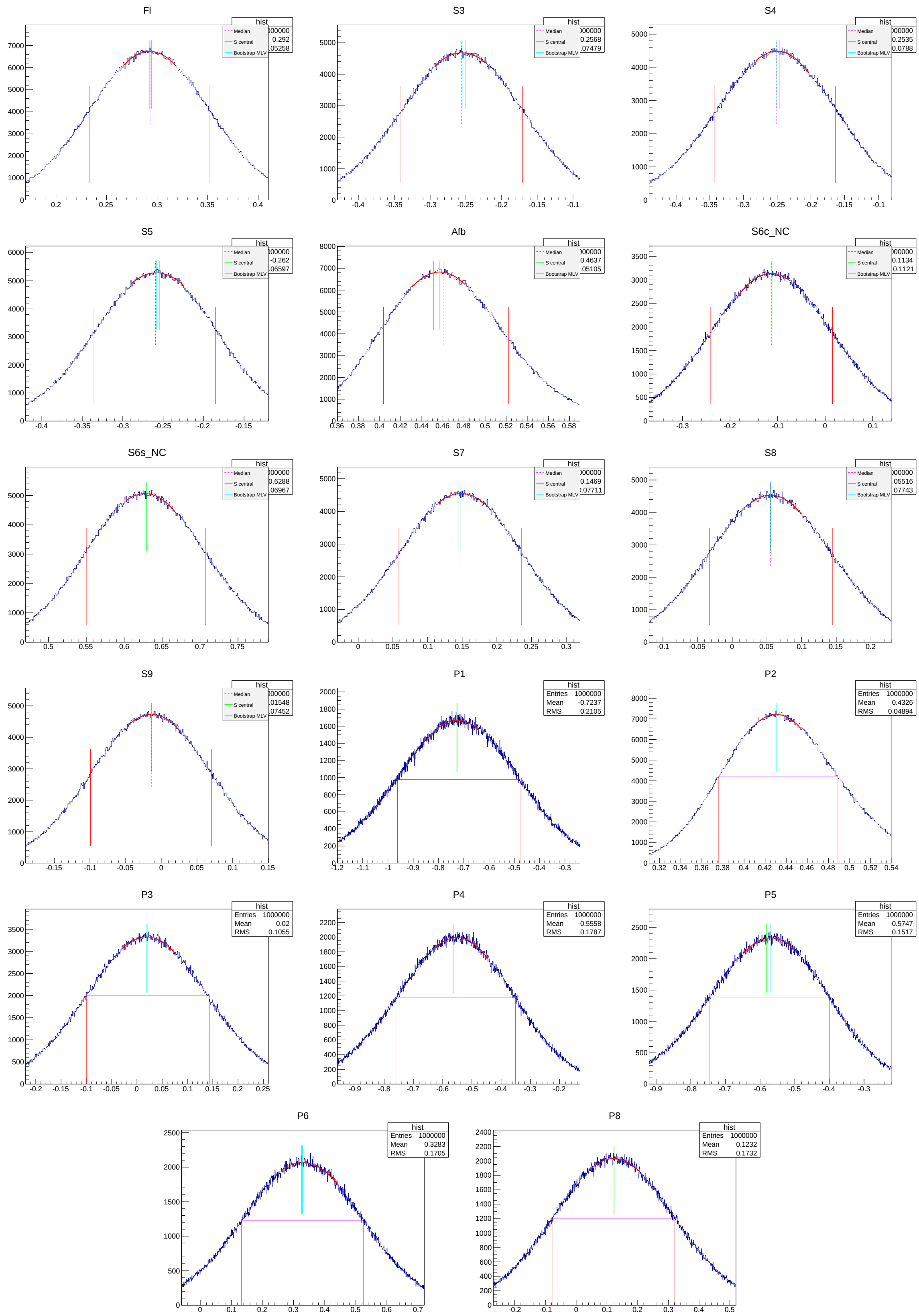

Figure 195: Bootstraps distribution in $17.0 < q^2 < 18.0\,\mathrm{GeV}^2/c^4$ bin

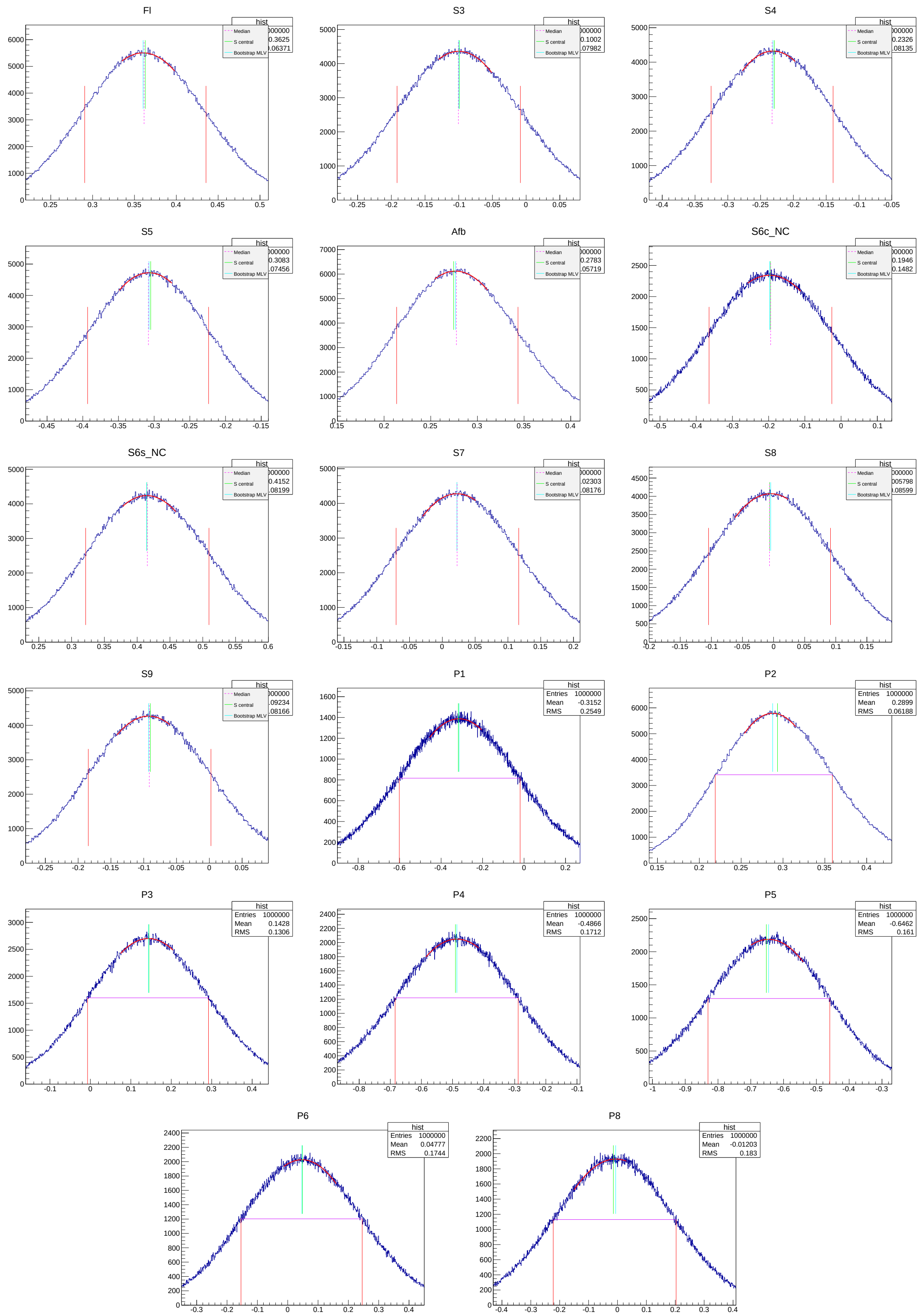

Figure 196: Bootstraps distribution in $18.0 < q^2 < 19.0\,\mathrm{GeV}^2/c^4$ bin

1867

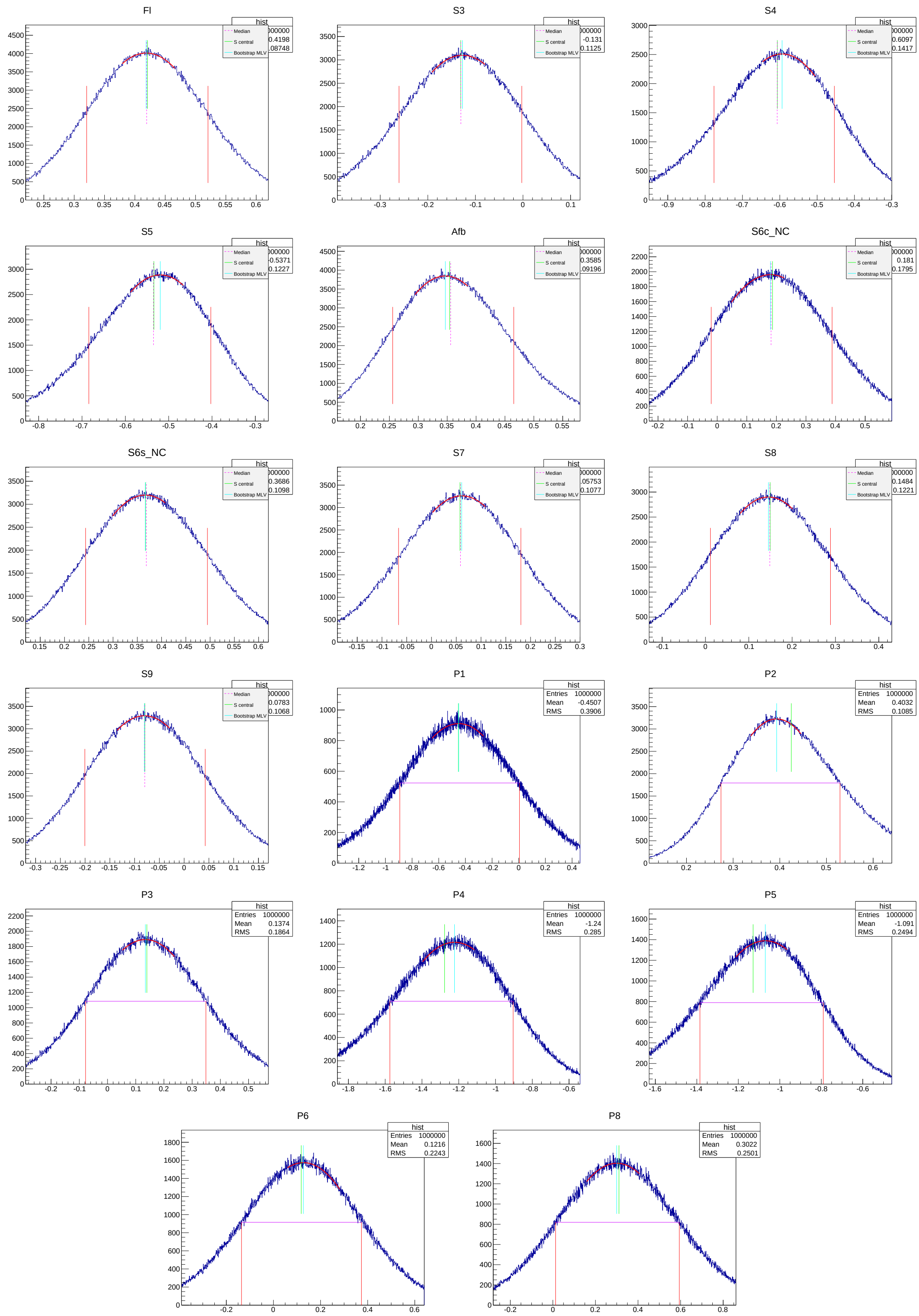

Figure 197: Bootstraps distribution in $1.1 < q^2 < 2.5\,\mathrm{GeV}^2/c^4$ bin

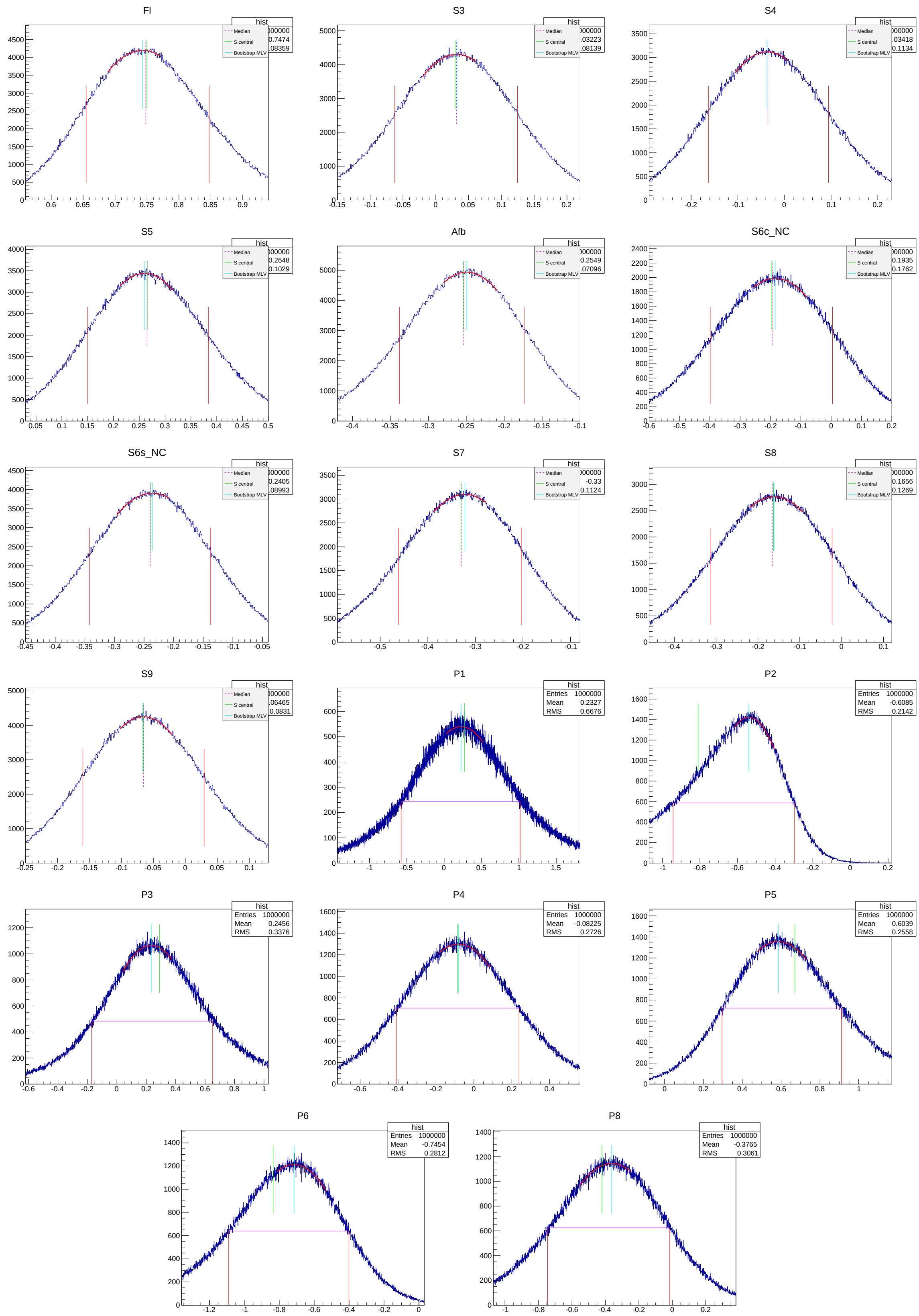

Figure 198: Bootstraps distribution in $2.5 < q^2 < 4.0\,\mathrm{GeV}^2/c^4$ bin

1869

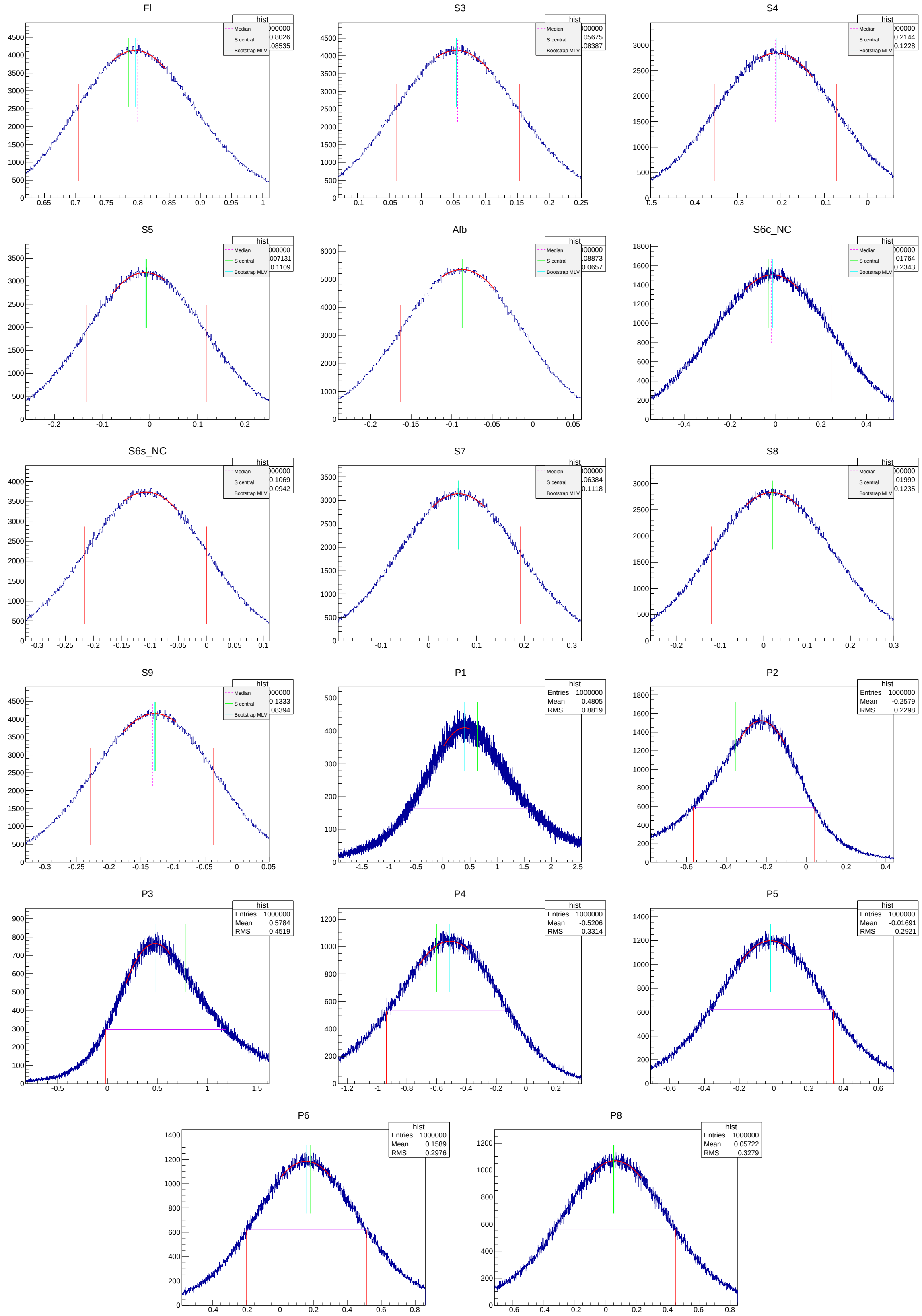

Figure 199: Bootstraps distribution in $4.0 < q^2 < 6.0\,\mathrm{GeV}^2/c^4$ bin

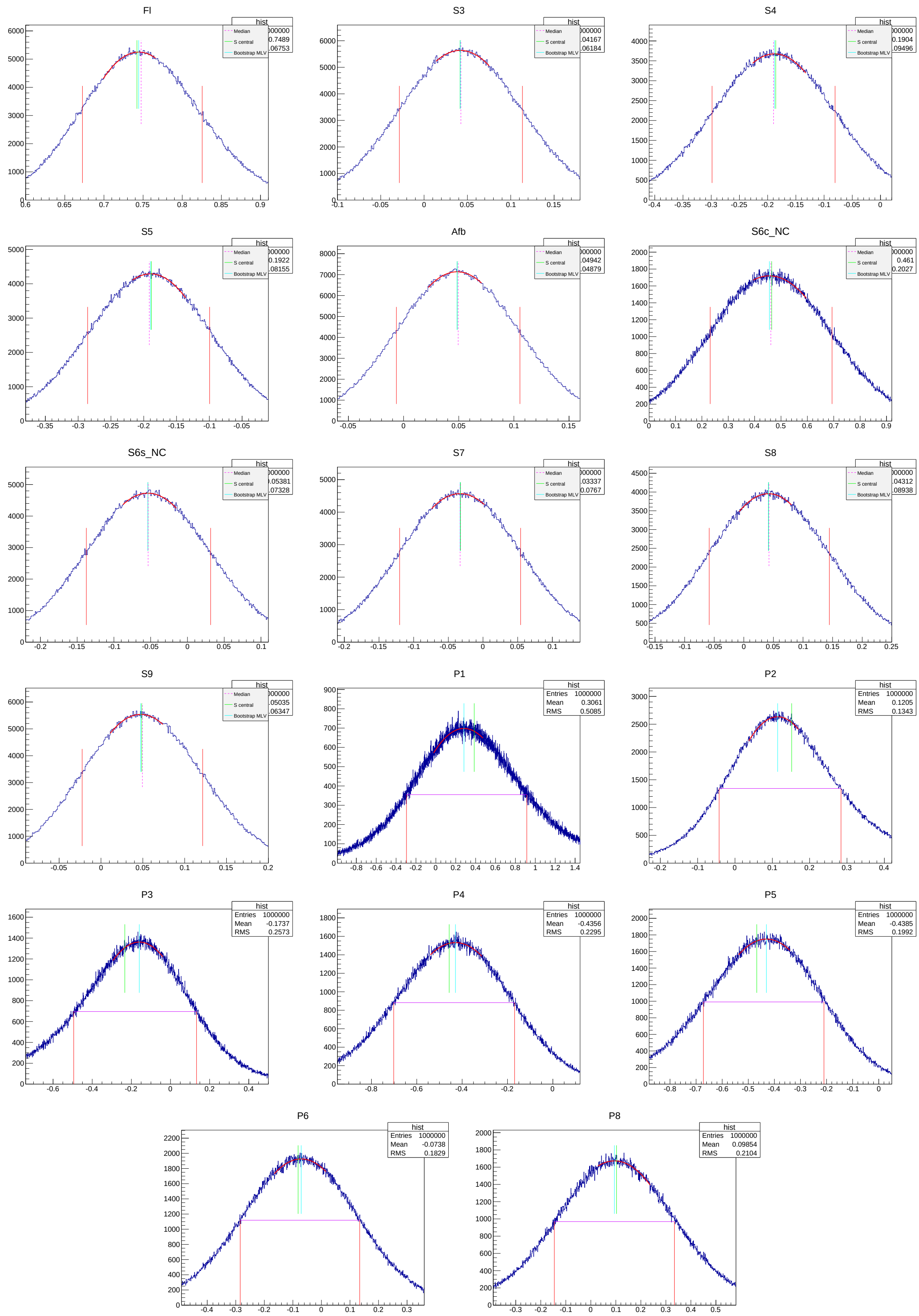

Figure 200: Bootstraps distribution in $6.0 < q^2 < 8.0\,\mathrm{GeV}^2/c^4$ bin

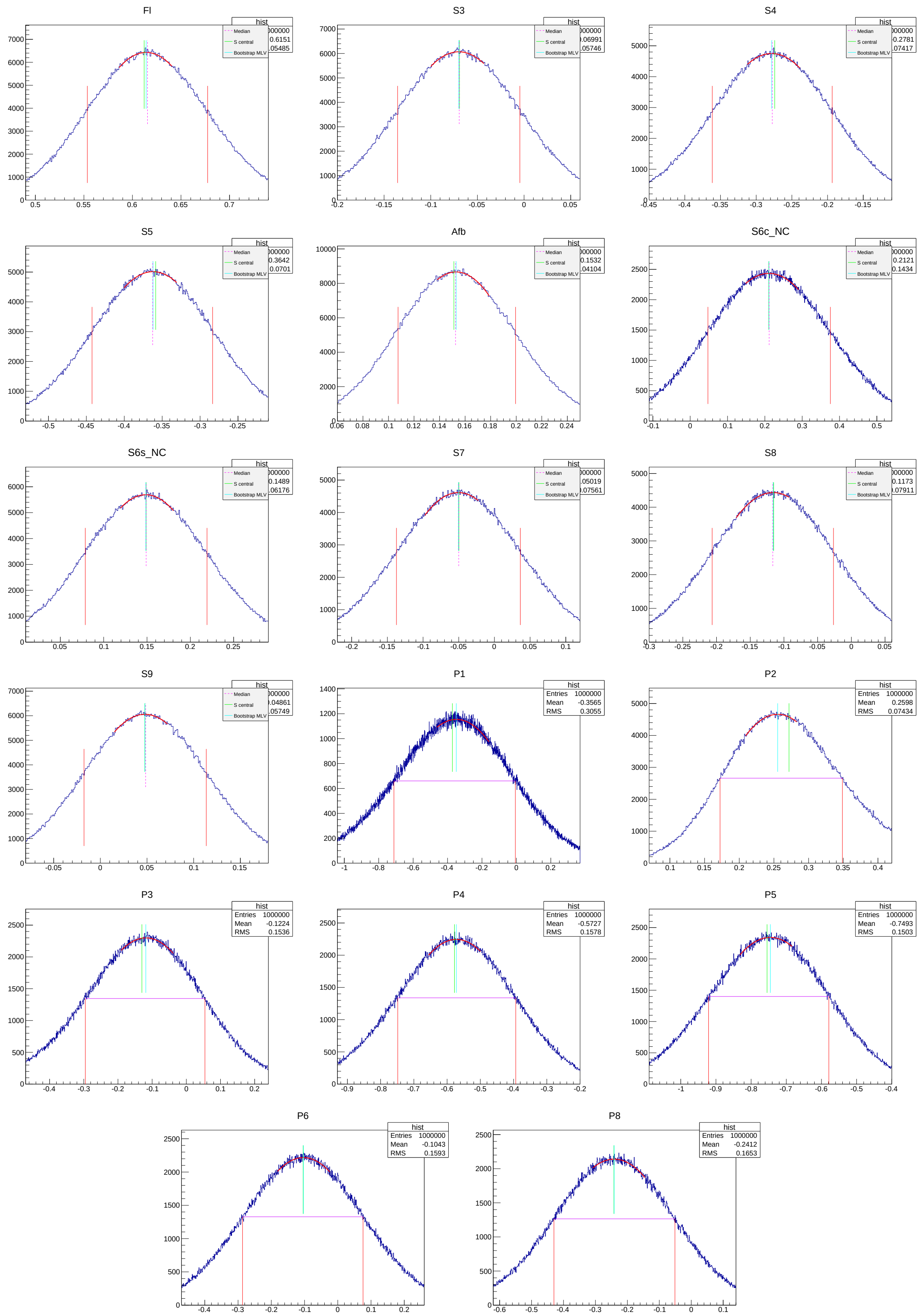

Figure 201: Bootstraps distribution in $11.0 < q^2 < 12.5\,\mathrm{GeV}^2/c^4$ bin

1872

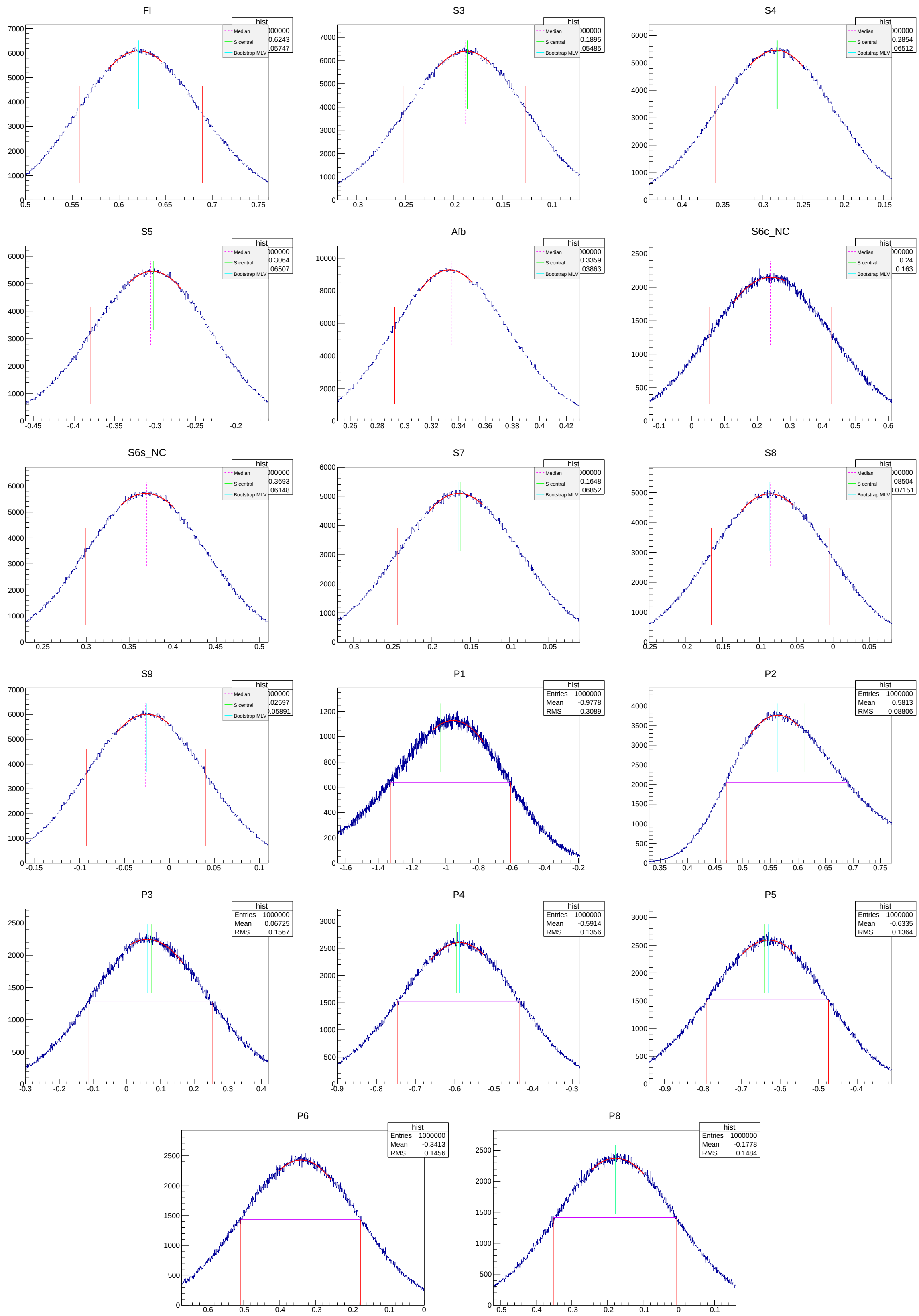

Figure 202: Bootstraps distribution in $15.0 < q^2 < 17.0\,\mathrm{GeV}^2/c^4$ bin

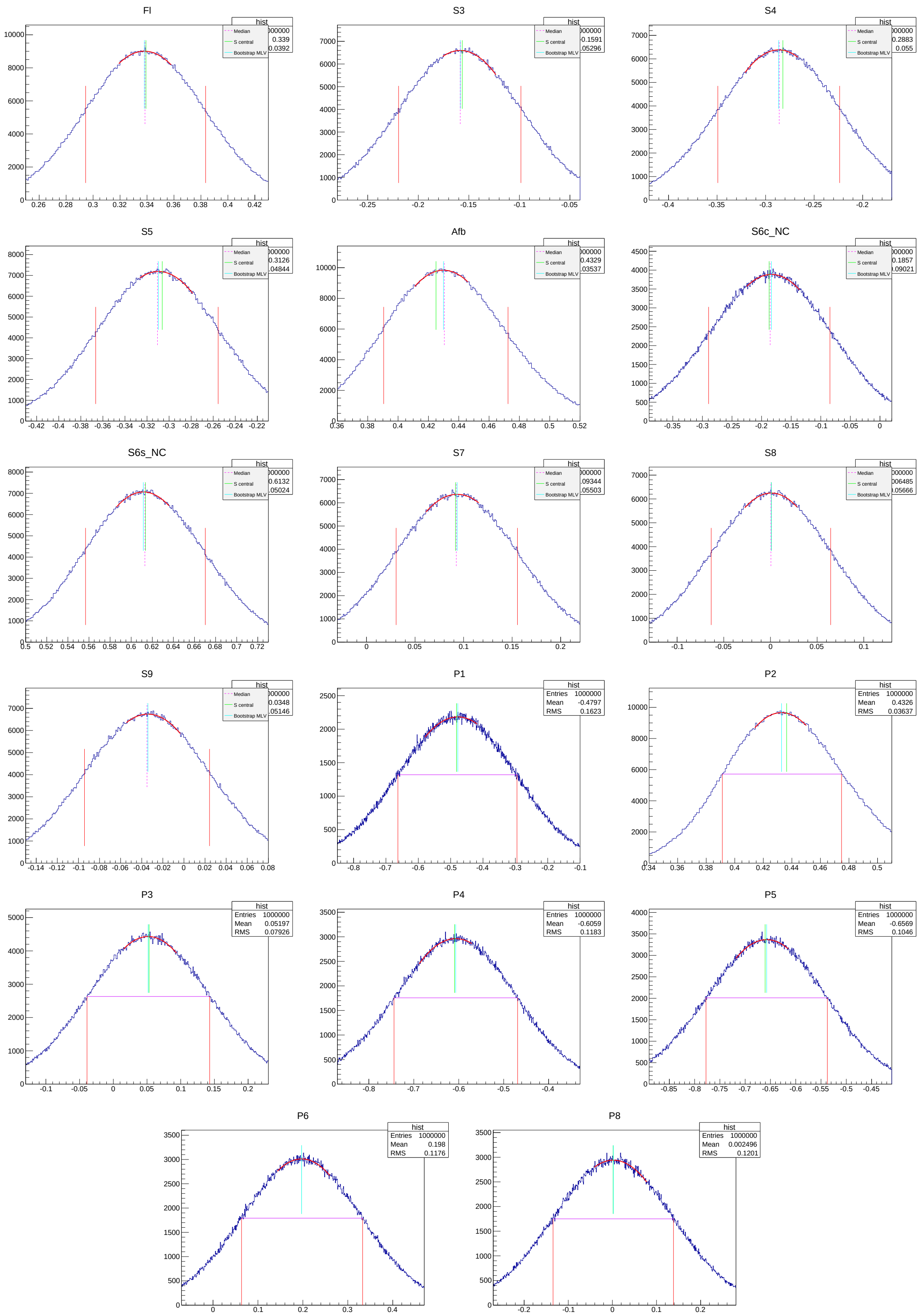

Figure 203: Bootstraps distribution in $17.0 < q^2 < 19.0\,\mathrm{GeV}^2/c^4$ bin

1874

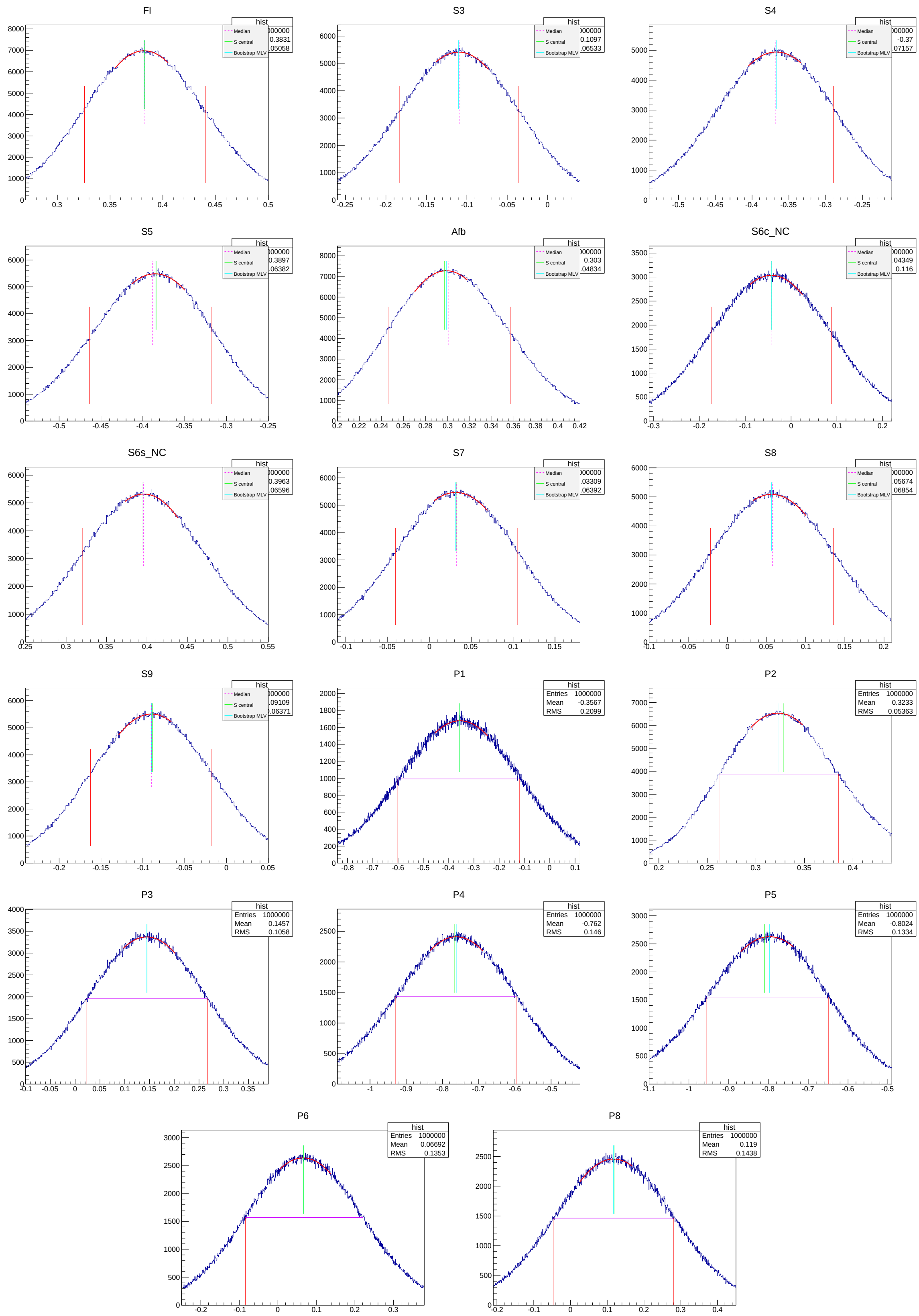

Figure 204: Bootstraps distribution in $0.1 < q^2 < 0.98\,\mathrm{GeV}^2/c^4$ bin

1875

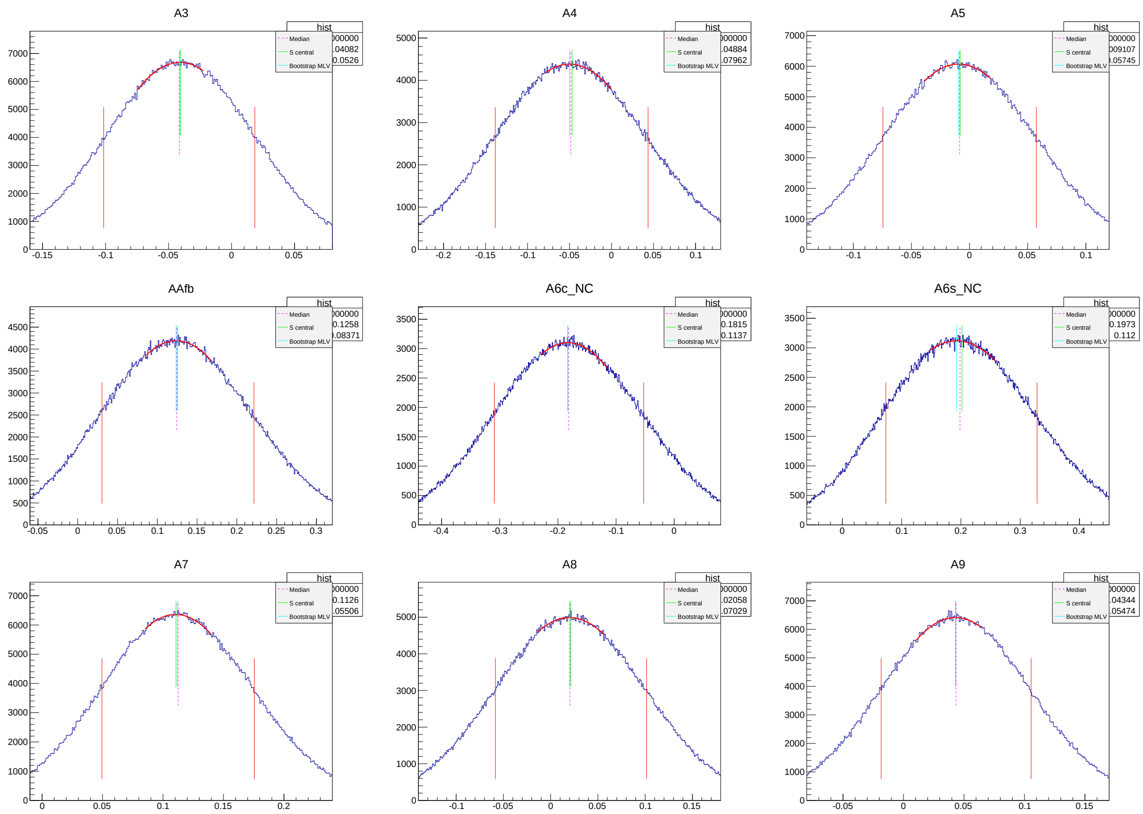

Figure 205: Bootstraps distribution in $1.1 < q^2 < 2.0\,\mathrm{GeV}^2/c^4$ bin

1876

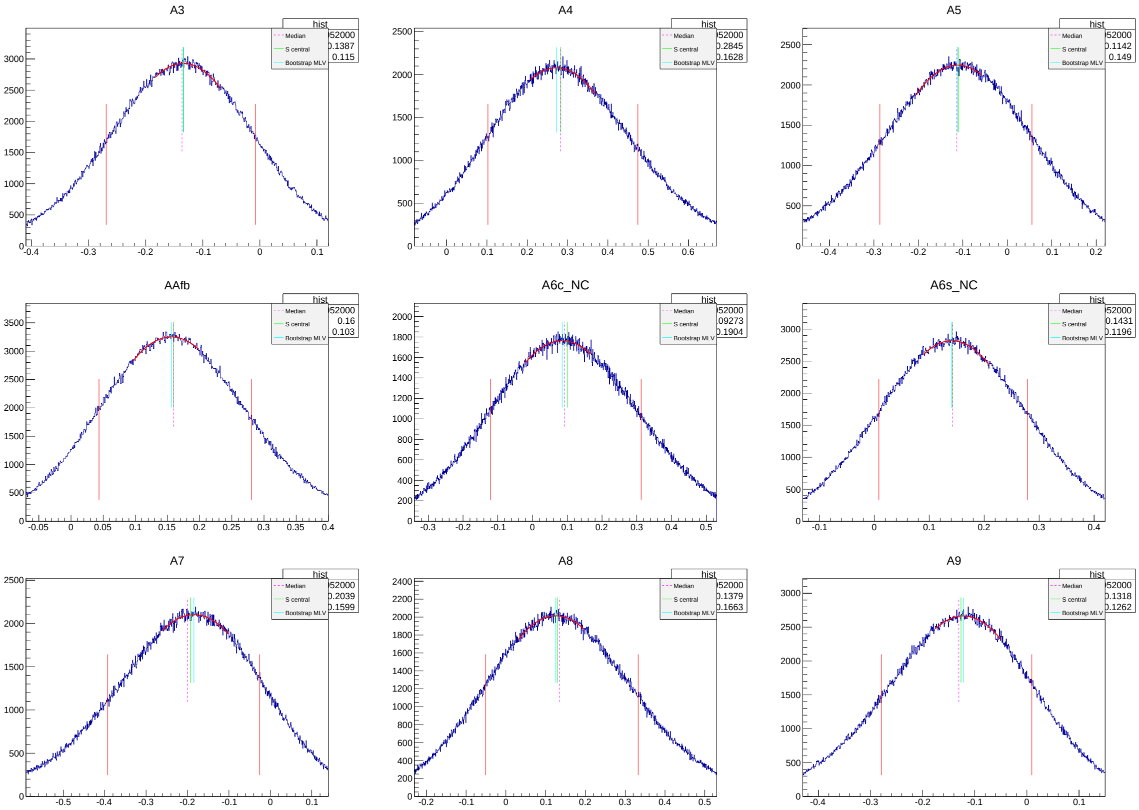

Figure 206: Bootstraps distribution in $2.0 < q^2 < 3.0\,\text{GeV}^2/c^4$ bin

1877

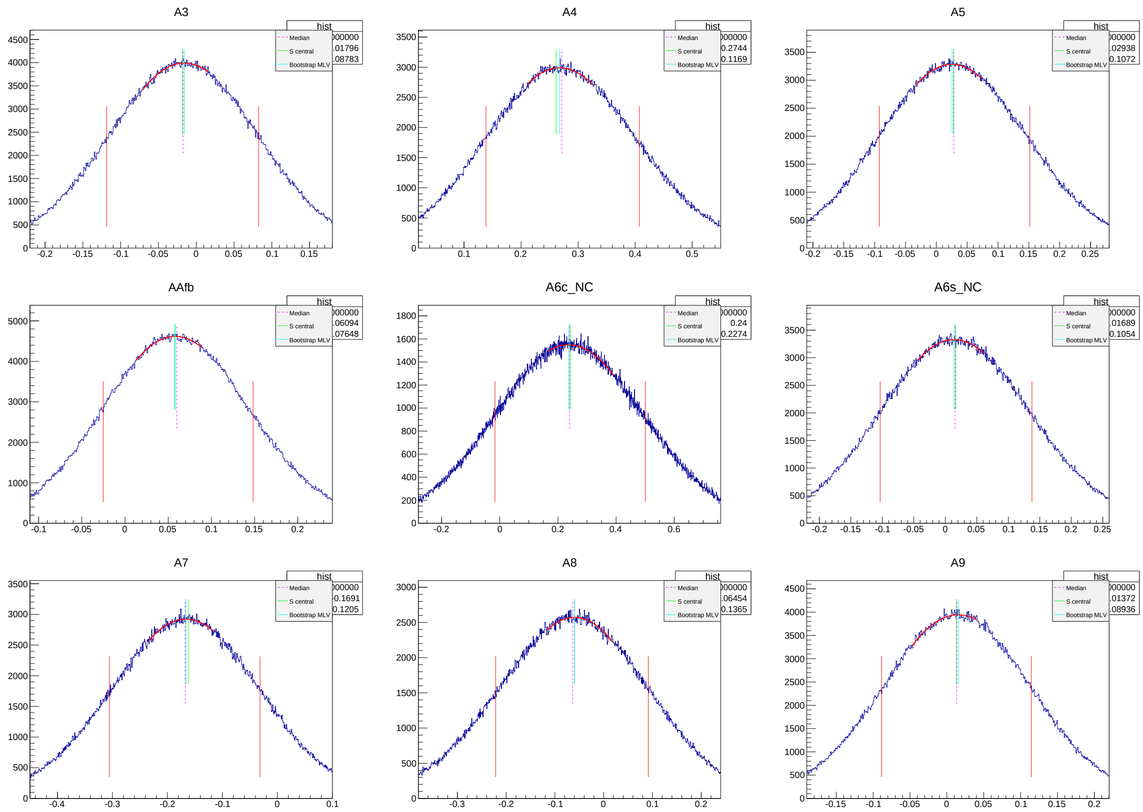

Figure 207: Bootstraps distribution in $3.0 < q^2 < 4.0\,\mathrm{GeV}^2/c^4$ bin

1878

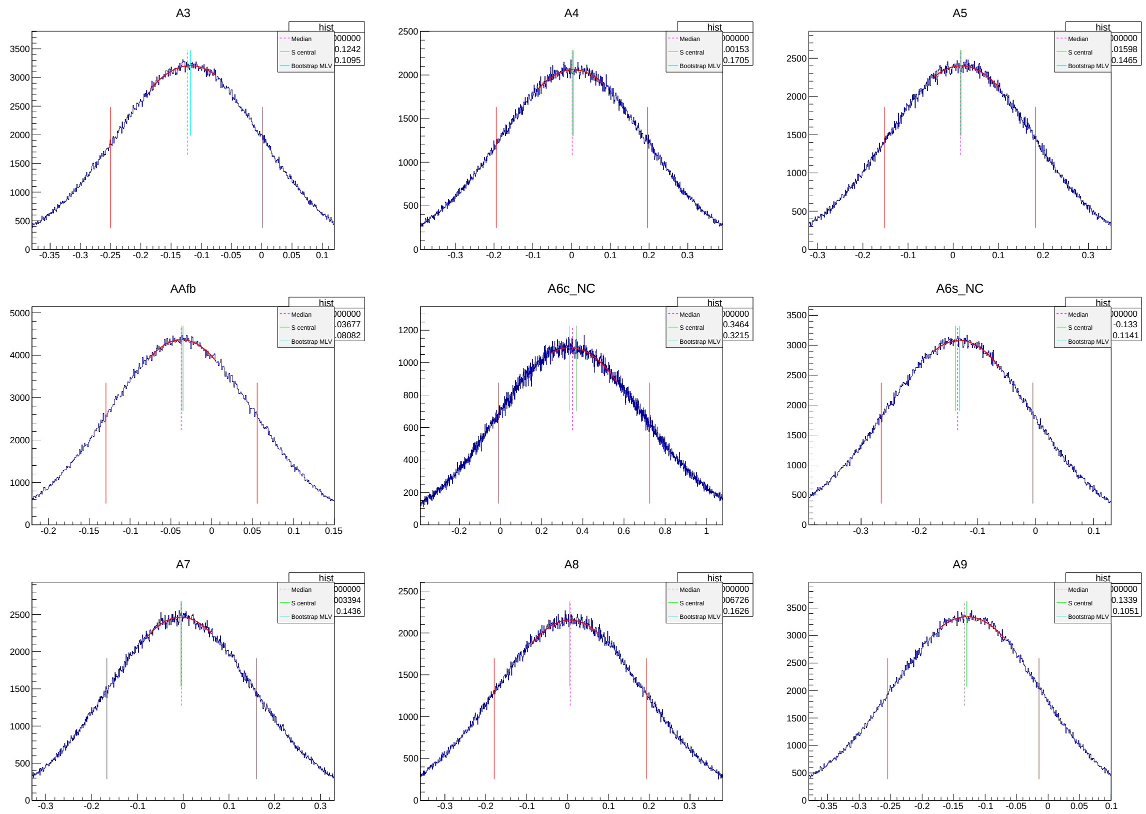

Figure 208: Bootstraps distribution in $4.0 < q^2 < 5.0\,\mathrm{GeV}^2/c^4$ bin

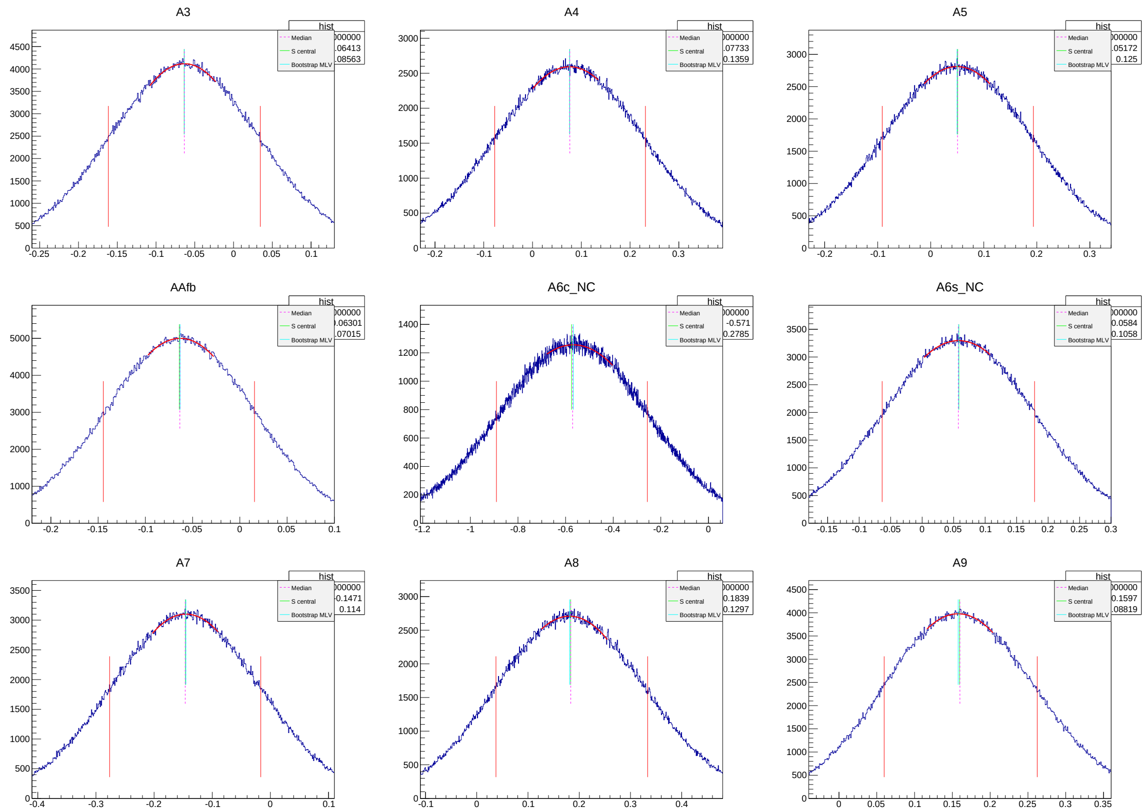

Figure 209: Bootstraps distribution in $5.0 < q^2 < 6.0\,\mathrm{GeV}^2/c^4$ bin

1880

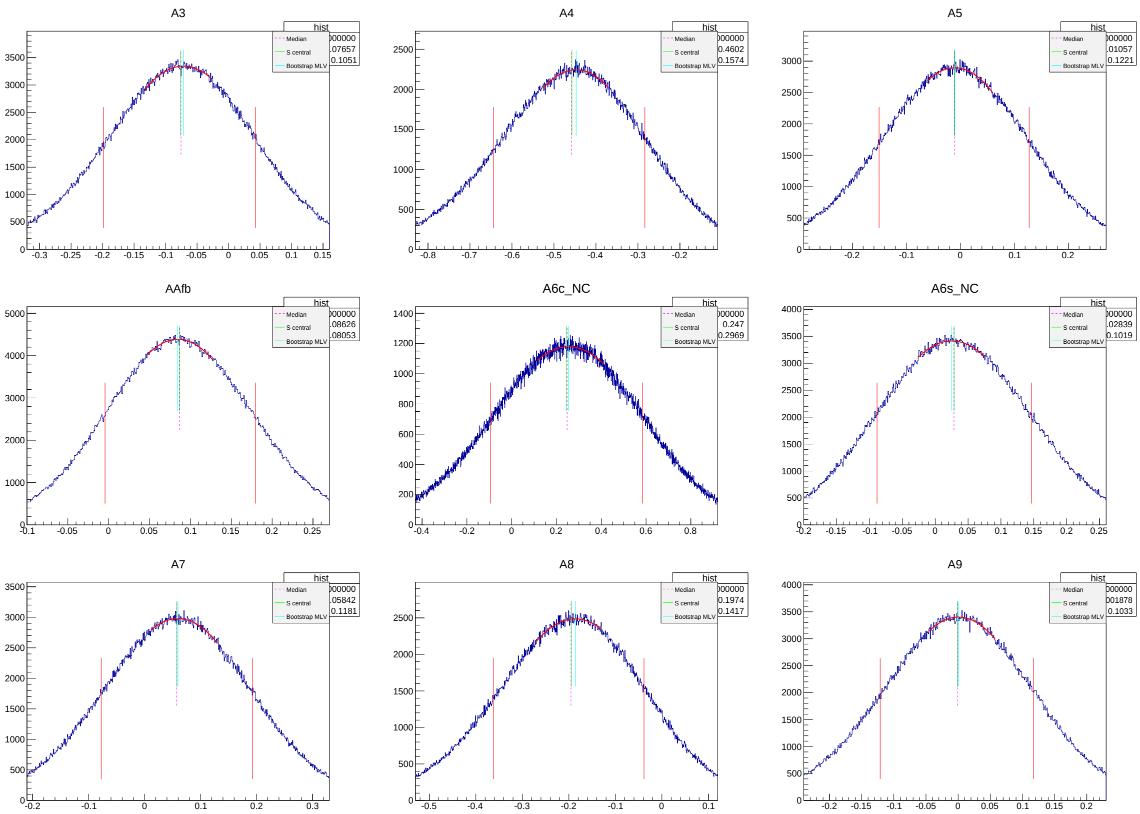

Figure 210: Bootstraps distribution in $6.0 < q^2 < 7.0\,\mathrm{GeV}^2/c^4$ bin

1881

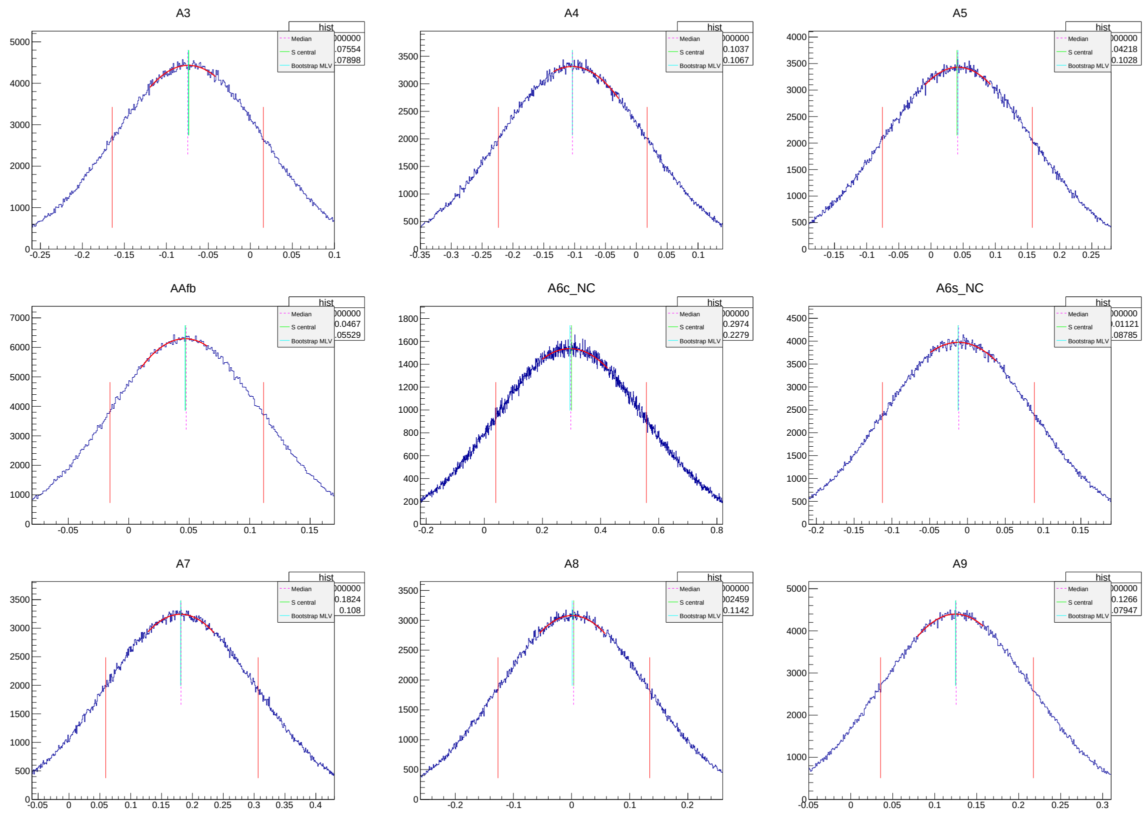

Figure 211: Bootstraps distribution in $7.0 < q^2 < 8.0\,\mathrm{GeV}^2/c^4$ bin

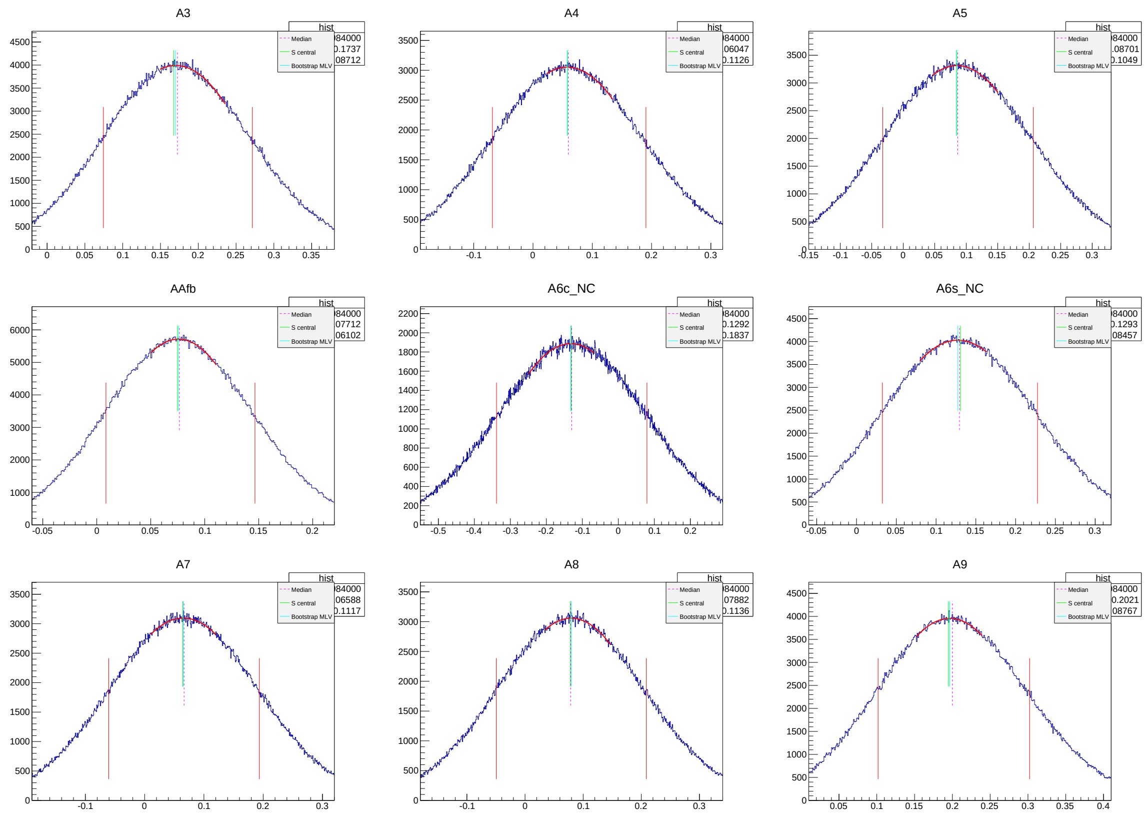

Figure 212: Bootstraps distribution in $11.0 < q^2 < 11.75\,\mathrm{GeV}^2/c^4$ bin

1883 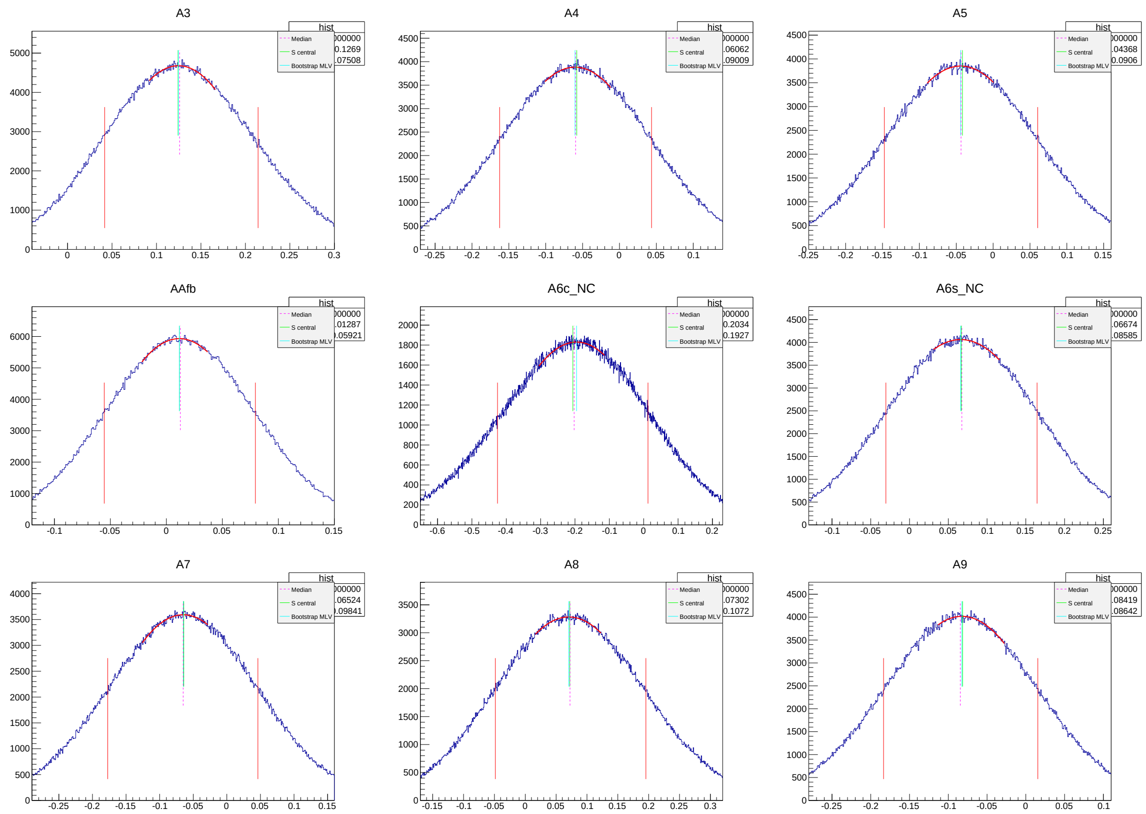

Figure 213: Bootstraps distribution in $11.75 < q^2 < 12\,\mathrm{GeV}^2/c^4$ bin

1884

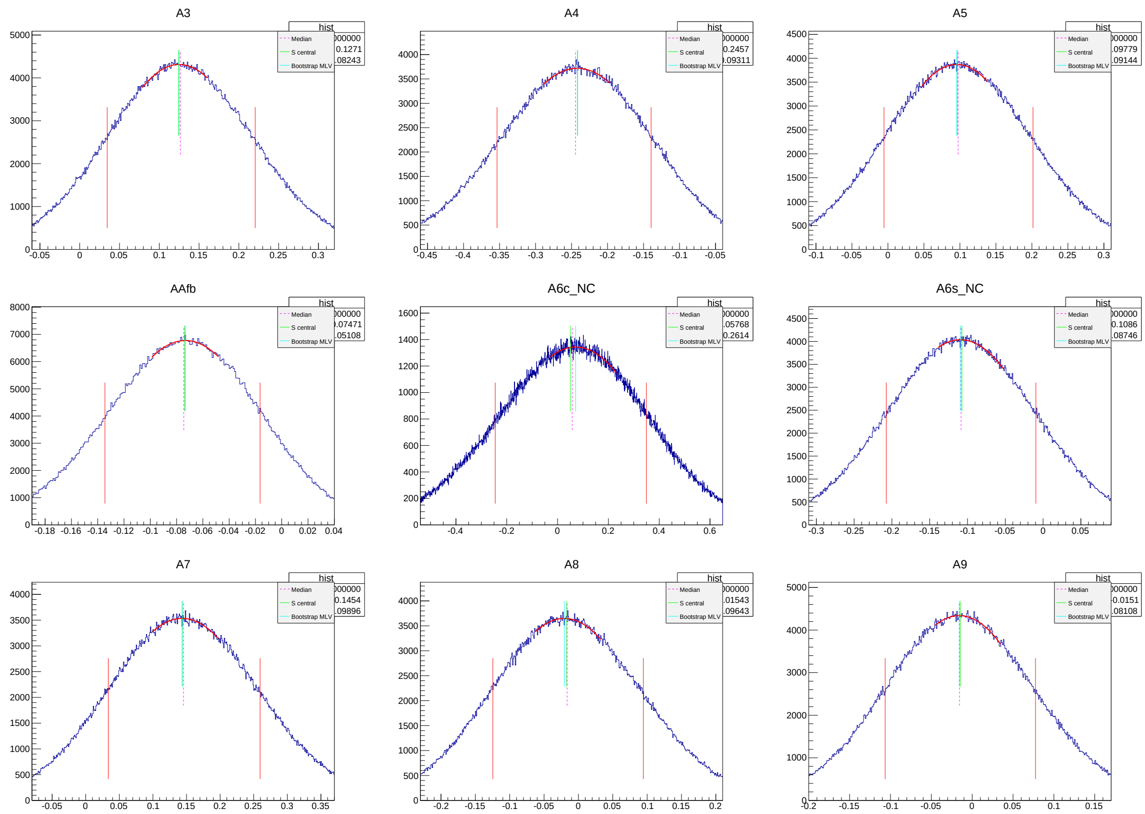

Figure 214: Bootstraps distribution in $15.0 < q^2 < 16.0\,\mathrm{GeV}^2/c^4$ bin

1885

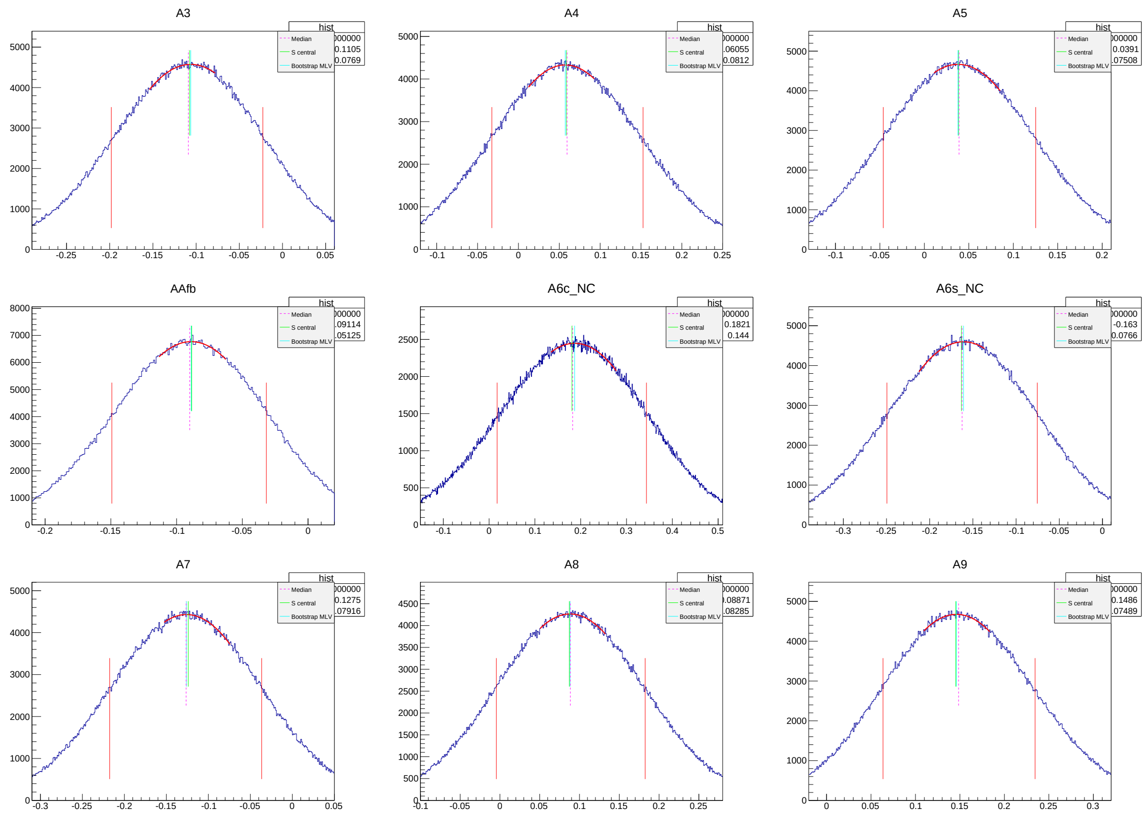

Figure 215: Bootstraps distribution in $16.0 < q^2 < 17.0\,\mathrm{GeV}^2/c^4$ bin

1886

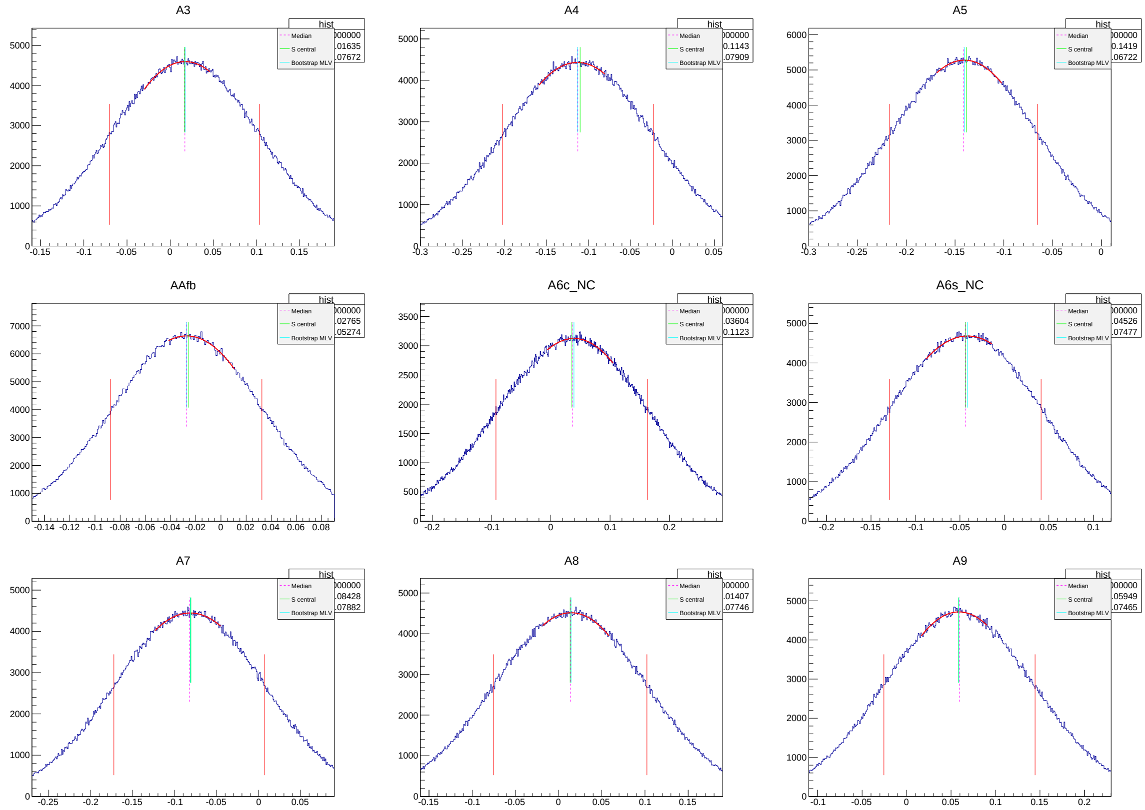

Figure 216: Bootstraps distribution in $17.0 < q^2 < 18.0\,\mathrm{GeV}^2/c^4$ bin

1887

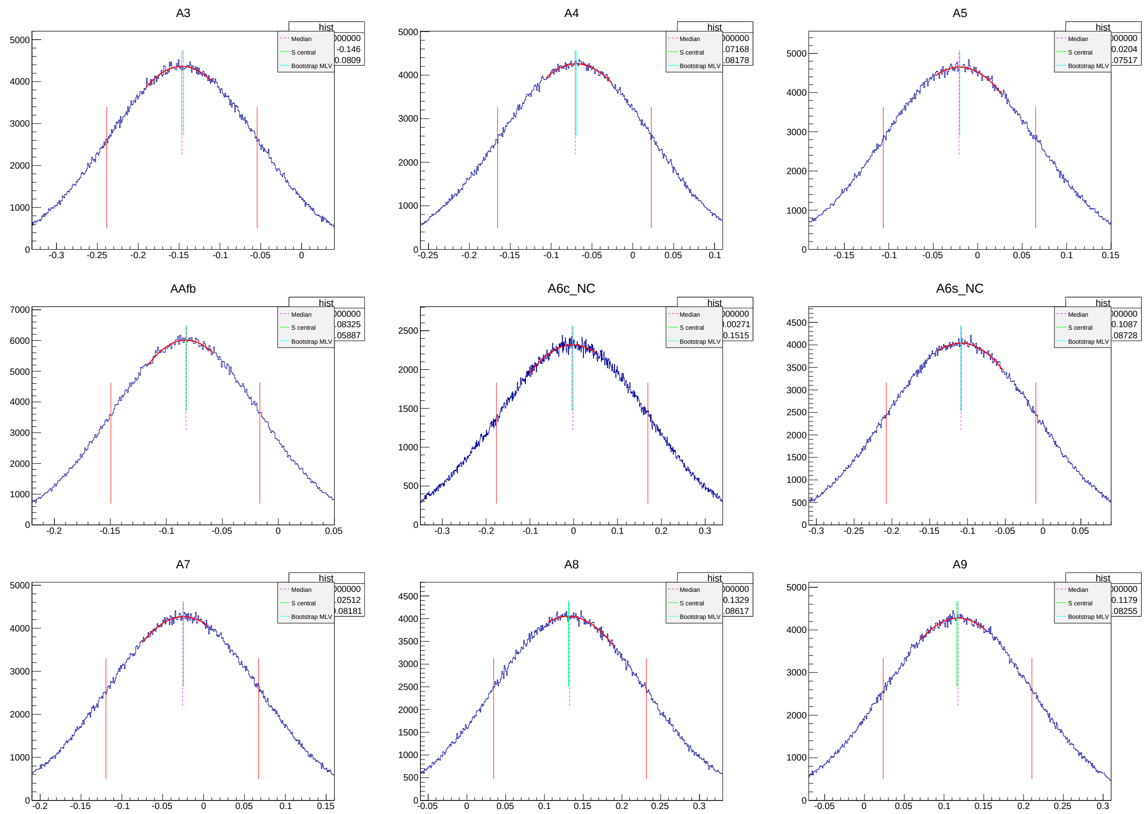

Figure 217: Bootstraps distribution in $18.0 < q^2 < 19.0\,\mathrm{GeV}^2/c^4$ bin

1888

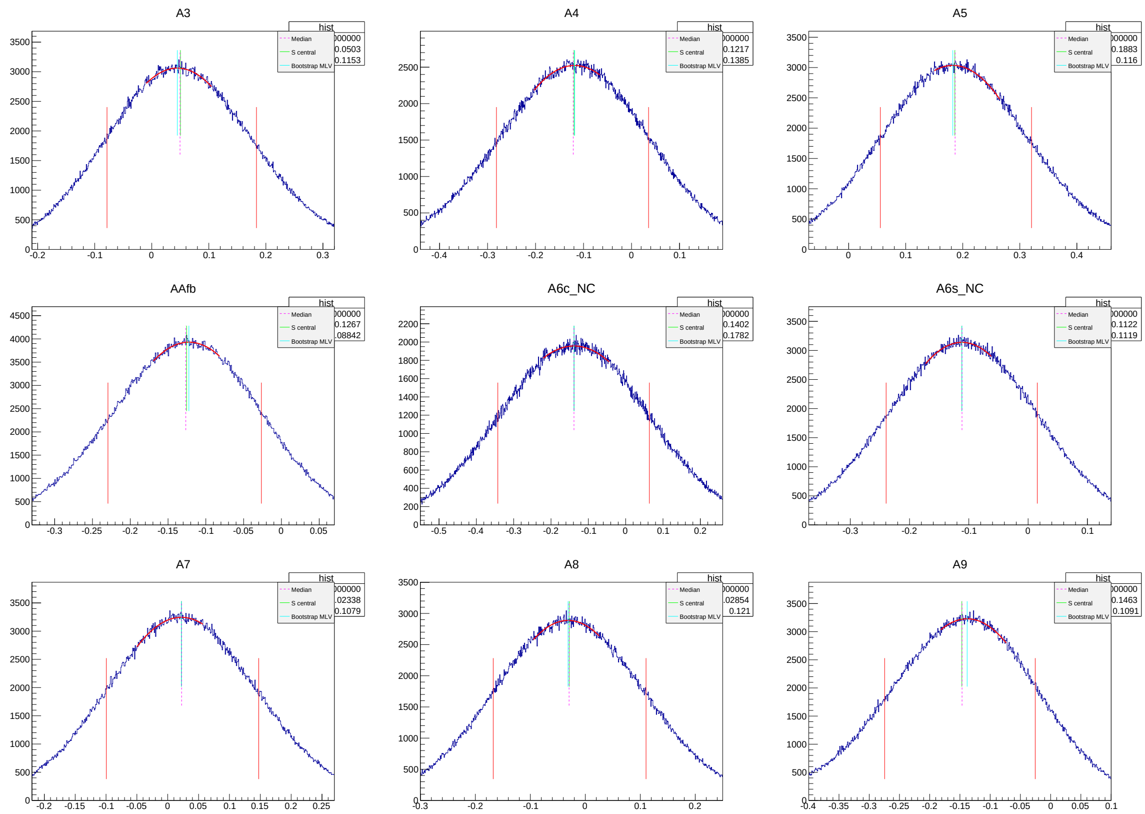

Figure 218: Bootstraps distribution in $1.1 < q^2 < 2.5\,\mathrm{GeV}^2/c^4$ bin

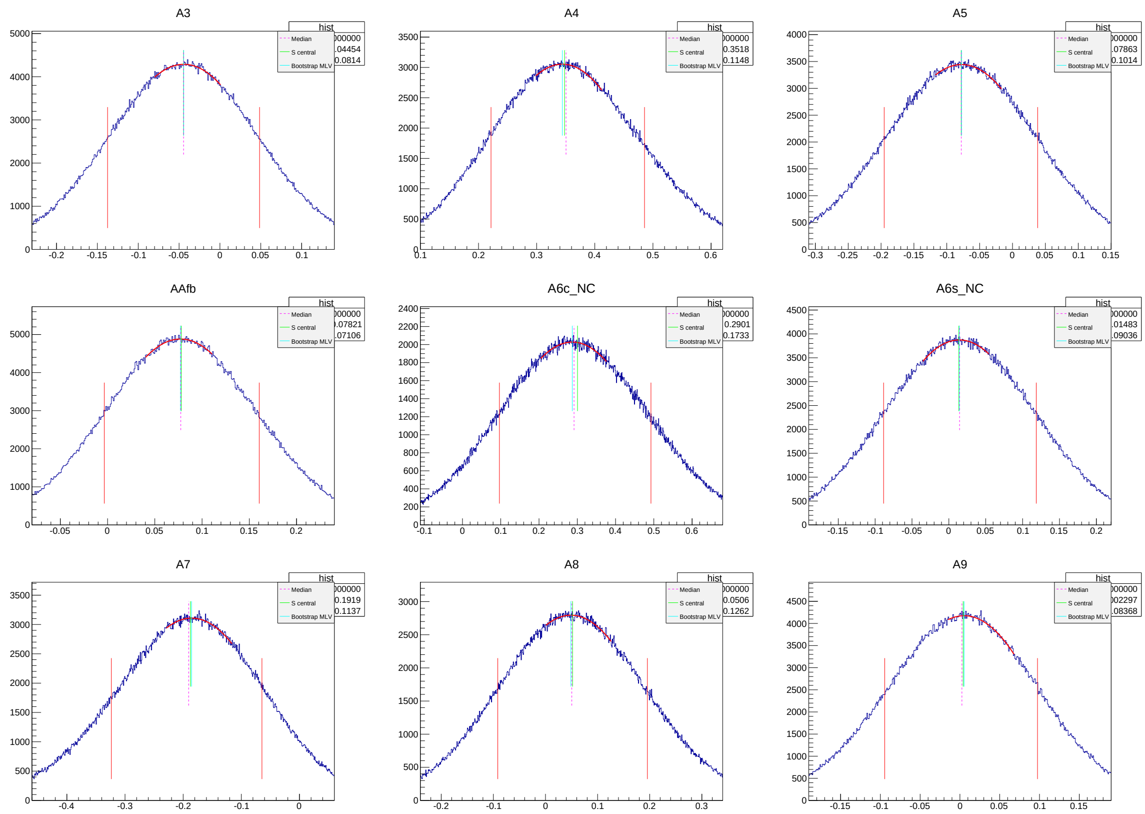

Figure 219: Bootstraps distribution in $2.5 < q^2 < 4.0\,\mathrm{GeV}^2/c^4$ bin

1890

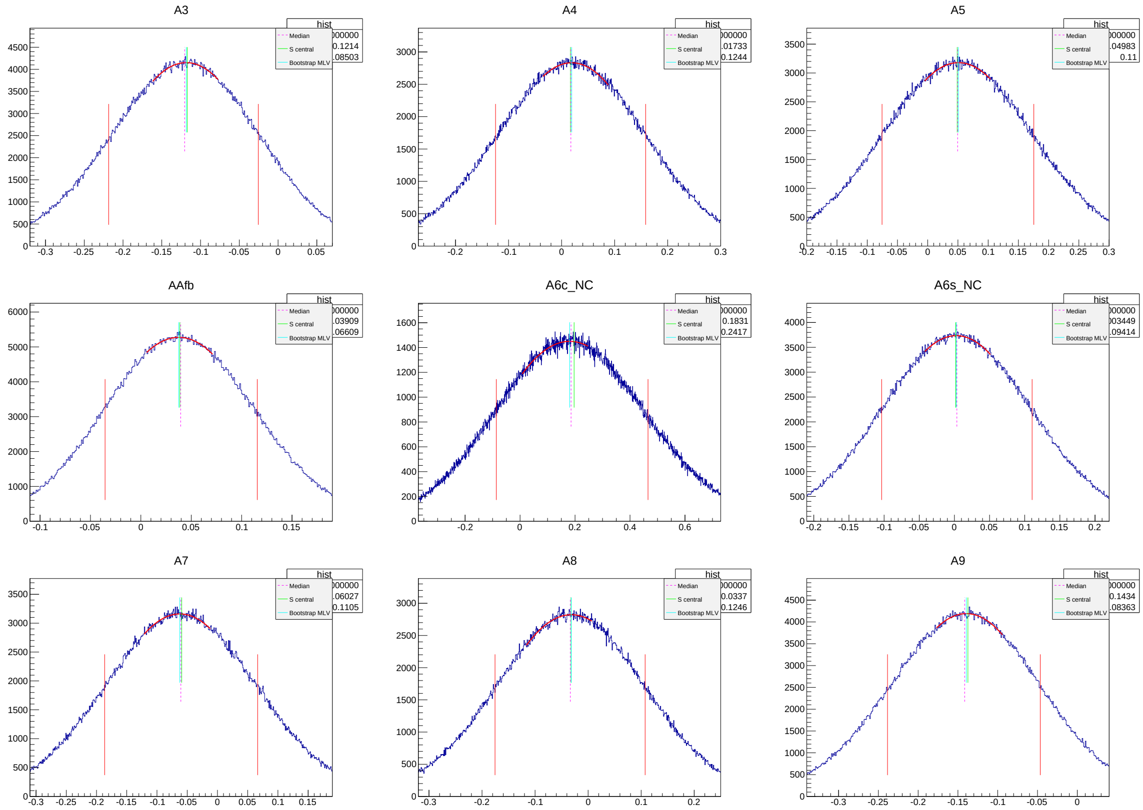

Figure 220: Bootstraps distribution in $4.0 < q^2 < 6.0\,\mathrm{GeV}^2/c^4$ bin

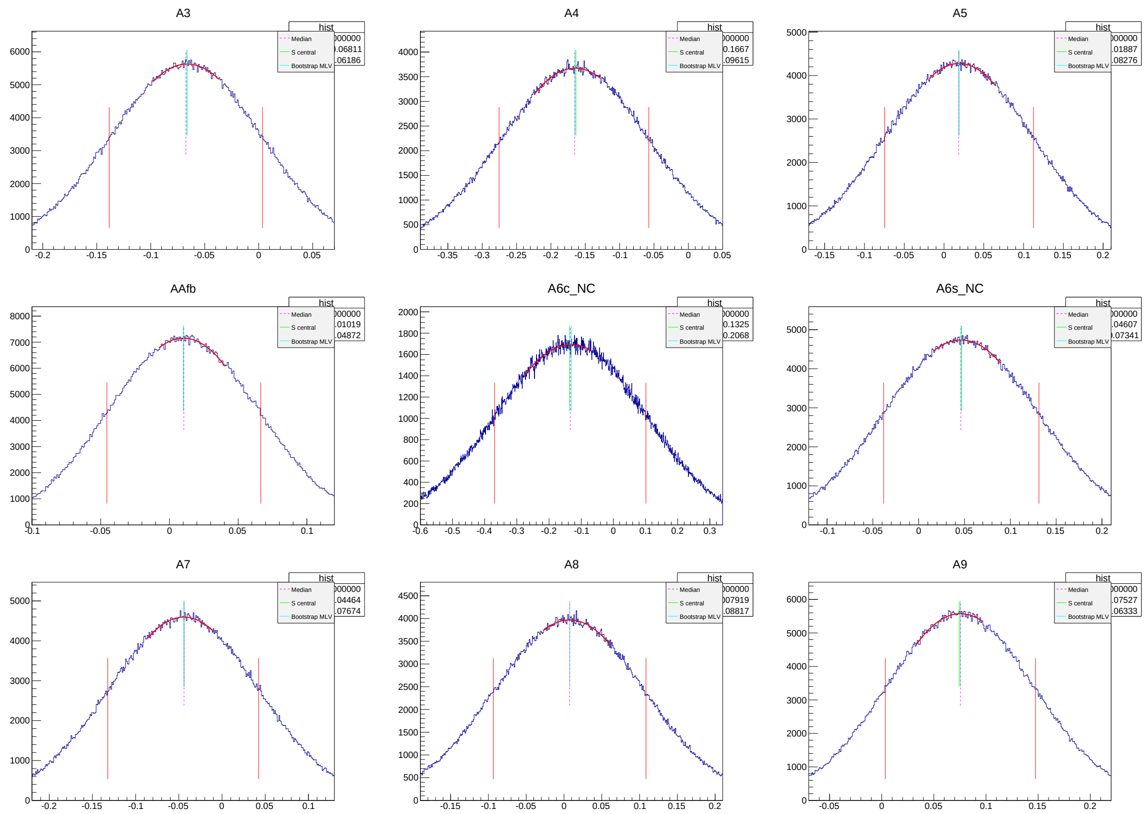

Figure 221: Bootstraps distribution in $6.0 < q^2 < 8.0\,\mathrm{GeV}^2/c^4$ bin

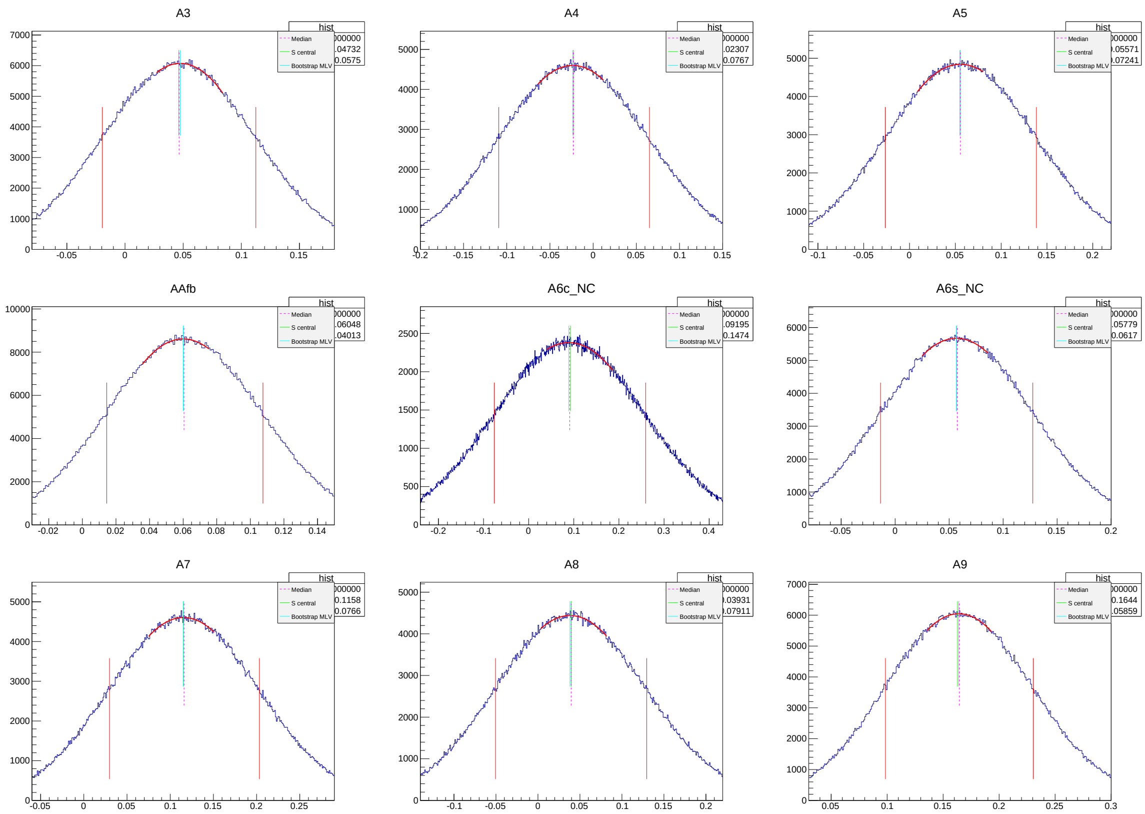

1892

Figure 222: Bootstraps distribution in $11.0 < q^2 < 12.5\,\mathrm{GeV}^2/c^4$ bin

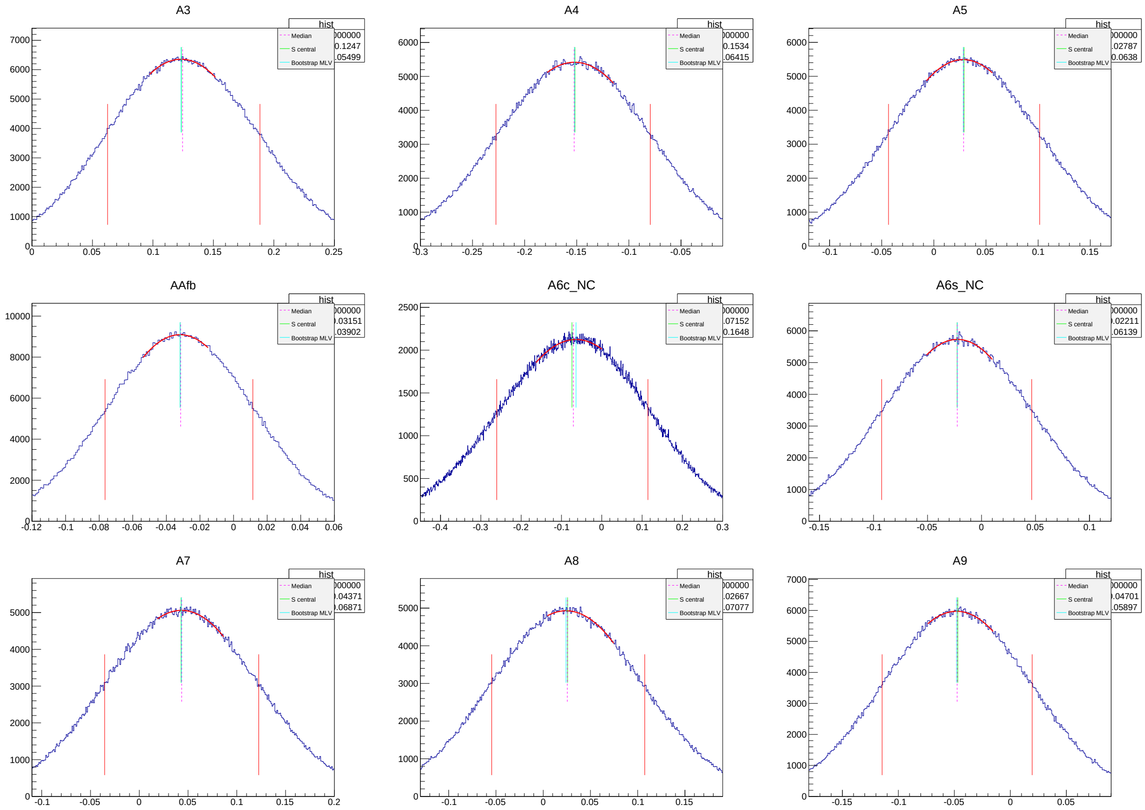

Figure 223: Bootstraps distribution in $15.0 < q^2 < 17\,\mathrm{GeV}^2/c^4$ bin

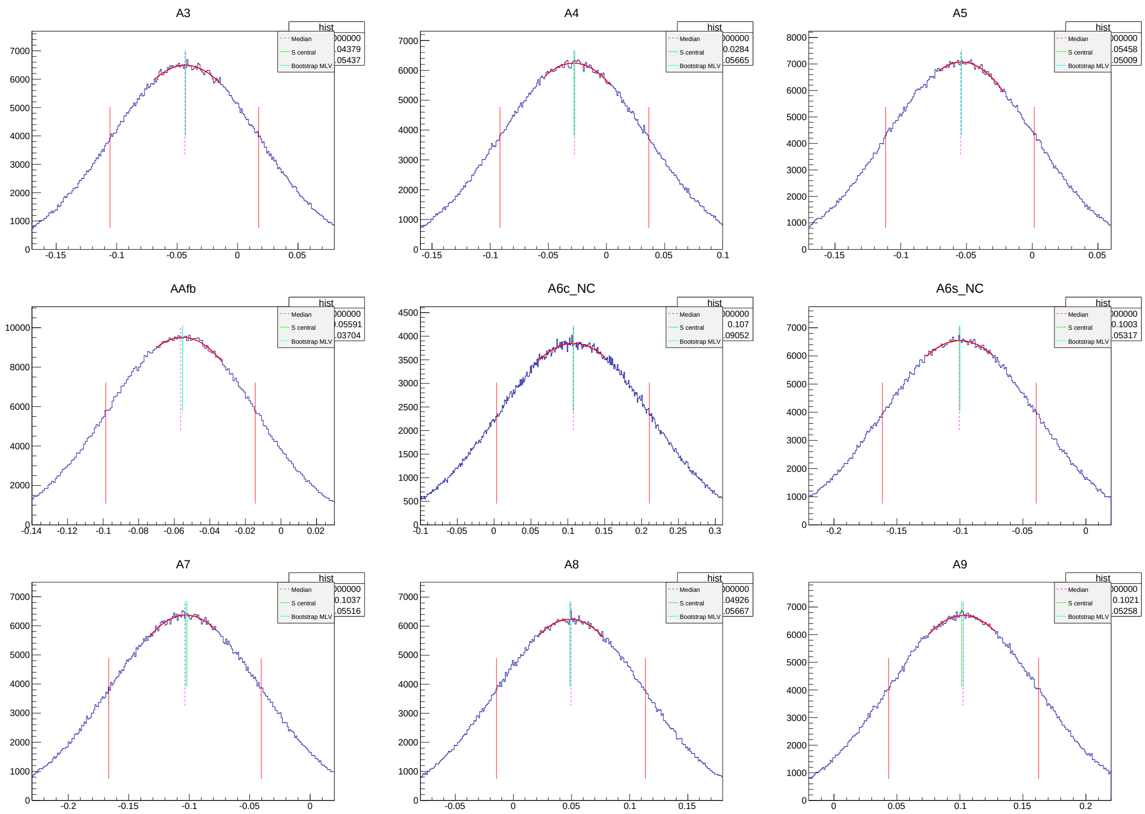

Figure 224: Bootstraps distribution in $17.0 < q^2 < 19\,\mathrm{GeV}^2/c^4$ bin

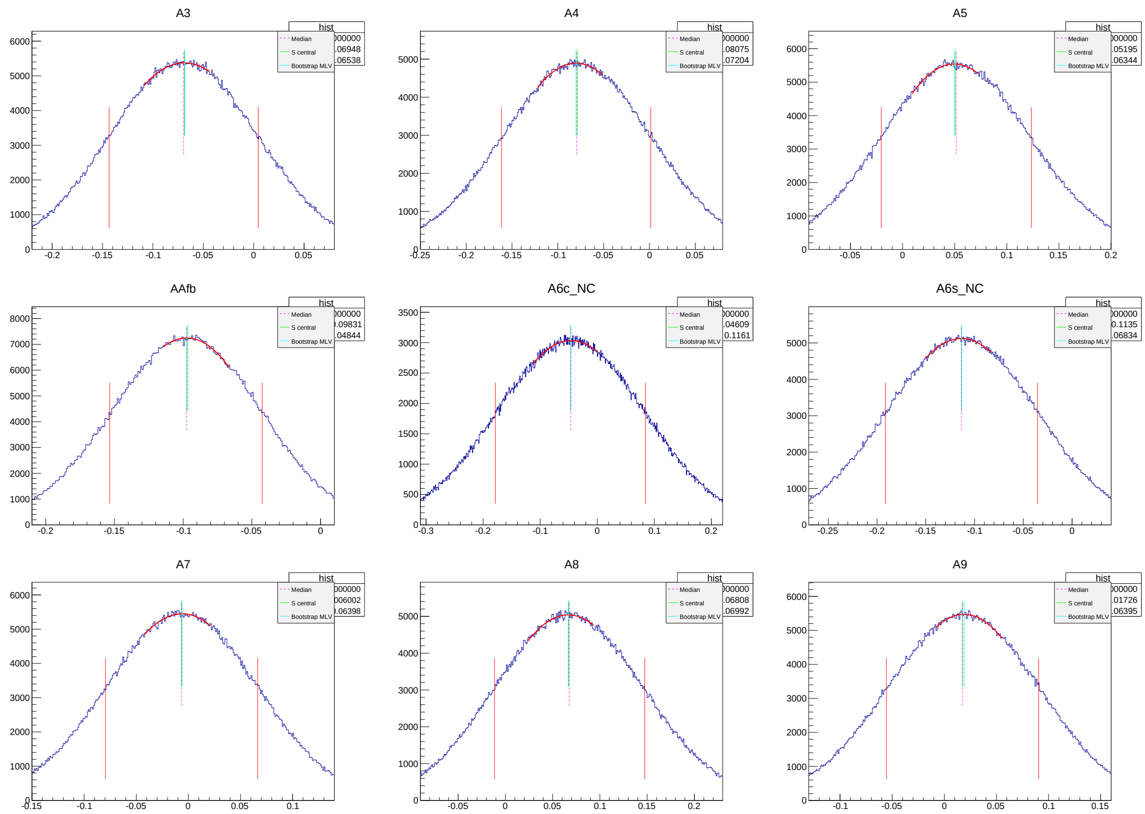

M Correlation matrices for the moment analysis

The correlation matrixes, obtained by bootstrapping the moments are given in Tables 128 through 193.

Table 128: Correlation matrix for $0.1 < q^2 < 0.98$ bin for the S_i observables.

F_{L}	S_3	S_4	S_5	A_{FB}	S_7	S_8	S_9	S_{6s}	S_{6c}
1.0	0.02	−0.0	−0.05	0.23	0.02	−0.01	0.05	0.25	−0.19
0.02	1.0	0.04	0.09	−0.01	0.01	−0.04	0.05	−0.01	−0.03
−0.0	0.04	1.0	−0.24	−0.05	−0.07	0.06	0.03	−0.0	−0.15
−0.05	0.09	−0.24	1.0	0.12	−0.0	−0.09	−0.02	0.11	0.02
0.23	−0.01	−0.05	0.12	1.0	0.09	−0.07	−0.04	0.96	−0.23
0.02	0.01	−0.07	−0.0	0.09	1.0	−0.09	0.1	0.07	0.04
−0.01	−0.04	0.06	−0.09	−0.07	−0.09	1.0	0.03	−0.04	−0.08
0.05	0.05	0.03	−0.02	−0.04	0.1	0.03	1.0	−0.03	−0.04
0.25	−0.01	−0.0	0.11	0.96	0.07	−0.04	−0.03	1.0	−0.47
−0.19	−0.03	−0.15	0.02	−0.23	0.04	−0.08	−0.04	−0.47	1.0

Table 129: Correlation matrix for $1.1 < q^2 < 2.0$ bin for the S_i observables.

F_{L}	S_3	S_4	S_5	A_{FB}	S_7	S_8	S_9	S_{6s}	S_{6c}
1.0	−0.02	0.06	0.16	−0.05	−0.03	−0.04	0.09	0.1	−0.05
−0.02	1.0	−0.01	0.03	0.08	0.1	−0.03	0.08	0.05	−0.02
0.06	−0.01	1.0	−0.0	−0.03	−0.13	−0.0	−0.06	−0.02	0.14
0.16	0.03	−0.0	1.0	−0.07	−0.05	−0.11	−0.06	0.01	−0.04
−0.05	0.08	−0.03	−0.07	1.0	0.04	−0.06	−0.1	0.81	−0.0
−0.03	0.1	−0.13	−0.05	0.04	1.0	−0.05	0.01	−0.04	0.01
−0.04	−0.03	−0.0	−0.11	−0.06	−0.05	1.0	−0.01	−0.09	−0.07
0.09	0.08	−0.06	−0.06	−0.1	0.01	−0.01	1.0	−0.06	−0.02
0.1	0.05	−0.02	0.01	0.81	−0.04	−0.09	−0.06	1.0	−0.44
−0.05	−0.02	0.14	−0.04	−0.0	0.01	−0.07	−0.02	−0.44	1.0

Table 130: Correlation matrix for $2.0 < q^2 < 3.0$ bin for the S_i observables.

F_{L}	S_3	S_4	S_5	A_{FB}	S_7	S_8	S_9	S_{6s}	S_{6c}
1.0	−0.12	−0.14	−0.04	0.11	−0.18	0.04	0.01	0.23	−0.19
−0.12	1.0	−0.09	0.06	0.04	0.08	−0.04	−0.01	0.02	0.0
−0.14	−0.09	1.0	−0.08	0.0	0.03	−0.05	−0.06	0.0	−0.01
−0.04	0.06	−0.08	1.0	−0.1	−0.08	0.04	−0.08	0.05	−0.24
0.11	0.04	0.0	−0.1	1.0	−0.01	−0.1	0.04	0.83	0.14
−0.18	0.08	0.03	−0.08	−0.01	1.0	−0.12	0.01	−0.06	0.03
0.04	−0.04	−0.05	0.04	−0.1	−0.12	1.0	−0.07	0.12	−0.39
0.01	−0.01	−0.06	−0.08	0.04	0.01	−0.07	1.0	0.03	0.01
0.23	0.02	0.0	0.05	0.83	−0.06	0.12	0.03	1.0	−0.43
−0.19	0.0	−0.01	−0.24	0.14	0.03	−0.39	0.01	−0.43	1.0

Table 131: Correlation matrix for $3.0 < q^2 < 4.0$ bin for the S_i observables.

F_{L}	S_3	S_4	S_5	A_{FB}	S_7	S_8	S_9	S_{6s}	S_{6c}
1.0	0.1	−0.01	−0.03	0.01	0.01	−0.16	0.05	−0.28	0.45
0.1	1.0	−0.01	−0.04	0.03	−0.08	−0.04	−0.11	0.02	0.01
−0.01	−0.01	1.0	0.18	0.05	0.01	−0.05	−0.02	0.1	−0.08
−0.03	−0.04	0.18	1.0	0.0	−0.01	0.02	−0.03	0.0	−0.0
0.01	0.03	0.05	0.0	1.0	0.04	−0.03	−0.01	0.76	0.15
0.01	−0.08	0.01	−0.01	0.04	1.0	0.18	−0.08	0.12	−0.12
−0.16	−0.04	−0.05	0.02	−0.03	0.18	1.0	−0.03	0.04	−0.11
0.05	−0.11	−0.02	−0.03	−0.01	−0.08	−0.03	1.0	−0.03	0.03
−0.28	0.02	0.1	0.0	0.76	0.12	0.04	−0.03	1.0	−0.53
0.45	0.01	−0.08	−0.0	0.15	−0.12	−0.11	0.03	−0.53	1.0

Table 132: Correlation matrix for $4.0 < q^2 < 5.0$ bin for the S_i observables.

F_{L}	S_3	S_4	S_5	A_{FB}	S_7	S_8	S_9	S_{6s}	S_{6c}
1.0	−0.01	0.03	−0.12	−0.02	−0.07	0.04	0.1	−0.14	0.19
−0.01	1.0	−0.1	−0.11	0.03	0.08	−0.12	0.07	0.02	0.01
0.03	−0.1	1.0	0.15	−0.03	−0.07	0.21	0.04	0.07	−0.15
−0.12	−0.11	0.15	1.0	−0.03	0.1	−0.02	−0.09	−0.03	0.0
−0.02	0.03	−0.03	−0.03	1.0	0.11	−0.15	0.0	0.77	0.16
−0.07	0.08	−0.07	0.1	0.11	1.0	0.07	−0.07	−0.02	0.18
0.04	−0.12	0.21	−0.02	−0.15	0.07	1.0	0.0	−0.03	−0.15
0.1	0.07	0.04	−0.09	0.0	−0.07	0.0	1.0	0.03	−0.05
−0.14	0.02	0.07	−0.03	0.77	−0.02	−0.03	0.03	1.0	−0.5
0.19	0.01	−0.15	0.0	0.16	0.18	−0.15	−0.05	−0.5	1.0

Table 133: Correlation matrix for $5.0 < q^2 < 6.0$ bin for the S_i observables.

F_L	S_3	S_4	S_5	A_{FB}	S_7	S_8	S_9	S_{6s}	S_{6c}
1.0	−0.03	−0.06	−0.04	−0.01	−0.03	−0.09	−0.02	−0.28	0.35
−0.03	1.0	−0.01	−0.06	−0.11	−0.05	0.02	0.11	−0.08	0.02
−0.06	−0.01	1.0	0.1	−0.03	0.08	0.02	0.01	0.02	−0.05
−0.04	−0.06	0.1	1.0	−0.08	−0.03	0.06	0.07	−0.02	−0.05
−0.01	−0.11	−0.03	−0.08	1.0	0.01	0.0	−0.0	0.69	0.14
−0.03	−0.05	0.08	−0.03	0.01	1.0	0.07	−0.09	0.07	−0.08
−0.09	0.02	0.02	0.06	0.0	0.07	1.0	−0.13	0.03	−0.04
−0.02	0.11	0.01	0.07	−0.0	−0.09	−0.13	1.0	−0.02	0.02
−0.28	−0.08	0.02	−0.02	0.69	0.07	0.03	−0.02	1.0	−0.6
0.35	0.02	−0.05	−0.05	0.14	−0.08	−0.04	0.02	−0.6	1.0

Table 134: Correlation matrix for $6.0 < q^2 < 7.0$ bin for the S_i observables.

F_L	S_3	S_4	S_5	A_{FB}	S_7	S_8	S_9	S_{6s}	S_{6c}
1.0	−0.0	−0.24	−0.14	−0.04	0.08	0.07	−0.03	−0.27	0.38
−0.0	1.0	−0.09	−0.17	−0.08	0.02	−0.04	−0.02	−0.09	0.02
−0.24	−0.09	1.0	0.13	−0.12	−0.03	−0.01	−0.04	0.07	−0.28
−0.14	−0.17	0.13	1.0	−0.07	−0.01	−0.01	−0.04	0.09	−0.24
−0.04	−0.08	−0.12	−0.07	1.0	0.02	−0.01	−0.05	0.78	0.08
0.08	0.02	−0.03	−0.01	0.02	1.0	0.21	−0.11	−0.03	0.09
0.07	−0.04	−0.01	−0.01	−0.01	0.21	1.0	−0.06	−0.02	0.03
−0.03	−0.02	−0.04	−0.04	−0.05	−0.11	−0.06	1.0	−0.04	−0.01
−0.27	−0.09	0.07	0.09	0.78	−0.03	−0.02	−0.04	1.0	−0.55
0.38	0.02	−0.28	−0.24	0.08	0.09	0.03	−0.01	−0.55	1.0

Table 135: Correlation matrix for $7.0 < q^2 < 8.0$ bin for the S_i observables.

F_L	S_3	S_4	S_5	A_{FB}	S_7	S_8	S_9	S_{6s}	S_{6c}
1.0	0.07	−0.13	−0.22	−0.08	−0.07	−0.01	0.09	−0.25	0.21
0.07	1.0	−0.12	−0.15	0.07	0.05	0.02	−0.01	0.03	0.03
−0.13	−0.12	1.0	0.15	−0.09	−0.05	0.06	−0.0	0.09	−0.25
−0.22	−0.15	0.15	1.0	−0.15	0.13	0.0	0.03	0.02	−0.18
−0.08	0.07	−0.09	−0.15	1.0	−0.02	−0.16	0.04	0.82	0.07
−0.07	0.05	−0.05	0.13	−0.02	1.0	0.07	−0.11	−0.02	0.0
−0.01	0.02	0.06	0.0	−0.16	0.07	1.0	−0.07	−0.11	−0.03
0.09	−0.01	−0.0	0.03	0.04	−0.11	−0.07	1.0	0.06	−0.04
−0.25	0.03	0.09	0.02	0.82	−0.02	−0.11	0.06	1.0	−0.46
0.21	0.03	−0.25	−0.18	0.07	0.0	−0.03	−0.04	−0.46	1.0

Table 136: Correlation matrix for $11.00 < q^2 < 11.75$ bin for the S_i observables.

F_{L}	S_3	S_4	S_5	A_{FB}	S_7	S_8	S_9	S_{6s}	S_{6c}
1.0	0.15	0.16	0.03	−0.34	−0.05	−0.12	−0.01	−0.52	0.33
0.15	1.0	−0.06	−0.21	−0.06	0.04	−0.0	−0.02	−0.04	0.02
0.16	−0.06	1.0	0.19	−0.19	−0.11	−0.15	−0.04	−0.09	−0.04
0.03	−0.21	0.19	1.0	−0.11	−0.13	−0.1	−0.09	−0.09	0.08
−0.34	−0.06	−0.19	−0.11	1.0	0.03	−0.03	−0.04	0.78	0.01
−0.05	0.04	−0.11	−0.13	0.03	1.0	0.24	−0.03	0.09	−0.1
−0.12	−0.0	−0.15	−0.1	−0.03	0.24	1.0	−0.1	0.11	−0.22
−0.01	−0.02	−0.04	−0.09	−0.04	−0.03	−0.1	1.0	−0.01	−0.02
−0.52	−0.04	−0.09	−0.09	0.78	0.09	0.11	−0.01	1.0	−0.55
0.33	0.02	−0.04	0.08	0.01	−0.1	−0.22	−0.02	−0.55	1.0

Table 137: Correlation matrix for $11.75 < q^2 < 12.50$ bin for the S_i observables.

F_{L}	S_3	S_4	S_5	A_{FB}	S_7	S_8	S_9	S_{6s}	S_{6c}
1.0	0.04	−0.05	−0.01	−0.17	−0.08	0.05	−0.0	−0.33	0.15
0.04	1.0	−0.13	−0.14	0.0	0.02	−0.0	0.05	0.03	0.01
−0.05	−0.13	1.0	0.16	−0.22	0.1	0.18	−0.02	0.0	−0.16
−0.01	−0.14	0.16	1.0	−0.17	0.16	0.08	−0.1	0.02	−0.11
−0.17	0.0	−0.22	−0.17	1.0	−0.08	−0.12	0.07	0.62	0.07
−0.08	0.02	0.1	0.16	−0.08	1.0	0.16	−0.16	−0.01	0.01
0.05	−0.0	0.18	0.08	−0.12	0.16	1.0	−0.08	−0.07	−0.03
−0.0	0.05	−0.02	−0.1	0.07	−0.16	−0.08	1.0	0.02	0.0
−0.33	0.03	0.0	0.02	0.62	−0.01	−0.07	0.02	1.0	−0.69
0.15	0.01	−0.16	−0.11	0.07	0.01	−0.03	0.0	−0.69	1.0

Table 138: Correlation matrix for $15.0 < q^2 < 16.0$ bin for the S_i observables.

F_{L}	S_3	S_4	S_5	A_{FB}	S_7	S_8	S_9	S_{6s}	S_{6c}
1.0	0.05	−0.01	−0.09	−0.34	0.01	0.03	−0.01	−0.27	−0.06
0.05	1.0	−0.15	−0.29	0.06	−0.03	0.02	−0.09	0.05	0.03
−0.01	−0.15	1.0	0.33	−0.06	−0.02	−0.17	−0.01	0.09	−0.23
−0.09	−0.29	0.33	1.0	−0.1	−0.13	−0.02	−0.05	0.04	−0.16
−0.34	0.06	−0.06	−0.1	1.0	−0.01	−0.03	−0.04	0.82	0.04
0.01	−0.03	−0.02	−0.13	−0.01	1.0	0.12	−0.1	−0.01	0.01
0.03	0.02	−0.17	−0.02	−0.03	0.12	1.0	−0.12	−0.03	0.01
−0.01	−0.09	−0.01	−0.05	−0.04	−0.1	−0.12	1.0	−0.02	0.0
−0.27	0.05	0.09	0.04	0.82	−0.01	−0.03	−0.02	1.0	−0.46
−0.06	0.03	−0.23	−0.16	0.04	0.01	0.01	0.0	−0.46	1.0

Table 139: Correlation matrix for $16.0 < q^2 < 17.0$ bin for the S_i observables.

F_{L}	S_3	S_4	S_5	A_{FB}	S_7	S_8	S_9	S_{6s}	S_{6c}
1.0	0.16	−0.02	0.01	−0.33	0.16	0.03	−0.01	−0.31	0.03
0.16	1.0	−0.12	−0.13	0.04	0.05	−0.01	−0.03	0.1	−0.01
−0.02	−0.12	1.0	0.21	−0.2	0.08	−0.02	0.06	−0.07	−0.16
0.01	−0.13	0.21	1.0	−0.14	0.02	0.07	0.2	−0.02	−0.14
−0.33	0.04	−0.2	−0.14	1.0	−0.05	0.01	−0.02	0.86	0.01
0.16	0.05	0.08	0.02	−0.05	1.0	0.15	−0.13	−0.07	0.05
0.03	−0.01	−0.02	0.07	0.01	0.15	1.0	−0.08	−0.04	0.11
−0.01	−0.03	0.06	0.2	−0.02	−0.13	−0.08	1.0	−0.03	0.03
−0.31	0.1	−0.07	−0.02	0.86	−0.07	−0.04	−0.03	1.0	−0.41
0.03	−0.01	−0.16	−0.14	0.01	0.05	0.11	0.03	−0.41	1.0

Table 140: Correlation matrix for $17.0 < q^2 < 18.0$ bin for the S_i observables.

F_L	S_3	S_4	S_5	A_{FB}	S_7	S_8	S_9	S_{6s}	S_{6c}
1.0	0.06	−0.08	0.05	−0.21	−0.05	0.06	0.0	−0.07	−0.27
0.06	1.0	−0.12	−0.19	0.03	0.09	0.01	−0.08	0.03	−0.01
−0.08	−0.12	1.0	0.14	−0.07	0.05	−0.12	0.0	−0.05	−0.01
0.05	−0.19	0.14	1.0	−0.06	−0.17	0.07	0.06	0.05	−0.18
−0.21	0.03	−0.07	−0.06	1.0	0.01	0.03	0.03	0.88	0.03
−0.05	0.09	0.05	−0.17	0.01	1.0	0.11	−0.2	−0.01	0.05
0.06	0.01	−0.12	0.07	0.03	0.11	1.0	−0.05	0.09	−0.11
0.0	−0.08	0.0	0.06	0.03	−0.2	−0.05	1.0	0.03	0.0
−0.07	0.03	−0.05	0.05	0.88	−0.01	0.09	0.03	1.0	−0.42
−0.27	−0.01	−0.01	−0.18	0.03	0.05	−0.11	0.0	−0.42	1.0

Table 141: Correlation matrix for $18.0 < q^2 < 19.$ bin for the S_i observables.

F_L	S_3	S_4	S_5	A_{FB}	S_7	S_8	S_9	S_{6s}	S_{6c}
1.0	0.2	−0.21	−0.16	−0.21	0.01	0.1	0.02	−0.31	0.29
0.2	1.0	−0.18	−0.21	−0.03	−0.0	0.05	−0.02	−0.04	0.07
−0.21	−0.18	1.0	0.36	−0.18	0.03	0.0	−0.0	0.03	−0.16
−0.16	−0.21	0.36	1.0	−0.24	−0.01	−0.03	0.02	0.04	−0.25
−0.21	−0.03	−0.18	−0.24	1.0	−0.04	0.02	0.05	0.85	−0.03
0.01	−0.0	0.03	−0.01	−0.04	1.0	0.19	−0.17	−0.06	0.09
0.1	0.05	0.0	−0.03	0.02	0.19	1.0	−0.01	−0.03	0.06
0.02	−0.02	−0.0	0.02	0.05	−0.17	−0.01	1.0	0.02	−0.0
−0.31	−0.04	0.03	0.04	0.85	−0.06	−0.03	0.02	1.0	−0.42
0.29	0.07	−0.16	−0.25	−0.03	0.09	0.06	−0.0	−0.42	1.0

Table 142: Correlation matrix for $1.10 < q^2 < 2.5$ bin for the S_i observables.

F_L	S_3	S_4	S_5	A_{FB}	S_7	S_8	S_9	S_{6s}	S_{6c}
1.0	−0.05	−0.02	0.1	0.02	−0.13	−0.03	0.11	0.18	−0.14
−0.05	1.0	−0.04	0.08	0.08	0.11	−0.01	0.01	0.04	−0.01
−0.02	−0.04	1.0	0.02	0.01	−0.08	−0.0	−0.1	−0.01	0.09
0.1	0.08	0.02	1.0	−0.07	−0.04	−0.05	−0.09	0.04	−0.13
0.02	0.08	0.01	−0.07	1.0	0.01	−0.1	−0.05	0.82	0.05
−0.13	0.11	−0.08	−0.04	0.01	1.0	−0.03	−0.02	−0.07	−0.0
−0.03	−0.01	−0.0	−0.05	−0.1	−0.03	1.0	−0.02	0.01	−0.31
0.11	0.01	−0.1	−0.09	−0.05	−0.02	−0.02	1.0	−0.02	−0.01
0.18	0.04	−0.01	0.04	0.82	−0.07	0.01	−0.02	1.0	−0.45
−0.14	−0.01	0.09	−0.13	0.05	−0.0	−0.31	−0.01	−0.45	1.0

Table 143: Correlation matrix for $2.5 < q^2 < 4.0$ bin for the S_i observables.

F_{L}	S_3	S_4	S_5	A_{FB}	S_7	S_8	S_9	S_{6s}	S_{6c}
1.0	−0.0	−0.04	−0.04	0.06	−0.04	−0.11	−0.01	−0.13	0.32
−0.0	1.0	−0.04	−0.03	0.02	−0.06	−0.07	−0.04	0.02	−0.0
−0.04	−0.04	1.0	0.06	0.04	0.03	−0.06	−0.0	0.06	−0.05
−0.04	−0.03	0.06	1.0	−0.04	−0.05	0.03	−0.03	0.0	−0.06
0.06	0.02	0.04	−0.04	1.0	0.02	−0.03	0.01	0.79	0.16
−0.04	−0.06	0.03	−0.05	0.02	1.0	0.04	0.0	0.07	−0.08
−0.11	−0.07	−0.06	0.03	−0.03	0.04	1.0	−0.05	0.07	−0.15
−0.01	−0.04	−0.0	−0.03	0.01	0.0	−0.05	1.0	−0.01	0.03
−0.13	0.02	0.06	0.0	0.79	0.07	0.07	−0.01	1.0	−0.48
0.32	−0.0	−0.05	−0.06	0.16	−0.08	−0.15	0.03	−0.48	1.0

Table 144: Correlation matrix for $4.0 < q^2 < 6.0$ bin for the S_i observables.

F_{L}	S_3	S_4	S_5	A_{FB}	S_7	S_8	S_9	S_{6s}	S_{6c}
1.0	0.02	−0.01	−0.11	−0.0	−0.07	−0.01	0.06	−0.21	0.28
0.02	1.0	−0.08	−0.1	−0.03	0.0	−0.04	0.08	−0.04	0.02
−0.01	−0.08	1.0	0.13	−0.03	−0.0	0.12	0.02	0.04	−0.1
−0.11	−0.1	0.13	1.0	−0.06	0.06	0.0	−0.02	−0.02	−0.03
−0.0	−0.03	−0.03	−0.06	1.0	0.06	−0.06	0.0	0.73	0.15
−0.07	0.0	−0.0	0.06	0.06	1.0	0.05	−0.09	0.03	0.04
−0.01	−0.04	0.12	0.0	−0.06	0.05	1.0	−0.06	0.0	−0.08
0.06	0.08	0.02	−0.02	0.0	−0.09	−0.06	1.0	0.0	−0.0
−0.21	−0.04	0.04	−0.02	0.73	0.03	0.0	0.0	1.0	−0.56
0.28	0.02	−0.1	−0.03	0.15	0.04	−0.08	−0.0	−0.56	1.0

Table 145: Correlation matrix for $6.0 < q^2 < 8.0$ bin for the S_i observables.

F_{L}	S_3	S_4	S_5	A_{FB}	S_7	S_8	S_9	S_{6s}	S_{6c}
1.0	0.03	−0.16	−0.16	−0.11	0.0	0.04	0.04	−0.29	0.31
0.03	1.0	−0.11	−0.15	0.01	0.04	0.01	−0.02	−0.01	0.02
−0.16	−0.11	1.0	0.15	−0.08	−0.04	0.02	−0.02	0.09	−0.27
−0.16	−0.15	0.15	1.0	−0.08	0.07	−0.03	−0.0	0.06	−0.21
−0.11	0.01	−0.08	−0.08	1.0	−0.01	−0.08	0.01	0.81	0.06
0.0	0.04	−0.04	0.07	−0.01	1.0	0.15	−0.12	−0.03	0.04
0.04	0.01	0.02	−0.03	−0.08	0.15	1.0	−0.07	−0.07	0.01
0.04	−0.02	−0.02	−0.0	0.01	−0.12	−0.07	1.0	0.03	−0.02
−0.29	−0.01	0.09	0.06	0.81	−0.03	−0.07	0.03	1.0	−0.52
0.31	0.02	−0.27	−0.21	0.06	0.04	0.01	−0.02	−0.52	1.0

Table 146: Correlation matrix for $11.0 < q^2 < 12.5$ bin for the S_i observables.

F_L	S_3	S_4	S_5	A_{FB}	S_7	S_8	S_9	S_{6s}	S_{6c}
1.0	0.1	0.03	0.01	−0.25	−0.05	−0.03	−0.0	−0.42	0.22
0.1	1.0	−0.1	−0.17	−0.03	0.02	−0.0	0.02	−0.0	0.01
0.03	−0.1	1.0	0.17	−0.2	0.0	0.01	−0.03	−0.03	−0.11
0.01	−0.17	0.17	1.0	−0.14	0.02	−0.01	−0.1	−0.02	−0.03
−0.25	−0.03	−0.2	−0.14	1.0	−0.03	−0.07	0.01	0.69	0.04
−0.05	0.02	0.0	0.02	−0.03	1.0	0.21	−0.09	0.04	−0.04
−0.03	−0.0	0.01	−0.01	−0.07	0.21	1.0	−0.09	0.01	−0.11
−0.0	0.02	−0.03	−0.1	0.01	−0.09	−0.09	1.0	0.0	−0.0
−0.42	−0.0	−0.03	−0.02	0.69	0.04	0.01	0.0	1.0	−0.63
0.22	0.01	−0.11	−0.03	0.04	−0.04	−0.11	−0.0	−0.63	1.0

Table 147: Correlation matrix for $15.0 < q^2 < 17.0$ bin for the S_i observables.

F_L	S_3	S_4	S_5	A_{FB}	S_7	S_8	S_9	S_{6s}	S_{6c}
1.0	0.11	−0.01	−0.05	−0.33	0.08	0.03	−0.02	−0.28	−0.03
0.11	1.0	−0.14	−0.21	0.06	0.0	0.0	−0.06	0.07	0.01
−0.01	−0.14	1.0	0.26	−0.13	0.04	−0.09	0.03	0.01	−0.19
−0.05	−0.21	0.26	1.0	−0.11	−0.05	0.02	0.07	0.01	−0.15
−0.33	0.06	−0.13	−0.11	1.0	−0.03	−0.01	−0.03	0.85	0.03
0.08	0.0	0.04	−0.05	−0.03	1.0	0.14	−0.11	−0.05	0.03
0.03	0.0	−0.09	0.02	−0.01	0.14	1.0	−0.1	−0.03	0.05
−0.02	−0.06	0.03	0.07	−0.03	−0.11	−0.1	1.0	−0.02	0.02
−0.28	0.07	0.01	0.01	0.85	−0.05	−0.03	−0.02	1.0	−0.43
−0.03	0.01	−0.19	−0.15	0.03	0.03	0.05	0.02	−0.43	1.0

Table 148: Correlation matrix for $17.0 < q^2 < 19.0$ bin for the S_i observables.

F_L	S_3	S_4	S_5	A_{FB}	S_7	S_8	S_9	S_{6s}	S_{6c}
1.0	0.12	−0.14	−0.04	−0.21	−0.02	0.07	0.01	−0.18	−0.04
0.12	1.0	−0.15	−0.19	0.0	0.05	0.03	−0.06	0.0	0.02
−0.14	−0.15	1.0	0.23	−0.1	0.03	−0.05	0.01	0.01	−0.11
−0.04	−0.19	0.23	1.0	−0.14	−0.1	0.03	0.05	0.06	−0.22
−0.21	0.0	−0.1	−0.14	1.0	−0.02	0.01	0.03	0.86	0.01
−0.02	0.05	0.03	−0.1	−0.02	1.0	0.14	−0.19	−0.03	0.07
0.07	0.03	−0.05	0.03	0.01	0.14	1.0	−0.04	0.03	−0.04
0.01	−0.06	0.01	0.05	0.03	−0.19	−0.04	1.0	0.02	0.0
−0.18	0.0	0.01	0.06	0.86	−0.03	0.03	0.02	1.0	−0.42
−0.04	0.02	−0.11	−0.22	0.01	0.07	−0.04	0.0	−0.42	1.0

Table 149: Correlation matrix for $15.0 < q^2 < 19.0$ bin for the S_i observables.

F_L	S_3	S_4	S_5	A_{FB}	S_7	S_8	S_9	S_{6s}	S_{6c}
1.0	0.11	−0.07	−0.04	−0.28	0.04	0.04	−0.01	−0.23	−0.04
0.11	1.0	−0.15	−0.21	0.04	0.02	0.01	−0.06	0.04	0.01
−0.07	−0.15	1.0	0.24	−0.11	0.04	−0.07	0.02	0.0	−0.16
−0.04	−0.21	0.24	1.0	−0.11	−0.08	0.03	0.07	0.03	−0.19
−0.28	0.04	−0.11	−0.11	1.0	−0.02	0.0	−0.0	0.86	0.02
0.04	0.02	0.04	−0.08	−0.02	1.0	0.14	−0.15	−0.04	0.05
0.04	0.01	−0.07	0.03	0.0	0.14	1.0	−0.07	−0.0	0.01
−0.01	−0.06	0.02	0.07	−0.0	−0.15	−0.07	1.0	0.0	0.01
−0.23	0.04	0.0	0.03	0.86	−0.04	−0.0	0.0	1.0	−0.43
−0.04	0.01	−0.16	−0.19	0.02	0.05	0.01	0.01	−0.43	1.0

Table 150: Correlation matrix for $0.1 < q^2 < 0.98$ bin for the A_i observables.

A_3	A_4	A_5	$A(A_{FB})$	A_7	A_8	A_9	A_{6s}	A_{6c}
1.0	0.04	0.09	−0.02	0.01	−0.04	0.05	−0.0	−0.04
0.04	1.0	−0.24	−0.07	−0.08	0.07	0.02	−0.02	−0.17
0.09	−0.24	1.0	0.07	0.0	−0.07	−0.01	0.06	0.02
−0.02	−0.07	0.07	1.0	0.08	−0.11	0.0	0.96	−0.16
0.01	−0.08	0.0	0.08	1.0	−0.09	0.12	0.05	0.08
−0.04	0.07	−0.07	−0.11	−0.09	1.0	0.01	−0.09	−0.07
0.05	0.02	−0.01	0.0	0.12	0.01	1.0	−0.0	−0.02
−0.0	−0.02	0.06	0.96	0.05	−0.09	−0.0	1.0	−0.41
−0.04	−0.17	0.02	−0.16	0.08	−0.07	−0.02	−0.41	1.0

Table 151: Correlation matrix for $1.1 < q^2 < 2.0$ bin for the A_i observables.

A_3	A_4	A_5	$A(A_{FB})$	A_7	A_8	A_9	A_{6s}	A_{6c}
1.0	−0.01	0.04	0.06	0.12	−0.05	0.08	0.07	−0.0
−0.01	1.0	−0.06	0.04	−0.16	0.04	−0.1	−0.04	0.12
0.04	−0.06	1.0	−0.05	0.01	−0.11	−0.07	−0.02	−0.03
0.06	0.04	−0.05	1.0	−0.06	−0.07	−0.09	0.89	−0.04
0.12	−0.16	0.01	−0.06	1.0	−0.12	0.1	−0.0	0.0
−0.05	0.04	−0.11	−0.07	−0.12	1.0	−0.04	−0.05	−0.08
0.08	−0.1	−0.07	−0.09	0.1	−0.04	1.0	−0.04	−0.02
0.07	−0.04	−0.02	0.89	−0.0	−0.05	−0.04	1.0	−0.43
−0.0	0.12	−0.03	−0.04	0.0	−0.08	−0.02	−0.43	1.0

Table 152: Correlation matrix for $2.0 < q^2 < 3.0$ bin for the A_x observables.

A_3	A_4	A_5	$A_(A_{\mathrm{FB}})$	A_7	A_8	A_9	A_{6s}	A_{6c}
1.0	−0.1	0.06	0.03	0.07	−0.04	−0.02	0.02	0.01
−0.1	1.0	−0.07	0.07	0.06	−0.06	−0.05	0.06	−0.01
0.06	−0.07	1.0	−0.1	−0.07	0.04	−0.07	0.03	−0.23
0.03	0.07	−0.1	1.0	−0.03	−0.11	0.04	0.84	0.14
0.07	0.06	−0.07	−0.03	1.0	−0.15	0.02	−0.05	0.06
−0.04	−0.06	0.04	−0.11	−0.15	1.0	−0.07	0.12	−0.39
−0.02	−0.05	−0.07	0.04	0.02	−0.07	1.0	0.02	0.02
0.02	0.06	0.03	0.84	−0.05	0.12	0.02	1.0	−0.41
0.01	−0.01	−0.23	0.14	0.06	−0.39	0.02	−0.41	1.0

Table 153: Correlation matrix for $3.0 < q^2 < 4.0$ bin for the A_i observables.

A_3	A_4	A_5	$A(A_{\mathrm{FB}})$	A_7	A_8	A_9	A_{6s}	A_{6c}
1.0	0.0	−0.04	0.03	−0.12	−0.05	−0.06	0.02	−0.01
0.0	1.0	0.18	0.06	0.01	−0.05	−0.01	0.1	−0.07
−0.04	0.18	1.0	0.01	−0.01	0.01	−0.01	0.02	−0.02
0.03	0.06	0.01	1.0	0.03	−0.05	−0.0	0.72	0.21
−0.12	0.01	−0.01	0.03	1.0	0.18	−0.05	0.11	−0.1
−0.05	−0.05	0.01	−0.05	0.18	1.0	−0.03	0.04	−0.11
−0.06	−0.01	−0.01	−0.0	−0.05	−0.03	1.0	−0.03	0.03
0.02	0.1	0.02	0.72	0.11	0.04	−0.03	1.0	−0.52
−0.01	−0.07	−0.02	0.21	−0.1	−0.11	0.03	−0.52	1.0

Table 154: Correlation matrix for $4.0 < q^2 < 5.0$ bin for the A_i observables.

A_3	A_4	A_5	$A(A_{\mathrm{FB}})$	A_7	A_8	A_9	A_{6s}	A_{6c}
1.0	−0.12	−0.11	0.02	0.06	−0.12	0.06	0.01	0.01
−0.12	1.0	0.17	−0.03	−0.06	0.19	0.03	0.08	−0.17
−0.11	0.17	1.0	−0.04	0.14	−0.06	−0.09	−0.01	−0.04
0.02	−0.03	−0.04	1.0	0.1	−0.14	−0.0	0.77	0.17
0.06	−0.06	0.14	0.1	1.0	0.04	−0.08	−0.01	0.14
−0.12	0.19	−0.06	−0.14	0.04	1.0	0.02	−0.04	−0.13
0.06	0.03	−0.09	−0.0	−0.08	0.02	1.0	0.01	−0.02
0.01	0.08	−0.01	0.77	−0.01	−0.04	0.01	1.0	−0.5
0.01	−0.17	−0.04	0.17	0.14	−0.13	−0.02	−0.5	1.0

Table 155: Correlation matrix for $5.0 < q^2 < 6.0$ bin for the A_i observables.

A_3	A_4	A_5	$A(A_{\mathrm{FB}})$	A_7	A_8	A_9	A_{6s}	A_{6c}
1.0	−0.03	−0.07	−0.09	−0.04	0.03	0.11	−0.09	0.04
−0.03	1.0	0.1	−0.03	0.08	0.07	0.03	0.02	−0.03
−0.07	0.1	1.0	−0.08	−0.04	0.07	0.07	−0.01	−0.06
−0.09	−0.03	−0.08	1.0	0.01	−0.01	−0.01	0.69	0.14
−0.04	0.08	−0.04	0.01	1.0	0.07	−0.09	0.07	−0.08
0.03	0.07	0.07	−0.01	0.07	1.0	−0.12	0.03	−0.03
0.11	0.03	0.07	−0.01	−0.09	−0.12	1.0	−0.02	0.02
−0.09	0.02	−0.01	0.69	0.07	0.03	−0.02	1.0	−0.6
0.04	−0.03	−0.06	0.14	−0.08	−0.03	0.02	−0.6	1.0

Table 156: Correlation matrix for $6.0 < q^2 < 7.0$ bin for the A_i observables.

A_3	A_4	A_5	$A(A_{\mathrm{FB}})$	A_7	A_8	A_9	A_{6s}	A_{6c}
1.0	−0.08	−0.15	−0.09	0.02	−0.05	−0.02	−0.09	0.01
−0.08	1.0	0.21	−0.15	−0.03	−0.04	−0.04	0.1	−0.34
−0.15	0.21	1.0	−0.1	−0.02	−0.03	−0.05	0.11	−0.31
−0.09	−0.15	−0.1	1.0	0.03	0.0	−0.05	0.76	0.12
0.02	−0.03	−0.02	0.03	1.0	0.22	−0.11	−0.04	0.09
−0.05	−0.04	−0.03	0.0	0.22	1.0	−0.05	−0.03	0.05
−0.02	−0.04	−0.05	−0.05	−0.11	−0.05	1.0	−0.04	−0.0
−0.09	0.1	0.11	0.76	−0.04	−0.03	−0.04	1.0	−0.55
0.01	−0.34	−0.31	0.12	0.09	0.05	−0.0	−0.55	1.0

Table 157: Correlation matrix for $7.0 < q^2 < 8.0$ bin for the A_i observables.

A_3	A_4	A_5	$A(A_{\mathrm{FB}})$	A_7	A_8	A_9	A_{6s}	A_{6c}
1.0	−0.07	−0.11	0.04	0.06	0.04	−0.01	0.02	0.02
−0.07	1.0	0.18	−0.07	−0.02	0.05	0.01	0.08	−0.28
−0.11	0.18	1.0	−0.11	0.14	−0.02	0.02	0.02	−0.22
0.04	−0.07	−0.11	1.0	−0.03	−0.14	0.07	0.84	0.1
0.06	−0.02	0.14	−0.03	1.0	0.07	−0.11	−0.02	−0.01
0.04	0.05	−0.02	−0.14	0.07	1.0	−0.08	−0.1	−0.03
−0.01	0.01	0.02	0.07	−0.11	−0.08	1.0	0.07	−0.03
0.02	0.08	0.02	0.84	−0.02	−0.1	0.07	1.0	−0.45
0.02	−0.28	−0.22	0.1	−0.01	−0.03	−0.03	−0.45	1.0

Table 158: Correlation matrix for $11.00 < q^2 < 11.75$ bin for the A_i observables.

A_3	A_4	A_5	$A(A_{\mathrm{FB}})$	A_7	A_8	A_9	A_{6s}	A_{6c}
1.0	−0.08	−0.2	−0.1	0.06	0.03	−0.02	−0.09	−0.0
−0.08	1.0	0.16	−0.14	−0.1	−0.15	−0.04	−0.08	−0.07
−0.2	0.16	1.0	−0.09	−0.11	−0.09	−0.1	−0.11	0.05
−0.1	−0.14	−0.09	1.0	−0.02	−0.07	−0.05	0.83	0.09
0.06	−0.1	−0.11	−0.02	1.0	0.25	−0.02	0.05	−0.12
0.03	−0.15	−0.09	−0.07	0.25	1.0	−0.09	0.07	−0.23
−0.02	−0.04	−0.1	−0.05	−0.02	−0.09	1.0	−0.03	−0.04
−0.09	−0.08	−0.11	0.83	0.05	0.07	−0.03	1.0	−0.48
−0.0	−0.07	0.05	0.09	−0.12	−0.23	−0.04	−0.48	1.0

Table 159: Correlation matrix for $11.75 < q^2 < 12.50$ bin for the A_i observables.

A_3	A_4	A_5	$A(A_{\mathrm{FB}})$	A_7	A_8	A_9	A_{6s}	A_{6c}
1.0	−0.12	−0.16	0.01	0.01	0.03	0.06	0.0	0.0
−0.12	1.0	0.17	−0.21	0.08	0.15	−0.05	−0.01	−0.21
−0.16	0.17	1.0	−0.17	0.14	0.12	−0.09	−0.02	−0.13
0.01	−0.21	−0.17	1.0	−0.07	−0.17	0.05	0.66	0.1
0.01	0.08	0.14	−0.07	1.0	0.19	−0.15	−0.05	−0.0
0.03	0.15	0.12	−0.17	0.19	1.0	−0.08	−0.09	−0.04
0.06	−0.05	−0.09	0.05	−0.15	−0.08	1.0	0.02	0.02
0.0	−0.01	−0.02	0.66	−0.05	−0.09	0.02	1.0	−0.67
0.0	−0.21	−0.13	0.1	−0.0	−0.04	0.02	−0.67	1.0

Table 160: Correlation matrix for $15.0 < q^2 < 16.0$ bin for the A_i observables.

A_3	A_4	A_5	$A(A_{\mathrm{FB}})$	A_7	A_8	A_9	A_{6s}	A_{6c}
1.0	−0.14	−0.26	0.05	−0.02	0.02	−0.1	0.02	0.04
−0.14	1.0	0.36	−0.12	−0.02	−0.17	0.0	−0.01	−0.19
−0.26	0.36	1.0	−0.16	−0.12	−0.02	−0.04	−0.08	−0.12
0.05	−0.12	−0.16	1.0	−0.02	−0.03	−0.05	0.88	0.01
−0.02	−0.02	−0.12	−0.02	1.0	0.13	−0.09	−0.03	0.02
0.02	−0.17	−0.02	−0.03	0.13	1.0	−0.12	−0.03	0.01
−0.1	0.0	−0.04	−0.05	−0.09	−0.12	1.0	−0.04	0.0
0.02	−0.01	−0.08	0.88	−0.03	−0.03	−0.04	1.0	−0.47
0.04	−0.19	−0.12	0.01	0.02	0.01	0.0	−0.47	1.0

Table 161: Correlation matrix for $16.0 < q^2 < 17.0$ bin for the A_i observables.

A_3	A_4	A_5	$A(A_{\mathrm{FB}})$	A_7	A_8	A_9	A_{6s}	A_{6c}
1.0	−0.08	−0.09	−0.0	0.01	−0.03	−0.04	−0.01	0.01
−0.08	1.0	0.21	−0.22	0.05	−0.02	0.06	−0.15	−0.14
−0.09	0.21	1.0	−0.14	−0.01	0.05	0.19	−0.09	−0.13
−0.0	−0.22	−0.14	1.0	0.02	0.02	−0.01	0.93	−0.03
0.01	0.05	−0.01	0.02	1.0	0.15	−0.13	0.01	0.04
−0.03	−0.02	0.05	0.02	0.15	1.0	−0.08	−0.02	0.11
−0.04	0.06	0.19	−0.01	−0.13	−0.08	1.0	−0.02	0.04
−0.01	−0.15	−0.09	0.93	0.01	−0.02	−0.02	1.0	−0.4
0.01	−0.14	−0.13	−0.03	0.04	0.11	0.04	−0.4	1.0

Table 162: Correlation matrix for $17.0 < q^2 < 18.0$ bin for the A_i observables.

A_3	A_4	A_5	$A(A_{\mathrm{FB}})$	A_7	A_8	A_9	A_{6s}	A_{6c}
1.0	−0.1	−0.16	−0.01	0.1	0.0	−0.06	−0.01	0.02
−0.1	1.0	0.18	−0.1	0.07	−0.14	0.03	−0.1	0.03
−0.16	0.18	1.0	−0.1	−0.16	0.05	0.09	−0.03	−0.13
−0.01	−0.1	−0.1	1.0	0.0	0.05	0.01	0.9	−0.02
0.1	0.07	−0.16	0.0	1.0	0.09	−0.2	−0.03	0.06
0.0	−0.14	0.05	0.05	0.09	1.0	−0.06	0.1	−0.13
−0.06	0.03	0.09	0.01	−0.2	−0.06	1.0	0.0	0.02
−0.01	−0.1	−0.03	0.9	−0.03	0.1	0.0	1.0	−0.46
0.02	0.03	−0.13	−0.02	0.06	−0.13	0.02	−0.46	1.0

Table 163: Correlation matrix for $18.0 < q^2 < 19.0$ bin for the A_i observables.

A_3	A_4	A_5	$A(A_{\mathrm{FB}})$	A_7	A_8	A_9	A_{6s}	A_{6c}
1.0	−0.18	−0.2	−0.06	−0.01	0.04	−0.03	−0.06	0.06
−0.18	1.0	0.28	−0.1	−0.02	0.01	0.07	−0.01	−0.23
−0.2	0.28	1.0	−0.15	−0.05	−0.0	0.04	−0.0	−0.31
−0.06	−0.1	−0.15	1.0	−0.01	−0.01	0.03	0.9	0.0
−0.01	−0.02	−0.05	−0.01	1.0	0.21	−0.19	−0.04	0.1
0.04	0.01	−0.0	−0.01	0.21	1.0	−0.03	−0.03	0.07
−0.03	0.07	0.04	0.03	−0.19	−0.03	1.0	0.01	−0.02
−0.06	−0.01	−0.0	0.9	−0.04	−0.03	0.01	1.0	−0.4
0.06	−0.23	−0.31	0.0	0.1	0.07	−0.02	−0.4	1.0

Table 164: Correlation matrix for $1.1 < q^2 < 2.5$ bin for the A_i observables.

A_3	A_4	A_5	$A(A_{\mathrm{FB}})$	A_7	A_8	A_9	A_{6s}	A_{6c}
1.0	−0.04	0.08	0.06	0.1	−0.02	0.01	0.05	0.0
−0.04	1.0	−0.02	0.07	−0.08	0.01	−0.1	0.01	0.07
0.08	−0.02	1.0	−0.05	−0.0	−0.03	−0.1	0.01	−0.12
0.06	0.07	−0.05	1.0	−0.05	−0.12	−0.03	0.87	0.04
0.1	−0.08	−0.0	−0.05	1.0	−0.09	0.02	−0.03	0.04
−0.02	0.01	−0.03	−0.12	−0.09	1.0	−0.02	0.03	−0.3
0.01	−0.1	−0.1	−0.03	0.02	−0.02	1.0	−0.01	−0.02
0.05	0.01	0.01	0.87	−0.03	0.03	−0.01	1.0	−0.44
0.0	0.07	−0.12	0.04	0.04	−0.3	−0.02	−0.44	1.0

Table 165: Correlation matrix for $2.5 < q^2 < 4.0$ bin for the A_i observables.

A_3	A_4	A_5	$A(A_{\mathrm{FB}})$	A_7	A_8	A_9	A_{6s}	A_{6c}
1.0	−0.03	−0.04	0.01	−0.07	−0.06	−0.02	0.02	−0.01
−0.03	1.0	0.07	0.05	0.03	−0.06	−0.0	0.07	−0.04
−0.04	0.07	1.0	−0.03	−0.05	0.03	−0.01	0.02	−0.07
0.01	0.05	−0.03	1.0	0.03	−0.04	−0.01	0.77	0.19
−0.07	0.03	−0.05	0.03	1.0	0.04	0.0	0.06	−0.07
−0.06	−0.06	0.03	−0.04	0.04	1.0	−0.04	0.07	−0.16
−0.02	−0.0	−0.01	−0.01	0.0	−0.04	1.0	−0.01	0.02
0.02	0.07	0.02	0.77	0.06	0.07	−0.01	1.0	−0.47
−0.01	−0.04	−0.07	0.19	−0.07	−0.16	0.02	−0.47	1.0

Table 166: Correlation matrix for $4.0 < q^2 < 6.0$ bin for the A_i observables.

A_3	A_4	A_5	$A(A_{\mathrm{FB}})$	A_7	A_8	A_9	A_{6s}	A_{6c}
1.0	−0.08	−0.1	−0.03	0.0	−0.05	0.08	−0.04	0.03
−0.08	1.0	0.14	−0.03	0.0	0.12	0.02	0.06	−0.12
−0.1	0.14	1.0	−0.06	0.06	−0.0	−0.02	−0.01	−0.06
−0.03	−0.03	−0.06	1.0	0.06	−0.07	−0.0	0.72	0.16
0.0	0.0	0.06	0.06	1.0	0.05	−0.09	0.03	0.03
−0.05	0.12	−0.0	−0.07	0.05	1.0	−0.06	−0.0	−0.07
0.08	0.02	−0.02	−0.0	−0.09	−0.06	1.0	−0.0	0.0
−0.04	0.06	−0.01	0.72	0.03	−0.0	−0.0	1.0	−0.56
0.03	−0.12	−0.06	0.16	0.03	−0.07	0.0	−0.56	1.0

Table 167: Correlation matrix for $6.0 < q^2 < 8.0$ bin for the A_i observables.

A_3	A_4	A_5	$A(A_{\mathrm{FB}})$	A_7	A_8	A_9	A_{6s}	A_{6c}
1.0	−0.08	−0.13	−0.01	0.04	0.01	−0.02	−0.01	0.01
−0.08	1.0	0.2	−0.1	−0.03	0.02	−0.02	0.1	−0.32
−0.13	0.2	1.0	−0.1	0.07	−0.03	−0.01	0.06	−0.26
−0.01	−0.1	−0.1	1.0	−0.01	−0.07	0.02	0.8	0.1
0.04	−0.03	0.07	−0.01	1.0	0.15	−0.12	−0.03	0.02
0.01	0.02	−0.03	−0.07	0.15	1.0	−0.06	−0.07	0.02
−0.02	−0.02	−0.01	0.02	−0.12	−0.06	1.0	0.03	−0.02
−0.01	0.1	0.06	0.8	−0.03	−0.07	0.03	1.0	−0.51
0.01	−0.32	−0.26	0.1	0.02	0.02	−0.02	−0.51	1.0

Table 168: Correlation matrix for $11.0 < q^2 < 12.5$ bin for the A_i observables.

A_3	A_4	A_5	$A(A_{\mathrm{FB}})$	A_7	A_8	A_9	A_{6s}	A_{6c}
1.0	−0.11	−0.17	−0.05	0.03	0.03	0.03	−0.04	0.0
−0.11	1.0	0.16	−0.18	−0.0	0.01	−0.05	−0.05	−0.15
−0.17	0.16	1.0	−0.13	0.02	0.01	−0.1	−0.06	−0.06
−0.05	−0.18	−0.13	1.0	−0.04	−0.11	0.0	0.74	0.1
0.03	−0.0	0.02	−0.04	1.0	0.22	−0.09	0.0	−0.05
0.03	0.01	0.01	−0.11	0.22	1.0	−0.09	−0.01	−0.12
0.03	−0.05	−0.1	0.0	−0.09	−0.09	1.0	0.01	−0.01
−0.04	−0.05	−0.06	0.74	0.0	−0.01	0.01	1.0	−0.59
0.0	−0.15	−0.06	0.1	−0.05	−0.12	−0.01	−0.59	1.0

Table 169: Correlation matrix for $15.0 < q^2 < 17.0$ bin for the A_i observables.

A_3	A_4	A_5	$A(A_{\mathrm{FB}})$	A_7	A_8	A_9	A_{6s}	A_{6c}
1.0	−0.11	−0.17	0.02	−0.01	−0.01	−0.07	0.01	0.02
−0.11	1.0	0.29	−0.17	0.01	−0.09	0.03	−0.09	−0.16
−0.17	0.29	1.0	−0.15	−0.07	0.02	0.08	−0.09	−0.12
0.02	−0.17	−0.15	1.0	0.0	−0.0	−0.03	0.9	−0.01
−0.01	0.01	−0.07	0.0	1.0	0.14	−0.11	−0.01	0.02
−0.01	−0.09	0.02	−0.0	0.14	1.0	−0.1	−0.03	0.05
−0.07	0.03	0.08	−0.03	−0.11	−0.1	1.0	−0.03	0.02
0.01	−0.09	−0.09	0.9	−0.01	−0.03	−0.03	1.0	−0.44
0.02	−0.16	−0.12	−0.01	0.02	0.05	0.02	−0.44	1.0

Table 170: Correlation matrix for $17.0 < q^2 < 19.0$ bin for the A_i observables.

A_3	A_4	A_5	$A(A_{\mathrm{FB}})$	A_7	A_8	A_9	A_{6s}	A_{6c}
1.0	−0.13	−0.18	−0.02	0.05	0.03	−0.04	−0.03	0.03
−0.13	1.0	0.22	−0.1	0.02	−0.07	0.04	−0.06	−0.09
−0.18	0.22	1.0	−0.12	−0.11	0.02	0.07	−0.01	−0.22
−0.02	−0.1	−0.12	1.0	−0.0	0.02	0.02	0.9	−0.01
0.05	0.02	−0.11	−0.0	1.0	0.14	−0.2	−0.03	0.07
0.03	−0.07	0.02	0.02	0.14	1.0	−0.04	0.04	−0.04
−0.04	0.04	0.07	0.02	−0.2	−0.04	1.0	0.01	0.01
−0.03	−0.06	−0.01	0.9	−0.03	0.04	0.01	1.0	−0.43
0.03	−0.09	−0.22	−0.01	0.07	−0.04	0.01	−0.43	1.0

Table 171: Correlation matrix for $17.0 < q^2 < 19.0$ bin for the A_i observables.

A_3	A_4	A_5	$A(A_{\mathrm{FB}})$	A_7	A_8	A_9	A_{6s}	A_{6c}
1.0	−0.12	−0.18	0.0	0.01	0.01	−0.05	−0.01	0.03
−0.12	1.0	0.26	−0.14	0.02	−0.08	0.03	−0.07	−0.13
−0.18	0.26	1.0	−0.13	−0.09	0.02	0.07	−0.05	−0.16
0.0	−0.14	−0.13	1.0	0.0	0.01	−0.01	0.9	−0.01
0.01	0.02	−0.09	0.0	1.0	0.14	−0.15	−0.02	0.04
0.01	−0.08	0.02	0.01	0.14	1.0	−0.07	0.0	0.01
−0.05	0.03	0.07	−0.01	−0.15	−0.07	1.0	−0.01	0.02
−0.01	−0.07	−0.05	0.9	−0.02	0.0	−0.01	1.0	−0.43
0.03	−0.13	−0.16	−0.01	0.04	0.01	0.02	−0.43	1.0

Table 172: Correlation matrix for $0.1 < q^2 < 0.98$ bin for the P_i observables.

F_{L}	P_1	P_2	P_3	P_4	P_5	P_6	P_8
1.0	−0.0	0.12	0.09	−0.04	−0.23	−0.04	−0.08
−0.0	1.0	−0.02	−0.05	0.04	0.08	0.01	−0.04
0.12	−0.02	1.0	0.06	−0.05	0.11	0.08	−0.08
0.09	−0.05	0.06	1.0	−0.04	−0.01	−0.1	−0.03
−0.04	0.04	−0.05	−0.04	1.0	−0.22	−0.07	0.07
−0.23	0.08	0.11	−0.01	−0.22	1.0	0.01	−0.07
−0.04	0.01	0.08	−0.1	−0.07	0.01	1.0	−0.08
−0.08	−0.04	−0.08	−0.03	0.07	−0.07	−0.08	1.0

Table 173: Correlation matrix for $1.1 < q^2 < 2.0$ bin for the P_i observables.

F_{L}	P_1	P_2	P_3	P_4	P_5	P_6	P_8
1.0	0.02	−0.09	0.03	0.21	0.44	−0.35	−0.17
0.02	1.0	−0.17	0.03	0.01	0.08	0.04	−0.04
−0.09	−0.17	1.0	−0.31	−0.17	−0.4	0.31	0.11
0.03	0.03	−0.31	1.0	0.1	0.18	−0.1	−0.04
0.21	0.01	−0.17	0.1	1.0	0.16	−0.24	−0.07
0.44	0.08	−0.4	0.18	0.16	1.0	−0.32	−0.21
−0.35	0.04	0.31	−0.1	−0.24	−0.32	1.0	0.09
−0.17	−0.04	0.11	−0.04	−0.07	−0.21	0.09	1.0

Table 174: Correlation matrix for $2.0 < q^2 < 3.0$ bin for the P_i observables.

F_L	P_1	P_2	P_3	P_4	P_5	P_6	P_8
1.0	−0.09	−0.39	−0.0	−0.45	0.2	−0.4	−0.12
−0.09	1.0	0.11	0.01	−0.03	0.02	0.11	−0.01
−0.39	0.11	1.0	−0.03	0.35	−0.24	0.31	0.04
−0.0	0.01	−0.03	1.0	0.04	0.07	−0.01	0.06
−0.45	−0.03	0.35	0.04	1.0	−0.23	0.3	0.08
0.2	0.02	−0.24	0.07	−0.23	1.0	−0.23	−0.03
−0.4	0.11	0.31	−0.01	0.3	−0.23	1.0	0.0
−0.12	−0.01	0.04	0.06	0.08	−0.03	0.0	1.0

Table 175: Correlation matrix for $3.0 < q^2 < 4.0$ bin for the P_i observables.

F_L	P_1	P_2	P_3	P_4	P_5	P_6	P_8
1.0	−0.23	0.08	−0.33	−0.08	−0.23	0.3	0.07
−0.23	1.0	−0.11	0.38	−0.01	−0.05	−0.04	−0.03
0.08	−0.11	1.0	−0.28	0.06	0.07	−0.05	−0.05
−0.33	0.38	−0.28	1.0	−0.03	−0.11	0.18	0.04
−0.08	−0.01	0.06	−0.03	1.0	0.18	−0.03	−0.06
−0.23	−0.05	0.07	−0.11	0.18	1.0	−0.14	−0.03
0.3	−0.04	−0.05	0.18	−0.03	−0.14	1.0	0.21
0.07	−0.03	−0.05	0.04	−0.06	−0.03	0.21	1.0

Table 176: Correlation matrix for $4.0 < q^2 < 5.0$ bin for the P_i observables.

F_L	P_1	P_2	P_3	P_4	P_5	P_6	P_8
1.0	−0.34	−0.08	0.24	−0.27	−0.55	−0.24	0.25
−0.34	1.0	0.31	−0.64	−0.14	−0.24	−0.03	−0.0
−0.08	0.31	1.0	−0.37	−0.13	−0.23	−0.01	−0.01
0.24	−0.64	−0.37	1.0	0.13	0.38	0.17	−0.13
−0.27	−0.14	−0.13	0.13	1.0	0.36	0.07	0.03
−0.55	−0.24	−0.23	0.38	0.36	1.0	0.28	−0.25
−0.24	−0.03	−0.01	0.17	0.07	0.28	1.0	−0.05
0.25	−0.0	−0.01	−0.13	0.03	−0.25	−0.05	1.0

Table 177: Correlation matrix for $5.0 < q^2 < 6.0$ bin for the P_i observables.

F_L	P_1	P_2	P_3	P_4	P_5	P_6	P_8
1.0	−0.28	0.14	0.19	−0.25	−0.14	0.01	−0.13
−0.28	1.0	−0.18	−0.21	0.08	−0.0	−0.04	0.06
0.14	−0.18	1.0	0.13	−0.14	−0.11	0.01	−0.04
0.19	−0.21	0.13	1.0	−0.11	−0.11	0.08	0.07
−0.25	0.08	−0.14	−0.11	1.0	0.17	0.06	0.06
−0.14	−0.0	−0.11	−0.11	0.17	1.0	−0.04	0.07
0.01	−0.04	0.01	0.08	0.06	−0.04	1.0	0.07
−0.13	0.06	−0.04	0.07	0.06	0.07	0.07	1.0

Table 178: Correlation matrix for $6.0 < q^2 < 7.0$ bin for the P_i observables.

F_L	P_1	P_2	P_3	P_4	P_5	P_6	P_8
1.0	−0.21	0.2	−0.15	−0.41	−0.33	0.09	0.12
−0.21	1.0	−0.13	0.06	0.02	−0.07	0.0	−0.07
0.2	−0.13	1.0	0.0	−0.22	−0.16	0.05	0.02
−0.15	0.06	0.0	1.0	0.12	0.1	0.09	0.04
−0.41	0.02	−0.22	0.12	1.0	0.25	−0.04	−0.05
−0.33	−0.07	−0.16	0.1	0.25	1.0	−0.03	−0.04
0.09	0.0	0.05	0.09	−0.04	−0.03	1.0	0.21
0.12	−0.07	0.02	0.04	−0.05	−0.04	0.21	1.0

Table 179: Correlation matrix for $7.0 < q^2 < 8.0$ bin for the P_i observables.

F_L	P_1	P_2	P_3	P_4	P_5	P_6	P_8
1.0	−0.08	0.58	−0.18	−0.26	−0.41	−0.13	−0.16
−0.08	1.0	−0.01	0.03	−0.08	−0.09	0.06	0.03
0.58	−0.01	1.0	−0.19	−0.28	−0.45	−0.12	−0.26
−0.18	0.03	−0.19	1.0	0.05	0.06	0.12	0.11
−0.26	−0.08	−0.28	0.05	1.0	0.26	−0.01	0.13
−0.41	−0.09	−0.45	0.06	0.26	1.0	0.17	0.11
−0.13	0.06	−0.12	0.12	−0.01	0.17	1.0	0.1
−0.16	0.03	−0.26	0.11	0.13	0.11	0.1	1.0

Table 180: Correlation matrix for $11.0 < q^2 < 11.75$ bin for the P_i observables.

F_{L}	P_1	P_2	P_3	P_4	P_5	P_6	P_8
1.0	−0.32	0.6	0.17	0.15	0.02	−0.06	−0.13
−0.32	1.0	−0.24	−0.05	−0.12	−0.19	0.06	0.06
0.6	−0.24	1.0	0.16	−0.03	−0.09	−0.03	−0.14
0.17	−0.05	0.16	1.0	0.05	0.09	0.01	0.07
0.15	−0.12	−0.03	0.05	1.0	0.19	−0.11	−0.14
0.02	−0.19	−0.09	0.09	0.19	1.0	−0.12	−0.1
−0.06	0.06	−0.03	0.01	−0.11	−0.12	1.0	0.24
−0.13	0.06	−0.14	0.07	−0.14	−0.1	0.24	1.0

Table 181: Correlation matrix for $11.75 < q^2 < 12.5$ bin for the P_i observables.

F_{L}	P_1	P_2	P_3	P_4	P_5	P_6	P_8
1.0	−0.41	0.55	−0.1	−0.46	−0.47	−0.37	−0.1
−0.41	1.0	−0.48	0.05	0.15	0.16	0.2	0.04
0.55	−0.48	1.0	−0.19	−0.55	−0.57	−0.4	−0.13
−0.1	0.05	−0.19	1.0	0.11	0.18	0.2	0.09
−0.46	0.15	−0.55	0.11	1.0	0.52	0.4	0.23
−0.47	0.16	−0.57	0.18	0.52	1.0	0.45	0.16
−0.37	0.2	−0.4	0.2	0.4	0.45	1.0	0.22
−0.1	0.04	−0.13	0.09	0.23	0.16	0.22	1.0

Table 182: Correlation matrix for $15.0 < q^2 < 16.0$ bin for the P_i observables.

F_{L}	P_1	P_2	P_3	P_4	P_5	P_6	P_8
1.0	−0.03	0.41	0.09	0.12	0.06	−0.0	0.05
−0.03	1.0	0.07	0.09	−0.15	−0.28	−0.03	0.01
0.41	0.07	1.0	0.08	−0.02	−0.11	−0.01	−0.01
0.09	0.09	0.08	1.0	0.02	0.06	0.1	0.12
0.12	−0.15	−0.02	0.02	1.0	0.34	−0.02	−0.16
0.06	−0.28	−0.11	0.06	0.34	1.0	−0.13	−0.02
−0.0	−0.03	−0.01	0.1	−0.02	−0.13	1.0	0.12
0.05	0.01	−0.01	0.12	−0.16	−0.02	0.12	1.0

Table 183: Correlation matrix for $16.0 < q^2 < 17.0$ bin for the P_i observables.

F_L	P_1	P_2	P_3	P_4	P_5	P_6	P_8
1.0	−0.09	0.33	0.03	0.17	0.23	0.06	−0.01
−0.09	1.0	0.07	0.03	−0.12	−0.14	0.01	−0.02
0.33	0.07	1.0	0.04	−0.15	−0.06	0.02	0.02
0.03	0.03	0.04	1.0	−0.06	−0.18	0.13	0.08
0.17	−0.12	−0.15	−0.06	1.0	0.25	0.09	−0.02
0.23	−0.14	−0.06	−0.18	0.25	1.0	0.02	0.06
0.06	0.01	0.02	0.13	0.09	0.02	1.0	0.14
−0.01	−0.02	0.02	0.08	−0.02	0.06	0.14	1.0

Table 184: Correlation matrix for $17.0 < q^2 < 18.0$ bin for the P_i observables.

F_L	P_1	P_2	P_3	P_4	P_5	P_6	P_8
1.0	−0.07	0.28	0.11	0.04	0.21	−0.06	0.06
−0.07	1.0	0.02	0.07	−0.12	−0.2	0.1	−0.0
0.28	0.02	1.0	0.0	−0.07	0.01	−0.01	0.06
0.11	0.07	0.0	1.0	0.0	−0.03	0.19	0.05
0.04	−0.12	−0.07	0.0	1.0	0.15	0.04	−0.12
0.21	−0.2	0.01	−0.03	0.15	1.0	−0.17	0.08
−0.06	0.1	−0.01	0.19	0.04	−0.17	1.0	0.11
0.06	−0.0	0.06	0.05	−0.12	0.08	0.11	1.0

Table 185: Correlation matrix for $18.0 < q^2 < 19.0$ bin for the P_i observables.

F_L	P_1	P_2	P_3	P_4	P_5	P_6	P_8
1.0	0.03	0.39	0.1	−0.06	−0.01	−0.0	0.06
0.03	1.0	0.02	0.03	−0.14	−0.18	−0.0	0.03
0.39	0.02	1.0	0.0	−0.27	−0.29	−0.03	0.07
0.1	0.03	0.0	1.0	−0.01	−0.03	0.17	0.02
−0.06	−0.14	−0.27	−0.01	1.0	0.38	0.03	0.01
−0.01	−0.18	−0.29	−0.03	0.38	1.0	−0.01	−0.03
−0.0	−0.0	−0.03	0.17	0.03	−0.01	1.0	0.19
0.06	0.03	0.07	0.02	0.01	−0.03	0.19	1.0

Table 186: Correlation matrix for $1.1 < q^2 < 2.5$ bin for the P_i observables.

F_{L}	P_1	P_2	P_3	P_4	P_5	P_6	P_8
1.0	0.05	−0.47	0.11	−0.07	0.43	−0.48	−0.23
0.05	1.0	−0.03	0.0	−0.04	0.09	0.05	−0.02
−0.47	−0.03	1.0	−0.17	0.06	−0.43	0.46	0.17
0.11	0.0	−0.17	1.0	0.07	0.17	−0.1	−0.04
−0.07	−0.04	0.06	0.07	1.0	−0.03	−0.01	0.03
0.43	0.09	−0.43	0.17	−0.03	1.0	−0.38	−0.23
−0.48	0.05	0.46	−0.1	−0.01	−0.38	1.0	0.18
−0.23	−0.02	0.17	−0.04	0.03	−0.23	0.18	1.0

Table 187: Correlation matrix for $2.5 < q^2 < 4.0$ bin for the P_i observables.

F_{L}	P_1	P_2	P_3	P_4	P_5	P_6	P_8
1.0	0.1	−0.16	0.23	−0.35	−0.05	0.08	−0.07
0.1	1.0	−0.11	0.17	−0.09	−0.04	−0.04	−0.07
−0.16	−0.11	1.0	−0.38	0.25	0.01	−0.04	0.02
0.23	0.17	−0.38	1.0	−0.2	−0.01	0.04	−0.0
−0.35	−0.09	0.25	−0.2	1.0	0.07	−0.05	−0.02
−0.05	−0.04	0.01	−0.01	0.07	1.0	−0.06	0.03
0.08	−0.04	−0.04	0.04	−0.05	−0.06	1.0	0.03
−0.07	−0.07	0.02	−0.0	−0.02	0.03	0.03	1.0

Table 188: Correlation matrix for $4.0 < q^2 < 6.0$ bin for the P_i observables.

F_{L}	P_1	P_2	P_3	P_4	P_5	P_6	P_8
1.0	0.2	0.25	−0.27	−0.24	−0.37	−0.13	0.05
0.2	1.0	0.07	−0.15	−0.13	−0.17	−0.02	−0.03
0.25	0.07	1.0	−0.17	−0.16	−0.23	−0.01	−0.02
−0.27	−0.15	−0.17	1.0	0.09	0.17	0.13	0.02
−0.24	−0.13	−0.16	0.09	1.0	0.27	0.05	0.08
−0.37	−0.17	−0.23	0.17	0.27	1.0	0.12	−0.04
−0.13	−0.02	−0.01	0.13	0.05	0.12	1.0	0.04
0.05	−0.03	−0.02	0.02	0.08	−0.04	0.04	1.0

Table 189: Correlation matrix for $6.0 < q^2 < 8.0$ bin for the P_i observables.

F_{L}	P_1	P_2	P_3	P_4	P_5	P_6	P_8
1.0	−0.15	0.41	−0.16	−0.27	−0.3	−0.01	−0.0
−0.15	1.0	−0.06	0.05	−0.05	−0.09	0.04	0.01
0.41	−0.06	1.0	−0.09	−0.21	−0.22	−0.02	−0.07
−0.16	0.05	−0.09	1.0	0.06	0.05	0.12	0.07
−0.27	−0.05	−0.21	0.06	1.0	0.2	−0.04	0.03
−0.3	−0.09	−0.22	0.05	0.2	1.0	0.07	−0.02
−0.01	0.04	−0.02	0.12	−0.04	0.07	1.0	0.15
−0.0	0.01	−0.07	0.07	0.03	−0.02	0.15	1.0

Table 190: Correlation matrix for $11.0 < q^2 < 12.5$ bin for the P_i observables.

F_{L}	P_1	P_2	P_3	P_4	P_5	P_6	P_8
1.0	−0.42	0.75	0.08	−0.12	−0.16	−0.14	−0.07
−0.42	1.0	−0.37	−0.06	−0.03	−0.06	0.09	0.04
0.75	−0.37	1.0	0.06	−0.23	−0.23	−0.15	−0.1
0.08	−0.06	0.06	1.0	0.02	0.08	0.08	0.08
−0.12	−0.03	−0.23	0.02	1.0	0.2	0.03	0.03
−0.16	−0.06	−0.23	0.08	0.2	1.0	0.05	−0.0
−0.14	0.09	−0.15	0.08	0.03	0.05	1.0	0.21
−0.07	0.04	−0.1	0.08	0.03	−0.0	0.21	1.0

Table 191: Correlation matrix for $15.0 < q^2 < 17.0$ bin for the P_i observables.

F_{L}	P_1	P_2	P_3	P_4	P_5	P_6	P_8
1.0	−0.07	0.37	0.06	0.13	0.13	0.03	0.03
−0.07	1.0	0.07	0.06	−0.14	−0.21	−0.01	−0.0
0.37	0.07	1.0	0.06	−0.08	−0.08	0.0	0.01
0.06	0.06	0.06	1.0	−0.02	−0.07	0.11	0.1
0.13	−0.14	−0.08	−0.02	1.0	0.28	0.04	−0.09
0.13	−0.21	−0.08	−0.07	0.28	1.0	−0.04	0.03
0.03	−0.01	0.0	0.11	0.04	−0.04	1.0	0.14
0.03	−0.0	0.01	0.1	−0.09	0.03	0.14	1.0

Table 192: Correlation matrix for $17.0 < q^2 < 19.0$ bin for the P_i observables.

$F_{\rm L}$	P_1	P_2	P_3	P_4	P_5	P_6	P_8
1.0	−0.02	0.3	0.11	0.0	0.11	−0.03	0.05
−0.02	1.0	0.02	0.05	−0.14	−0.19	0.06	0.02
0.3	0.02	1.0	0.0	−0.13	−0.11	−0.03	0.04
0.11	0.05	0.0	1.0	−0.01	−0.04	0.19	0.04
0.0	−0.14	−0.13	−0.01	1.0	0.23	0.03	−0.04
0.11	−0.19	−0.11	−0.04	0.23	1.0	−0.1	0.04
−0.03	0.06	−0.03	0.19	0.03	−0.1	1.0	0.14
0.05	0.02	0.04	0.04	−0.04	0.04	0.14	1.0

Table 193: Correlation matrix for $15.0 < q^2 < 19.0$ bin for the P_i observables.

$F_{\rm L}$	P_1	P_2	P_3	P_4	P_5	P_6	P_8
1.0	−0.05	0.33	0.08	0.08	0.13	0.01	0.03
−0.05	1.0	0.05	0.05	−0.14	−0.21	0.02	0.01
0.33	0.05	1.0	0.03	−0.1	−0.07	−0.01	0.02
0.08	0.05	0.03	1.0	−0.02	−0.06	0.15	0.07
0.08	−0.14	−0.1	−0.02	1.0	0.24	0.04	−0.07
0.13	−0.21	−0.07	−0.06	0.24	1.0	−0.07	0.03
0.01	0.02	−0.01	0.15	0.04	−0.07	1.0	0.14
0.03	0.01	0.02	0.07	−0.07	0.03	0.14	1.0

N Difference between Reco12 and Reco14

N.1 Overlap between Reco12 and Reco14

The difference between the angular distributions in $B^0 \to J/\psi K^{*0}$ for `Reco12-Stripping17` and `Reco14-Stripping20r1` were checked on data using the `Reco12-Stripping17` stripped candidates, where either the `Reco12` or `Reco14` reconstruction was rerun. For more details see Ref. [13]. A simplified selection was used to select a pure sample of $B^0 \to J/\psi K^{*0}$ events, with cuts on the p_{T} of the final state particles, the B^0 flight direction and the PID variables of the π^- and the K^+ applied. Furthermore only one candidate per event was allowed. The comparison of the B^0 mass and helicity angles for events which are unique in their corresponding sample is shown in Fig. 225. The B^0 candidate mass and the angular distributions are compatible, however in Fig. 226 one can see that the value of these distributions can differ on an event-by-event basis.

In Fig. 227 the event-by-event difference is shown for q^2 and the helicity angles in the overlapping dataset for $B^0 \to K^{*0}\mu^+\mu^-$. These plots are made using the `Reco12-Stripping17` and the 2011 part of the `Reco14-Stripping20r1` tuple of the $B^0 \to K^{*0}\mu^+\mu^-$ analysis, *i.e.* in addition to the changes in the reconstruction shown in the other two figures, also the changes in the selection and the BDT are included. Still, one can see that the differences are of the same order as for the re-reconstructed $B^0 \to J/\psi K^{*0}$ events. When assuming a difference of $10\,\mathrm{MeV}/c^2$ in the reconstructed mass for the calculation of q^2 at a q^2 of $9\,\mathrm{GeV}^2/c^4$ (as seen in $B^0 \to J/\psi K^{*0}$), this leads to a difference in q^2 of: $3^2\,\mathrm{GeV}^2/c^4 - (3-0.01)^2\,\mathrm{GeV}^2/c^4 \approx 0.06\,\mathrm{GeV}^2/c^4$, which is well compatible with what is seen in $B^0 \to K^{*0}\mu^+\mu^-$.

N.2 Observables from a counting method

To check the impact of the differences between the `Reco12-Stripping17` and the `Reco14-Stripping20r1` $B^0 \to K^{*0}\mu^+\mu^-$ dataset, the results for the observables S_4, S_5, S_7 and S_8, obtained with a "counting experiment" (for details, see Ref. [50]) were compared on the `Reco12-Stripping17` dataset and on the 2011 part of the `Reco14-Stripping20(r1)` data set. The results are shown in Figs. 228, 229, 230, and 231. All events were weighted with an event-weight accounting for the acceptance. The B^0 candidate mass distribution was fitted with the mass shape taken from $B^0 \to J/\psi K^{*0}$ used in Ref. [50] for both datasets. Note that the binning scheme is not the same as in the 2011 analysis, as not exactly the same cuts were used to cut out the contributions from the J/ψ the $\psi(2S)$ resonances, and that there are more unique events in the `Reco14-Stripping20` sample than in the `Reco12-Stripping17` sample. This, in addition to the fact the the unique events are more dominated by background events, can lead to difficulties in the mass fit, as observed in some bins.

As can be seen from these plots, all distributions with the unique events show an agreement compatible with the fact that these datasets are statistically independent but follow the same underlying distribution, while the overlapping datasets show a very good

Figure 225: Angular distributions and B^0 candidate mass for $B^0 \to J/\psi K^{*0}$ with `Reco12-Stripping17` and `Reco12-Stripping20r1` for events unique in the corresponding data sets.

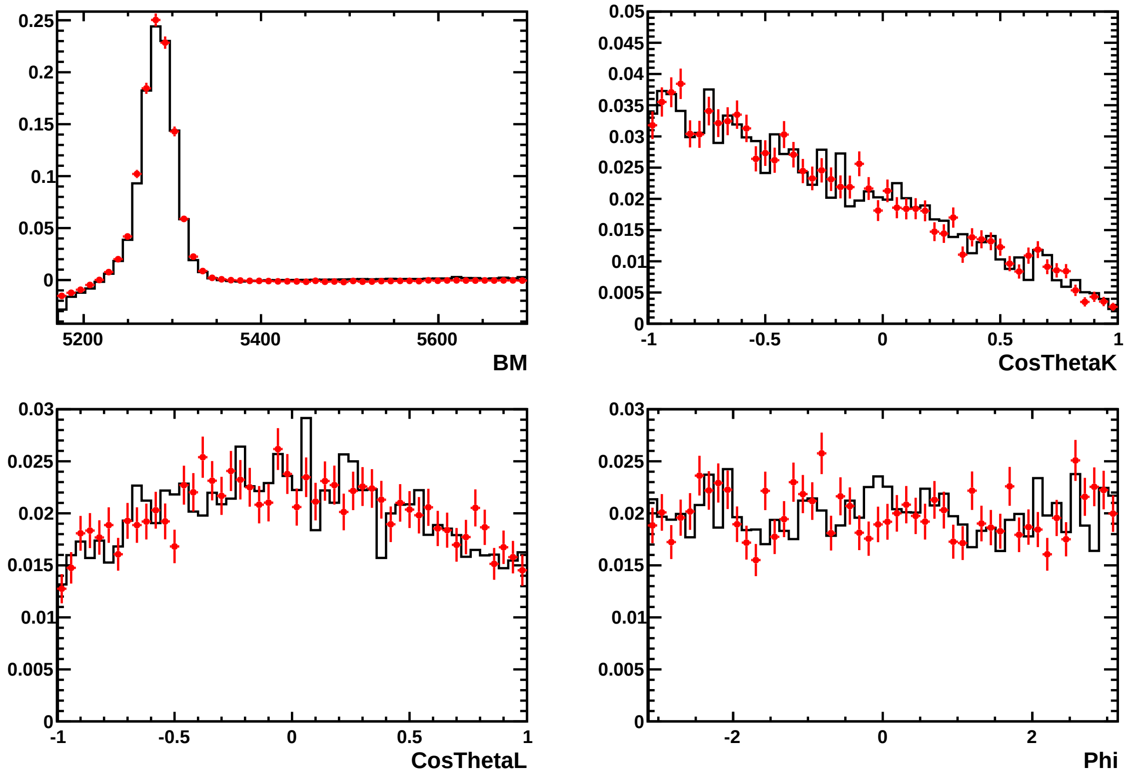

agreement.

N.3 Observables from the folded fit

In order to cross check that the differences between Reco12 and Reco14 does not give sizable effects for the angular observables, the analysis performed last year is repeated using the folding technique for the 2011 data reconstructed using `Reco12` and `Reco14`. Since about 35% of the events are unique in each reconstruction version we expect to observe statistical deviations in this comparison. Three kinds of comparison have been performed: analysis of the full 2011 dataset for Reco12 and Reco14 (Fig. 232); analysis of the full Reco12 dataset compared with unique events in Reco14 (Fig. 234); analysis of overlapping events in Reco12 and Reco14 (Fig. 233). As can be observed in the figures perfect agreement (almost exact) is observed for overlapping events. Small differences are expected in this case due to the angular and q^2 resolution. Statistical agreement is observed in the comparison of the two statistically independent sample full Reco12 and unique events in Reco14. It should be noted that some of the fit do not converge nicely given the small statistics, however this does not change our conclusions. The only

Figure 226: Difference of angular observables and B^0 candidate mass for $B^0 \to J/\psi K^{*0}$ with `Reco12-Stripping17` and `Reco12-Stripping20r1` for events that are in both datasets.

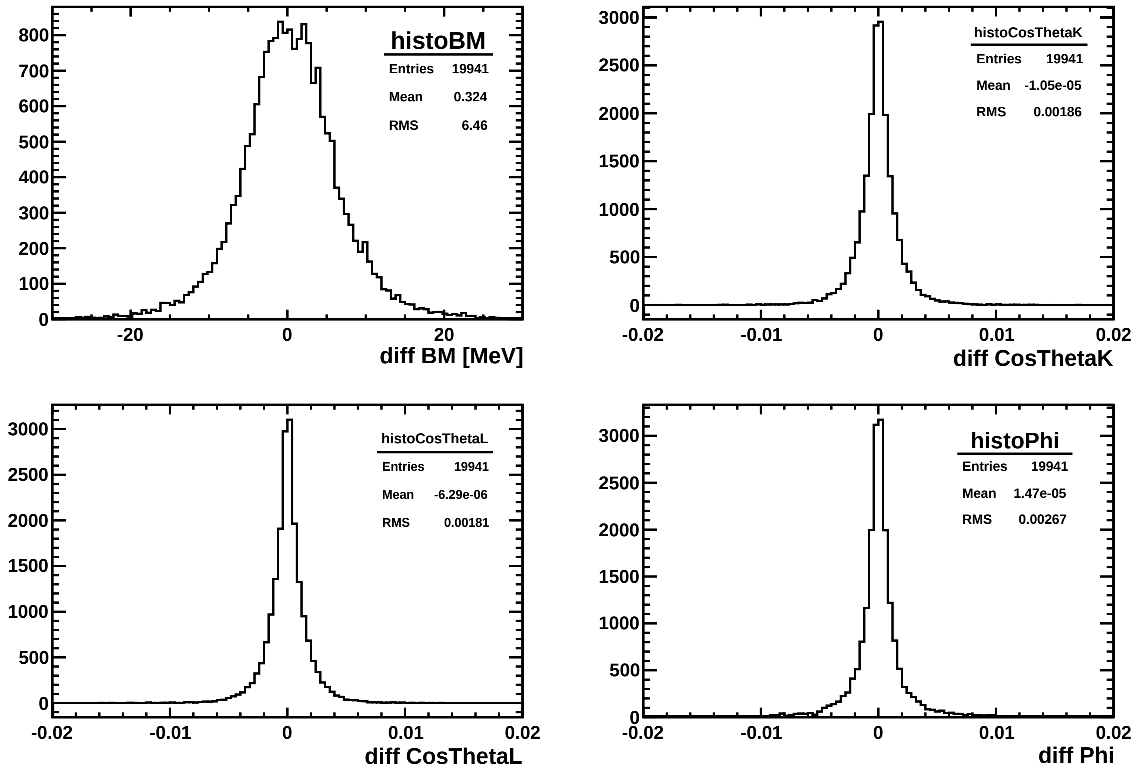

1953 exception is the fourth bin of the observable P_4' at large q^2 which show a significant larger
1954 than expected disagreement. This effect is currently under investigation.

Figure 227: Difference of angular observables and q^2 candidate mass for $B^0 \to K^{*0}\mu^+\mu^-$ with `Reco12-Stripping17` and `Reco12-Stripping20r1` for events that are in both datasets.

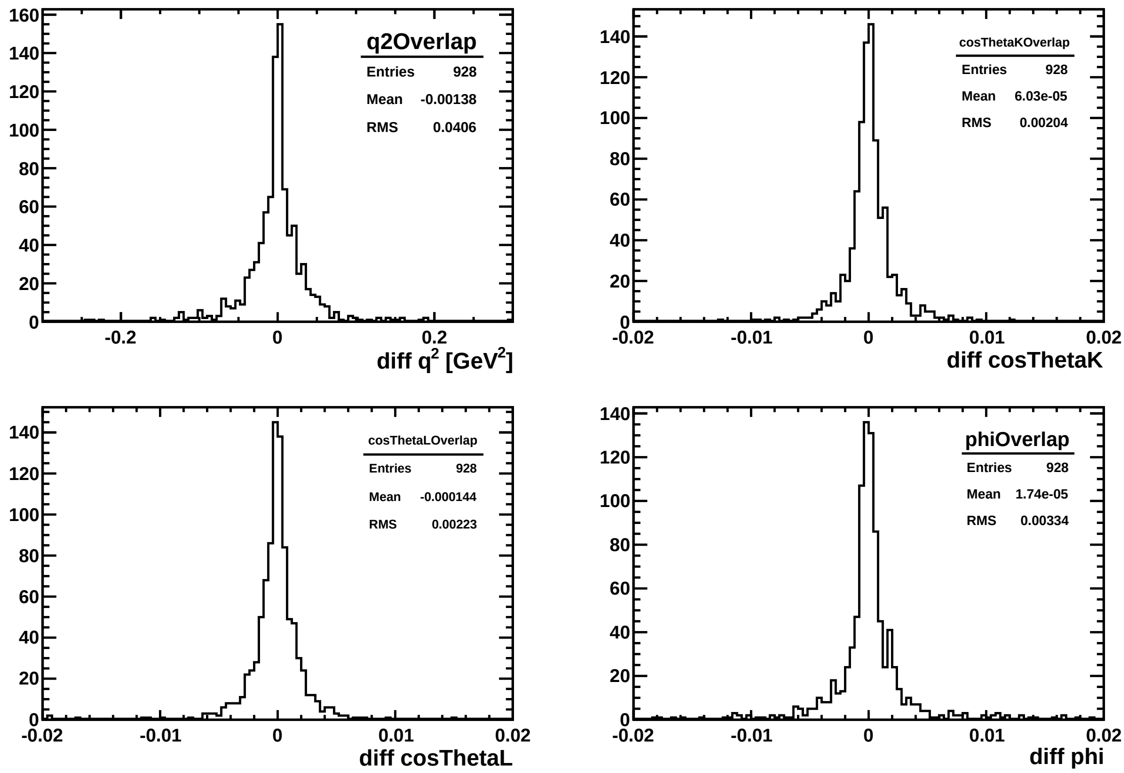

Figure 228: Results for S_4 using a counting experiment for overlapping events (left) and unique events (right) of the Reco12 and Reco14 datasets. In red are the Reco14 events, in black the Reco12 events.

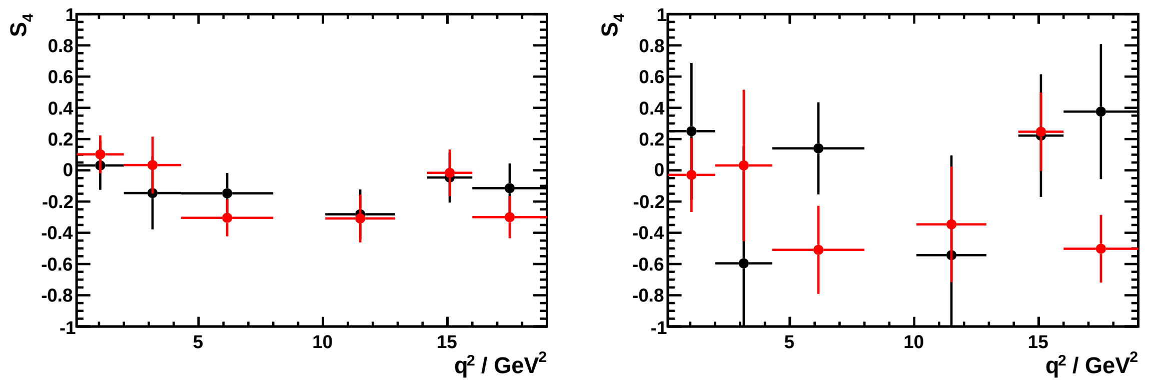

Figure 229: Results for S_5 using a counting experiment for overlapping events (left) and unique events (right) of the Reco12 and Reco14 datasets. In red are the Reco14 events, in black the Reco12 events.

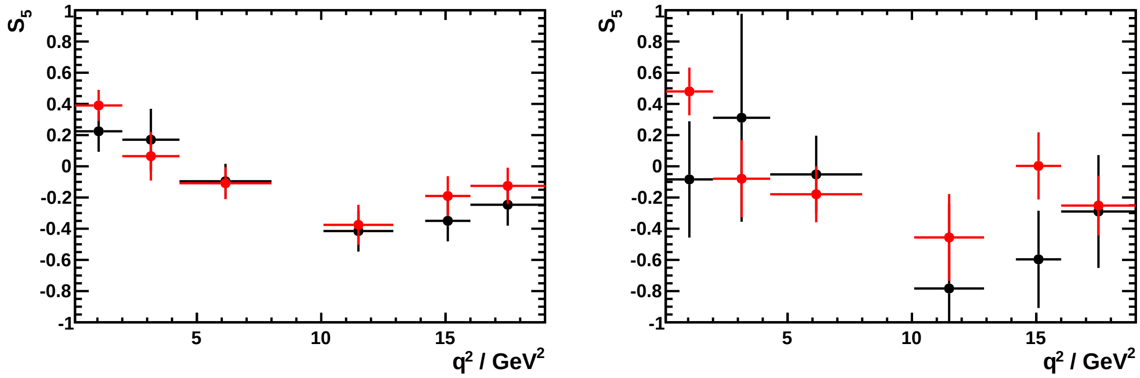

Figure 230: Results for S_7 using a counting experiment for overlapping events (left) and unique events (right) of the Reco12 and Reco14 datasets. In red are the Reco14 events, in black the Reco12 events.

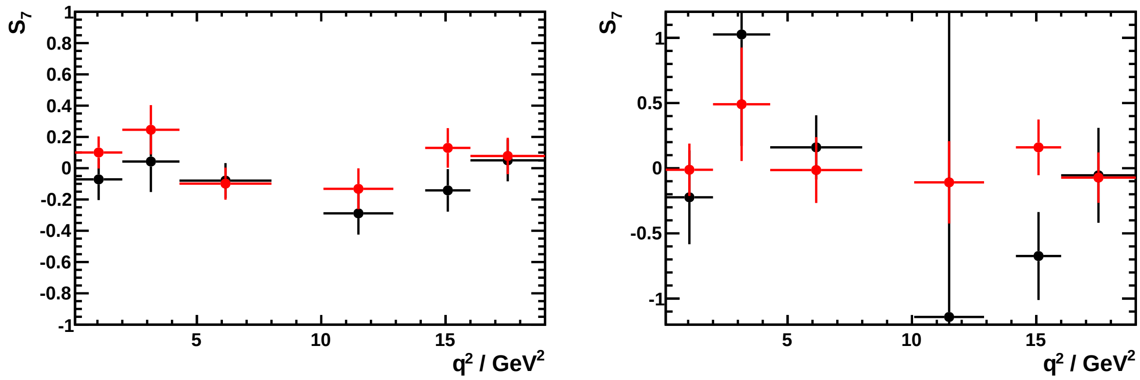

Figure 231: Results for S_8 using a counting experiment for overlapping events (left) and unique events (right) of the Reco12 and Reco14 datasets. In red are the Reco14 events, in black the Reco12 events.

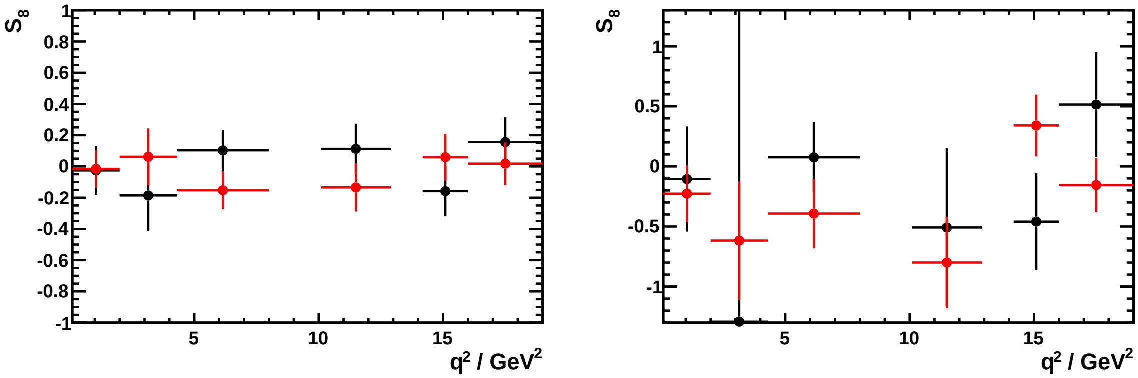

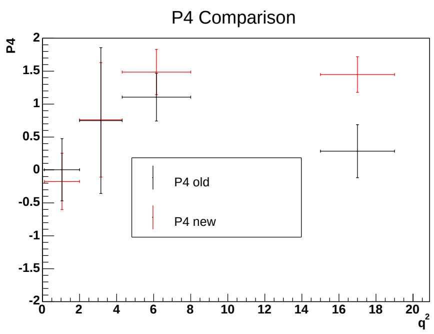

(a) P_4'

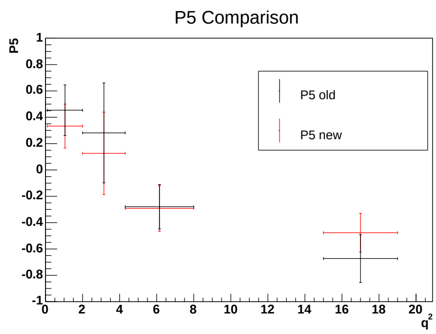

(b) P_5'

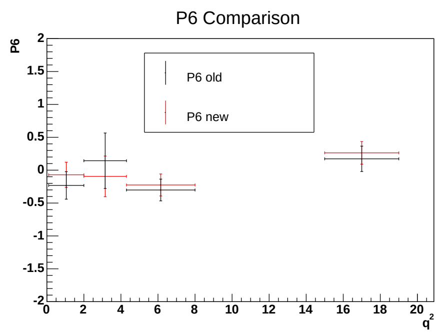

(c) P_6'

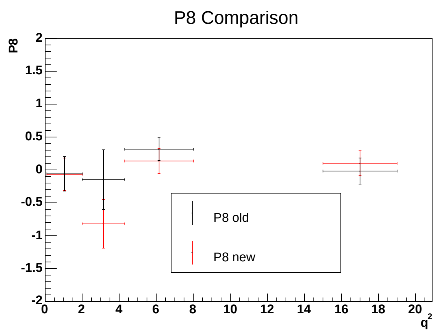

(d) P_8'

Figure 232: Comparison between the P_i' observables for full (2011) Reco12 dataset and full (2011) Reco14 dataset.

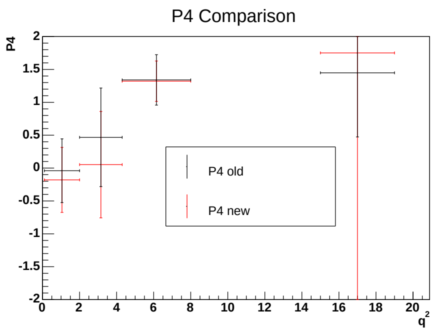

(a) P_4'

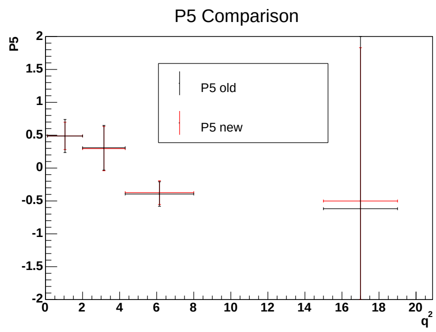

(b) P_5'

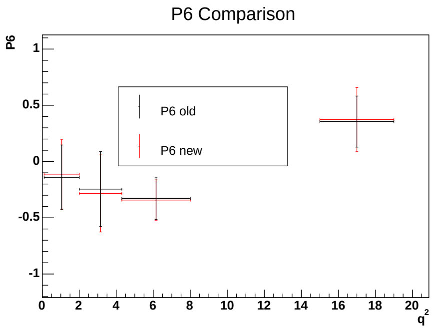

(c) P_6'

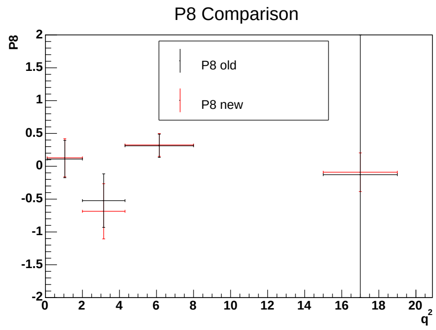

(d) P_8'

Figure 233: Comparison between the P_i' observables for overlapping events in (2011) Reco12 dataset and in (2011) Reco14 dataset.

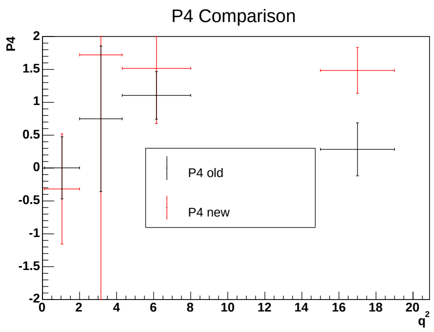

(a) P_4'

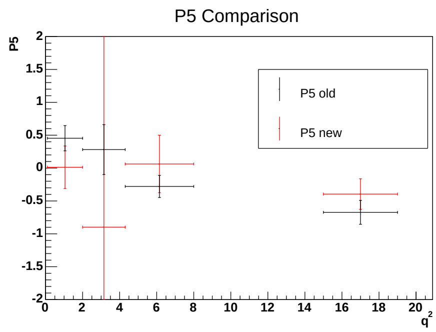

(b) P_5'

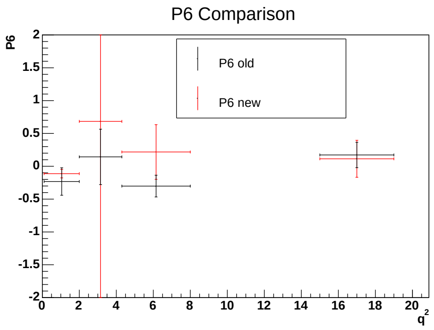

(c) P_6'

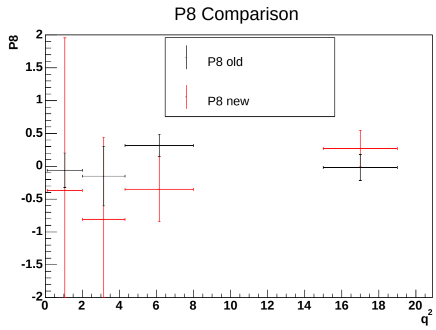

(d) P_8'

Figure 234: Comparison between the P_i' observables for full (2011) Reco12 dataset and unique events in (2011) Reco14 dataset.

O Performance comparison for determination of observables

Several toy studies are performed to evaluate the performance of the fitter. For the following studies the nomial fitter for the observables is used. A detailed comparison with a `RooFit` based fitter was done and no major differences were found. For the toy studies the `EOS` MC sample including background, but without acceptance correction is used (see Sec. 3.2). The large sample is divided into subsets which correspond to the yields shown in Tab. 12.

In each subset the angular observables are determined separately and compared to the values which were used for the generation (see Tab 3). In the following three different methods are compared: The nominal fit, the folded fit and the method of moments. The sensitivity is determined from the widths of the distribution of the angular observables (σ from a fit of a Gaussian). The values which were obtained for different q^2 regions can be seen in Fig. 235. The dependence on q^2 is introduced due to a different number of signal events and different values of the parameters in each bin. In general the folded fit and the full fit have similar sensitivities and the method of moments performs around 10% worse.

To check the bias of the methods pull distributions are generated ($(S_{i,\text{fitted}} - S_{i,\text{generated}})/\sigma_{S_i}$) and fitted with a Gaussian. The mean of these Gaussians is shown in Fig. 236 and the width in Fig. 237. The mean of the Gaussians is ideally zero. Whereas the Method of Moments is most stable and is in every q^2 bin unbiased the fits show in some bins statistical significant deviations. The bias depends on the number of events in each bin and it is tested that the bias gets insignificant if the number of events is enhanced. A detailed discussion of the bias was done in Sec. 6.2.9. The widths of the Gaussians is expected to be one. A larger width means that the error in the Fit is underestimated. To guarantee a correct error the method of coverage correction is applied for the real fit on data as described in Sec. 6.2.10.

P Treatment of S-wave for determination of observables

The toys studies done in the last subsection do not include a possible S-wave contribution. However, a priori the S-wave contribution (including all interferences terms) in the $B^0 \to K^{*0}\mu^+\mu^-$ channel is not known.

As the `EOS` MC does not include a S-wave contribution, toy events are generated according to a pdf including 10% S-wave fraction (thus $F_S = 0.1$, all interference terms are set to zero). Two possible scenarios are compared. In the first case, events are generated including the S-wave contribution, however in the fit pdf the S-wave is ignored. In the second case, the S-wave is generated and also fitted for. Both cases are compared to the nominal case, where the S-wave is neither generated nor fitted for.

The mean and sigma of the pulls for the different methods are shown in Fig. 238 and

Fig. 239. If the S-wave is ignored, this results in an extreme bias of the mean of up to 80%. If the S-wave is included into the fit, the additional bias gets statistical insignificant. However, in the latter case the statistical sensitivity of the methods is reduced, as can be seen in Fig. 240. What also can be seen is that an additional prior to F_S would reduce this sensitivity loss significantly. Nevertheless, also without this prior, it is possible to include the S-wave in the Fit to $B^0 \to K^{*0}\mu^+\mu^-$.

Q Angular observables from the decay $B^0 \to J/\psi\, K^{*0}$

A fit to the full data sample of 2011 and 2012 data (± 60 MeV around the nominal J/ψ mass) is performed comparing the different methods to determine the angular observables. The fit is the nominal four-dimensional unbinned maximum likelihood fit in $m(K^+\pi^+\mu^+\mu^-)$ and the three decay angles $\cos\theta_l$, $\cos\theta_K$ and ϕ. The mass shapes are parametrized as discussed in Sec. 5.1. For the angular distribution of the signal, the full PDF including S-wave as given in Sec. 6.2.1 is used. The background is parametrized using Chebyshev polynomials.

There are two possibilities how to implement the angular acceptance. One possibility is to include it using weights which are shown in Fig. 241. The weights are derived on an event-by-event basis and are the inverse of the efficiency for given combination of $\cos\theta_\ell, \cos\theta_K, \phi$ and q^2 which is described in Chapt. 8. These weights are also used to account for the angular acceptance in the method of moments. In this case each weight is additionaly multiplied by the *sWeight* to statistically separate the signal component. The second possibility is to implement the acceptance directly in the PDF of the fit. In this case the differential decay rate is multiplied by the expected efficency in this phase space region, as described in Sec. 6.2.3.

The result for the two fits and the method of moments is given in Tab. 194. The projections of the mass of the three methods (for the MoM the fit to get the sWeights) is shown in Fig. 242.

There is a good agreement betweem all three methods compared to the expected statistical uncertainty expected for the fits of the signal decay $B^0 \to K^{*0}\mu^+\mu^-$. The projections of the weighted fit are shown in Fig. 243 and 244. Furthermore two-dimensional pulls are shown in Figs. 245– 247, showing that, accounting for the acceptance effect, the data is well described by the PDF.

Table 194: Result of the observables fit and the method of moments for $B^0 \to J/\psi K^{*0}$ data of 2011+2012. In the fit the angular acceptance is either folded into the pdf (no weights) or implemented using weights (weights). For the method of moments events are weighted with the product of the *sWeight* times the acceptance weight. All methods agree to a level which is sufficient for the $B^0 \to K^{*0}\mu\mu$ analysis.

parameter	Full Fit (no weights)	Full Fit (weights)	MoM (weights)
f_{sig}	0.9485 ± 0.0009	0.9430 ± 0.0010	0.9467 ± 0.0011
m_{B^0}	5284.33 ± 0.04	5284.32 ± 0.04	5284.32 ± 0.05
$f_{CB1/CB2}$	0.745 ± 0.024	0.746 ± 0.030	0.725 ± 0.028
$\sigma_{CB\mathrm{m},1}$	15.61 ± 0.17	15.68 ± 0.20	15.56 ± 0.19
$\sigma_{CB\mathrm{m},2}$	27.45 ± 0.86	$27.5 \pm 1.$	26.94 ± 0.87
n_{CB}(fixed)	5.2	5.2	5.2
α_{CB1}	1.493 ± 0.018	1.477 ± 0.020	1.469 ± 0.020
α_{CB2}	1.780 ± 0.067	1.837 ± 0.096	1.683 ± 0.060
α_{bkg}	0.00503 ± 0.00009	0.00543 ± 0.00009	0.00522 ± 0.00010
$\Delta m_{B^0_s}$	90.23 ± 0.85	89.51 ± 0.92	89.11 ± 0.83
$f_{B^0_s/B^0}$	0.01088 ± 0.00042	0.01125 ± 0.00049	0.0123 ± 0.0005
S_{1s}	0.3309 ± 0.0010	0.3332 ± 0.0011	0.3340 ± 0.0011
S_3	0.0015 ± 0.0019	0.0015 ± 0.0020	0.0012 ± 0.0021
S_4	-0.2774 ± 0.0020	-0.2773 ± 0.0021	-0.2813 ± 0.0024
S_5	-0.0018 ± 0.0020	-0.0018 ± 0.0020	-0.0033 ± 0.0023
S_{6s}	0.0017 ± 0.0016	0.0017 ± 0.0018	0.0012 ± 0.0017
S_7	0.0009 ± 0.0020	0.0014 ± 0.0021	0.0013 ± 0.0024
S_8	-0.0507 ± 0.0020	-0.0510 ± 0.0021	-0.0534 ± 0.0024
S_9	-0.0874 ± 0.0019	-0.0883 ± 0.0020	-0.0878 ± 0.0021
F_s	0.0833 ± 0.0031	0.0860 ± 0.0033	0.0834 ± 0.0040
S_{S1}	-0.2292 ± 0.0034	-0.2361 ± 0.0033	-0.2363 ± 0.0040
S_{S2}	0.0003 ± 0.0022	0.0016 ± 0.0024	0.0023 ± 0.0025
S_{S3}	0.0024 ± 0.0021	0.0025 ± 0.0022	0.0035 ± 0.0024
S_{S4}	0.0013 ± 0.0021	0.0016 ± 0.0023	0.0018 ± 0.0024
S_{S5}	-0.0655 ± 0.0023	-0.0661 ± 0.0025	-0.0653 ± 0.0025
$c_{l,1}$	-0.013 ± 0.018	-0.017 ± 0.018	–
$c_{l,2}$	-0.450 ± 0.021	-0.469 ± 0.021	–
$c_{K,1}$	0.557 ± 0.018	0.572 ± 0.018	–
$c_{K,2}$	0.261 ± 0.016	0.296 ± 0.015	–
$c_{\phi,1}$	-0.0096 ± 0.0059	-0.0126 ± 0.0058	–
$c_{\phi,2}$	0.0001 ± 0.0018	0.0005 ± 0.0018	–

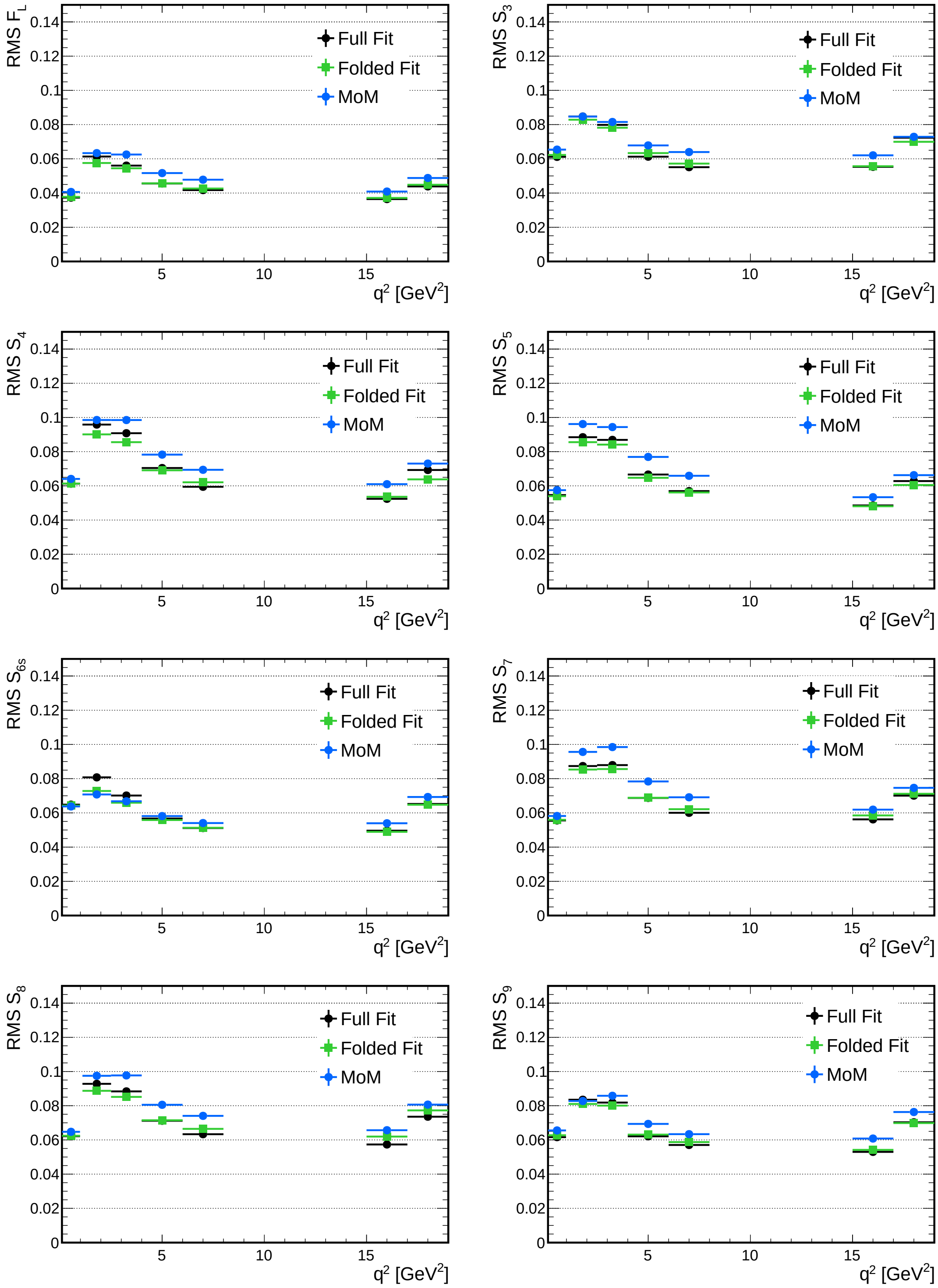

Figure 235: RMS of the P-wave observables vs q^2 for the full and folded fit, and the method of moments.

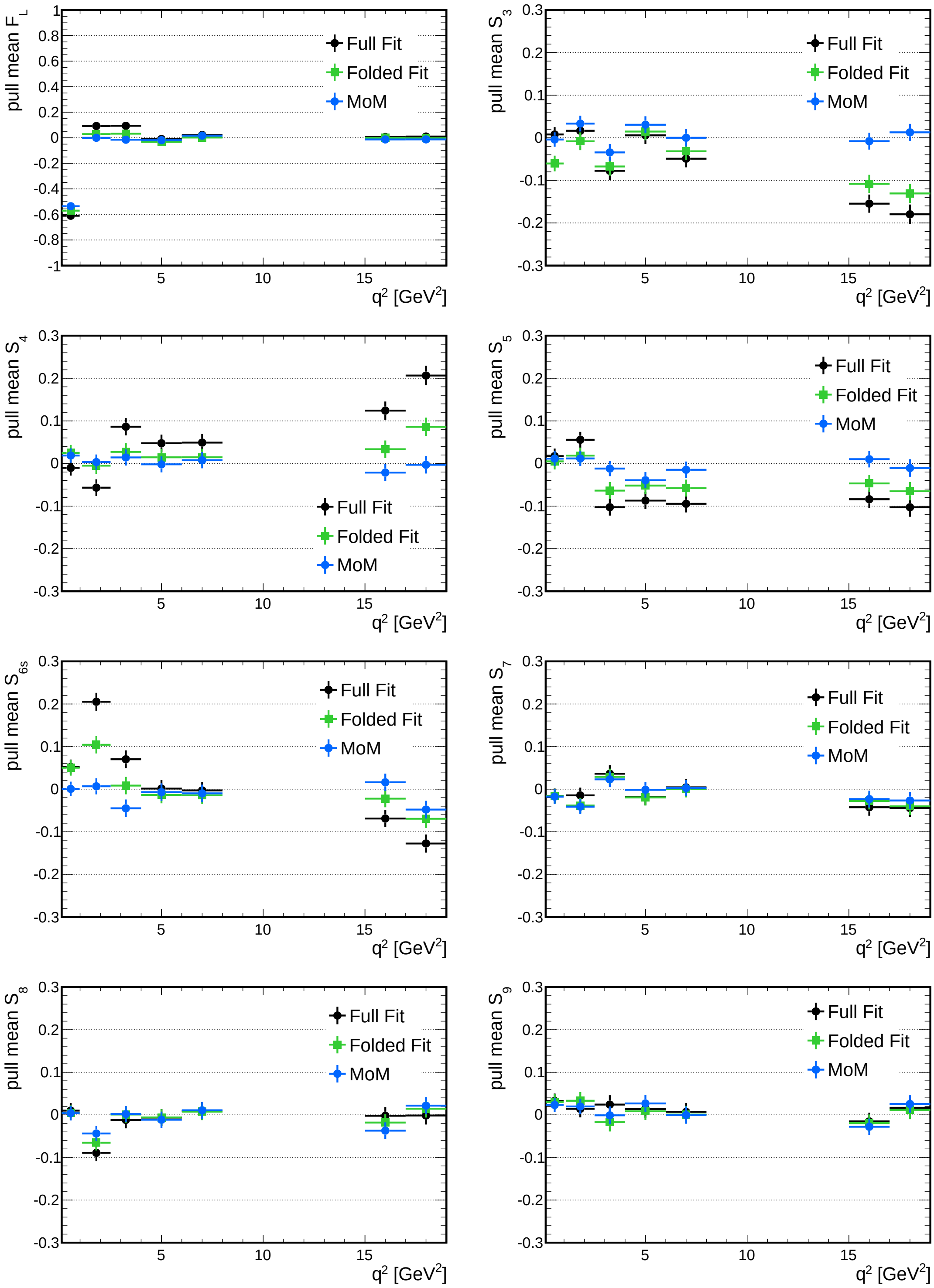

Figure 236: Mean of the pulls of the P-wave observables vs q^2 for the full and the folded fit, and the method of moments.

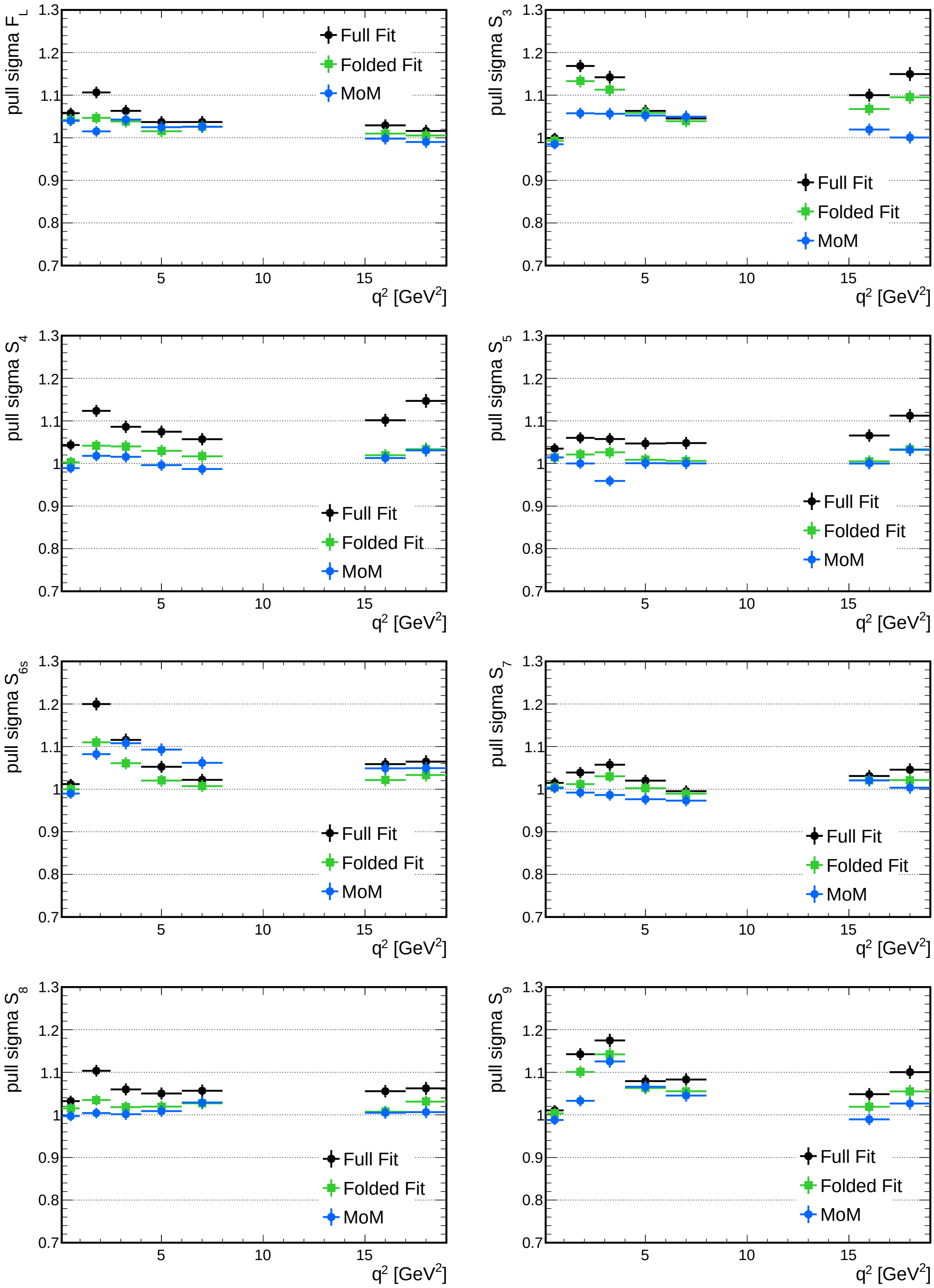

Figure 237: Sigma of the pulls of the P-wave observables vs q^2 for the full and the folded fit, and the method of moments.

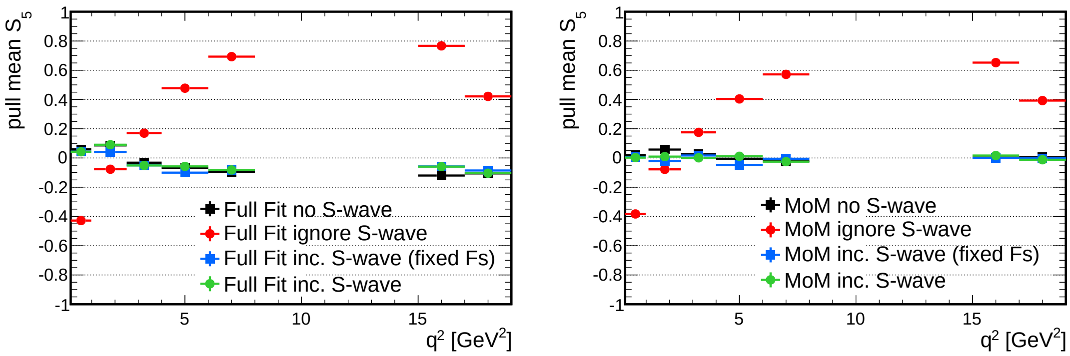

Figure 238: Mean of the pull distributions for the Full Fit (left) and the Method of Moments (right) vs. q^2. In the 'no S-wave' case the S-wave is neither generated nor fitted. In the 'ignore' case the S-wave is generated and neglected in the fit. In the case 'inc. S-wave' the S-wave is both generated and fitted. The main challenge in fitting the S-wave is the determination of F_S, which is illustrated by the case 'inc. S-wave (fixed F_S)', in which case F_S is fixed to the generated value.

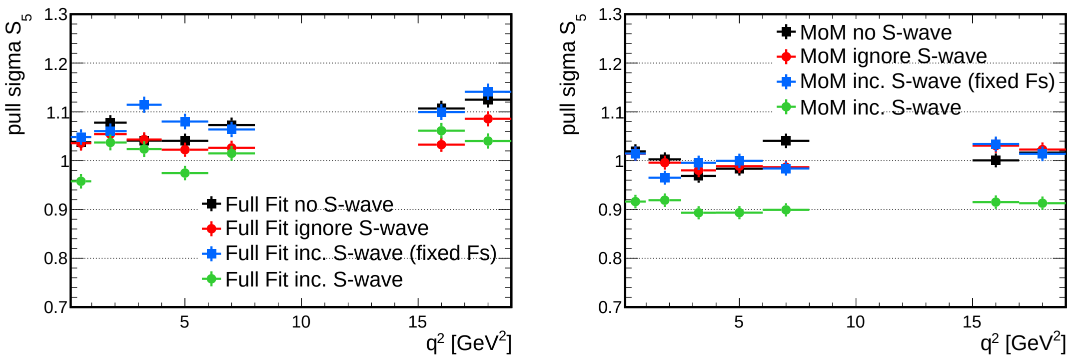

Figure 239: Sigma of the pull distributions for the Full Fit (left) and the Method of Moments (right) vs. q^2. In the 'no S-wave' case the S-wave is neither generated nor fitted. In the 'ignore' case the S-wave is generated and neglected in the fit. In the case 'inc. S-wave' the S-wave is both generated and fitted. The main challenge in fitting the S-wave is the determination of F_S, which is illustrated by the case 'inc. S-wave (fixed F_S)', in which case F_S is fixed to the generated value.

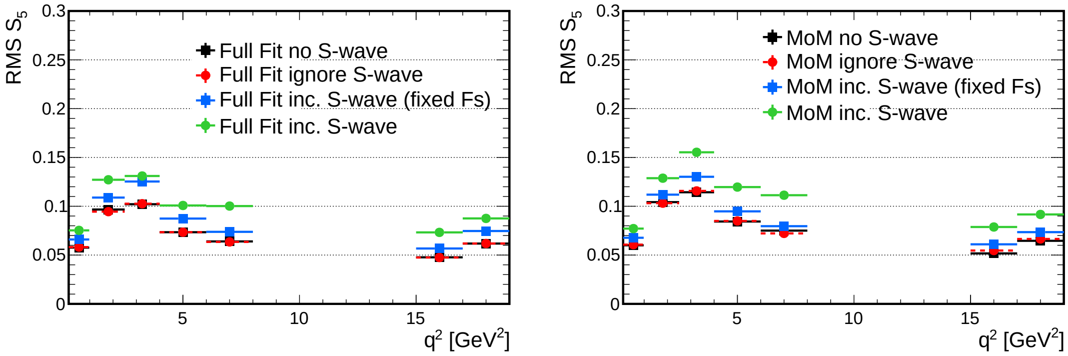

Figure 240: RMS for the different methods vs. q^2. In the 'no S-wave' case the S-wave is neither generated nor fitted. In the 'ignore' case the S-wave is generated and neglected in the fit. In the case 'inc. S-wave' the S-wave is both generated and fitted. The main challenge in fitting the S-wave is the determination of F_S, which is illustrated by the case 'inc. S-wave (fixed F_S)', in which case F_S is fixed to the generated value.

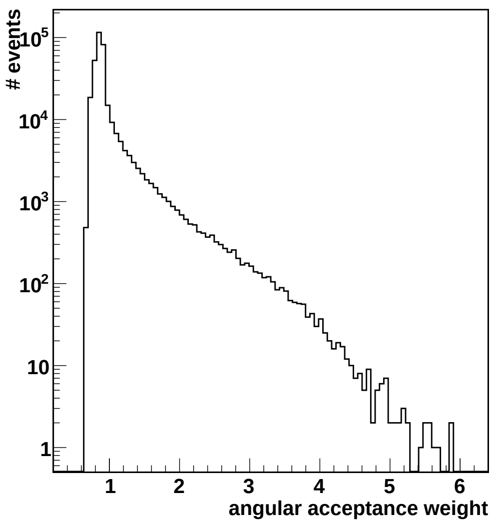

Figure 241: Weights for the $B^0 \to J/\psi K^{*0}$ events to take the angular acceptance int account. The angular acceptance is described in Chapt. 8, the weights are the inverse of the expected efficiency of the data event for a given point in the phase-space.

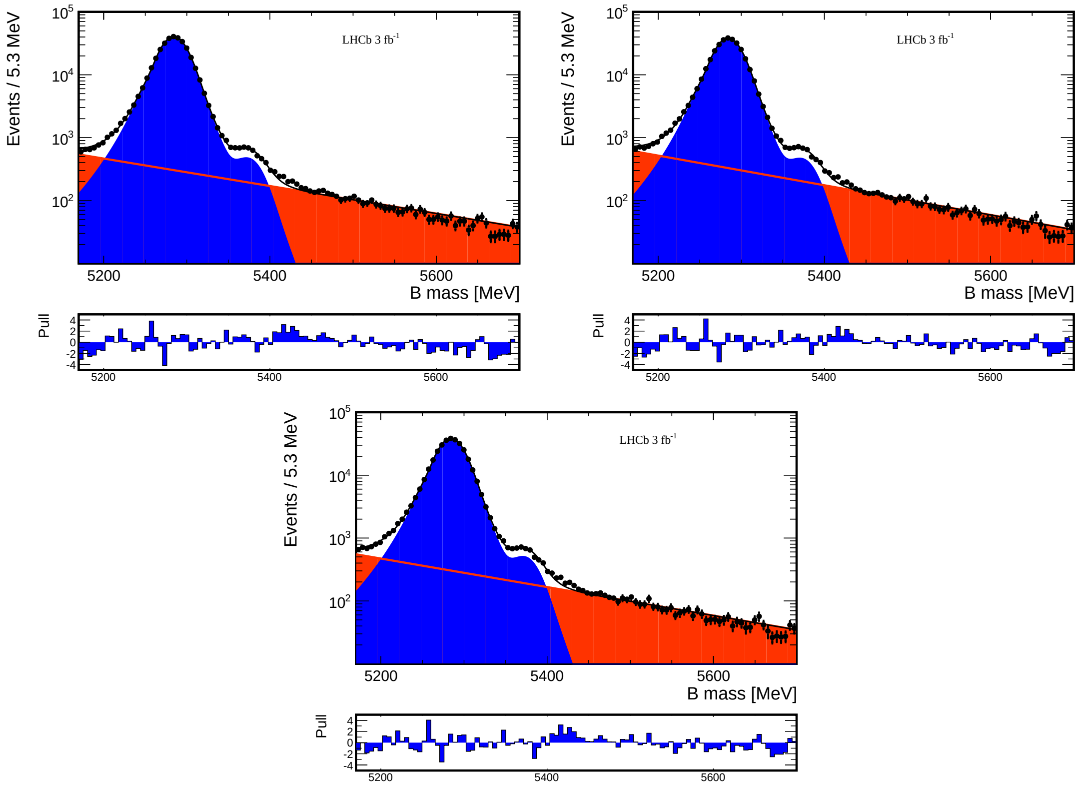

Figure 242: Projections of the mass for the three methods to extract the angular parameters from the decay $B^0 \to J/\psi K^{*0}$ (compare Tab. 194). The top left plots shows the non-weighted fit, the top right the weighted fit, and the lower plot the fit to get the sWeights for the Method of Moments.

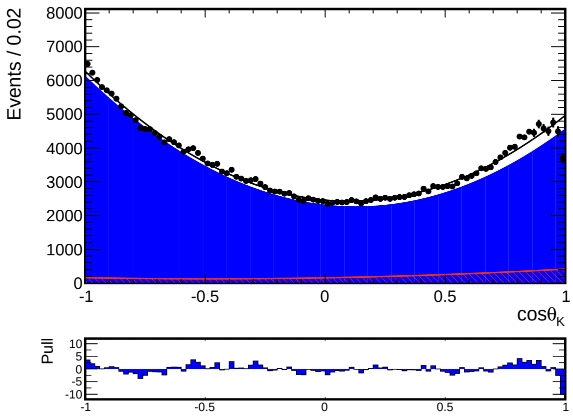

Figure 243: Projections of the full (weighted) fit to $B^0 \to J/\psi K^{*0}$ for $\cos\theta_K$ for all available data of 2011+2012.

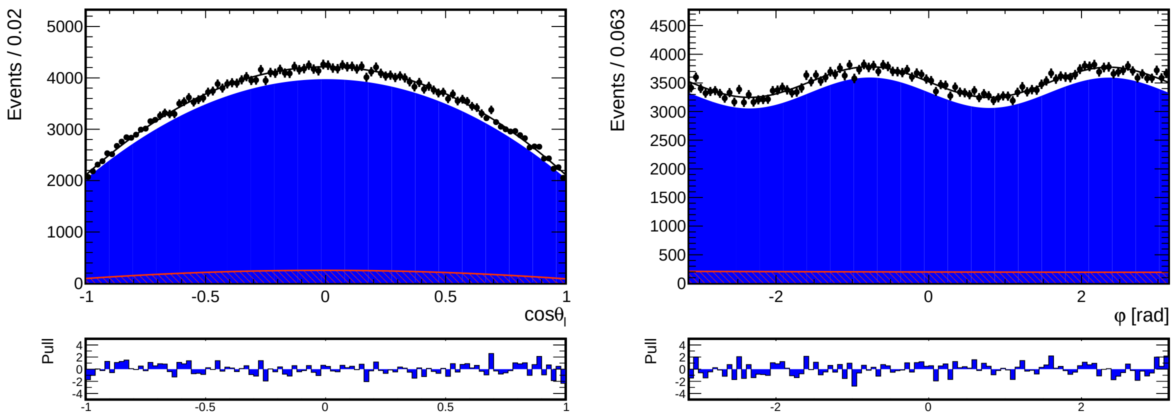

Figure 244: Projections of the full (weighted) fit to $B^0 \to J/\psi\, K^{*0}$ for ϕ and $\cos\theta_\ell$ for all available data of 2011+2012.

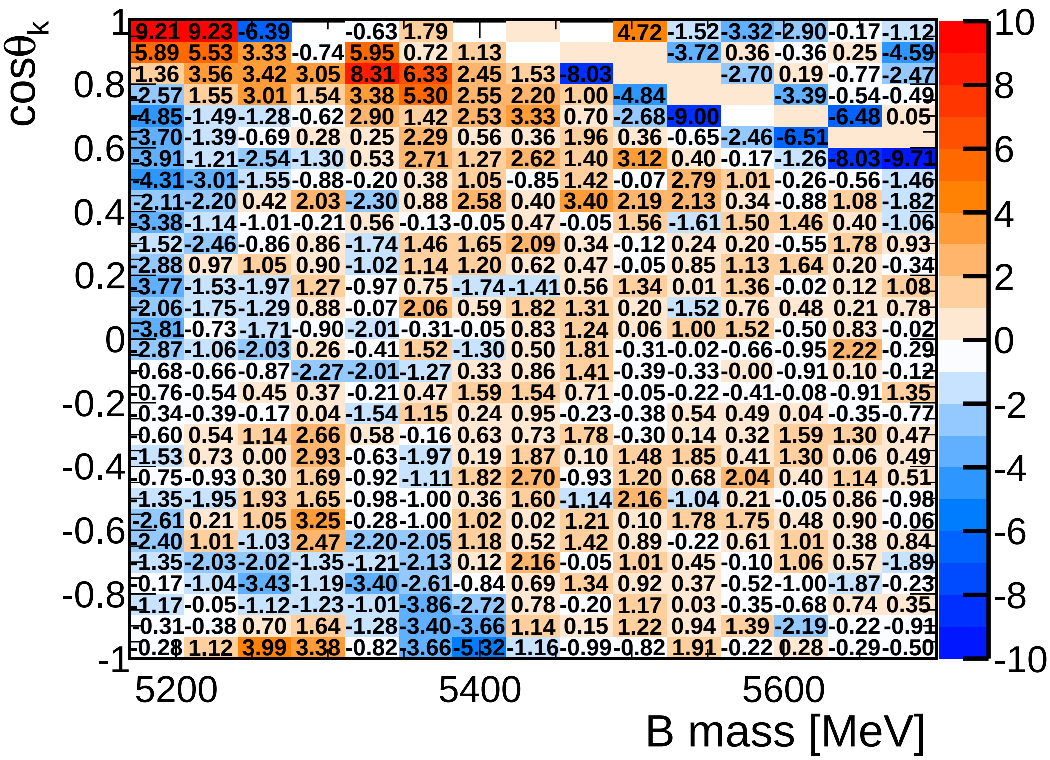

Figure 245: 2D pull of $\cos\theta_K$ vs mass of the full (weighted) fit to $B^0 \to J/\psi\, K^{*0}$ for all available data of 2011+2012. The diagonal region with no events stems from the veto-cut on $B^+ \to K^+\mu^+\mu^-$.

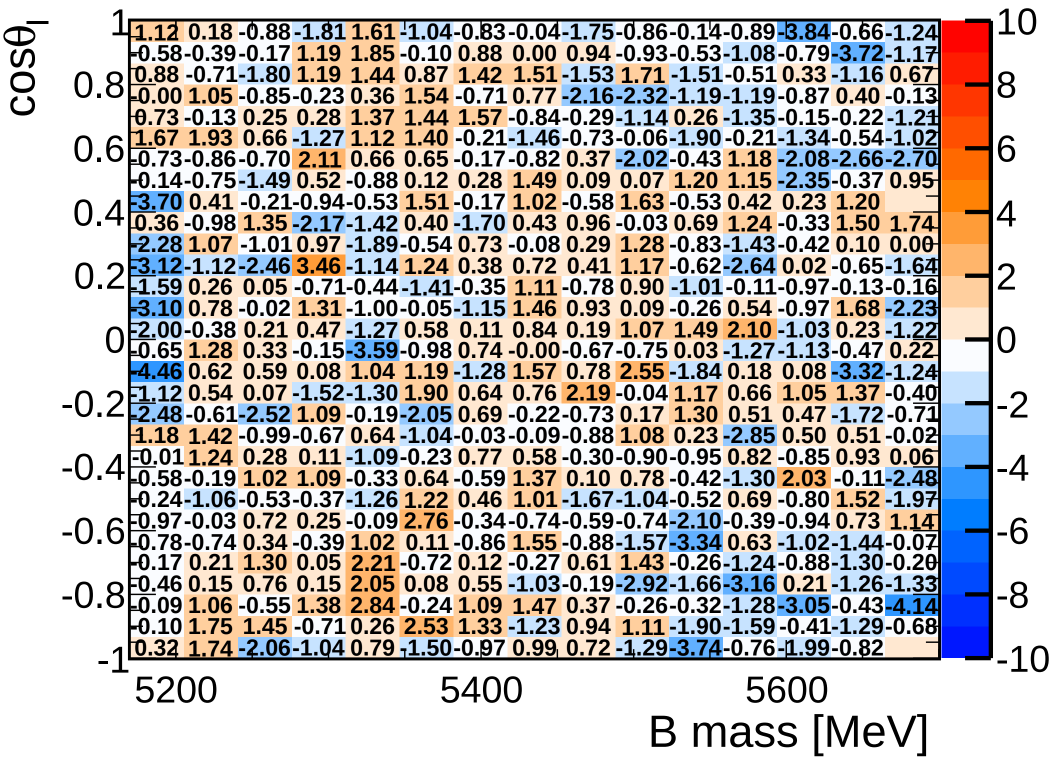

Figure 246: 2D pull of $\cos\theta_\ell$ vs mass of the full (weighted) fit to $B^0 \to J/\psi\, K^{*0}$ for all available data of 2011+2012.

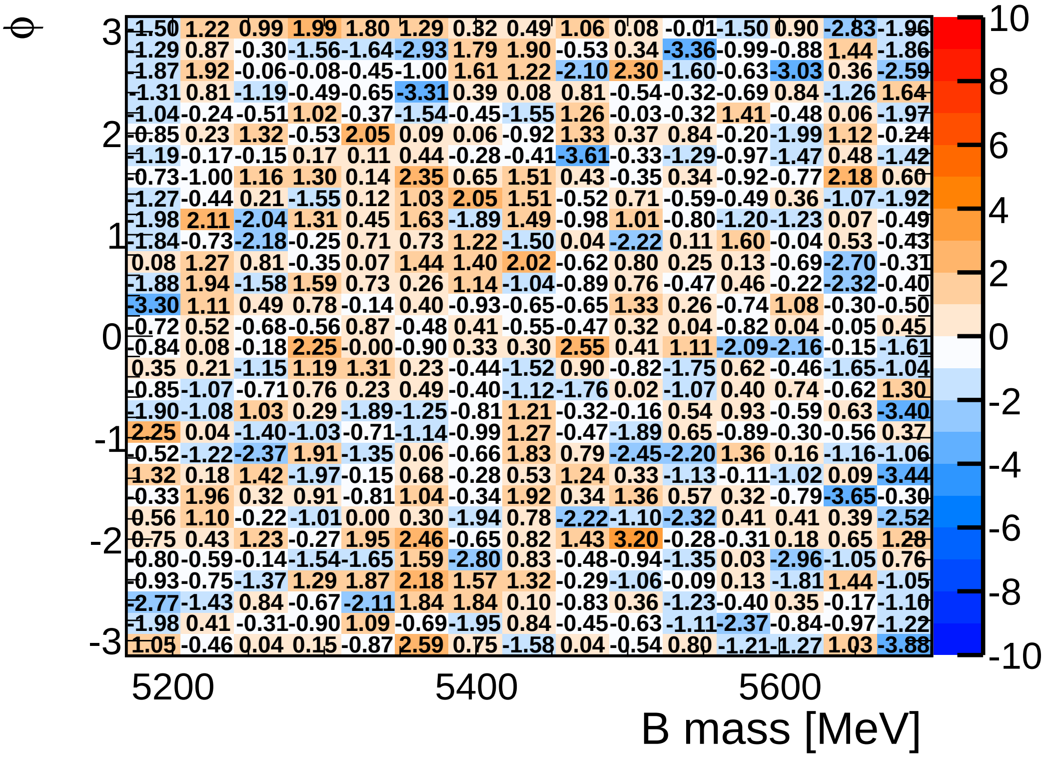

Figure 247: 2D pull of ϕ vs mass of the full (weighted) fit to $B^0 \to J/\psi\, K^{*0}$ for all available data of 2011+2012.

R Fitting $B^0 \to J/\psi\, K^{*0}$ with a single set of decay amplitudes

For the $B^0 \to J/\psi\, K^{*0}$ decay there are really only a single set of K^{*0} decay amplitudes, rather than different left- and right-handed amplitudes as is the case for the $B^0 \to K^{*0}\mu^+\mu^-$ decay. For $B^0 \to J/\psi\, K^{*0}$, $A^L_{\|,\perp,0} = A^R_{\|,\perp,0} = A_{\|,\perp,0}$. Applying this relationship forces $S_{5,6,7}$ (and $A_{5,6,7}$) to be identical to zero. In this basis the 4 symmetries of the $B^0 \to K^{*0}\mu^+\mu^-$ decay are also reduced to one, a global phase rotation that can be used to fix one of the amplitudes to be real, e.g. $\Im(A_0) = 0$.

As a cross-check a fit has also been performed to the $B^0 \to J/\psi\, K^{*0}$ decay using this reduced number of amplitudes. As was the case for the q^2 dependent amplitude fit, the scale of the amplitudes is fixed by applying a constraint on the number of signal candidates in the fit,

$$N_{\rm sig} = \int_{-1}^{+1}\int_{-1}^{+1}\int_{-\pi}^{+\pi} \frac{\mathrm{d}^3\Gamma[\mathrm{Sig}]}{\mathrm{d}\cos\theta_\ell\,\mathrm{d}\cos\theta_K\,\mathrm{d}\phi}\epsilon(\cos\theta_\ell,\cos\theta_K,\phi)\mathrm{d}\cos\theta_\ell\,\mathrm{d}\cos\theta_K\,\mathrm{d}\phi\ . \quad (115)$$

The result of this fit is compatible with the more general amplitude fit where left- and right-handed amplitudes are floated separately. The shift seen for S_4 between the "full" amplitude fit and the observable fit is also present. See Table 195 for details.

Observable	Fitting $A^{\rm L,R}_{0,\|,\perp}$	Fitting $A^{\rm L}_{0,\|,\perp} = A^{\rm R}_{0,\|,\perp}$	LHCb-PAPER-2013-023
S_{1c}	$+0.563 \pm 0.001$	$+0.563 \pm 0.001$	$+0.572 \pm 0.020$
S_3	-0.012 ± 0.002	-0.012 ± 0.002	$-0.0130 \pm XX$
S_4	-0.248 ± 0.001	-0.248 ± 0.001	-0.250 ± 0.008
S_5	-0.008 ± 0.002	–	–
S_6	$+0.003 \pm 0.002$	–	–
S_7	$+0.001 \pm 0.002$	–	–
S_8	-0.049 ± 0.002	-0.049 ± 0.002	-0.048 ± 0.007
S_9	-0.091 ± 0.002	-0.091 ± 0.002	-0.084 ± 0.010

Table 195: Result of fitting $B^0 \to J/\psi\, K^{*0}$ data for constant decay amplitudes in two configurations, first where separate left- and right-hand amplitudes are considered and second when the left- and right-handed amplitudes are forced to be identical. The two fits are compared to the result from LHCb-PAPER-2013-024 [51]. The S-wave observables have been omitted.

S Fitting run periods and B flavour separately

As an additional cross-check the data for $B^0 \to K^{*0}\mu^+\mu^-$ has been split by run-period and by B flavour and fit separately. The result of these fits is shown in Fig. 248. The four sub-samples (corresponding to different combinations of year and B flavour) are compatible.

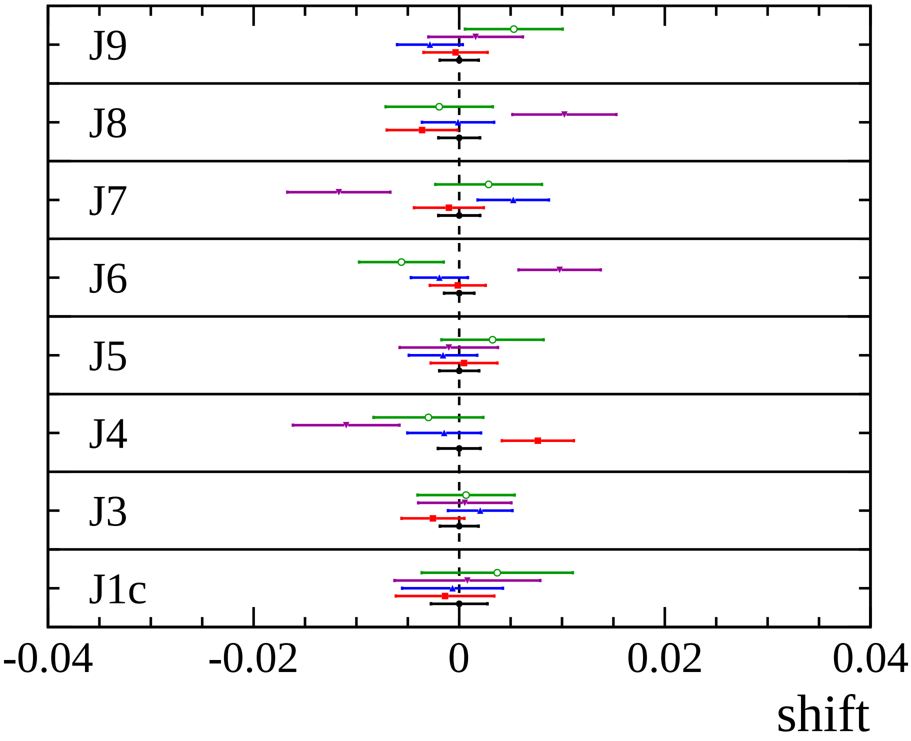

Figure 248: Comparison of fit results for the J_i/Γ (as opposed to S_i or A_i) for $B^0 \to J/\psi K^{*0}$ fitting separately for: B^0 in 2012 (red square), $\overline{B}^0$ in 2012 (blue triangular), B^0 in 2011 (inverted purple triangle) and $\overline{B}^0$ in 2011 (green open circle). The J_i are determined from a fit to the observables and are plotted with respect to a combined fit to the full run 1 dataset (black circle).

T Peaking backgrounds

After applying the full selection criteria, peaking backgrounds are reduced to $\lesssim 1\%$ of the level of the signal. These backgrounds will however have a different angular distribution to the signal and in the case of $\Lambda_b^0 \to pK\mu^+\mu^-$ the angular distribution of the background is essentially unknown.

The mass and angular distributions of $B_s^0 \to \phi\mu^+\mu^-$ and $\Lambda_b^0 \to pK^-\mu^+\mu^-$ candidates reconstructed as $B^0 \to K^{*0}\mu^+\mu^-$, with $m(K^+\pi^-)$ within $\pm 100\,\mathrm{MeV}/c^2$ of the nominal K^{*0} mass, in the data are shown in Figs. 249–252. In order to produce these distributions, the PID requirements from the pre-selection have been removed and a second BDT has been trained without the K^+ and π^- PID information. The candidates are then selected by inverting the PID requirements such that

- the pion in the $B^0 \to K^{*0}\mu^+\mu^-$ decay is kaon-like for the $B^0_s \to \phi\mu^+\mu^-$ decay, by requiring that the pion and the kaon have `ProbNNK` > 0.4;
- the pion in the $B^0 \to K^{*0}\mu^+\mu^-$ decay is proton-like for the $\Lambda^0_b \to pK^-\mu^+\mu^-$ decay, by requiring that the kaon has `ProbNNK` > 0.4 and the pion `ProbNNp` > 0.4.

These requirements suppress the background from the $B^0 \to K^{*0}\mu^+\mu^-$ signal. The $\cos\theta_l$ and ϕ distributions of these backgrounds are reasonably compatible with the signal, however the $\cos\theta_K$ distribution is strongly peaked towards $\cos\theta_K \sim -1$. The distributions in Figs. 249-252 are only illustrative, the distribution in the data will be further influenced by the PID requirements in the pre-selection and by the inclusion of PID in the BDT.

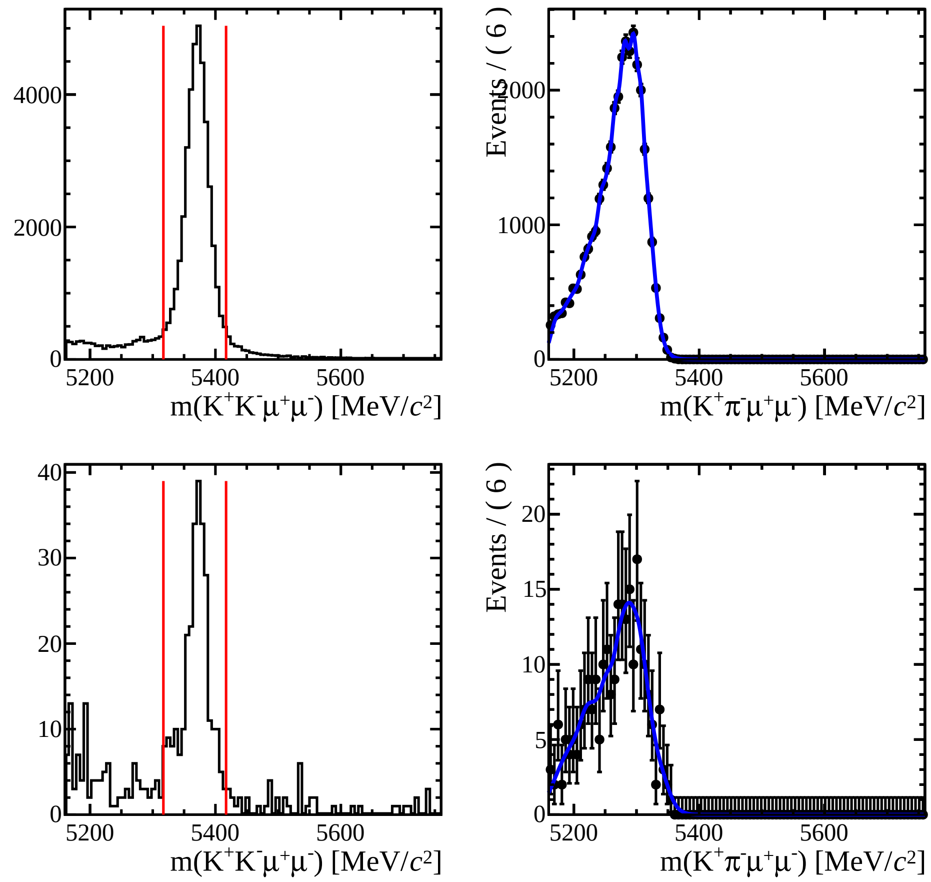

Figure 249: The $K^+K^-\mu^+\mu^-$ invariant mass of candidates after requiring the pion `ProbNNK` > 0.4 (left) and the $K^+\pi^-\mu^+\mu^-$ invariant mass of the candidates that are compatible with originating from $B_s^0 \to \phi\mu^+\mu^-$ (right). The top pair of plots corresponds to the J/ψ window and the lower plots to candidates with $q^2 < 6\,\mathrm{GeV}^2/c^4$ or $q^2 > 15\,\mathrm{GeV}^2/c^4$.

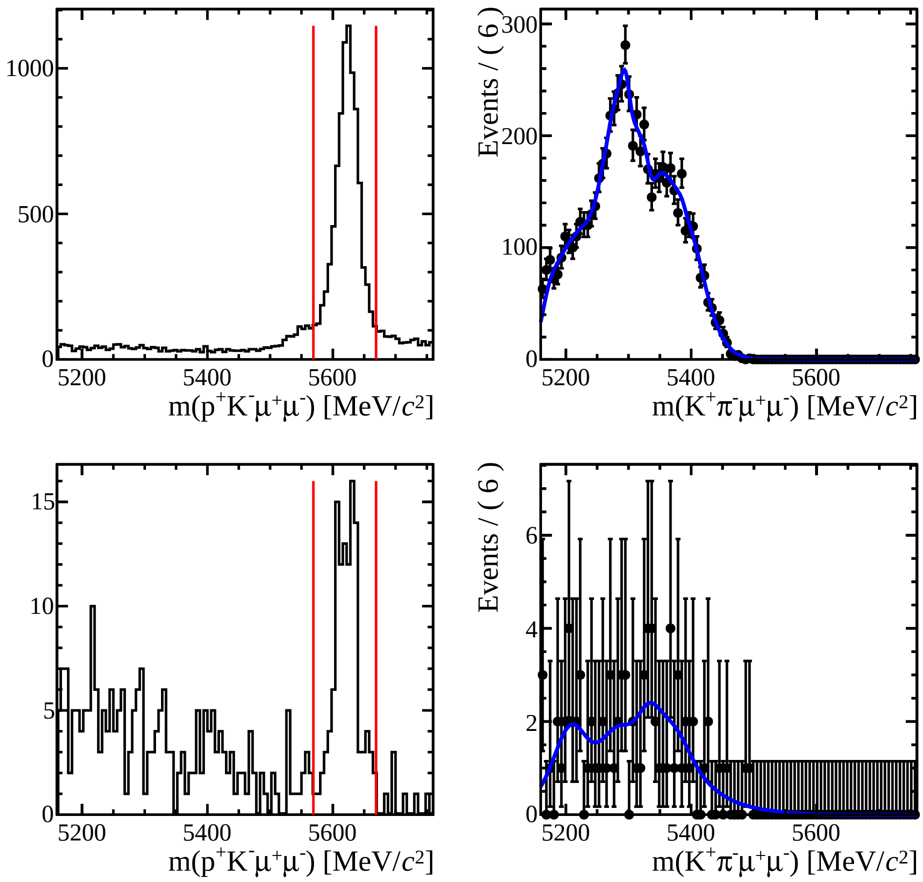

Figure 250: The $pK^-\mu^+\mu^-$ invariant mass of candidates after requiring the pion `ProbNNp` $>$ 0.4 and kaon `ProbNNK` > 0.4 (left) and the $K^+\pi^-\mu^+\mu^-$ invariant mass of the candidates that are compatible with originating from $\Lambda_b^0 \to pK^-\mu^+\mu^-$ (right). The top pair of plots corresponds to the J/ψ window and the lower plots to candidates with $q^2 < 6\,\mathrm{GeV}^2/c^4$ or $q^2 > 15\,\mathrm{GeV}^2/c^4$.

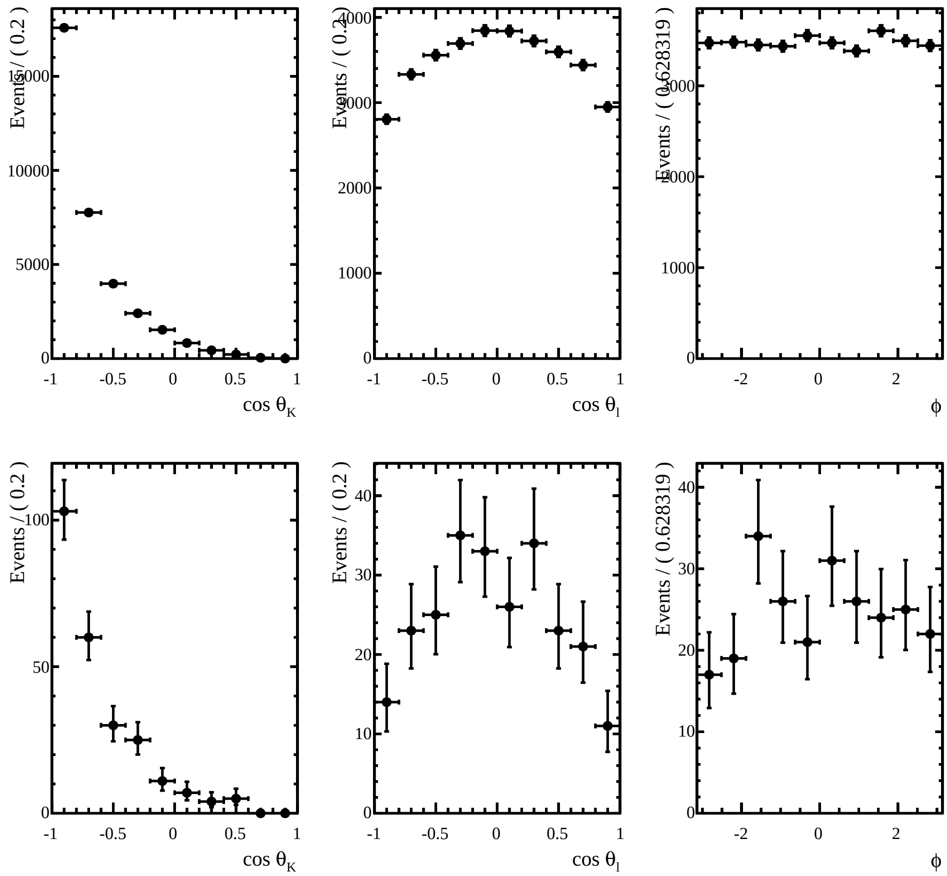

Figure 251: Angular distribution of $B_s^0 \to \phi\mu^+\mu^-$ candidates reconstructed as $B^0 \to K^{*0}\mu^+\mu^-$. The top plots correspond to the J/ψ window and the lower plots to candidates with $q^2 < 6\,\mathrm{GeV}^2/c^4$ or $q^2 > 15\,\mathrm{GeV}^2/c^4$.

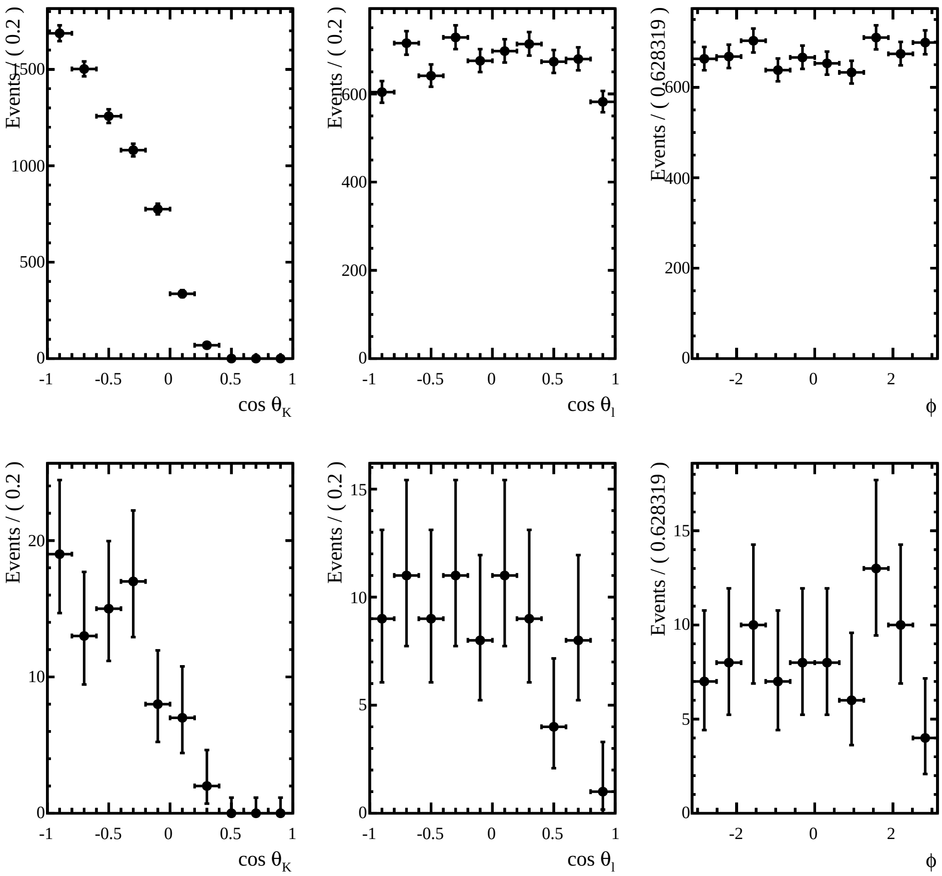

Figure 252: Angular distribution of $\Lambda_b^0 \to pK^-\mu^+\mu^-$ candidates reconstructed as $B^0 \to K^{*0}\mu^+\mu^-$. The top plots correspond to the J/ψ window and the lower plots to candidates with $q^2 < 6\,\mathrm{GeV}^2/c^4$ or $q^2 > 15\,\mathrm{GeV}^2/c^4$.

U Background angular distribution from the ABCD method

In the analysis, the background angular distribution in the signal region is determined using the events in the upper mass sideband. To test and to validate this choice the ABCD method [52] is used as a crosscheck and a comparison between the background angular distribution of these two methods is made.

The goal of the ABCD method is to infer the distribution of the background in the signal region (A) using the distributions from three control regions (B - D). The candidates in a 2D plane defined by the BDT variable and the B^0 mass are divided into four regions as follows and shown in Fig. 253.

A. $\texttt{BDT} > 0.2$ and $m(K^+\pi^-\mu^+\mu^-) < 5350\,\mathrm{MeV}/c^2$

B. $\texttt{BDT} > 0.2$ and $m(K^+\pi^-\mu^+\mu^-) > 5350\,\mathrm{MeV}/c^2$

C. $\texttt{BDT} < -0.4$ and $m(K^+\pi^-\mu^+\mu^-) < 5350\,\mathrm{MeV}/c^2$

D. $\texttt{BDT} < -0.4$ and $m(K^+\pi^-\mu^+\mu^-) > 5350\,\mathrm{MeV}/c^2$

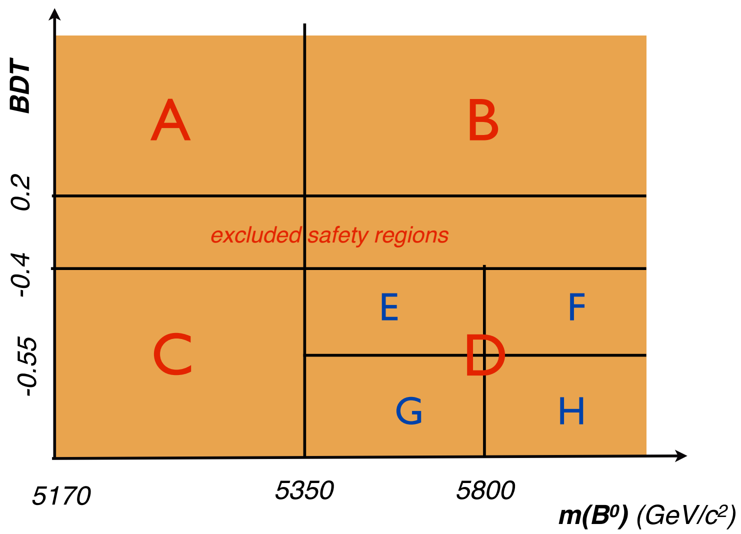

Figure 253: 2D plane defining the different regions of the ABCD method.

The region A corresponds to the signal region and the region B to the commonly called upper mass sideband region. With the ABCD method, the background angular distribution in the signal region A, is obtained from the background angular distributions of the three other regions by

$$A = \frac{B \times C}{D} \tag{116}$$

The method relies on two hypothesis:

1. region B,C,D contain only background events;
2. and there is no correlation between the BDT variable and the reconstructed mass of the candidate.

To ensure that the first hypothesis is true, events with $-0.4 < BDT < 0.2$ are excluded from the regions B and D. The leakage of signal events into region B is then $\lesssim 1$ in every q^2 bin. The advantage of this approach is that there is no assumption that the angular distribution of the background is the same in the sideband and the signal mass window. The ABCD method can then be used to test this assumption.

U.1 Validation of the ABCD method

Unfortunately, when the `BDT` requirement is relaxed, there can be a correlation between the `BDT` response and the mass of the candidate. To take into account this correlation, a correction to the angular distribution in the A region is applied.

The correction factor is computed as the following:

$$R = \frac{E \times H}{F \times G} \tag{117}$$

where E,F,G and H are subsets of region D, defined as:

E. $-0.55 < \texttt{BDT} < -0.4$ and $5350 < m(K^+\pi^-\mu^+\mu^-) < 5800\,\text{MeV}/c^2$;

F. $-0.55 < \texttt{BDT} < -0.4$ and $m(K^+\pi^-\mu^+\mu^-) > 5800\,\text{MeV}/c^2$;

G. $\texttt{BDT} < -0.55$ and $5350 < m(K^+\pi^-\mu^+\mu^-) < 5800\,\text{MeV}/c^2$;

H. and $\texttt{BDT} < -0.55$ and $m(K^+\pi^-\mu^+\mu^-) > 5800\,\text{MeV}/c^2$.

The correction factors for the different q^2 bins are given in Table 196. It has been checked that this correction factor has a negligible angular dependence, see Sec. U.2.

A comparison of the background angular distributions in the A region, obtained from the ABCD method, to the upper mass sideband has been done for each q^2 bin in both binning schemes and for the three angles. All comparisons are given in Fig. 254, Fig. 255, Fig. 256, Fig. 257 and in Sec. U.2. The resulting distributions for region A are in excellent agreement with the distributions in the upper mass sideband.

$q^2\,[\,\mathrm{GeV}^2]$	Correction factor R
$[0.1, 0.98]$	1.304
$[1.1, 2.0]$	1.584
$[2.0, 3.0]$	1.259
$[3.0, 4.0]$	1.366
$[4.0, 5.0]$	1.281
$[5.0, 6.0]$	1.276
$[6.0, 7.0]$	1.324
$[7.0, 8.0]$	1.282
$[11.0, 11.75]$	1.435
$[11.75, 12.5]$	1.007
$[15.0, 16.0]$	1.438
$[16.0, 17.0]$	0.994
$[17.0, 18.0]$	1.057
$[18.0, 19.0]$	0.902

$q^2\,[\,\mathrm{GeV}^2]$	Correction factor R
$[0.1, 0.98]$	1.034
$[1.1, 2.5]$	1.517
$[2.5, 4.0]$	1.301
$[4.0, 6.0]$	1.282
$[6.0, 8.0]$	1.304
$[11.0, 12.5]$	1.206
$[15.0, 17.0]$	1.176
$[17.0, 19.0]$	0.968

Table 196: Correction factor R with the two q^2 binnings: (left) $1\,\mathrm{GeV}^2/c^4$ and (right) $2\,\mathrm{GeV}^2/c^4$ bins.

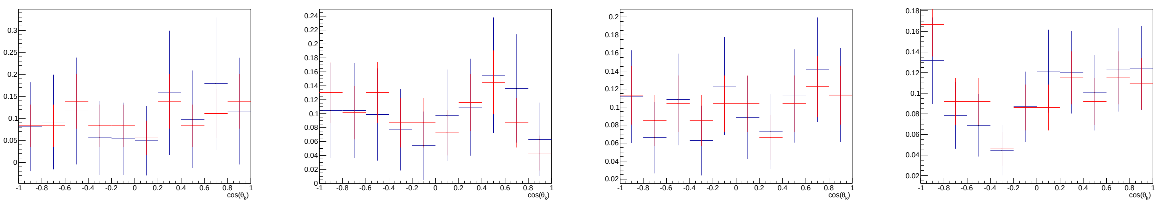

(a) $[0.1, 0.98]$ (b) $[1.1, 2.5]$ (c) $[2.5, 4]$ (d) $[4, 6]$

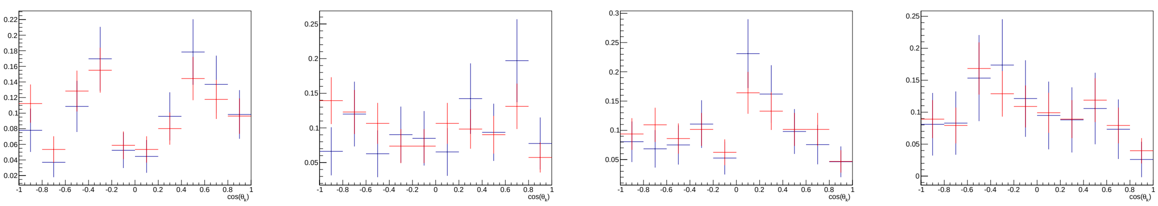

(e) $[6, 8]$ (f) $[11, 12.5]$ (g) $[15, 17]$ (h) $[17, 19]$

Figure 254: Comparison of the $\cos(\theta_k)$ distribution for the ABCD method (blue) and the upper mass sideband (red) in the 2 GeV^2/c^4 binning scheme

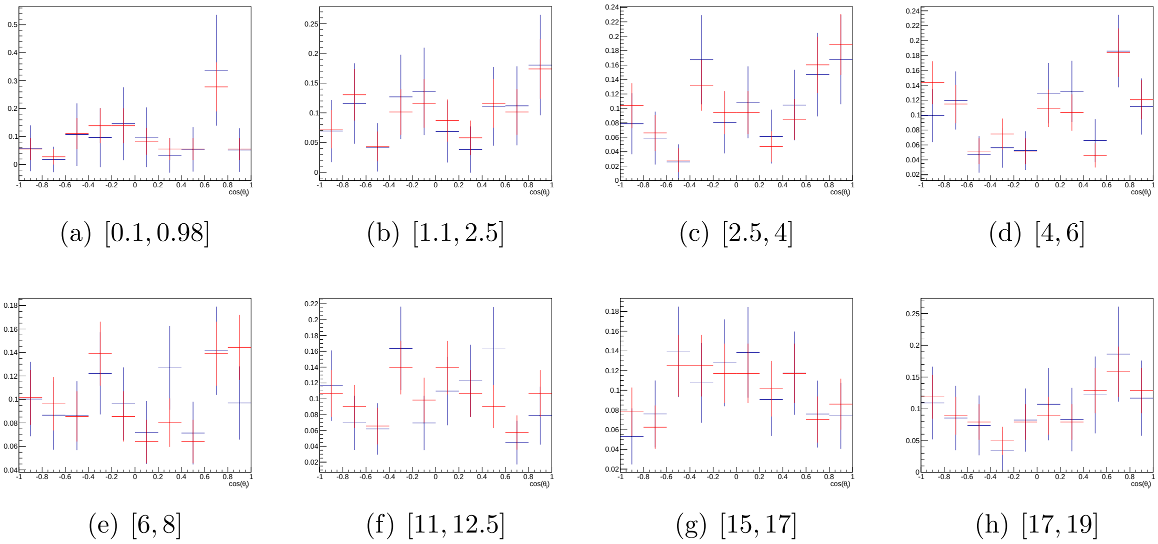

(a) [0.1, 0.98] (b) [1.1, 2.5] (c) [2.5, 4] (d) [4, 6]

(e) [6, 8] (f) [11, 12.5] (g) [15, 17] (h) [17, 19]

Figure 255: Comparison of the $\cos(\theta_l)$ distribution for the ABCD method (blue) and the upper mass sideband (red) in the 2 GeV^2/c^4 binning scheme

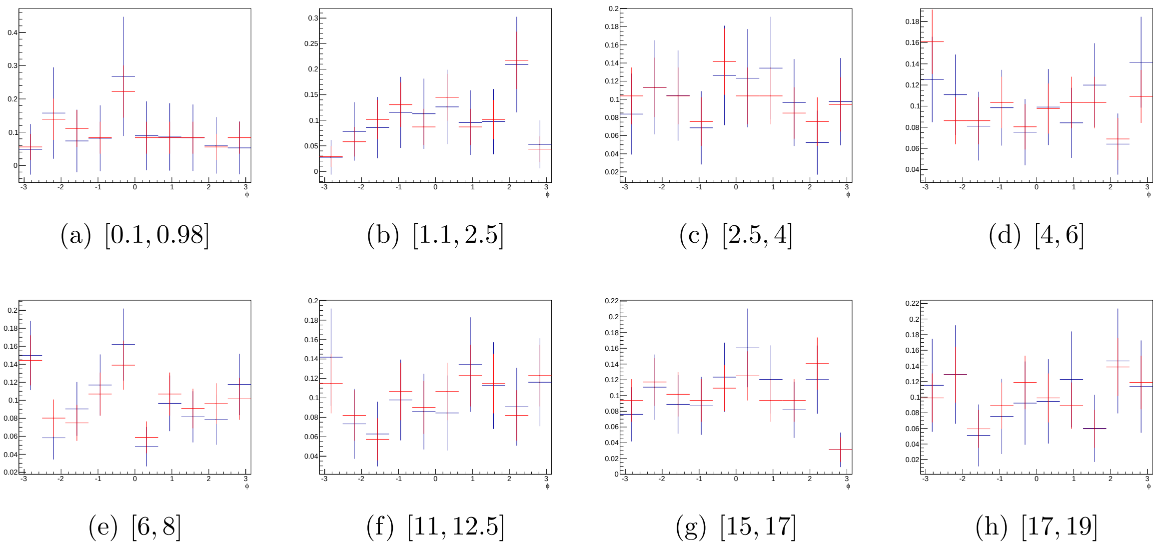

(a) [0.1, 0.98] (b) [1.1, 2.5] (c) [2.5, 4] (d) [4, 6]

(e) [6, 8] (f) [11, 12.5] (g) [15, 17] (h) [17, 19]

Figure 256: Comparison of the ϕ distribution for the ABCD method (blue) and the upper mass sideband (red) in the 2 GeV^2/c^4 binning scheme

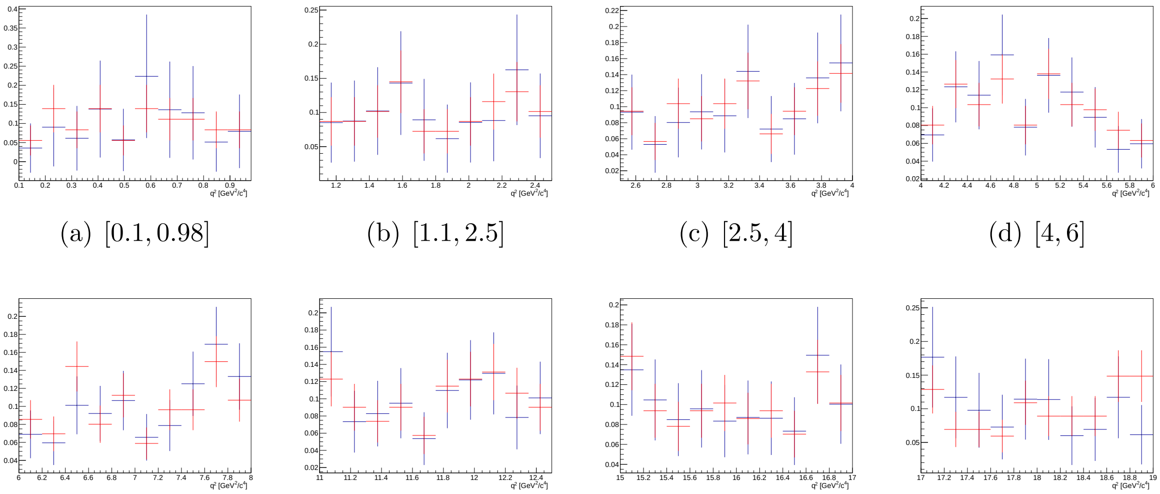

(a) $[0.1, 0.98]$ (b) $[1.1, 2.5]$ (c) $[2.5, 4]$ (d) $[4, 6]$

(e) $[6, 8]$ (f) $[11, 12.5]$ (g) $[15, 17]$ (h) $[17, 19]$

Figure 257: Comparison of the q^2 distribution for the ABCD method (blue) and the upper mass sideband (red) in the 2 GeV$^2/c^4$ binning scheme

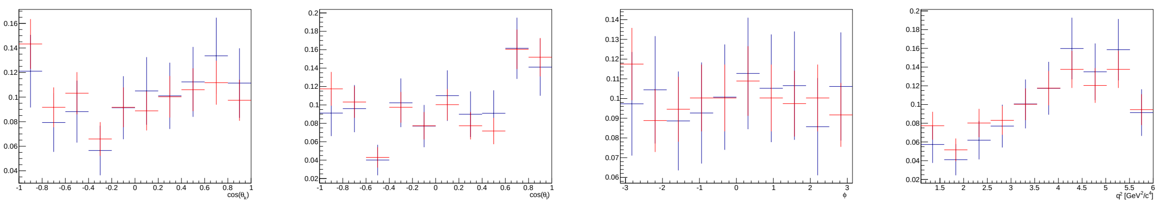

(a) $\cos(\theta_k)$ (b) $\cos(\theta_l)$ (c) ϕ (d) q^2

Figure 258: Comparison of the $\cos(\theta_k)$ 258(a) ,$\cos(\theta_l)$ 258(b), ϕ 258(c) and q^2 258(d) distribution for the ABCD method (blue) and the upper mass sideband (red) in the large bin 1-6 GeV$^2/c^4$.

U.2 Correlation correction factor

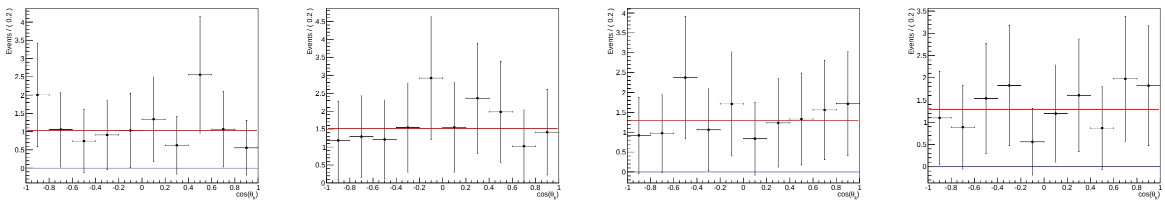

(a) $[0.1, 0.98]$ (b) $[1.1, 2.5]$ (c) $[2.5, 4]$ (d) $[4, 6]$

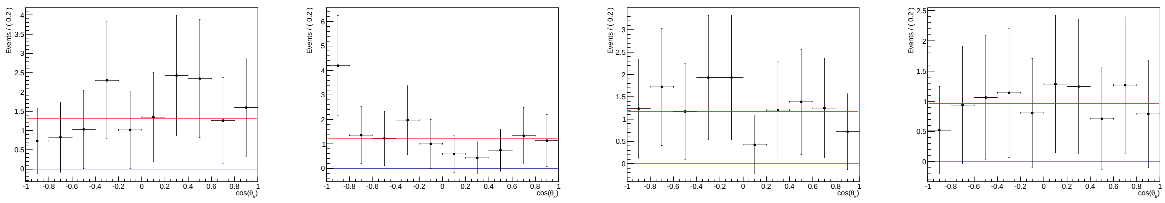

(e) $[6, 8]$ (f) $[11, 12.5]$ (g) $[15, 17]$ (h) $[17, 19]$

Figure 259: Correction factor R for the $\cos(\theta_k)$ distribution for the 2 GeV^2/c^4 bin width.

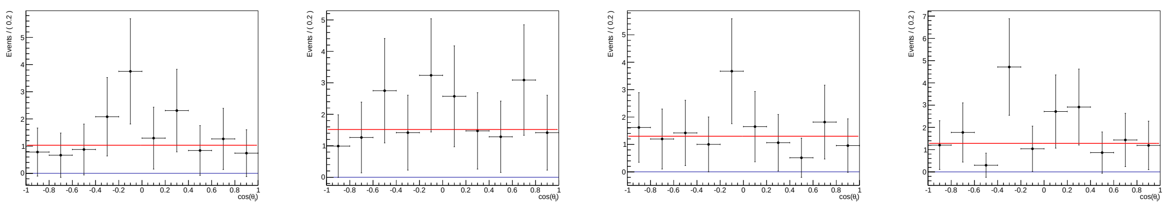

(a) $[0.1, 0.98]$ (b) $[1.1, 2.5]$ (c) $[2.5, 4]$ (d) $[4, 6]$

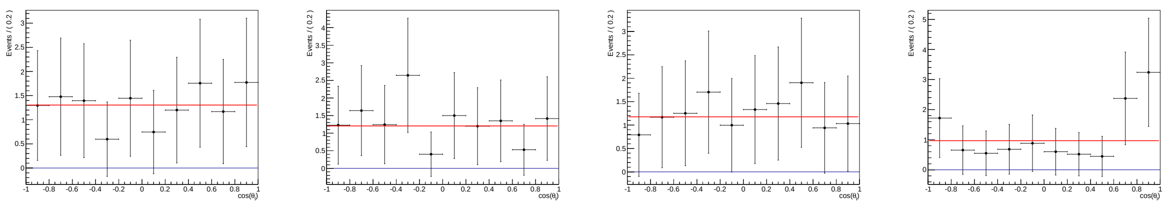

(e) $[6, 8]$ (f) $[11, 12.5]$ (g) $[15, 17]$ (h) $[17, 19]$

Figure 260: Correction factor R for the $\cos(\theta_l)$ distribution for the 2 GeV^2/c^4 bin width.

U.3 Comparison with upper mass sideband

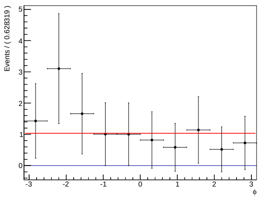

(a) $[0.1, 0.98]$

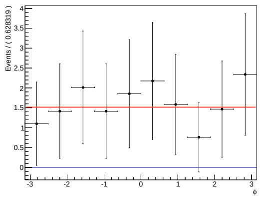

(b) $[1.1, 2.5]$

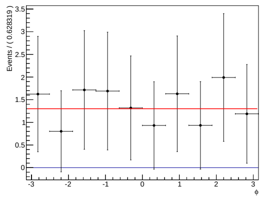

(c) $[2.5, 4]$

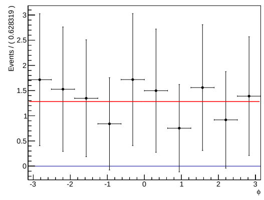

(d) $[4, 6]$

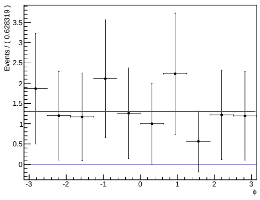

(e) $[6, 8]$

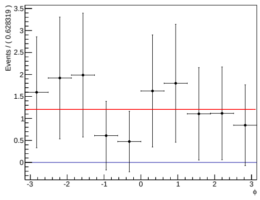

(f) $[11, 12.5]$

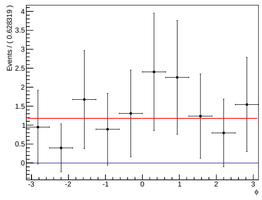

(g) $[15, 17]$

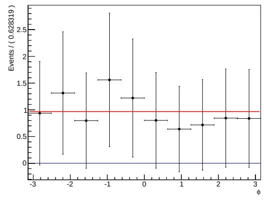

(h) $[17, 19]$

Figure 261: Correction factor R for the ϕ distribution for the 2 GeV$^2/c^4$ bin width.

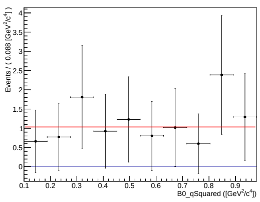

(a) $[0.1, 0.98]$

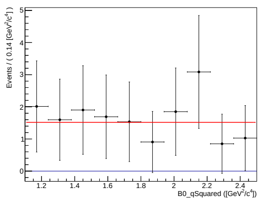

(b) $[1.1, 2.5]$

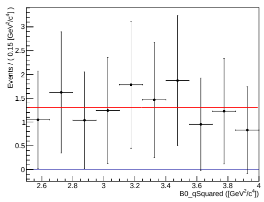

(c) $[2.5, 4]$

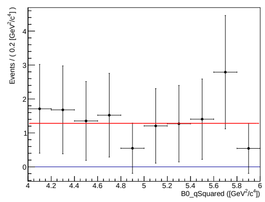

(d) $[4, 6]$

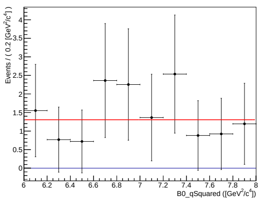

(e) $[6, 8]$

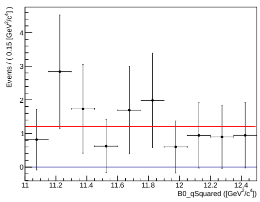

(f) $[11, 12.5]$

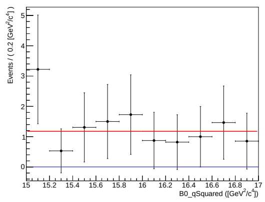

(g) $[15, 17]$

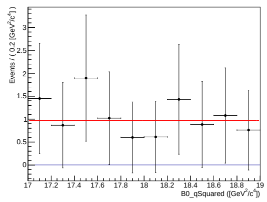

(h) $[17, 19]$

Figure 262: Correction factor R for the q^2 distribution for the 2 GeV$^2/c^4$ bin width.

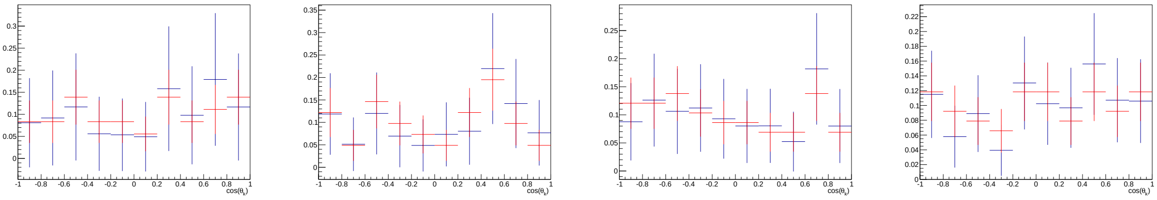

(a) $[0.1, 0.98]$ (b) $[1.1, 2]$ (c) $[2, 3]$ (d) $[3, 4]$

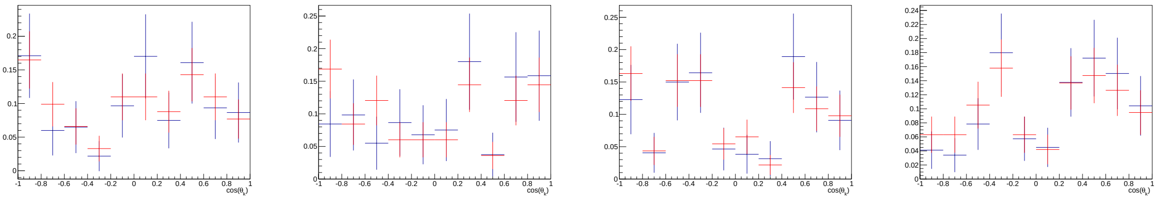

(e) $[4, 5]$ (f) $[5, 6]$ (g) $[6, 7]$ (h) $[7, 8]$

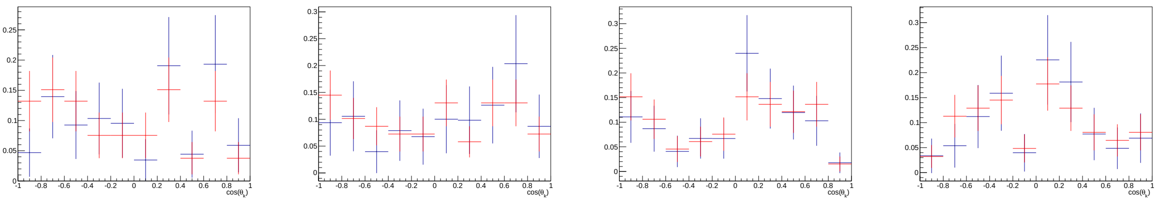

(i) $[11, 11.75]$ (j) $[11.75, 12.5]$ (k) $[15, 16]$ (l) $[16, 17]$

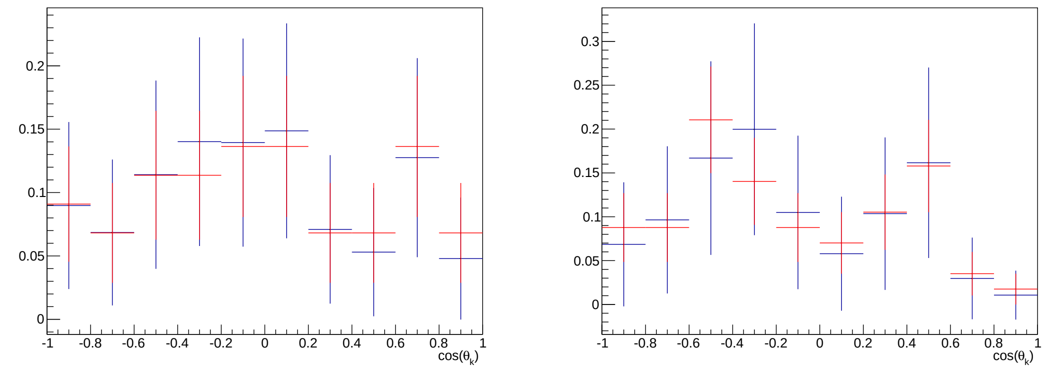

(m) $[17, 18]$ (n) $[18, 19]$

Figure 263: Comparison of the $\cos(\theta_k)$ distribution for the ABCD method (blue) and the upper mass sideband (red) in the 1 GeV$^2/c^4$ binning scheme.

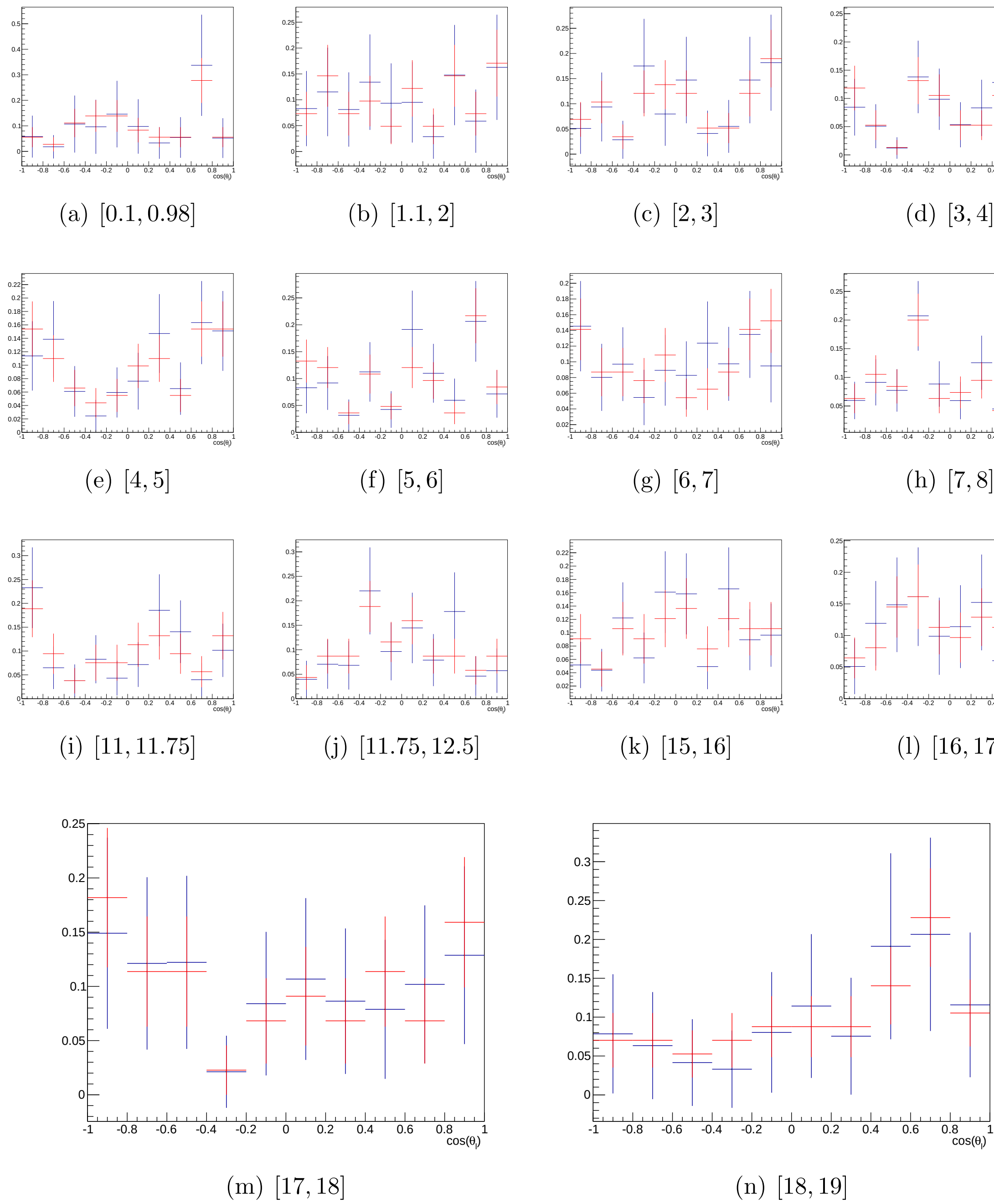

(a) $[0.1, 0.98]$ (b) $[1.1, 2]$ (c) $[2, 3]$ (d) $[3, 4]$

(e) $[4, 5]$ (f) $[5, 6]$ (g) $[6, 7]$ (h) $[7, 8]$

(i) $[11, 11.75]$ (j) $[11.75, 12.5]$ (k) $[15, 16]$ (l) $[16, 17]$

(m) $[17, 18]$ (n) $[18, 19]$

Figure 264: Comparison of the $\cos(\theta_l)$ distribution for the ABCD method (blue) and the upper mass sideband (red) in the 1 GeV^2/c^4 binning scheme.

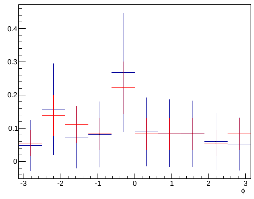

(a) $[0.1, 0.98]$

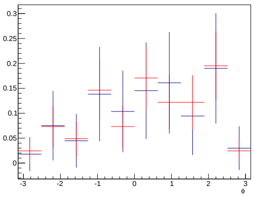

(b) $[1.1, 2]$

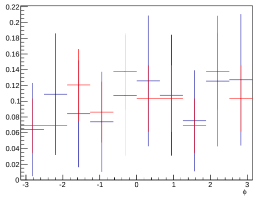

(c) $[2, 3]$

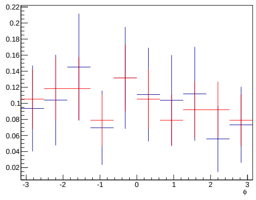

(d) $[3, 4]$

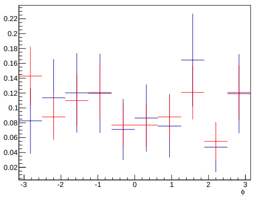

(e) $[4, 5]$

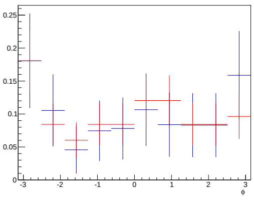

(f) $[5, 6]$

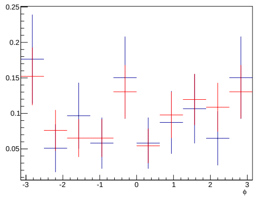

(g) $[6, 7]$

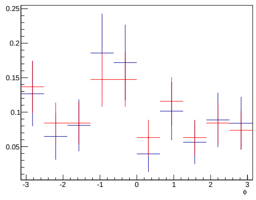

(h) $[7, 8]$

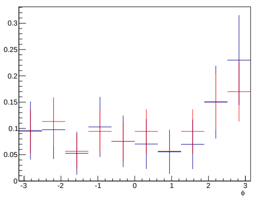

(i) $[11, 11.75]$

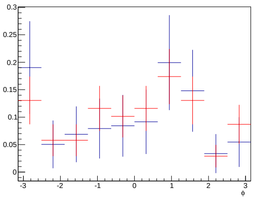

(j) $[11.75, 12.5]$

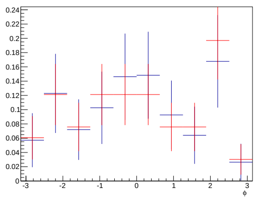

(k) $[15, 16]$

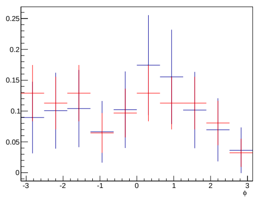

(l) $[16, 17]$

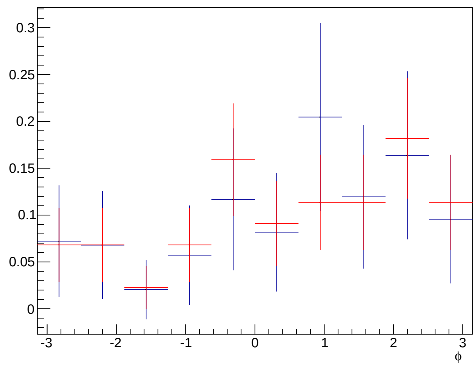

(m) $[17, 18]$

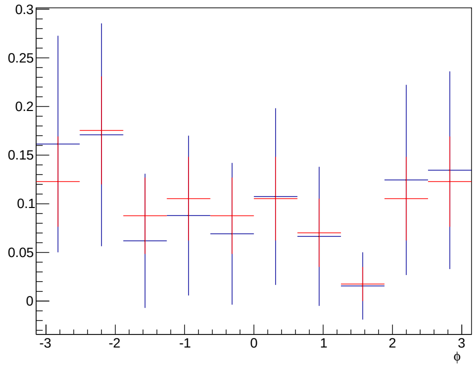

(n) $[18, 19]$

Figure 265: Comparison of the ϕ distribution for the ABCD method (blue) and the upper mass sideband (red) in the 1 GeV$^2/c^4$ binning scheme.

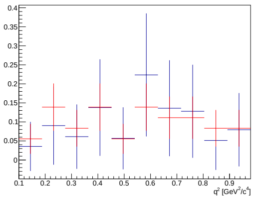

(a) $[0.1, 0.98]$

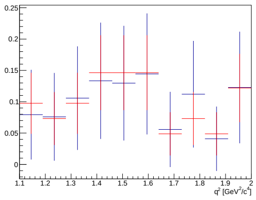

(b) $[1.1, 2]$

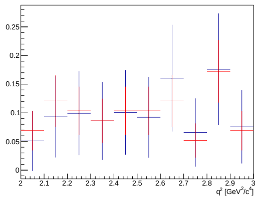

(c) $[2, 3]$

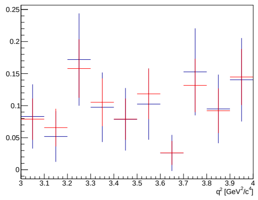

(d) $[3, 4]$

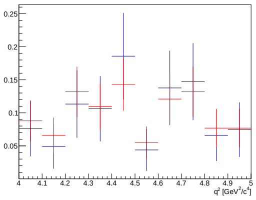

(e) $[4, 5]$

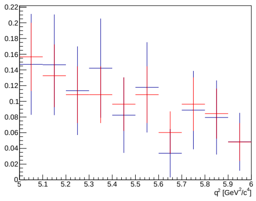

(f) $[5, 6]$

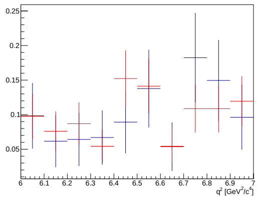

(g) $[6, 7]$

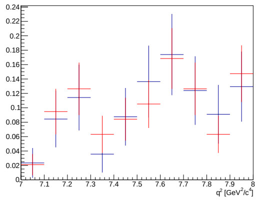

(h) $[7, 8]$

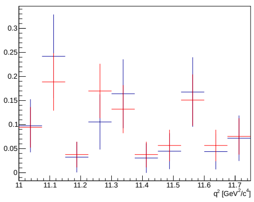

(i) $[11, 11.75]$

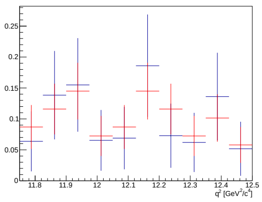

(j) $[11.75, 12.5]$

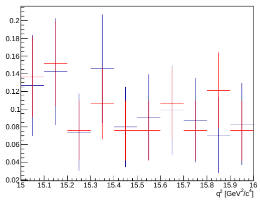

(k) $[15, 16]$

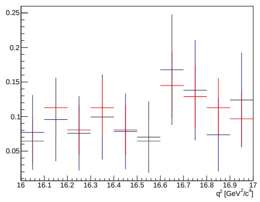

(l) $[16, 17]$

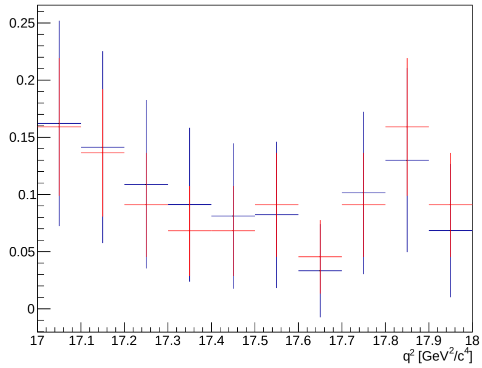

(m) $[17, 18]$

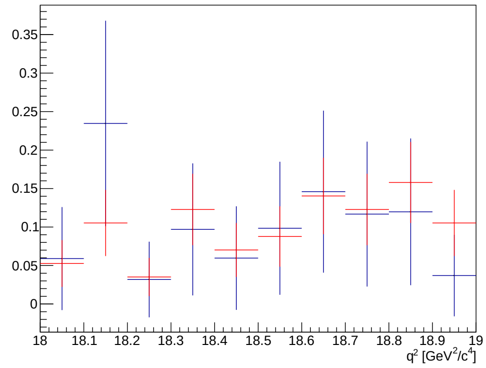

(n) $[18, 19]$

Figure 266: Comparison of the q^2 distribution for the ABCD method (blue) and the upper mass sideband (red) in the 1 GeV$^2/c^4$ binning scheme.

V The angular acceptances of the trigger lines

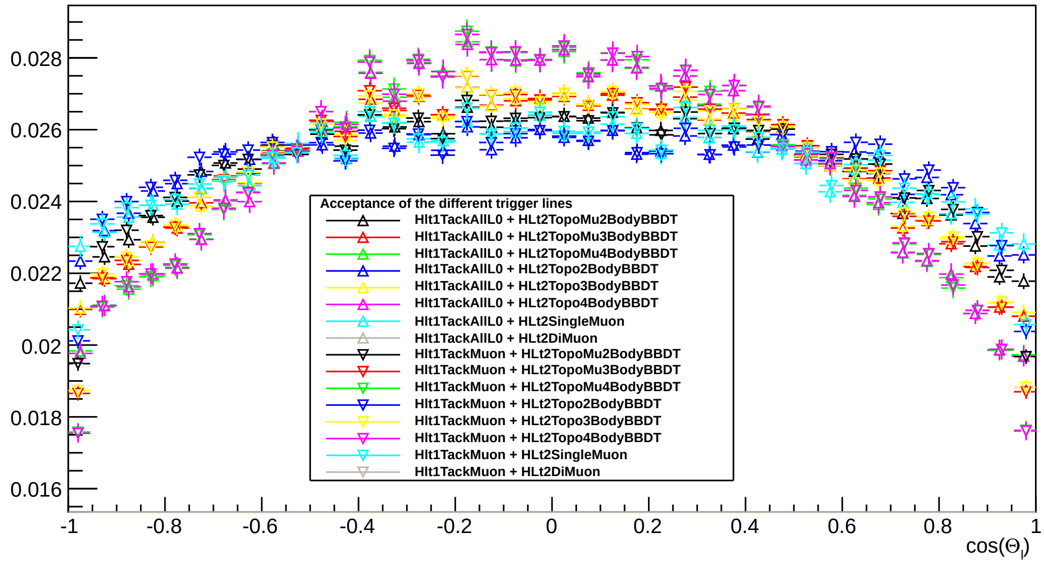

Figure 267: $\cos(\theta_l)$ acceptance of the different trigger lines determined using phase-space $K^{*0}\mu\mu$ MC.

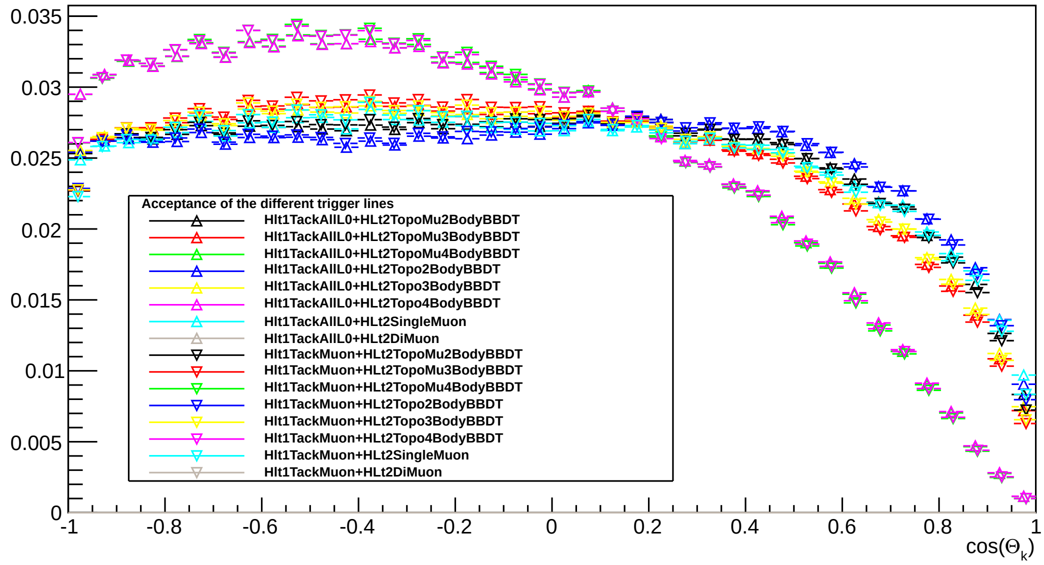

Figure 268: $\cos(\theta_k)$ acceptance of the different trigger lines determined using phase-space $K^{*0}\mu\mu$ MC.

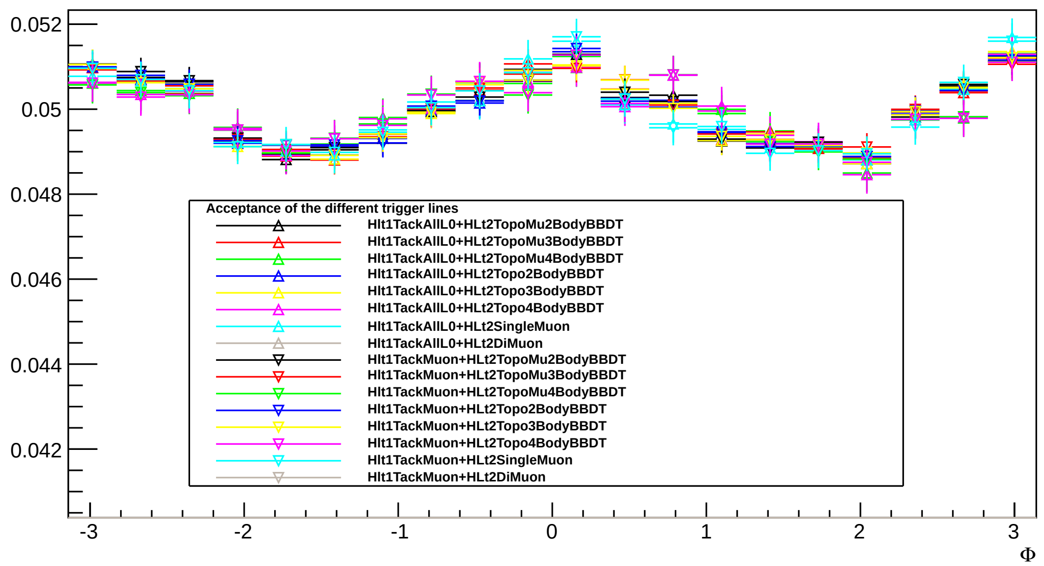

Figure 269: Φ acceptance of the different trigger lines determined using phase-space $K^{*0}\mu\mu$ MC.

W Correlation Formulas

As already discussed in Sec. 7 the correlation of the different angular terms can be calculated analytically using their moments:

$$\mathrm{cor}(S_i, S_k) = \frac{\langle f_i f_k \rangle - \langle f_i \rangle \langle f_k \rangle}{\sqrt{\langle f_i^2 \rangle - \langle f_i \rangle^2}\sqrt{\langle f_k^2 \rangle - \langle f_k \rangle^2}} \tag{118}$$

In the following calculations a different angular basis was used ($A_s = 0.5S_{S1}$, $A_{s4} = 2/3S_{S2}$, $A_{s5} = 2/3S_{S3}$, $A_{s7} = 2/3S_{S4}$, $A_{s8} = 2/3S_{S5}$).

The angular terms are defined as ($x = cos(\theta_k)$, $y = cos(\theta_l)$):

$$\begin{aligned}
f_1 &= x^2, \\
f_3 &= (1-x^2)(1-y^2)cos(2\phi), \\
f_4 &= 2x\sqrt{1-x^2}2y\sqrt{1-y^2}cos(\phi), \\
f_5 &= 2x\sqrt{1-x^2}\sqrt{1-y^2}cos(\phi), \\
f_6 &= (1-x^2)y, \\
f_7 &= 2x\sqrt{1-x^2}\sqrt{1-y^2}sin(\phi), \\
f_8 &= 2x\sqrt{1-x^2}2y\sqrt{1-y^2}sin(\phi), \\
f_9 &= (1-x^2)(1-y^2)sin(2\phi), \\
f_{F_s} &= 1-y^2, \\
f_{A_s} &= x(1-y^2), \\
f_{A_{s4}} &= \sqrt{1-x^2}2y\sqrt{1-y^2}cos(\phi), \\
f_{A_{s5}} &= \sqrt{1-x^2}\sqrt{1-y^2}cos(\phi), \\
f_{A_{s7}} &= \sqrt{1-x^2}\sqrt{1-y^2}sin(\phi), \\
f_{A_{s8}} &= \sqrt{1-x^2}2y\sqrt{1-y^2}sin(\phi)
\end{aligned} \tag{119}$$

The corresponding moments are:

$$
\begin{aligned}
\langle f_1 \rangle &= 2/15(6 + 3F_l(F_s - 1) - F_s),\\
\langle f_3 \rangle &= -8/25(-1 + F_s)S_3,\\
\langle f_4 \rangle &= -8/25(-1 + F_s)S_4,\\
\langle f_5 \rangle &= -2/5(-1 + F_s)S_5,\\
\langle f_6 \rangle &= -2/5(-1 + F_s)S_{6s},\\
\langle f_7 \rangle &= -2/5(-1 + F_s)S_7,\\
\langle f_8 \rangle &= -8/25(-1 + F_s)S_8,\\
\langle f_9 \rangle &= -8/25(-1 + F_s)S_9,\\
\langle f_{F_s} \rangle &= 1/5(3 + F_l + F_s - F_l F_s),\\
\langle f_{A_s} \rangle &= 8/15A_s,\\
\langle f_{A_{s4}} \rangle &= 2/5A_{s4},\\
\langle f_{A_{s5}} \rangle &= 1/2A_{s5},\\
\langle f_{A_{s7}} \rangle &= 1/2A_{s7},\\
\langle f_{A_{s8}} \rangle &= 2/5A_{s8}
\end{aligned}
\tag{120}
$$

$$
\begin{aligned}
\langle f_1 f_1 \rangle &= 8/105(9 + 6F_l(-1 + F_s) - 2F_s),\\
\langle f_1 f_3 \rangle &= -(48/175)(-1 + F_s)S_3,\\
\langle f_1 f_4 \rangle &= -(32/175)(-1 + F_s)S_4,\\
\langle f_1 f_5 \rangle &= -(8/35)(-1 + F_s)S_5,\\
\langle f_1 f_6 \rangle &= -(12/35)(-1 + F_s)S_{6s},\\
\langle f_1 f_7 \rangle &= -(8/35)(-1 + F_s)S_7,\\
\langle f_1 f_8 \rangle &= -(32/175)(-1 + F_s)S_8,\\
\langle f_1 f_9 \rangle &= -(48/175)(-1 + F_s)S_9,\\
\langle f_1 f_{F_s} \rangle &= 4/75(9 + 3F_l(-1 + F_s) + F_s),\\
\langle f_1 f_{A_s} \rangle &= (16A_s)/75,\\
\langle f_1 f_{A_{s4}} \rangle &= (8A_{s4})/25,\\
\langle f_1 f_{A_{s5}} \rangle &= (2A_{s5})/5,\\
\langle f_1 f_{A_{s7}} \rangle &= (2A_{s7})/5,\\
\langle f_1 f_{A_{s8}} \rangle &= (8A_{s8})/25
\end{aligned}
$$

$$
\begin{aligned}
\langle f_3 f_3\rangle &= (32(6+3F_l(-1+F_s)+F_s))/1225,\\
\langle f_3 f_4\rangle &= -((64(-1+F_s)S_4)/1225),\\
\langle f_3 f_5\rangle &= -(16/175)(-1+F_s)S_5,\\
\langle f_3 f_6\rangle &= 0,\\
\langle f_3 f_7\rangle &= (16/175)(-1+F_s)S_7,\\
\langle f_3 f_8\rangle &= (64(-1+F_s)S_8)/1225,\\
\langle f_3 f_9\rangle &= 0,\\
\langle f_3 f_{F_s}\rangle &= -(48/175)(-1+F_s)S_3,\\
\langle f_3 f_{A_s}\rangle &= 0,\\
\langle f_3 f_{A_{s4}}\rangle &= (16A_{s4})/175,\\
\langle f_3 f_{A_{s5}}\rangle &= (4A_{s5})/25,\\
\langle f_3 f_{A_{s7}}\rangle &= -((4A_{s7})/25),\\
\langle f_3 f_{A_{s8}}\rangle &= -((16A_{s8})/175)
\end{aligned}
\tag{121}
$$

$$
\begin{aligned}
\langle f_4 f_4\rangle &= -32/3675(-15+3F_l(-1+F_s)+F_s-6S_3+6F_sS_3),\\
\langle f_4 f_5\rangle &= -(16/175)(-1+F_s)S_{6s},\\
\langle f_4 f_6\rangle &= -(16/175)(-1+F_s)S_5,\\
\langle f_4 f_7\rangle &= 0,\\
\langle f_4 f_8\rangle &= -(64(-1+F_s)S_9)/1225,\\
\langle f_4 f_9\rangle &= -(64(-1+F_s)S_8)/1225,\\
\langle f_4 f_{F_s}\rangle &= 0,\\
\langle f_4 f_{A_s}\rangle &= (16A_{s4})/175,\\
\langle f_4 f_{A_{s4}}\rangle &= (64A_s)/525,\\
\langle f_4 f_{A_{s5}}\rangle &= 0,\\
\langle f_4 f_{A_{s7}}\rangle &= 0,\\
\langle f_4 f_{A_{s8}}\rangle &= 0
\end{aligned}
$$

$$
\begin{aligned}
\langle f_5 f_5\rangle &= -(8/525)(-9+9F_l(-1+F_s)-6S_3+F_s(-5+6S_3)),\\
\langle f_5 f_6\rangle &= -(16/175)(-1+F_s)S_4,\\
\langle f_5 f_7\rangle &= -(16/175)(-1+F_s)S_9,\\
\langle f_5 f_8\rangle &= 0,\\
\langle f_5 f_9\rangle &= -(16/175)(-1+F_s)S_7,\\
\langle f_5 f_{F_s}\rangle &= -(8/25)(-1+F_s)S_5,\\
\langle f_5 f_{A_s}\rangle &= (4A_{s5})/25,\\
\langle f_5 f_{A_{s4}}\rangle &= 0,\\
\langle f_5 f_{A_{s5}}\rangle &= (16A_s)/75,\\
\langle f_5 f_{A_{s7}}\rangle &= 0,\\
\langle f_5 f_{A_{s8}}\rangle &= 0\\
\\
\langle f_6 f_6\rangle &= 8/525(18+15F_l(-1+F_s)-11F_s),\\
\langle f_6 f_7\rangle &= -(16/175)(-1+F_s)S_8,\\
\langle f_6 f_8\rangle &= -(16/175)(-1+F_s)S_7,\\
\langle f_6 f_9\rangle &= 0,\\
\langle f_6 f_{F_s}\rangle &= -(4/25)(-1+F_s)S_{6s},\\
\langle f_6 f_{A_s}\rangle &= 0,\\
\langle f_6 f_{A_{s4}}\rangle &= (4A_{s5})/25,\\
\langle f_6 f_{A_{s5}}\rangle &= (4A_{s4})/25,\\
\langle f_6 f_{A_{s7}}\rangle &= (4A_{s8})/25,\\
\langle f_6 f_{A_{s8}}\rangle &= (4A_{s7})/25\\
\\
\langle f_7 f_7\rangle &= -(8/525)(-9+9F_l(-1+F_s)+6S_3-F_s(5+6S_3)),\\
\langle f_7 f_8\rangle &= -(16/175)(-1+F_s)S_{6s},\\
\langle f_7 f_9\rangle &= -(16/175)(-1+F_s)S_5,\\
\langle f_7 f_{F_s}\rangle &= -(8/25)(-1+F_s)S_7,\\
\langle f_7 f_{A_s}\rangle &= (4A_{s7})/25,\\
\langle f_7 f_{A_{s4}}\rangle &= 0,\\
\langle f_7 f_{A_{s5}}\rangle &= 0,\\
\langle f_7 f_{A_{s7}}\rangle &= (16A_s)/75,\\
\langle f_7 f_{A_{s8}}\rangle &= 0
\end{aligned}
\tag{122}
$$

$$
\begin{aligned}
\langle f_8 f_8\rangle &= -32/3675(-15+3F_l(-1+F_s)+F_s+6S_3-6F_sS_3),\\
\langle f_8 f_9\rangle &= -(64(-1+F_s)S_4)/1225,\\
\langle f_8 f_{F_s}\rangle &= -(32/175)(-1+F_s)S_8,\\
\langle f_8 f_{A_s}\rangle &= (16A_{s8})/175,\\
\langle f_8 f_{A_{s4}}\rangle &= 0,\\
\langle f_8 f_{A_{s5}}\rangle &= 0,\\
\langle f_8 f_{A_{s7}}\rangle &= 0,\\
\langle f_8 f_{A_{s8}}\rangle &= (64A_s)/525\\
\\
\langle f_9 f_9\rangle &= (32(6+3F_l(-1+F_s)+F_s))/1225,\\
\langle f_9 f_{F_s}\rangle &= -(48/175)(-1+F_s)S_9,\\
\langle f_9 f_{A_s}\rangle &= 0,\\
\langle f_9 f_{A_{s4}}\rangle &= (16A_{s8})/175,\\
\langle f_9 f_{A_{s5}}\rangle &= (4A_{s7})/25,\\
\langle f_9 f_{A_{s7}}\rangle &= (4A_{s5})/25,\\
\langle f_9 f_{A_{s8}}\rangle &= (16A_{s4})/175\\
\\
\langle f_{F_s} f_{F_s}\rangle &= 8/35(2+F_l+F_s-F_lF_s),\\
\langle f_{F_s} f_{A_s}\rangle &= (16A_s)/35,\\
\langle f_{F_s} f_{A_{s4}}\rangle &= (8A_{s4})/35,\\
\langle f_{F_s} f_{A_{s5}}\rangle &= (2A_{s5})/5,\\
\langle f_{F_s} f_{A_{s7}}\rangle &= (2A_{s7})/5,\\
\langle f_{F_s} f_{A_{s8}}\rangle &= (8A_{s8})/35\\
\\
\langle f_{A_s} f_{A_s}\rangle &= 8/175(2-7F_l(-1+F_s)+3F_s),\\
\langle f_{A_s} f_{A_{s4}}\rangle &= -(16/175)(-1+F_s)S_4,\\
\langle f_{A_s} f_{A_{s5}}\rangle &= -(4/25)(-1+F_s)S_5,\\
\langle f_{A_s} f_{A_{s7}}\rangle &= -(4/25)(-1+F_s)S_7,\\
\langle f_{A_s} f_{A_{s8}}\rangle &= -(16/175)(-1+F_s)S_8\\
\\
\langle f_{A_{s4}} f_{A_{s4}}\rangle &= 8/525(15+9F_l(-1+F_s)+6S_3-F_s(5+6S_3)),\\
\langle f_{A_{s4}} f_{A_{s5}}\rangle &= -(4/25)(-1+F_s)S_{6s},\\
\langle f_{A_{s4}} f_{A_{s7}}\rangle &= 0,\\
\langle f_{A_{s4}} f_{A_{s8}}\rangle &= -(16/175)(-1+F_s)S_9
\end{aligned}
\tag{123}
$$

$$
\begin{aligned}
\langle f_{A_{s5}} f_{A_{s5}} \rangle &= 2/75(9 + 3F_l(-1 + F_s) + F_s + 6S_3 - 6F_sS_3), \\
\langle f_{A_{s5}} f_{A_{s7}} \rangle &= -(4/25)(-1 + F_s)S_9, \\
\langle f_{A_{s5}} f_{A_{s8}} \rangle &= 0 \\
\\
\langle f_{A_{s7}} f_{A_{s7}} \rangle &= 2/75(9 + 3F_l(-1 + F_s) + F_s - 6S_3 + 6F_sS_3), \\
\langle f_{A_{s7}} f_{A_{s8}} \rangle &= -(4/25)(-1 + F_s)S_{6s} \\
\\
\langle f_{A_{s8}} f_{A_{s8}} \rangle &= 8/525(15 + 9F_l(-1 + F_s) - 6S_3 + F_s(-5 + 6S_3))
\end{aligned}
\tag{124}
$$

X 2D plots of right sideband

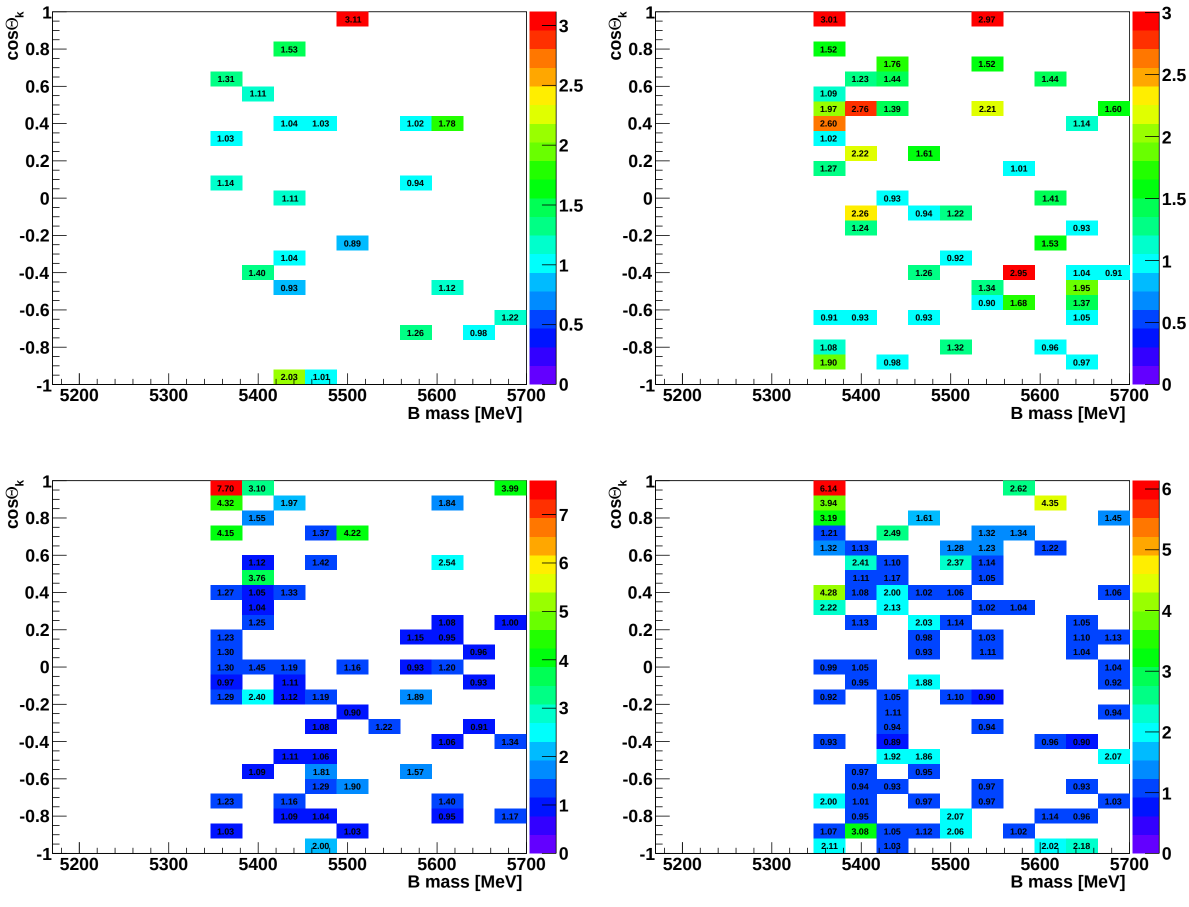

Figure 270: Distribution of B mass vs. $cos(\theta_l)$ of events in the right sideband. Events are weighted according to their angular acceptance. The plots are corresponding to different q^2 regions: top left: $0.1 - 0.98\,\mathrm{GeV}^2/c^4$, top right: $1.1 - 2.5\,\mathrm{GeV}^2/c^4$, bottom left: $2.5 - 4.0\,\mathrm{GeV}^2/c^4$, bottom right: $4.0 - 6.0\,\mathrm{GeV}^2/c^4$ In the control sample $B^0 \to J/\psi\, K^{*0}$ in the upper right corner a structure is visible. However, for the real analysis the expected number of events is small enough to neglect this.

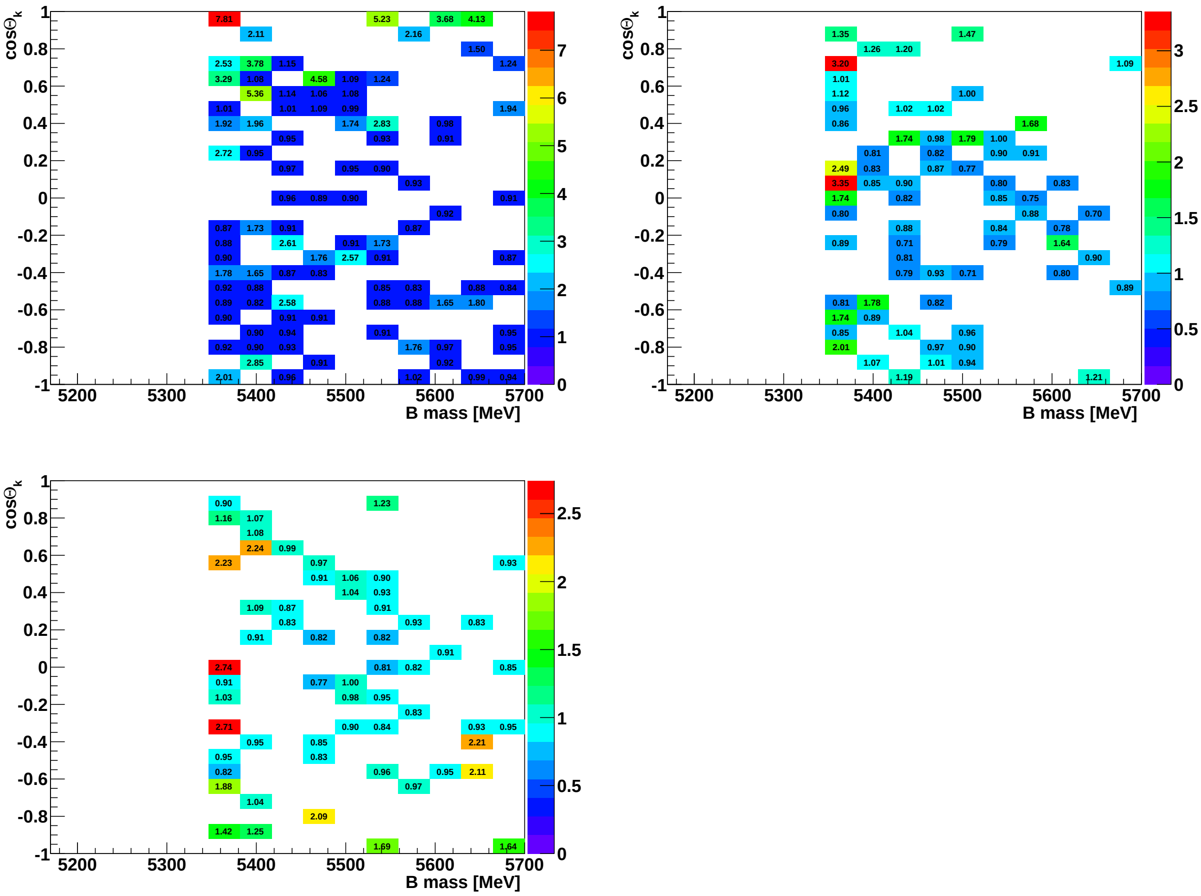

Figure 271: Distribution of B mass vs. $cos(\theta_l)$ of events in the right sideband. Events are weighted according to their angular acceptance. The plots are corresponding to different q^2 regions: top left: $6.0 - 8.0\,\mathrm{GeV}^2/c^4$, top right: $15.0 - 17.0\,\mathrm{GeV}^2/c^4$, bottom: $17.0 - 19.0\,\mathrm{GeV}^2/c^4$ In the control sample $B^0 \to J/\psi\, K^{*0}$ in the upper right corner a structure is visible. However, for the real analysis the expected number of events is small enough to neglect this.

Y Goodness of Fit

A detailed comparison of different goodness of fit methods can be found in Ref. [53]. The goodness of fit of the one-dimensional mass fits can be checked by looking at the pull distribution. However, due to the high dimensionality (mass and three angles) of the four-dimensional fit and the small number of events it is not possible to use the binned χ^2 method to determine the goodness of the fits. Instead the point-to-point dissimilarity method (P2PD) will be used to test the agreement of the fits with data. However, it must be noted that also this method only has limited power to distinguish "good" and "bad" fits. Due to the very limited statistics, small disagreements between fitted PDF and data can not be detected. Only if there is a clear disagreement between data and the fitted PDF a significantly lower p-value can be expected. This will be discussed in detail in the following sections.

Y.1 Point-to-point dissimilarity method

The point-to-point dissimilarity method [53] is designed to test if two data sets origin from the same PDF. A comparison of the fitted PDF with data can be performed by generating toy MC events according to the PDF. It is then tested if the data events agree with the generated toy MC events. To reduce statistical fluctuations, the number of generated MC events should be significantly larger than the number of data events. As a result this method is rather time consuming for a large number of events.

The test statistic T for the point-to-point dissimilarity method is calculated according to the following formula:

$$T = \frac{1}{n_d^2} \sum_{i,j>i}^{n_d} \Psi(|x_i^d - x_j^d|) - \frac{1}{n_d n_{mc}} \sum_{i,j}^{n_d,n_{mc}} \Psi(|x_i^d - x_j^{mc}|) \tag{125}$$

with n_d data and n_{mc} MC events and a function Ψ of the distance between two points. The first term means that Ψ is evaluated and summed up for all data points. In the second term Ψ is calculated for all data and MC events. A third term which calculates the distance between all MC events is usually neglected.

There is no strict rule for the choice of the distance function Ψ. As discussed in Ref. [53] a Gaussian function provides good results. The widths of the multidimensional Gaussian must be tuned with simulation to deliver the best results. Nevertheless the results should not strongly depend on this tuning parameter. In the following a Gaussian function is used for Ψ. As the fit is done in four dimensions, a four-dimensional Gaussian function is used:

$$\Psi(x_i, x_j) = e^{-\frac{(m_i-m_j)^2}{2\sigma_m^2} - \frac{(\phi_i-\phi_j)^2}{2\sigma_\phi^2} - \frac{(\theta_{l,i}-\theta_{l,i})^2}{2\sigma_{\theta_l}^2} - \frac{(\theta_{k,i}-\theta_{k,i})^2}{2\sigma_{\theta_k}^2}} \tag{126}$$

The four tuning parameters (σ_i) must be tuned such the influence of all four terms is balanced. If one term would be dominating, the effect of the other terms would vanish and only the agreement of the dominating variable would be tested.

The p-value is determined in the following way. First, the test statistic of the data sample is calculated. Afterwards, the data events are replaced by the same number of toy MC events and T is calculated again[7]. This is repeated several times until the T distribution is known for the specific case. The p-value is the fraction of toys, where the value of T is lower than the one calculated on data. For the toy studies in the next sections the following settings are used:

- $n_{mc}/n_d = 75$
- N_{toys} to determine p-value $= 500$
- $\sigma_m = 40\,\text{MeV}$
- $\sigma_{phi} = \pi/2$
- $\sigma_{\theta_l} = 1$
- $\sigma_{\theta_k} = 1$

Y.2 Comparison of χ^2 method and P2PD method

To check the performance of the point-to-point dissimilarity method it is compared to the χ^2 method. The test scenario is chosen such that the χ^2 method is still possible (one dimension, no empty bins) and the P2PD method provides a result in a reasonable computing time. It was chosen to look at 500 events in a broad mass peak (see Fig. 272). The χ^2 value is calculated for 10 bins, as shown in the figure. It is tested, that for this case this gives slightly better results than using 20 bins. Events are generated according to the PDF. Afterwards the p-value of the events are calculated with both methods. No fitting procedure is applied.

The resulting p-value distribution can be seen in Fig. 273(top left). There is only a small deviation to the ideal flat distribution and within the desired precision there is no bias. To check the power of both methods to identify wrong PDFs, the PDFs are changed before calculating the p-value. Namely the position of the B^0 mass peak is shifted to higher values by 10, 25, 50 MeV. In these cases the p-values of both methods get significantly smaller. The P2PD method shows a better discrimination power than the χ^2 method.

Y.3 Testing P2PD method in a realistic scenario

The performance of the P2PD method is tested in scenarios similar to what is expected to be present in the $B^0 \to K^{*0}\mu^+\mu^-$ fit (see Fig 274). The mass and angular distribution is taken from a $B^0 \to J/\psi K^{*0}$ data fit . The signal fraction parameter is reduced to 0.80, to account for the significantly larger background fraction which is expected in $B^0 \to K^{*0}\mu^+\mu^-$ compared to $B^0 \to J/\psi K^{*0}$. In each toy 200 events are generated.

[7] Actually due to timing no new MC events are generated, but a subsample is randomly drawn from the combined pool of MC and data events

In a first test the power of the P2PD method to identify a shifted mass peak is tested, similar to what was done in the last subsection. Events are generated according to a PDF and afterwards the B^0 mass in the PDF is changed. Compared to the last subsection the mass peak is now much better defined and smaller mass shifts are used (namely 1, 5, 15 MeV). Two different options are compared. In one case the test statistic is calculated using only the mass, in the second case all four variables (mass and 3 angles) are considered. Because only the mass is modified, it is expected that also testing the mass alone provides better results. The results of this test can be seen in Fig. 275. The P2PD method shows an unbiased performance in this scenario and shows only p values significantly below 1% for a mass shift of 15 MeV. The 1D case performs only slightly better than the 4D case.

In a second test the capability to identify a wrong angular distribution is tested. The signal fraction is reduced from originally 0.8 to 0.5,0.3 and 0.1 which affects the angular pdf as signal and background are differently distributed. Again two different options are compared. In the first case the test statistic is calculated using the angles only. In the second case all four variables are used. Modifying the signal fraction has the largest impact on the mass peak. Thus it can be expected, that in this test the option also using mass information performs best, what can be seen in Fig. 276. Nevertheless also the option using only the angular variables is sensitive to a wrong PDF.

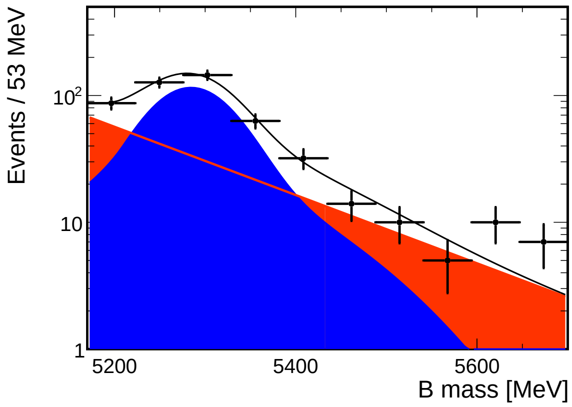

Figure 272: PDF distribution to test both the P2PD and χ^2 method. As a test scenario a broad peak in one dimension with 500 events is chosen. The data points show one possible toy.

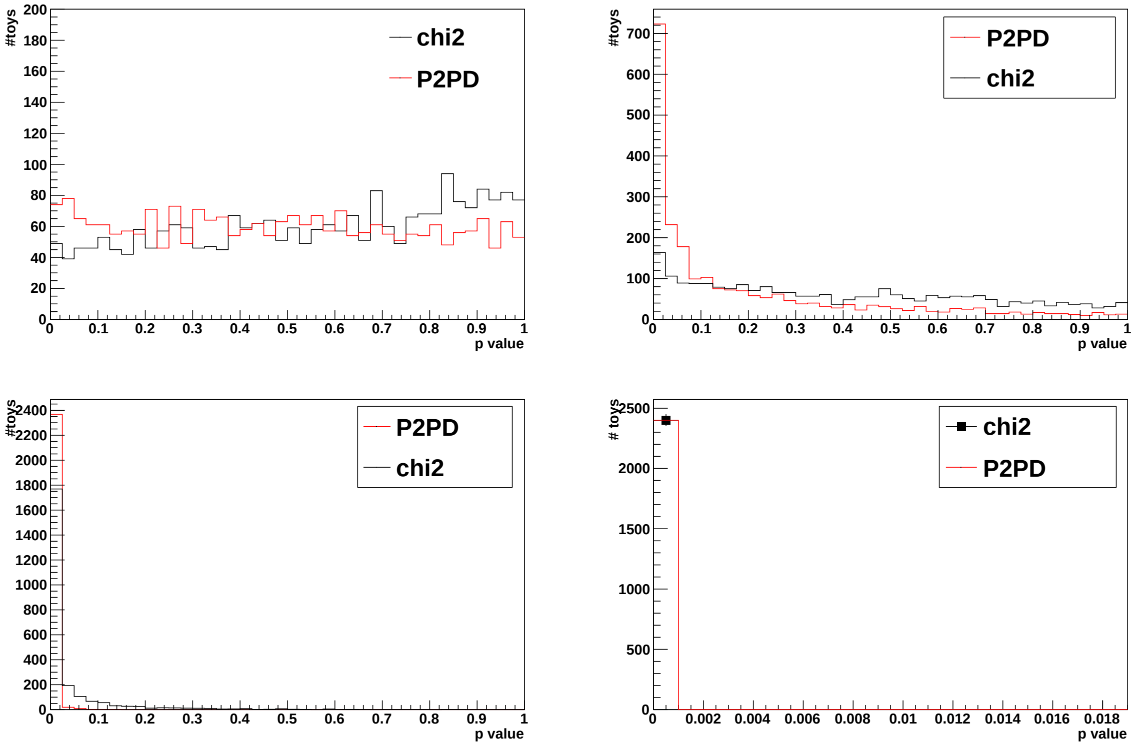

Figure 273: Distribution of the p value for four different tests. On the top left the agreement of the data points to the generated PDF is tested. On the top right the mass peak is shifted after the generation by 10 MeV, bottom left by 25 MeV, bottom right by 50 MeV.

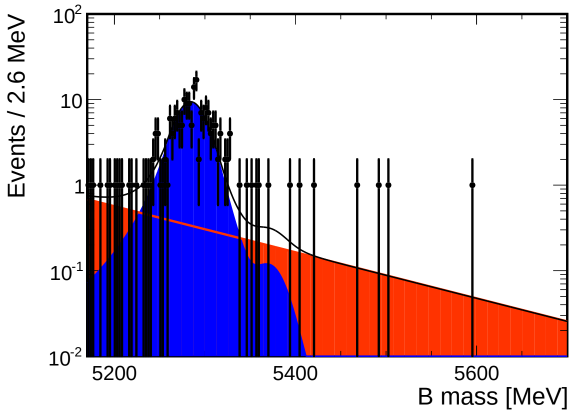

Figure 274: PDF distribution to test the P2PD method on a realistic scenario. The mass and angular distribution is taken from a fit to $B^0 \to J/\psi\, K^{*0}$ data. The signal fraction is set to 0.8 and the number of events is 200. The data points show one possible toy.

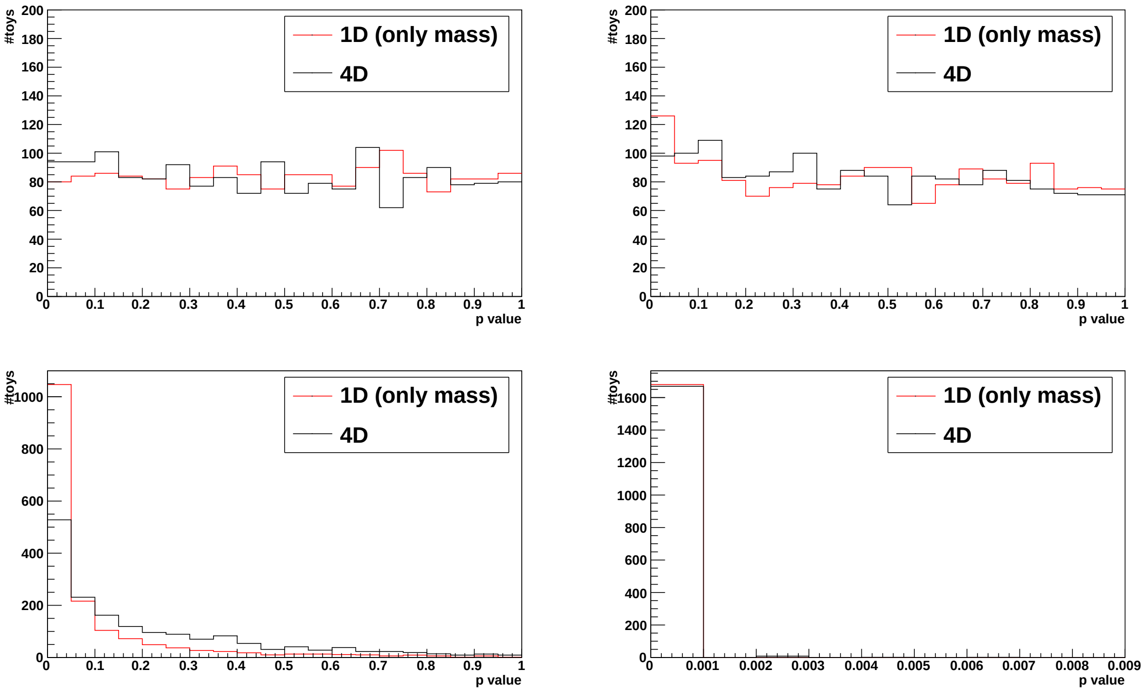

Figure 275: Distribution of the p value for four different tests. On the top left the agreement of the data points to the generated PDF is tested. On the top right the mass peak is shifted after the generation by 1 MeV, bottom left by 5 MeV, bottom right by 15 MeV.

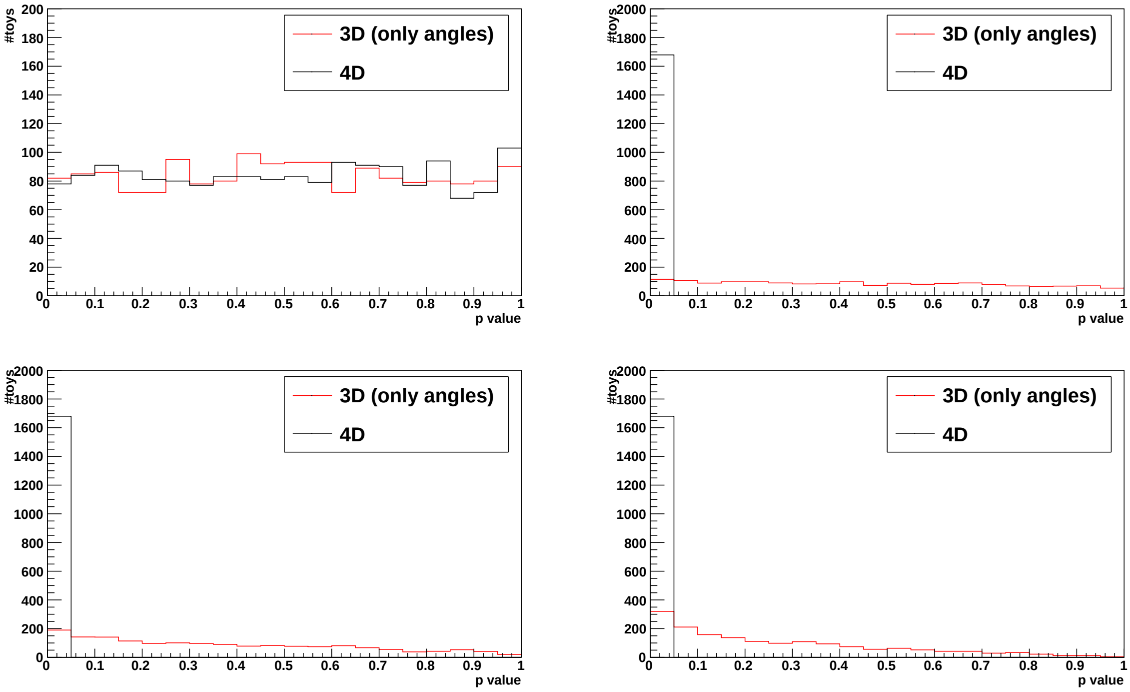

Figure 276: Distribution of the p value for four different tests. On the top left the agreement of the data points to the generated PDF is tested ($f_{sig} = 0.8$). On the top right the signal fraction is set after generation to $f_{sig} = 0.5$, bottom left $f_{sig} = 0.3$, bottom right $f_{sig} = 0.1$.

Z Exotic charmonium states in $B^0 \to J/\psi K^+\pi^-$

The Belle experiment sees evidence for two exotic charmonium states, $Z_c^+(4200)$ and $Z_c^+(4430)$, decaying to $J/\psi\pi^+$ in an amplitude analysis of $B^0 \to J/\psi K^+\pi^-$ decays [54]. The two states have a favoured J^P of 1^+. The $Z_c^+(4430)$ is consistent with what LHCb sees in it amplitude analysis of $B^0 \to \psi(2S)K^+\pi^-$ [55].

To study the possible impact of these Z_c^+ states in the $795 < m(K^+\pi^-) < 995\,\mathrm{MeV}/c^2$ mass window used in the analysis, toy experiments were generated using a matrix element squared,

$$|\mathcal{M}|^2 = \sum_{\lambda_\psi=-1,0,1} \Bigg| \sum_k A_{k,\lambda_\psi} R(m_{K^+\pi^-}|m_k,\Gamma_k) d^{J_k}_{\lambda_\psi,0}(\theta_K) + \tag{127}$$

$$\sum_{\lambda^Z_\psi=-1,0,1} d^1_{\lambda^z_\psi,\lambda_\psi}(\theta_{K,Z}) A_{Z,\lambda^Z_\psi} R(m_{\psi\pi^-}|m_Z,\Gamma_Z) d^{J_Z}_{0,\lambda^z_\psi}(\theta_Z) \Bigg|. \tag{128}$$

$$\tag{129}$$

Here, the $d^J_{m',m}$ are Wigner d-functions and the functions R are relativistic Breit-Wigner functions describing the line shapes of the different states. The amplitudes A_{k,λ_ψ} and A_{Z,λ^Z_ψ} were taken from Belles result. By parity conservation

$$A_{Z,-1} = A_{Z,+1} \tag{130}$$

for a $J^P = 1^+$ state. This is the same model used in LHCb's Z_c^+ analysis.

The P-wave observables are not significantly effected by the presence of the Z_c^+, but a sizeable difference is seen in the S-wave fraction, F_S. Interestingly in toys included the Z_c^+ states, a difference is seen between the value of F_S estimated by the angular fit/moments and the $m(K^+\pi^-)$ mass fit (see Table 197). This difference is consistent with what is seen in data. The $\cos\theta_K$ and $m(K^+\pi^-)$ distribution of toys with and without the Z are included in Fig. 277. Small differences are seen in the $795 < m(K^+\pi^-) < 995\,\mathrm{MeV}/c^2$ mass window.

Table 197: Result of fitting either the angular or $m(K^+\pi^-)$ distribution of toy experiments for the S-wave fraction, F_S, in three configurations: one in which only the $K^*(892)$, $K_0(800)$ and $K_0(1430)$ were included in the toy; one in which K^* states up-to $J = 4$ were included; and finally one in which the Z_c^+ states were added.

model	angular	$m(K^+\pi^-)$
$J \leq 4$ + $Z(4200)$ + $Z(4430)$	0.067 ± 0.002	0.050 ± 0.002
$J \leq 4$	0.057 ± 0.002	0.053 ± 0.002
$K^*(892) + K_0(800) + K_0(1430)$	0.052 ± 0.002	0.047 ± 0.02

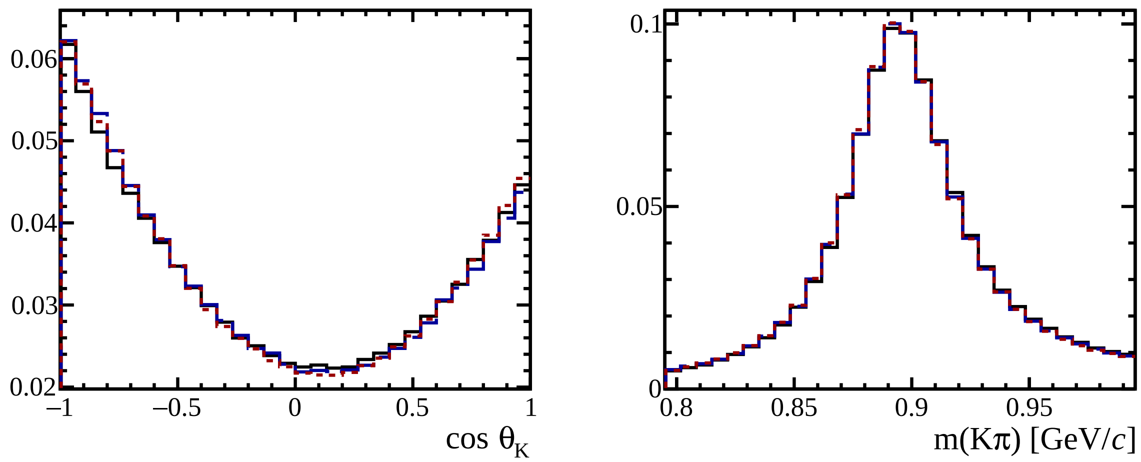

Figure 277: The $\cos\theta_K$ and $m(K^+\pi^-)$ distributions of toy experiments produced with: only the $K^*(892)$, $K_0(800)$ and $K_0(1430)$ (red short-dashed); all K^* states up to $J = 4$ (blue long-dashed); and adding the two Z_c^+ states observed by Belle (black solid-line). In each case only events in the $795 < m(K^+\pi^-) < 995\,\mathrm{MeV}/c^2$ mass window are shown.

References

[1] LHCb collaboration, R. Aaij *et al.*, *Differential branching fraction and angular analysis of the decay $B^0 \to K^{*0}\mu^+\mu^-$*, JHEP **08** (2013) 131, `arXiv:1304.6325`.

[2] LHCb collaboration, R. Aaij *et al.*, *Measurement of form-factor-independent observables in the decay $B^0 \to K^{*0}\mu^+\mu^-$*, Phys. Rev. Lett. **111** (2013) 191801, `arXiv:1308.1707`.

[3] W. Altmannshofer *et al.*, *Symmetries and Asymmetries of $B \to K^*\mu^+\mu^-$ Decays in the Standard Model and Beyond*, JHEP **0901** (2009) 019, `arXiv:0811.1214`.

[4] S. Descotes-Genon, T. Hurth, J. Matias, and J. Virto, *Optimizing the basis of $B \to K^*\ell^+\ell^-$ observables in the full kinematic range*, JHEP **1305** (2013) 137, `arXiv:1303.5794`.

[5] S. Descotes-Genon, J. Matias, and J. Virto, *Understanding the $B \to K^*\mu^+\mu^-$ Anomaly*, Phys. Rev. **D88** (2013), no. 7 074002, `arXiv:1307.5683`.

[6] W. Altmannshofer and D. M. Straub, *New physics in $B \to K^*\mu\mu$?*, Eur. Phys. J. **C73** (2013) 2646, `arXiv:1308.1501`.

[7] F. Beaujean, C. Bobeth, and D. van Dyk, *Comprehensive Bayesian analysis of rare (semi)leptonic and radiative B decays*, Eur. Phys. J. **C74** (2014) 2897, `arXiv:1310.2478`.

[8] T. Hurth and F. Mahmoudi, *On the LHCb anomaly in $B \to K^*\ell^+\ell^-$*, JHEP **1404** (2014) 097, `arXiv:1312.5267`.

[9] S. Jäger and J. Martin Camalich, *On $B \to Vll$ at small dilepton invariant mass, power corrections, and new physics*, JHEP **1305** (2013) 043, `arXiv:1212.2263`.

[10] S. Descotes-Genon, L. Hofer, J. Matias, and J. Virto, *On the impact of power corrections in the prediction of $B^0 \to K^{*0}\mu^+\mu^-$ observables*, `arXiv:1407.8526`.

[11] J. Lyon and R. Zwicky, *Resonances gone topsy turvy - the charm of QCD or new physics in $b \to s\ell^+\ell^-$?*, `arXiv:1406.0566`.

[12] LHCb collaboration, R. Aaij *et al.*, *Differential branching fractions and isospin asymmetry of $B \to K^{(*)}\mu^+\mu^+$ decays*, JHEP **06** (2014) 133, `arXiv:1403.8044`.

[13] $B^0 \to K^{*0}\mu^+\mu^-$ WG, *$B^0 \to K^{*0}\mu^+\mu^-$ selection*, LHCb-INT-2013-058, 2013.

[14] C. Bobeth, G. Hiller, and D. van Dyk, *The Benefits of $\bar{B} \to \bar{K}^*l^+l^-$ Decays at Low Recoil*, JHEP **1007** (2010) 098, `arXiv:1006.5013`.

[15] C. Bobeth, G. Hiller, D. van Dyk, and C. Wacker, *The Decay $B \to K l^+ l^-$ at Low Hadronic Recoil and Model-Independent Delta B = 1 Constraints*, JHEP **1201** (2012) 107, `arXiv:1111.2558`.

[16] F. Beaujean, C. Bobeth, D. van Dyk, and C. Wacker, *The EOS software package*, http://project.het.physik.tu-dortmund.de/eos/, 2014.

[17] T. Blake *et al.*, *Angular analysis of $B^0 \to K^{*0}\mu^+\mu^-$ at LHCb with 1 fb^{-1}*, LHCb-ANA-2012-051.

[18] C. Bobeth, G. Hiller, and G. Piranishvili, *CP Asymmetries in bar $B \to \bar{K}^*(\to \bar{K}\pi)\bar{\ell}\ell$ and Untagged $\bar{B}_s$, $B_s \to \phi(\to K^+K^-)\bar{\ell}\ell$ Decays at NLO*, JHEP **0807** (2008) 106, `arXiv:0805.2525`.

[19] T. Blake and C. Langenbruch, *Angular conventions for the decays $B^0 \to K^{*0}\mu^+\mu^-$ and $B^0_s \to \phi\mu^+\mu^-$*, LHCb-INT-2012-021, 2012.

[20] LHCb collaboration, R. Aaij *et al.*, *Measurement of the polarization amplitudes in $B^0 \to J/\psi K^*(892)^0$ decays*, Phys. Rev. **D88** (2013) 052002, `arXiv:1307.2782`.

[21] D. Becirevic and E. Schneider, *On transverse asymmetries in $B^0 \to K^{*0}\ell^+\ell^-$*, Nucl. Phys. **B854** (2012) 321, `arXiv:1106.3283`.

[22] F. Krüger and J. Matias, *Probing new physics via the transverse amplitudes of $B^0 \to \overline{K}^{*0}(\to K^-\pi^+)\ell^+\ell-$ at large recoil*, Phys. Rev. **D71** (2005) 094009, `arXiv:hep-ph/0502060`.

[23] W. Verkerke and D. Kirkby, *The RooFit toolkit for data modeling*, ArXiv Physics e-prints (2003) `arXiv:physics/0306116`.

[24] G. J. Feldman and R. D. Cousins, *Unified approach to the classical statistical analysis of small signals*, Phys. Rev. D **57** (1998) 3873, `arXiv:physics/9711021`.

[25] B. Sen, M. Walker, and M. Woodroofe, *On the unified method with nuisance parameters*, Statistica Sinica **19** (2009) 301.

[26] BaBar collaboration, B. Aubert *et al.*, *Measurement of decay amplitudes of $B \to J/\psi K^*, \psi(2S)K^*$, and $\chi_{c1}K^*$ with an angular analysis*, Phys. Rev. **D76** (2007) 031102, `arXiv:0704.0522`.

[27] Belle collaboration, R. Itoh *et al.*, *Studies of CP violation in $B^0 \to J/\psi K^*$ decays*, Phys. Rev. Lett. **95** (2005) 091601, `arXiv:hep-ex/0504030`.

[28] CDF collaboration, *Angular analysis of $B^0_s \to J/\psi\phi$ and $B^0 \to J/\psi K^*$ decays and measurement of $\Delta\Gamma_s$ and ϕ_s*, CDF public note 8950, www-cdf.fnal.gov/physics/new/bottom/bottom.html.

[29] D. Becirevic and A. Tayduganov, *Impact of* $B \to K_0^* \ell^+ \ell^-$ *on the New Physics search in* $B \to K^* \ell^+ \ell^-$ *decay*, Nucl. Phys. **B868** (2013) 368, `arXiv:1207.4004`.

[30] J. Bressieux, G. Cowan, M. Kreps, O. Schneider, T. Skwarnicki, Q. Wenbin, *Evidence for the resonant character of the* $Z(4430)^- \to \psi(2S)\pi^-$ *mass peak observed in* $B^0 \to \psi(2S)K^+\pi^-$ *decays, and determination of the* $Z(4430)^-$ *spin-parity* , LHCb-ANA-2013-053, 2013.

[31] D. Aston *et al.*, *A Study of K- pi+ Scattering in the Reaction K- p —¿ K- pi+ n at 11-GeV/c*, Nucl. Phys. **B296** (1988) 493.

[32] F. James, *Statistical methods in experimental physics*, .

[33] A. S. Dighe, I. Dunietz, and R. Fleischer, *Extracting CKM phases and* $B_s - \bar{B}_s$ *mixing parameters from angular distributions of nonleptonic B decays*, Eur. Phys. J. **C6** (1999) 647, `arXiv:hep-ph/9804253`.

[34] B. Efron, *Bootstrap methods: Another look at the jackknife*, The Annals of Statistics **7** (1979), no. 1 1.

[35] U. Egede *et al.*, *On the new physics reach of the decay mode* $\bar{B}_d \to \bar{K}^{*0}\ell^+\ell^-$, Journal of High Energy Physics **2010** (2010), no. 10 .

[36] T. Blake, U. Egede, and A. Shires, *The effect of s-wave interference on the* $\bar{b}_d \to \bar{k}^{*0}\ell^+\ell^-$ *angular observables*, Journal of High Energy Physics **2013** (2013), no. 3 .

[37] D. Beirevi and A. Tayduganov, *Impact of on the new physics search in decay*, Nuclear Physics B **868** (2013), no. 2 368 .

[38] D. Das, G. Hiller, M. Jung, and A. Shires, *The* $\bar{B} \to \bar{K}\pi\ell^+\ell^-$ *and* $\bar{B}_s \to \bar{K}K\ell^+\ell^-$ *distributions at low hadronic recoi*, Journal of High Energy Physics **2014** (2014), no. 9 .

[39] S. Descotes-Genon, T. Hurth, J. Matias, and J. Virto, $\bar{b}_d \to \bar{k}^{*0}\ell^+\ell^-$ *observables in the full kinematic range*, Journal of High Energy Physics **2013** (2013), no. 5 .

[40] Particle Data Group, J. Beringer *et al.*, *Review of particle physics*, Phys. Rev. **D86** (2012) 010001.

[41] C.-D. Lü and W. Wang, *Analysis of* $B \to K_J^*(\to K\pi)\mu^+\mu^-$ *in the higher kaon resonance region*, Phys. Rev. D **85** (2012) 034014.

[42] U.-G. Meiner and W. Wang, *Generalized heavy-to-light form factors in light-cone sum rules*, Physics Letters B **730** (2014), no. 0 336 .

[43] LHCb collaboration, R. Aaij *et al.*, *Measurement of the* $\bar{B}^0_{(s)} - B^0_{(s)}$ *production asymmetry in 7 TeV pp collisions*, `arXiv:1408.0275`, submitted to Phys. Lett. B.

[44] S. Stahl *et al.*, *Search for CP violation in* $D^0 \to KK^+, \pi\pi^+$ *using semileptonic B decays on 3 fb*$^{-}$1, .

[45] LHCb collaboration, R. Aaij *et al.*, *Measurement of CP asymmetry in* $D^0 \to K^-K^+$ *and* $D^0 \to \pi^-\pi^+$ *decays*, JHEP **07** (2014) 041, arXiv:1405.2797.

[46] W. Altmannshofer and D. M. Straub, *New physics in* $b \to s$ *transitions after LHC run 1*, arXiv:1411.3161.

[47] A. Bharucha, D. M. Straub, and R. Zwicky, $B \to V\ell^+\ell^-$ *in the Standard Model from Light-Cone Sum Rules*, arXiv:1503.0553.

[48] A. Khodjamirian, T. Mannel, A. Pivovarov, and Y.-M. Wang, *Charm-loop effect in* $B \to K^{(*)}\ell^+\ell^-$ *and* $B \to K^*\gamma$, JHEP **1009** (2010) 089, arXiv:1006.4945.

[49] P. Ball and R. Zwicky, *B(D,S) —¿ rho, omega, K*, phi decay form-factors from light-cone sum rules revisited*, Phys. Rev. **D71** (2005) 014029, arXiv:hep-ph/0412079.

[50] M. De Cian *et al.*, *Measurement of new angular observables in the decay* $B^0 \to K^{*0}\mu^+\mu^-$, LHCb-ANA-2013-016.

[51] LHCb collaboration, R. Aaij *et al.*, *Observation of* $B_s^0 \to \chi_{c1}\phi$ *decay and study of* $B^0 \to \chi_{c1,2}K^{*0}$ *decays*, Nucl. Phys. **B874** (2013) 663, arXiv:1305.6511.

[52] ATLAS collaboration, G. A. et al, *Measurement of the inclusive isolated prompt photon cross section in pp collisions at* $\sqrt{7}$ *TeV with the ATLAS detector*, ArXiv Physics e-prints (2010) arXiv:1012.4389.

[53] M. Williams, *How good are your fits? Unbinned multivariate goodness-of-fit tests in high energy physics*, JINST **5** (2010) P09004, arXiv:1006.3019.

[54] Belle Collaboration, K. Chilikin *et al.*, *Observation of a new charged charmoniumlike state in* $\bar{B}^0 J/K^{-+}$ *decays*, Phys. Rev. **D90** (2014), no. 11 112009, arXiv:1408.6457.

[55] LHCb collaboration, R. Aaij *et al.*, *Observation of the resonant character of the* $Z(4430)^-$ *state*, Phys. Rev. Lett. **112** (2014), no. 22 222002, arXiv:1404.1903.